

Georgia State University

ScholarWorks @ Georgia State University

Physics and Astronomy Dissertations

Department of Physics and Astronomy

8-8-2005

Rest Frame Variability Characteristics of Blazars

John Patrick McFarland

Follow this and additional works at: https://scholarworks.gsu.edu/phy_astr_diss



Part of the [Astrophysics and Astronomy Commons](#), and the [Physics Commons](#)

Recommended Citation

McFarland, John Patrick, "Rest Frame Variability Characteristics of Blazars." Dissertation, Georgia State University, 2005.

doi: <https://doi.org/10.57709/1059803>

This Dissertation is brought to you for free and open access by the Department of Physics and Astronomy at ScholarWorks @ Georgia State University. It has been accepted for inclusion in Physics and Astronomy Dissertations by an authorized administrator of ScholarWorks @ Georgia State University. For more information, please contact scholarworks@gsu.edu.

REST FRAME VARIABILITY CHARACTERISTICS OF BLAZARS

by

JOHN PATRICK MCFARLAND

Under the Direction of H. Richard Miller

ABSTRACT

Blazars exhibit the most extreme variability of the class of objects known as active galactic nuclei (AGN). They are characterized by a featureless continuum, high polarization, and variability at all wavelengths and time-scales. The amplitude of optical variations can range from less than 0.1 magnitude on time-scales of minutes to hours, to greater than 5.0 magnitudes on time-scales of months to years. Gamma-ray variability amplitudes can span a range of as much as three orders of magnitude on a time-scale as short as a few days. These characteristics are consistent with a supermassive black hole accreting matter at the heart of the host galaxy. However, the observed properties of these objects don't necessarily reflect the intrinsic properties because the emissions have been modified by their propagation over cosmological distances.

The intrinsic variability of 7 blazars, which have very different redshifts, have been investigated using several different analytical approaches; i.e., structure function analysis, variability index analysis, and light curve analysis. By transforming observed measurements into the rest frame of the source, the intrinsic properties of the variability can be compared. These variability characteristics of blazars, as seen in their rest frame, and as a function of

state, are discussed in reference to their general characteristics and classification schemes.

In addition to the intrinsic variability investigation, a multi-color variability investigation has been undertaken. This investigation utilizes new data collected through the SMARTS (Small and Moderate Aperture Research Telescope System) consortium simultaneously in both the optical and near-infrared (near-IR) wavebands. The 11 objects in this sample, which have very different redshifts, are investigated using light curve analysis and color index analysis to determine if there exists any changes in color as a function of time (leads or lags) or variability amplitude.

The results from both investigations impose constraints on the nature and structure of the emitting regions (e.g. variability originating from turbulence in the jet versus flares in an accretion disk, and size limits of emission regions).

INDEX WORDS: Blazar, Active galaxy, Rest frame, Variability

REST FRAME VARIABILITY CHARACTERISTICS OF BLAZARS

by

JOHN PATRICK MCFARLAND

A Dissertation Submitted in Partial Fulfillment of the Requirements for the degree of

Doctor of Philosophy

Georgia State University

2005

Copyright by
John Patrick McFarland
2005

REST FRAME VARIABILITY CHARACTERISTICS OF BLAZARS

by

JOHN PATRICK MCFARLAND

| | |
|-----------------|--------------------------------------------------------------------------------------|
| Major Professor | H. Richard Miller |
| Committee | William G. Bagnuolo, Jr. D. Michael Crenshaw Steven T. Manson Paul J. Wiita |

Electronic Version Approved:

Office of Graduate Studies
College of Arts and Sciences
Georgia State University
May 2005

For Heather

Acknowledgements

A dissertation . . . is a dance. And as in a dance, one needs partners. Every partner moves the dance forward until its great finale. I would like to thank all those partners for what they contributed. First and foremost, I would like to thank my future wife Heather, if she'll still have me, for putting up with all my moods and helping in too many ways to count during the completion of this monumental work. You have stood by me through the smooth times and the rough times, through the delays and the charges, and through the rights and the wrongs. Thank you only scratches the surface. And next to my advisor, Dick Miller for always believing it could be done if I tried hard enough. Your talks have helped move mountains and also added new ones that were well worth climbing. Thank you the rest of my committee, Bill Bagnuolo, Mike Crenshaw, Steve Manson, and Paul Wiita, for their various suggestions and most of all, their patience. Thank you to Bill for being there, to Paul for filling in wonderfully when Dick wasn't available, to Mike for keeping me honest and suggesting new ways of looking at the same old things, and to Steve for filling in at the last possible moment. Thank you to Bill Nelson for being a committee member until scheduling forced you off. And many thanks to Doug Gies, a committee member in spirit, for the countless talks over the years—you have always had the best advice.

Many thanks go to the PEGAns past and present: to Elizabeth Ferrara for getting me

started in all this and forcing me to learn the ins and outs of data reduction and inspiring more than one very useful script; to Amy Campbell for giving moral and technical support just when I needed it most; to Angela Osterman for her hours and hours of tireless data reduction before she had a good idea what it all was really for; to Kevin Marshall and Wes Ryle for carrying on the tradition and continuing to improve what I have built upon from previous generations of PEGAns.

Any dissertation requires data, and I would like to acknowledge the many sources of that data. For the most recent, Todd Henry through the SMARTS consortium has provided access to multiple telescopes from which a very large proportion of data used here has been acquired. Lowell Observatory has kindly provided access to several of their telescopes, and the vast majority of archival data has been collected through them over many years. The late Bob Fried collected data with and allowed access to Braeside Observatory, supplementing the large dataset used here.

This research has made use of the NASA/IPAC Extragalactic Database (NED) which is operated by the Jet Propulsion Laboratory, California Institute of Technology, under contract with the National Aeronautics and Space Administration. This research was supported in part by a grant from the Research Corporation and the PEGA-RPE program at Georgia State University.

And finally I'd like to thank my family. Their love and support through all my years of education, 24 by last count, has made all of this possible. And last, but absolutely not least, thank you to my grandmother who always believed I could do it, but unfortunately could not be here in person to celebrate.

Contents

| | |
|-----------------------------------------------|-------------|
| Acknowledgements | v |
| List of Tables | viii |
| List of Figures | ix |
| List of Abbreviations | x |
| 1 Introduction | 1 |
| 1.1 AGN History | 2 |
| 1.1.1 Discovery | 2 |
| 1.1.2 Classification | 3 |
| 1.1.3 Unified Model | 4 |
| 1.2 Blazars | 6 |
| 1.2.1 Classification | 7 |
| 1.2.2 Morphology | 8 |
| 1.2.3 Continuum Emission | 8 |
| 1.3 Blazar Variability | 10 |
| 1.3.1 Optical Variability | 11 |
| 1.3.2 X-ray/Gamma-ray Variability | 14 |
| 1.3.3 Radio Variability | 14 |
| 1.4 Blazar Selection Effects | 15 |
| 1.5 Research Direction | 15 |
| 2 The Data: Acquisition and Reductions | 18 |
| 2.1 Data Sources | 18 |
| 2.2 Reduction Software | 20 |
| 2.2.1 IRAF | 20 |
| 2.2.2 CCDPhot | 21 |
| 2.3 Data Sorting and Mining | 22 |
| 2.4 The Dataset | 24 |
| 3 Rest Frame Analysis | 54 |
| 3.1 Shifting to the Rest Frame | 54 |
| 3.1.1 Relativistic Effects | 54 |
| 3.1.2 BL Lacertae, the Baseline | 57 |

| | | |
|----------|------------------------------------------------|------------|
| 3.2 | Archival Data | 58 |
| 3.2.1 | 0235 + 164 | 60 |
| 3.2.2 | 1156 + 295 | 86 |
| 3.2.3 | 1622 − 297 | 94 |
| 3.2.4 | 1633 + 382 | 105 |
| 3.2.5 | 1641 + 399 | 128 |
| 3.2.6 | 2200 + 420 | 152 |
| 3.2.7 | 2223 − 052 | 212 |
| 3.2.8 | Comparison in the Rest Frame | 241 |
| 3.3 | Analysis Methods | 243 |
| 3.3.1 | Light Curves | 244 |
| 3.3.2 | Structure Function | 247 |
| 3.3.3 | Variability Index | 249 |
| 3.4 | Rest Frame Analysis Results | 250 |
| 3.4.1 | Variability and State | 255 |
| 3.4.2 | Structure Function in the Rest Frame | 261 |
| 3.4.3 | Variability Index in the Rest Frame | 280 |
| 4 | Multi-color Analysis | 296 |
| 4.1 | SMARTS Data | 297 |
| 4.1.1 | 0420 − 014 | 298 |
| 4.1.2 | 0818 − 128 | 301 |
| 4.1.3 | 1226 + 023 | 303 |
| 4.1.4 | 1253 − 055 | 305 |
| 4.1.5 | 1510 − 089 | 307 |
| 4.1.6 | 1514 − 241 | 309 |
| 4.1.7 | 1622 − 297 | 311 |
| 4.1.8 | 2005 − 489 | 313 |
| 4.1.9 | 2155 − 304 | 315 |
| 4.1.10 | 2223 − 052 | 317 |
| 4.1.11 | 2345 − 167 | 319 |
| 4.2 | Analysis Methods | 321 |
| 4.2.1 | Cross Correlation Function | 321 |
| 4.3 | Multi-color Analysis Results | 322 |
| 4.3.1 | Amplitudes of Colors | 322 |
| 4.3.2 | Leads and Lags | 323 |
| 4.3.3 | Rest Frame Correlations | 327 |
| 5 | Discussion and Future Work | 330 |
| 5.1 | Discussion | 330 |
| 5.1.1 | Variability in the Rest Frame | 331 |
| 5.1.2 | Color variability | 336 |
| 5.2 | Future Work | 339 |

| | | |
|----------|----------------------|------------|
| A | Scripts | 341 |
| A.1 | pegasort | 341 |
| A.2 | pegaplot | 346 |
| A.3 | pegacalib | 363 |
| B | Analysis Code | 366 |
| B.1 | pegabin | 366 |
| B.2 | mag2flux | 370 |
| B.3 | obs2ref | 374 |
| B.4 | strfun | 376 |
| B.5 | varind | 379 |
| B.6 | ccfdcf | 382 |
| B.7 | functions | 385 |

List of Tables

| | | |
|-----|----------------------------------------------------------------|-----|
| 1.1 | Simple Unification Model | 4 |
| 1.2 | The Archival Sample | 16 |
| 1.3 | The SMARTS Sample | 17 |
| 2.1 | CCD/IR Detectors | 19 |
| 3.1 | Magnitude to Flux Conversion Factors | 55 |
| 3.2 | Variability Characteristic Classification Scheme | 245 |
| 3.4 | Structure Function and Variability Index Time-scales | 278 |
| 4.1 | Source Region Size Estimates | 327 |

List of Figures

| | | |
|------|------------------------------------------------------------|----|
| 1.1 | Unified model of AGN | 5 |
| 1.2 | Spectral Energy Distribution of Blazars | 9 |
| 1.3 | Gamma-ray variability of 1622 – 297 | 10 |
| 1.4 | Optical Microvariability of 2200 + 420 | 12 |
| 1.5 | Optical Microvariability of OF 038 | 13 |
| 1.6 | Long term Optical Variability of 2200 + 420 | 14 |
| 3.1 | 2200 + 420 Rest Frame Example | 58 |
| 3.2 | Complete V and R band light curve of 0235 + 164 | 61 |
| 3.3 | Detail of V and R band light curve of 0235 + 164 | 62 |
| 3.4 | Microvariability of 0235 + 164 on 13 Oct 1986 | 63 |
| 3.5 | Microvariability of 0235 + 164 on 11 Nov 1987 | 64 |
| 3.6 | Microvariability of 0235 + 164 on 27 Oct 1990 | 65 |
| 3.7 | Microvariability of 0235 + 164 on 28 Oct 1990 | 66 |
| 3.8 | Microvariability of 0235 + 164 on 29 Oct 1990 | 67 |
| 3.9 | Microvariability of 0235 + 164 on 30 Oct 1990 | 68 |
| 3.10 | Microvariability of 0235 + 164 on 31 Oct 1990 | 69 |
| 3.11 | Microvariability of 0235 + 164 on 05 Nov 1991 | 70 |
| 3.12 | Microvariability of 0235 + 164 on 06 Nov 1991 | 71 |
| 3.13 | Microvariability of 0235 + 164 on 07 Nov 1991 | 72 |
| 3.14 | Microvariability of 0235 + 164 on 08 Nov 1991 | 73 |
| 3.15 | Microvariability of 0235 + 164 on 09 Nov 1997 | 74 |
| 3.16 | Microvariability of 0235 + 164 on 25 Nov 1997 | 75 |
| 3.17 | Microvariability of 0235 + 164 on 09 Mar 1998 | 76 |
| 3.18 | Microvariability of 0235 + 164 on 18 Oct 1998 | 77 |
| 3.19 | Microvariability of 0235 + 164 on 19 Oct 1998 | 78 |
| 3.20 | Microvariability of 0235 + 164 on 13 Jan 2004 | 79 |
| 3.21 | Microvariability of 0235 + 164 on 27 Jan 2004 | 80 |
| 3.22 | Microvariability of 0235 + 164 on 09 Feb 2004 | 81 |
| 3.23 | Microvariability of 0235 + 164 on 11 Feb 2004 | 82 |
| 3.24 | Microvariability of 0235 + 164 on 12 Feb 2004 | 83 |
| 3.25 | Microvariability of 0235 + 164 on 14 Feb 2004 | 84 |
| 3.26 | Microvariability of 0235 + 164 on 16 Feb 2004 | 85 |
| 3.27 | Complete R band light curve of 1156 + 295 | 87 |
| 3.28 | Microvariability of 1156 + 295 on 19 Jan 1994 | 88 |

| | | |
|------|---------------------------------------------------------|-----|
| 3.29 | Microvariability of 1156 + 295 on 20 Jan 1994 | 89 |
| 3.30 | Microvariability of 1156 + 295 on 21 Jan 1994 | 90 |
| 3.31 | Microvariability of 1156 + 295 on 22 Jan 1994 | 91 |
| 3.32 | Microvariability of 1156 + 295 on 23 Jan 1994 | 92 |
| 3.33 | Microvariability of 1156 + 295 on 24 Jan 1994 | 93 |
| 3.34 | Complete R band light curve of 1622 – 297 | 95 |
| 3.35 | Microvariability of 1622 – 297 on 16 May 1997 | 96 |
| 3.36 | Microvariability of 1622 – 297 on 23 Aug 1997 | 97 |
| 3.37 | Microvariability of 1622 – 297 on 24 Aug 1997 | 98 |
| 3.38 | Microvariability of 1622 – 297 on 25 Aug 1997 | 99 |
| 3.39 | Microvariability of 1622 – 297 on 26 Aug 1997 | 100 |
| 3.40 | Microvariability of 1622 – 297 on 27 Aug 1997 | 101 |
| 3.41 | Microvariability of 1622 – 297 on 08 Jun 2000 | 102 |
| 3.42 | Microvariability of 1622 – 297 on 09 Jun 2000 | 103 |
| 3.43 | Microvariability of 1622 – 297 on 20 May 2002 | 104 |
| 3.44 | Complete R band light curve of 1633 + 382 | 106 |
| 3.45 | Microvariability of 1633 + 382 on 01 Apr 1996 | 107 |
| 3.46 | Microvariability of 1633 + 382 on 02 Apr 1996 | 108 |
| 3.47 | Microvariability of 1633 + 382 on 03 Apr 1996 | 109 |
| 3.48 | Microvariability of 1633 + 382 on 26 Apr 1996 | 110 |
| 3.49 | Microvariability of 1633 + 382 on 27 Apr 1996 | 111 |
| 3.50 | Microvariability of 1633 + 382 on 28 Apr 1996 | 112 |
| 3.51 | Microvariability of 1633 + 382 on 29 Apr 1996 | 113 |
| 3.52 | Microvariability of 1633 + 382 on 30 Apr 1996 | 114 |
| 3.53 | Microvariability of 1633 + 382 on 01 May 1996 | 115 |
| 3.54 | Microvariability of 1633 + 382 on 17 May 1998 | 116 |
| 3.55 | Microvariability of 1633 + 382 on 18 May 1998 | 117 |
| 3.56 | Microvariability of 1633 + 382 on 08 Jun 2000 | 118 |
| 3.57 | Microvariability of 1633 + 382 on 09 Jun 2000 | 119 |
| 3.58 | Microvariability of 1633 + 382 on 20 May 2003 | 120 |
| 3.59 | Microvariability of 1633 + 382 on 21 May 2003 | 121 |
| 3.60 | Microvariability of 1633 + 382 on 22 May 2003 | 122 |
| 3.61 | Microvariability of 1633 + 382 on 23 May 2003 | 123 |
| 3.62 | Microvariability of 1633 + 382 on 24 May 2003 | 124 |
| 3.63 | Microvariability of 1633 + 382 on 21 May 2004 | 125 |
| 3.64 | Microvariability of 1633 + 382 on 22 May 2004 | 126 |
| 3.65 | Microvariability of 1633 + 382 on 23 May 2004 | 127 |
| 3.66 | Complete R band light curve of 1641 + 399 | 129 |
| 3.67 | Microvariability of 1641 + 399 on 10 Jun 1992 | 130 |
| 3.68 | Microvariability of 1641 + 399 on 01 Apr 1996 | 131 |
| 3.69 | Microvariability of 1641 + 399 on 03 Apr 1996 | 132 |
| 3.70 | Microvariability of 1641 + 399 on 19 May 1997 | 133 |
| 3.71 | Microvariability of 1641 + 399 on 17 May 1998 | 134 |
| 3.72 | Microvariability of 1641 + 399 on 18 May 1998 | 135 |

| | | |
|-------|---------------------------------------------------------|-----|
| 3.73 | Microvariability of 1641 + 399 on 19 May 1998 | 136 |
| 3.74 | Microvariability of 1641 + 399 on 14 Apr 2000 | 137 |
| 3.75 | Microvariability of 1641 + 399 on 15 Apr 2000 | 138 |
| 3.76 | Microvariability of 1641 + 399 on 16 Apr 2000 | 139 |
| 3.77 | Microvariability of 1641 + 399 on 17 Apr 2000 | 140 |
| 3.78 | Microvariability of 1641 + 399 on 06 Jun 2000 | 141 |
| 3.79 | Microvariability of 1641 + 399 on 21 May 2001 | 142 |
| 3.80 | Microvariability of 1641 + 399 on 15 Jun 2001 | 143 |
| 3.81 | Microvariability of 1641 + 399 on 16 Jun 2001 | 144 |
| 3.82 | Microvariability of 1641 + 399 on 17 Jun 2001 | 145 |
| 3.83 | Microvariability of 1641 + 399 on 18 Jun 2001 | 146 |
| 3.84 | Microvariability of 1641 + 399 on 20 May 2003 | 147 |
| 3.85 | Microvariability of 1641 + 399 on 21 May 2003 | 148 |
| 3.86 | Microvariability of 1641 + 399 on 22 May 2003 | 149 |
| 3.87 | Microvariability of 1641 + 399 on 23 May 2003 | 150 |
| 3.88 | Microvariability of 1641 + 399 on 24 May 2003 | 151 |
| 3.89 | Complete V and R band light curve of BL Lac | 153 |
| 3.90 | Detail of V and R band light curve of BL Lac | 154 |
| 3.91 | Microvariability of 2200 + 420 on 18 Sep 1991 | 155 |
| 3.92 | Microvariability of 2200 + 420 on 15 Sep 1995 | 156 |
| 3.93 | Microvariability of 2200 + 420 on 16 Sep 1995 | 157 |
| 3.94 | Microvariability of 2200 + 420 on 17 Sep 1995 | 158 |
| 3.95 | Microvariability of 2200 + 420 on 18 Sep 1995 | 159 |
| 3.96 | Microvariability of 2200 + 420 on 19 Sep 1995 | 160 |
| 3.97 | Microvariability of 2200 + 420 on 31 Oct 1995 | 161 |
| 3.98 | Microvariability of 2200 + 420 on 19 Sep 1996 | 162 |
| 3.99 | Microvariability of 2200 + 420 on 20 Sep 1996 | 163 |
| 3.100 | Microvariability of 2200 + 420 on 21 Sep 1996 | 164 |
| 3.101 | Microvariability of 2200 + 420 on 18 Jul 1997 | 165 |
| 3.102 | Microvariability of 2200 + 420 on 19 Jul 1997 | 166 |
| 3.103 | Microvariability of 2200 + 420 on 19 Aug 1997 | 167 |
| 3.104 | Microvariability of 2200 + 420 on 27 Sep 1997 | 168 |
| 3.105 | Microvariability of 2200 + 420 on 27 Sep 1997 | 169 |
| 3.106 | Microvariability of 2200 + 420 on 28 Sep 1997 | 170 |
| 3.107 | Microvariability of 2200 + 420 on 28 Sep 1997 | 171 |
| 3.108 | Microvariability of 2200 + 420 on 29 Sep 1997 | 172 |
| 3.109 | Microvariability of 2200 + 420 on 12 Dec 1997 | 174 |
| 3.110 | Microvariability of 2200 + 420 on 13 Jul 1998 | 175 |
| 3.111 | Microvariability of 2200 + 420 on 14 Jul 1998 | 176 |
| 3.112 | Microvariability of 2200 + 420 on 27 Jul 1998 | 177 |
| 3.113 | Microvariability of 2200 + 420 on 01 Aug 1998 | 178 |
| 3.114 | Microvariability of 2200 + 420 on 03 Aug 1998 | 179 |
| 3.115 | Microvariability of 2200 + 420 on 17 Aug 1998 | 180 |
| 3.116 | Microvariability of 2200 + 420 on 19 Aug 1998 | 181 |

| | | |
|-------|---------------------------------------------------------|-----|
| 3.117 | Microvariability of 2200 + 420 on 20 Aug 1998 | 182 |
| 3.118 | Microvariability of 2200 + 420 on 19 Oct 1998 | 183 |
| 3.119 | Microvariability of 2200 + 420 on 21 Jul 2000 | 184 |
| 3.120 | Microvariability of 2200 + 420 on 23 Jul 2000 | 185 |
| 3.121 | Microvariability of 2200 + 420 on 25 Jul 2000 | 186 |
| 3.122 | Microvariability of 2200 + 420 on 01 Aug 2000 | 187 |
| 3.123 | Microvariability of 2200 + 420 on 05 Aug 2000 | 188 |
| 3.124 | Microvariability of 2200 + 420 on 06 Aug 2000 | 189 |
| 3.125 | Microvariability of 2200 + 420 on 08 Aug 2000 | 190 |
| 3.126 | Microvariability of 2200 + 420 on 11 Aug 2000 | 191 |
| 3.127 | Microvariability of 2200 + 420 on 15 Aug 2000 | 192 |
| 3.128 | Microvariability of 2200 + 420 on 17 Aug 2000 | 193 |
| 3.129 | Microvariability of 2200 + 420 on 19 Aug 2000 | 194 |
| 3.130 | Microvariability of 2200 + 420 on 14 Jun 2001 | 195 |
| 3.131 | Microvariability of 2200 + 420 on 15 Jun 2001 | 196 |
| 3.132 | Microvariability of 2200 + 420 on 17 Jun 2001 | 197 |
| 3.133 | Microvariability of 2200 + 420 on 18 Jun 2001 | 198 |
| 3.134 | Microvariability of 2200 + 420 on 02 Oct 2002 | 199 |
| 3.135 | Microvariability of 2200 + 420 on 04 Oct 2002 | 200 |
| 3.136 | Microvariability of 2200 + 420 on 08 Oct 2002 | 201 |
| 3.137 | Microvariability of 2200 + 420 on 19 Oct 2002 | 202 |
| 3.138 | Microvariability of 2200 + 420 on 21 Sep 2004 | 203 |
| 3.139 | Microvariability of 2200 + 420 on 22 Sep 2004 | 204 |
| 3.140 | Microvariability of 2200 + 420 on 23 Sep 2004 | 205 |
| 3.141 | Microvariability of 2200 + 420 on 04 Oct 2004 | 206 |
| 3.142 | Microvariability of 2200 + 420 on 05 Oct 2004 | 207 |
| 3.143 | Microvariability of 2200 + 420 on 06 Oct 2004 | 208 |
| 3.144 | Microvariability of 2200 + 420 on 07 Oct 2004 | 209 |
| 3.145 | Microvariability of 2200 + 420 on 08 Oct 2004 | 210 |
| 3.146 | Microvariability of 2200 + 420 on 09 Oct 2004 | 211 |
| 3.147 | Complete R band light curve of 2223 – 052 | 213 |
| 3.148 | Microvariability of 2223 – 052 on 10 Aug 1988 | 214 |
| 3.149 | Microvariability of 2223 – 052 on 29 Sep 1988 | 216 |
| 3.150 | Microvariability of 2223 – 052 on 30 Sep 1988 | 217 |
| 3.151 | Microvariability of 2223 – 052 on 01 Oct 1988 | 218 |
| 3.152 | Microvariability of 2223 – 052 on 25 Oct 1988 | 219 |
| 3.153 | Microvariability of 2223 – 052 on 27 Aug 1998 | 220 |
| 3.154 | Microvariability of 2223 – 052 on 28 Aug 1998 | 221 |
| 3.155 | Microvariability of 2223 – 052 on 29 Aug 1998 | 222 |
| 3.156 | Microvariability of 2223 – 052 on 30 Aug 1998 | 223 |
| 3.157 | Microvariability of 2223 – 052 on 18 Oct 1998 | 224 |
| 3.158 | Microvariability of 2223 – 052 on 19 Oct 1998 | 225 |
| 3.159 | Microvariability of 2223 – 052 on 20 Oct 1998 | 226 |
| 3.160 | Microvariability of 2223 – 052 on 08 Sep 2000 | 227 |

| | | |
|-------|------------------------------------------------------------------|-----|
| 3.161 | Microvariability of 2223 – 052 on 09 Sep 2000 | 228 |
| 3.162 | Microvariability of 2223 – 052 on 10 Sep 2000 | 229 |
| 3.163 | Microvariability of 2223 – 052 on 11 Sep 2000 | 230 |
| 3.164 | Microvariability of 2223 – 052 on 26 Oct 2000 | 231 |
| 3.165 | Microvariability of 2223 – 052 on 27 Oct 2000 | 232 |
| 3.166 | Microvariability of 2223 – 052 on 04 Oct 2001 | 233 |
| 3.167 | Microvariability of 2223 – 052 on 05 Oct 2001 | 234 |
| 3.168 | Microvariability of 2223 – 052 on 05 Aug 2003 | 235 |
| 3.169 | Microvariability of 2223 – 052 on 06 Aug 2003 | 236 |
| 3.170 | Microvariability of 2223 – 052 on 08 Aug 2003 | 237 |
| 3.171 | Microvariability of 2223 – 052 on 09 Aug 2003 | 238 |
| 3.172 | Microvariability of 2223 – 052 on 10 Aug 2003 | 239 |
| 3.173 | Microvariability of 2223 – 052 on 06 Oct 2004 | 240 |
| 3.174 | Examples of Characteristics of Microvariability | 246 |
| 3.175 | Skematic of “ideal” Structure Function | 248 |
| 3.176 | Percentage of Microvariability | 256 |
| 3.177 | Characteristics of Microvariability | 257 |
| 3.178 | Microvariability and State I | 258 |
| 3.179 | Microvariability Amplitudes (Flux Density) | 259 |
| 3.180 | Energetics of Microvariability | 259 |
| 3.181 | Duty Cycle of LBLs Versus 5 GHz Radio Flux | 260 |
| 3.182 | Duty Cycle of LBLs Versus Apparent Speed $\beta = v/c$ | 261 |
| 3.183 | Structure Functions | 263 |
| 3.184 | Variability Indexes | 281 |
| 4.1 | SMARTS Light Curve of 0420 – 014 | 300 |
| 4.2 | SMARTS Light Curve of 0818 – 128 | 302 |
| 4.3 | SMARTS Light Curve of 1226 + 023 | 304 |
| 4.4 | SMARTS Light Curve of 1253 – 055 | 306 |
| 4.5 | SMARTS Light Curve of 1510 – 089 | 308 |
| 4.6 | SMARTS Light Curve of 1514 – 241 | 310 |
| 4.7 | SMARTS Light Curve of 1622 – 297 | 312 |
| 4.8 | SMARTS Light Curve of 2005 – 489 | 314 |
| 4.9 | SMARTS Light Curve of 2155 – 304 | 316 |
| 4.10 | SMARTS Light Curve of 2223 – 052 | 318 |
| 4.11 | SMARTS Light Curve of 2345 – 167 | 320 |
| 4.12 | Cross Correlation Function of 0420 – 014 | 324 |
| 4.13 | Cross Correlation Function of 1622 – 297 | 325 |
| 4.14 | Cross Correlation Function of 2005 – 489 | 326 |
| 4.15 | Cross Correlation Function of 2345 – 167 | 326 |
| 4.16 | SMARTS Auto-Correlation Functions | 328 |

List of Abbreviations

| | |
|-------|--------------------------------------------------------------|
| AGN | Active Galactic Nuclei |
| AO | Arecibo Observatory |
| BLRG | Broad Line Radio Galaxy |
| CCD | Charge Coupled Device |
| CTIO | Cerro Tololo Inter-American Observatory |
| DEC | Declination |
| FR I | Fanaroff-Riley type I |
| FR II | Fanaroff-Riley type II |
| FWHM | Full Width at Half Maximum |
| HBL | High-energy-cutoff BL Lacertae object |
| HLCO | Hard Labor Creek Observatory |
| IDL | Interactive Data Language |
| IR | Infrared |
| IRAF | Image Reduction and Analysis Facility |
| JD | Julian Date |
| KPNO | Kitt Peak National Observatory |
| LBL | Low-energy-cutoff BL Lacertae object |
| NLRG | Narrow Line Radio Galaxy |
| OVV | Optically Violent Variable |
| PKS | Parkes catalogue |
| PEGA | Program in Extragalactic Astronomy, Georgia State University |
| PG | Palomar-Green catalogue |
| QSO | Quasi-stellar Object |
| RA | Right Ascension |
| RBL | Radio Selected Blazar |
| SED | Spectral Energy Distribution |
| SMBH | Supermassive Black Hole |
| UT | Universal Time |
| VLBA | Very Long Baseline Array |
| XBL | X-Ray Selected Blazar |

Chapter 1

Introduction

Active Galactic Nuclei (AGN) exhibit the most powerful, sustained emissions of any objects currently known. They can be seen to the edge of the visible universe and thus can act as candles to illuminate intervening material. The leading model describes the mechanism at the heart of AGN to be a supermassive black hole accreting matter from a surrounding disk. It is the gravitational energy resulting from this accretion which powers AGN and gives rise to their emissions. Current techniques are unable to resolve the inner cores of even the nearest AGN, so only by studying how their emissions change over time in both continuum and line flux can we hope to understand the nature and location of the emissions and what mechanisms are involved in their creation.

In this dissertation, I have investigated the optical and near-IR flux variations of the most variable class of AGN, known as blazars, in the observed frame and transform them into the rest frame of the emission source. These flux variations were analyzed and have provided new insight into the physical properties and emission mechanisms of AGNs in general, and blazars in particular.

1.1 AGN History

AGN have a long and unusual history. Distant AGN were first thought to be stars, but when their broad- and narrow-band emissions were analyzed, it was noted that they had both an ultraviolet and infrared excess, and that their spectra contained unusual emission and absorption lines. It wasn't until later that astronomers determined the unidentified spectral features were in fact normal spectral features which were highly broadened and at very large redshifts. It was also noted by Carl Seyfert (1943) that some nearby spiral galaxies had unusually bright nuclei with a non-thermal component and similarly wide spectral features. These two classes of distant and nearby objects were eventually seen to be related, but were at very different distances.

1.1.1 Discovery

Early in the twentieth century, the first AGN spectrum was obtained for the object NGC 1068. This was done in 1908 by Lick Observatory's E. A. Fath while studying "spiral nebula", and later by V. M. Slipher of Lowell Observatory who obtained a higher resolution spectrum (Fath, 1908; Slipher, 1917). It showed extremely strong and broad emission lines that puzzled astronomers. Carl Seyfert noted similar features in several other nearby galaxies, which are now part of the class of objects known as Seyfert galaxies, named in his honor. By the mid-twentieth century, the resolution of radio observations improved sufficiently to allow one to identify various radio sources associated with unusual optical sources. These quasi-stellar radio sources, later called "quasars", were then known only as "radio stars". It wasn't until 1963 that Maarten Schmidt noted that the unusual emission lines in the spectra of these

objects were simply the well-known emission lines of hydrogen at large redshifts. (Schmidt, 1963)

1.1.2 Classification

All classes of AGN exhibit at least some common characteristics. It was Schmidt (1968) who defined a list of characteristics he noted in quasars:

- Optically stellar appearing radio sources
- Continuum flux variability over time
- Large ultraviolet excess
- Broad emission lines
- Large redshifts

Today, it is the broad spectral energy distribution (SED) of AGN that are their most uniquely defining characteristic. Whereas the SEDs of normal galaxies can be described as the combined thermal black-body spectrum of all member stars, active galaxies contain a distinctive non-thermal component to their spectrum. In many cases, this is the primary component observed.

AGN can be classified into many different types based on differences in observed properties. It was not understood at first what could cause such differences if in fact these objects were part of the same family of objects. It was not until near the end of the twentieth century before plausible theories began to explain these differences.

1.1.3 Unified Model

In the leading theory (see e.g., Urry and Padovani (1995)), AGN emissions are believed to originate from a central supermassive black hole (SMBH) and surrounding accretion disk. An optically thick dust torus or similar structure is posited to exist farther from the center. This torus serves many functions, from collimating the outflow of material along its axis to obscuring the central region. The natural result of such an arrangement are anisotropic emissions concentrated orthogonal to the plane of the accretion disk. These emissions can be thermal (e.g., accretion disk), non-thermal (e.g., radio jet), or some combination of both.

There is a large body of evidence, with observations covering the electromagnetic spectrum, that demonstrates these anisotropic emissions of AGN. All of this implies that viewing angle plays a prominent role for the differences in observed characteristics of AGN and that the way AGN have been classified is strongly dependent on orientation. This is the primary evidence that supports the unified model. The different classes are summarized in Table 1.1 where the acronyms are: OVV (optically violent variable), BLRG (broad line radio galaxy), QSO (quasi stellar object), FR I/II (Fanaroff-Riley type I/II), NLRG (narrow line radio galaxy), FIR (far infrared).

Table 1.1: Simple Unification Model (Peterson, 1997)

| Radio Properties | Orientation | |
|------------------|------------------------------|-------------------------|
| | Face-On | Edge-On |
| Radio Loud | BL Lac Quasar/OVV BLRG | FR I FR II NLRG |
| Radio Quiet | Seyfert 1 QSO | Seyfert 2 FIR galaxy |

To account for the broad permitted and narrow forbidden lines in the spectra of AGN, two regions are envisaged: a broad-line region (BLR) and a narrow-line region (NLR). The BLR region exists near to the SMBH and within the dust torus. The material here is dense and fast moving. The NLR exists farther out beyond any obscuration from the disk, and is composed of less dense, slower moving gas. Observational evidence shows that both regions have low filling factors, which implies a clumpy nature for the material (Peterson, 1997). Figure 1.1 illustrates the geometry of the inner $\sim 10^{20}$ cm of the core of an active galaxy.

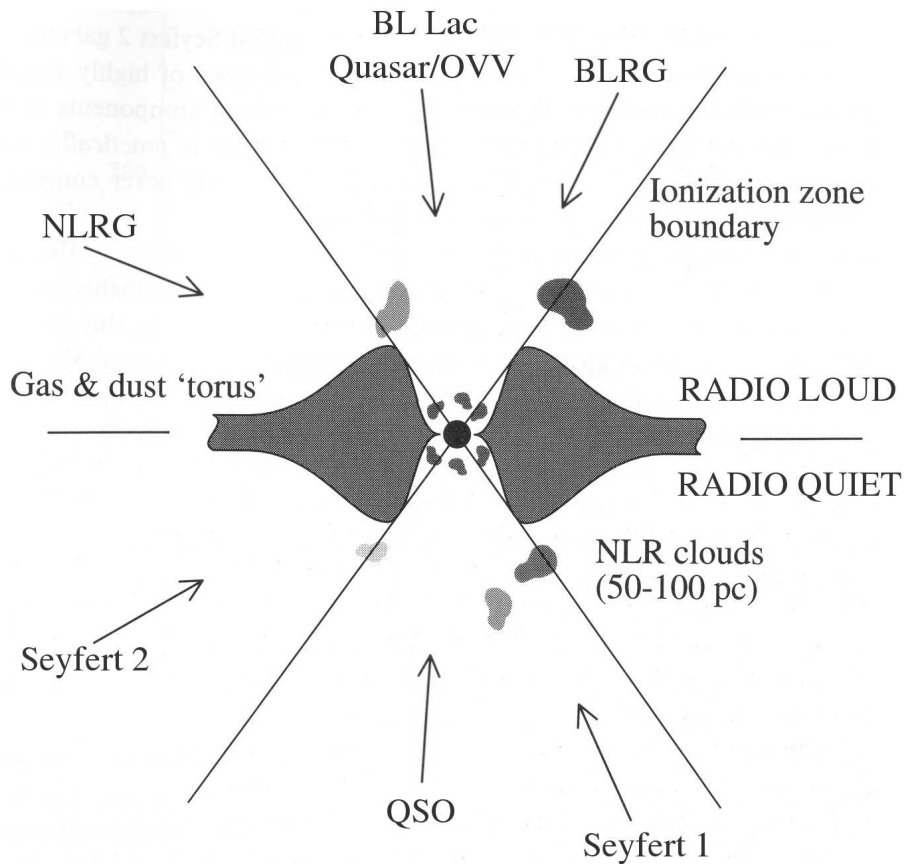


Figure 1.1: Unified model of AGN (Urry and Padovani, 1995). Figure adapted from Peterson (1997)

1.2 Blazars

It is well-established that blazars are among the most variable AGN observed at any wavelength, and rapid, large-amplitude variations are common. The continuum emission of blazars is dominated by radiation from a relativistic jet that is oriented so that the axis of the jet is pointed near the line-of-sight to the observer (Urry and Padovani, 1995).

The term “blazar” was first coined by Spiegel (1978). Like all other AGN, they have a defining set of characteristics based on models and observations. These characteristics are summarized below:

- Continuum variability at all wavelengths and time scales
- A “featureless” continuum
- High polarization variability

Blazars are highly variable in both their emission flux and their polarization. Because these objects are believed to have their relativistic jet axis oriented very close to the line of sight of the observer (see §1.1), there are profound implications on what is actually observed (e.g., amplification of emissions by Doppler boosting described in §3.1.1).

The continuum variability is thought to arise mainly from bulk relativistic motions within the jet and the propagation of resulting shock fronts, and interaction with the surrounding medium. As these shocks propagate down the jet, the resulting emissions are frequency dependent. Higher frequency emissions tend to vary more in amplitude and the timing with respect to other frequency regimes is dependent on the actual mechanisms involved.

The featureless continuum refers to the fact that blazars, in general, have very weak nebular emissions or stellar absorption features, if they are observed at all. This is due to the non-thermal nature of emissions and their distance. Intervening material may be one source of these features. There are exceptions to this rule which will be discussed in §1.2.1.

Lastly, blazars exhibit high polarization, on the order of 3-4%, but it can be as high as 20%. The polarization arises from the nature of the emission mechanism (e.g., synchrotron and synchrotron self-Compton, see §1.2.3) and, like the continuum flux, can be highly variable.

1.2.1 Classification

Blazars can be classified into two main groups: BL Lacertae (or BL Lac) objects after the prototype of the class, BL Lac; and optically violent variable, or OVV, quasars. It is this latter group that differs in the appearance of their continuum. OVV quasars, in a high luminosity state, resemble BL Lac objects because there is little contrast between the broad emission lines, usually prominent in lower luminosity states, and the non-thermal continuum. These two groups are believed to be the Doppler boosted versions of the Fanaroff-Riley (FR) class of radio galaxies: BL Lacs are associated with the lower luminosity FR Is and OVVs with the FR IIs.

Blazars can also be subdivided by how they were first identified. X-ray selected blazars, or XBLs, and radio selected blazars, or RBLs, differ mainly by the flux band in which they were discovered. They do exhibit other differences, which will be the subject of one of the investigations to be discussed later in this dissertation.

1.2.2 Morphology

Due to the high amplification of the beaming processes in the relativistic jet, blazars can be seen at very large distances. As a result, in most cases, the galaxy contribution to the flux is negligible. There are, of course, exceptions in the case of some relatively nearby blazars ($z \lesssim 0.3$). BL Lac, at $z = 0.069$, does show some slight nebulosity; however, it is believed that the dilution of microvariability due to the host galaxy contribution is minimal and acceptable for this investigation.

It has been noted that the host galaxies morphology is related to the AGN morphology. Seyfert galaxies are hosted primarily by spiral galaxies. Blazars and other radio loud quasars, to the extent that it can be determined, generally reside in ellipticals (Wurtz et al., 1996).

1.2.3 Continuum Emission

It is believed that the origin of the dominant emission mechanism of blazars is the relativistic jet. There is evidence for this when one compares the continuum of a blazar with that of a stellar blackbody continuum. The blazar continuum shows a distinct excess in flux in both the infrared (IR) and the ultraviolet (UV) implying a non-thermal (power law) continuum. The jet is responsible for emissions from radio through γ -ray. Given this picture, it is almost certain that the main intrinsic source of any flux variability resides in the jet or in the feeding mechanisms of the jet (see §1.3).

The continuum of any AGN can be described with a spectral energy distribution, or SED. For blazars, it is their main defining characteristic. The classic view was that the SED was a power law ($F_\nu \propto \nu^{-\alpha}; \alpha > 0$) over the narrow wavelength range that it was

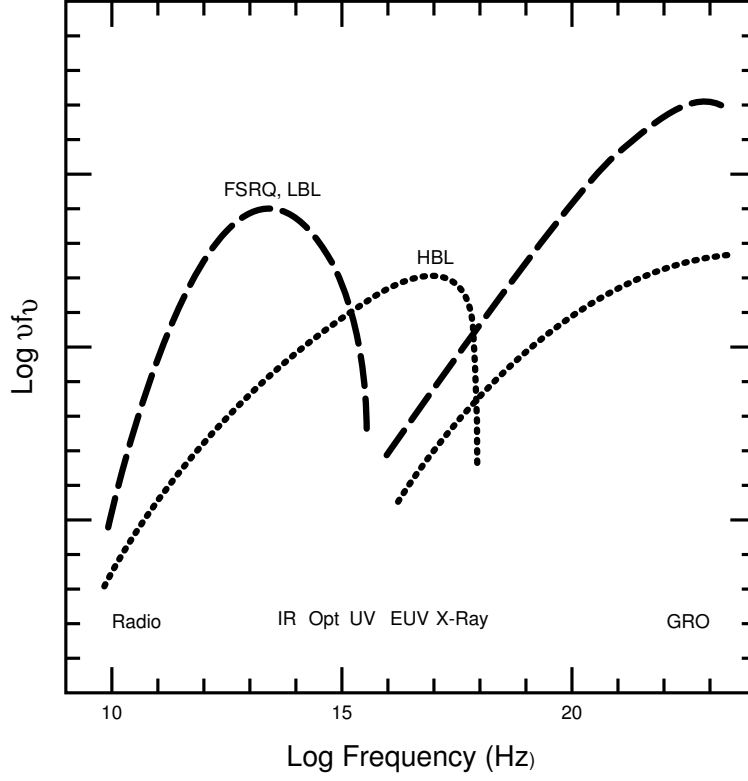


Figure 1.2: Spectral Energy Distribution (SED) for typical blazars. The dashed and dotted lines indicate the SED for two different classes of blazars: LBLs (low-energy-cutoff BL Lac objects, a.k.a RBLs or radio selected BL Lac objects) and HBLs (high-energy-cutoff BL Lac objects, a.k.a XBLs or x-ray selected BL Lac objects), respectively. (see §1.4). (Urry, 1996)

observed. Today, with the wide range of observatories looking at blazars from the radio to the γ -ray regime, the picture is significantly different. Figure 1.2 illustrates the nominal SED for blazars. According to the standard model, the first, lower frequency “hump” in the radio through optical regime is due to beamed synchrotron emission originating in the relativistic jet. The second hump originating in the UV and extending through the γ -ray regime is due to inverse-Compton emissions. It is a subject of some debate where the seed photons for this segment of the SED originate. One possibility is that photons from the relativistic electrons responsible for the synchrotron emissions are inverse-Compton boosted

by the same electrons. This so-called synchrotron self-Compton (SSC) model is thought to be the dominant inverse Compton process. The other model, external Compton, has thermal photons from the accretion disk and reprocessed photons from the BLR as possible sources of seed photons.

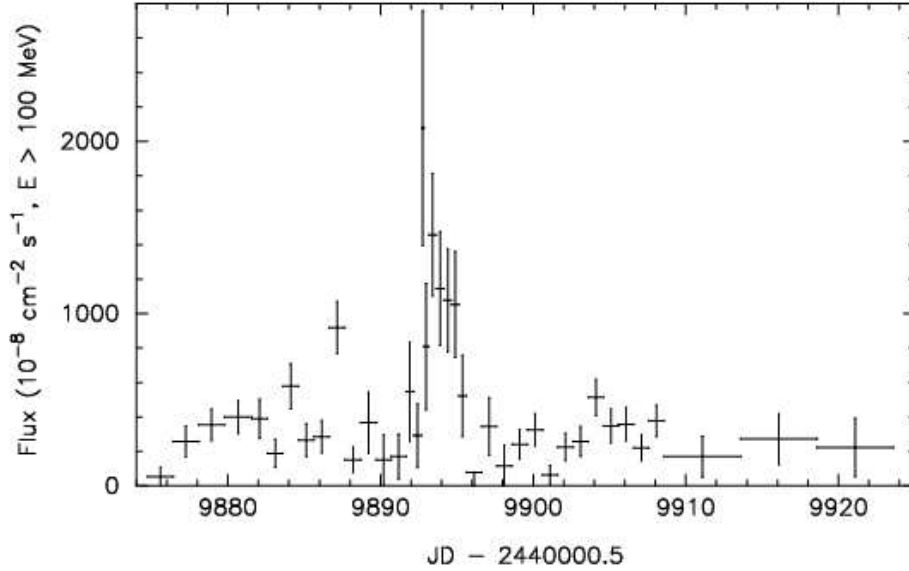


Figure 1.3: Example of gamma-ray variability for 1622–297. Note the amplitude of the event is several orders of magnitude in flux space. (Mattox and Wagner, 1996)

1.3 Blazar Variability

Blazars vary on all timescales and at all wavelengths. They are seen to change at rates faster than 0.1 magnitude per hour and up to ~ 5 magnitudes over several years in the optical. In the X-ray and gamma-ray regime, the variability rates can be as high as several orders of magnitude (in flux) over several days (see Figure 1.3). In the following sections, I will give detailed examples of variability in several wavelength regimes.

1.3.1 Optical Variability

The sources of blazar optical variability are many. Long term variability (months to years) is believed to be caused by relativistic bulk motions within the jet and shocks resulting from these motions; by jet precession away from and toward the observer's line of sight; and by changes in the accretion rate. Shorter term, lower amplitude microvariability (minutes to hours) may be caused by small scale disturbances or turbulence in the jet.

Other origins of microvariability have been investigated. For example, Wiita (1996) has summarized investigations of microvariations which might be produced from some mechanisms other than the jet. In this picture, instabilities and flares in the accretion disk can be strong and rapid enough to account for at least some of the observed microvariability. One of the goals of this dissertation is to investigate whether the microvariability is primarily of thermal (e.g., accretion disk flares) or non-thermal origin. By looking at how the flux variations change as a function of state, one may place limits on the possible origin of the microvariability.

If the flux variability amplitude scales with luminosity state (i.e., constant variability amplitude in magnitude space), the processes behind the variations would be primarily jet-based. The reason for this is that as the luminosity of the jet increases, the amount of energy in the turbulent event also increases. This can be thought of as a conservation of the change in luminosity ($\Delta L \propto L$). If the microvariability were caused by the thermal emissions from the accretion disk, it would be unaffected by the state of the jet. In this latter case, one would see the flux variability amplitude to remain constant with increasing luminosity state (i.e., decreasing variability amplitude in magnitude space).

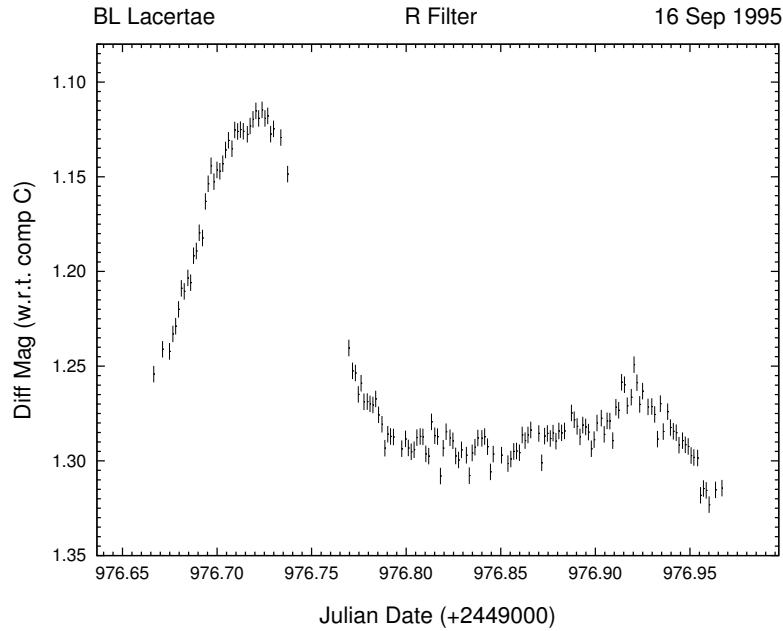


Figure 1.4: Example of the optical microvariability (R band) of 2200 + 420 on the night of 16 Sep 1995. Note the duration of the primary event is ~ 3 hours and the amplitude is ~ 0.2 mag.

In Figure 1.4, there is an excellent example of the microvariability of BL Lac in the optical. The symbol size indicates the error ($\pm 1\sigma$). The events consist of a large symmetrical event of ~ 0.2 mag for ~ 3 hours duration and a smaller, possibly incomplete event of similar duration, but only ~ 0.05 mag amplitude.

Another good example of microvariability comes from the object OF 038 (see Figure 1.5). This figure illustrates a single event of only 20 minutes duration, yet an amplitude of variation of ~ 0.2 magnitude. In this case it is unclear if the event is intrinsic to the source or if it is caused by intervening material along the line of sight.

Simple light time travel arguments (see §3.3.1) can give an upper limit to the size of emitting region, assuming that the minimum light crossing time is equivalent to the duration of the event. To be able to apply this argument to blazars, relativistic considerations, such

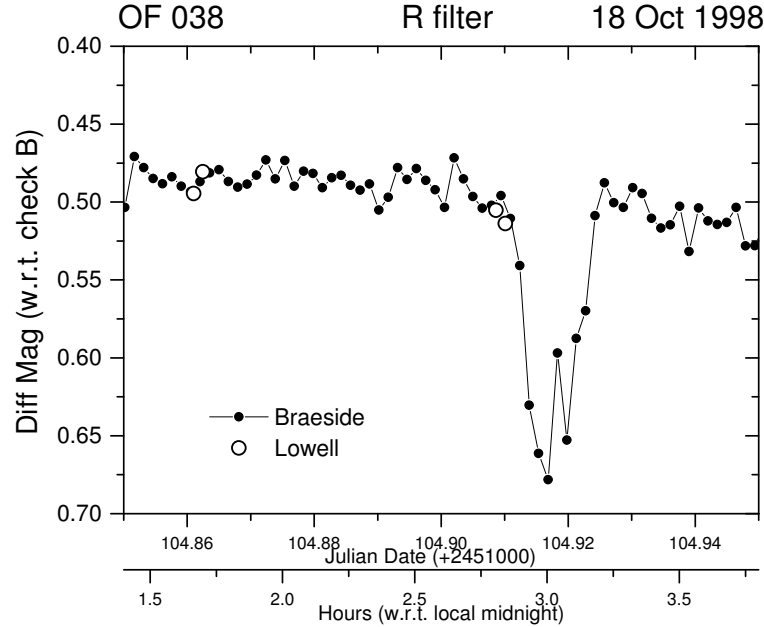


Figure 1.5: Example of the optical microvariability of OF 038 on the night of 18 Oct 1998. Note that the duration of the event is ~ 20 minutes and the amplitude is ~ 0.2 mag, and that the Braeside Observatory observations (connected dots) are very well correlated with the sparser Lowell Observatory observations (open circles). (McFarland et al., 1999)

and beaming and cosmological redshift, must be taken into account. When this is done for the BL Lac light curve in Figure 1.4, for example, a value of $\sim 10^{15}$ cm or roughly 1 light day is derived.

In addition to microvariability, blazars exhibit large amplitude variability over larger timescales. Figure 1.6 illustrates this with a 13-year light curve of BL Lac in the R band. This light curve demonstrates a variability amplitude of roughly 2.5 mag, with large variations occurring over months, and in some cases, days.

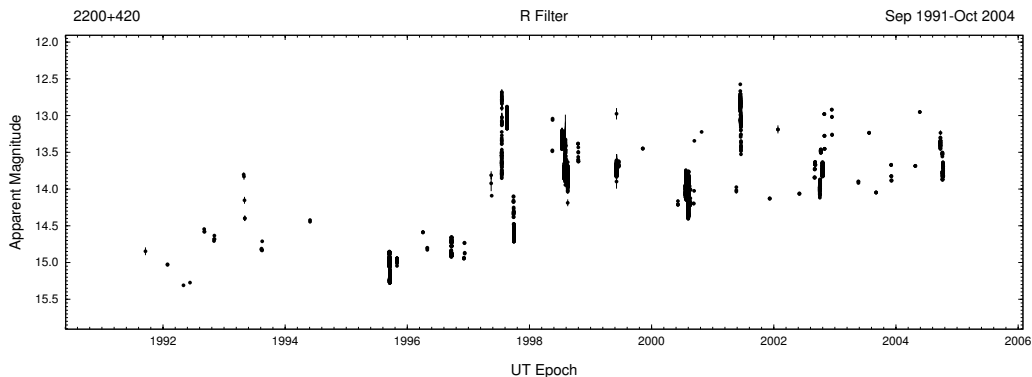


Figure 1.6: Example of the long term optical variability (R band) of 2200 + 420 from 1991 to 2004. The amplitude of variability is ~ 3 mag.

1.3.2 X-ray/Gamma-ray Variability

The X-ray selected subset of blazars are highly variable in the X-ray and TeV gamma-rays (see e.g., Figure 1.3). This is expected because these wavelength regimes are where their synchrotron and inverse-Compton peaks occur respectively (see Figure 1.2).

1.3.3 Radio Variability

All blazars are radio loud. It is at these wavelengths that they have been most readily detected and their variability most thoroughly studied (see e.g., Aller (1999)). The radio emissions are non-thermal and variable, therefore, they can be used to investigate the synchrotron processes at the very heart of the blazar. As mentioned earlier, variations in jet emission are most likely due to bulk relativistic motions along the jet creating shocks. The emissions from these shocks are then amplified by relativistic beaming (Blandford et al., 1977).

Evidence for these bulk motions comes from superluminal studies of radio galaxies and

blazars. In fact, it is the blazars that most often exhibit superluminal motion (Urry and Padovani, 1995).

1.4 Blazar Selection Effects

The main selection effect is related to how various blazars populations were first detected. Blazars have historically been investigated as X-ray-selected blazars (XBLs) and radio-selected blazars (RBLs) based upon the wavelength location of the synchrotron peak in their spectral energy distribution (SED). Padovani and Giommi (1995) have suggested that one should reserve the RBL/XBL designation for the discrete survey populations and have suggested a new notation based on spectral characteristics. They suggested the notation LBL for “low-energy-cutoff BL Lac object” and HBL for “high-energy-cutoff BL Lac object” for RBL-like and XBL-like objects respectively. Another important selection effect to consider is that the highly beamed emissions of blazars are relativistically amplified by Doppler boosting. The consequence of this is that these objects can be seen out to great distances in the Universe.

1.5 Research Direction

There are two main goals for the research described in this dissertation. The first goal is to characterize the optical variability in the rest frame of the object. The second goal is to investigate the nature of the optical/near-IR variability for a sample of 11 blazars using SMARTS¹ telescopes.

¹Small and Moderate Aperture Research Telescope System

The first goal will be accomplished by shifting the observations (in flux space) into the rest frame of the emission source. Various methods will be employed to analyze the resulting data in both the observed and rest frame. This will be discussed in Chapters 2 & 3.1. The methods utilized will include construction and examination of simple light curves, structure function analysis, and variability index analysis.

Table 1.2: The Archival Sample

| OBJECT | Type | RA | DEC | TYPE | z | #OBS |
|------------|------|------------|-----------|------|-------|------|
| 0235 + 164 | LBL | 02 38 39.0 | +16 36 59 | BLL | 0.940 | 3149 |
| 1156 + 295 | LBL | 11 59 31.9 | +29 14 44 | QSO | 0.729 | 474 |
| 1622 − 297 | LBL | 16 26 06.1 | −29 51 27 | QSO | 0.815 | 280 |
| 1633 + 382 | LBL | 16 35 15.6 | +38 08 05 | QSO | 1.814 | 497 |
| 1641 + 399 | LBL | 16 42 58.9 | +39 48 37 | QSO | 0.593 | 1247 |
| 2200 + 420 | LBL | 22 02 43.4 | +42 16 40 | BLL | 0.069 | 6881 |
| 2223 − 052 | LBL | 22 25 47.3 | −04 57 01 | QSO | 1.404 | 1299 |

Another goal is to investigate the nature of the variability. Comparing how the variations change as a function of luminosity state provides clues to the nature and locations of the emitting regions. To determine if a relationship exists between the amplitude of microvariability and the redshift can also give clues to the nature of the emitting regions. Thus far, no such relationship has been found. (Miller and Noble, 1996)

Table 1.2 lists the sample of objects being used for the rest frame studies. Column 1 is the RA/DEC name of the object derived from B1950 coordinates, column 2 lists the class, LBL/HBL, followed by the right ascension (RA) and declination (DEC) in columns 3 and 4, respectively, in J2000.0 coordinates. Column 5 lists the type of blazar: BL Lac (BLL) or OVV (OVV, QSO). Column 6 contains the redshift (z), and column 7 the number of observations (individual frames) of each object.

Table 1.3: The SMARTS Sample

| OBJECT | Type | RA | DEC | TYPE | z | #OBS |
|------------|------|------------|-----------|------|-------|------|
| 0420 – 014 | LBL | 04 23 15.9 | –01 20 33 | QSO | 0.915 | 167 |
| 0818 – 128 | LBL | 08 20 57.5 | –12 58 59 | BLL | ... | 229 |
| 1226 + 023 | LBL | 12 29 06.7 | +02 03 09 | QSO | 0.158 | 191 |
| 1253 – 055 | LBL | 12 56 11.2 | –05 47 22 | OVV | 0.538 | 165 |
| 1510 – 089 | LBL | 15 12 50.6 | –09 06 00 | QSO | 0.360 | 540 |
| 1514 – 241 | LBL | 15 17 41.8 | –24 22 19 | BLL | 0.049 | 673 |
| 1622 – 297 | LBL | 16 26 06.1 | –29 51 27 | QSO | 0.815 | 512 |
| 2005 – 489 | HBL | 20 09 25.5 | –48 49 54 | BLL | 0.071 | 408 |
| 2155 – 304 | HBL | 21 58 52.1 | –30 13 32 | BLL | 0.117 | 933 |
| 2223 – 052 | LBL | 22 25 47.3 | –04 57 01 | QSO | 1.454 | 275 |
| 2345 – 167 | LBL | 23 48 02.7 | –16 31 12 | QSO | 0.576 | 403 |

To accomplish the second main goal, there exists a new set of simultaneous multi-frequency observations in the optical/near-IR with 3-day time resolution. This data is the result of two years of monitoring 15 objects, mostly blazars, with a time resolution of 3 days. This data-set is unique in that the sample rate is very uniform, the spectral coverage is relatively broad, and the objects in it cover a large range of redshifts. It allows virtual simultaneous sampling in 6 wavebands (B, V, R, J, H, and K) to determine first if there are any lags or leads between the lower and higher frequency bands, and second if there is a color dependence on the observed variability. The former will help in testing various jet models and in putting constraints on them. The objects to be used in this investigation are listed in Table 1.3. The columns here are the same as Table 1.2.

Chapter 2

The Data: Acquisition and Reductions

Ideally, evenly sampled observations are needed in order to optimize any investigation of AGN variability. However, due to observing constraints and unforeseeable circumstances (e.g., weather, instrument problems, etc.), evenly sampled data over useful time intervals are rarely available. Optical variability studies of blazars, as with other AGN, also require data sampled over a wide range of timescales. This current investigation utilizes data gathered on timescales ranging from seconds to years.

In general, variability studies can use data gathered over many timescales, but microvariability¹ studies require data with high temporal sampling over an extended amount of time. It has been shown that in order to optimize the likely detection of microvariability, one observation every 5 minutes with a minimum duration of 4 hours of monitoring is required (Carini, 1990). A large portion of the data used here is of this type.

2.1 Data Sources

A large number of telescopes and detector combinations were used to gather data for this dissertation. All recent observations were made with direct CCD (charge coupled device) im-

¹Microvariability refers to the the timescale of variations being on the order of minutes to hours.

agers in the optical or a HgCdTe (Mercury-Cadmium-Telluride) detector in the near-infrared (near-IR) mounted rigidly to their respective telescope. The location and particulars of the combinations are as follows: Lowell observatory hosts the 1.8m (72-inch) Perkins telescope, the 1.07m (42-inch) Hall telescope, the 0.79m (31-inch) telescope; Kitt Peak National Observatory hosts the 0.9m (36-inch) telescope; Cerro Tololo Inter-American Observatory hosts the 0.9m (36-inch) SMARTS consortium telescope and the SMARTS 1.3m (52-inch) telescope (formerly the 2MASS survey telescope); Hard Labor Creek Observatory hosts the 0.4m (16-inch) B&C telescope; and Braeside Observatory hosts a 0.6m (16-inch) telescope. Characteristics of the CCD detectors used is summarized in Table 2.1.

Table 2.1: CCD/IR Detectors

| Telescope | CCD | chip size (pixels) | gain e^- /DN | noise e^- |
|-------------------------|-----------------|-----------------------|-------------------|----------------|
| Hall 1.07m/Perkins 1.8m | RCA | 320 x 512 | 11.5 | 79.0 |
| Braeside 0.4m | THOMPSON | 512 x 512 | 5.0 | 5.0 |
| HLCO 0.4m | THOMPSON | 512 x 512 | 5.0 | 5.0 |
| Lowell 0.79m | THOMPSON | 512 x 512 | 5.0 | 5.0 |
| Hall 1.07m/Perkins 1.8m | USNO | 800 x 800 | 2.3 | 9.0 |
| Hall 1.07m/Perkins 1.8m | SITe | 2048 x 2048 | 3.9 | 11.0 |
| Hall 1.07m/Perkins 1.8m | LORAL | 2048 x 2048 | 3.1 | 17 |
| KPNO 0.9m | T2KA | 2048 x 2046 | 3.0 | 5.4 |
| CTIO 0.9m | SITe | 2048 x 2048 | 10.5 | 4.0 |
| SMARTS 1.3m | FAIRCHILD 447 | 2048 x 2048 | 2.3 | 6.5 |
| Perkins 1.8m | PRISM | 2048 x 2048 | 2.8 | 15 |
| Telescope | HgCdTe Array | chip size (pixels) | gain e^- /DN | noise e^- |
| SMARTS 1.3m | Rockwell | 1024 x 1024 | 7.2 | 20 |

2.2 Reduction Software

Data reduction is the single most important step in producing the final photometric database and the process most prone to problems. Great care must be taken in every step to insure that systematic errors do not contaminate the final result. To this end, a variety of software, custom and prepackaged, has been used to take the data in raw form, calibrate it, measure it, and produce a final output in the most usable form.

2.2.1 IRAF

The Image Reduction and Analysis Facility² (IRAF) was used for all calibration of both the CCD and near-IR data. CCD images were overscan (bias level) corrected, zero (read noise) corrected, dark corrected (where applicable), and flat field corrected to reduce any instrumental effects to their minimum. The near-IR frames were treated slightly differently. The method of Cowie, Gardner, Lilly, and McLean, (1990) was used to flat field correct and subtract the sky contribution from all frames. The nominal procedure requires a relatively sparse field with dithered observations. For each frame to be calibrated, 4 preceding and 4 following frames are used to construct both the flat field and sky correction frames through the use of median filtering. These are then applied in the standard way to achieve near perfect results. All frames, CCD and near-IR, are then run through a cosmic ray cleaning routine to reduce the cosmic ray impact on the photometry.

All these procedures have been incorporated into a data reduction pipeline utilizing the

²IRAF is written and maintained by the National Optical Astronomy Observatories (NOAO), <http://iraf.noao.edu/>

IRAF Command Language in scripts. The pipeline takes the data from completely raw form and outputs fully calibrated frames ready for photometry.

2.2.2 CCDPhot

The calibrated data is photometered with an IDL³ program called CCDPHOT⁴ written by Marc Buie of Lowell Observatory. Photometry is achieved through the use of a synthetic aperture for the point sources and a pair of concentric annuli for the sky. This method can be applied to as many objects in the field as necessary, with the results identical to a multi-aperture photometer. The relative instrumental magnitudes of the object of interest and several calibrated comparison stars in the same field of view are measured simultaneously. This has the advantage of simplicity and precision. No separate standards need to be observed and with the standards in such close proximity to the object of interest, sky conditions and airmass play almost no role in the derived differential magnitudes. Because airmass changes insignificantly across the detector (less than 0.2% for a typical 10 arcmin field), the first- and second-order extinction coefficients are also insignificant in this case. By Equation (2.1), the measured magnitude can be corrected for extinction:

$$m_{\lambda 0} = m_{\lambda} - (k'_{\lambda} + k''_{\lambda}c)X , \quad (2.1)$$

where $m_{\lambda 0}$ is the extinction corrected magnitude, m_{λ} is the measured magnitude, k'_{λ} and k''_{λ} are the first- and second-order extinction coefficients, c is the color index, and X is the

³Interactive Data Language by Research Systems Inc.

⁴<http://www.lowell.edu/users/buie/idl/ccdphot.html>

airmass

CCDPHOT uses object templates and a centering algorithm to automate the photometry of a large number of observations of the same field yielding quick, yet accurate, results. CCDPHOT does not output the results in the most optimal form for analysis, so several scripts have been written to convert and plot the data.

2.3 Data Sorting and Mining

The first task to be accomplished with the fully reduced data is to convert it into a form that can be analyzed. The `pegasort` script (all scripts and source code written for use in this dissertation will be distinguished by a `typeset` font and can be found in Appendix A and B) takes the CCDPHOT output and converts it into such a form. It takes the CCDPHOT output file which has a separate line per object per frame and converts it into a form where there is only one line per frame, each consisting of the frame name, date, filter, exposure time, aperture, and information specific to each object in turn: full width at half maximum (FWHM), peak counts, and instrumental magnitude.

Once the data in the file is sorted, it is ready to be either visualized or calibrated. To visualize the data, the `pegaplot` script was created. It plots the differential magnitude of the science object with respect to the two most stable comparison stars in the field. They are selected based on the standard deviation of the distribution of their difference in magnitude, which is generally less than 0.05 magnitude.

The `pegacalib` script can be used to convert the instrumental magnitudes to real magnitudes. This is done by applying a zero-point offset magnitude for each data point derived

from the two most stable comparison stars (in many cases, more than two) within the field of view of the CCD. These comparison stars are chosen such that the stars are as close in magnitude to the object as possible. The errors of the comparison stars are averaged in quadrature with the sample standard deviation of the determined zero-point offsets of the comparison stars. The resulting error estimate represents both the error in calibrated magnitudes and the spread in how well they each predict the actual photometric solution for a particular frame. It should be noted that the photon statistics ($1/N_{photons}$) of the dimmest object used in the calibration (source or comparisons) sets the minimum for the error estimate, and is used if the above error estimate drops below this minimum (e.g., when the object is very faint).

To use the `pegacalib` script, the apparent magnitudes of a calibrated comparison sequence for a given object need to be known. The website⁵ for the Program in Extragalactic Astronomy (PEGA) hosts a large set of finding charts which include these sequences. There are links at the bottom of each finding chart webpage that give the magnitudes in the exact form needed by the `pegacalib` script.

If the error in a particular dataset is unacceptably large (e.g., due to small telescope aperture or short time exposures), the data can be combined into bins containing n -points to increase the signal-to-noise ratio (S/N). The contents of each bin would then be averaged such that the time and observable (e.g., flux or magnitude) are averaged linearly (i.e., $(f_1 + f_2 + \dots + f_n)/n$), and the error is averaged in quadrature (i.e. $(e_1^2 + e_2^2 + \dots + e_n^2)^{1/2}/n$) with an extra factor to compensate for the spread in the observable. The extra factor is simply

⁵<http://www.chara.gsu.edu/PEGA/>

the sample standard deviation of the observables used in the average. This value is averaged in quadrature with the associated errors. The result is a realistic estimate of the error for the combined data. The C program `pegabin` was written to implement this.

2.4 The Dataset

There are 16 objects in the sample: 7 in the archival sample and 11 in the SMARTS sample, 2 of which are common to both (see Tables 1.2 & 1.3). The objects range in redshift from 0.069 to 1.814 and exhibit amplitudes of their variations that range from the detection limit (~ 0.03 magnitude) to ~ 6 magnitudes. The reference names used for the objects follow the IAU standard format for truncated 1950 Equinox coordinates: HHMM+DDd, where “HHMM” are the hours and minutes of right ascension and the “+DDd” are the signed 2 digit degrees and one decimal degree of declination. When an object is referred to outside of tables, this reference name will be used preferably except when a common name is more familiar (e.g 2200+420 will be referred to as BL Lac). Inside tables and figures, the reference name will be used for uniformity

In this section, data from all objects are displayed in the form of a nightly average in Table 2.2. All data is in the R or V band. Columns 1 and 2 give the reference name for each object and the filter name respectively; columns 3 and 4 give the date in Julian format and Epoch respectively; and the last column gives the apparent magnitude of the object. The errors on individual points within a night are typically $\lesssim 0.05$ mag. The error on the nightly averages are similar.

Table 2.2: Nightly Avaraged Data

| Object | Filter | Julian Date | UT Epoch | Mag |
|------------|--------|---------------|----------|-------|
| 0235 + 164 | V | 2446716.92315 | 1986.783 | 17.38 |
| 0235 + 164 | V | 2447110.92793 | 1987.862 | 17.92 |
| 0235 + 164 | V | 2448191.85844 | 1990.821 | 16.56 |
| 0235 + 164 | V | 2448192.81154 | 1990.824 | 16.50 |
| 0235 + 164 | V | 2448193.82327 | 1990.826 | 16.42 |
| 0235 + 164 | V | 2448194.81528 | 1990.829 | 16.16 |
| 0235 + 164 | V | 2448195.74153 | 1990.832 | 16.44 |
| 0235 + 164 | V | 2448308.97560 | 1991.142 | 17.73 |
| 0235 + 164 | V | 2448565.85382 | 1991.845 | 14.48 |
| 0235 + 164 | V | 2448566.80901 | 1991.848 | 14.48 |
| 0235 + 164 | V | 2448567.80265 | 1991.850 | 14.55 |
| 0235 + 164 | V | 2448568.76712 | 1991.853 | 14.19 |
| 0235 + 164 | V | 2448622.61336 | 1992.000 | 15.97 |
| 0235 + 164 | R | 2448649.58685 | 1992.074 | 16.30 |
| 0235 + 164 | R | 2448868.90954 | 1992.675 | 15.16 |
| 0235 + 164 | V | 2448868.92486 | 1992.675 | 15.91 |
| 0235 + 164 | R | 2448869.95426 | 1992.677 | 14.70 |
| 0235 + 164 | R | 2448870.98756 | 1992.680 | 15.02 |
| 0235 + 164 | V | 2448870.99453 | 1992.680 | 15.75 |
| 0235 + 164 | V | 2448927.76853 | 1992.836 | 17.51 |
| 0235 + 164 | V | 2448930.79174 | 1992.844 | 16.96 |
| 0235 + 164 | R | 2448930.79981 | 1992.844 | 16.19 |
| 0235 + 164 | R | 2448988.62154 | 1993.002 | 15.41 |
| 0235 + 164 | R | 2449212.90356 | 1993.616 | 18.25 |
| 0235 + 164 | R | 2450420.71106 | 1996.923 | 19.10 |
| 0235 + 164 | R | 2450421.68332 | 1996.926 | 18.96 |
| 0235 + 164 | R | 2450424.68667 | 1996.934 | 18.36 |
| 0235 + 164 | R | 2450425.68298 | 1996.937 | 18.36 |
| 0235 + 164 | R | 2450718.76927 | 1997.739 | 17.28 |
| 0235 + 164 | V | 2450761.86396 | 1997.857 | 16.79 |
| 0235 + 164 | V | 2450777.80843 | 1997.901 | 17.60 |
| 0235 + 164 | R | 2450827.71992 | 1998.038 | 15.64 |
| 0235 + 164 | R | 2450828.70745 | 1998.040 | 14.97 |
| 0235 + 164 | R | 2450881.61169 | 1998.185 | 15.46 |
| 0235 + 164 | V | 2450882.61336 | 1998.188 | 16.20 |
| 0235 + 164 | R | 2451104.87206 | 1998.796 | 16.13 |
| 0235 + 164 | R | 2451105.91824 | 1998.799 | 16.65 |
| 0235 + 164 | R | 2451106.76151 | 1998.802 | 16.87 |
| 0235 + 164 | R | 2451491.82063 | 1999.856 | 17.32 |
| 0235 + 164 | R | 2451843.82053 | 2000.819 | 18.97 |

Table 2.2: continued...

| Object | Filter | Julian Date | UT Epoch | Mag |
|------------|--------|---------------|----------|-------|
| 0235 + 164 | R | 2452250.65092 | 2001.933 | 18.54 |
| 0235 + 164 | R | 2452577.88230 | 2002.829 | 17.23 |
| 0235 + 164 | R | 2452578.87460 | 2002.832 | 17.12 |
| 0235 + 164 | R | 2452976.74668 | 2003.921 | 17.11 |
| 0235 + 164 | R | 2452977.72128 | 2003.924 | 16.98 |
| 0235 + 164 | R | 2453014.74491 | 2004.025 | 17.55 |
| 0235 + 164 | R | 2453015.65937 | 2004.028 | 17.59 |
| 0235 + 164 | R | 2453017.68645 | 2004.033 | 18.26 |
| 0235 + 164 | R | 2453031.70463 | 2004.072 | 18.18 |
| 0235 + 164 | R | 2453044.66801 | 2004.107 | 17.80 |
| 0235 + 164 | R | 2453046.67759 | 2004.113 | 17.59 |
| 0235 + 164 | R | 2453047.66135 | 2004.115 | 17.76 |
| 0235 + 164 | R | 2453049.67150 | 2004.121 | 17.90 |
| 0235 + 164 | R | 2453051.64818 | 2004.126 | 18.01 |
| 0235 + 164 | R | 2453270.93079 | 2004.727 | 18.41 |
| 0235 + 164 | R | 2453271.92821 | 2004.729 | 18.40 |
| 0235 + 164 | R | 2453282.95809 | 2004.760 | 17.69 |
| 0235 + 164 | R | 2453283.92637 | 2004.762 | 17.80 |
| 0235 + 164 | R | 2453284.85400 | 2004.765 | 17.85 |
| 0235 + 164 | R | 2453286.90116 | 2004.770 | 18.14 |
| 0235 + 164 | R | 2453287.87516 | 2004.773 | 18.18 |
| | | | | |
| 0420 − 014 | R | 2452963.62961 | 2003.885 | 15.44 |
| 0420 − 014 | R | 2452981.67731 | 2003.935 | 16.32 |
| 0420 − 014 | R | 2452996.65374 | 2003.976 | 16.51 |
| 0420 − 014 | R | 2453012.61196 | 2004.019 | 15.95 |
| 0420 − 014 | R | 2453018.63424 | 2004.036 | 16.03 |
| 0420 − 014 | R | 2453032.62560 | 2004.074 | 16.40 |
| 0420 − 014 | R | 2453053.57338 | 2004.132 | 16.03 |
| 0420 − 014 | R | 2453057.52123 | 2004.142 | 16.39 |
| 0420 − 014 | R | 2453060.54623 | 2004.151 | 16.54 |
| 0420 − 014 | R | 2453063.54392 | 2004.159 | 16.60 |
| 0420 − 014 | R | 2453066.54475 | 2004.167 | 16.73 |
| 0420 − 014 | R | 2453069.52498 | 2004.175 | 16.97 |
| 0420 − 014 | R | 2453072.52201 | 2004.183 | 17.07 |
| 0420 − 014 | R | 2453075.53326 | 2004.192 | 16.96 |
| 0420 − 014 | R | 2453078.50948 | 2004.200 | 16.97 |
| 0420 − 014 | R | 2453082.52628 | 2004.211 | 17.01 |
| 0420 − 014 | R | 2453089.48765 | 2004.230 | 17.03 |
| 0420 − 014 | R | 2453092.48775 | 2004.238 | 17.09 |
| 0420 − 014 | R | 2453097.47918 | 2004.252 | 17.07 |

Table 2.2: continued...

| Object | Filter | Julian Date | UT Epoch | Mag |
|------------|--------|---------------|----------|-------|
| 0420 – 014 | R | 2453102.47535 | 2004.266 | 17.07 |
| 0420 – 014 | R | 2453105.47094 | 2004.274 | 17.11 |
| 0420 – 014 | R | 2453108.47520 | 2004.282 | 17.13 |
| 0420 – 014 | R | 2453111.47066 | 2004.290 | 17.18 |
| 0420 – 014 | R | 2453277.76904 | 2004.745 | 17.01 |
| 0420 – 014 | R | 2453301.72567 | 2004.811 | 16.76 |
| 0420 – 014 | R | 2453334.61988 | 2004.901 | 17.00 |
| 0420 – 014 | R | 2453337.64160 | 2004.909 | 17.09 |
| 0420 – 014 | R | 2453340.65228 | 2004.918 | 17.35 |
| 0420 – 014 | R | 2453344.58348 | 2004.928 | 17.26 |
| 0420 – 014 | R | 2453349.67459 | 2004.942 | 17.35 |
| 0420 – 014 | R | 2453352.63927 | 2004.950 | 17.31 |
| 0420 – 014 | R | 2453355.63735 | 2004.959 | 17.45 |
| 0420 – 014 | R | 2453358.61919 | 2004.967 | 17.48 |
| 0420 – 014 | R | 2453361.61184 | 2004.975 | 17.51 |
| 0420 – 014 | R | 2453366.56924 | 2004.989 | 17.54 |
| 0420 – 014 | R | 2453369.60814 | 2004.997 | 17.68 |
| 0420 – 014 | R | 2453373.61596 | 2005.008 | 17.66 |
| 0420 – 014 | R | 2453379.61052 | 2005.024 | 17.62 |
| 0420 – 014 | R | 2453382.56494 | 2005.032 | 17.36 |
| 0420 – 014 | R | 2453385.60815 | 2005.041 | 17.48 |
| | | | | |
| 0818 – 128 | V | 2452963.73185 | 2003.886 | 17.85 |
| 0818 – 128 | V | 2452990.77877 | 2003.960 | 17.83 |
| 0818 – 128 | V | 2453002.79008 | 2003.993 | 17.68 |
| 0818 – 128 | V | 2453012.77591 | 2004.020 | 17.79 |
| 0818 – 128 | V | 2453018.74968 | 2004.036 | 17.80 |
| 0818 – 128 | V | 2453031.74654 | 2004.072 | 17.63 |
| 0818 – 128 | V | 2453056.72913 | 2004.140 | 17.88 |
| 0818 – 128 | V | 2453059.62906 | 2004.148 | 17.98 |
| 0818 – 128 | V | 2453062.68424 | 2004.157 | 18.07 |
| 0818 – 128 | V | 2453068.59406 | 2004.173 | 18.02 |
| 0818 – 128 | V | 2453071.63510 | 2004.181 | 18.00 |
| 0818 – 128 | V | 2453074.63664 | 2004.189 | 17.95 |
| 0818 – 128 | V | 2453077.57794 | 2004.197 | 17.98 |
| 0818 – 128 | V | 2453081.69139 | 2004.209 | 17.99 |
| 0818 – 128 | V | 2453088.52191 | 2004.227 | 18.07 |
| 0818 – 128 | V | 2453091.54794 | 2004.236 | 18.08 |
| 0818 – 128 | V | 2453096.56975 | 2004.249 | 18.08 |
| 0818 – 128 | V | 2453099.52481 | 2004.257 | 18.13 |
| 0818 – 128 | V | 2453103.65626 | 2004.269 | 18.05 |

Table 2.2: continued...

| Object | Filter | Julian Date | UT Epoch | Mag |
|------------|--------|---------------|----------|-------|
| 0818 – 128 | V | 2453106.53369 | 2004.277 | 18.08 |
| 0818 – 128 | V | 2453109.55221 | 2004.285 | 18.07 |
| 0818 – 128 | V | 2453113.54116 | 2004.296 | 18.09 |
| 0818 – 128 | V | 2453116.53174 | 2004.304 | 18.03 |
| 0818 – 128 | V | 2453123.48404 | 2004.323 | 18.05 |
| 0818 – 128 | V | 2453126.46209 | 2004.331 | 18.07 |
| 0818 – 128 | V | 2453132.51568 | 2004.348 | 18.05 |
| 0818 – 128 | V | 2453135.46618 | 2004.356 | 17.99 |
| 0818 – 128 | V | 2453138.45979 | 2004.364 | 18.03 |
| 0818 – 128 | V | 2453141.50249 | 2004.372 | 17.79 |
| 0818 – 128 | V | 2453145.47709 | 2004.383 | 17.95 |
| 0818 – 128 | V | 2453151.51626 | 2004.400 | 17.88 |
| 0818 – 128 | V | 2453154.49331 | 2004.408 | 17.91 |
| 0818 – 128 | V | 2453156.46265 | 2004.413 | 17.86 |
| 0818 – 128 | V | 2453160.44500 | 2004.424 | 17.85 |
| 0818 – 128 | V | 2453163.45985 | 2004.432 | 17.92 |
| 0818 – 128 | V | 2453167.47443 | 2004.443 | 17.87 |
| 0818 – 128 | V | 2453172.46221 | 2004.457 | 17.87 |
| 0818 – 128 | V | 2453176.44493 | 2004.468 | 17.73 |
| 0818 – 128 | V | 2453180.44117 | 2004.479 | 17.88 |
| 0818 – 128 | V | 2453183.45100 | 2004.487 | 17.85 |
| 0818 – 128 | V | 2453187.45413 | 2004.498 | 17.83 |
| 0818 – 128 | V | 2453281.83337 | 2004.757 | 17.86 |
| 0818 – 128 | V | 2453339.72380 | 2004.915 | 17.98 |
| 0818 – 128 | V | 2453342.73122 | 2004.923 | 17.98 |
| 0818 – 128 | V | 2453351.74741 | 2004.948 | 18.04 |
| 0818 – 128 | V | 2453354.74508 | 2004.956 | 18.11 |
| 0818 – 128 | V | 2453357.67949 | 2004.964 | 18.12 |
| 0818 – 128 | V | 2453360.74672 | 2004.973 | 18.24 |
| 0818 – 128 | V | 2453363.72941 | 2004.981 | 18.28 |
| 0818 – 128 | V | 2453371.62333 | 2005.002 | 18.21 |
| 0818 – 128 | V | 2453374.66072 | 2005.011 | 18.26 |
| 0818 – 128 | V | 2453377.71419 | 2005.019 | 18.26 |
| 0818 – 128 | V | 2453380.68936 | 2005.027 | 18.30 |
| 0818 – 128 | V | 2453383.67657 | 2005.035 | 18.33 |
| 0818 – 128 | V | 2453386.68541 | 2005.044 | 18.31 |
| 1156 + 295 | R | 2448648.84585 | 1992.072 | 16.98 |
| 1156 + 295 | R | 2449371.94200 | 1994.052 | 13.82 |
| 1156 + 295 | R | 2449372.95763 | 1994.055 | 13.81 |
| 1156 + 295 | R | 2449373.94145 | 1994.057 | 13.76 |

Table 2.2: continued...

| Object | Filter | Julian Date | UT Epoch | Mag |
|------------|--------|---------------|----------|-------|
| 1156 + 295 | R | 2449374.91519 | 1994.060 | 14.21 |
| 1156 + 295 | R | 2449375.93953 | 1994.063 | 14.15 |
| 1156 + 295 | R | 2449376.88317 | 1994.065 | 14.40 |
| 1156 + 295 | R | 2450950.71414 | 1998.374 | 15.18 |
| 1156 + 295 | R | 2452016.83187 | 2001.293 | 15.79 |
| 1156 + 295 | R | 2453147.73308 | 2004.389 | 18.10 |
| | | | | |
| 1226 + 023 | R | 2453060.73424 | 2004.151 | 12.49 |
| 1226 + 023 | R | 2453063.72186 | 2004.159 | 12.58 |
| 1226 + 023 | R | 2453071.68613 | 2004.181 | 12.51 |
| 1226 + 023 | R | 2453077.60110 | 2004.197 | 12.52 |
| 1226 + 023 | R | 2453092.62602 | 2004.239 | 12.53 |
| 1226 + 023 | R | 2453101.66997 | 2004.263 | 12.58 |
| 1226 + 023 | R | 2453104.59503 | 2004.271 | 12.57 |
| 1226 + 023 | R | 2453107.64229 | 2004.280 | 12.54 |
| 1226 + 023 | R | 2453111.68380 | 2004.291 | 12.55 |
| 1226 + 023 | R | 2453114.63111 | 2004.299 | 12.58 |
| 1226 + 023 | R | 2453121.62542 | 2004.318 | 12.56 |
| 1226 + 023 | R | 2453124.58811 | 2004.326 | 12.55 |
| 1226 + 023 | R | 2453130.59525 | 2004.342 | 12.56 |
| 1226 + 023 | R | 2453133.50086 | 2004.350 | 12.60 |
| 1226 + 023 | R | 2453139.54990 | 2004.367 | 12.55 |
| 1226 + 023 | R | 2453142.48378 | 2004.375 | 12.55 |
| 1226 + 023 | R | 2453146.60902 | 2004.386 | 12.55 |
| 1226 + 023 | R | 2453152.52725 | 2004.403 | 12.57 |
| 1226 + 023 | R | 2453156.51027 | 2004.413 | 12.57 |
| 1226 + 023 | R | 2453160.47877 | 2004.424 | 12.55 |
| 1226 + 023 | R | 2453163.51858 | 2004.433 | 12.54 |
| 1226 + 023 | R | 2453167.51420 | 2004.444 | 12.56 |
| 1226 + 023 | R | 2453172.53069 | 2004.457 | 12.57 |
| 1226 + 023 | R | 2453180.51514 | 2004.479 | 12.61 |
| 1226 + 023 | R | 2453184.51444 | 2004.490 | 12.57 |
| 1226 + 023 | R | 2453188.52046 | 2004.501 | 12.57 |
| 1226 + 023 | R | 2453191.45934 | 2004.509 | 12.58 |
| 1226 + 023 | R | 2453194.48648 | 2004.517 | 12.57 |
| 1226 + 023 | R | 2453197.55277 | 2004.526 | 12.56 |
| 1226 + 023 | R | 2453202.46950 | 2004.539 | 12.58 |
| 1226 + 023 | R | 2453206.49736 | 2004.550 | 12.58 |
| 1226 + 023 | R | 2453211.48017 | 2004.564 | 12.50 |
| 1226 + 023 | R | 2453218.51088 | 2004.583 | 12.53 |
| 1226 + 023 | R | 2453224.46723 | 2004.599 | 12.55 |

Table 2.2: continued...

| Object | Filter | Julian Date | UT Epoch | Mag |
|------------|--------|---------------|----------|-------|
| 1226 + 023 | R | 2453229.47027 | 2004.613 | 12.54 |
| 1253 − 055 | R | 2453060.74366 | 2004.151 | 15.06 |
| 1253 − 055 | R | 2453063.73080 | 2004.159 | 15.02 |
| 1253 − 055 | R | 2453071.70872 | 2004.181 | 15.21 |
| 1253 − 055 | R | 2453078.65846 | 2004.200 | 15.22 |
| 1253 − 055 | R | 2453097.60826 | 2004.252 | 15.60 |
| 1253 − 055 | R | 2453102.66510 | 2004.266 | 15.69 |
| 1253 − 055 | R | 2453105.60205 | 2004.274 | 15.78 |
| 1253 − 055 | R | 2453108.61772 | 2004.282 | 15.73 |
| 1253 − 055 | R | 2453112.58127 | 2004.293 | 15.79 |
| 1253 − 055 | R | 2453115.64735 | 2004.302 | 15.56 |
| 1253 − 055 | R | 2453122.60541 | 2004.321 | 15.55 |
| 1253 − 055 | R | 2453125.58679 | 2004.329 | 15.83 |
| 1253 − 055 | R | 2453130.61836 | 2004.343 | 15.70 |
| 1253 − 055 | R | 2453134.51446 | 2004.353 | 15.57 |
| 1253 − 055 | R | 2453137.58470 | 2004.362 | 15.66 |
| 1253 − 055 | R | 2453140.60365 | 2004.370 | 15.26 |
| 1253 − 055 | R | 2453144.58596 | 2004.381 | 15.32 |
| 1253 − 055 | R | 2453150.53860 | 2004.397 | 14.99 |
| 1253 − 055 | R | 2453153.53395 | 2004.405 | 14.93 |
| 1253 − 055 | R | 2453158.54605 | 2004.419 | 15.16 |
| 1253 − 055 | R | 2453161.55346 | 2004.427 | 15.10 |
| 1253 − 055 | R | 2453164.49275 | 2004.435 | 15.11 |
| 1253 − 055 | R | 2453168.59463 | 2004.447 | 14.98 |
| 1253 − 055 | R | 2453174.51292 | 2004.463 | 14.79 |
| 1253 − 055 | R | 2453177.51157 | 2004.471 | 14.51 |
| 1253 − 055 | R | 2453184.56296 | 2004.490 | 14.47 |
| 1253 − 055 | R | 2453188.52846 | 2004.501 | 14.01 |
| 1253 − 055 | R | 2453191.46721 | 2004.509 | 14.29 |
| 1253 − 055 | R | 2453194.50731 | 2004.517 | 14.40 |
| 1253 − 055 | R | 2453197.56807 | 2004.526 | 14.54 |
| 1253 − 055 | R | 2453202.48219 | 2004.539 | 14.90 |
| 1253 − 055 | R | 2453206.53065 | 2004.550 | 15.27 |
| 1253 − 055 | R | 2453212.46802 | 2004.567 | 15.61 |
| 1253 − 055 | R | 2453223.51749 | 2004.597 | 15.46 |
| 1253 − 055 | R | 2453225.46666 | 2004.602 | 15.47 |
| 1253 − 055 | R | 2453230.48326 | 2004.616 | 15.77 |
| 1253 − 055 | R | 2453243.46808 | 2004.652 | 15.58 |
| 1253 − 055 | R | 2453377.79690 | 2005.019 | 15.04 |
| 1253 − 055 | R | 2453380.78545 | 2005.027 | 15.63 |

Table 2.2: continued...

| Object | Filter | Julian Date | UT Epoch | Mag |
|------------|--------|---------------|----------|-------|
| 1253 – 055 | R | 2453383.79640 | 2005.036 | 15.55 |
| 1510 – 089 | R | 2452675.85831 | 2003.097 | 16.79 |
| 1510 – 089 | R | 2452676.88987 | 2003.100 | 16.79 |
| 1510 – 089 | R | 2452677.83060 | 2003.103 | 16.79 |
| 1510 – 089 | R | 2452678.80286 | 2003.106 | 16.76 |
| 1510 – 089 | R | 2452679.83421 | 2003.108 | 16.86 |
| 1510 – 089 | R | 2452680.84299 | 2003.111 | 16.81 |
| 1510 – 089 | R | 2452681.84039 | 2003.114 | 16.83 |
| 1510 – 089 | R | 2452682.82979 | 2003.117 | 16.83 |
| 1510 – 089 | R | 2452683.80275 | 2003.119 | 16.80 |
| 1510 – 089 | R | 2452684.82204 | 2003.122 | 16.87 |
| 1510 – 089 | R | 2452687.77911 | 2003.130 | 16.80 |
| 1510 – 089 | R | 2452690.78537 | 2003.138 | 16.70 |
| 1510 – 089 | R | 2452694.81963 | 2003.149 | 16.76 |
| 1510 – 089 | R | 2452696.82455 | 2003.155 | 16.76 |
| 1510 – 089 | R | 2452699.83743 | 2003.163 | 16.84 |
| 1510 – 089 | R | 2452702.82991 | 2003.171 | 16.87 |
| 1510 – 089 | R | 2452705.80942 | 2003.179 | 16.81 |
| 1510 – 089 | R | 2452708.77010 | 2003.188 | 16.87 |
| 1510 – 089 | R | 2452711.75282 | 2003.196 | 16.89 |
| 1510 – 089 | R | 2452714.84752 | 2003.204 | 16.95 |
| 1510 – 089 | R | 2452717.84427 | 2003.212 | 16.90 |
| 1510 – 089 | R | 2452723.78037 | 2003.229 | 16.91 |
| 1510 – 089 | R | 2452729.74689 | 2003.245 | 16.93 |
| 1510 – 089 | R | 2452732.72881 | 2003.253 | 16.87 |
| 1510 – 089 | R | 2452735.73941 | 2003.261 | 16.92 |
| 1510 – 089 | R | 2452738.73256 | 2003.270 | 16.89 |
| 1510 – 089 | R | 2452741.70193 | 2003.278 | 16.94 |
| 1510 – 089 | R | 2452744.70894 | 2003.286 | 16.89 |
| 1510 – 089 | R | 2452750.75714 | 2003.303 | 16.89 |
| 1510 – 089 | R | 2452753.82608 | 2003.311 | 16.94 |
| 1510 – 089 | R | 2452756.75035 | 2003.319 | 16.93 |
| 1510 – 089 | R | 2452758.71278 | 2003.324 | 16.89 |
| 1510 – 089 | R | 2452761.68568 | 2003.332 | 16.95 |
| 1510 – 089 | R | 2452764.58921 | 2003.340 | 16.88 |
| 1510 – 089 | R | 2452766.78948 | 2003.346 | 16.83 |
| 1510 – 089 | R | 2452770.74449 | 2003.357 | 16.92 |
| 1510 – 089 | R | 2452773.59661 | 2003.365 | 16.90 |
| 1510 – 089 | R | 2452776.58920 | 2003.373 | 16.87 |
| 1510 – 089 | R | 2452782.57885 | 2003.390 | 16.83 |

Table 2.2: continued...

| Object | Filter | Julian Date | UT Epoch | Mag |
|------------|--------|---------------|----------|-------|
| 1510 – 089 | R | 2452785.56163 | 2003.398 | 16.71 |
| 1510 – 089 | R | 2452788.54801 | 2003.406 | 16.80 |
| 1510 – 089 | R | 2452789.52851 | 2003.409 | 16.81 |
| 1510 – 089 | R | 2452792.57523 | 2003.417 | 16.94 |
| 1510 – 089 | R | 2452797.67822 | 2003.431 | 16.82 |
| 1510 – 089 | R | 2452804.69013 | 2003.450 | 17.63 |
| 1510 – 089 | R | 2452809.61179 | 2003.464 | 16.82 |
| 1510 – 089 | R | 2452812.47888 | 2003.472 | 16.83 |
| 1510 – 089 | R | 2452815.47204 | 2003.480 | 16.79 |
| 1510 – 089 | R | 2452818.48441 | 2003.488 | 16.72 |
| 1510 – 089 | R | 2452821.51861 | 2003.496 | 16.74 |
| 1510 – 089 | R | 2452831.47273 | 2003.524 | 16.60 |
| 1510 – 089 | R | 2452833.51934 | 2003.529 | 16.82 |
| 1510 – 089 | R | 2452836.49844 | 2003.537 | 16.61 |
| 1510 – 089 | R | 2452839.59735 | 2003.546 | 16.64 |
| 1510 – 089 | R | 2452842.53233 | 2003.554 | 16.60 |
| 1510 – 089 | R | 2452845.51399 | 2003.562 | 16.70 |
| 1510 – 089 | R | 2452847.58309 | 2003.568 | 16.71 |
| 1510 – 089 | R | 2452852.55069 | 2003.581 | 16.69 |
| 1510 – 089 | R | 2452854.57145 | 2003.587 | 16.62 |
| 1510 – 089 | R | 2452860.56922 | 2003.603 | 16.77 |
| 1510 – 089 | R | 2452864.52652 | 2003.614 | 16.69 |
| 1510 – 089 | R | 2452867.52744 | 2003.622 | 16.67 |
| 1510 – 089 | R | 2452870.49466 | 2003.630 | 16.66 |
| 1510 – 089 | R | 2452873.51271 | 2003.639 | 16.70 |
| 1510 – 089 | R | 2452876.53554 | 2003.647 | 16.68 |
| 1510 – 089 | R | 2452879.49387 | 2003.655 | 16.72 |
| 1510 – 089 | R | 2452883.53031 | 2003.666 | 16.71 |
| 1510 – 089 | R | 2453121.68671 | 2004.318 | 16.78 |
| 1510 – 089 | R | 2453124.62647 | 2004.326 | 16.75 |
| 1510 – 089 | R | 2453127.60817 | 2004.334 | 16.76 |
| 1510 – 089 | R | 2453131.67541 | 2004.345 | 16.82 |
| 1510 – 089 | R | 2453134.56455 | 2004.353 | 16.52 |
| 1510 – 089 | R | 2453137.60485 | 2004.362 | 16.54 |
| 1510 – 089 | R | 2453140.61273 | 2004.370 | 16.72 |
| 1510 – 089 | R | 2453144.77417 | 2004.381 | 16.73 |
| 1510 – 089 | R | 2453149.69168 | 2004.395 | 16.76 |
| 1510 – 089 | R | 2453153.60802 | 2004.405 | 16.71 |
| 1510 – 089 | R | 2453155.52538 | 2004.411 | 16.69 |
| 1510 – 089 | R | 2453159.62656 | 2004.422 | 16.68 |
| 1510 – 089 | R | 2453162.57049 | 2004.430 | 16.72 |

Table 2.2: continued...

| Object | Filter | Julian Date | UT Epoch | Mag |
|------------|--------|---------------|----------|-------|
| 1510 – 089 | R | 2453165.59441 | 2004.438 | 16.71 |
| 1510 – 089 | R | 2453169.65633 | 2004.449 | 16.68 |
| 1510 – 089 | R | 2453175.57931 | 2004.466 | 16.58 |
| 1510 – 089 | R | 2453178.60300 | 2004.474 | 16.57 |
| 1510 – 089 | R | 2453182.62227 | 2004.485 | 16.50 |
| 1510 – 089 | R | 2453186.64447 | 2004.496 | 16.58 |
| 1510 – 089 | R | 2453189.54681 | 2004.504 | 16.54 |
| 1510 – 089 | R | 2453195.55854 | 2004.520 | 16.38 |
| 1510 – 089 | R | 2453199.62735 | 2004.531 | 16.48 |
| 1510 – 089 | R | 2453203.50395 | 2004.542 | 16.46 |
| 1510 – 089 | R | 2453207.52406 | 2004.553 | 16.25 |
| 1510 – 089 | R | 2453217.53436 | 2004.581 | 15.75 |
| 1510 – 089 | R | 2453224.57571 | 2004.600 | 15.70 |
| 1510 – 089 | R | 2453229.55333 | 2004.613 | 16.18 |
| 1510 – 089 | R | 2453242.58878 | 2004.649 | 16.40 |
| 1510 – 089 | R | 2453247.52829 | 2004.663 | 16.44 |
| 1510 – 089 | R | 2453254.50230 | 2004.682 | 16.45 |
| 1510 – 089 | R | 2453264.48436 | 2004.709 | 16.60 |
| 1510 – 089 | R | 2453268.48656 | 2004.720 | 16.62 |
| | | | | |
| 1514 – 241 | R | 2452675.86428 | 2003.098 | 14.65 |
| 1514 – 241 | R | 2452677.83541 | 2003.103 | 14.65 |
| 1514 – 241 | R | 2452678.80781 | 2003.106 | 14.63 |
| 1514 – 241 | R | 2452679.83892 | 2003.108 | 14.57 |
| 1514 – 241 | R | 2452680.84758 | 2003.111 | 14.64 |
| 1514 – 241 | R | 2452681.84509 | 2003.114 | 14.62 |
| 1514 – 241 | R | 2452682.83499 | 2003.117 | 14.59 |
| 1514 – 241 | R | 2452683.80753 | 2003.119 | 14.62 |
| 1514 – 241 | R | 2452684.82894 | 2003.122 | 14.57 |
| 1514 – 241 | R | 2452687.79052 | 2003.130 | 14.59 |
| 1514 – 241 | R | 2452690.79719 | 2003.138 | 14.56 |
| 1514 – 241 | R | 2452694.83420 | 2003.149 | 14.63 |
| 1514 – 241 | R | 2452696.83305 | 2003.155 | 14.63 |
| 1514 – 241 | R | 2452699.84657 | 2003.163 | 14.64 |
| 1514 – 241 | R | 2452702.83859 | 2003.171 | 14.62 |
| 1514 – 241 | R | 2452705.81770 | 2003.180 | 14.56 |
| 1514 – 241 | R | 2452708.77843 | 2003.188 | 14.58 |
| 1514 – 241 | R | 2452711.76108 | 2003.196 | 14.64 |
| 1514 – 241 | R | 2452714.85614 | 2003.204 | 14.54 |
| 1514 – 241 | R | 2452717.85328 | 2003.212 | 14.54 |
| 1514 – 241 | R | 2452723.78864 | 2003.229 | 14.50 |

Table 2.2: continued...

| Object | Filter | Julian Date | UT Epoch | Mag |
|------------|--------|---------------|----------|-------|
| 1514 – 241 | R | 2452729.75619 | 2003.245 | 14.40 |
| 1514 – 241 | R | 2452732.73765 | 2003.253 | 14.47 |
| 1514 – 241 | R | 2452735.74788 | 2003.261 | 14.42 |
| 1514 – 241 | R | 2452738.74135 | 2003.270 | 14.48 |
| 1514 – 241 | R | 2452741.71055 | 2003.278 | 14.40 |
| 1514 – 241 | R | 2452744.71978 | 2003.286 | 14.44 |
| 1514 – 241 | R | 2452750.76595 | 2003.303 | 14.55 |
| 1514 – 241 | R | 2452753.83432 | 2003.311 | 14.51 |
| 1514 – 241 | R | 2452756.75907 | 2003.319 | 14.51 |
| 1514 – 241 | R | 2452758.72218 | 2003.324 | 14.50 |
| 1514 – 241 | R | 2452761.69444 | 2003.332 | 14.54 |
| 1514 – 241 | R | 2452764.60035 | 2003.340 | 14.67 |
| 1514 – 241 | R | 2452766.79806 | 2003.346 | 14.72 |
| 1514 – 241 | R | 2452770.75266 | 2003.357 | 14.69 |
| 1514 – 241 | R | 2452773.60502 | 2003.365 | 14.72 |
| 1514 – 241 | R | 2452776.59758 | 2003.373 | 14.67 |
| 1514 – 241 | R | 2452782.58754 | 2003.390 | 14.68 |
| 1514 – 241 | R | 2452785.56991 | 2003.398 | 14.57 |
| 1514 – 241 | R | 2452788.55777 | 2003.406 | 14.56 |
| 1514 – 241 | R | 2452789.53710 | 2003.409 | 14.58 |
| 1514 – 241 | R | 2452792.58355 | 2003.417 | 14.58 |
| 1514 – 241 | R | 2452797.66702 | 2003.431 | 14.63 |
| 1514 – 241 | R | 2452804.68077 | 2003.450 | 14.80 |
| 1514 – 241 | R | 2452809.62034 | 2003.464 | 14.69 |
| 1514 – 241 | R | 2452812.47041 | 2003.472 | 14.63 |
| 1514 – 241 | R | 2452815.48065 | 2003.480 | 14.55 |
| 1514 – 241 | R | 2452818.47608 | 2003.488 | 14.50 |
| 1514 – 241 | R | 2452821.50954 | 2003.496 | 14.55 |
| 1514 – 241 | R | 2452831.47959 | 2003.524 | 14.64 |
| 1514 – 241 | R | 2452833.50498 | 2003.529 | 14.55 |
| 1514 – 241 | R | 2452836.50741 | 2003.537 | 14.56 |
| 1514 – 241 | R | 2452839.58696 | 2003.546 | 14.55 |
| 1514 – 241 | R | 2452842.54093 | 2003.554 | 14.61 |
| 1514 – 241 | R | 2452845.52238 | 2003.562 | 14.58 |
| 1514 – 241 | R | 2452847.59178 | 2003.568 | 14.63 |
| 1514 – 241 | R | 2452852.55945 | 2003.581 | 14.55 |
| 1514 – 241 | R | 2452854.57969 | 2003.587 | 14.55 |
| 1514 – 241 | R | 2452860.57779 | 2003.603 | 14.43 |
| 1514 – 241 | R | 2452864.54095 | 2003.614 | 14.45 |
| 1514 – 241 | R | 2452867.53577 | 2003.622 | 14.45 |
| 1514 – 241 | R | 2452870.50324 | 2003.630 | 14.48 |

Table 2.2: continued...

| Object | Filter | Julian Date | UT Epoch | Mag |
|------------|--------|---------------|----------|-------|
| 1514 – 241 | R | 2452873.52146 | 2003.639 | 14.47 |
| 1514 – 241 | R | 2452876.54402 | 2003.647 | 14.53 |
| 1514 – 241 | R | 2452879.54729 | 2003.655 | 14.53 |
| 1514 – 241 | R | 2452883.53977 | 2003.666 | 14.38 |
| 1514 – 241 | R | 2453122.62707 | 2004.321 | 14.38 |
| 1514 – 241 | R | 2453125.60885 | 2004.329 | 14.46 |
| 1514 – 241 | R | 2453127.58943 | 2004.334 | 14.47 |
| 1514 – 241 | R | 2453133.54767 | 2004.351 | 14.42 |
| 1514 – 241 | R | 2453136.58289 | 2004.359 | 14.41 |
| 1514 – 241 | R | 2453139.61992 | 2004.367 | 14.39 |
| 1514 – 241 | R | 2453142.68245 | 2004.376 | 14.37 |
| 1514 – 241 | R | 2453146.63708 | 2004.386 | 14.44 |
| 1514 – 241 | R | 2453152.61498 | 2004.403 | 14.42 |
| 1514 – 241 | R | 2453155.53392 | 2004.411 | 14.37 |
| 1514 – 241 | R | 2453159.63484 | 2004.422 | 14.39 |
| 1514 – 241 | R | 2453162.57878 | 2004.430 | 14.28 |
| 1514 – 241 | R | 2453165.60943 | 2004.438 | 14.39 |
| 1514 – 241 | R | 2453169.68285 | 2004.450 | 14.39 |
| 1514 – 241 | R | 2453175.59326 | 2004.466 | 14.38 |
| 1514 – 241 | R | 2453178.61109 | 2004.474 | 14.47 |
| 1514 – 241 | R | 2453183.54975 | 2004.487 | 14.53 |
| 1514 – 241 | R | 2453187.64434 | 2004.499 | 14.52 |
| 1514 – 241 | R | 2453190.57259 | 2004.507 | 14.53 |
| 1514 – 241 | R | 2453193.61689 | 2004.515 | 14.43 |
| 1514 – 241 | R | 2453196.55804 | 2004.523 | 14.50 |
| 1514 – 241 | R | 2453201.57307 | 2004.537 | 14.37 |
| 1514 – 241 | R | 2453205.60454 | 2004.548 | 14.35 |
| 1514 – 241 | R | 2453210.54806 | 2004.561 | 14.53 |
| 1514 – 241 | R | 2453217.55477 | 2004.581 | 14.45 |
| 1514 – 241 | R | 2453230.58309 | 2004.616 | 14.43 |
| 1514 – 241 | R | 2453242.59698 | 2004.649 | 14.38 |
| 1514 – 241 | R | 2453250.50543 | 2004.671 | 14.45 |
| 1514 – 241 | R | 2453258.51036 | 2004.693 | 14.44 |
| 1514 – 241 | R | 2453263.51046 | 2004.706 | 14.59 |
| 1514 – 241 | R | 2453269.49325 | 2004.723 | 14.42 |
| 1622 – 297 | R | 2449913.71881 | 1995.535 | 16.89 |
| 1622 – 297 | R | 2450584.83436 | 1997.373 | 16.76 |
| 1622 – 297 | R | 2450587.80315 | 1997.381 | 16.76 |
| 1622 – 297 | R | 2450683.65156 | 1997.643 | 17.14 |
| 1622 – 297 | R | 2450684.94317 | 1997.647 | 17.12 |

Table 2.2: continued...

| Object | Filter | Julian Date | UT Epoch | Mag |
|------------|--------|---------------|----------|-------|
| 1622 – 297 | R | 2450685.72834 | 1997.649 | 16.98 |
| 1622 – 297 | R | 2450686.65837 | 1997.651 | 16.99 |
| 1622 – 297 | R | 2450687.57355 | 1997.654 | 17.15 |
| 1622 – 297 | R | 2450880.00930 | 1998.181 | 15.90 |
| 1622 – 297 | R | 2451702.82229 | 2000.433 | 17.70 |
| 1622 – 297 | R | 2451703.78728 | 2000.436 | 17.27 |
| 1622 – 297 | R | 2451704.75126 | 2000.439 | 17.65 |
| 1622 – 297 | R | 2452075.81394 | 2001.455 | 17.99 |
| 1622 – 297 | R | 2452076.78804 | 2001.457 | 17.41 |
| 1622 – 297 | R | 2452413.66983 | 2002.380 | 18.16 |
| 1622 – 297 | R | 2452414.68831 | 2002.382 | 17.86 |
| 1622 – 297 | R | 2452436.68163 | 2002.443 | 17.92 |
| 1622 – 297 | R | 2452441.65289 | 2002.456 | 17.85 |
| 1622 – 297 | R | 2452443.60231 | 2002.462 | 17.84 |
| 1622 – 297 | R | 2452456.57383 | 2002.497 | 17.89 |
| 1622 – 297 | R | 2452461.64744 | 2002.511 | 17.82 |
| 1622 – 297 | R | 2452675.88422 | 2003.098 | 19.23 |
| 1622 – 297 | R | 2452677.85446 | 2003.103 | 19.18 |
| 1622 – 297 | R | 2452678.82727 | 2003.106 | 19.15 |
| 1622 – 297 | R | 2452679.84463 | 2003.108 | 19.38 |
| 1622 – 297 | R | 2452680.85295 | 2003.111 | 19.37 |
| 1622 – 297 | R | 2452681.85053 | 2003.114 | 19.17 |
| 1622 – 297 | R | 2452682.84075 | 2003.117 | 19.11 |
| 1622 – 297 | R | 2452683.83819 | 2003.119 | 19.11 |
| 1622 – 297 | R | 2452684.83660 | 2003.122 | 19.23 |
| 1622 – 297 | R | 2452687.83463 | 2003.130 | 19.18 |
| 1622 – 297 | R | 2452690.84413 | 2003.139 | 19.08 |
| 1622 – 297 | R | 2452695.83170 | 2003.152 | 19.22 |
| 1622 – 297 | R | 2452696.84317 | 2003.155 | 19.09 |
| 1622 – 297 | R | 2452699.85583 | 2003.163 | 19.20 |
| 1622 – 297 | R | 2452702.88933 | 2003.171 | 19.22 |
| 1622 – 297 | R | 2452705.82729 | 2003.180 | 19.35 |
| 1622 – 297 | R | 2452708.80594 | 2003.188 | 19.32 |
| 1622 – 297 | R | 2452711.81071 | 2003.196 | 19.26 |
| 1622 – 297 | R | 2452714.86601 | 2003.204 | 19.22 |
| 1622 – 297 | R | 2452717.86804 | 2003.213 | 19.17 |
| 1622 – 297 | R | 2452723.82646 | 2003.229 | 19.34 |
| 1622 – 297 | R | 2452729.79436 | 2003.245 | 19.16 |
| 1622 – 297 | R | 2452732.79179 | 2003.253 | 19.19 |
| 1622 – 297 | R | 2452735.78156 | 2003.262 | 19.10 |
| 1622 – 297 | R | 2452738.78442 | 2003.270 | 19.15 |

Table 2.2: continued...

| Object | Filter | Julian Date | UT Epoch | Mag |
|------------|--------|---------------|----------|-------|
| 1622 – 297 | R | 2452741.73544 | 2003.278 | 19.22 |
| 1622 – 297 | R | 2452744.75590 | 2003.286 | 19.08 |
| 1622 – 297 | R | 2452750.81398 | 2003.303 | 18.66 |
| 1622 – 297 | R | 2452753.86204 | 2003.311 | 19.06 |
| 1622 – 297 | R | 2452756.81323 | 2003.319 | 19.02 |
| 1622 – 297 | R | 2452758.81399 | 2003.325 | 19.03 |
| 1622 – 297 | R | 2452761.70304 | 2003.333 | 19.14 |
| 1622 – 297 | R | 2452764.60917 | 2003.340 | 19.13 |
| 1622 – 297 | R | 2452766.80685 | 2003.346 | 19.20 |
| 1622 – 297 | R | 2452771.62720 | 2003.360 | 19.10 |
| 1622 – 297 | R | 2452773.65043 | 2003.365 | 18.69 |
| 1622 – 297 | R | 2452777.75840 | 2003.376 | 18.53 |
| 1622 – 297 | R | 2452782.65081 | 2003.390 | 18.11 |
| 1622 – 297 | R | 2452785.57852 | 2003.398 | 18.08 |
| 1622 – 297 | R | 2452788.56662 | 2003.406 | 18.17 |
| 1622 – 297 | R | 2452789.54669 | 2003.409 | 18.40 |
| 1622 – 297 | R | 2452792.63191 | 2003.417 | 18.02 |
| 1622 – 297 | R | 2452797.68681 | 2003.431 | 17.91 |
| 1622 – 297 | R | 2452808.67257 | 2003.461 | 18.72 |
| 1622 – 297 | R | 2452812.62247 | 2003.472 | 18.56 |
| 1622 – 297 | R | 2452815.53249 | 2003.480 | 18.48 |
| 1622 – 297 | R | 2452818.49284 | 2003.488 | 18.46 |
| 1622 – 297 | R | 2452821.55620 | 2003.496 | 18.30 |
| 1622 – 297 | R | 2452827.54956 | 2003.513 | 19.08 |
| 1622 – 297 | R | 2452830.53067 | 2003.521 | 18.68 |
| 1622 – 297 | R | 2452833.52777 | 2003.529 | 19.44 |
| 1622 – 297 | R | 2452836.53309 | 2003.537 | 18.88 |
| 1622 – 297 | R | 2452839.60653 | 2003.546 | 18.91 |
| 1622 – 297 | R | 2452843.52463 | 2003.557 | 18.91 |
| 1622 – 297 | R | 2452845.53112 | 2003.562 | 19.05 |
| 1622 – 297 | R | 2452847.60053 | 2003.568 | 18.88 |
| 1622 – 297 | R | 2452852.67752 | 2003.582 | 18.81 |
| 1622 – 297 | R | 2452854.63718 | 2003.587 | 18.91 |
| 1622 – 297 | R | 2452857.58382 | 2003.595 | 19.03 |
| 1622 – 297 | R | 2452860.61153 | 2003.603 | 18.85 |
| 1622 – 297 | R | 2452870.58527 | 2003.631 | 19.07 |
| 1622 – 297 | R | 2452873.53601 | 2003.639 | 19.12 |
| 1622 – 297 | R | 2452876.57723 | 2003.647 | 19.13 |
| 1622 – 297 | R | 2452879.57253 | 2003.655 | 19.15 |
| 1622 – 297 | R | 2452883.60687 | 2003.666 | 19.08 |
| 1622 – 297 | R | 2452893.52895 | 2003.693 | 19.14 |

Table 2.2: continued...

| Object | Filter | Julian Date | UT Epoch | Mag |
|------------|--------|---------------|----------|-------|
| 1622 − 297 | R | 2453124.70590 | 2004.326 | 19.05 |
| 1622 − 297 | R | 2453127.70949 | 2004.335 | 19.15 |
| 1622 − 297 | R | 2453133.59576 | 2004.351 | 19.25 |
| 1622 − 297 | R | 2453138.70068 | 2004.365 | 19.18 |
| 1622 − 297 | R | 2453146.70378 | 2004.387 | 19.18 |
| 1622 − 297 | R | 2453152.70234 | 2004.403 | 19.18 |
| 1622 − 297 | R | 2453160.71561 | 2004.425 | 18.98 |
| 1622 − 297 | R | 2453165.67794 | 2004.439 | 19.24 |
| 1622 − 297 | R | 2453175.68623 | 2004.466 | 19.20 |
| 1622 − 297 | R | 2453193.65735 | 2004.515 | 19.19 |
| 1622 − 297 | R | 2453201.60963 | 2004.537 | 19.15 |
| 1622 − 297 | R | 2453205.61829 | 2004.548 | 19.12 |
| 1622 − 297 | R | 2453211.53010 | 2004.564 | 19.07 |
| 1622 − 297 | R | 2453218.61662 | 2004.583 | 19.11 |
| 1622 − 297 | R | 2453231.59178 | 2004.619 | 18.86 |
| 1622 − 297 | R | 2453243.61138 | 2004.652 | 18.98 |
| 1622 − 297 | R | 2453250.54681 | 2004.671 | 19.08 |
| 1622 − 297 | R | 2453258.57016 | 2004.693 | 18.96 |
| 1622 − 297 | R | 2453263.52538 | 2004.706 | 19.03 |
| 1622 − 297 | R | 2453267.53698 | 2004.717 | 18.97 |
| 1622 − 297 | R | 2453270.52605 | 2004.726 | 18.74 |
| 1622 − 297 | R | 2453280.52515 | 2004.753 | 18.57 |
| 1622 − 297 | R | 2453288.49617 | 2004.775 | 18.19 |
| | | | | |
| 1633 + 382 | R | 2450174.87458 | 1996.250 | 16.53 |
| 1633 + 382 | R | 2450175.86341 | 1996.253 | 16.72 |
| 1633 + 382 | R | 2450176.91031 | 1996.256 | 16.81 |
| 1633 + 382 | R | 2450199.92610 | 1996.319 | 17.35 |
| 1633 + 382 | R | 2450200.91612 | 1996.321 | 17.36 |
| 1633 + 382 | R | 2450201.90385 | 1996.324 | 17.33 |
| 1633 + 382 | R | 2450202.90644 | 1996.327 | 17.32 |
| 1633 + 382 | R | 2450203.89364 | 1996.330 | 17.30 |
| 1633 + 382 | R | 2450204.89151 | 1996.332 | 17.26 |
| 1633 + 382 | R | 2450719.59666 | 1997.742 | 16.13 |
| 1633 + 382 | R | 2450881.01386 | 1998.183 | 17.31 |
| 1633 + 382 | R | 2450950.85948 | 1998.375 | 17.32 |
| 1633 + 382 | R | 2450951.84818 | 1998.377 | 17.24 |
| 1633 + 382 | R | 2451701.89781 | 2000.431 | 17.30 |
| 1633 + 382 | R | 2451703.87575 | 2000.436 | 17.31 |
| 1633 + 382 | R | 2451704.79551 | 2000.439 | 17.27 |
| 1633 + 382 | R | 2452075.81076 | 2001.455 | 17.05 |

Table 2.2: continued...

| Object | Filter | Julian Date | UT Epoch | Mag |
|------------|--------|---------------|----------|-------|
| 1633 + 382 | R | 2452397.79827 | 2002.336 | 17.12 |
| 1633 + 382 | R | 2452427.74499 | 2002.418 | 17.33 |
| 1633 + 382 | R | 2452517.67128 | 2002.664 | 17.35 |
| 1633 + 382 | R | 2452753.89299 | 2003.311 | 17.26 |
| 1633 + 382 | R | 2452755.86247 | 2003.317 | 17.22 |
| 1633 + 382 | R | 2452779.85782 | 2003.382 | 17.34 |
| 1633 + 382 | R | 2452780.82512 | 2003.385 | 17.34 |
| 1633 + 382 | R | 2452781.78848 | 2003.388 | 17.34 |
| 1633 + 382 | R | 2452782.80880 | 2003.390 | 17.36 |
| 1633 + 382 | R | 2452783.79326 | 2003.393 | 17.29 |
| 1633 + 382 | R | 2452844.73851 | 2003.560 | 17.41 |
| 1633 + 382 | R | 2453146.87151 | 2004.387 | 17.08 |
| 1633 + 382 | R | 2453147.82059 | 2004.390 | 17.10 |
| 1633 + 382 | R | 2453148.74922 | 2004.392 | 17.13 |
| 1633 + 382 | R | 2453269.62967 | 2004.723 | 17.35 |
| | | | | |
| 1641 + 399 | R | 2448782.81762 | 1992.439 | 15.46 |
| 1641 + 399 | R | 2448783.83199 | 1992.442 | 15.42 |
| 1641 + 399 | R | 2449207.71191 | 1993.602 | 16.65 |
| 1641 + 399 | R | 2449501.72802 | 1994.407 | 17.26 |
| 1641 + 399 | R | 2449913.84385 | 1995.536 | 17.10 |
| 1641 + 399 | R | 2450174.91381 | 1996.250 | 17.13 |
| 1641 + 399 | R | 2450175.85678 | 1996.253 | 17.10 |
| 1641 + 399 | R | 2450176.91329 | 1996.256 | 17.16 |
| 1641 + 399 | R | 2450203.98624 | 1996.330 | 17.25 |
| 1641 + 399 | R | 2450204.86253 | 1996.332 | 17.21 |
| 1641 + 399 | R | 2450587.83527 | 1997.381 | 16.98 |
| 1641 + 399 | R | 2450719.60712 | 1997.742 | 16.54 |
| 1641 + 399 | R | 2450880.02108 | 1998.181 | 16.45 |
| 1641 + 399 | R | 2450950.91374 | 1998.375 | 15.42 |
| 1641 + 399 | R | 2450951.86676 | 1998.377 | 15.33 |
| 1641 + 399 | R | 2450952.81806 | 1998.380 | 15.35 |
| 1641 + 399 | R | 2451347.83053 | 1999.462 | 16.42 |
| 1641 + 399 | R | 2451648.95358 | 2000.286 | 16.09 |
| 1641 + 399 | R | 2451649.91375 | 2000.289 | 16.09 |
| 1641 + 399 | R | 2451650.89415 | 2000.291 | 16.08 |
| 1641 + 399 | R | 2451651.84990 | 2000.294 | 16.10 |
| 1641 + 399 | R | 2451701.86013 | 2000.431 | 16.02 |
| 1641 + 399 | R | 2452050.89572 | 2001.386 | 15.13 |
| 1641 + 399 | R | 2452075.80504 | 2001.455 | 15.14 |
| 1641 + 399 | R | 2452076.77454 | 2001.457 | 15.15 |

Table 2.2: continued...

| Object | Filter | Julian Date | UT Epoch | Mag |
|------------|--------|---------------|----------|-------|
| 1641 + 399 | R | 2452077.74544 | 2001.460 | 15.14 |
| 1641 + 399 | R | 2452078.85880 | 2001.463 | 15.31 |
| 1641 + 399 | R | 2452427.75958 | 2002.418 | 16.04 |
| 1641 + 399 | R | 2452517.65736 | 2002.664 | 16.45 |
| 1641 + 399 | R | 2452705.00239 | 2003.177 | 16.02 |
| 1641 + 399 | R | 2452706.01091 | 2003.180 | 16.04 |
| 1641 + 399 | R | 2452779.86960 | 2003.382 | 16.42 |
| 1641 + 399 | R | 2452780.82771 | 2003.385 | 16.41 |
| 1641 + 399 | R | 2452781.83407 | 2003.388 | 16.41 |
| 1641 + 399 | R | 2452782.88141 | 2003.391 | 16.39 |
| 1641 + 399 | R | 2452783.79193 | 2003.393 | 16.39 |
| 1641 + 399 | R | 2452844.75028 | 2003.560 | 16.27 |
| 1641 + 399 | R | 2453147.94686 | 2004.390 | 16.44 |
| 1641 + 399 | R | 2453150.70735 | 2004.398 | 16.43 |
| | | | | |
| 2005 − 489 | R | 2452891.70421 | 2003.688 | 13.39 |
| 2005 − 489 | R | 2452894.67142 | 2003.697 | 13.41 |
| 2005 − 489 | R | 2452897.69436 | 2003.705 | 13.37 |
| 2005 − 489 | R | 2452900.68992 | 2003.713 | 13.41 |
| 2005 − 489 | R | 2452903.70884 | 2003.721 | 13.39 |
| 2005 − 489 | R | 2452907.63940 | 2003.732 | 13.40 |
| 2005 − 489 | R | 2452910.63493 | 2003.740 | 13.43 |
| 2005 − 489 | R | 2452913.60713 | 2003.748 | 13.46 |
| 2005 − 489 | R | 2452916.64990 | 2003.757 | 13.45 |
| 2005 − 489 | R | 2452920.61700 | 2003.768 | 13.45 |
| 2005 − 489 | R | 2452924.57765 | 2003.778 | 13.42 |
| 2005 − 489 | R | 2452927.64317 | 2003.787 | 13.48 |
| 2005 − 489 | R | 2452930.60629 | 2003.795 | 13.43 |
| 2005 − 489 | R | 2452933.61967 | 2003.803 | 13.45 |
| 2005 − 489 | R | 2452937.57658 | 2003.814 | 13.49 |
| 2005 − 489 | R | 2452940.56815 | 2003.822 | 13.50 |
| 2005 − 489 | R | 2452943.54755 | 2003.830 | 13.51 |
| 2005 − 489 | R | 2452946.54794 | 2003.839 | 13.52 |
| 2005 − 489 | R | 2452949.53511 | 2003.847 | 13.54 |
| 2005 − 489 | R | 2452952.52939 | 2003.855 | 13.53 |
| 2005 − 489 | R | 2452955.53264 | 2003.863 | 13.50 |
| 2005 − 489 | R | 2452958.53202 | 2003.871 | 13.50 |
| 2005 − 489 | R | 2452962.52211 | 2003.882 | 13.54 |
| 2005 − 489 | R | 2452965.51150 | 2003.891 | 13.59 |
| 2005 − 489 | R | 2452970.51692 | 2003.904 | 13.58 |
| 2005 − 489 | R | 2452973.51693 | 2003.912 | 13.54 |

Table 2.2: continued...

| Object | Filter | Julian Date | UT Epoch | Mag |
|------------|--------|---------------|----------|-------|
| 2005 – 489 | R | 2452976.51652 | 2003.921 | 13.54 |
| 2005 – 489 | R | 2452979.51235 | 2003.929 | 13.60 |
| 2005 – 489 | R | 2452985.51853 | 2003.945 | 13.57 |
| 2005 – 489 | R | 2453124.83892 | 2004.327 | 13.73 |
| 2005 – 489 | R | 2453127.88117 | 2004.335 | 13.79 |
| 2005 – 489 | R | 2453131.80354 | 2004.346 | 13.71 |
| 2005 – 489 | R | 2453134.78648 | 2004.354 | 13.75 |
| 2005 – 489 | R | 2453138.84242 | 2004.365 | 13.69 |
| 2005 – 489 | R | 2453146.89068 | 2004.387 | 13.82 |
| 2005 – 489 | R | 2453156.91826 | 2004.415 | 13.89 |
| 2005 – 489 | R | 2453159.79662 | 2004.422 | 13.87 |
| 2005 – 489 | R | 2453162.89260 | 2004.431 | 13.76 |
| 2005 – 489 | R | 2453174.86171 | 2004.464 | 13.66 |
| 2005 – 489 | R | 2453191.80661 | 2004.510 | 13.71 |
| 2005 – 489 | R | 2453193.85170 | 2004.516 | 13.61 |
| 2005 – 489 | R | 2453196.82538 | 2004.524 | 13.61 |
| 2005 – 489 | R | 2453204.81564 | 2004.546 | 13.66 |
| 2005 – 489 | R | 2453211.81073 | 2004.565 | 13.68 |
| 2005 – 489 | R | 2453223.79109 | 2004.598 | 13.74 |
| 2005 – 489 | R | 2453224.79015 | 2004.600 | 13.73 |
| 2005 – 489 | R | 2453237.77181 | 2004.636 | 13.67 |
| 2005 – 489 | R | 2453239.80692 | 2004.641 | 13.64 |
| 2005 – 489 | R | 2453241.78512 | 2004.647 | 13.56 |
| 2005 – 489 | R | 2453243.74530 | 2004.652 | 13.57 |
| 2005 – 489 | R | 2453246.72998 | 2004.660 | 13.54 |
| 2005 – 489 | R | 2453249.68870 | 2004.669 | 13.49 |
| 2005 – 489 | R | 2453253.69779 | 2004.680 | 13.56 |
| 2005 – 489 | R | 2453259.64396 | 2004.696 | 13.50 |
| 2005 – 489 | R | 2453263.69282 | 2004.707 | 13.55 |
| 2005 – 489 | R | 2453266.67201 | 2004.715 | 13.52 |
| 2005 – 489 | R | 2453267.69998 | 2004.718 | 13.50 |
| 2005 – 489 | R | 2453270.72120 | 2004.726 | 13.47 |
| 2005 – 489 | R | 2453272.65935 | 2004.731 | 13.40 |
| 2005 – 489 | R | 2453277.67401 | 2004.745 | 13.43 |
| 2005 – 489 | R | 2453281.64513 | 2004.756 | 13.55 |
| 2005 – 489 | R | 2453288.64295 | 2004.775 | 13.54 |
| 2005 – 489 | R | 2453296.52728 | 2004.797 | 13.60 |
| 2005 – 489 | R | 2453298.54149 | 2004.802 | 13.57 |
| 2005 – 489 | R | 2453301.59803 | 2004.811 | 13.50 |
| 2005 – 489 | R | 2453307.58162 | 2004.827 | 13.54 |
| 2005 – 489 | R | 2453311.56369 | 2004.838 | 13.50 |

Table 2.2: continued...

| Object | Filter | Julian Date | UT Epoch | Mag |
|------------|--------|---------------|----------|-------|
| 2005 – 489 | R | 2453324.54434 | 2004.873 | 13.59 |
| 2005 – 489 | R | 2453328.51959 | 2004.884 | 13.56 |
| 2005 – 489 | R | 2453331.51491 | 2004.893 | 13.56 |
| 2005 – 489 | R | 2453336.54241 | 2004.906 | 13.50 |
| 2005 – 489 | R | 2453339.51718 | 2004.914 | 13.48 |
| 2005 – 489 | R | 2453343.51372 | 2004.925 | 13.52 |
| 2005 – 489 | R | 2453351.51988 | 2004.947 | 13.55 |
| | | | | |
| 2155 – 304 | R | 2452732.90803 | 2003.254 | 13.29 |
| 2155 – 304 | R | 2452735.91764 | 2003.262 | 13.33 |
| 2155 – 304 | R | 2452738.90598 | 2003.270 | 13.36 |
| 2155 – 304 | R | 2452741.90594 | 2003.278 | 13.32 |
| 2155 – 304 | R | 2452744.89907 | 2003.287 | 13.38 |
| 2155 – 304 | R | 2452750.90336 | 2003.303 | 13.31 |
| 2155 – 304 | R | 2452756.87750 | 2003.319 | 13.29 |
| 2155 – 304 | R | 2452758.89167 | 2003.325 | 13.29 |
| 2155 – 304 | R | 2452761.89224 | 2003.333 | 13.24 |
| 2155 – 304 | R | 2452764.86193 | 2003.341 | 13.39 |
| 2155 – 304 | R | 2452766.89710 | 2003.347 | 13.46 |
| 2155 – 304 | R | 2452771.82626 | 2003.360 | 13.39 |
| 2155 – 304 | R | 2452774.87041 | 2003.369 | 13.35 |
| 2155 – 304 | R | 2452776.87732 | 2003.374 | 13.43 |
| 2155 – 304 | R | 2452782.88848 | 2003.391 | 13.47 |
| 2155 – 304 | R | 2452786.83745 | 2003.401 | 13.46 |
| 2155 – 304 | R | 2452789.83513 | 2003.410 | 13.44 |
| 2155 – 304 | R | 2452793.86919 | 2003.421 | 13.57 |
| 2155 – 304 | R | 2452796.87257 | 2003.429 | 13.58 |
| 2155 – 304 | R | 2452804.91067 | 2003.451 | 13.61 |
| 2155 – 304 | R | 2452809.89613 | 2003.464 | 13.45 |
| 2155 – 304 | R | 2452812.88543 | 2003.473 | 13.56 |
| 2155 – 304 | R | 2452815.85803 | 2003.481 | 13.58 |
| 2155 – 304 | R | 2452818.88957 | 2003.489 | 13.59 |
| 2155 – 304 | R | 2452821.86462 | 2003.497 | 13.67 |
| 2155 – 304 | R | 2452824.91554 | 2003.506 | 13.67 |
| 2155 – 304 | R | 2452826.87535 | 2003.511 | 13.67 |
| 2155 – 304 | R | 2452829.89315 | 2003.519 | 13.69 |
| 2155 – 304 | R | 2452832.79153 | 2003.527 | 13.70 |
| 2155 – 304 | R | 2452833.82333 | 2003.530 | 13.77 |
| 2155 – 304 | R | 2452836.85353 | 2003.538 | 13.66 |
| 2155 – 304 | R | 2452839.79914 | 2003.546 | 13.64 |
| 2155 – 304 | R | 2452843.85325 | 2003.557 | 13.71 |

Table 2.2: continued...

| Object | Filter | Julian Date | UT Epoch | Mag |
|------------|--------|---------------|----------|-------|
| 2155 – 304 | R | 2452845.83066 | 2003.563 | 13.80 |
| 2155 – 304 | R | 2452847.83250 | 2003.568 | 13.86 |
| 2155 – 304 | R | 2452851.84982 | 2003.579 | 13.65 |
| 2155 – 304 | R | 2452854.78001 | 2003.587 | 13.64 |
| 2155 – 304 | R | 2452857.81800 | 2003.596 | 13.77 |
| 2155 – 304 | R | 2452860.84926 | 2003.604 | 13.76 |
| 2155 – 304 | R | 2452865.82453 | 2003.618 | 13.69 |
| 2155 – 304 | R | 2452867.76471 | 2003.623 | 13.58 |
| 2155 – 304 | R | 2452870.74340 | 2003.631 | 13.54 |
| 2155 – 304 | R | 2452873.78757 | 2003.639 | 13.60 |
| 2155 – 304 | R | 2452876.73063 | 2003.647 | 13.72 |
| 2155 – 304 | R | 2452879.73583 | 2003.656 | 13.78 |
| 2155 – 304 | R | 2452890.70140 | 2003.686 | 13.44 |
| 2155 – 304 | R | 2452893.69802 | 2003.694 | 13.50 |
| 2155 – 304 | R | 2452895.67383 | 2003.699 | 13.48 |
| 2155 – 304 | R | 2452898.62233 | 2003.707 | 13.41 |
| 2155 – 304 | R | 2452901.68525 | 2003.716 | 13.39 |
| 2155 – 304 | R | 2452904.63256 | 2003.724 | 13.43 |
| 2155 – 304 | R | 2452907.68584 | 2003.732 | 13.54 |
| 2155 – 304 | R | 2452910.64256 | 2003.740 | 13.55 |
| 2155 – 304 | R | 2452912.67479 | 2003.746 | 13.66 |
| 2155 – 304 | R | 2452915.64871 | 2003.754 | 13.52 |
| 2155 – 304 | R | 2452920.65109 | 2003.768 | 13.53 |
| 2155 – 304 | R | 2452924.61115 | 2003.779 | 13.41 |
| 2155 – 304 | R | 2452927.66109 | 2003.787 | 13.48 |
| 2155 – 304 | R | 2452931.56196 | 2003.798 | 13.37 |
| 2155 – 304 | R | 2452935.57076 | 2003.809 | 13.37 |
| 2155 – 304 | R | 2452939.61350 | 2003.820 | 13.25 |
| 2155 – 304 | R | 2452942.59680 | 2003.828 | 13.30 |
| 2155 – 304 | R | 2452946.57986 | 2003.839 | 13.29 |
| 2155 – 304 | R | 2452949.56714 | 2003.847 | 13.27 |
| 2155 – 304 | R | 2452952.53810 | 2003.855 | 13.21 |
| 2155 – 304 | R | 2452956.53143 | 2003.866 | 13.23 |
| 2155 – 304 | R | 2452961.55530 | 2003.880 | 13.20 |
| 2155 – 304 | R | 2452964.51967 | 2003.888 | 13.23 |
| 2155 – 304 | R | 2452968.52108 | 2003.899 | 13.25 |
| 2155 – 304 | R | 2452972.52215 | 2003.910 | 13.12 |
| 2155 – 304 | R | 2452975.53492 | 2003.918 | 13.01 |
| 2155 – 304 | R | 2452978.52189 | 2003.926 | 13.07 |
| 2155 – 304 | R | 2452982.54227 | 2003.937 | 13.12 |
| 2155 – 304 | R | 2452985.55139 | 2003.945 | 13.00 |

Table 2.2: continued...

| Object | Filter | Julian Date | UT Epoch | Mag |
|------------|--------|---------------|----------|-------|
| 2155 – 304 | R | 2452988.54610 | 2003.954 | 13.06 |
| 2155 – 304 | R | 2452991.53978 | 2003.962 | 13.05 |
| 2155 – 304 | R | 2452994.53584 | 2003.970 | 12.96 |
| 2155 – 304 | R | 2452999.54417 | 2003.984 | 13.07 |
| 2155 – 304 | R | 2453003.53446 | 2003.995 | 13.12 |
| 2155 – 304 | R | 2453125.86789 | 2004.330 | 12.93 |
| 2155 – 304 | R | 2453131.86497 | 2004.346 | 12.95 |
| 2155 – 304 | R | 2453135.82499 | 2004.357 | 12.83 |
| 2155 – 304 | R | 2453142.89725 | 2004.376 | 12.78 |
| 2155 – 304 | R | 2453156.92837 | 2004.415 | 12.88 |
| 2155 – 304 | R | 2453159.83419 | 2004.423 | 12.90 |
| 2155 – 304 | R | 2453167.90079 | 2004.445 | 13.03 |
| 2155 – 304 | R | 2453175.84514 | 2004.466 | 13.07 |
| 2155 – 304 | R | 2453188.83851 | 2004.502 | 13.08 |
| 2155 – 304 | R | 2453192.85021 | 2004.513 | 12.97 |
| 2155 – 304 | R | 2453195.81898 | 2004.521 | 12.82 |
| 2155 – 304 | R | 2453203.84127 | 2004.543 | 12.97 |
| 2155 – 304 | R | 2453206.84312 | 2004.551 | 13.07 |
| 2155 – 304 | R | 2453223.81840 | 2004.598 | 13.32 |
| 2155 – 304 | R | 2453224.82483 | 2004.600 | 13.25 |
| 2155 – 304 | R | 2453239.81602 | 2004.642 | 12.73 |
| 2155 – 304 | R | 2453243.73841 | 2004.652 | 12.76 |
| 2155 – 304 | R | 2453247.76594 | 2004.663 | 12.75 |
| 2155 – 304 | R | 2453248.72450 | 2004.666 | 12.75 |
| 2155 – 304 | R | 2453250.72692 | 2004.671 | 12.70 |
| 2155 – 304 | R | 2453254.80422 | 2004.683 | 12.54 |
| 2155 – 304 | R | 2453257.82510 | 2004.691 | 12.52 |
| 2155 – 304 | R | 2453262.70677 | 2004.704 | 12.62 |
| 2155 – 304 | R | 2453271.70784 | 2004.729 | 12.69 |
| 2155 – 304 | R | 2453275.66924 | 2004.740 | 12.79 |
| 2155 – 304 | R | 2453279.65977 | 2004.751 | 12.84 |
| 2155 – 304 | R | 2453283.62907 | 2004.761 | 12.82 |
| 2155 – 304 | R | 2453292.65997 | 2004.786 | 12.94 |
| 2155 – 304 | R | 2453297.55494 | 2004.800 | 12.95 |
| 2155 – 304 | R | 2453299.66133 | 2004.805 | 13.11 |
| 2155 – 304 | R | 2453303.61182 | 2004.816 | 13.13 |
| 2155 – 304 | R | 2453308.57819 | 2004.830 | 13.02 |
| 2155 – 304 | R | 2453314.61563 | 2004.846 | 12.97 |
| 2155 – 304 | R | 2453321.66442 | 2004.866 | 13.18 |
| 2155 – 304 | R | 2453329.60889 | 2004.887 | 12.96 |
| 2155 – 304 | R | 2453334.57454 | 2004.901 | 13.10 |

Table 2.2: continued...

| Object | Filter | Julian Date | UT Epoch | Mag |
|------------|--------|---------------|----------|-------|
| 2155 − 304 | R | 2453337.56441 | 2004.909 | 13.17 |
| 2155 − 304 | R | 2453340.57311 | 2004.917 | 13.13 |
| 2155 − 304 | R | 2453344.52100 | 2004.928 | 12.99 |
| 2155 − 304 | R | 2453349.55951 | 2004.942 | 13.04 |
| 2155 − 304 | R | 2453353.54289 | 2004.953 | 13.12 |
| 2155 − 304 | R | 2453356.54747 | 2004.961 | 13.15 |
| 2155 − 304 | R | 2453359.53619 | 2004.969 | 13.11 |
| 2155 − 304 | R | 2453363.52907 | 2004.980 | 13.06 |
| 2155 − 304 | R | 2453367.53265 | 2004.991 | 13.11 |
| 2155 − 304 | R | 2453370.52970 | 2004.999 | 13.03 |
| | | | | |
| 2200 + 420 | R | 2448517.78266 | 1991.713 | 14.85 |
| 2200 + 420 | V | 2448517.79676 | 1991.713 | 15.53 |
| 2200 + 420 | V | 2448519.92381 | 1991.719 | 15.70 |
| 2200 + 420 | V | 2448521.00035 | 1991.722 | 15.70 |
| 2200 + 420 | R | 2448649.57532 | 1992.074 | 15.03 |
| 2200 + 420 | R | 2448744.96693 | 1992.335 | 15.31 |
| 2200 + 420 | V | 2448782.94881 | 1992.439 | 16.35 |
| 2200 + 420 | R | 2448783.89084 | 1992.442 | 15.27 |
| 2200 + 420 | V | 2448783.90060 | 1992.442 | 16.23 |
| 2200 + 420 | V | 2448868.72126 | 1992.674 | 15.39 |
| 2200 + 420 | R | 2448868.73977 | 1992.674 | 14.55 |
| 2200 + 420 | R | 2448869.84321 | 1992.677 | 14.58 |
| 2200 + 420 | V | 2448869.84822 | 1992.677 | 15.27 |
| 2200 + 420 | V | 2448870.71163 | 1992.680 | 15.29 |
| 2200 + 420 | R | 2448870.71686 | 1992.680 | 14.58 |
| 2200 + 420 | V | 2448927.69571 | 1992.836 | 15.48 |
| 2200 + 420 | R | 2448927.70721 | 1992.836 | 14.71 |
| 2200 + 420 | V | 2448928.56234 | 1992.838 | 15.45 |
| 2200 + 420 | R | 2448928.57322 | 1992.838 | 14.68 |
| 2200 + 420 | V | 2448929.57993 | 1992.841 | 15.41 |
| 2200 + 420 | R | 2448929.59527 | 1992.841 | 14.63 |
| 2200 + 420 | V | 2448930.61956 | 1992.844 | 15.39 |
| 2200 + 420 | R | 2448930.62654 | 1992.844 | 14.68 |
| 2200 + 420 | V | 2449064.02642 | 1993.209 | 14.32 |
| 2200 + 420 | V | 2449065.03699 | 1993.212 | 14.21 |
| 2200 + 420 | V | 2449066.01642 | 1993.214 | 14.43 |
| 2200 + 420 | R | 2449104.97450 | 1993.321 | 13.80 |
| 2200 + 420 | V | 2449104.97453 | 1993.321 | 13.88 |
| 2200 + 420 | V | 2449106.96128 | 1993.326 | 13.92 |
| 2200 + 420 | R | 2449106.96130 | 1993.326 | 13.83 |

Table 2.2: continued...

| Object | Filter | Julian Date | UT Epoch | Mag |
|------------|--------|---------------|----------|-------|
| 2200 + 420 | V | 2449109.92666 | 1993.335 | 14.24 |
| 2200 + 420 | R | 2449109.92670 | 1993.335 | 14.15 |
| 2200 + 420 | R | 2449111.97855 | 1993.340 | 14.40 |
| 2200 + 420 | R | 2449210.77859 | 1993.611 | 14.82 |
| 2200 + 420 | V | 2449210.78455 | 1993.611 | 15.55 |
| 2200 + 420 | V | 2449211.92588 | 1993.614 | 15.65 |
| 2200 + 420 | R | 2449211.93061 | 1993.614 | 14.81 |
| 2200 + 420 | V | 2449212.65016 | 1993.616 | 15.57 |
| 2200 + 420 | R | 2449212.65576 | 1993.616 | 14.83 |
| 2200 + 420 | R | 2449213.87631 | 1993.619 | 14.83 |
| 2200 + 420 | V | 2449213.88684 | 1993.619 | 15.56 |
| 2200 + 420 | R | 2449214.71374 | 1993.621 | 14.84 |
| 2200 + 420 | V | 2449214.71749 | 1993.621 | 15.61 |
| 2200 + 420 | R | 2449215.67780 | 1993.624 | 14.71 |
| 2200 + 420 | V | 2449374.58696 | 1994.059 | 15.86 |
| 2200 + 420 | V | 2449501.95783 | 1994.408 | 15.21 |
| 2200 + 420 | R | 2449501.96679 | 1994.408 | 14.43 |
| 2200 + 420 | R | 2449975.87605 | 1995.705 | 15.02 |
| 2200 + 420 | R | 2449976.82478 | 1995.708 | 14.99 |
| 2200 + 420 | R | 2449977.76338 | 1995.711 | 14.97 |
| 2200 + 420 | R | 2449978.84290 | 1995.713 | 15.25 |
| 2200 + 420 | R | 2449979.83510 | 1995.716 | 15.17 |
| 2200 + 420 | R | 2450021.73517 | 1995.831 | 14.96 |
| 2200 + 420 | R | 2450176.99622 | 1996.256 | 14.59 |
| 2200 + 420 | R | 2450202.98765 | 1996.327 | 14.81 |
| 2200 + 420 | R | 2450345.80804 | 1996.718 | 14.85 |
| 2200 + 420 | R | 2450346.85161 | 1996.721 | 14.89 |
| 2200 + 420 | R | 2450347.83646 | 1996.724 | 14.71 |
| 2200 + 420 | R | 2450421.60026 | 1996.926 | 14.94 |
| 2200 + 420 | R | 2450422.56482 | 1996.928 | 14.94 |
| 2200 + 420 | R | 2450425.56319 | 1996.937 | 14.73 |
| 2200 + 420 | R | 2450426.57571 | 1996.939 | 14.87 |
| 2200 + 420 | R | 2450584.94422 | 1997.373 | 13.87 |
| 2200 + 420 | R | 2450587.92240 | 1997.381 | 14.09 |
| 2200 + 420 | R | 2450648.22179 | 1997.546 | 13.57 |
| 2200 + 420 | R | 2450648.78296 | 1997.548 | 12.91 |
| 2200 + 420 | R | 2450679.79160 | 1997.633 | 13.08 |
| 2200 + 420 | V | 2450718.66460 | 1997.739 | 15.03 |
| 2200 + 420 | R | 2450718.81139 | 1997.739 | 14.25 |
| 2200 + 420 | V | 2450719.70907 | 1997.742 | 15.11 |
| 2200 + 420 | R | 2450719.79585 | 1997.742 | 14.34 |

Table 2.2: continued...

| Object | Filter | Julian Date | UT Epoch | Mag |
|------------|--------|---------------|----------|-------|
| 2200 + 420 | V | 2450784.72373 | 1997.920 | 16.42 |
| 2200 + 420 | R | 2450720.74492 | 1997.745 | 14.62 |
| 2200 + 420 | R | 2450950.95294 | 1998.375 | 13.48 |
| 2200 + 420 | R | 2450951.94540 | 1998.378 | 13.05 |
| 2200 + 420 | R | 2451007.80939 | 1998.531 | 13.36 |
| 2200 + 420 | R | 2451008.82639 | 1998.533 | 13.31 |
| 2200 + 420 | R | 2451021.84512 | 1998.569 | 13.78 |
| 2200 + 420 | R | 2451026.84484 | 1998.583 | 13.64 |
| 2200 + 420 | R | 2451028.79006 | 1998.588 | 13.71 |
| 2200 + 420 | R | 2451042.81760 | 1998.626 | 13.85 |
| 2200 + 420 | R | 2451044.85936 | 1998.632 | 13.81 |
| 2200 + 420 | R | 2451104.60812 | 1998.796 | 13.38 |
| 2200 + 420 | R | 2451105.75785 | 1998.799 | 13.55 |
| 2200 + 420 | R | 2451106.68608 | 1998.801 | 13.62 |
| 2200 + 420 | R | 2451334.79486 | 1999.426 | 13.73 |
| 2200 + 420 | R | 2451346.89536 | 1999.459 | 13.68 |
| 2200 + 420 | R | 2451347.86385 | 1999.462 | 13.63 |
| 2200 + 420 | R | 2451491.61676 | 1999.855 | 13.45 |
| 2200 + 420 | R | 2451701.91017 | 2000.431 | 14.20 |
| 2200 + 420 | R | 2451747.36496 | 2000.555 | 14.03 |
| 2200 + 420 | R | 2451747.50744 | 2000.556 | 13.97 |
| 2200 + 420 | R | 2451749.37878 | 2000.561 | 13.85 |
| 2200 + 420 | R | 2451749.50018 | 2000.561 | 13.89 |
| 2200 + 420 | R | 2451751.37027 | 2000.566 | 14.06 |
| 2200 + 420 | R | 2451751.52058 | 2000.567 | 14.08 |
| 2200 + 420 | R | 2451758.33426 | 2000.585 | 13.95 |
| 2200 + 420 | R | 2451762.37646 | 2000.597 | 14.22 |
| 2200 + 420 | R | 2451763.29088 | 2000.599 | 14.30 |
| 2200 + 420 | R | 2451763.52515 | 2000.600 | 14.26 |
| 2200 + 420 | R | 2451765.36458 | 2000.605 | 14.02 |
| 2200 + 420 | R | 2451765.51909 | 2000.605 | 14.16 |
| 2200 + 420 | R | 2451768.39221 | 2000.613 | 14.14 |
| 2200 + 420 | R | 2451768.52595 | 2000.613 | 14.09 |
| 2200 + 420 | R | 2451771.79494 | 2000.622 | 14.06 |
| 2200 + 420 | R | 2451773.92939 | 2000.628 | 14.21 |
| 2200 + 420 | R | 2451775.77628 | 2000.633 | 14.18 |
| 2200 + 420 | R | 2451776.80353 | 2000.636 | 14.01 |
| 2200 + 420 | R | 2451795.68942 | 2000.688 | 14.20 |
| 2200 + 420 | R | 2451798.78105 | 2000.696 | 14.02 |
| 2200 + 420 | R | 2451799.82150 | 2000.699 | 13.34 |
| 2200 + 420 | R | 2451843.56249 | 2000.819 | 13.22 |

Table 2.2: continued...

| Object | Filter | Julian Date | UT Epoch | Mag |
|------------|--------|---------------|----------|-------|
| 2200 + 420 | R | 2452050.93064 | 2001.387 | 14.01 |
| 2200 + 420 | R | 2452074.87341 | 2001.452 | 12.83 |
| 2200 + 420 | R | 2452075.89953 | 2001.455 | 12.81 |
| 2200 + 420 | R | 2452076.79962 | 2001.457 | 13.28 |
| 2200 + 420 | R | 2452077.86220 | 2001.460 | 13.07 |
| 2200 + 420 | R | 2452078.92940 | 2001.463 | 13.41 |
| 2200 + 420 | R | 2452250.59300 | 2001.933 | 14.13 |
| 2200 + 420 | R | 2452299.57430 | 2002.067 | 13.19 |
| 2200 + 420 | R | 2452427.91848 | 2002.419 | 14.06 |
| 2200 + 420 | R | 2452518.79733 | 2002.667 | 13.84 |
| 2200 + 420 | R | 2452519.88853 | 2002.670 | 13.73 |
| 2200 + 420 | R | 2452520.71338 | 2002.673 | 13.66 |
| 2200 + 420 | R | 2452521.93651 | 2002.676 | 13.64 |
| 2200 + 420 | R | 2452522.89403 | 2002.679 | 13.67 |
| 2200 + 420 | R | 2452550.08657 | 2002.753 | 14.02 |
| 2200 + 420 | R | 2452552.06808 | 2002.759 | 13.92 |
| 2200 + 420 | R | 2452556.06670 | 2002.770 | 13.49 |
| 2200 + 420 | R | 2452566.75324 | 2002.799 | 13.76 |
| 2200 + 420 | R | 2452576.61951 | 2002.826 | 12.98 |
| 2200 + 420 | R | 2452577.60513 | 2002.828 | 13.28 |
| 2200 + 420 | R | 2452578.59581 | 2002.831 | 13.45 |
| 2200 + 420 | R | 2452621.59925 | 2002.949 | 12.92 |
| 2200 + 420 | R | 2452622.60759 | 2002.952 | 13.02 |
| 2200 + 420 | R | 2452623.61907 | 2002.954 | 13.26 |
| 2200 + 420 | R | 2452780.94215 | 2003.385 | 13.90 |
| 2200 + 420 | R | 2452844.93993 | 2003.560 | 13.23 |
| 2200 + 420 | R | 2452886.76984 | 2003.675 | 14.05 |
| 2200 + 420 | R | 2452976.72128 | 2003.921 | 13.67 |
| 2200 + 420 | R | 2452977.66713 | 2003.924 | 13.82 |
| 2200 + 420 | R | 2452978.61034 | 2003.926 | 13.88 |
| 2200 + 420 | R | 2453120.96262 | 2004.316 | 13.69 |
| 2200 + 420 | R | 2453147.92551 | 2004.390 | 12.95 |
| 2200 + 420 | R | 2453269.81321 | 2004.724 | 13.37 |
| 2200 + 420 | R | 2453270.76450 | 2004.726 | 13.40 |
| 2200 + 420 | R | 2453271.76414 | 2004.729 | 13.37 |
| 2200 + 420 | R | 2453272.66706 | 2004.731 | 13.36 |
| 2200 + 420 | R | 2453282.82892 | 2004.759 | 13.52 |
| 2200 + 420 | R | 2453283.75905 | 2004.762 | 13.81 |
| 2200 + 420 | R | 2453284.81473 | 2004.765 | 13.79 |
| 2200 + 420 | R | 2453285.76198 | 2004.767 | 13.79 |
| 2200 + 420 | R | 2453286.77518 | 2004.770 | 13.68 |

Table 2.2: continued...

| Object | Filter | Julian Date | UT Epoch | Mag |
|------------|--------|---------------|----------|-------|
| 2200 + 420 | R | 2453287.76829 | 2004.773 | 13.78 |
| 2223 − 052 | R | 2447383.86679 | 1988.609 | 15.27 |
| 2223 − 052 | R | 2447433.69000 | 1988.745 | 15.48 |
| 2223 − 052 | R | 2447434.62266 | 1988.748 | 15.90 |
| 2223 − 052 | R | 2447435.64822 | 1988.751 | 15.90 |
| 2223 − 052 | R | 2447459.69402 | 1988.816 | 16.07 |
| 2223 − 052 | R | 2448567.60560 | 1991.850 | 17.90 |
| 2223 − 052 | R | 2448869.82993 | 1992.677 | 18.09 |
| 2223 − 052 | R | 2449210.97311 | 1993.611 | 17.40 |
| 2223 − 052 | R | 2449975.77071 | 1995.705 | 16.56 |
| 2223 − 052 | R | 2450345.86300 | 1996.718 | 17.40 |
| 2223 − 052 | R | 2450421.61046 | 1996.926 | 17.59 |
| 2223 − 052 | R | 2450422.56930 | 1996.928 | 17.58 |
| 2223 − 052 | R | 2450425.56734 | 1996.937 | 17.61 |
| 2223 − 052 | R | 2450426.57059 | 1996.939 | 17.53 |
| 2223 − 052 | R | 2450587.93392 | 1997.381 | 17.74 |
| 2223 − 052 | R | 2450718.73707 | 1997.739 | 17.77 |
| 2223 − 052 | R | 2451052.82306 | 1998.654 | 17.37 |
| 2223 − 052 | R | 2451053.84562 | 1998.657 | 17.39 |
| 2223 − 052 | R | 2451054.85782 | 1998.659 | 17.35 |
| 2223 − 052 | R | 2451055.83009 | 1998.662 | 17.30 |
| 2223 − 052 | R | 2451104.69615 | 1998.796 | 17.08 |
| 2223 − 052 | R | 2451105.72363 | 1998.799 | 17.02 |
| 2223 − 052 | R | 2451106.69756 | 1998.801 | 16.95 |
| 2223 − 052 | R | 2451439.79611 | 1999.713 | 16.21 |
| 2223 − 052 | R | 2451491.64066 | 1999.855 | 16.71 |
| 2223 − 052 | R | 2451701.91727 | 2000.431 | 15.63 |
| 2223 − 052 | R | 2451795.81859 | 2000.688 | 15.73 |
| 2223 − 052 | R | 2451796.75205 | 2000.691 | 15.78 |
| 2223 − 052 | R | 2451797.76934 | 2000.693 | 15.86 |
| 2223 − 052 | R | 2451798.77701 | 2000.696 | 15.90 |
| 2223 − 052 | R | 2451843.72747 | 2000.819 | 15.83 |
| 2223 − 052 | R | 2451844.64226 | 2000.822 | 15.88 |
| 2223 − 052 | R | 2452165.71939 | 2001.701 | 17.37 |
| 2223 − 052 | R | 2452186.77516 | 2001.758 | 16.53 |
| 2223 − 052 | R | 2452187.70956 | 2001.761 | 16.38 |
| 2223 − 052 | R | 2452250.62037 | 2001.933 | 17.21 |
| 2223 − 052 | R | 2452414.86090 | 2002.383 | 17.89 |
| 2223 − 052 | R | 2452429.92843 | 2002.424 | 17.79 |
| 2223 − 052 | R | 2452518.82754 | 2002.668 | 17.97 |

Table 2.2: continued...

| Object | Filter | Julian Date | UT Epoch | Mag |
|------------|--------|---------------|----------|-------|
| 2223 – 052 | R | 2452576.63848 | 2002.826 | 17.90 |
| 2223 – 052 | R | 2452577.62041 | 2002.829 | 17.91 |
| 2223 – 052 | R | 2452578.60885 | 2002.831 | 17.88 |
| 2223 – 052 | R | 2452622.57951 | 2002.952 | 17.76 |
| 2223 – 052 | R | 2452623.58824 | 2002.954 | 17.68 |
| 2223 – 052 | R | 2452783.94872 | 2003.393 | 17.50 |
| 2223 – 052 | R | 2452844.93047 | 2003.560 | 17.96 |
| 2223 – 052 | R | 2452856.80781 | 2003.593 | 17.95 |
| 2223 – 052 | R | 2452857.76513 | 2003.596 | 17.96 |
| 2223 – 052 | R | 2452858.68187 | 2003.598 | 17.93 |
| 2223 – 052 | R | 2452859.76463 | 2003.601 | 17.94 |
| 2223 – 052 | R | 2452860.74811 | 2003.604 | 17.91 |
| 2223 – 052 | R | 2452861.76142 | 2003.606 | 17.91 |
| 2223 – 052 | R | 2452886.76192 | 2003.675 | 17.73 |
| 2223 – 052 | R | 2452888.72692 | 2003.680 | 17.77 |
| 2223 – 052 | R | 2452893.70854 | 2003.694 | 17.69 |
| 2223 – 052 | R | 2452895.68340 | 2003.699 | 17.75 |
| 2223 – 052 | R | 2452898.70033 | 2003.708 | 17.75 |
| 2223 – 052 | R | 2452901.69488 | 2003.716 | 17.72 |
| 2223 – 052 | R | 2452904.64206 | 2003.724 | 17.77 |
| 2223 – 052 | R | 2452907.70455 | 2003.732 | 17.80 |
| 2223 – 052 | R | 2452910.66261 | 2003.740 | 17.82 |
| 2223 – 052 | R | 2452914.57396 | 2003.751 | 17.85 |
| 2223 – 052 | R | 2452917.65332 | 2003.759 | 17.82 |
| 2223 – 052 | R | 2452921.64100 | 2003.770 | 17.67 |
| 2223 – 052 | R | 2452924.63356 | 2003.779 | 17.84 |
| 2223 – 052 | R | 2452927.67093 | 2003.787 | 17.81 |
| 2223 – 052 | R | 2452931.57202 | 2003.798 | 17.85 |
| 2223 – 052 | R | 2452935.60048 | 2003.809 | 17.86 |
| 2223 – 052 | R | 2452939.64287 | 2003.820 | 17.78 |
| 2223 – 052 | R | 2452942.60942 | 2003.828 | 17.75 |
| 2223 – 052 | R | 2452945.54685 | 2003.836 | 17.78 |
| 2223 – 052 | R | 2452948.56762 | 2003.844 | 17.79 |
| 2223 – 052 | R | 2452951.58121 | 2003.852 | 17.89 |
| 2223 – 052 | R | 2452954.56169 | 2003.861 | 17.90 |
| 2223 – 052 | R | 2452957.56202 | 2003.869 | 17.90 |
| 2223 – 052 | R | 2452961.56929 | 2003.880 | 17.84 |
| 2223 – 052 | R | 2452964.53327 | 2003.888 | 17.80 |
| 2223 – 052 | R | 2452968.53518 | 2003.899 | 17.77 |
| 2223 – 052 | R | 2452971.52006 | 2003.907 | 17.76 |
| 2223 – 052 | R | 2452975.54776 | 2003.918 | 17.70 |

Table 2.2: continued...

| Object | Filter | Julian Date | UT Epoch | Mag |
|------------|--------|---------------|----------|-------|
| 2223 – 052 | R | 2452977.65792 | 2003.924 | 17.72 |
| 2223 – 052 | R | 2452978.53485 | 2003.926 | 17.65 |
| 2223 – 052 | R | 2452982.55523 | 2003.937 | 17.58 |
| 2223 – 052 | R | 2452985.54171 | 2003.945 | 17.64 |
| 2223 – 052 | R | 2452988.53591 | 2003.954 | 17.44 |
| 2223 – 052 | R | 2452991.52977 | 2003.962 | 17.15 |
| 2223 – 052 | R | 2452994.52643 | 2003.970 | 16.93 |
| 2223 – 052 | R | 2452999.53408 | 2003.984 | 17.35 |
| 2223 – 052 | R | 2453269.84706 | 2004.724 | 17.66 |
| 2223 – 052 | R | 2453277.70345 | 2004.745 | 17.20 |
| 2223 – 052 | R | 2453280.66253 | 2004.753 | 16.81 |
| 2223 – 052 | R | 2453282.67893 | 2004.759 | 16.97 |
| 2223 – 052 | R | 2453283.66776 | 2004.762 | 16.94 |
| 2223 – 052 | R | 2453284.68820 | 2004.764 | 16.99 |
| 2223 – 052 | R | 2453285.64210 | 2004.767 | 16.88 |
| 2223 – 052 | R | 2453286.65442 | 2004.770 | 16.99 |
| 2223 – 052 | R | 2453287.64349 | 2004.772 | 16.95 |
| 2223 – 052 | R | 2453292.67411 | 2004.786 | 17.26 |
| 2223 – 052 | R | 2453297.58926 | 2004.800 | 16.94 |
| 2223 – 052 | R | 2453299.66994 | 2004.805 | 17.03 |
| 2223 – 052 | R | 2453306.59774 | 2004.824 | 17.12 |
| 2223 – 052 | R | 2453310.58383 | 2004.835 | 17.34 |
| 2223 – 052 | R | 2453315.57523 | 2004.849 | 17.33 |
| 2223 – 052 | R | 2453325.59091 | 2004.876 | 17.30 |
| 2223 – 052 | R | 2453330.58837 | 2004.890 | 17.28 |
| | | | | |
| 2345 – 167 | R | 2452890.71148 | 2003.686 | 17.50 |
| 2345 – 167 | R | 2452894.71834 | 2003.697 | 17.51 |
| 2345 – 167 | R | 2452897.71807 | 2003.705 | 16.55 |
| 2345 – 167 | R | 2452900.74798 | 2003.713 | 17.58 |
| 2345 – 167 | R | 2452903.73485 | 2003.721 | 17.67 |
| 2345 – 167 | R | 2452906.73165 | 2003.730 | 17.48 |
| 2345 – 167 | R | 2452909.64698 | 2003.738 | 17.46 |
| 2345 – 167 | R | 2452912.71476 | 2003.746 | 17.17 |
| 2345 – 167 | R | 2452915.67589 | 2003.754 | 16.76 |
| 2345 – 167 | R | 2452918.66986 | 2003.762 | 16.88 |
| 2345 – 167 | R | 2452921.66622 | 2003.770 | 16.78 |
| 2345 – 167 | R | 2452924.67775 | 2003.779 | 16.52 |
| 2345 – 167 | R | 2452927.68352 | 2003.787 | 16.43 |
| 2345 – 167 | R | 2452930.62860 | 2003.795 | 15.31 |
| 2345 – 167 | R | 2452933.68156 | 2003.803 | 15.28 |

Table 2.2: continued...

| Object | Filter | Julian Date | UT Epoch | Mag |
|------------|--------|---------------|----------|-------|
| 2345 – 167 | R | 2452937.59765 | 2003.814 | 16.54 |
| 2345 – 167 | R | 2452940.62749 | 2003.822 | 16.75 |
| 2345 – 167 | R | 2452943.64102 | 2003.831 | 16.66 |
| 2345 – 167 | R | 2452946.62053 | 2003.839 | 16.52 |
| 2345 – 167 | R | 2452949.59216 | 2003.847 | 16.61 |
| 2345 – 167 | R | 2452952.59253 | 2003.855 | 16.14 |
| 2345 – 167 | R | 2452955.56179 | 2003.863 | 17.07 |
| 2345 – 167 | R | 2452958.70034 | 2003.872 | 17.05 |
| 2345 – 167 | R | 2452962.54787 | 2003.882 | 16.75 |
| 2345 – 167 | R | 2452965.54858 | 2003.891 | 16.41 |
| 2345 – 167 | R | 2452970.60738 | 2003.904 | 16.67 |
| 2345 – 167 | R | 2452973.52512 | 2003.912 | 17.33 |
| 2345 – 167 | R | 2452976.53204 | 2003.921 | 17.05 |
| 2345 – 167 | R | 2452979.53241 | 2003.929 | 17.09 |
| 2345 – 167 | R | 2452983.54239 | 2003.940 | 17.33 |
| 2345 – 167 | R | 2452986.52659 | 2003.948 | 17.26 |
| 2345 – 167 | R | 2452989.52975 | 2003.956 | 17.39 |
| 2345 – 167 | R | 2452992.52972 | 2003.964 | 17.41 |
| 2345 – 167 | R | 2452995.52854 | 2003.973 | 17.19 |
| 2345 – 167 | R | 2452999.55873 | 2003.984 | 17.23 |
| 2345 – 167 | R | 2453003.57039 | 2003.995 | 17.21 |
| 2345 – 167 | R | 2453009.53499 | 2004.011 | 17.33 |
| 2345 – 167 | R | 2453012.53156 | 2004.019 | 18.33 |
| 2345 – 167 | R | 2453015.53688 | 2004.027 | 17.58 |
| 2345 – 167 | R | 2453018.53206 | 2004.036 | 17.40 |
| 2345 – 167 | R | 2453021.52733 | 2004.044 | 16.31 |
| 2345 – 167 | R | 2453024.53036 | 2004.052 | 16.72 |
| 2345 – 167 | R | 2453278.66396 | 2004.748 | 17.25 |
| 2345 – 167 | R | 2453283.69734 | 2004.762 | 17.47 |
| 2345 – 167 | R | 2453289.66580 | 2004.778 | 17.38 |
| 2345 – 167 | R | 2453296.65280 | 2004.797 | 17.62 |
| 2345 – 167 | R | 2453298.64522 | 2004.803 | 17.68 |
| 2345 – 167 | R | 2453305.61695 | 2004.822 | 17.48 |
| 2345 – 167 | R | 2453310.59242 | 2004.835 | 17.06 |
| 2345 – 167 | R | 2453316.63326 | 2004.852 | 16.78 |
| 2345 – 167 | R | 2453325.65847 | 2004.877 | 17.14 |
| 2345 – 167 | R | 2453331.61880 | 2004.893 | 17.94 |
| 2345 – 167 | R | 2453335.61895 | 2004.904 | 17.99 |
| 2345 – 167 | R | 2453338.61043 | 2004.912 | 17.93 |
| 2345 – 167 | R | 2453342.52868 | 2004.923 | 17.94 |
| 2345 – 167 | R | 2453348.54187 | 2004.939 | 18.28 |

Table 2.2: continued...

| Object | Filter | Julian Date | UT Epoch | Mag |
|------------|--------|---------------|----------|-------|
| 2345 – 167 | R | 2453352.57314 | 2004.950 | 18.19 |
| 2345 – 167 | R | 2453355.56588 | 2004.958 | 18.08 |
| 2345 – 167 | R | 2453358.55319 | 2004.967 | 18.01 |
| 2345 – 167 | R | 2453361.52747 | 2004.975 | 17.95 |
| 2345 – 167 | R | 2453366.53475 | 2004.988 | 17.81 |
| 2345 – 167 | R | 2453369.53379 | 2004.997 | 17.83 |
| 2345 – 167 | R | 2453372.52618 | 2005.005 | 17.98 |
| 2345 – 167 | R | 2453375.52948 | 2005.013 | 18.18 |
| 2345 – 167 | R | 2453378.53255 | 2005.021 | 18.59 |
| 2345 – 167 | R | 2453381.53965 | 2005.030 | 18.42 |

Chapter 3

Rest Frame Analysis

3.1 Shifting to the Rest Frame

One of the primary goals of this dissertation is to investigate blazar variability characteristics as a function of redshift. By shifting the observations into the rest frame of the source, the intrinsic character of the variability for each source becomes more apparent. Several effects are imposed onto the observed flux before it is measured and each must be dealt with. These effects include cosmological redshift of the individual photons, of the frequency interval, and of the time interval.

3.1.1 Relativistic Effects

Magnitude to Flux Conversion

The light curves for each of these blazars plots the apparent magnitude of the object versus time. In order to transform the light curves to the rest frame for each source, the apparent magnitudes must first be converted into fluxes using Equation (3.1), where m_1 and m_2 are the apparent magnitudes of an object and a reference star with known flux respectively, and f_1 and f_2 are the corresponding fluxes.

$$m_1 - m_2 = -2.5 \log \frac{f_1}{f_2} \quad (3.1)$$

If the reference star is chosen such that its apparent magnitude is 0.0 (e.g., an A0V star like α -Lyr) in a waveband of interest, Equation (3.1) can be converted into Equation (3.2)¹.

$$f_1 = f_2 10^{-0.4m_1} \quad (3.2)$$

Using more appropriate notation to reflect the units in the various terms, f_1 becomes F_ν , the unknown spectral flux density, f_2 becomes F_{ν_0} , the *zero-point* spectral flux density, and m_1 becomes m , the apparent magnitude to be converted. F_{ν_0} depends upon the filter through which the observation was taken (see Table 3.1 for the filters used here) and is in flux units of Janskys (Jy). The zero-point spectral flux densities were obtained from Allen (2001).

$$F_\nu \equiv \frac{dF}{d\nu} = F_{\nu_0} 10^{-0.4m} \quad (3.3)$$

Table 3.1: Magnitude to Flux Conversion Factors

| Filter | $F_{\nu_0}(\text{Jy})$ |
|----------|------------------------|
| <i>V</i> | 3781 |
| <i>R</i> | 2941 |

The fluxes for each object derived using Equations (3.1) through (3.3) must be trans-

¹It is to be noted that the magnitudes used here are not being calibrated absolutely to the flux of α -Lyr (Vega). Conversions of this type are inherently inaccurate, and can generally yield results no better than 2% accuracy. The magnitudes used here are being converted in exactly the same fashion, therefore they are *internally* consistent with respect to each other.

formed into the rest frame of the source using the redshift (z) for that source. Table 1.2 summarizes the redshifts (or lower bound) for each object. The redshift is applied to the observations of each object in 3 factors of $(1+z)$. One factor for cosmological redshift (photon energy), one for frequency/wavelength interval, and one for time interval² as illustrated in Equation (3.4), where F_{ν_e} and F_{ν_o} are the flux density in the emitted and observed fluxes respectively. It is important to note that the frequency interval in these two terms, denoted by ν_e for the rest frame and ν_o for the observed, is different in both spectral location and bandwidth.

$$F_{\nu_e} = F_{\nu_o}(1+z)^3 \quad (3.4)$$

Effects of Doppler Boosting

The large amplitude, short time-scale variations observed in blazars are believed to be produced by shocks propagating down a relativistic jet oriented close to the line of sight of the observer. These emissions are beamed in the forward direction and at very small angles ($< 10^\circ$) with respect to the line of sight. The variations are enhanced as shown in Equation (3.5) where the Doppler factor $\delta = \Gamma^{-1}(1 - \beta \cos \theta)^{-1}$, $\Gamma = (1 - \beta^2)^{-1/2}$, $\beta = v/c$, and θ is the angle with respect to the line of sight.

$$F_{\nu_o} \propto \delta^3 F_{\nu_e} \quad (3.5)$$

²The time interval is modified by the equation: $t_e = t_o(1+z)^{-1}$, where t_e and t_o are the time in the emitted and observed frames, respectively.

The Doppler boosting of the emissions is thus a function of both the speed of the bulk motions and their angle with respect to the line of sight of the observer. Because the Doppler boosting is related to these parameters (Γ , θ) which are difficult to determine accurately, and because these parameters aren't directly related to rest frame variations as they are investigated here, no correction will be made for it.

3.1.2 BL Lacertae, the Baseline

BL Lacertae (or more simply BL Lac), the prototype for the majority of objects known as blazars, will be used as the baseline for comparison to the rest frame variability observed for each object. Not only does it have the largest number of observations in our archive, but it is the closest of the objects in the sample with a redshift of only 0.069. BL Lac has shown large amplitude variability on all time scales investigated and has rarely exhibited an absence of microvariability. Examples of BL Lac's variability can be seen in Figures 1.4 & 1.6 and in §3.2.6.

When the observed variability is transformed to the rest frame, BL Lac, with its low redshift, shows very little enhancement. This enhancement is expected for any blazar not located at $z = 0$. As an example, consider the light curve in Figure 1.4 for 16 September 1995. Figure 3.1 shows this light curve converted to fluxes. Notice how the upper, rest frame, light curve is amplified only mildly. The flux is increased by just over 20% and the time over which the event occurred has decreased by less than 10%.

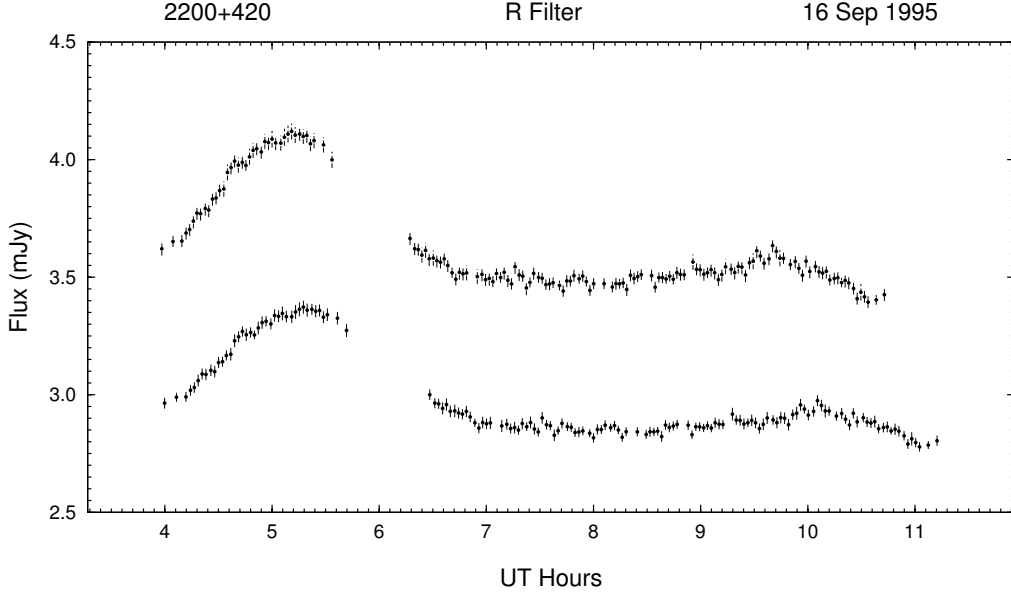


Figure 3.1: Example of the optical microvariability (R band) of $2200 + 420$ on the night of 16 Sep 1995 shifted into the rest frame. The lower curve is the observed frame flux and the upper curve is the rest frame flux.

3.2 Archival Data

The current repository of PEGAn archival data spans more than 30 years and includes photographic, photoelectric, and CCD observational data. The largest accessible portion of the archive is CCD data dating from about 1987, which is fully available in electronic format (i.e., CCD images and reduced data files). Many objects have data spanning this entire time window and most have at least some very high time density sampling.

The amount of objects regularly monitored numbers in the hundreds and covers the range of AGN classes: Seyfert 1 galaxies, Seyfert 2 galaxies, Narrow-line Seyfert 1 galaxies, BL Lacertae objects, and OVV quasars. All PEGA team members regularly add to this archive as they collect data for their own dissertations. There exists proprietary data in the archive; it is freely available for all team members to use in their own analysis.

Each microvariability light curve (i.e., light curves > 30 minutes and < 24 hours) has three panels: the upper panel shows the apparent magnitude versus UT hour as measured by the observer. The middle panel is the flux density light curve (in mJy) converted back into the rest frame of the object and uses open symbols for clarity, and the lower panel is the flux density light curve (also in mJy) measured by the observer, both versus UT hour. For low redshift objects, the scale of the lower two panels is the same, and for higher redshift objects, the scale of the lower panel is reduced by a factor of 1, 2, or 5 (indicated by the 1x, 2x, or 5x to the right of the panel) to allow more direct comparison between it and the magnitude light curve. This is done because of the large range of values in the flux densities that would normally be compensated for by using a logarithmic (i.e., magnitude) scale. Unfortunately that logarithmic scale would also eliminate the differences in variability amplitude expected between the observed and emitted (rest) frame of the source. Please see §2.3 for how the errors were calculated and for how the fluxes were converted from the apparent magnitudes, and see §3.1 for a complete discussion of the rest frame conversion. The object of the conversion is to allow comparison of the light curves as they would be seen in the rest frame of the source. It is expected that this will allow a more robust comparison of the *intrinsic* variability characteristics, so that all objects can be analyzed on equal footing.

Basic information about each object will be given in each of the following subsections followed by light curves as described above for both long term variability (magnitude versus Epoch) and short term microvariability (magnitude and flux density versus UT hour). The character of the microvariability will be discussed in magnitudes in reference to its amplitude and duration, ending with a short section describing how the shift back into the rest frame

has modified the light curves for the given object. At the end of this section, the results from all objects will be discussed with respect to their rest frame light curves, and compared to BL Lac specifically to show how the microvariability of each relates to this baseline object.

3.2.1 0235 + 164

The BL Lac object AO 0235 + 16 (also known as PKS 0235 + 164 or simply 0235 + 164) has a redshift of 0.940 and has exhibited a total variability amplitude range of just above 5 magnitudes (or mag) based on the observations for this investigation (see Figure 3.2). The observations used for AO 0235 + 16 were obtained in the R and V bands only, and were taken from the PEGA archives, and extend just over 18 years (roughly 12 years in each band overlapping for 6 years). No SMARTS data exists for this object.

In Figure 3.2, the complete V and R band light curve of AO 0235 + 16 is shown. The average color index $V - R = 0.81$ was adopted from Takalo et al. (1992) and Romero et al. (2000) to combine the V and R band observations. Their observations bracket the window of overlap of V and R band data. AO 0235 + 164 exhibits extremely large variations over the entire 18 years on the order of 5 mag. It was in the high, or outburst state twice: once between 1991 and 1993 and again throughout 1998. The remainder of the time was spent in either an intermediate or low (quiescent) state. A detailed look at the overlap region is shown in Figure 3.3. The amplitude of both the short and long term variability agree with the results of Raiteri et al. (2001).

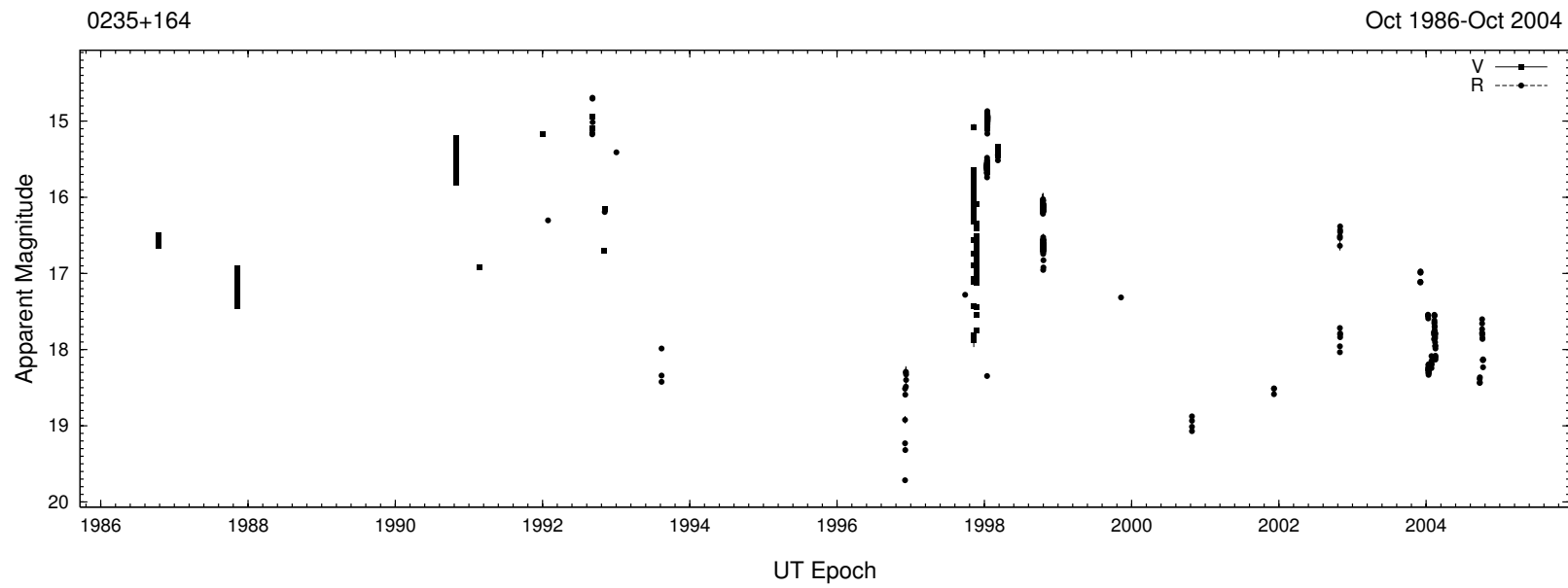


Figure 3.2: Complete V and R band light curve of 0235 + 164 from 1986 to 2004.
The amplitude of variability is ~ 5 mag.

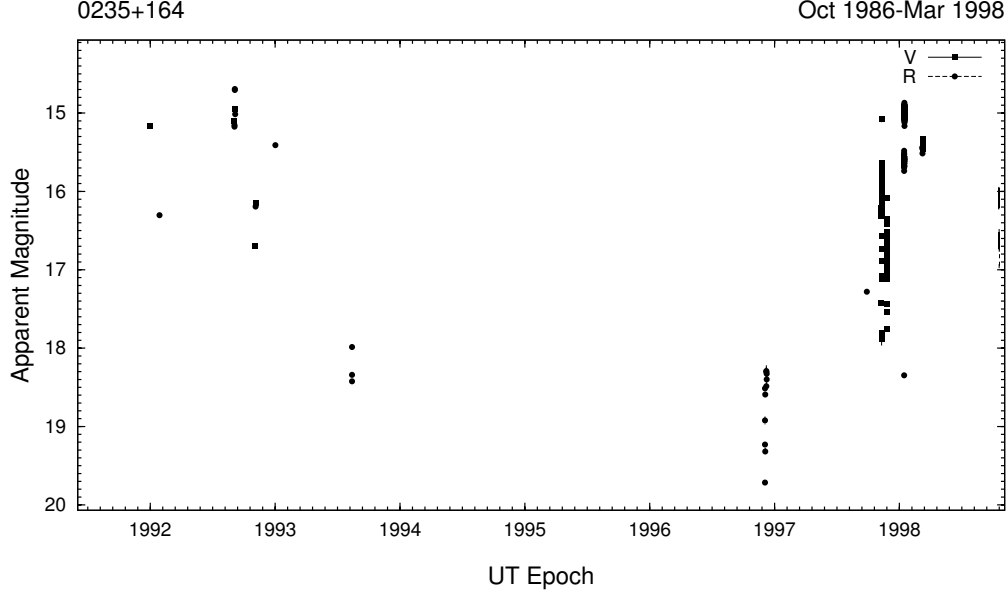


Figure 3.3: Detailed intersection of V and R band light curve of 0235 + 164 from 1992 to 1998. The amplitude of variability is ~ 5 mag.

The V band light curve shown in Figure 3.4 for AO 0235 + 16 obtained on the night of 13 Oct 1986. This light curve exhibits marked microvariability in an oscillatory fashion with a quasi-periodicity of approximately one hour and with a confidence level of 2.7σ . Visually it is clear that there is variability present and that it is statistically significant. Figure 3.5 shows a 5.6σ change on the night of 11 Nov 1987. These variations are more erratic in nature.

AO 0235 + 16 was monitored for five consecutive nights in late October 1990. The observations are presented in Figures 3.6 through 3.10. These observations were first reported by Noble (1995) and show very dramatic variations ($\sim 10 - 30\sigma$). During the first night (Figure 3.6), AO 0235 + 16 shows a steady increase in brightness without statistically significant evidence of microvariability superimposed on the rise. The second night, 28 Oct 1990 seen in Figure 3.7, AO 0235 + 16 showed a similar behavior, but with some evidence

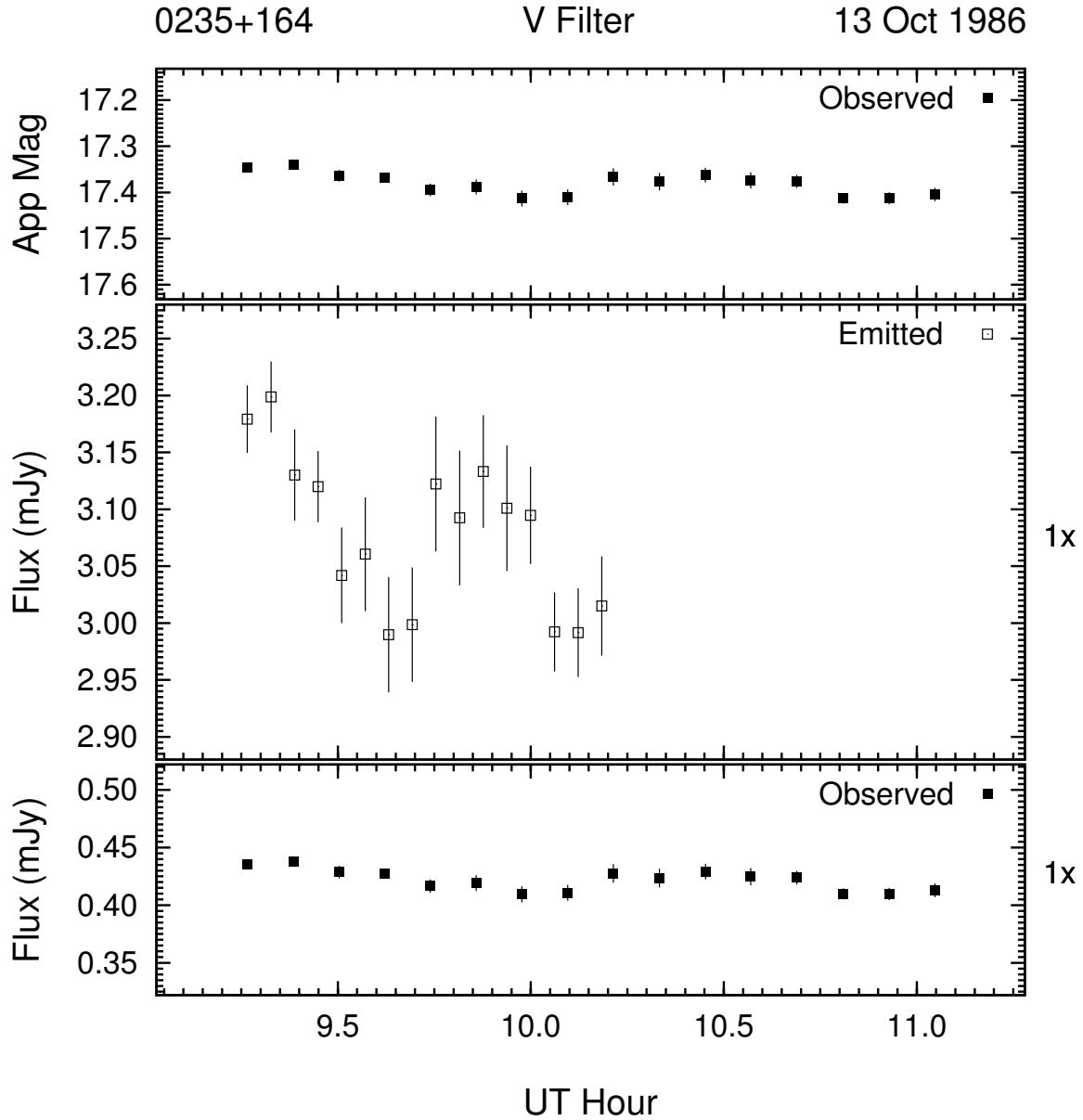


Figure 3.4: Example of the optical microvariability (V band) of 0235 + 164 on the night of 13 Oct 1986. This night's data was 4-point averaged to improve S/N .

of variations superimposed on the trend. On the third night (Figure 3.8), the upward trend continued with an apparent leveling off near the end of the night. The observations on this night show definite rapid variability superimposed on the trend at a $\geq 2.6\sigma$ significance level.

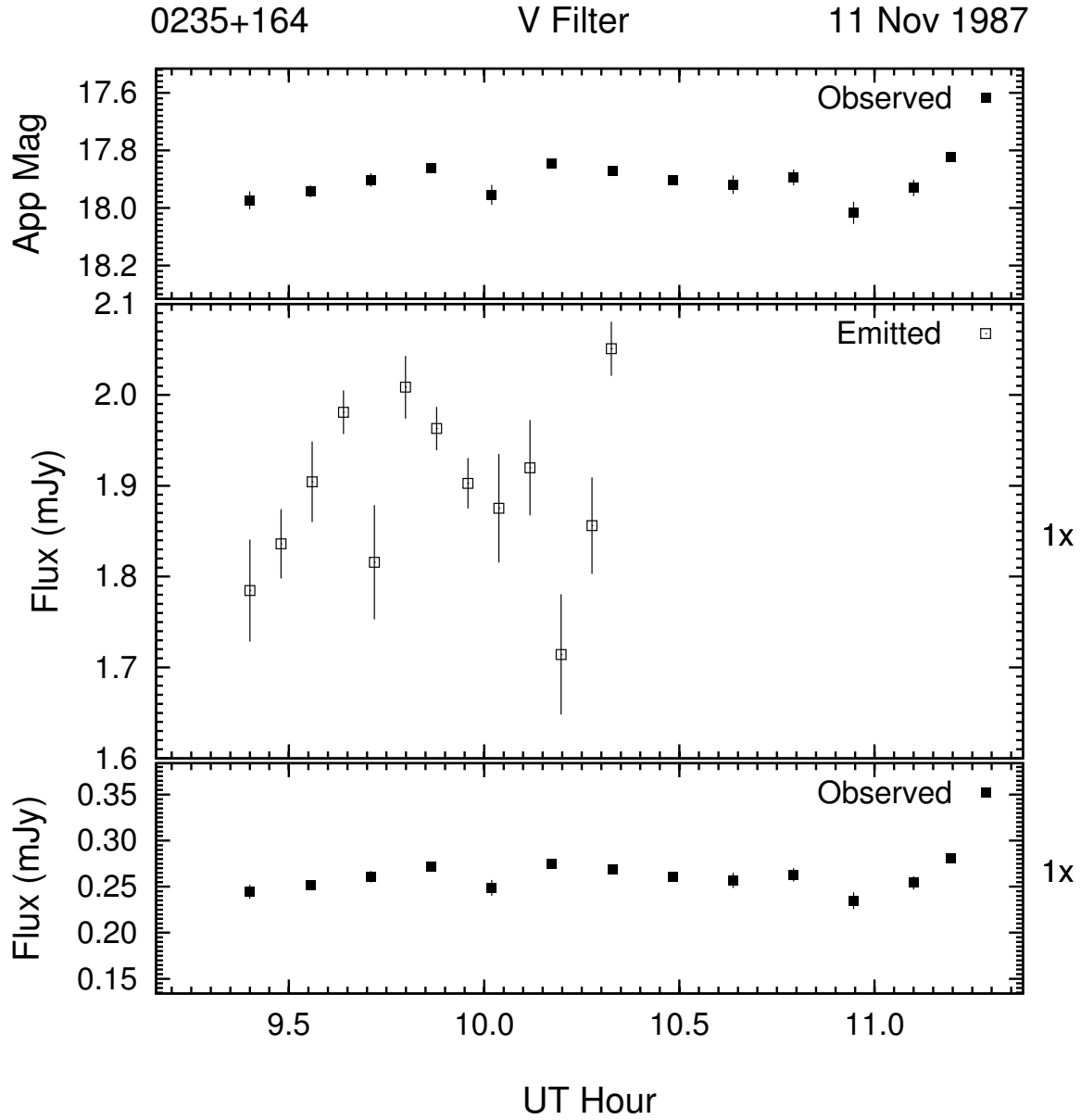


Figure 3.5: Example of the optical microvariability (V band) of 0235 + 164 on the night of 11 Nov 1987. This night's data was 4-point averaged to improve S/N .

The variations observed on the first three nights exhibit a very gentle rise in brightness from $V = 16.60$ to $V = 16.53$ for the first night, followed by a further brightening of 0.15 mag to $V = 16.40$ on 28 Oct 1990. On 29 Oct 1990, AO 0235 + 16 brightened from $V = 16.55$ more

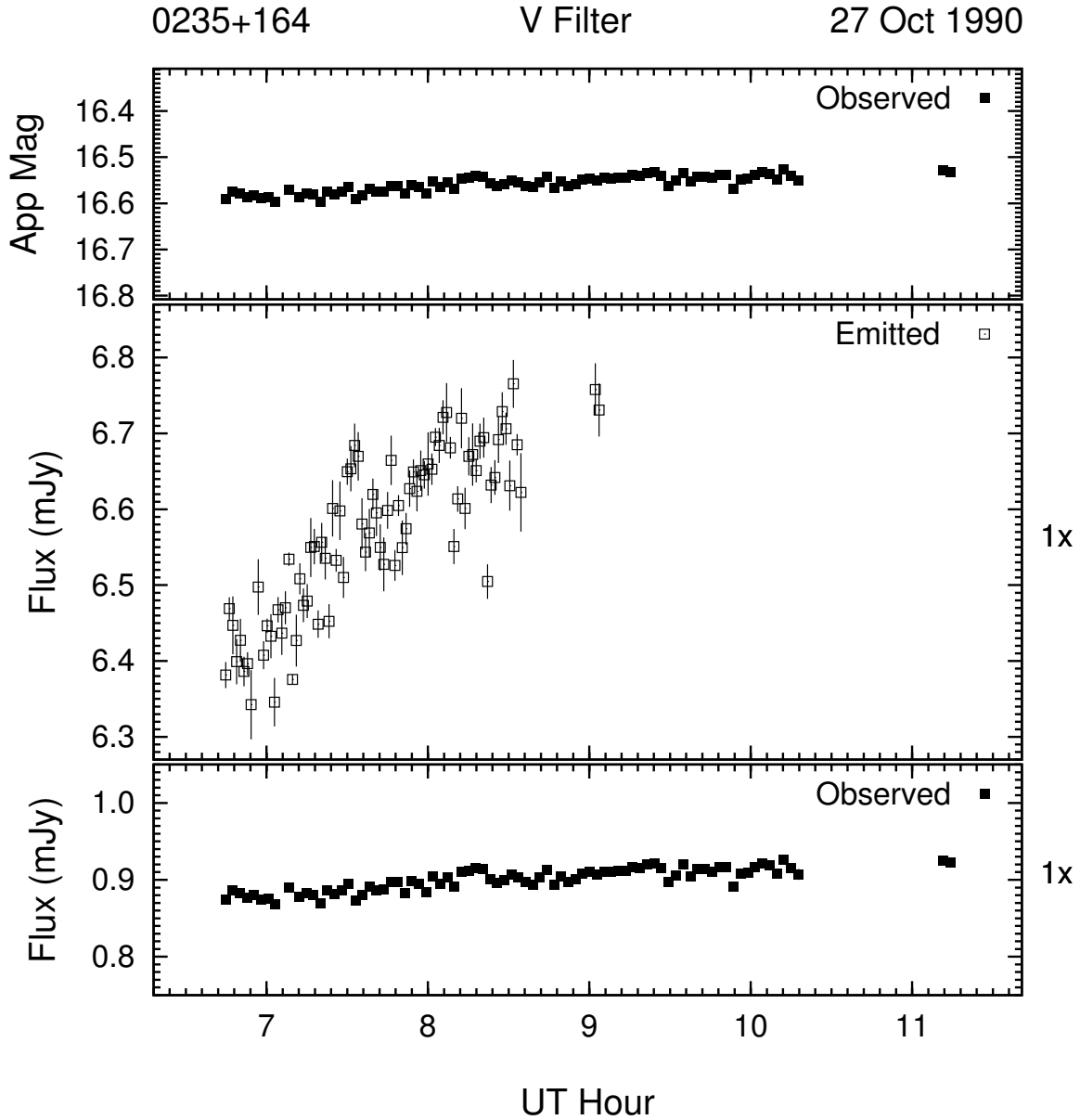


Figure 3.6: Example of the optical microvariability (V band) of 0235 + 164 on the night of 27 Oct 1990. This night's data was 3-point averaged to improve S/N .

than 0.2 mag to plateau at $V = 16.34$. This flare continued into the next night where the light curve of 30 Oct 1990 (Figure 3.9) starts out at $V = 16.07$. At this point, AO 0235 + 16 started to fade with small scale microvariability observed with an amplitude on the order of

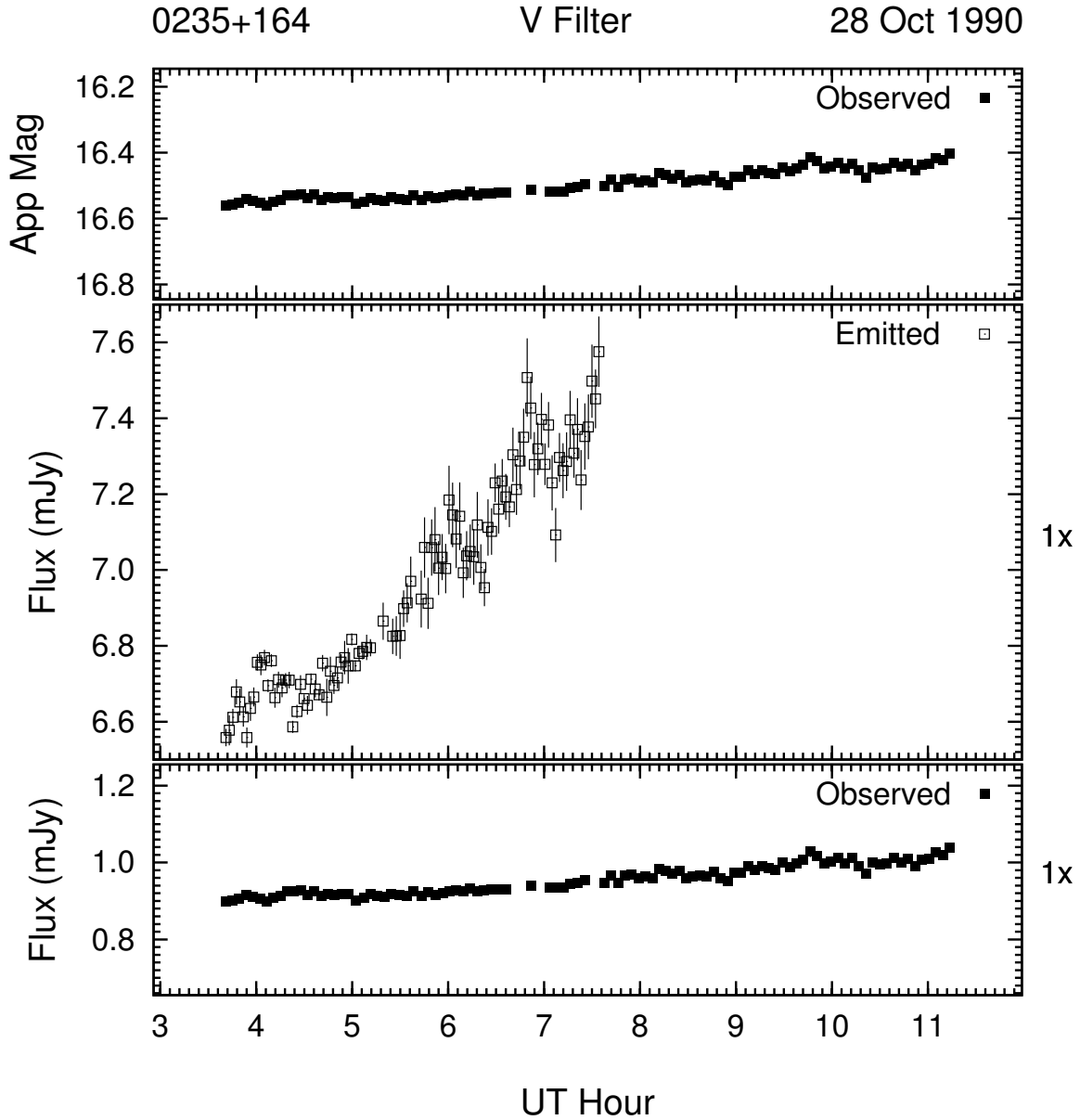


Figure 3.7: Example of the optical microvariability (V band) of 0235 + 164 on the night of 28 Oct 1990. This night's data was 5-point averaged to improve S/N .

< 0.1 mag on time scales of ~ 30 minutes. Overall, the source faded to $V = 16.25$, 0.18 mag dimmer than the start of this night. AO 0235 + 16 is found to have faded to $V = 16.45$ on the last night, 31 Oct 1990 (see Figure 3.10).

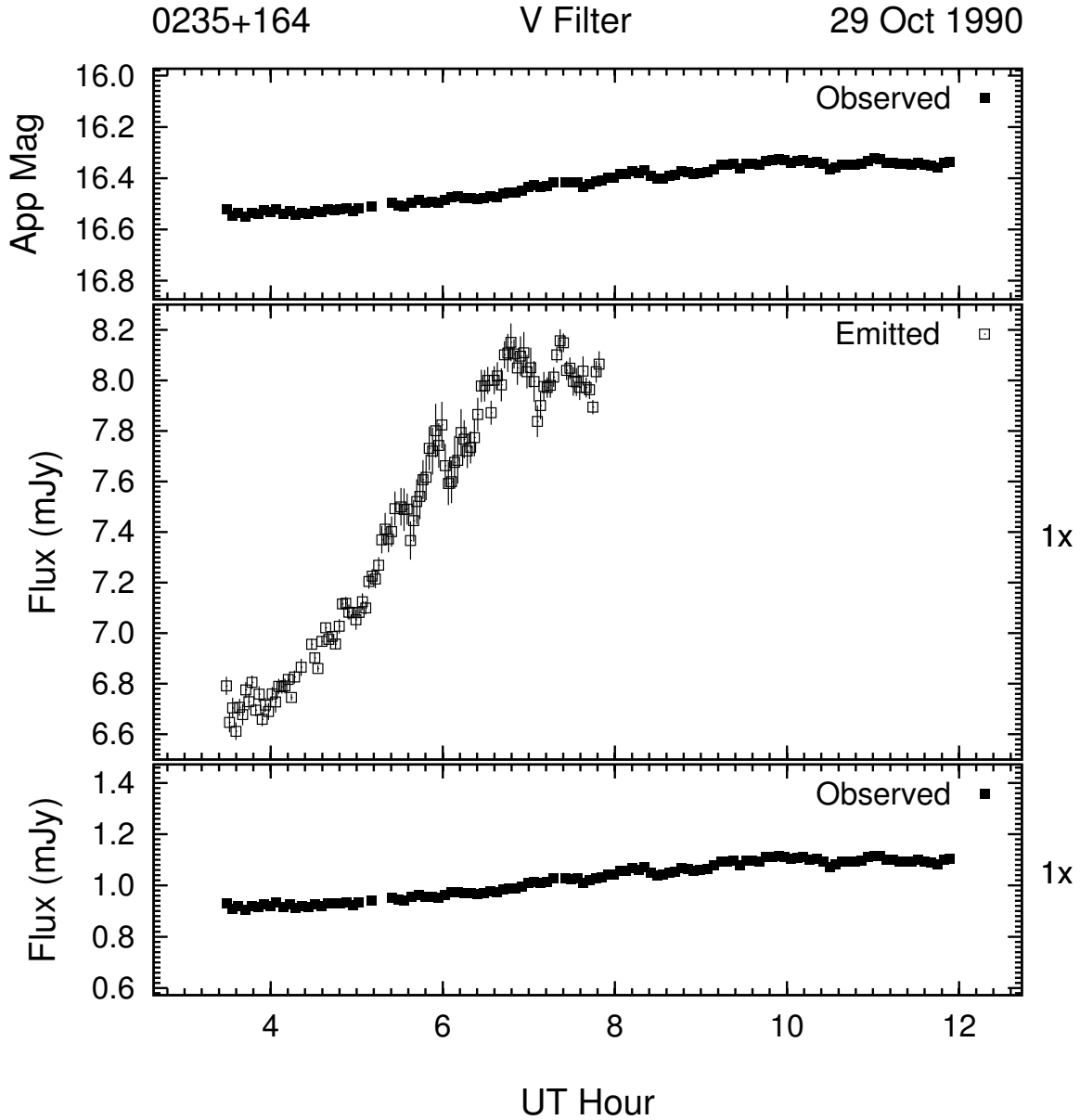


Figure 3.8: Example of the optical microvariability (V band) of 0235 + 164 on the night of 29 Oct 1990. This night's data was 5-point averaged to improve S/N .

AO 0235 + 16 was also monitored for 4 consecutive nights from 05 – 08 Nov 1991. The object was in a much brighter state than observed on the previous run (2 mag brighter) and exhibited a total range of variability of ~ 0.5 mag. On the first night, shown in Figure 3.11,

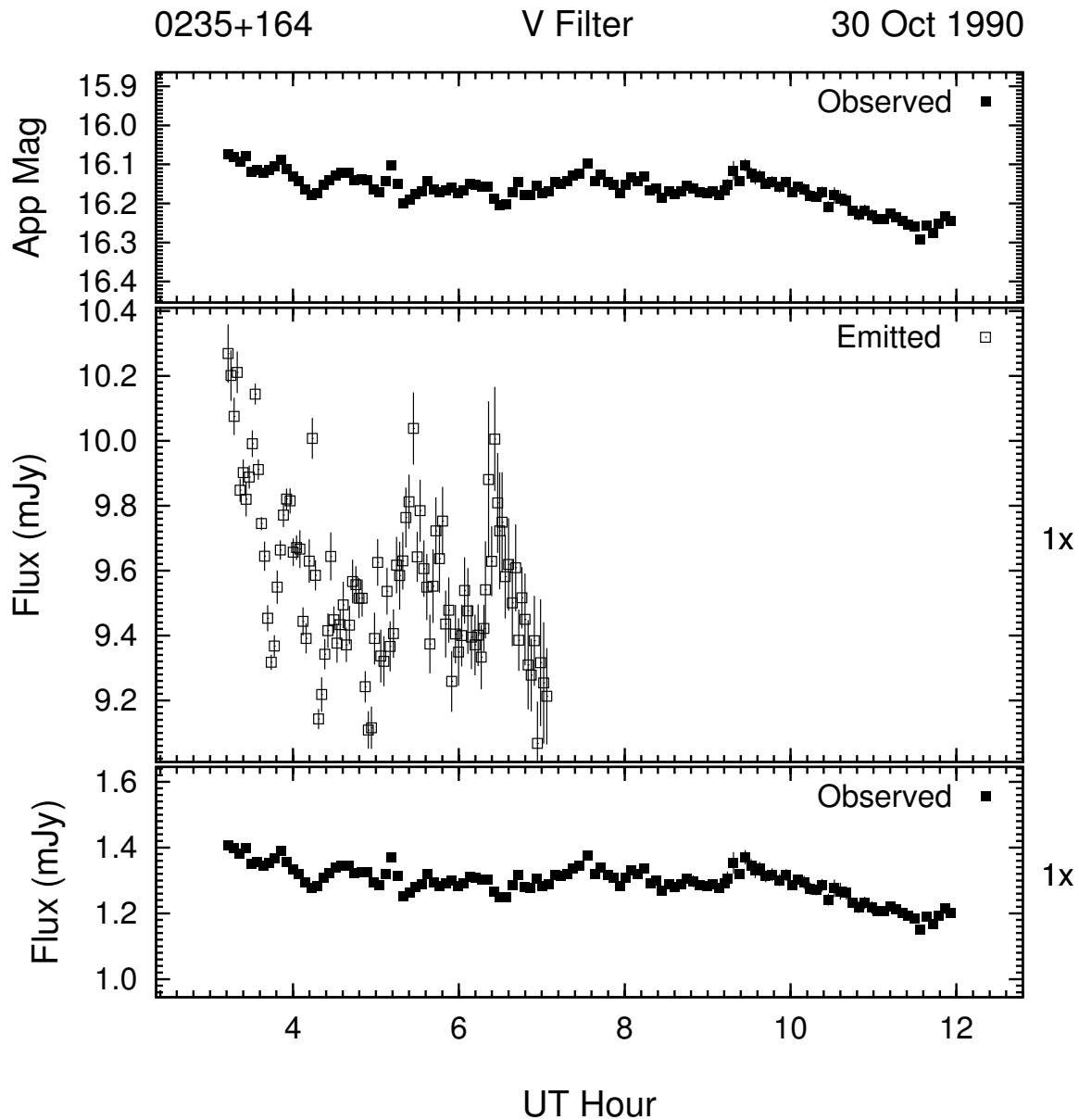


Figure 3.9: Example of the optical microvariability (V band) of 0235 + 164 on the night of 30 Oct 1990. This night's data was 5-point averaged to improve S/N .

AO 0235 + 16 exhibited a 0.2 mag rise over the duration of 6 hours. There are possible small amplitude variations superimposed on the trend, but the temporal sampling is too sparse to fully characterize them. On the following night, 06 Nov, the object was 0.05 mag

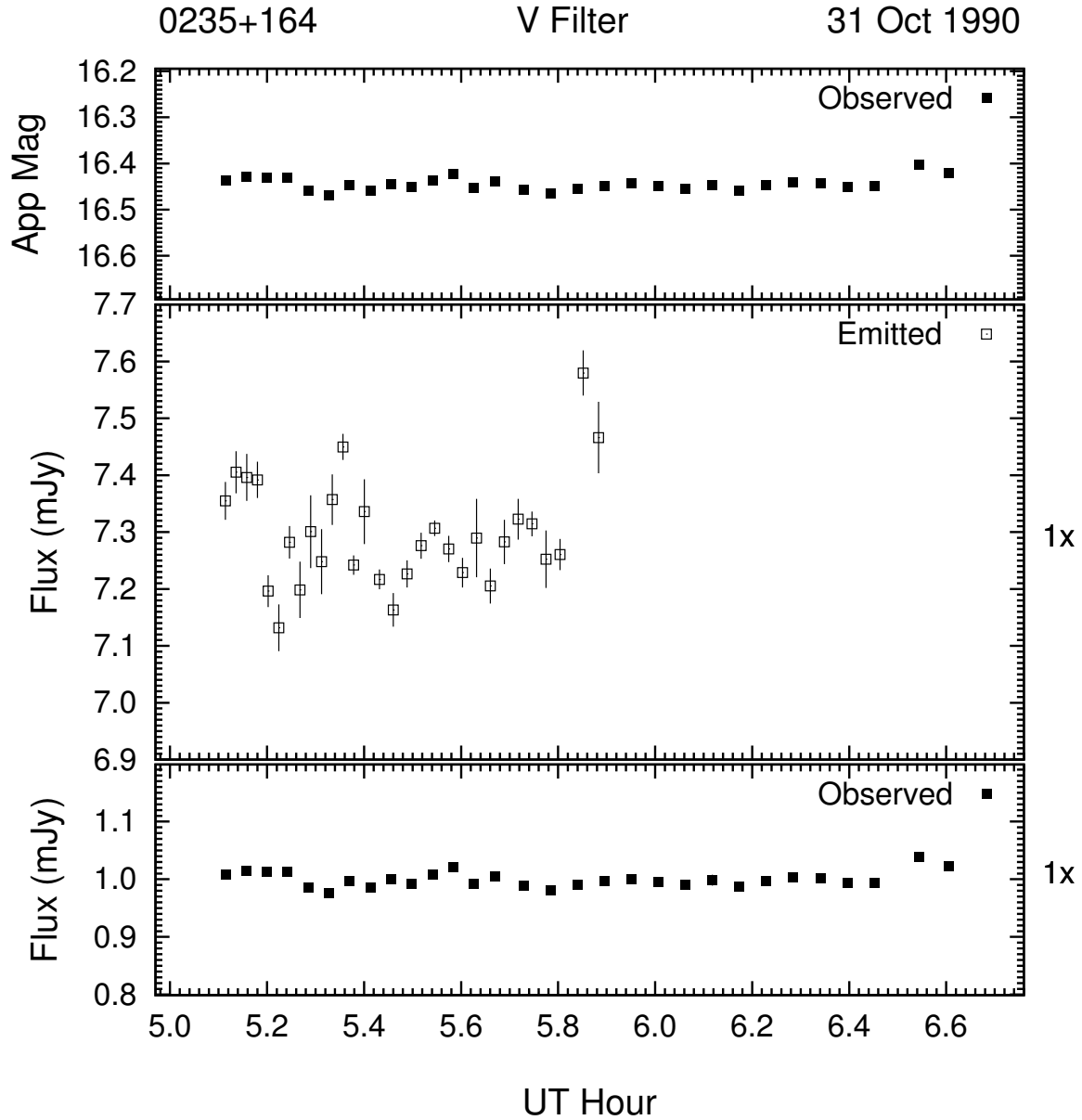


Figure 3.10: Example of the optical microvariability (V band) of 0235 + 164 on the night of 31 Oct 1990. This night's data was 3-point averaged to improve S/N .

fainter. This light curve (see Figure 3.12) shows modest variations, but no overall trend. The variations displayed in Figure 3.13 for the night of 07 Nov 1991 are similar in amplitude to those observed on 06 Nov 1991. AO 0235 + 16 showed only a moderate (5σ) increase

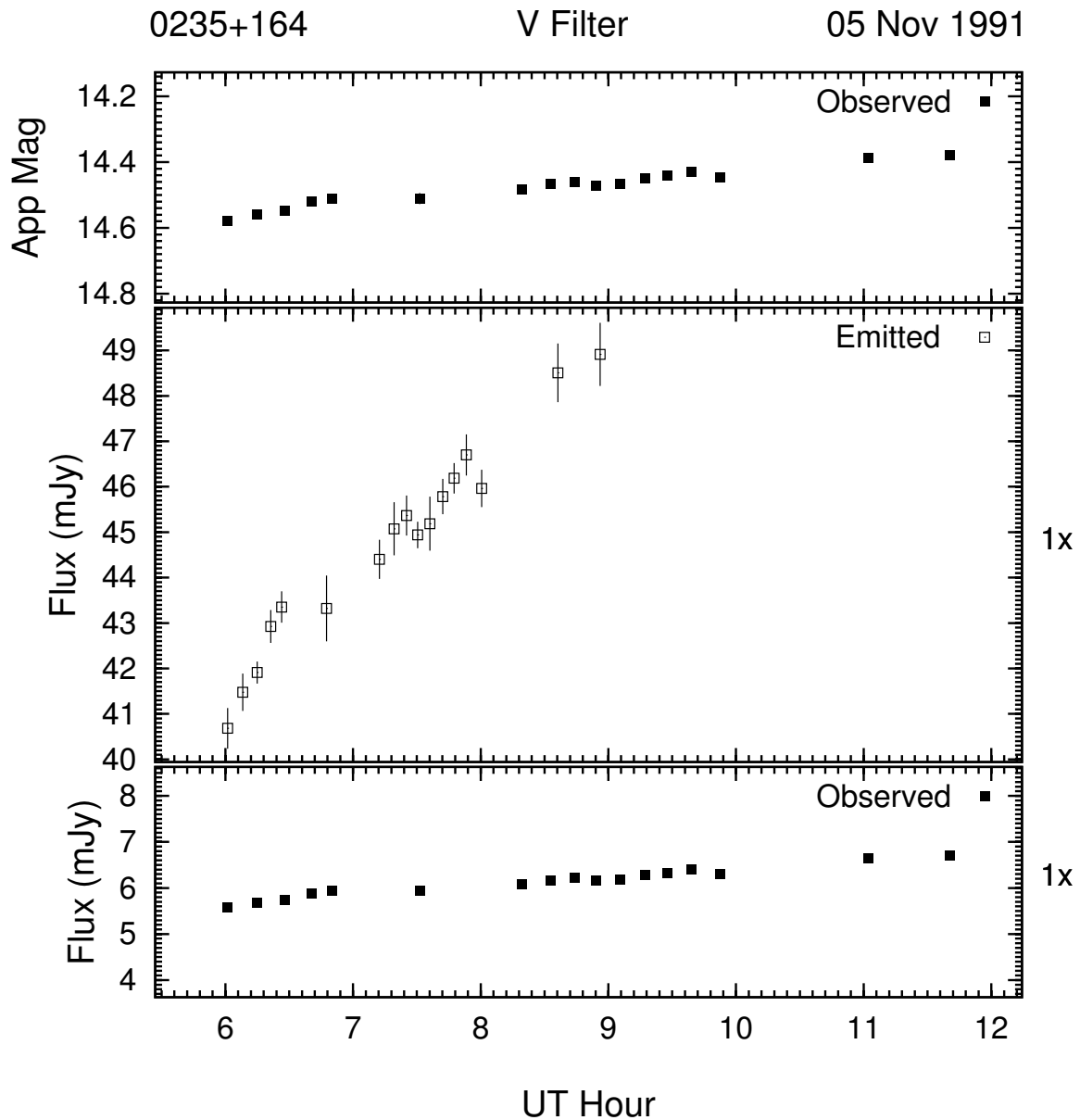


Figure 3.11: Example of the optical microvariability (V band) of 0235 + 164 on the night of 05 Nov 1991. This night's data was 2-point averaged to improve S/N .

followed by a similar decrease in brightness. The character of the variations exhibited by AO 0235 + 16 on the night of 08 Nov 1991 is dramatically different. Figure 3.14 shows that the object started at 0.5 mag brighter than the previous night, and remained quasi-steady

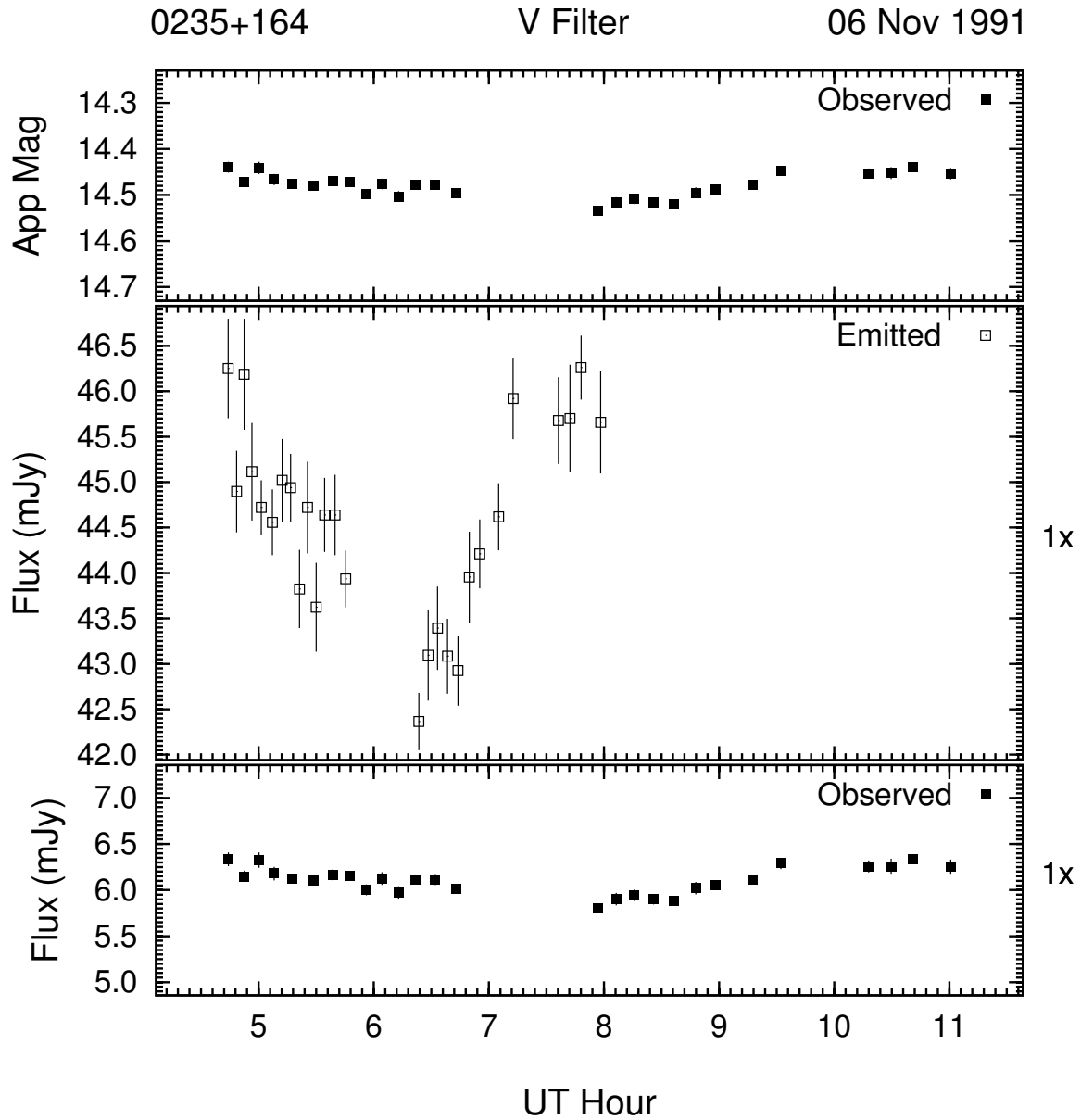


Figure 3.12: Example of the optical microvariability (V band) of 0235 + 164 on the night of 06 Nov 1991. This night's data was 2-point averaged to improve S/N .

until at 7.8 hours UT, it started a rapid decline of almost 0.2 mag over roughly 2 hours, and showed no evidence of variability for the remainder of the night.

The next 3 plots show observations of AO 0235 + 16 obtained from late 1997 to early

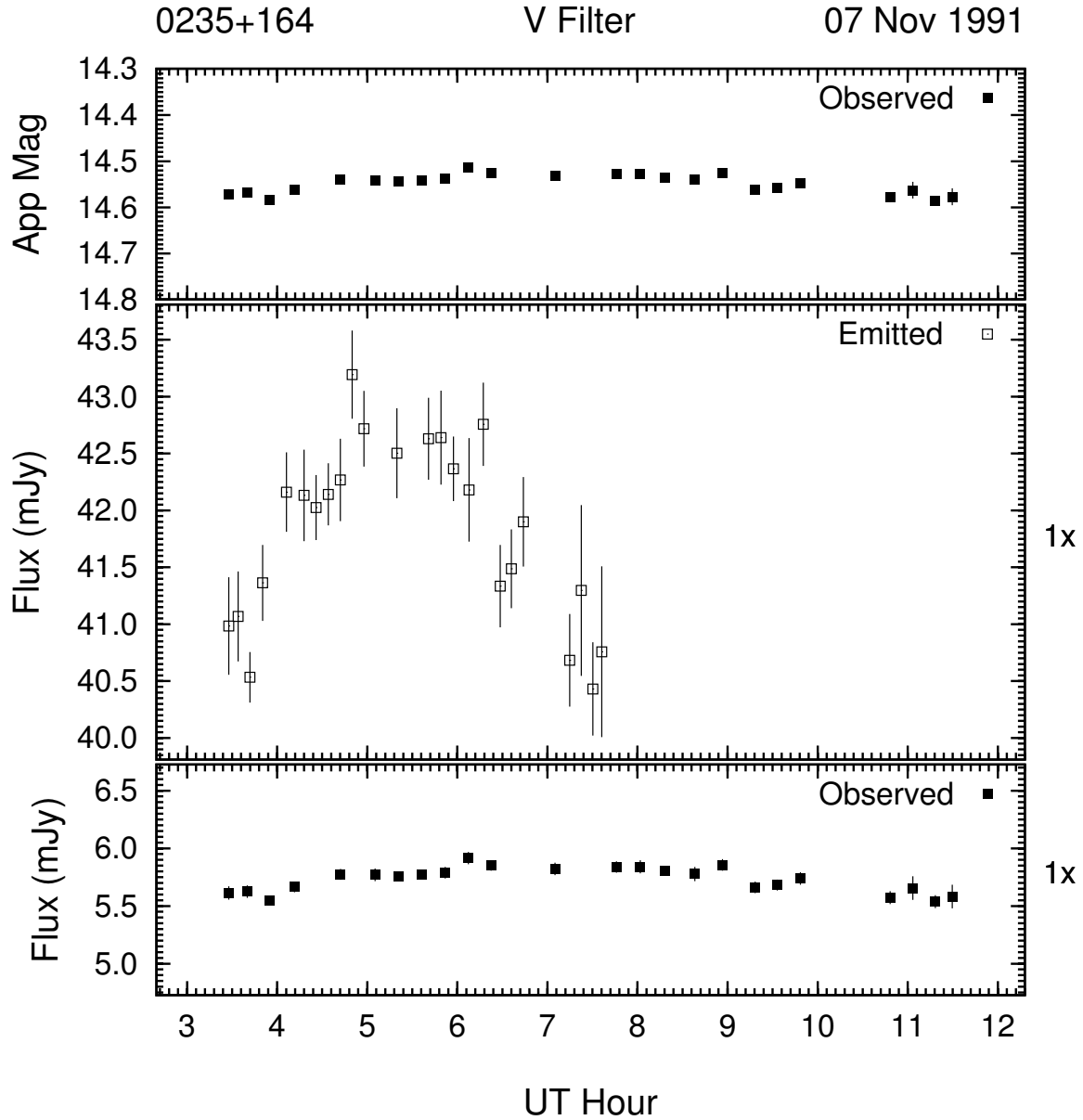


Figure 3.13: Example of the optical microvariability (V band) of 0235 + 164 on the night of 07 Nov 1991. This night's data was 2-point averaged to improve S/N .

1998. On the night of 09 Nov 1997, AO 0235 + 16 exhibited its most dramatic single night event. The light curve in Figure 3.15 started off with a brief plateau near $V = 17.1$ and quickly rose 0.6 mag in 3.5 hours, a change of 57.8σ ! It then leveled off and appeared to

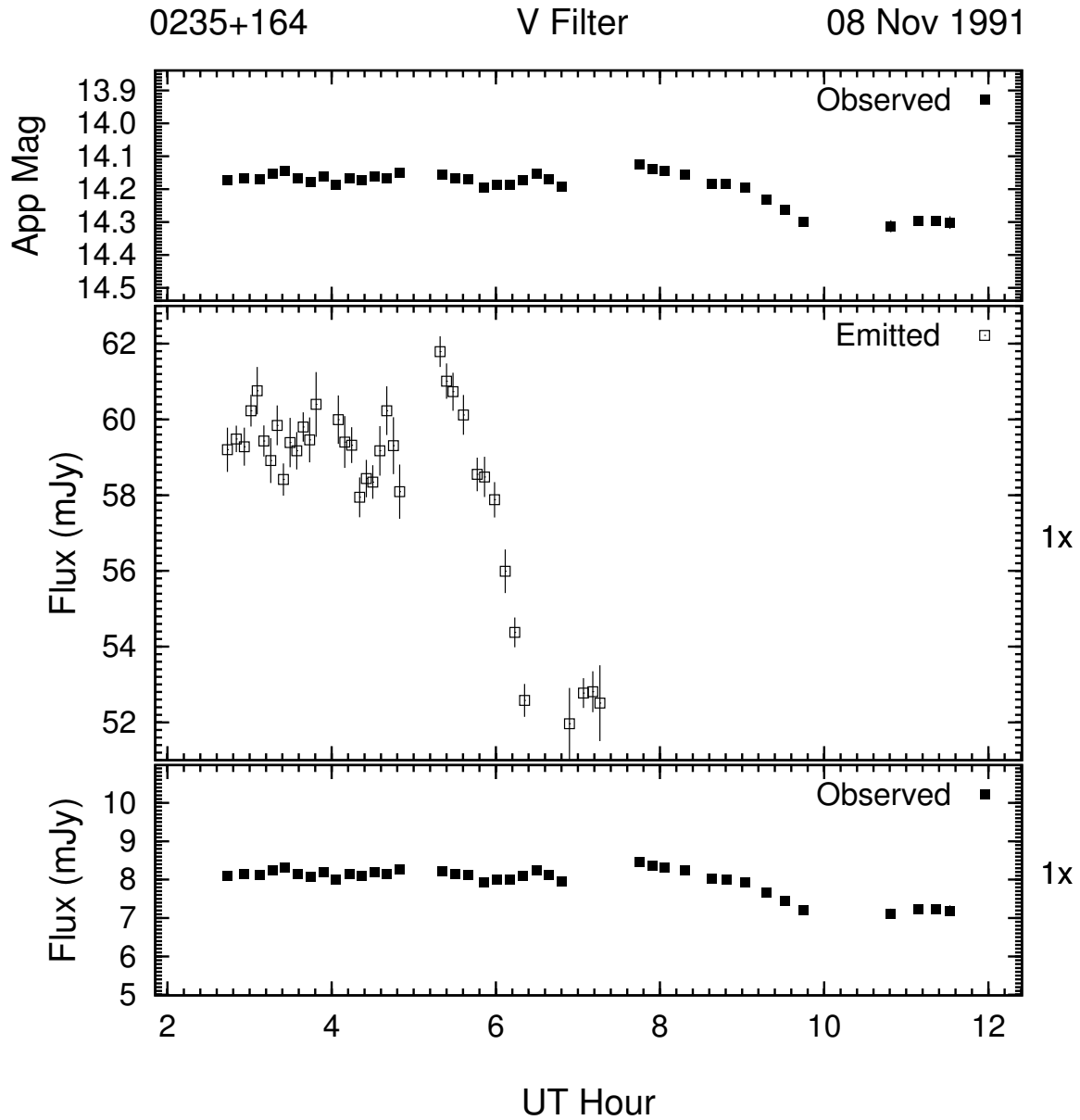


Figure 3.14: Example of the optical microvariability (V band) of 0235 + 164 on the night of 08 Nov 1991. This night's data was 2-point averaged to improve S/N .

begin to fade slowly, although this is at a level of $< 2.6\sigma$ significance. The larger error bars associated with individual data points in this and the following plot are an artifact of the 2- and 4-point averaging respectively (c.f. §2.3). In Figure 3.16, AO 0235 + 16 showed

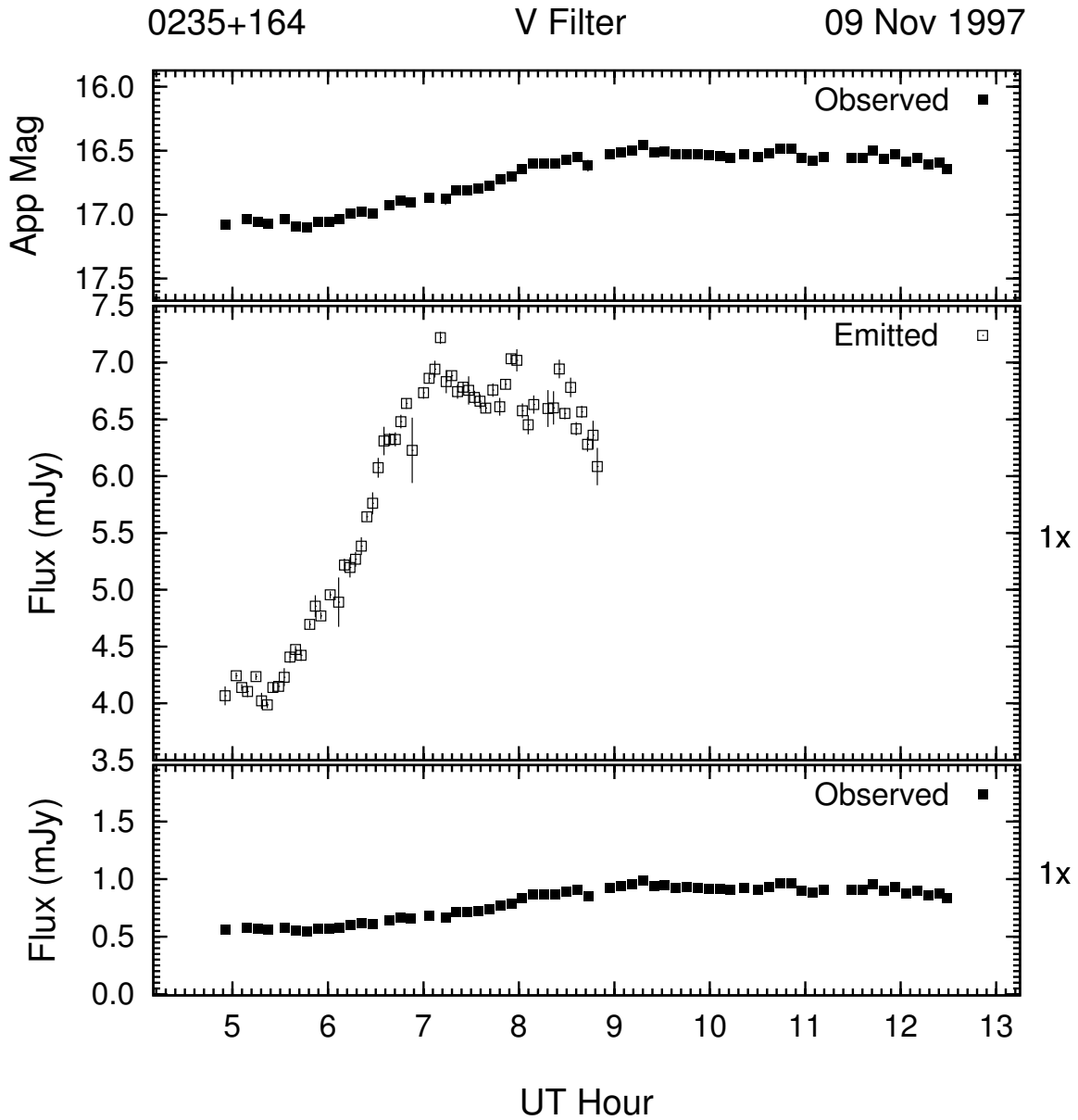


Figure 3.15: Example of the optical microvariability (V band) of 0235 + 164 on the night of 09 Nov 1997. This night's data was 2-point averaged to improve S/N .

variability that is nearly as dramatic, but is significantly different in character than that observed in the previous figure. The object's large decline in brightness is superimposed with large dips and peaks present with a significance on the order of $20 - 40\sigma$. The most

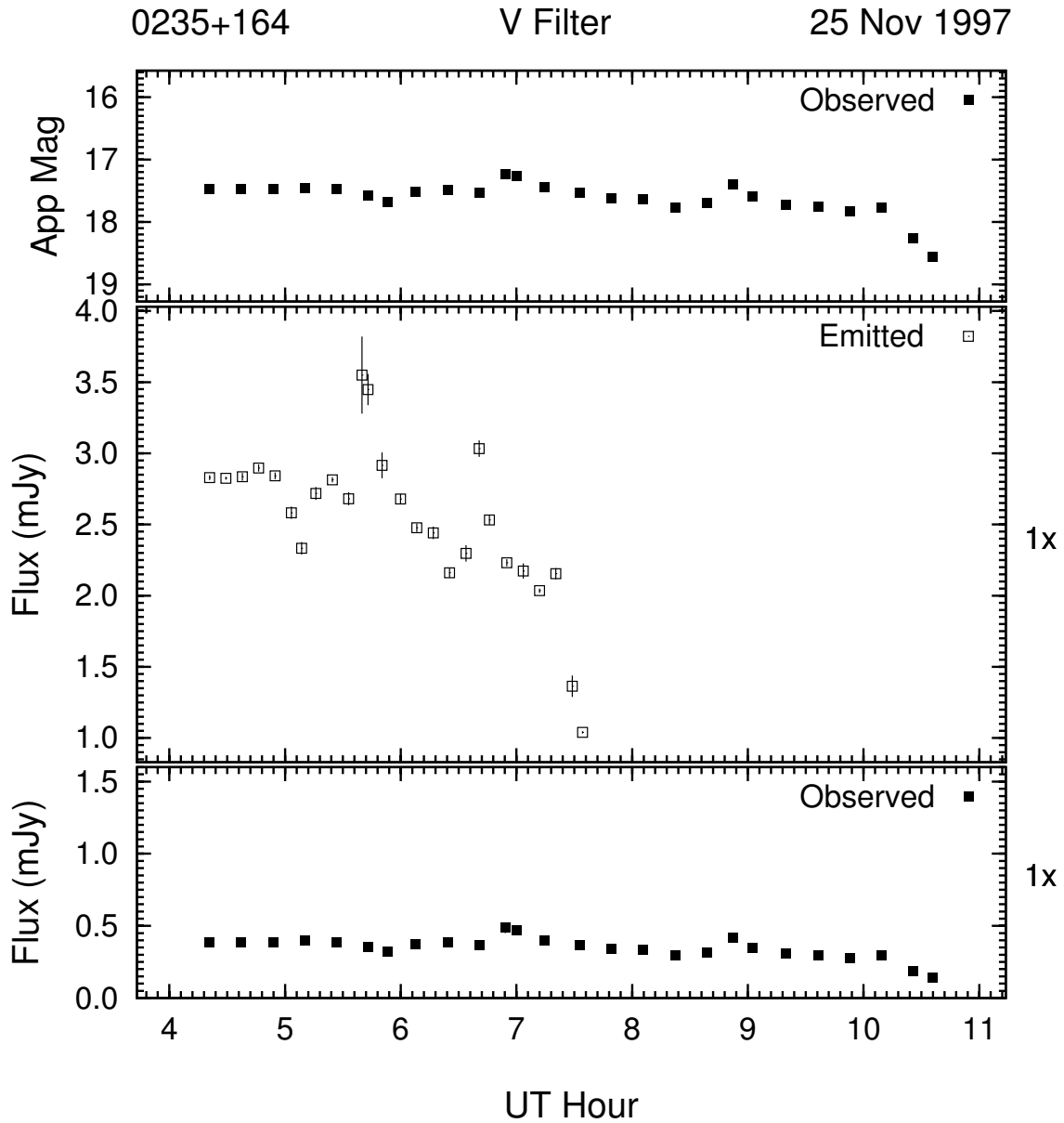


Figure 3.16: Example of the optical microvariability (V band) of 0235 + 164 on the night of 25 Nov 1997. This night's data was 4-point averaged to improve S/N .

dramatic of these is a flare of 0.5 mag with a duration of only 2 hours (i.e $6^h - 8^h$ UT). The final plot in this set, Figure 3.17, is the first example of a night during which no statistically significant microvariability was detected for AO 0235 + 16, but given the very short temporal

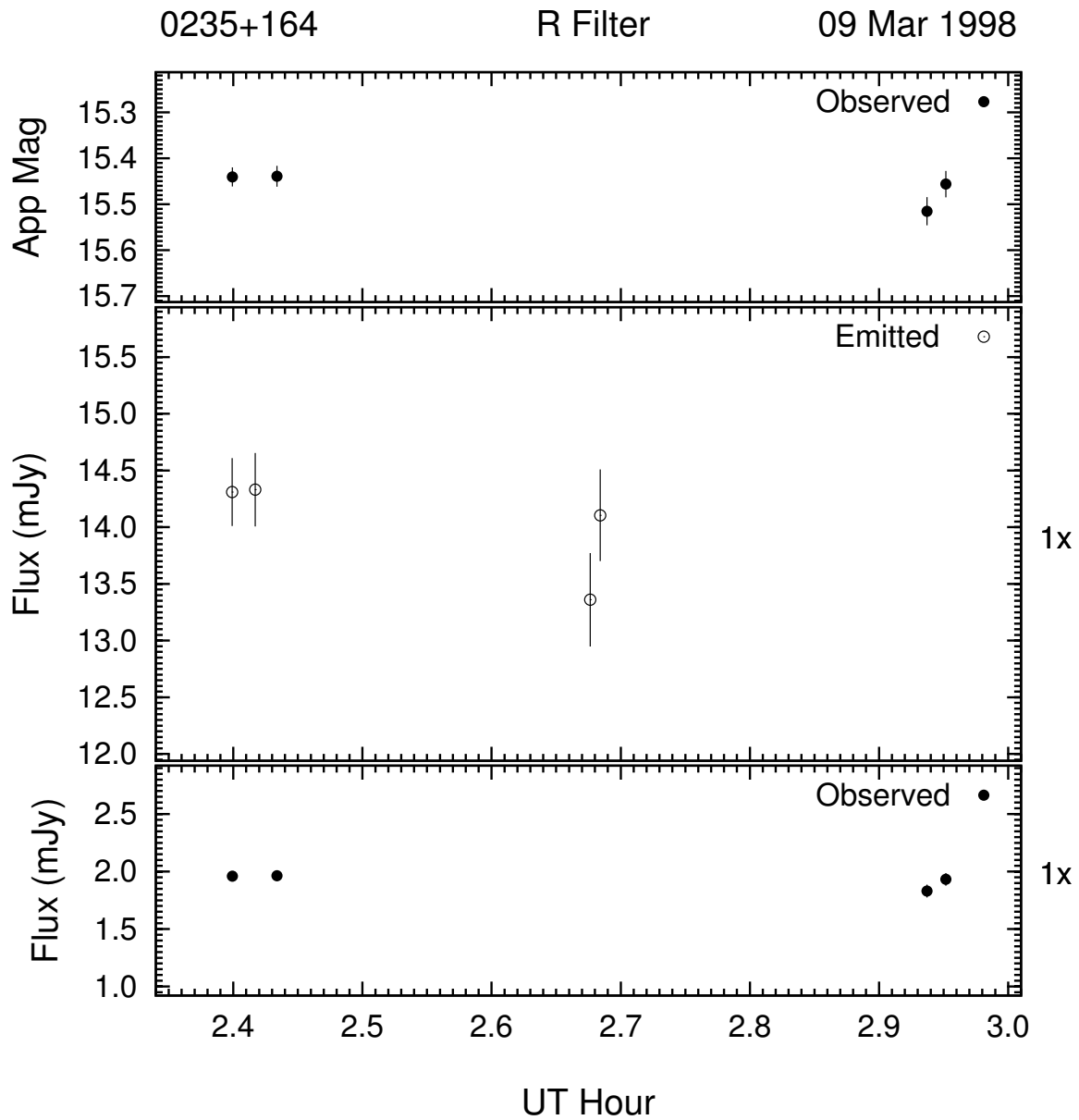


Figure 3.17: Example of the optical microvariability (R band) of 0235 + 164 on the night of 09 Mar 1998.

coverage, this is no surprise.

The next attempt to detect microvariability for AO 0235 + 16 occurred in late October of 1998. The light curves for two nights, 18 and 19 Oct 1998, are shown in Figures 3.18 and

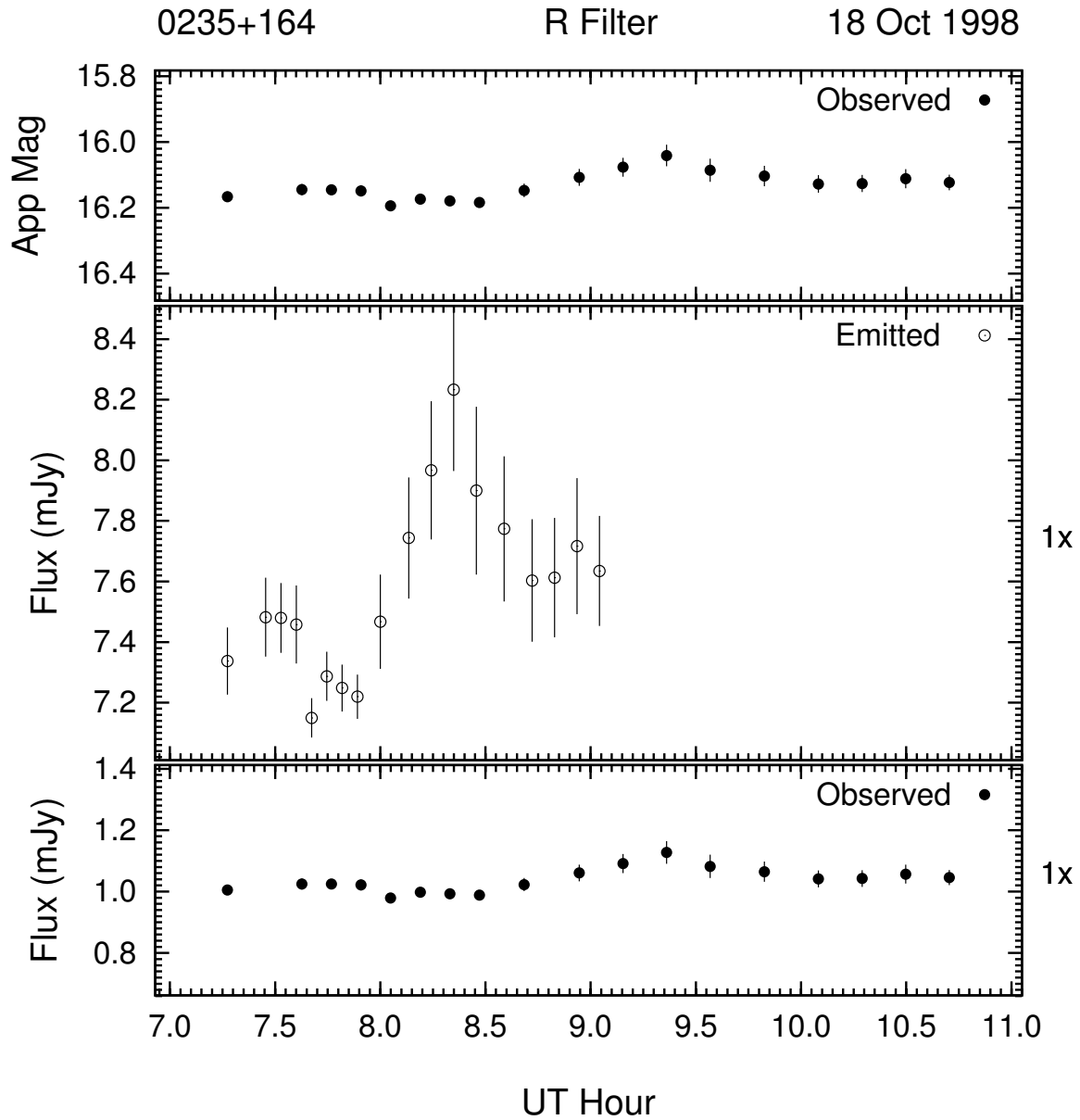


Figure 3.18: Example of the optical microvariability (R band) of 0235 + 164 on the night of 18 Oct 1998. This night's data was 4-point averaged to improve S/N .

3.19, respectively. On the first night a well defined event is detected with an amplitude of 0.15 mag (4.6σ) and a duration of only one hour. The following night is similar. The source exhibited complex variability with an amplitude of 0.2 mag.

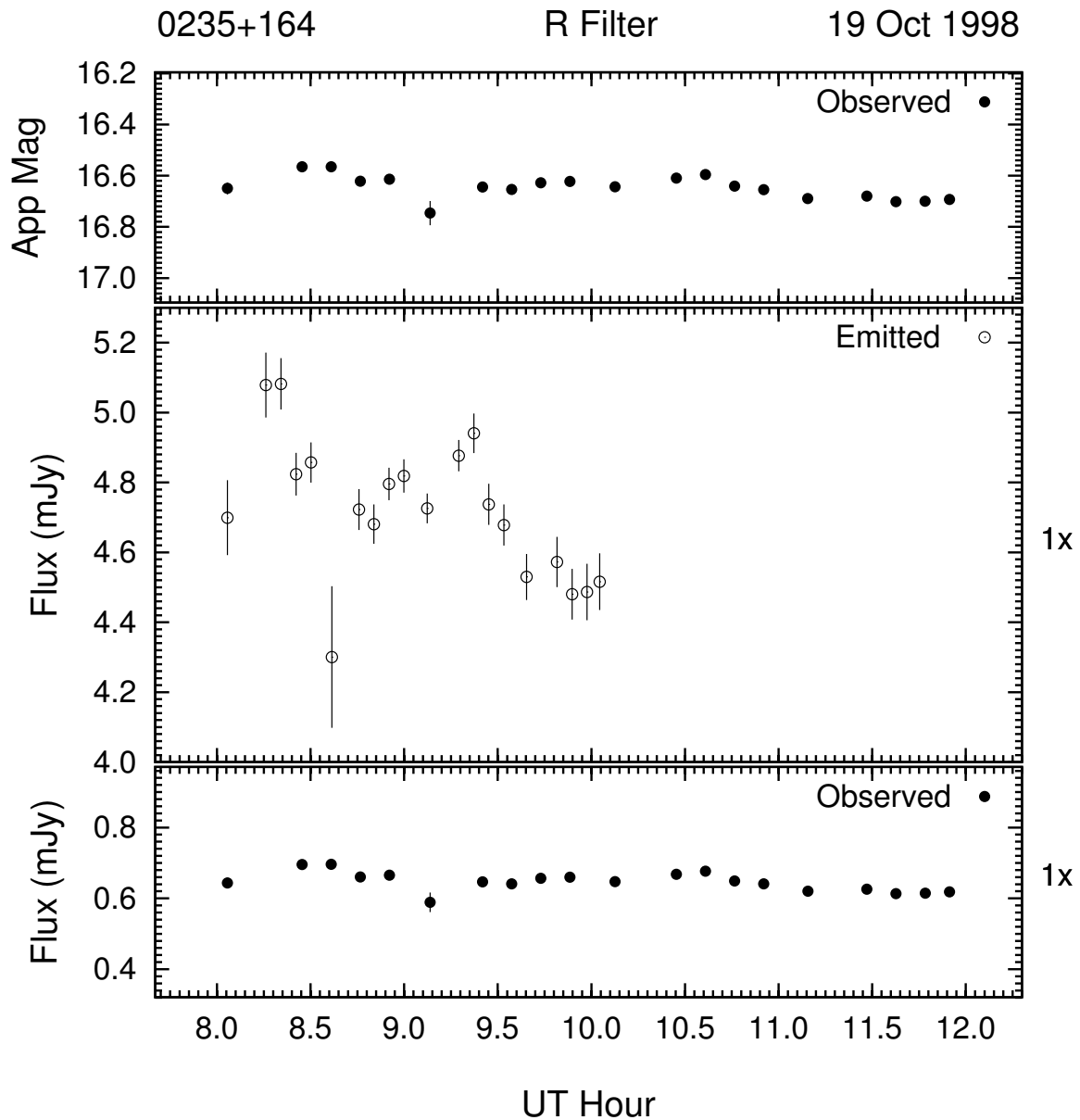


Figure 3.19: Example of the optical microvariability (R band) of 0235 + 164 on the night of 19 Oct 1998. This night's data was 3-point averaged to improve S/N .

The most recent attempt to detect microvariability for AO 0235 + 16 was in January and February of 2004. On the night of 13 Jan 2004 (Figure 3.20), AO 0235+16 exhibited complex variations superimposed on a longer term fading trend. At the time of these observations,

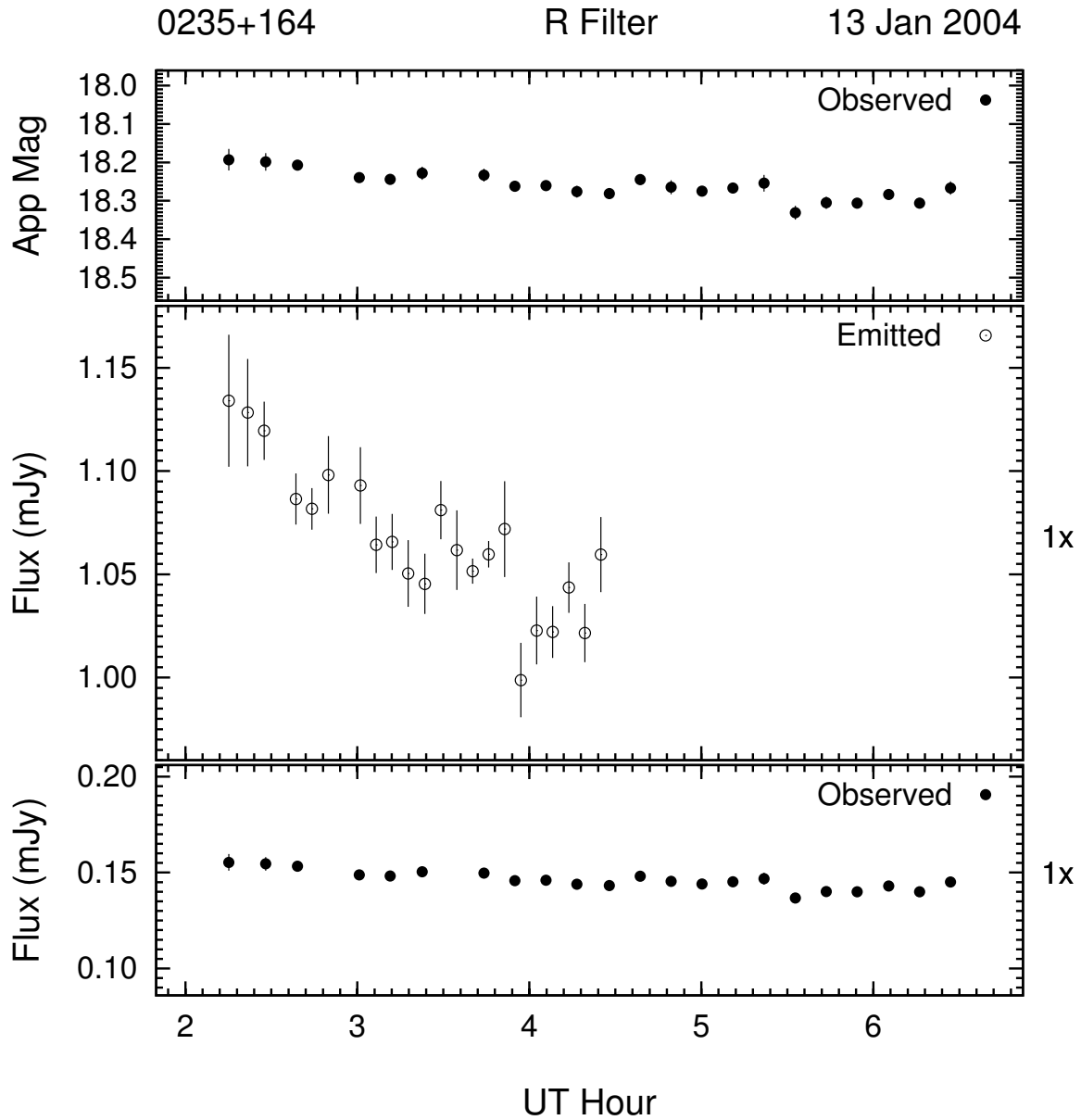


Figure 3.20: Example of the optical microvariability (R band) of 0235 + 164 on the night of 13 Jan 2004.

AO 0235+16 was more than 1.5 mag dimmer than at the end of 1998. On the night of 27 Jan 2004 and the next 5 nights, AO 0235 + 16 was observed to be fainter than $R = 17.5$. These observations were obtained with the 0.4m telescope. It is the low signal to noise from the

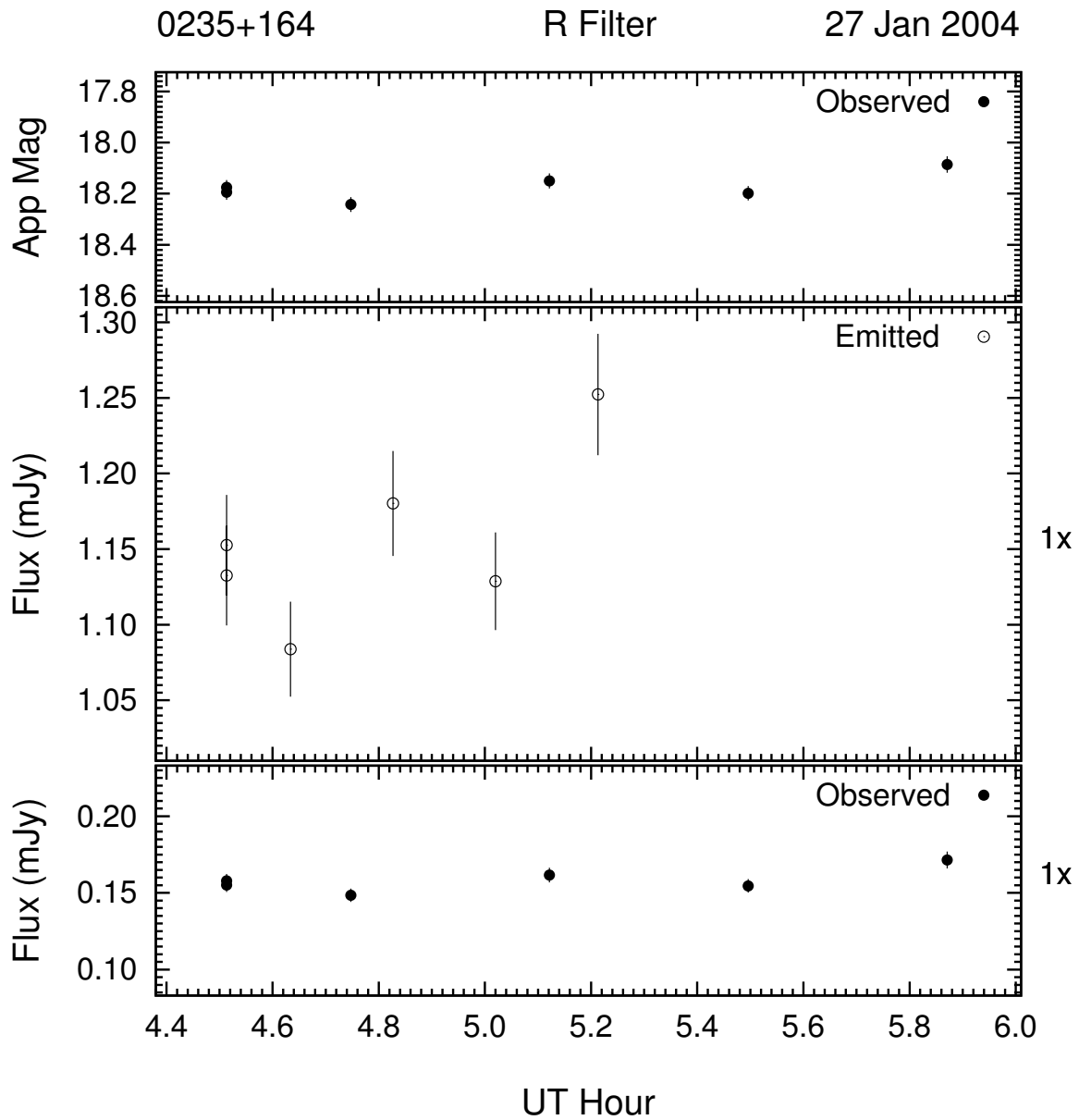


Figure 3.21: Example of the optical microvariability (R band) of 0235 + 164 on the night of 27 Jan 2004.

small collection aperture that caused the very poor errors in this set of data. In Figure 3.21, AO 0235 + 16 was still fainter than $R = 18$, and showed complex variability, but it should be noted that these variations are just significant at 2.9σ . The light curves for the next two

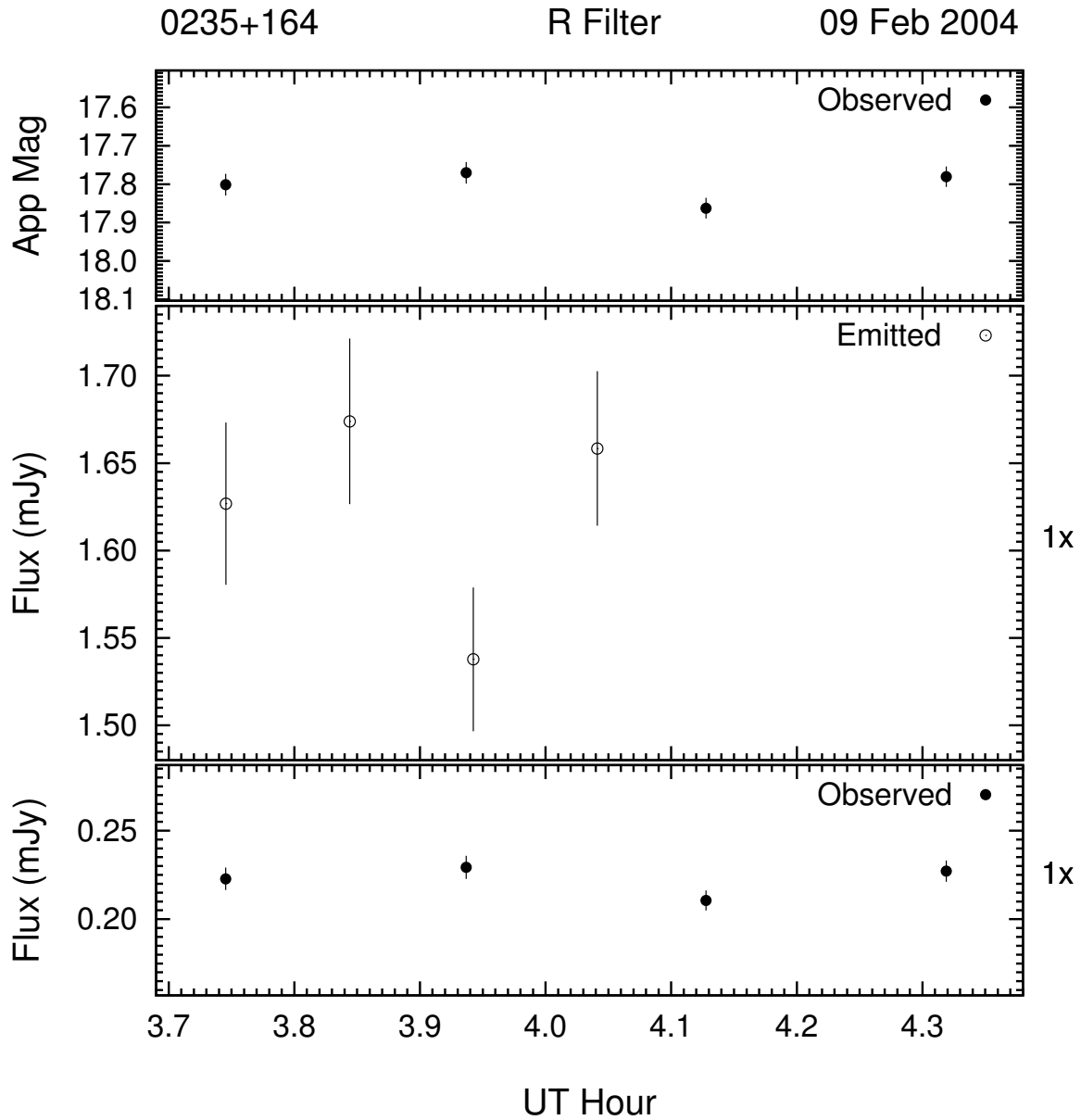


Figure 3.22: Example of the optical microvariability (R band) of 0235 + 164 on the night of 09 Feb 2004.

nights (Figures 3.22 and 3.23) show no statistically significant variability; although on the second night, AO 0235 + 16 is 0.2 mag brighter. On 12 Feb 2004, this trend changes. In Figure 3.24, the light curve shows a definite increase of 0.15 mag over 1 hour for the source.

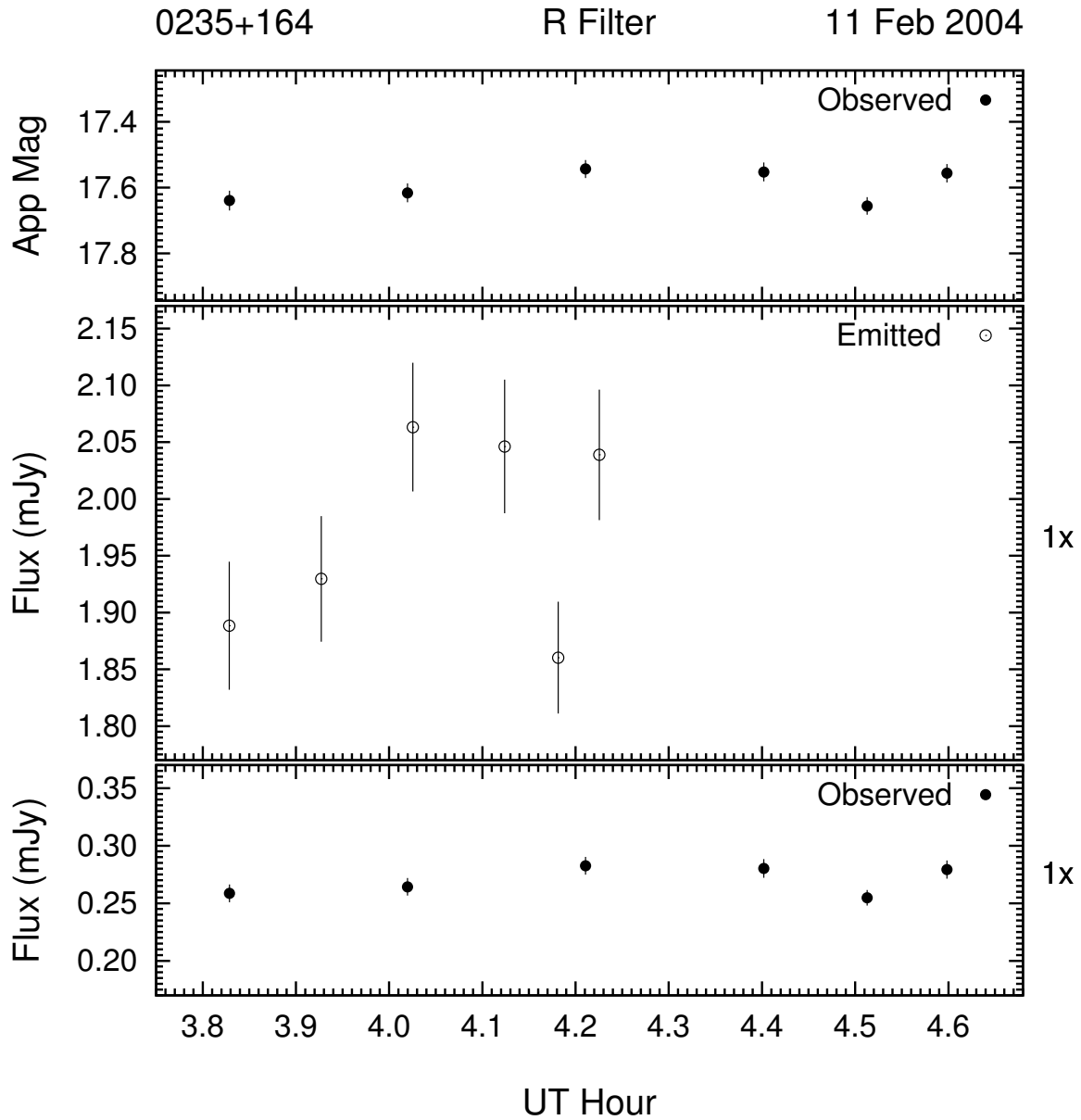


Figure 3.23: Example of the optical microvariability (R band) of 0235 + 164 on the night of 11 Feb 2004.

On the next night (Figure 3.25), AO 0235 + 16 showed a more dramatic drop in brightness of ~ 0.3 mag over 1.5 hours. The final night of observations, 16 Feb 2004, seen in Figure 3.26, the object showed complex variations that range over 0.3 mag.

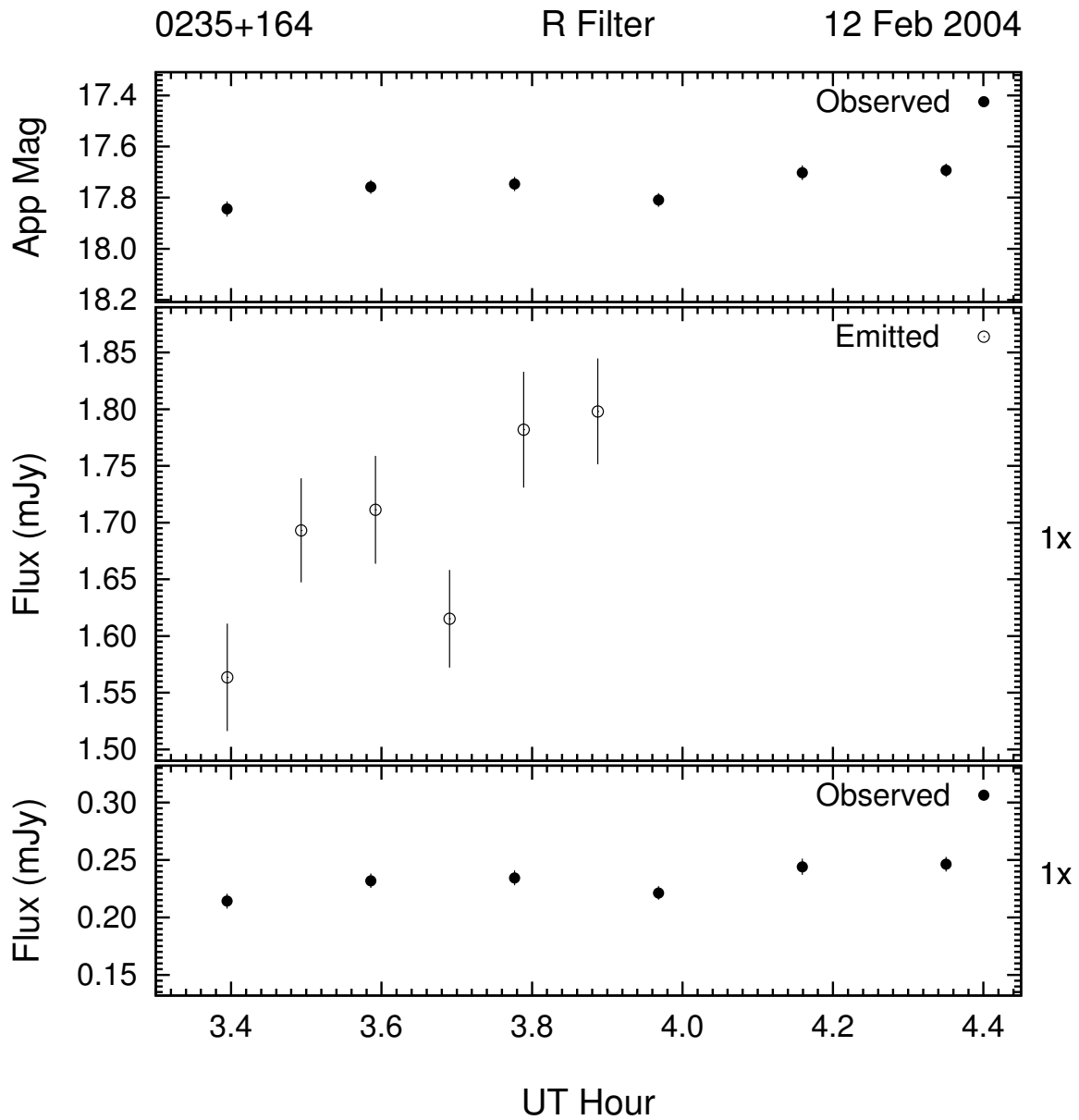


Figure 3.24: Example of the optical microvariability (R band) of 0235 + 164 on the night of 12 Feb 2004.

The enhancement of the amplitude of variation and the “time *undilation*” is clearly evident in the light curves of AO 0235 + 16 when comparing the lower, observed panels to the middle, emitted panels. With a redshift of 0.940, the amplitude of variation is enhanced

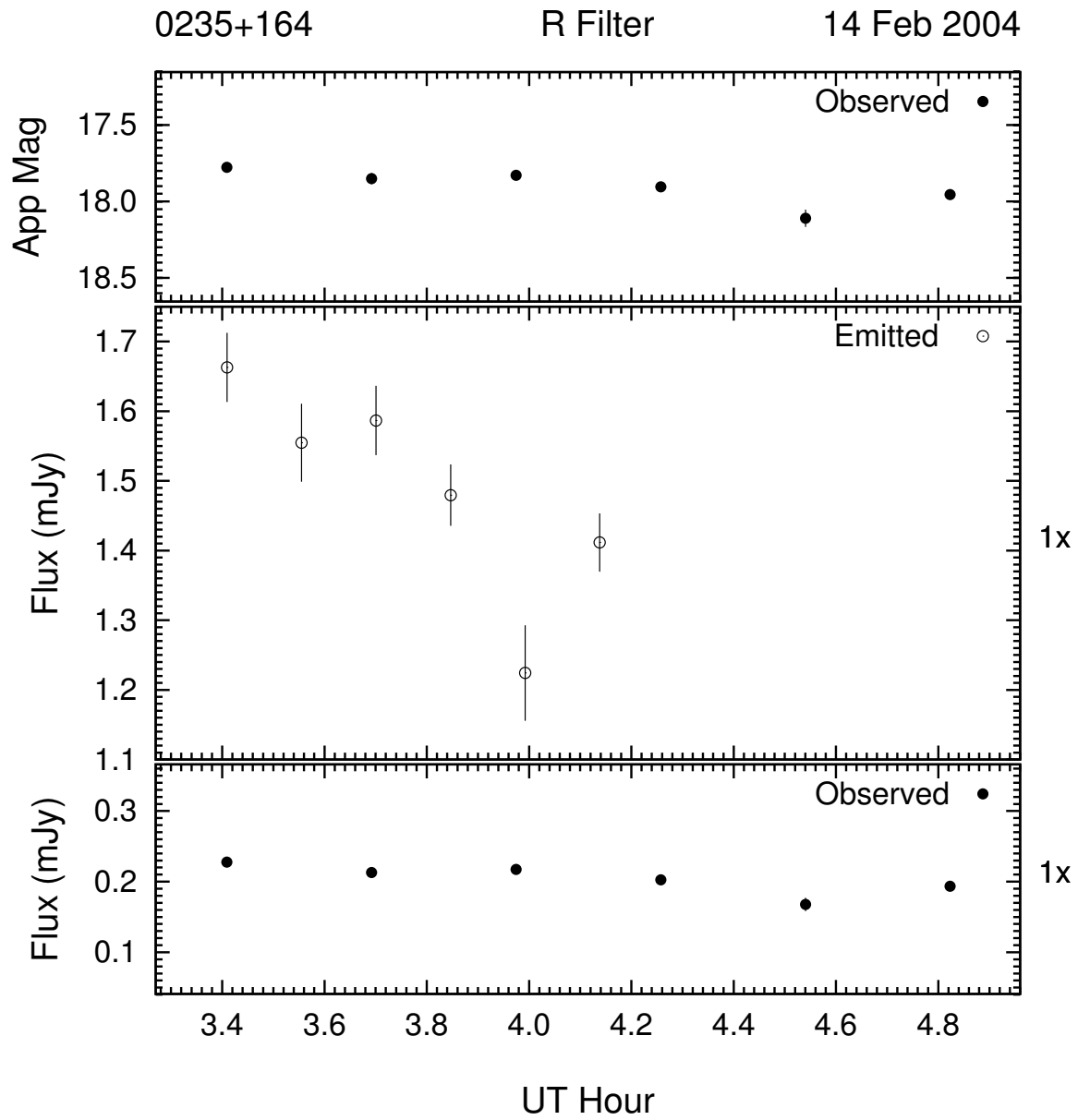


Figure 3.25: Example of the optical microvariability (R band) of 0235 + 164 on the night of 14 Feb 2004.

by a factor of 7.3 and the time-scale is compressed by almost 50%.

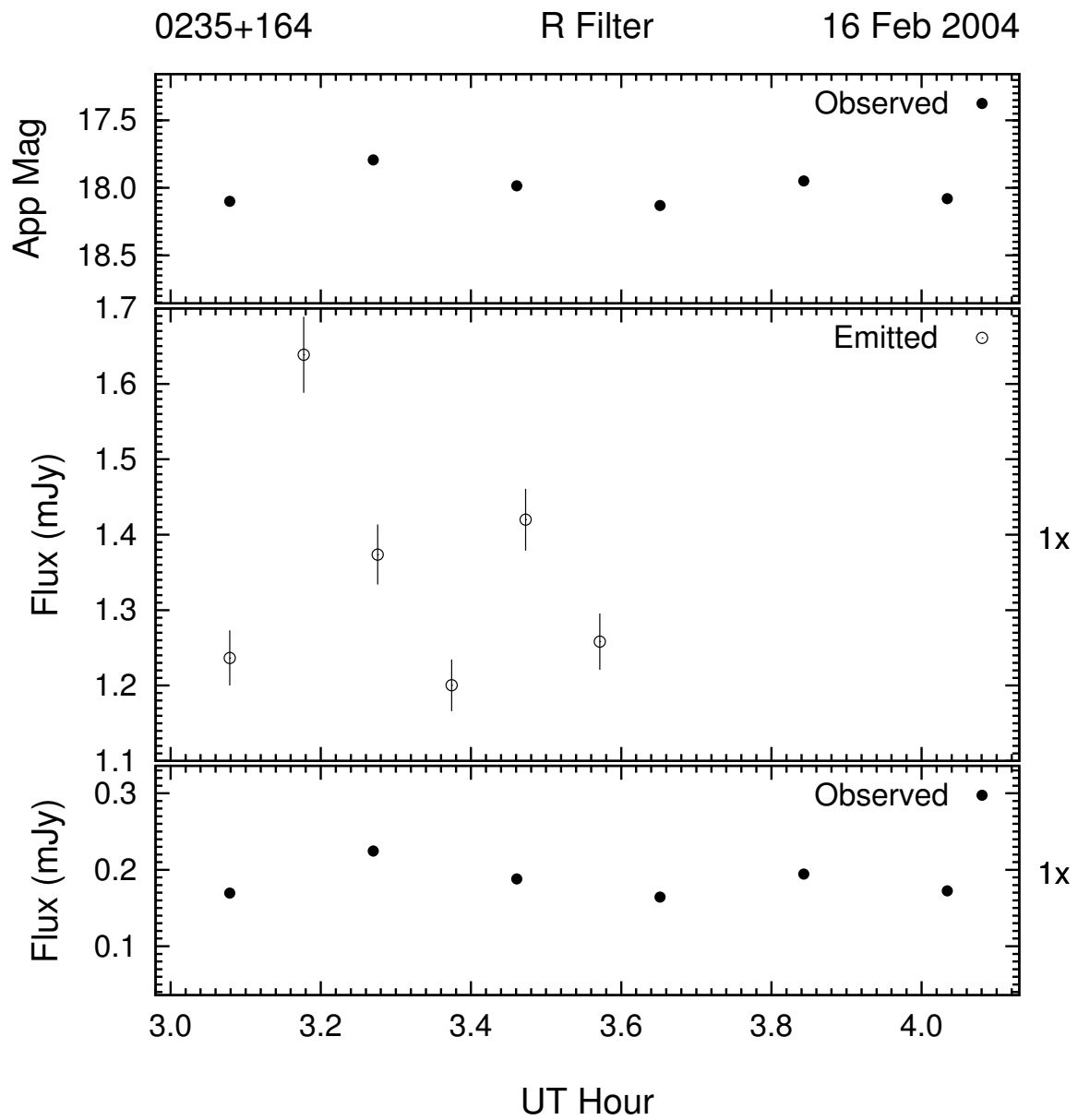


Figure 3.26: Example of the optical microvariability (R band) of 0235 + 164 on the night of 16 Feb 2004.

3.2.2 1156 + 295

The OVV Quasar 1156 + 295 (also known as PKS 1156 + 295 and 4C 29.45) has a redshift of 0.729 and has exhibited a variability amplitude range of just under 4.5 mag over the time that it has been monitored for this investigation (see Figure 3.27). The data used for 1156 + 295 is in the R band only, is taken from the PEGA archives, and covers a time period of just under 12 years. No SMARTS data exists for this object.

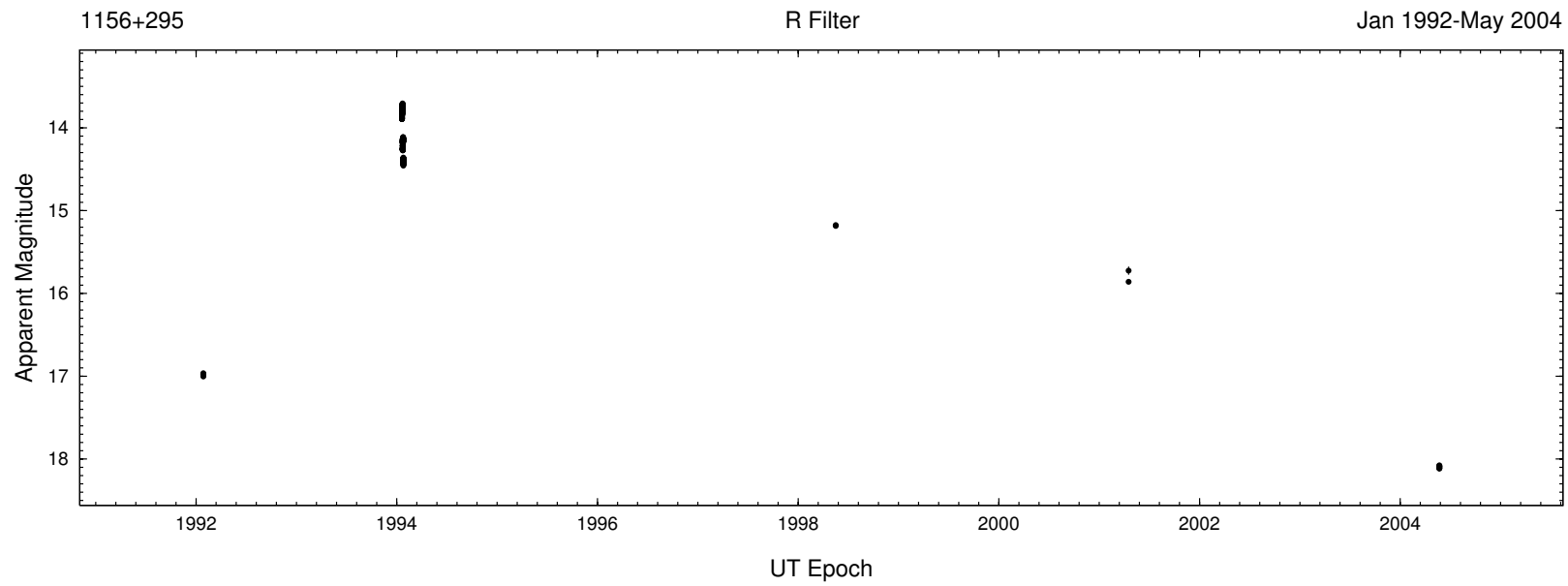


Figure 3.27: Complete R band light curve of 1156 + 295 from 1992 to 2004. The amplitude of variability is ~ 4.5 mag.

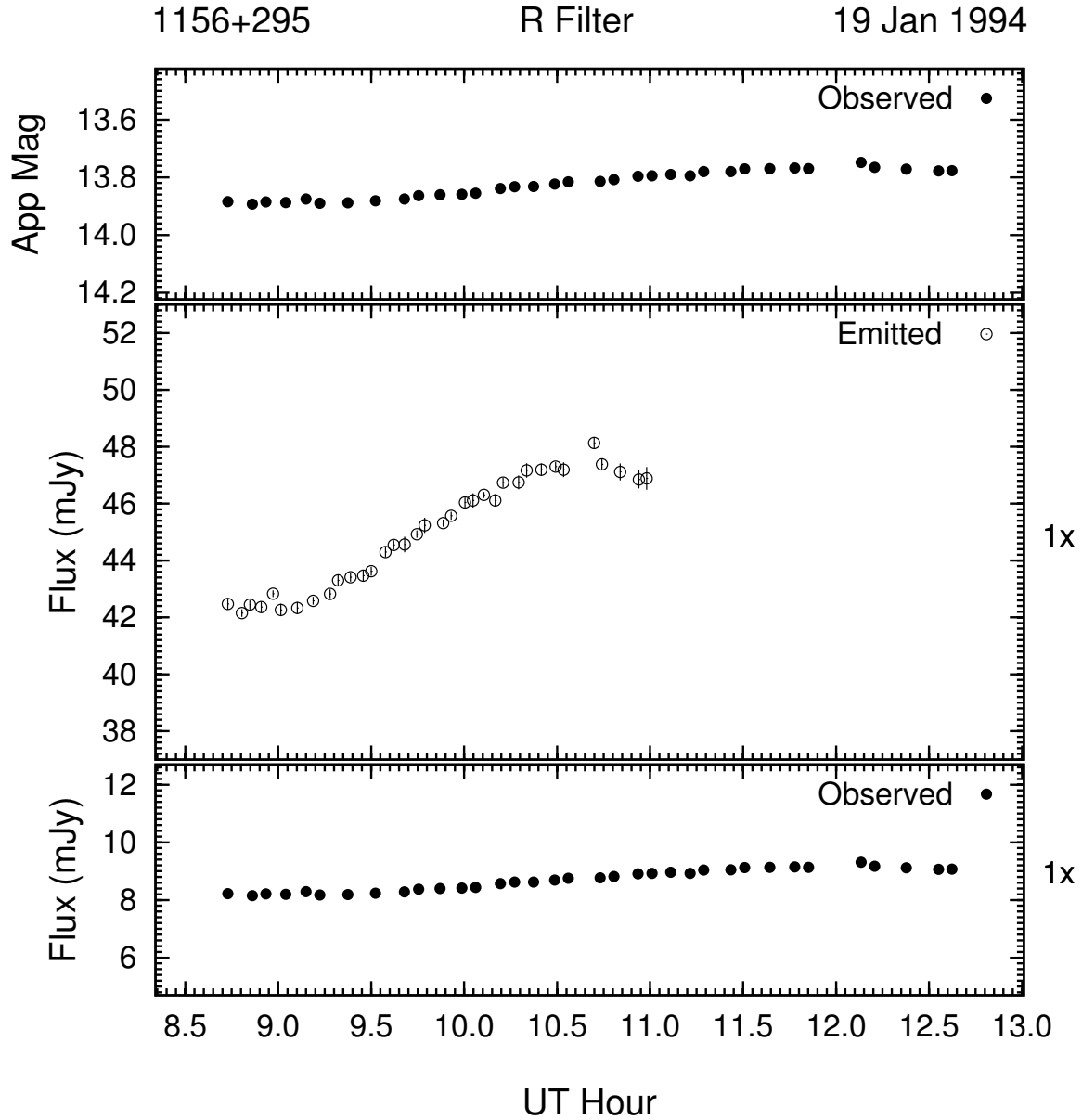


Figure 3.28: Example of the optical microvariability (R band) of 1156 + 295 on the night of 19 Jan 1994. This night's data was 2-point averaged to improve S/N .

The 12 year R band light curve of 1156 + 295 shown in Figure 3.27 is sparsely monitored, but exhibits a large range in brightness: well over 4 mag. The only microvariability searched for was during the 6 nights between 19 and 24 Jan 1994. The first light curve of this run

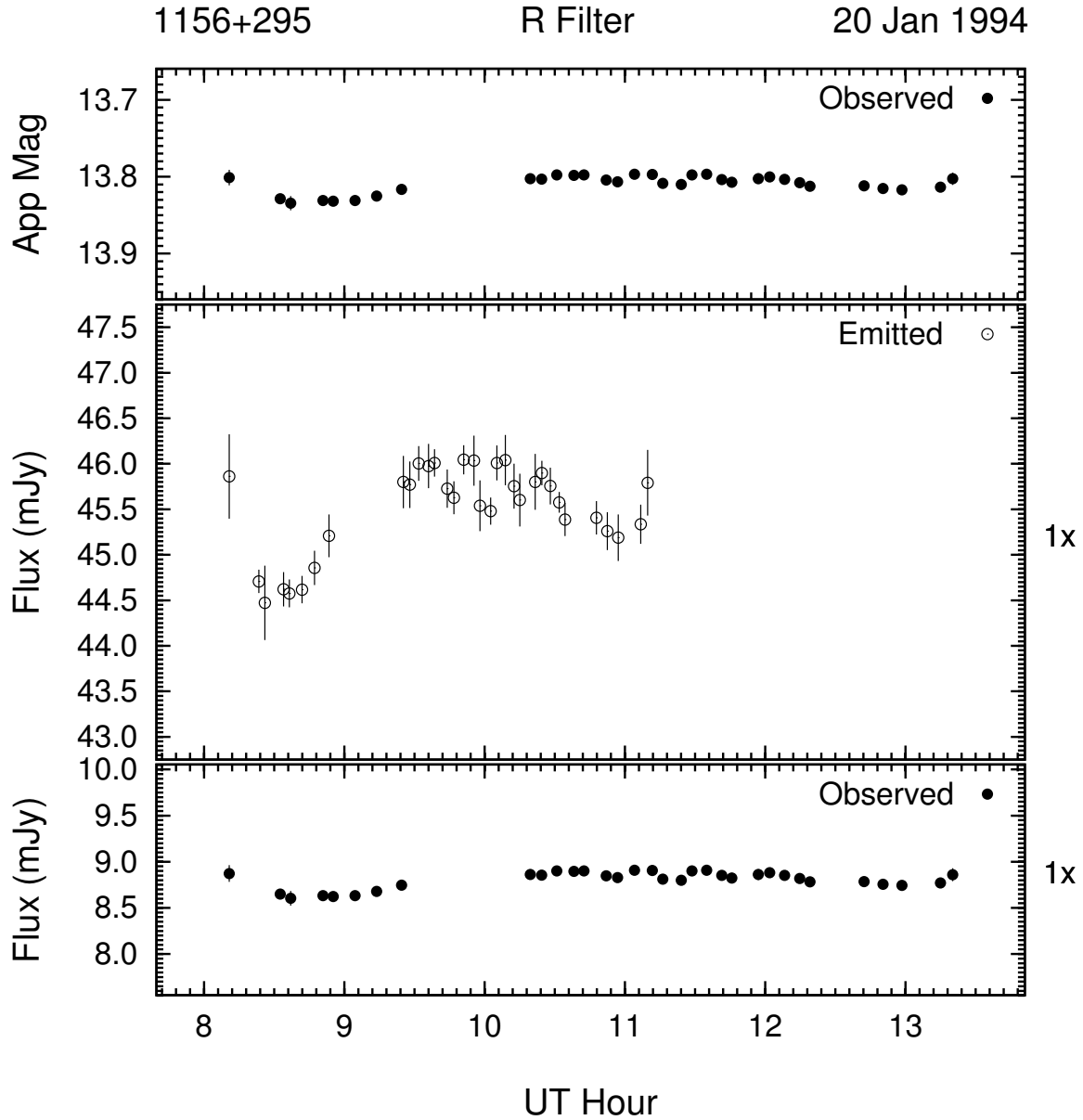


Figure 3.29: Example of the optical microvariability (R band) of 1156 + 295 on the night of 20 Jan 1994. This night's data was 2-point averaged to improve S/N .

(see Figure 3.28) shows that 1156 + 295 exhibited a modest brightening of 0.14 mag with a plateau at each end. This type of variation is common in BL Lac (§3.2.6), but only seen clearly in this light curve for 1156 + 295. The 28.0σ event covers roughly 3 hours. On the

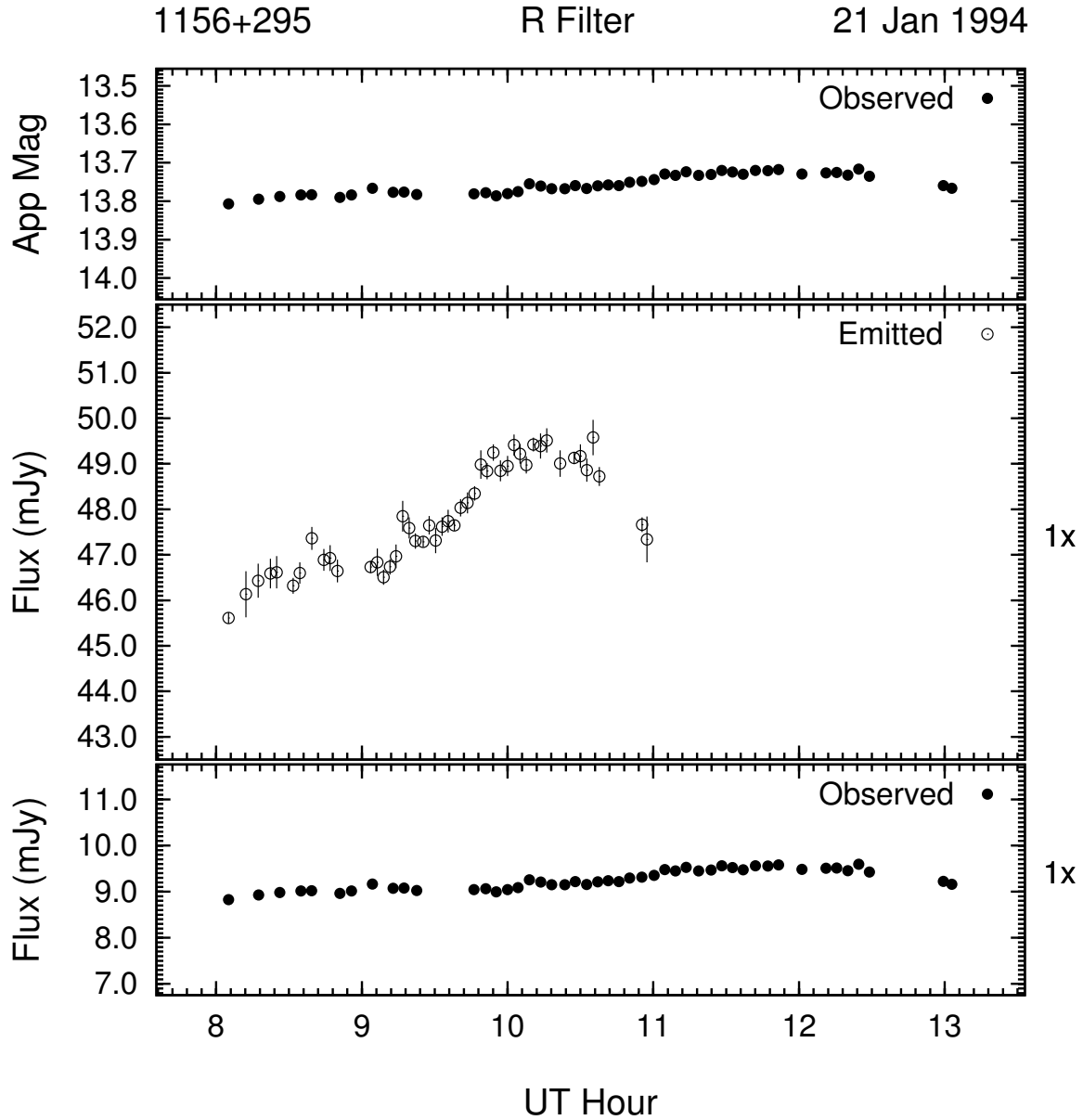


Figure 3.30: Example of the optical microvariability (R band) of 1156 + 295 on the night of 21 Jan 1994. This night's data was 2-point averaged to improve S/N .

next night, 20 Jan 1994, shown in Figure 3.29, 1156 + 295 started out at nearly the same level as the previous night, $R = 13.80$, and showed only a slight decrease then increase in brightness over 5 hours. There is no net change in the brightness at the end of this 5σ

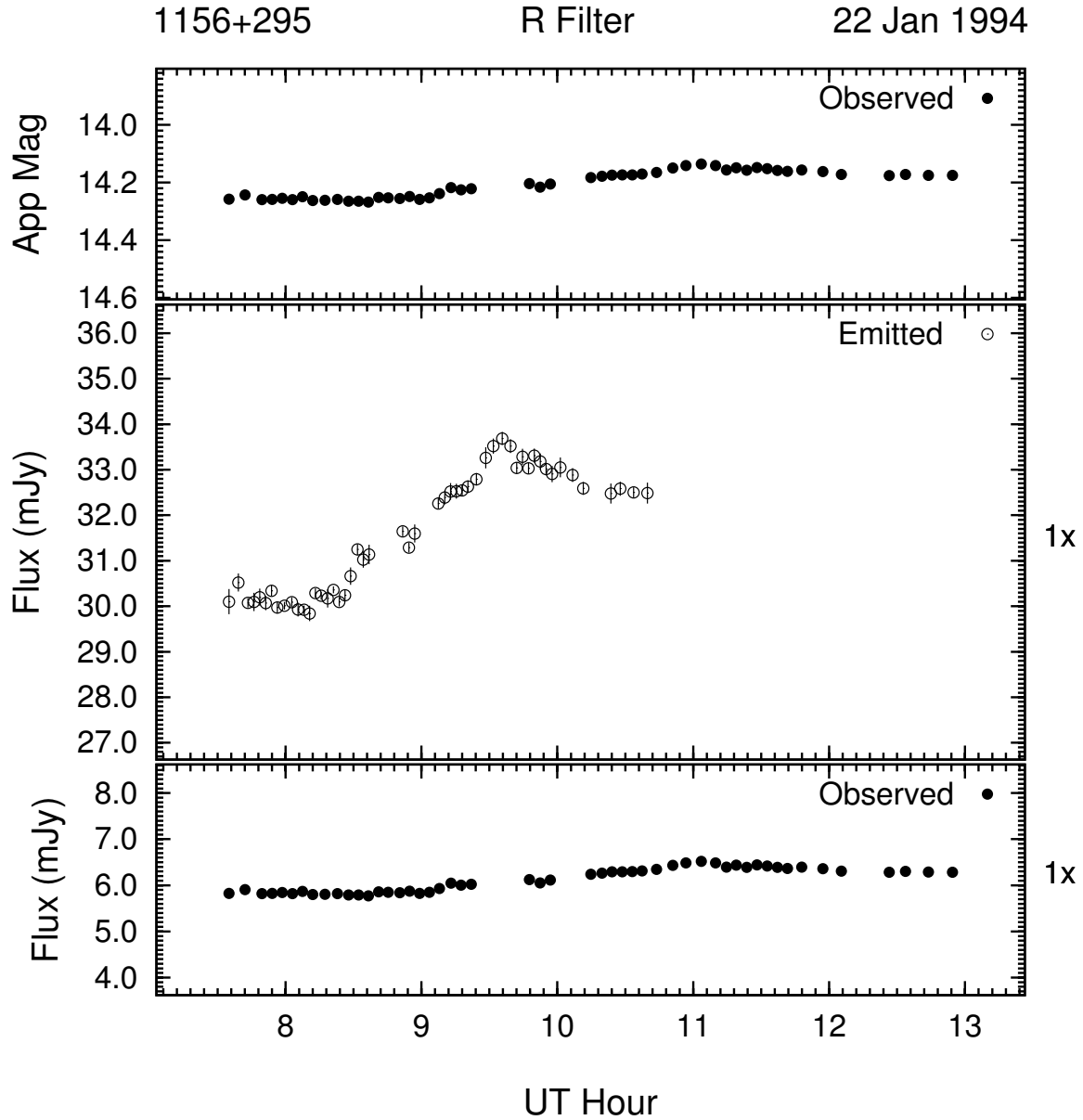


Figure 3.31: Example of the optical microvariability (R band) of 1156 + 295 on the night of 22 Jan 1994. This night's data was 2-point averaged to improve S/N .

event. The following night, shown in Figure 3.30, it picked up at the same level again, but brightened more significantly (14.5σ) to $R = 13.72$ in just 4 hours. 1156 + 295 then dimmed slightly to finish the night 0.05 mag fainter than at the peak. The second largest change in

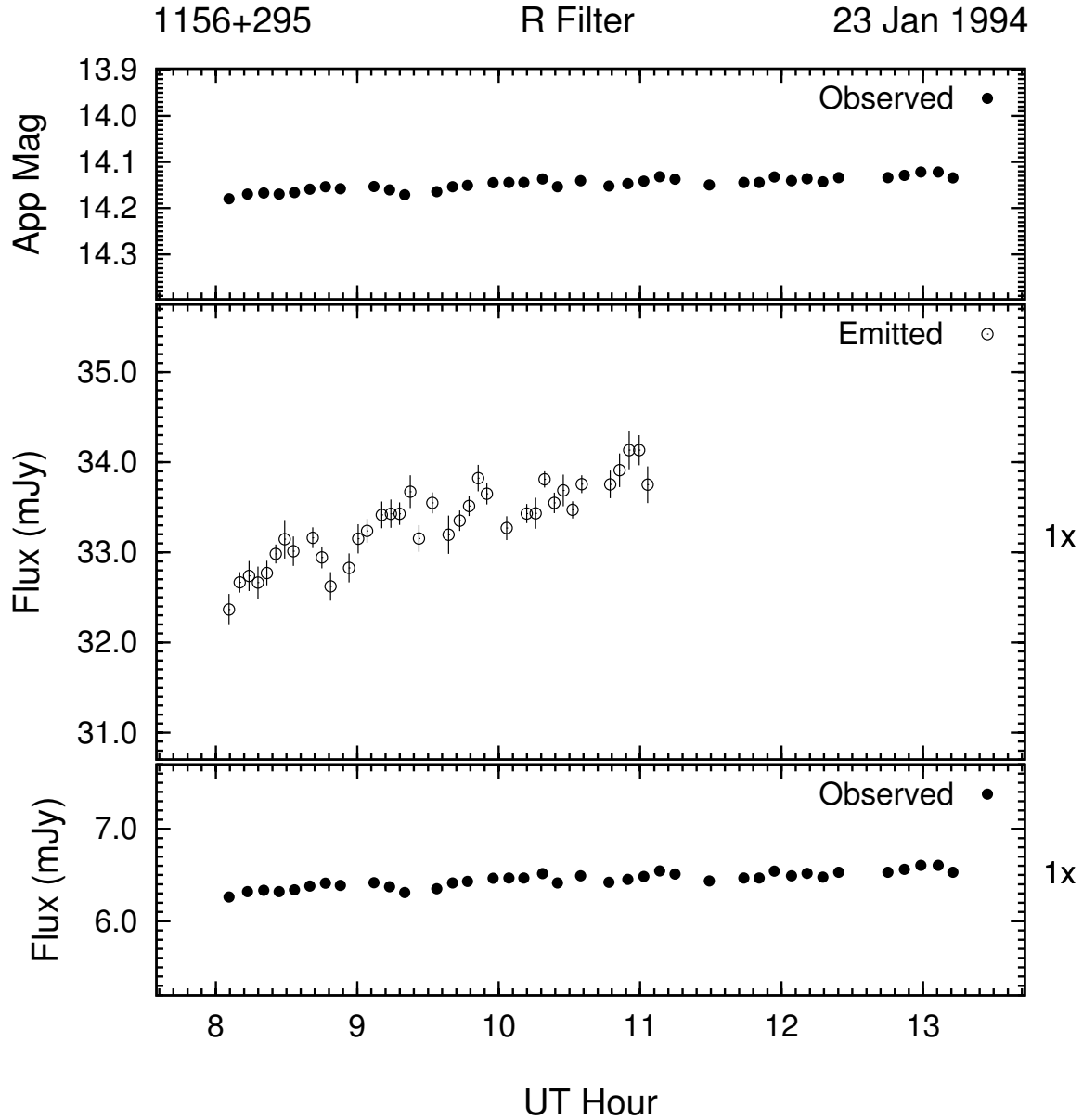


Figure 3.32: Example of the optical microvariability (R band) of 1156 + 295 on the night of 23 Jan 1994. This night's data was 2-point averaged to improve S/N .

brightness for 1156 + 295, 0.13 mag, can be seen on the night of 22 Jan 2004 in Figure 3.31.

It occurred after a 0.45 mag dimming from the previous night and has a character that is similar to the variability seen on 19 Jan, but is over a shorter temporal duration: only 2

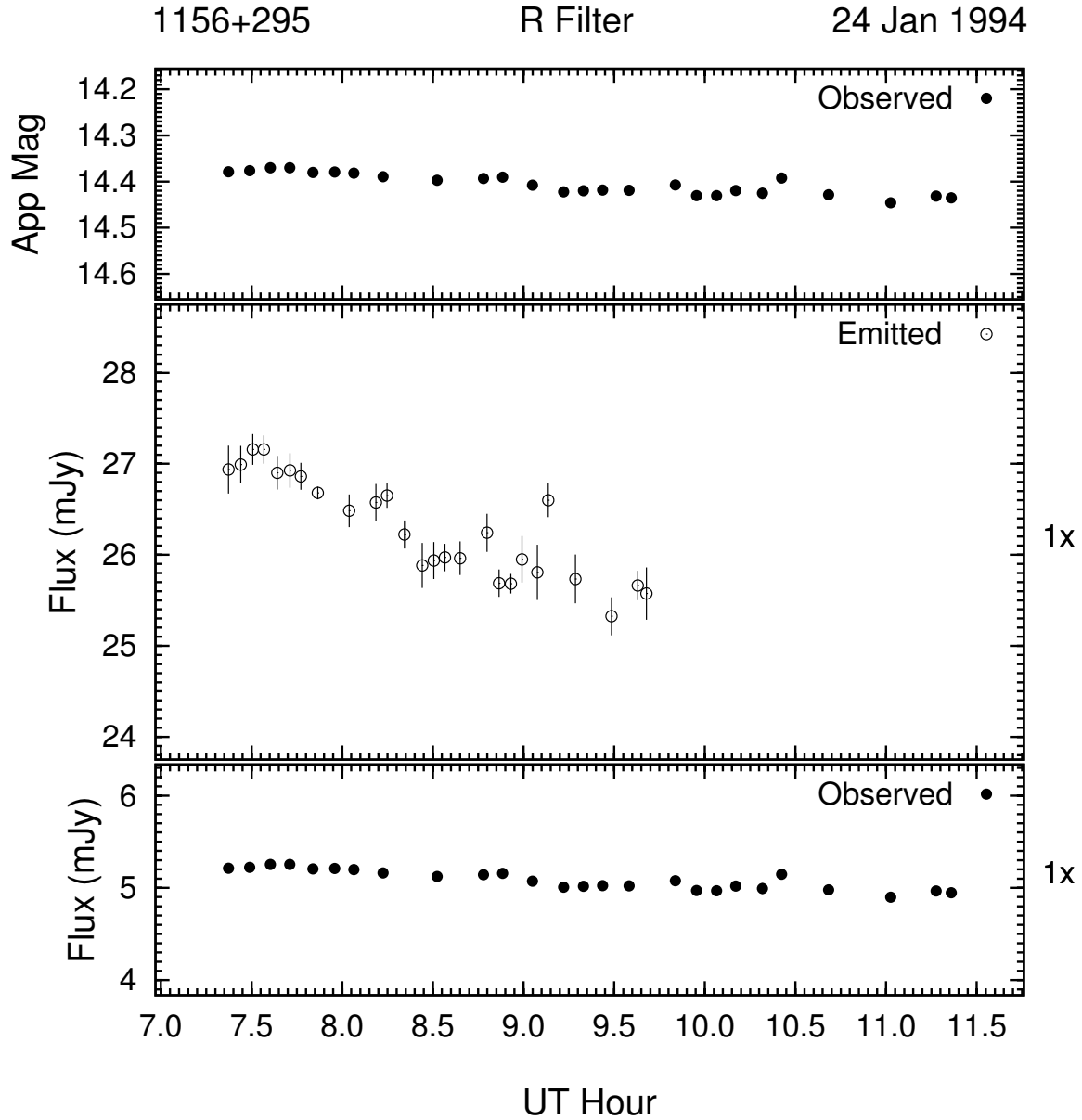


Figure 3.33: Example of the optical microvariability (R band) of 1156 + 295 on the night of 24 Jan 1994. This night's data was 2-point averaged to improve S/N .

hours. On the last two nights in this dataset (see Figures 3.32 and 3.33), 1156 + 295 showed similar variability characters: a brightening and a dimming trend respectively. The object then began the night of 23 Jan 1994 at about the same level where the previous night's light

curve left off, $R = 14.18$, and brightened 0.06 mag. On the night of 24 Jan 1994, 1156 + 295 starts 0.25 mag fainter and dimmed 0.08 mag further.

The emitted (rest frame) light curves of 1156 + 295 in the middle panel show similar enhancement of the amplitude of variation to those of AO 0235+16. The magnitude of the enhancement is ~ 5.2 due to a redshift of 0.729, and the time axis is *undilated* by just over 40%.

3.2.3 1622 – 297

The OVV quasar 1622 – 297 (also known as PKS 1622 – 297) has a redshift of 0.815 and has exhibited a variability amplitude range of approximately 4 mag over the time that it has been monitored for this investigation (see Figure 3.34). The data used for 1622 – 297 was taken from the PEGA archives (R band only), and covers a time period of just under 8 years. SMARTS data exists for this object and is exhibited in detail in §4.1.7.

The long term light curve of 1622 – 297 shows a general dimming trend with a peak of $R = 15.6$ in early 1997 and a low of $R = 19.4$ at the beginning of the SMARTS data in early 2003. Observations are somewhat sporadic, however, with most of them being high time density samples occurring over the course of one or several nights.

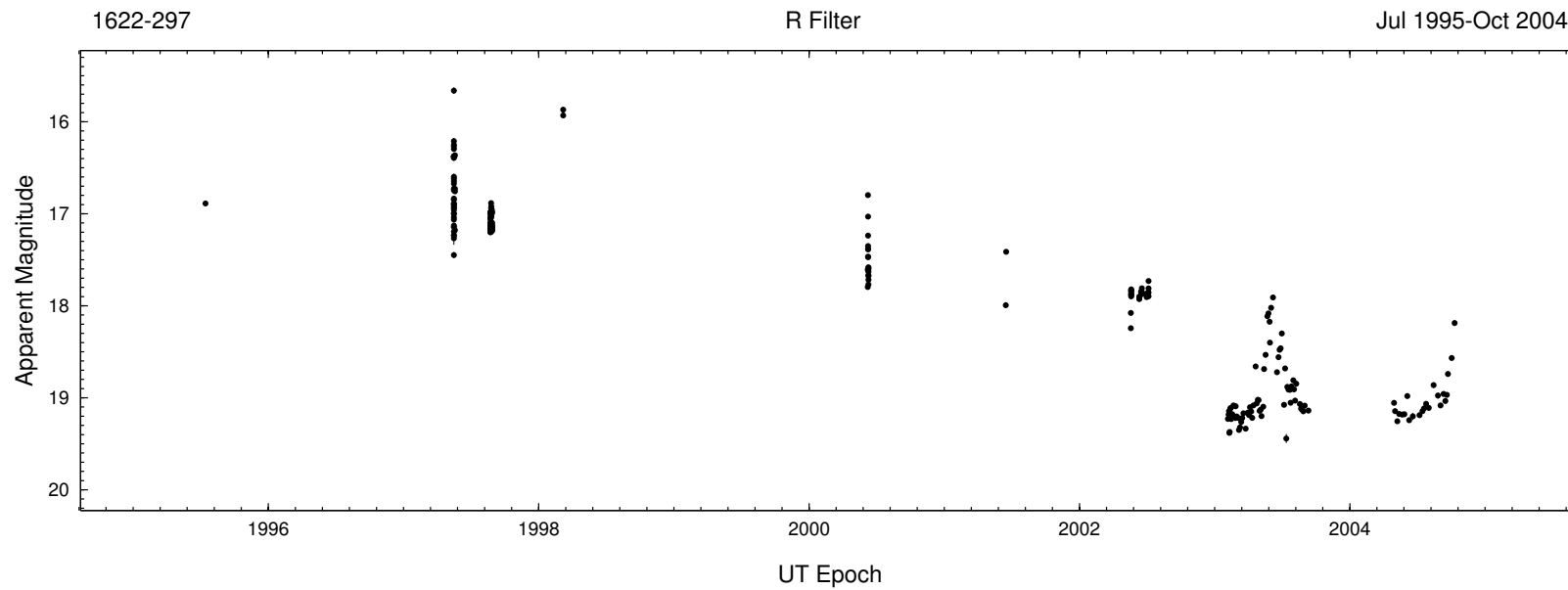


Figure 3.34: Complete R band light curve of 1622 – 297 from 1995 to 2004. The amplitude of variability is ~ 4 mag.

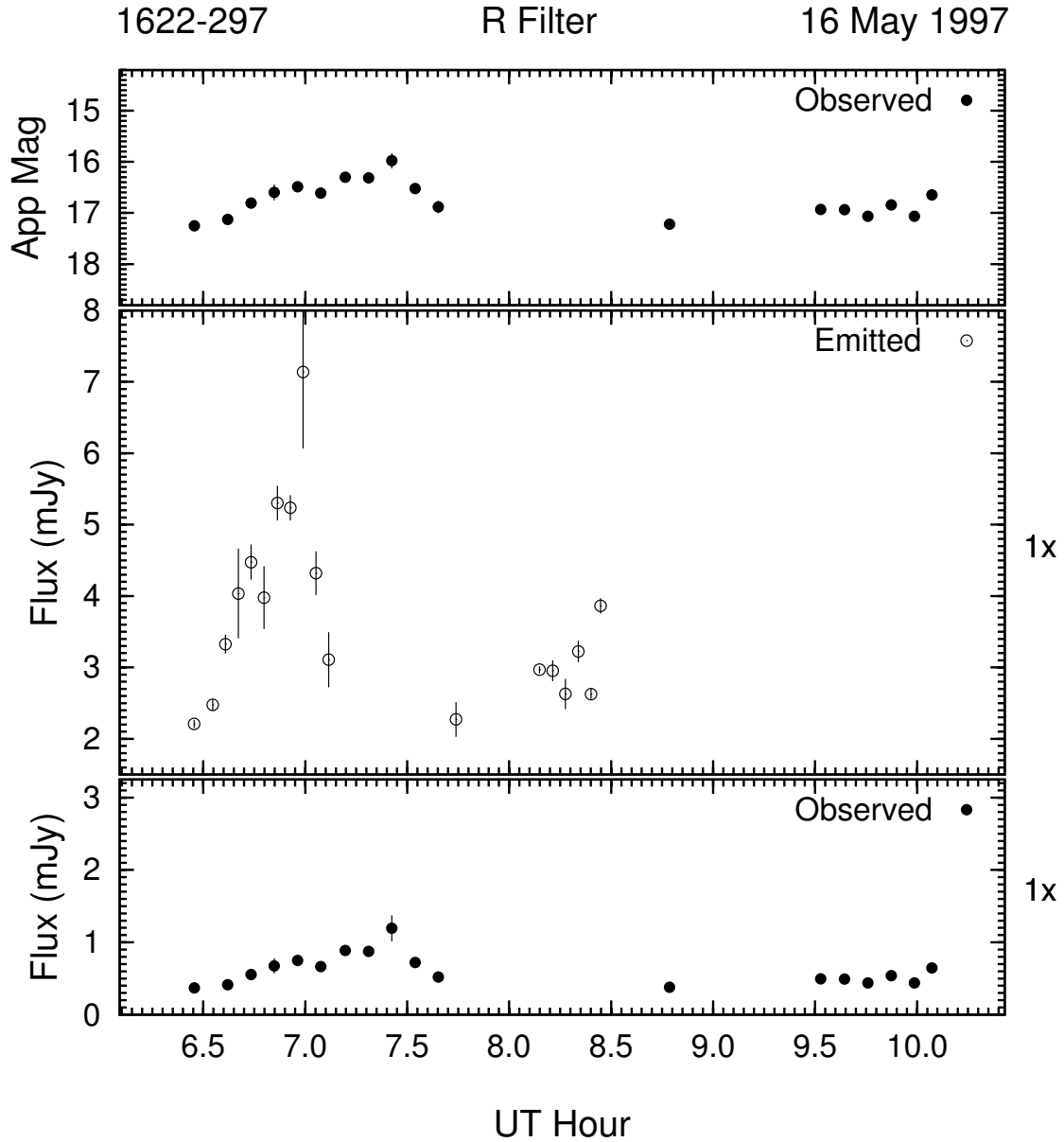


Figure 3.35: Example of the optical microvariability (R band) of 1622 – 297 on the night of 16 May 1997. This night's data was 2-point averaged to improve S/N .

The microvariability observations for 1622 – 297 began on the night of 16 May 1997 (Figure 3.35). On this night, 1622 – 297 exhibited a brightness change of ~ 1.2 mag (only 16.6σ given the large average error of ± 0.07 mag). This light curve exhibits an increasing

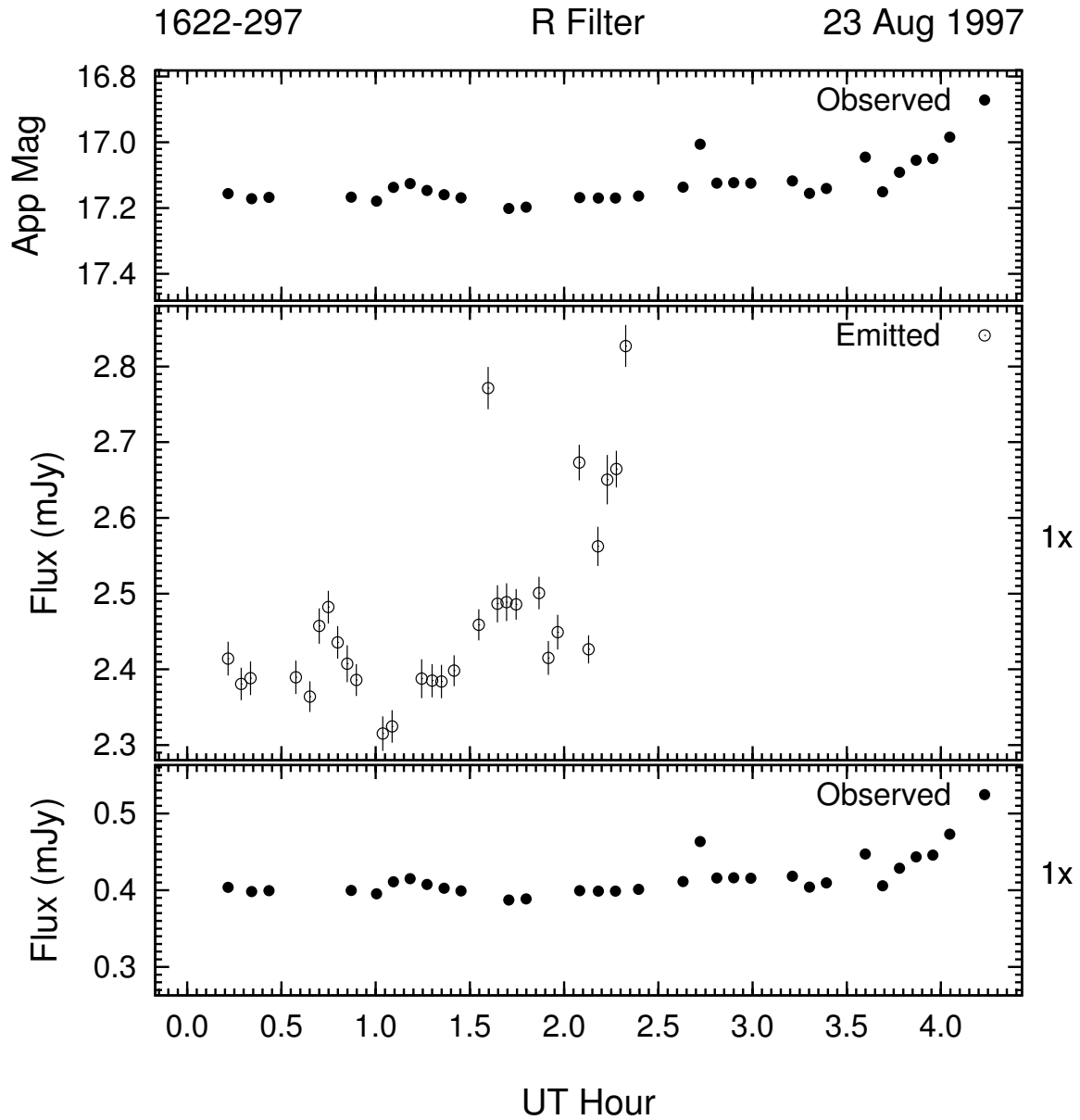


Figure 3.36: Example of the optical microvariability (R band) of 1622 – 297 on the night of 23 Aug 1997.

trend in brightness over 1 hour of ~ 1.2 mag followed by a dimming of ~ 1 mag over the next 0.5 hour. Following this extreme flare, 1622 – 297 showed another substantial increase in brightness over 2 hours of only 0.7 mag.

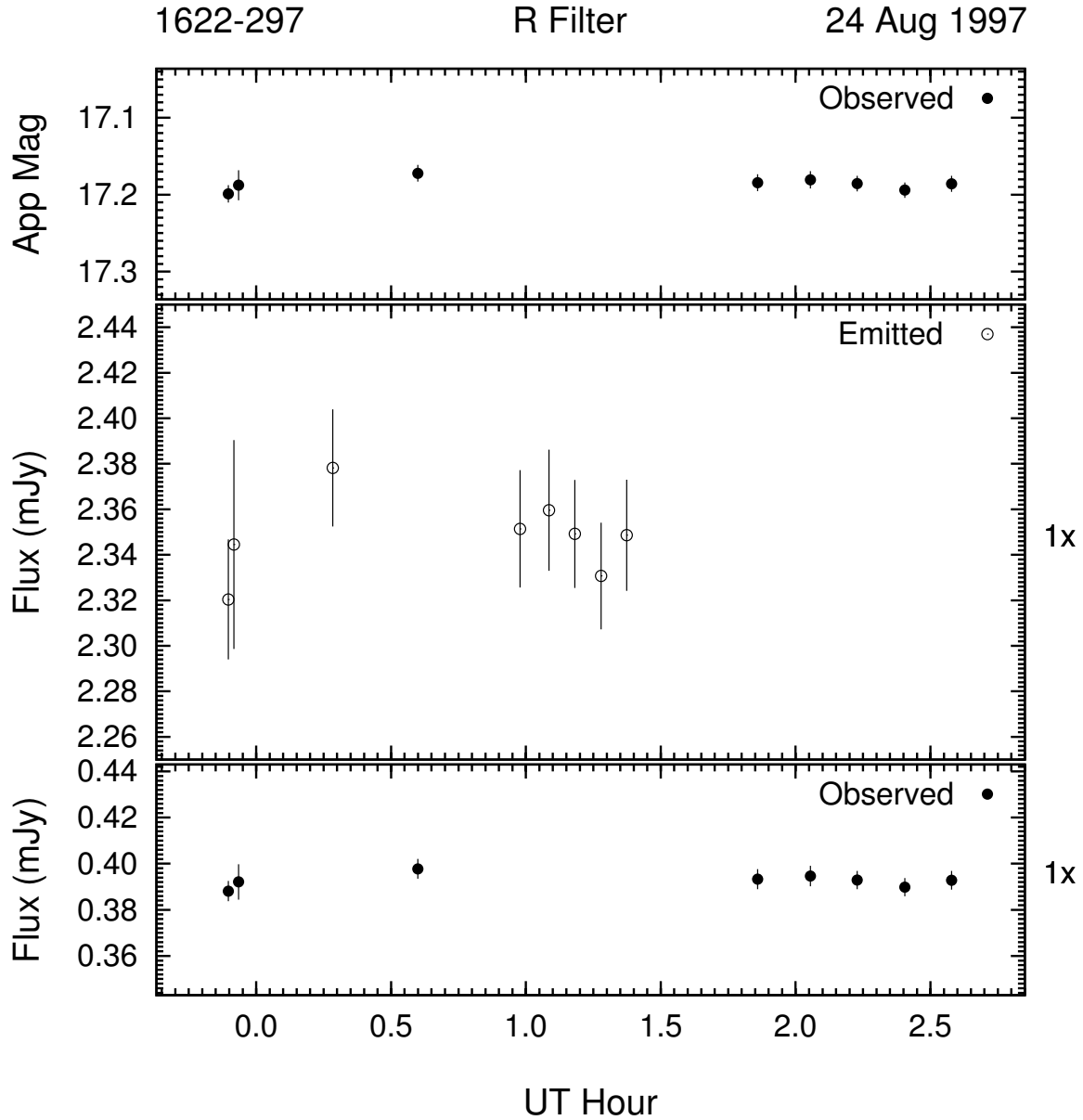


Figure 3.37: Example of the optical microvariability (R band) of 1622 – 297 on the night of 24 Aug 1997.

1622–297 is then monitored for 5 consecutive days in late August of 1997 shown in Figures 3.36 through 3.40. On the night of 23 Aug 1997, 1622 – 297 exhibited a brightness change of 0.2 mag ($\sigma_{20.2}$) after a slight brightening. The brightening trend lasted approximately

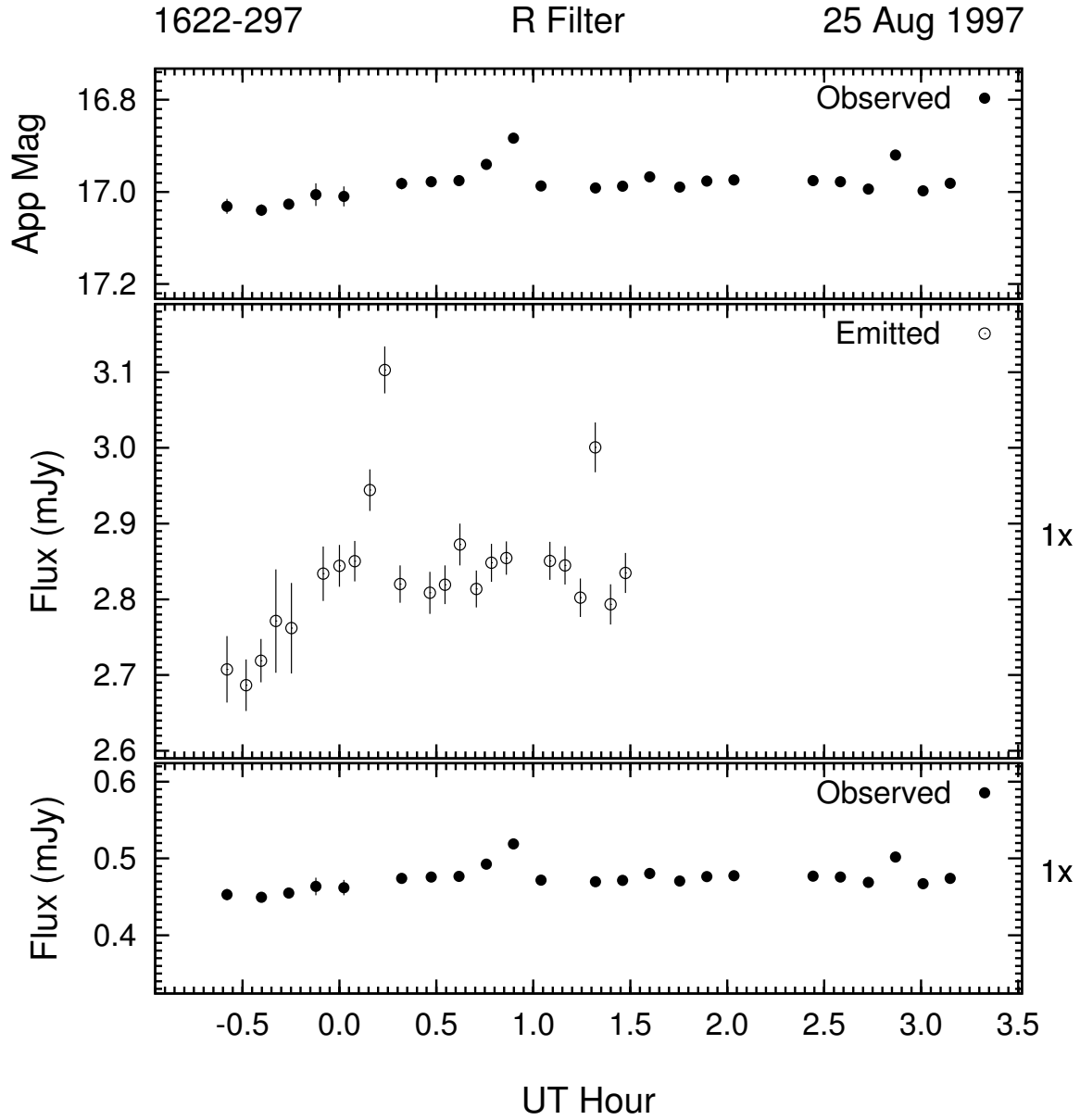


Figure 3.38: Example of the optical microvariability (R band) of 1622 – 297 on the night of 25 Aug 1997.

3.5 hours, ending in a moderate increase in brightness over only 0.5 hour. The average level for this first night is $R \simeq 17.1$. The following night, shown in Figure 3.37 (24 Aug 1997), 1622 – 297 exhibited no statistically significant microvariability, but dimmed 0.2 mag from

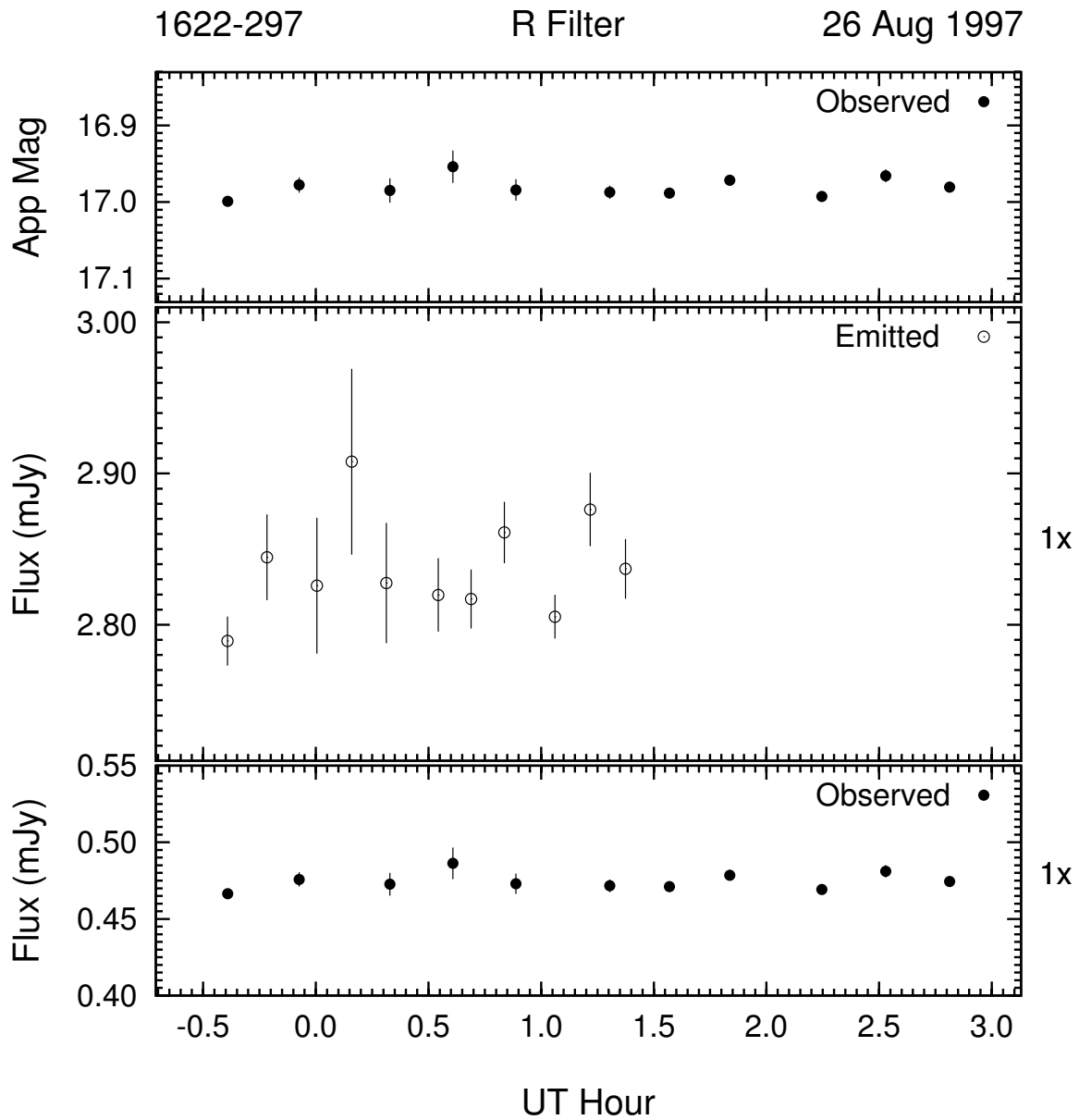


Figure 3.39: Example of the optical microvariability (R band) of 1622 – 297 on the night of 26 Aug 1997. This night's data was 2-point averaged to improve S/N .

the last level of the previous night. On the following night (25 Aug 1997, Figure 3.38), 1622 – 297 started almost 0.2 mag brighter and showed only two statistically significant events superimposed on a gentle rise in brightness. Figure 3.39 shows 1622 – 297 on the

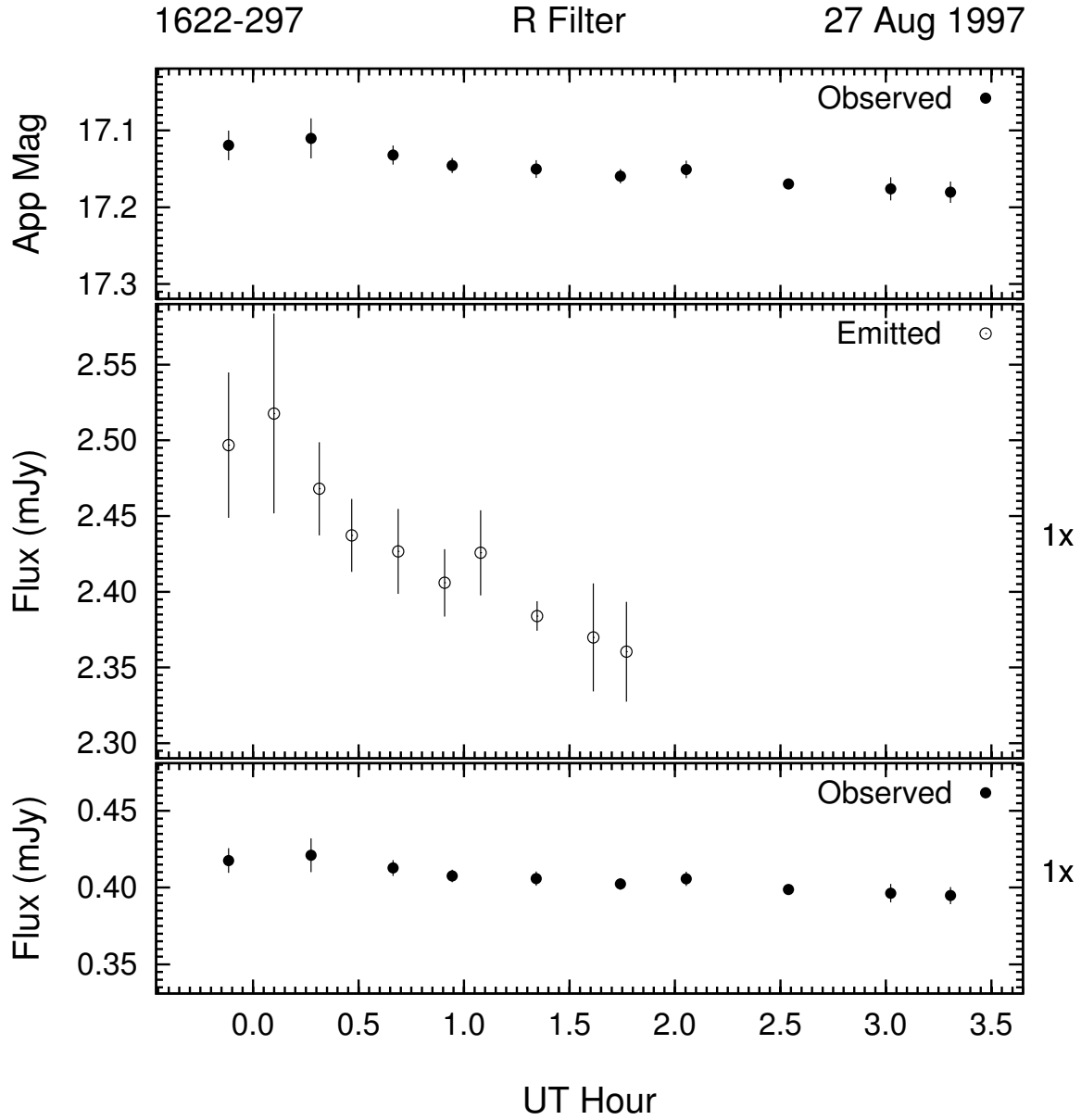


Figure 3.40: Example of the optical microvariability (R band) of 1622 – 297 on the night of 27 Aug 1997. This night's data was 2-point averaged to improve S/N .

night of 26 Aug 1997 at the same level of $R = 17.0$ with no significant microvariability.

The last night of this run (27 Aug 1997) shown in Figure 3.40, 1622 – 297 exhibits a slight dimming trend of only 0.1 mag (2.8σ).

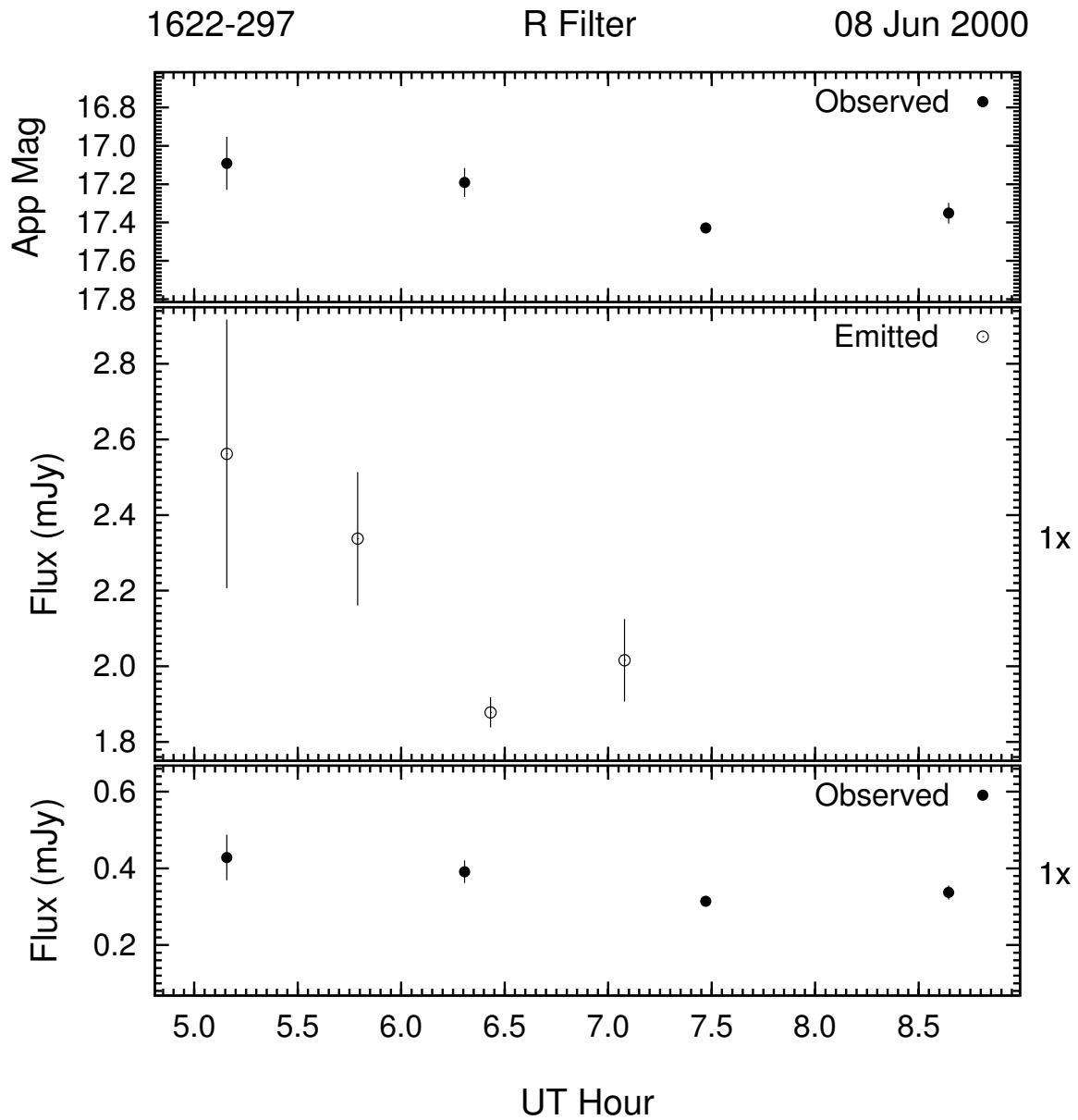


Figure 3.41: Example of the optical microvariability (R band) of 1622 – 297 on the night of 08 Jun 2000. This night's data was 2-point averaged to improve S/N .

Microvariability is searched for only three more times for 1622 – 297: one run of 2 nights in June of 2000 and one night in May of 2002. Figure 3.41 shows 1622 – 297 on the night of 08 Jun 2000 exhibiting variations on the order of 0.4 mag over the duration of 2.5 hours.

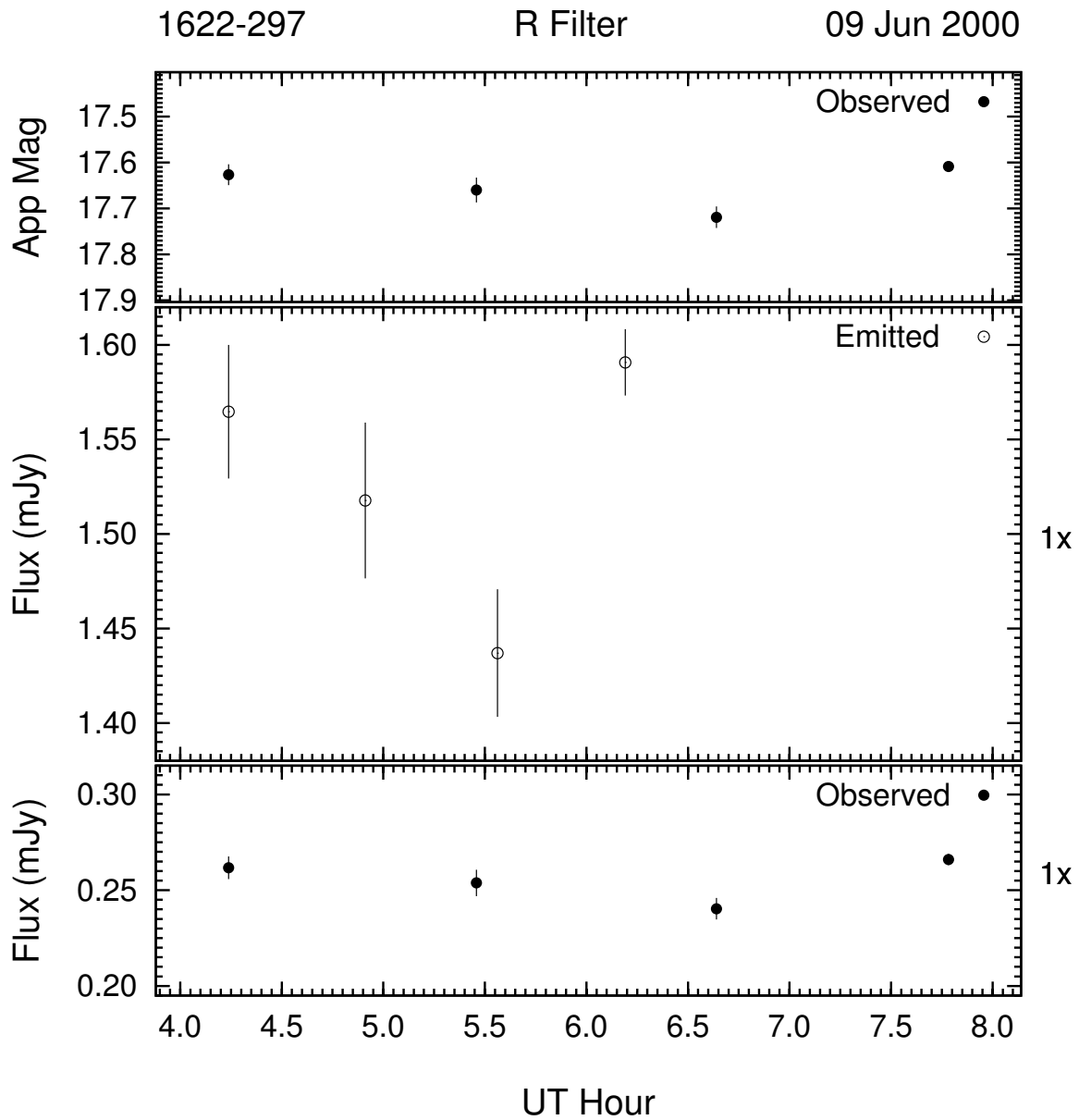


Figure 3.42: Example of the optical microvariability (R band) of 1622 – 297 on the night of 09 Jun 2000. This night's data was 2-point averaged to improve S/N .

On the following night, 1622 – 297 is 0.2 mag dimmer than at the end of the previous night at a level of $R = 17.6$. It was seen to have varied in a similar fashion, but with a change of only 0.1 mag (see Figure 3.42). Due to the large errors in the observations on 08 Jun 2000,

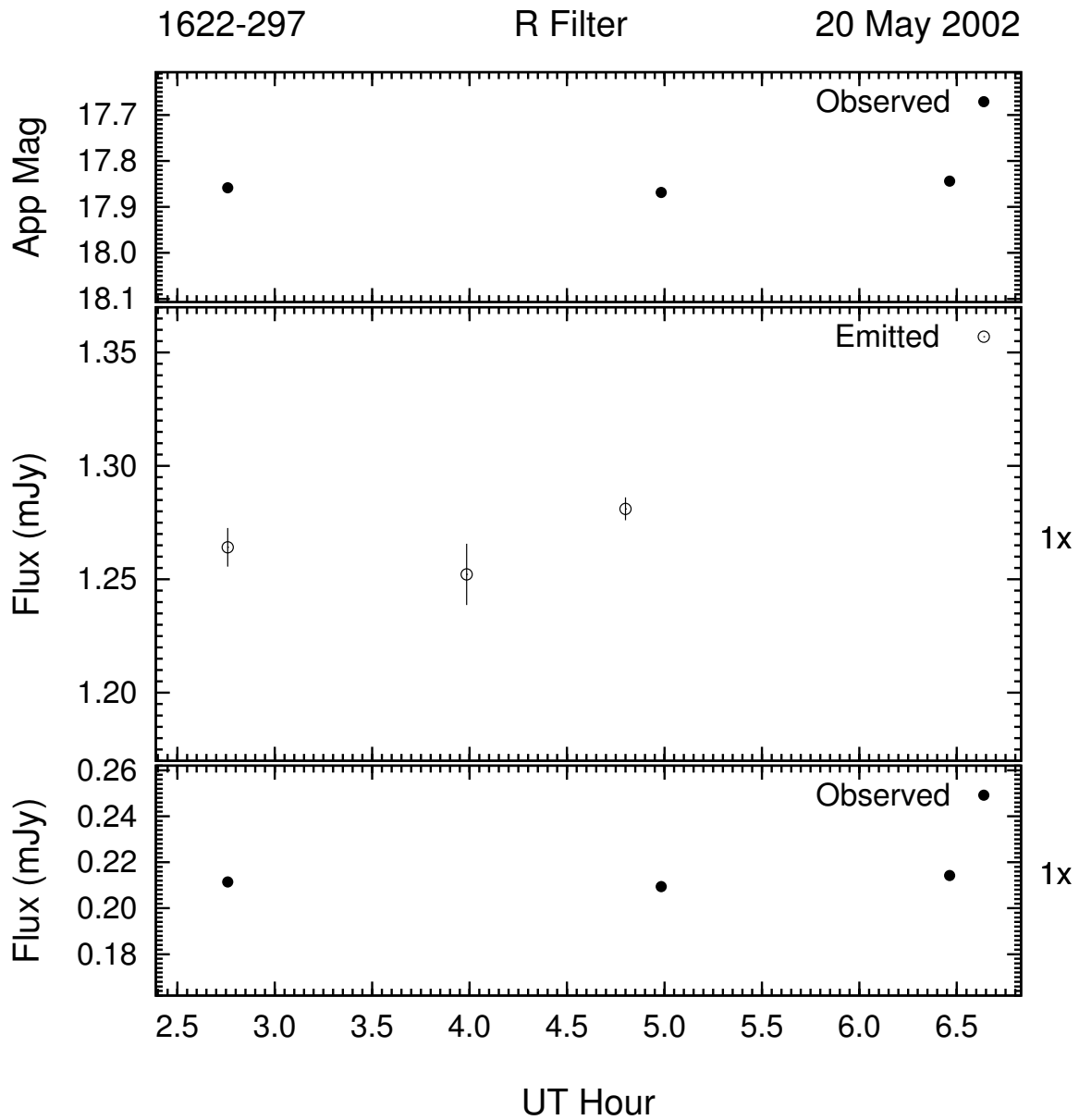


Figure 3.43: Example of the optical microvariability (R band) of 1622 – 297 on the night of 20 May 2002. This night’s data was 2-point averaged to improve S/N .

they are only at a level of 2.0σ , whereas those of 09 June 2000 are at a level of 2.8σ . The final time microvariability was searched for in 1622 – 297 was on the night of 20 May 2002 (Figure 3.43). It showed no statistically significant variability.

1622 – 297 is similar to both AO 0235 + 16 and 1156 + 295 in terms of enhancement of the amplitude of variation in the rest frame observations. The magnitude of the enhancement is ~ 6 with its redshift of 0.815, and the time-scale is *undilated* by approximately 45%.

3.2.4 1633 + 382

The OVV Quasar 1633 + 382 (also known as 4C 38.41) has a redshift of 1.814 and has exhibited a variability amplitude range of approximately 1.5 mag over the time that it has been monitored for this investigation (see Figure 3.44). The data used for 1633 + 382 is in the R band only, is taken from the PEGA archives, and covers a time period of just over 8 years. No SMARTS data exists for this object.

In Figure 3.44 the complete R band light curve for 1633 + 382 is displayed. With the exception of 2 flares in early 1996 and late 1997, this object was in a low state as determined by these observations. The microvariability observations start out with 2 runs in the beginning and end of April 1996, and are described below.

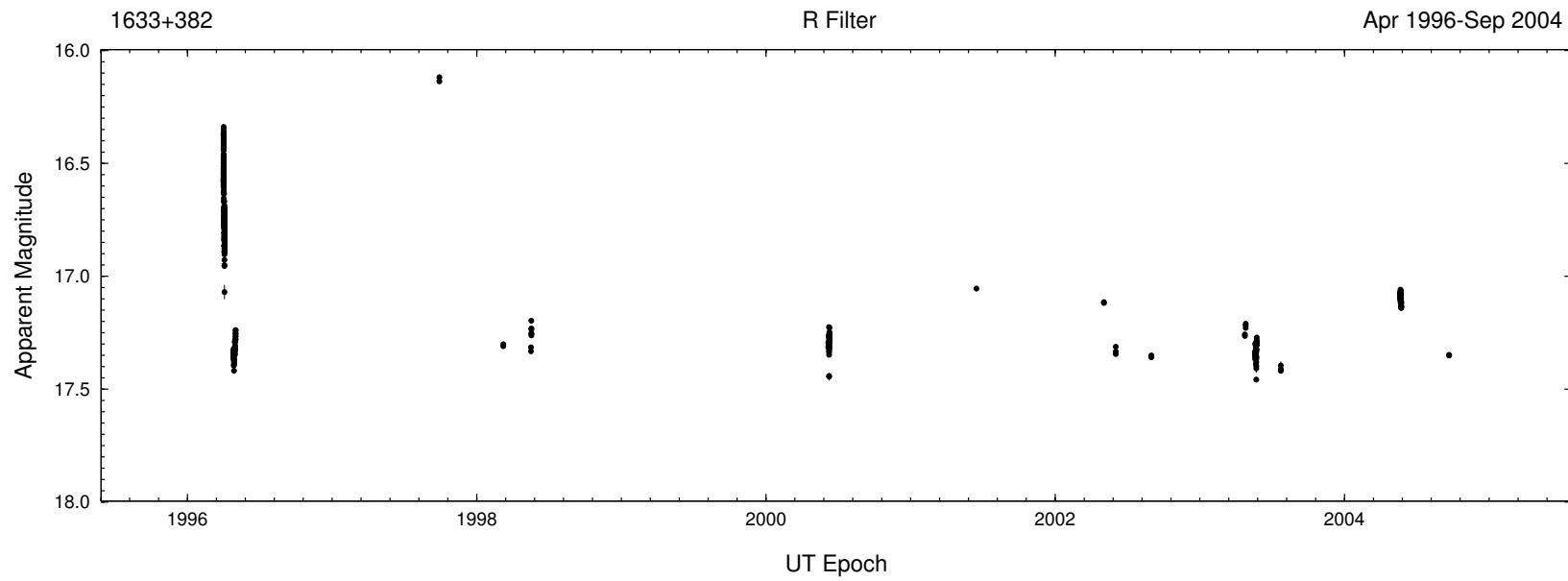


Figure 3.44: Complete R band light curve of 1633 + 382 from 1996 to 2004. The amplitude of variability is ~ 1.5 mag.

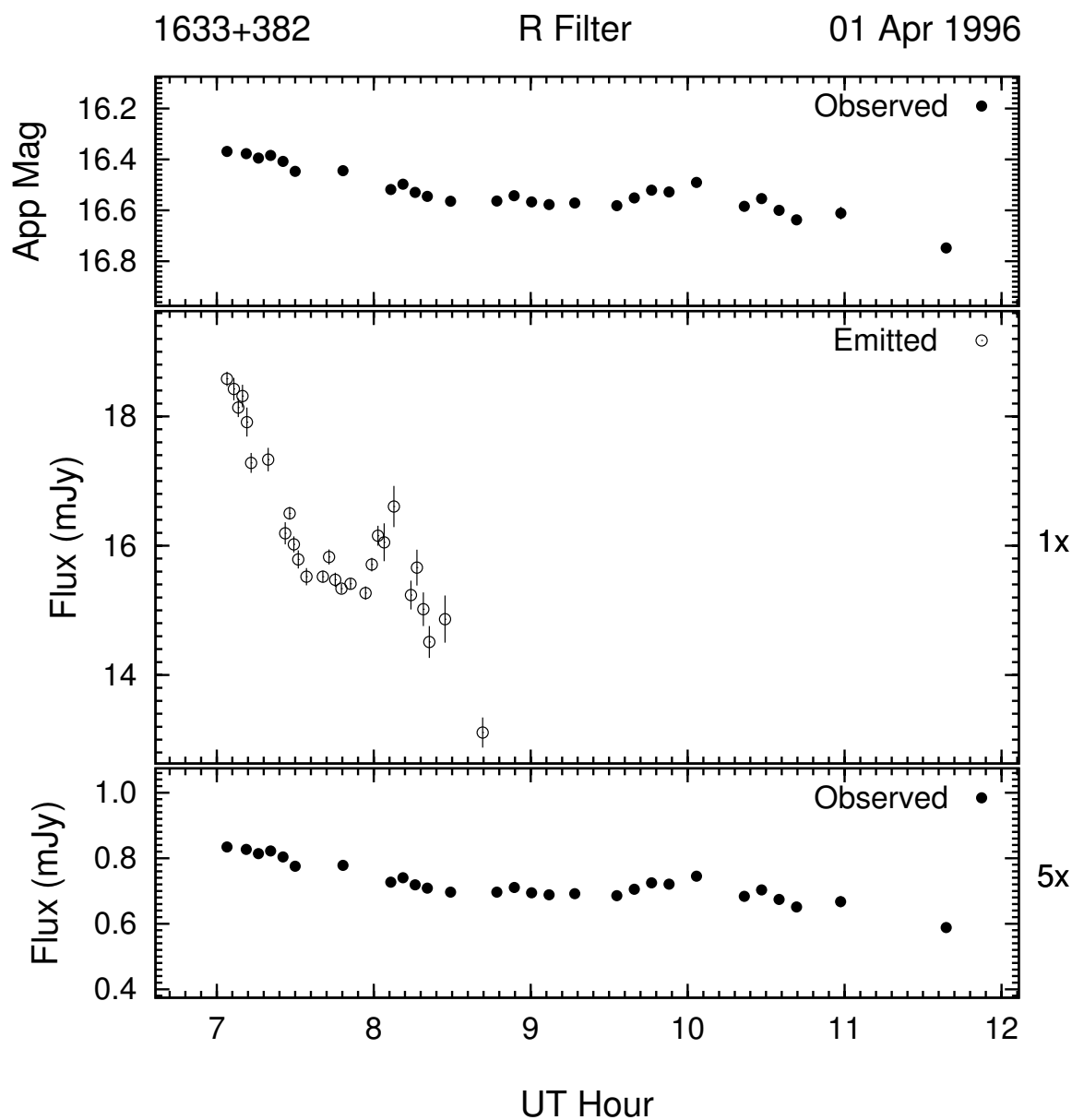


Figure 3.45: Example of the optical microvariability (R band) of 1633 + 382 on the night of 01 Apr 1996. This night's data was 4-point averaged to improve S/N .

Figures 3.45 through 3.47 show the state of 1633+382 over 3 days in the beginning of April 1996. On the night of 01 Apr 1996 (Figure 3.45), 1633 + 382 showed its largest single night change of 0.4 mag (29.4σ). It started at a level of $R \simeq 16.35$ and decreased in brightness in 2

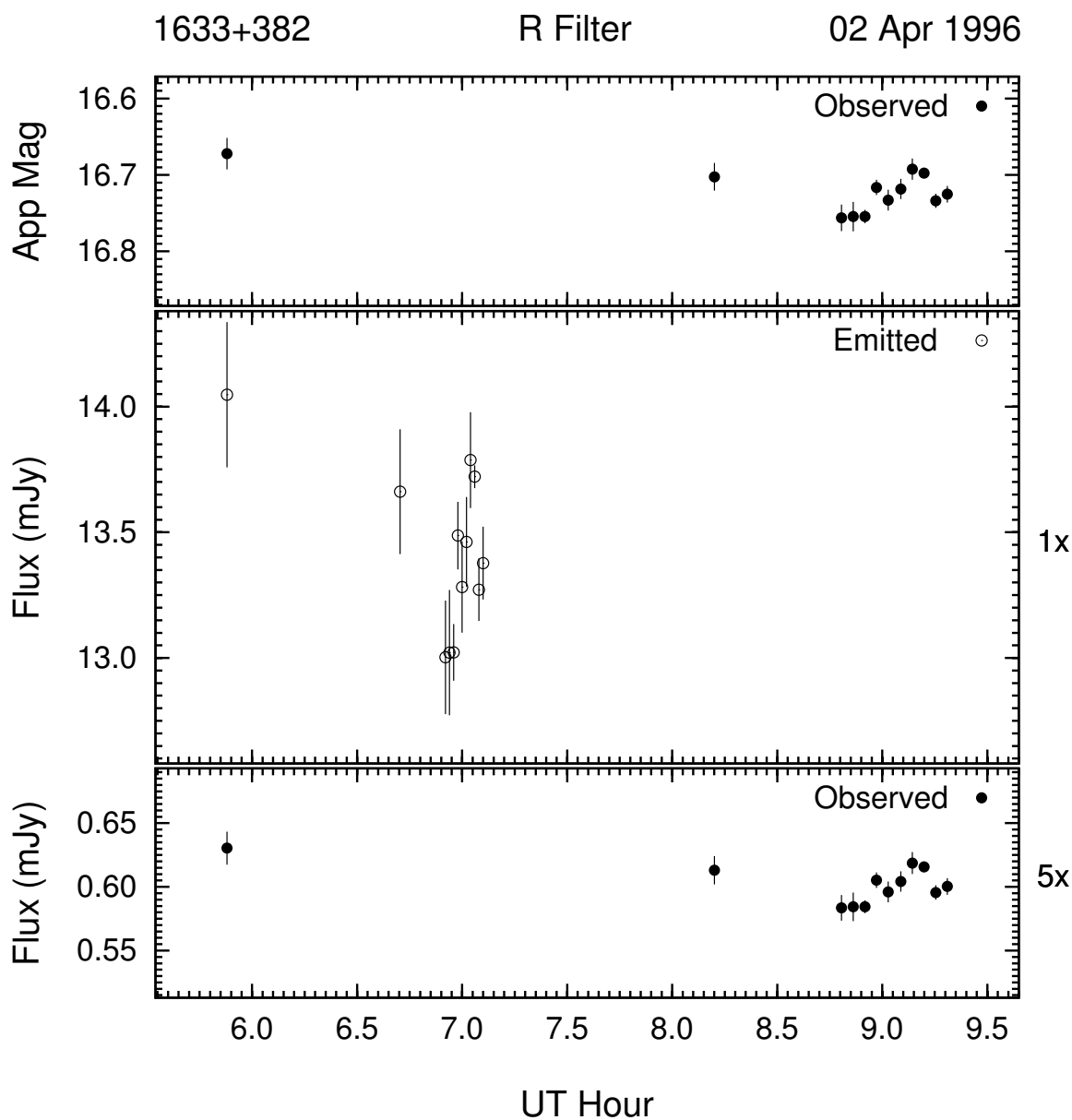


Figure 3.46: Example of the optical microvariability (R band) of 1633 + 382 on the night of 02 Apr 1996. This night's data was 2-point averaged to improve S/N .

steps over the time span of almost 5 hours. There does exist some superimposed variability that is statistically significant. The night of 02 Apr 1996, seen in Figure 3.46, shows that 1633 + 382 exhibited another downward trend in brightness with significant microvariability

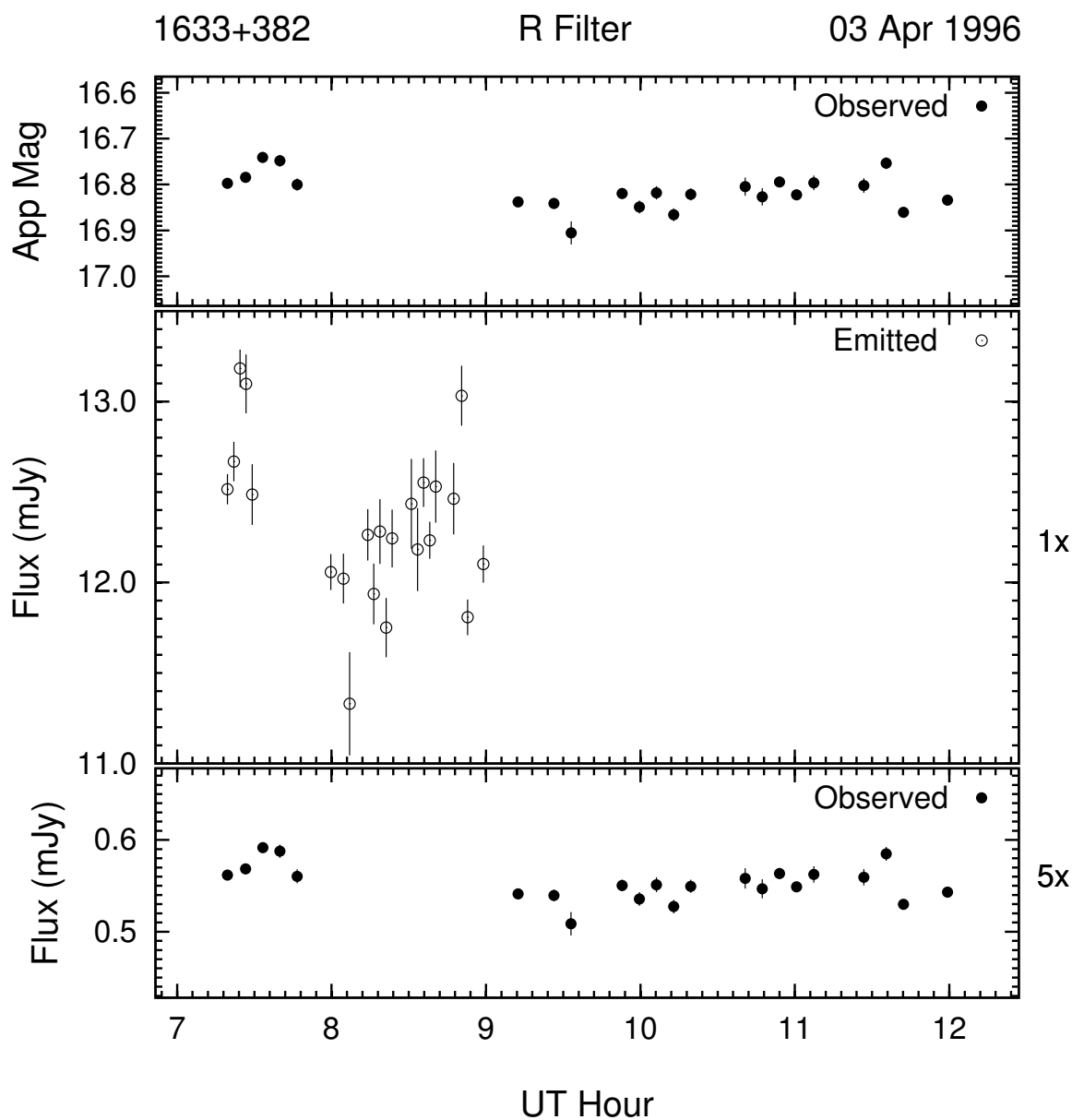


Figure 3.47: Example of the optical microvariability (R band) of 1633 + 382 on the night of 03 Apr 1996. This night's data was 4-point averaged to improve S/N .

superimposed on the very end of the night. The object's brightness level was roughly where it was at the end of the previous night. The character of the variability displayed by 1633+382 on the night of 03 Apr 1996 (Figure 3.47) is different in only that there is no trend visible.

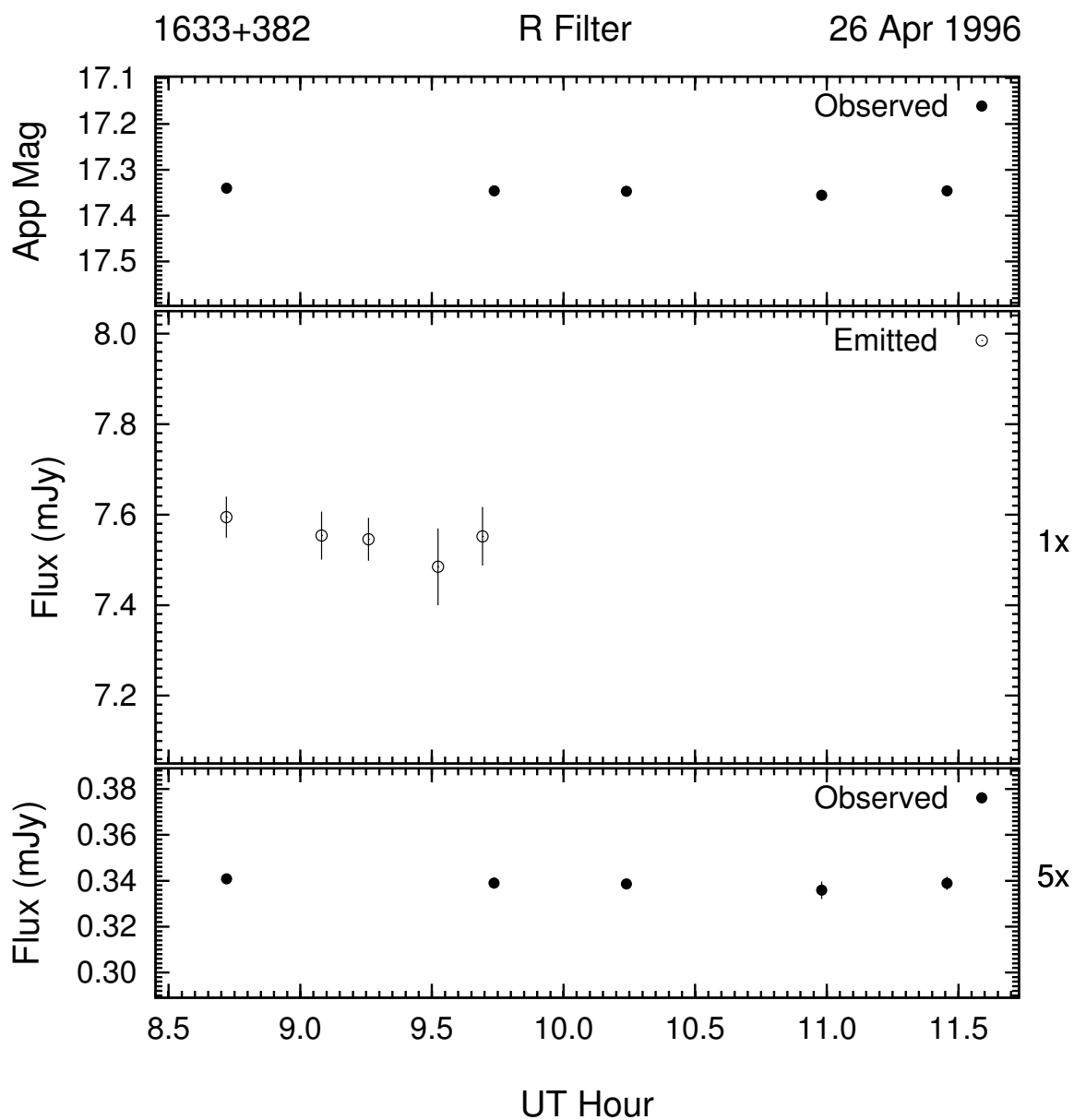


Figure 3.48: Example of the optical microvariability (R band) of 1633 + 382 on the night of 26 Apr 1996. This night's data was 3-point averaged to improve S/N .

The small scale microvariability, only some of which is significant, is still evident.

During the next run, 1633 + 382 exhibited no statistically significant variability on 3 of the 6 nights: 26, 28, and 29 Apr 1996 (Figures 3.48, 3.50, and 3.51, respectively). It also

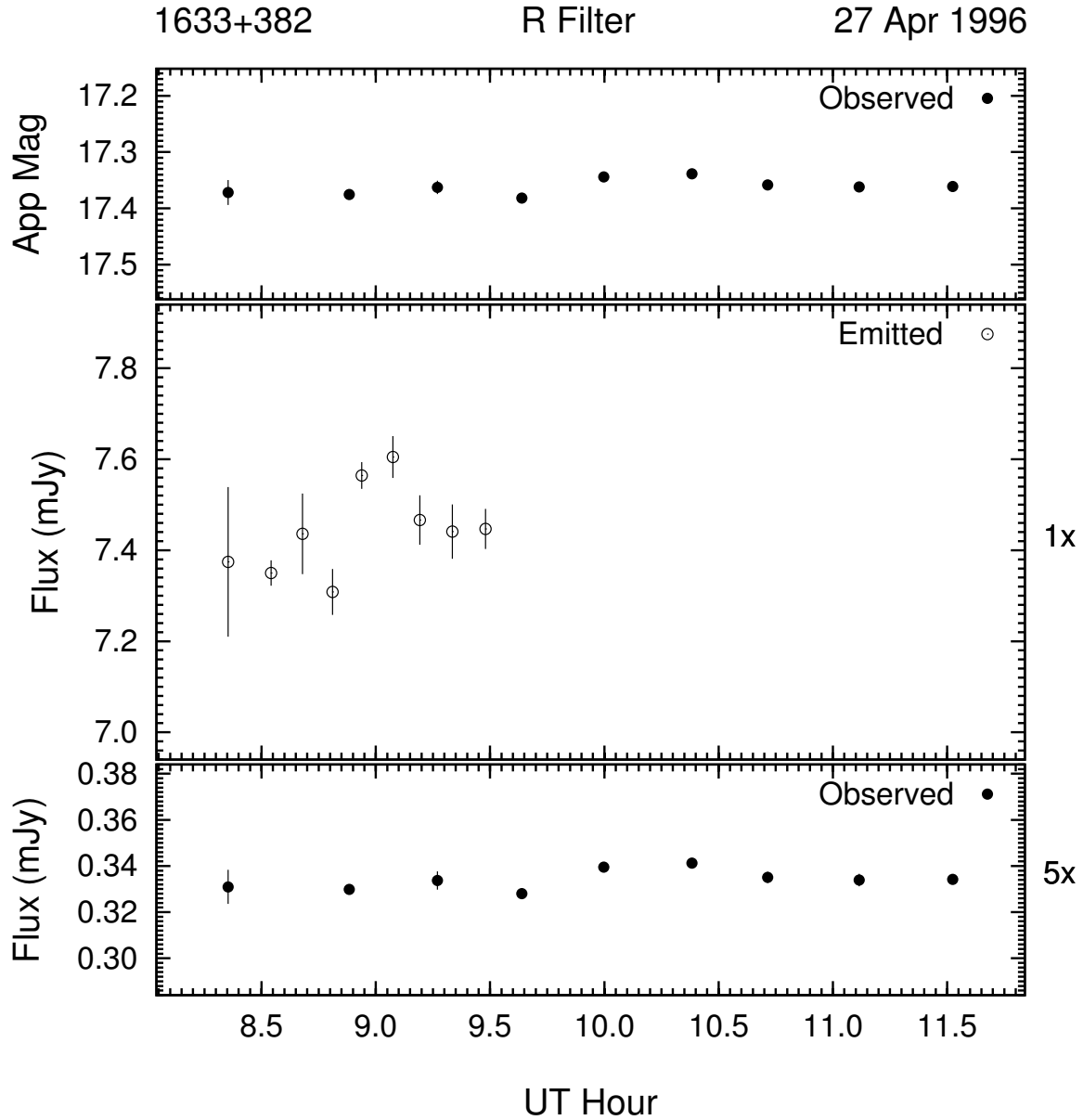


Figure 3.49: Example of the optical microvariability (R band) of 1633 + 382 on the night of 27 Apr 1996. This night's data was 2-point averaged to improve S/N .

stayed at a level of $R \simeq 17.3$, 0.5 mag dimmer than at the beginning of the month. On the remaining nights, 27 & 30 Apr and 01 May 1996, 1633 + 382 showed relatively similar, low level microvariability that is seen in Figures 3.49, 3.52 and 3.53, respectively.

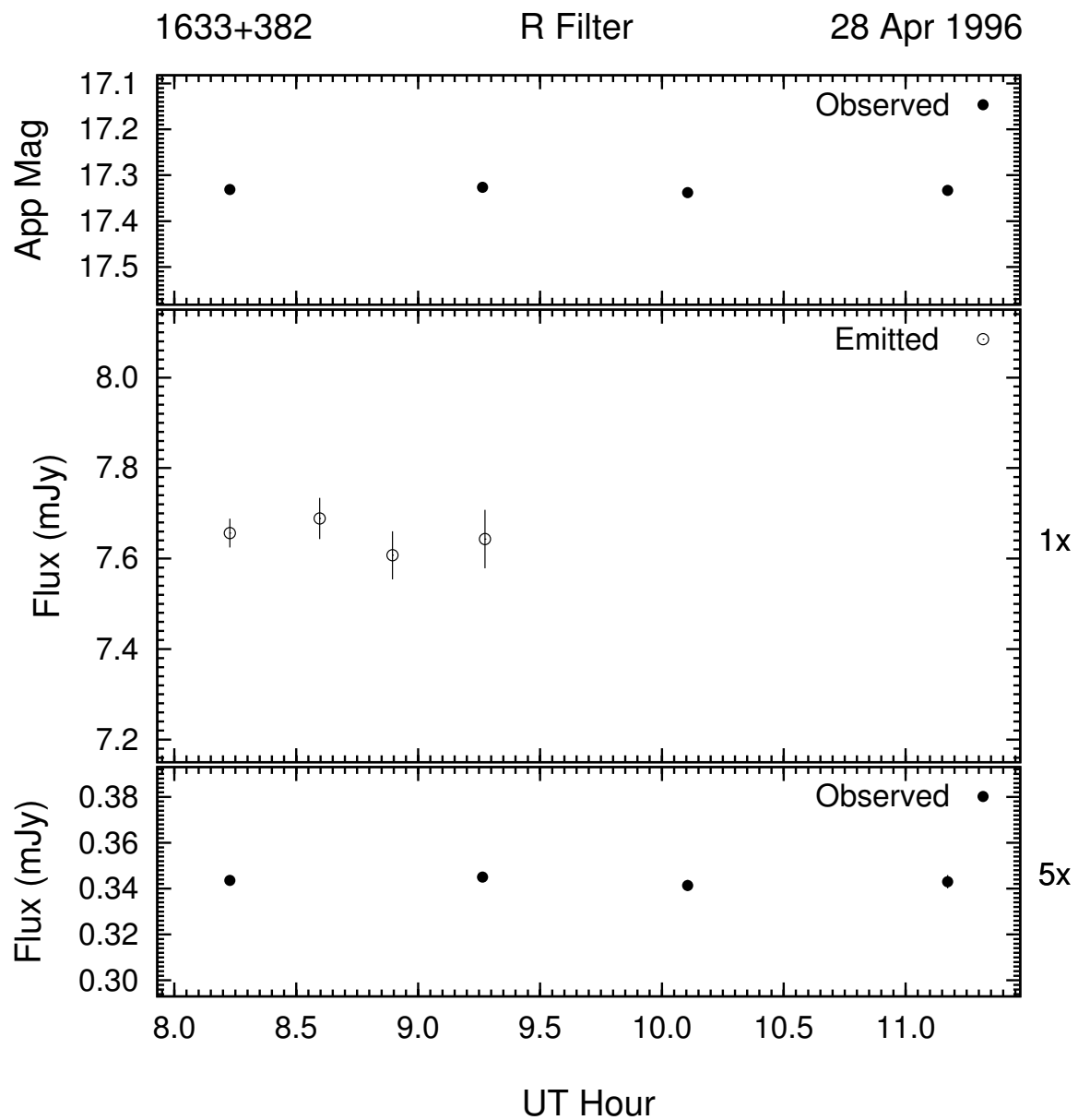


Figure 3.50: Example of the optical microvariability (R band) of 1633 + 382 on the night of 28 Apr 1996. This night's data was 2-point averaged to improve S/N .

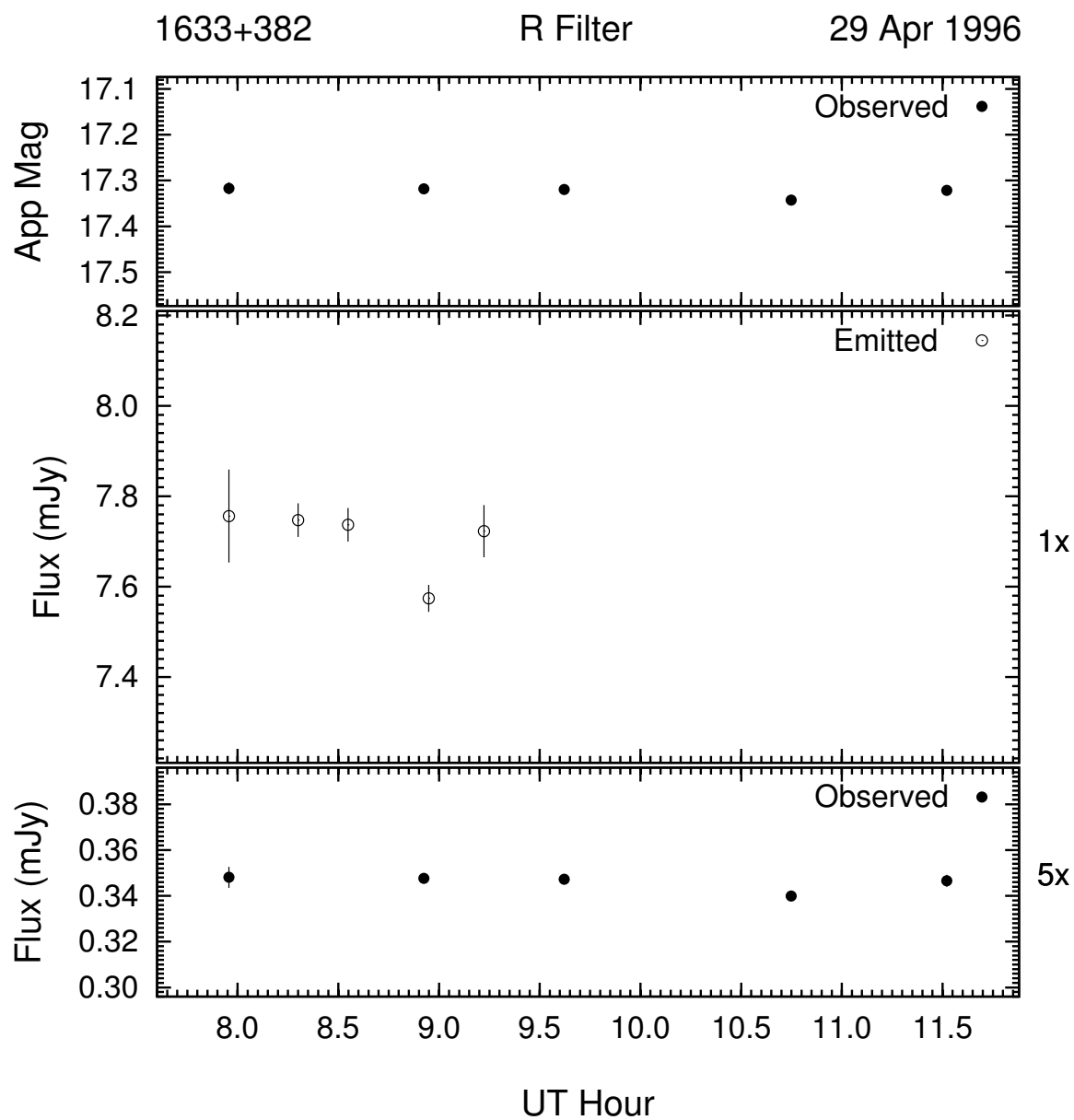


Figure 3.51: Example of the optical microvariability (R band) of 1633 + 382 on the night of 29 Apr 1996. This night's data was 2-point averaged to improve S/N .

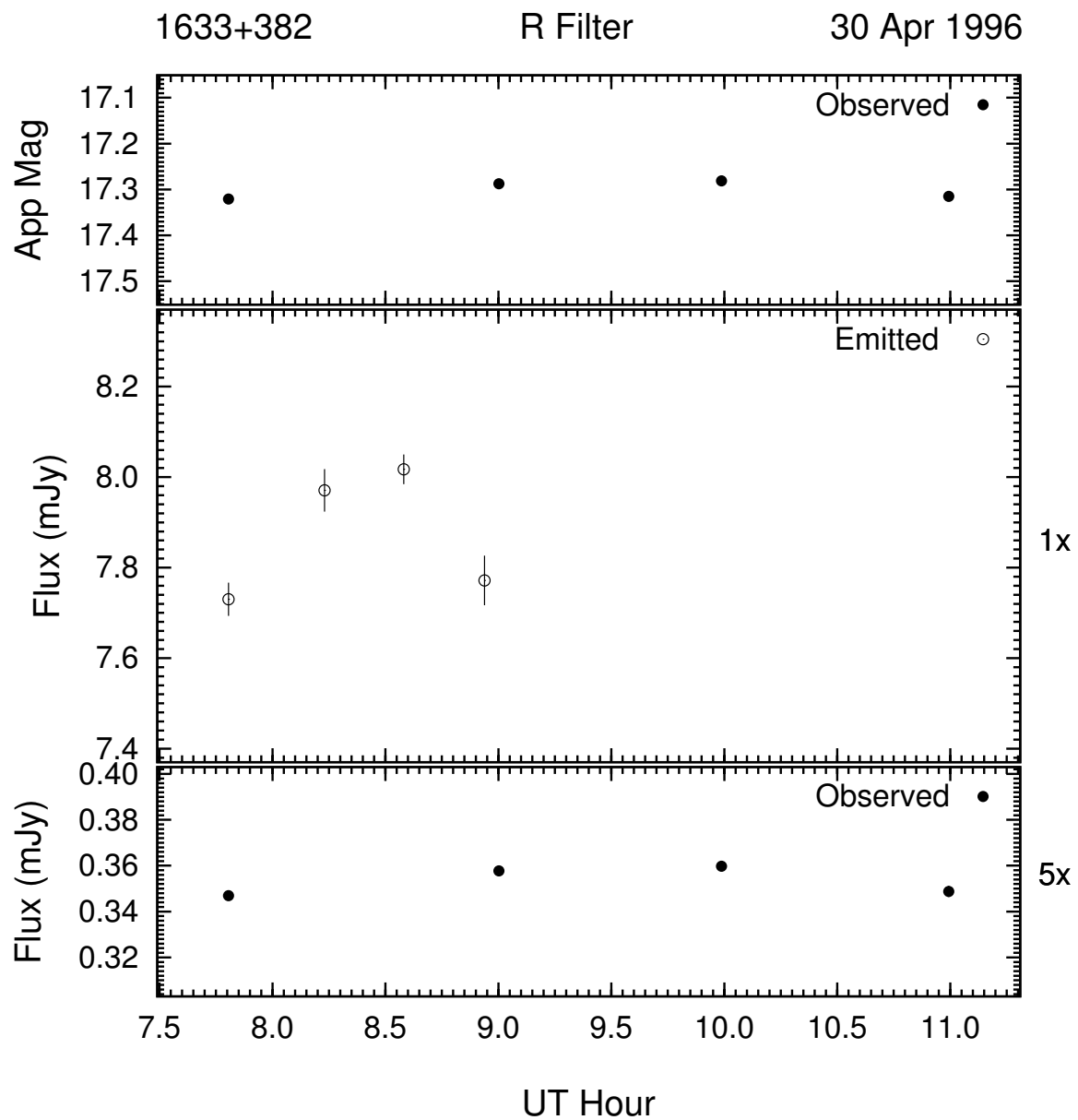


Figure 3.52: Example of the optical microvariability (R band) of 1633 + 382 on the night of 30 Apr 1996. This night's data was 2-point averaged to improve S/N .

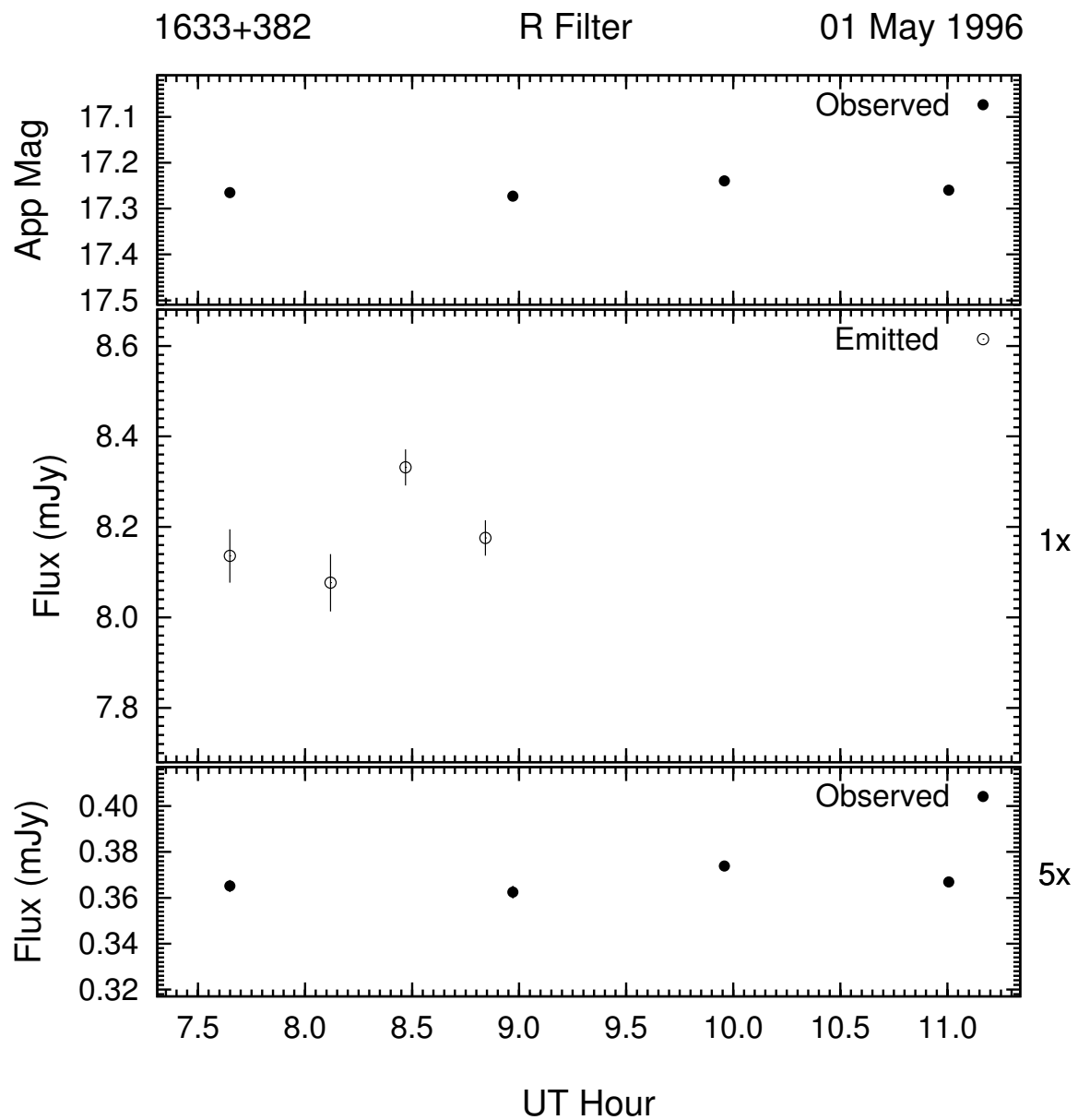


Figure 3.53: Example of the optical microvariability (R band) of 1633 + 382 on the night of 01 May 1996. This night's data was 2-point averaged to improve S/N .

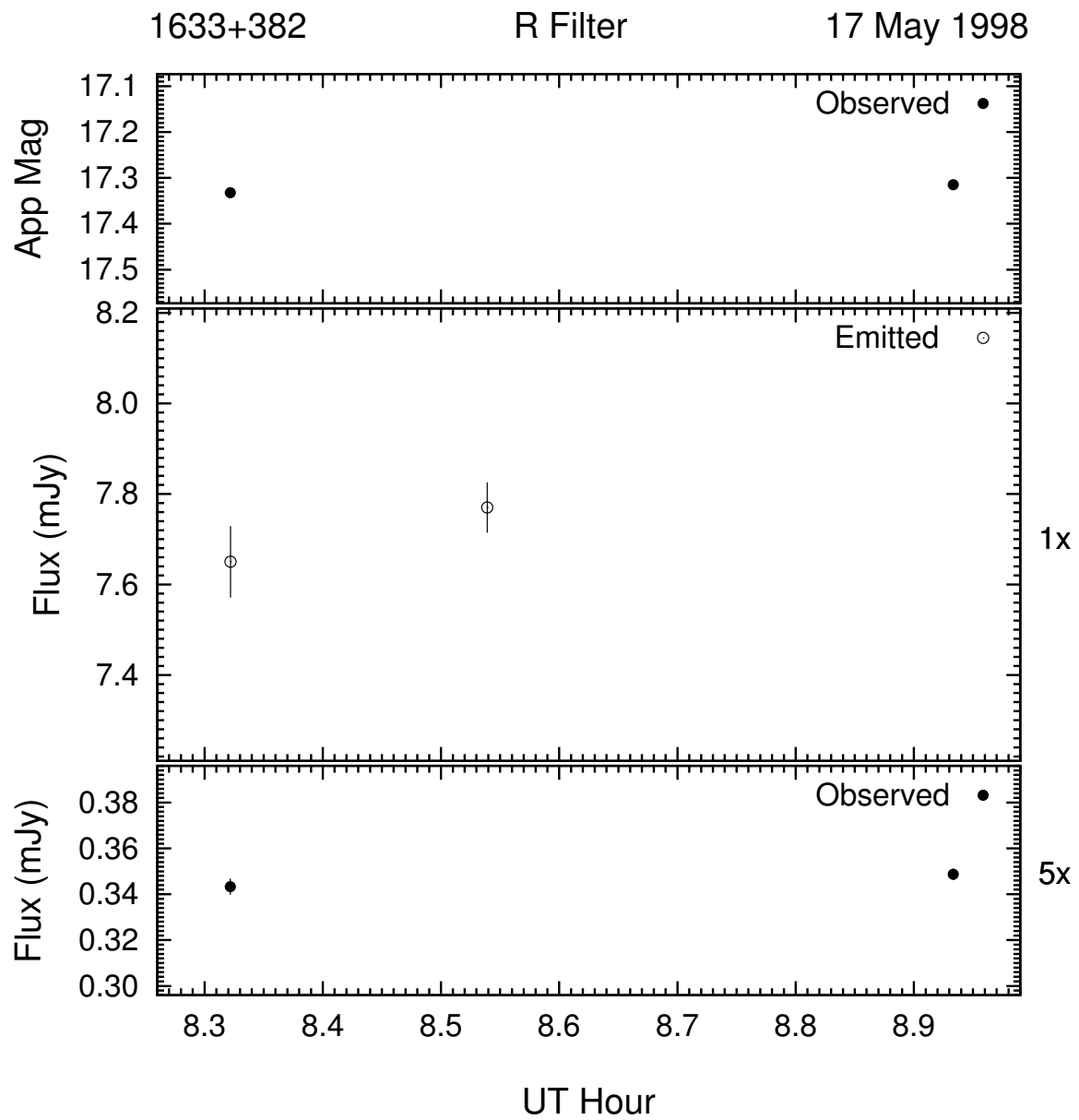


Figure 3.54: Example of the optical microvariability (R band) of 1633 + 382 on the night of 17 May 1998.

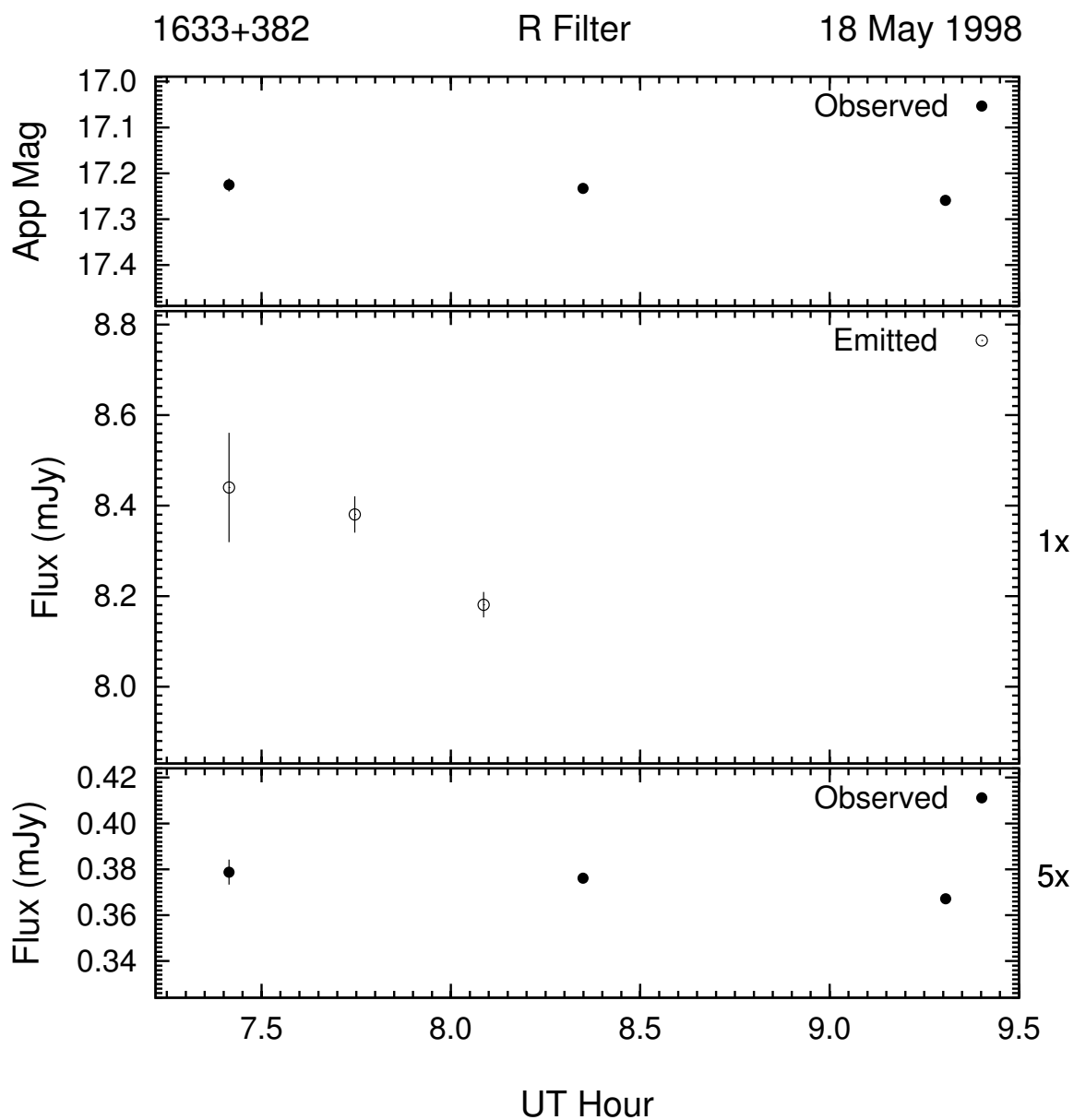


Figure 3.55: Example of the optical microvariability (R band) of 1633 + 382 on the night of 18 May 1998. This night's data was 2-point averaged to improve S/N .

The next 2 nights where 1633+382 was observed for microvariability were 17 and 18 May 1998 (Figures 3.54 & 3.55). There was no statistically significant microvariability detected for 1633 + 382 on either night, although it did brighten 0.1 mag between the two nights.

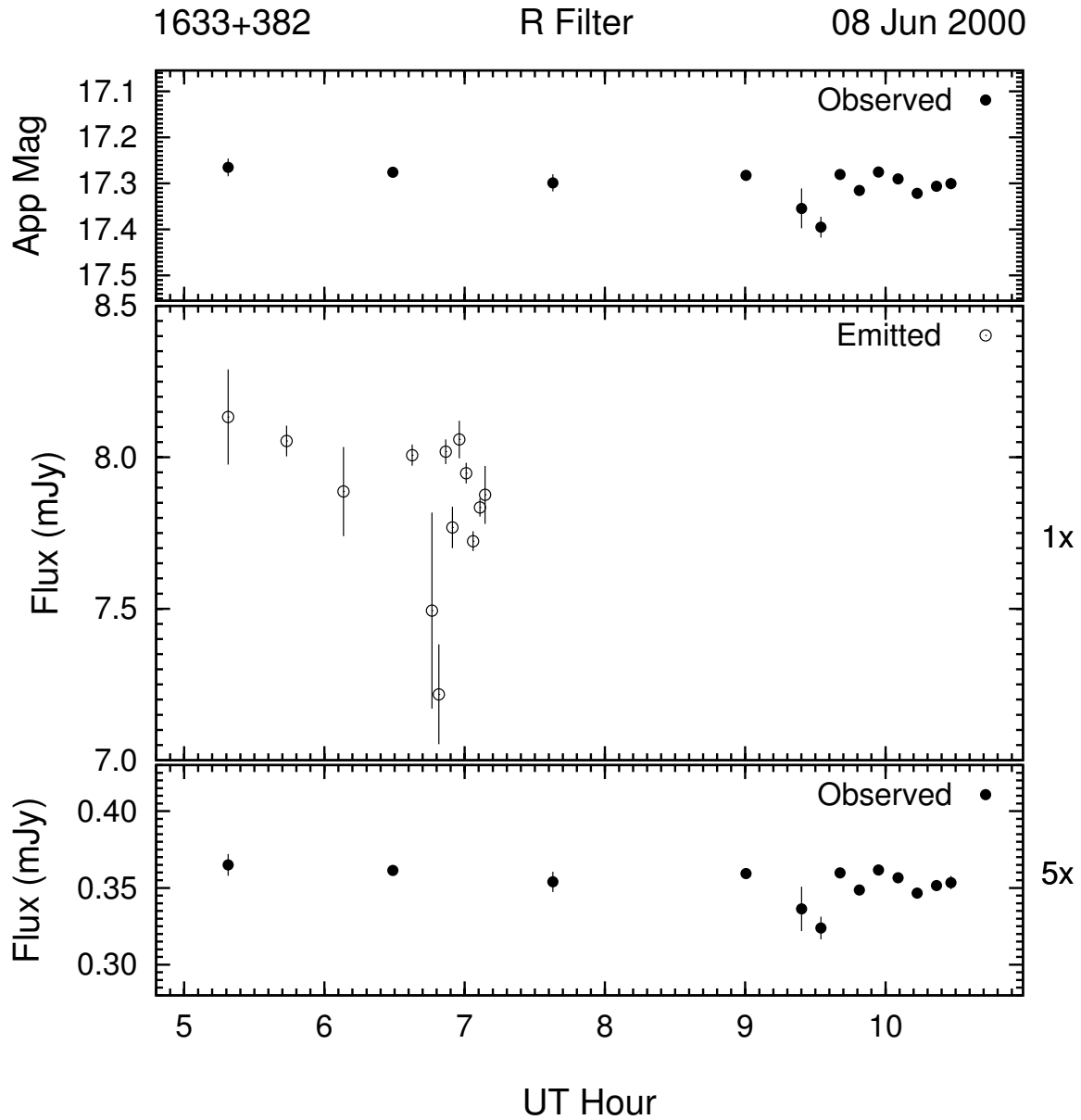


Figure 3.56: Example of the optical microvariability (R band) of 1633 + 382 on the night of 08 Jun 2000. This night's data was 2-point averaged to improve S/N .

Two nights of the following microvariability run for 1633 + 382 were 08 & 09 Jun 2000 (Figure 3.56 and Figure 3.57). 1633 + 382 exhibited a slight downward trend in brightness on the first night with one significant dimming event of ~ 0.15 mag (7.6σ) between 9^h and

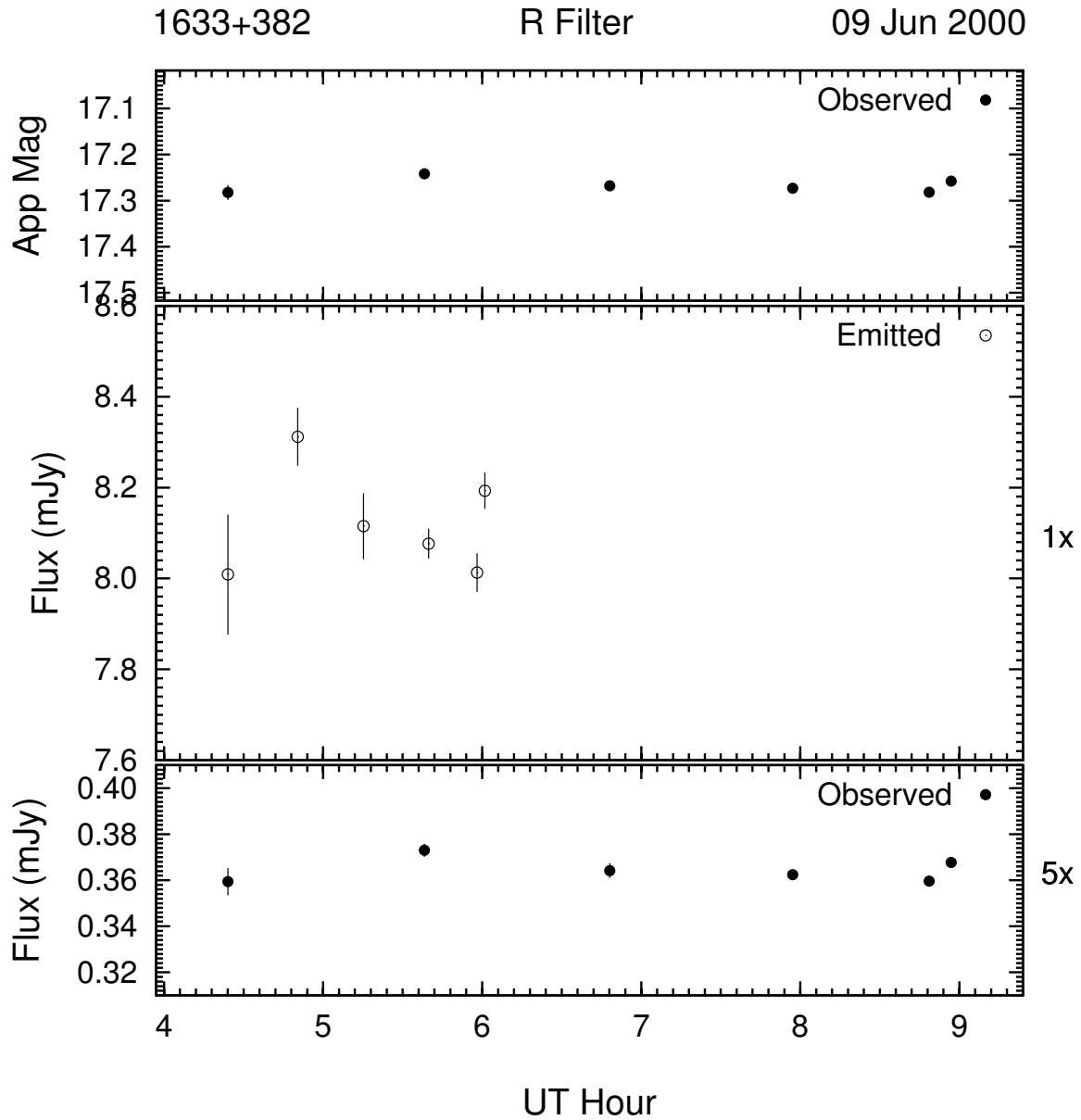


Figure 3.57: Example of the optical microvariability (R band) of 1633 + 382 on the night of 09 Jun 2000. This night's data was 2-point averaged to improve S/N .

10^h UT. On the following night, the object varied < 0.1 mag without any overall change in brightness.

Observations from 5 nights in late May 2003 are shown in Figures 3.58 through 3.62. All

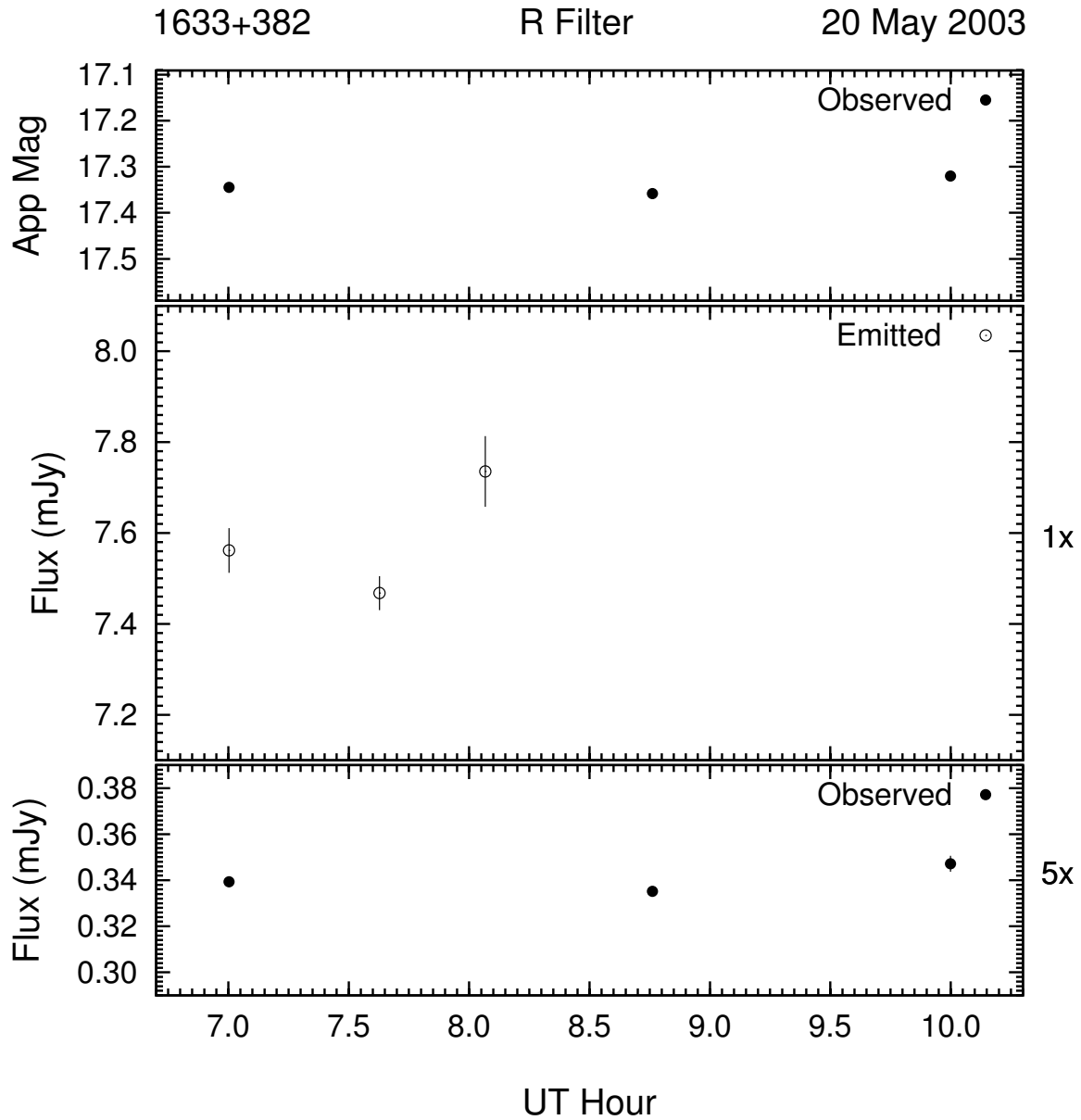


Figure 3.58: Example of the optical microvariability (R band) of 1633 + 382 on the night of 20 May 2003. This night's data was 2-point averaged to improve S/N .

five nights were at roughly the same level ($R \simeq 17.35$) and showed very slight variability. Only 2 nights stand out: 21 May (Figure 3.59) and 23 May (Figure 3.61). On the night of 21 May 2003, 1633 + 382 showed no statistically significant variability and on 23 May 2003,

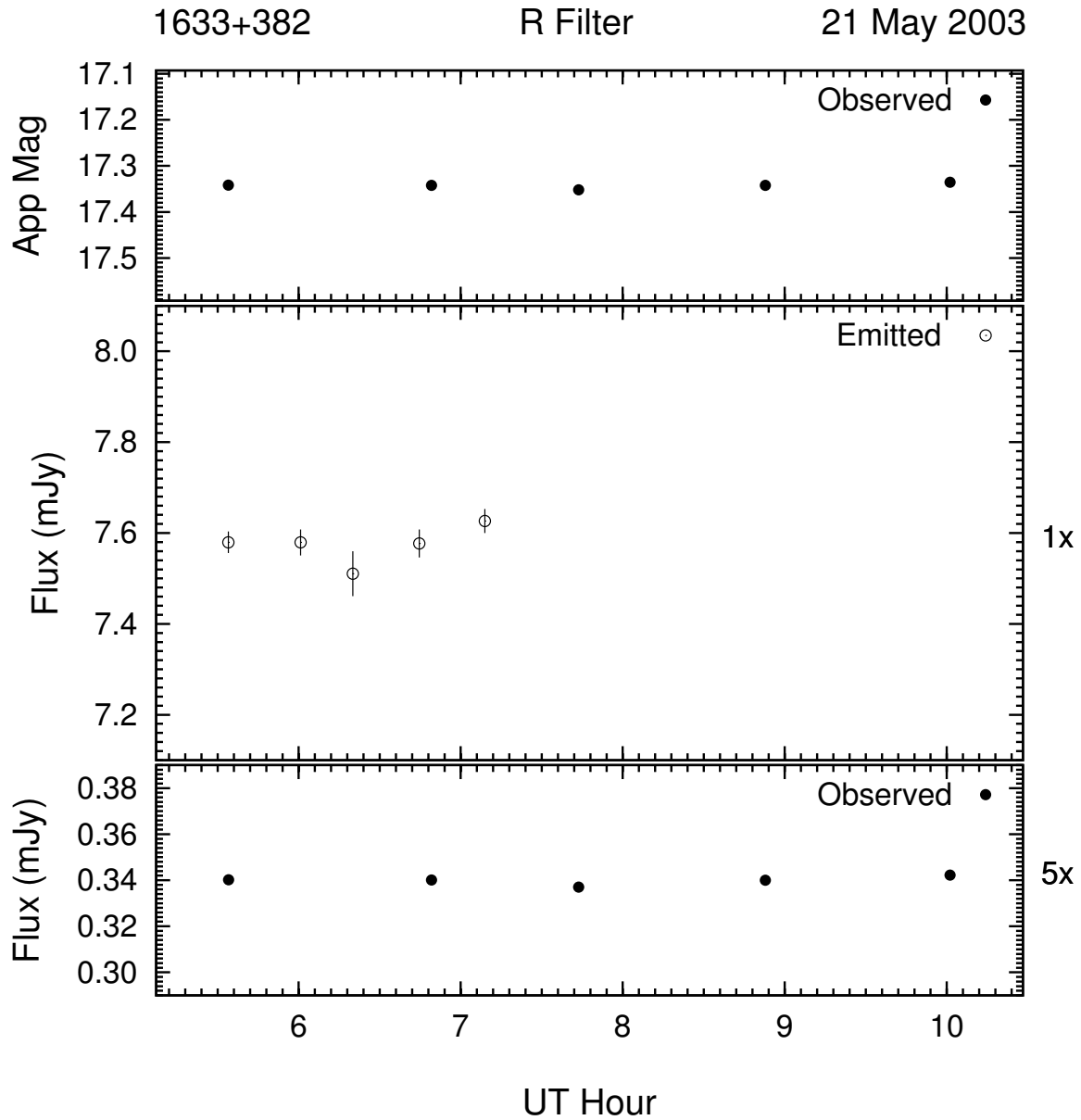


Figure 3.59: Example of the optical microvariability (R band) of 1633 + 382 on the night of 21 May 2003. This night's data was 2-point averaged to improve S/N .

it showed a definite increase in brightness over the 3 hours of 0.10 mag (6.7σ).

The last microvariability search for 1633 + 382 was in late May of 2004 (Figures 3.63 through 3.65). The sampling rate is higher, but the results are very similar to the previous

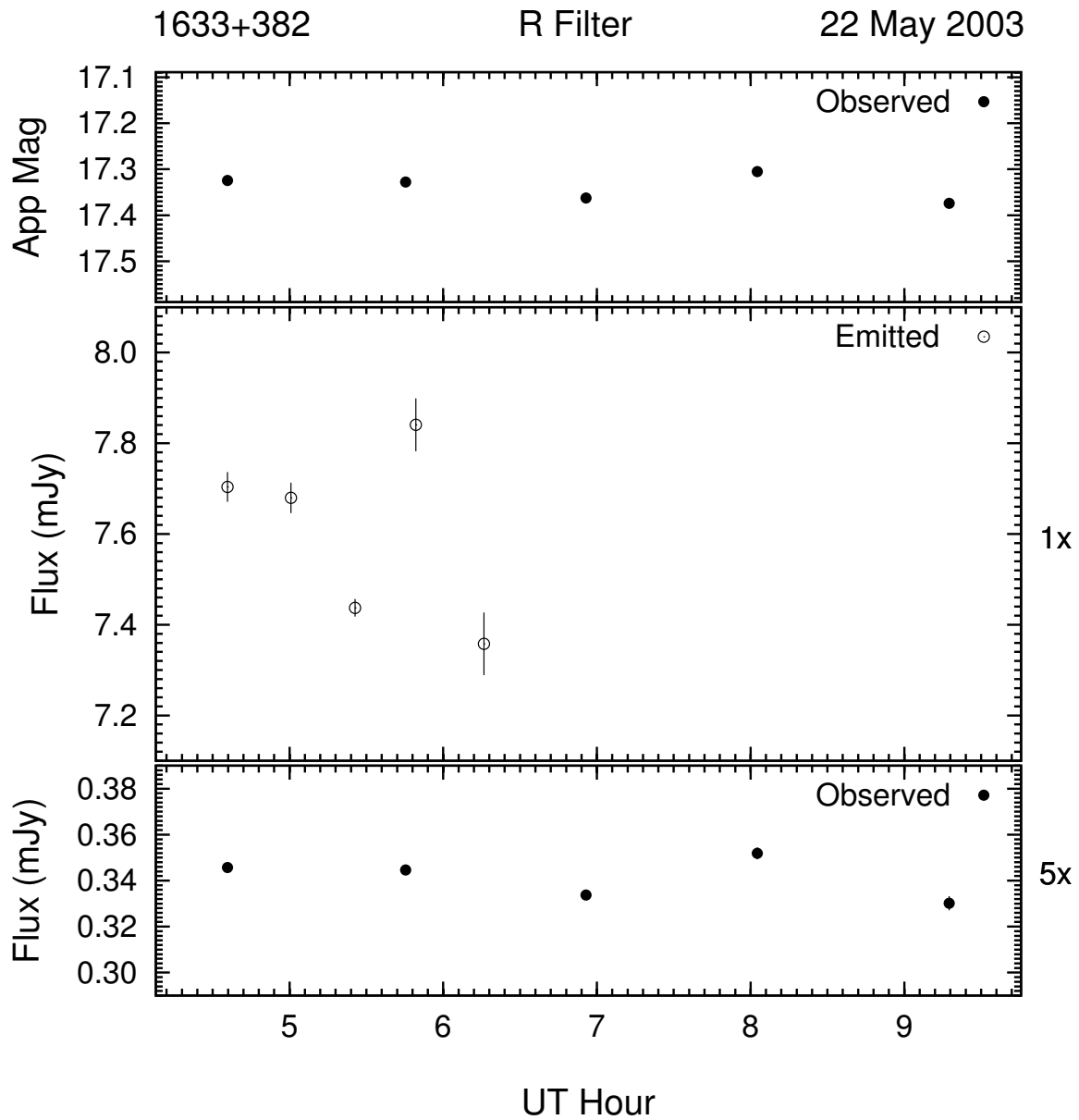


Figure 3.60: Example of the optical microvariability (R band) of 1633 + 382 on the night of 22 May 2003. This night's data was 2-point averaged to improve S/N .

year: low level microvariability with very little change in brightness (< 0.1 mag) from night to night. Figure 3.64 shows the most dramatic of these with a rise of only ~ 0.05 mag (5.7σ) over 5.5 hours.

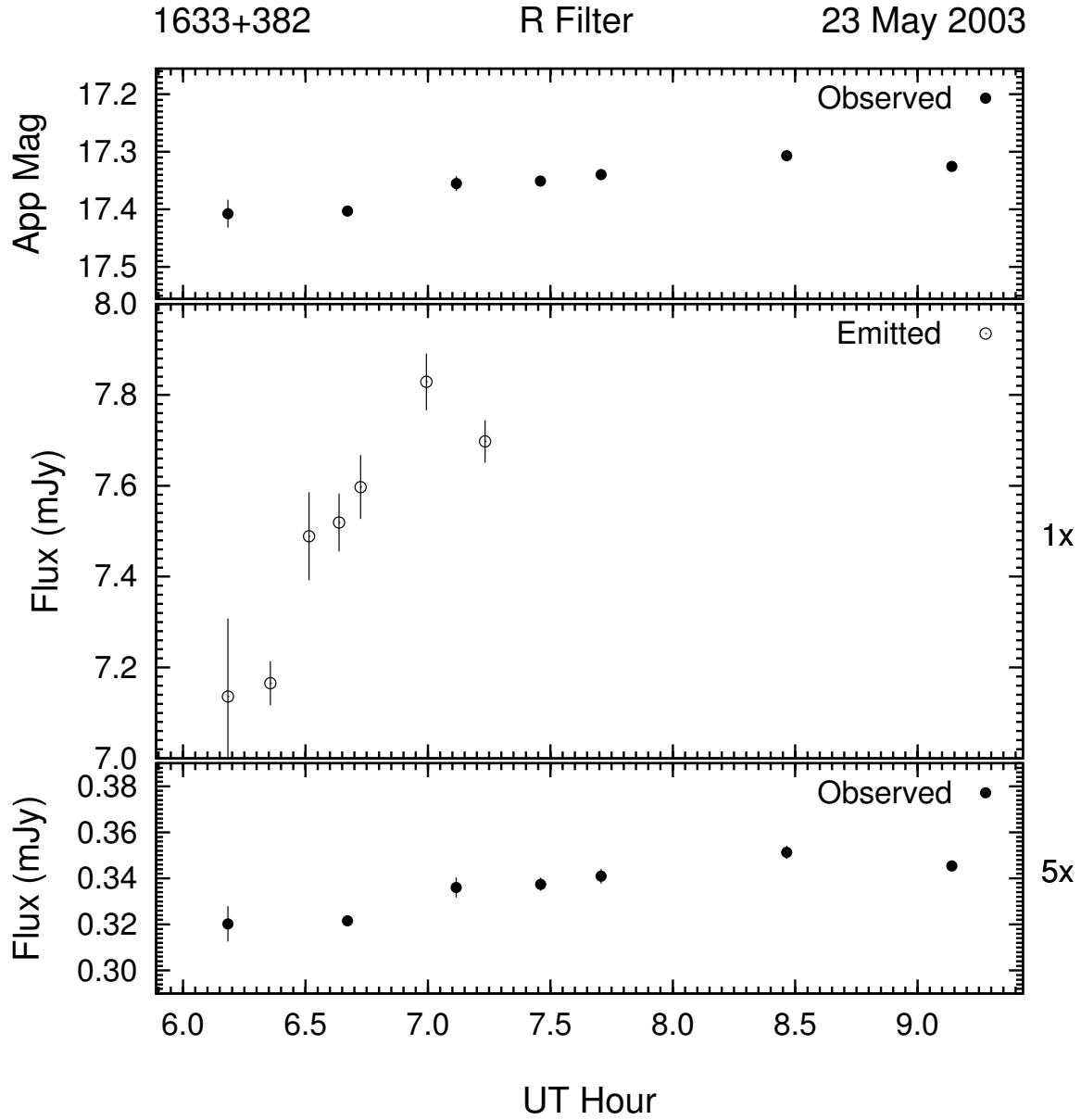


Figure 3.61: Example of the optical microvariability (R band) of 1633 + 382 on the night of 23 May 2003. This night's data was 2-point averaged to improve S/N .

With a redshift of 1.814, 1633 + 382 exhibits the greatest enhancement in variability amplitude by a factor of ~ 22 ! The rest frame time-scale at this redshift is only 35% the observed frame time-scale, giving the highest time sampling compression of all the objects.

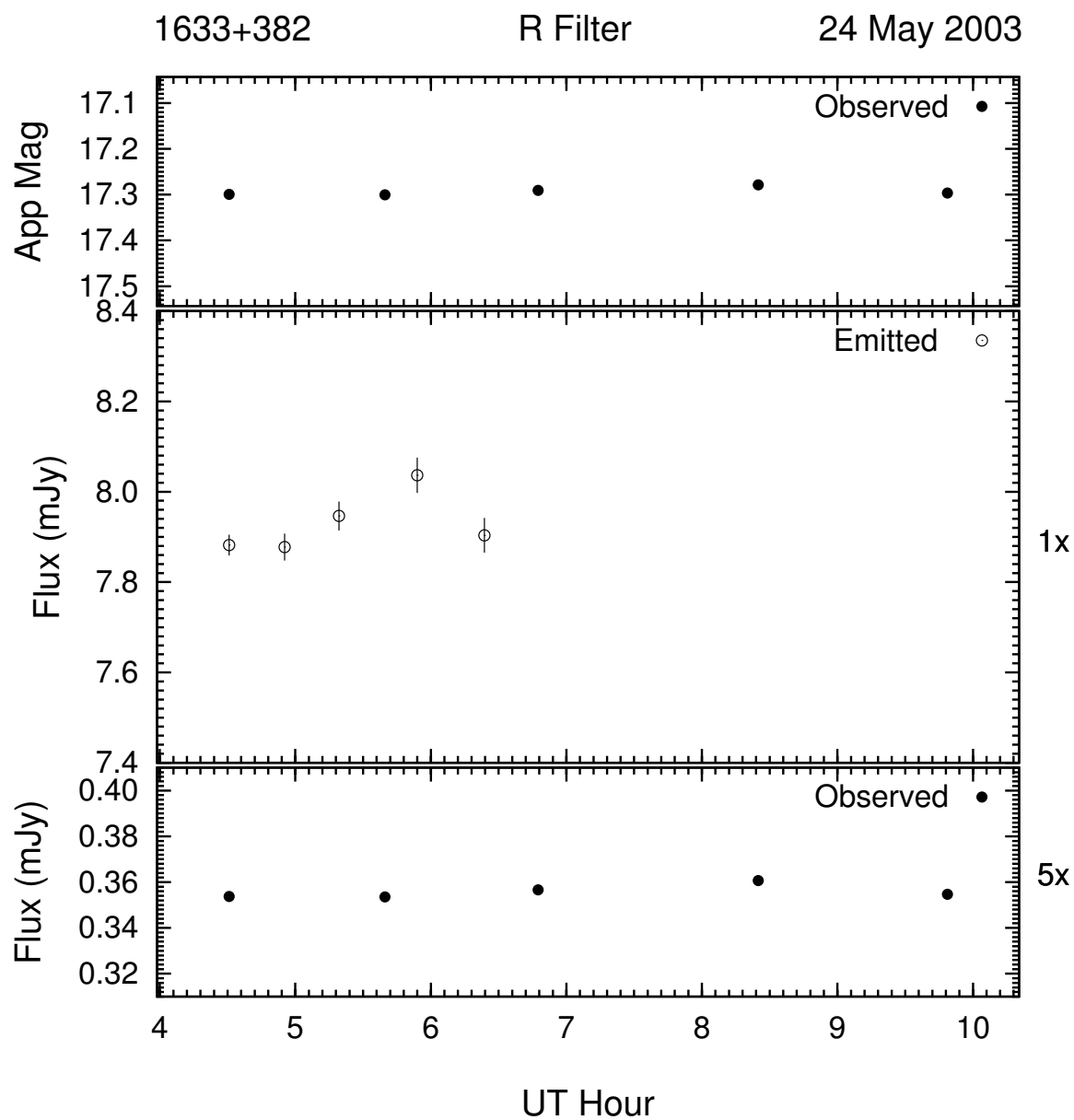


Figure 3.62: Example of the optical microvariability (R band) of 1633 + 382 on the night of 24 May 2003. This night's data was 2-point averaged to improve S/N .

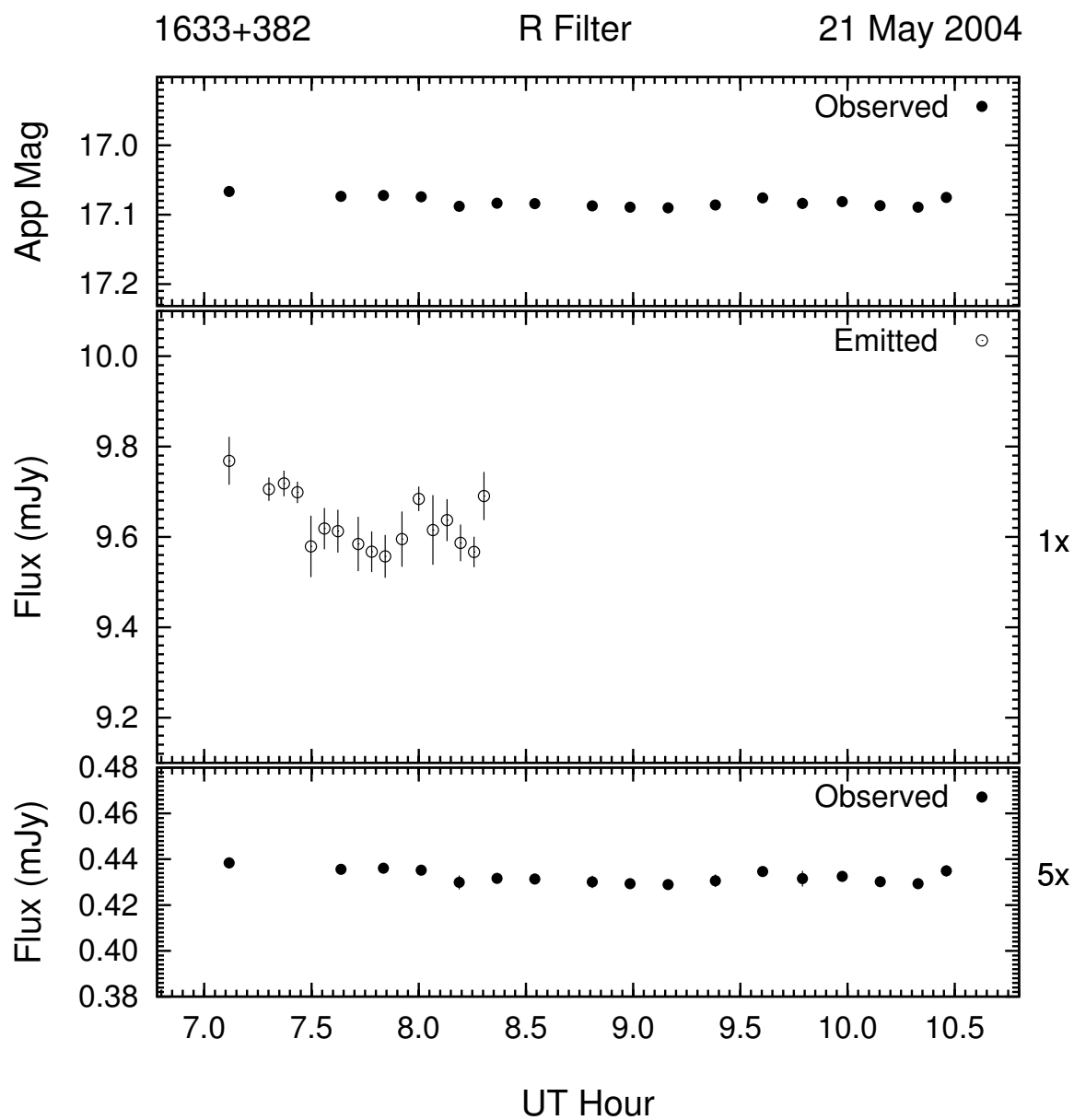


Figure 3.63: Example of the optical microvariability (R band) of 1633 + 382 on the night of 21 May 2004. This night's data was 2-point averaged to improve S/N .

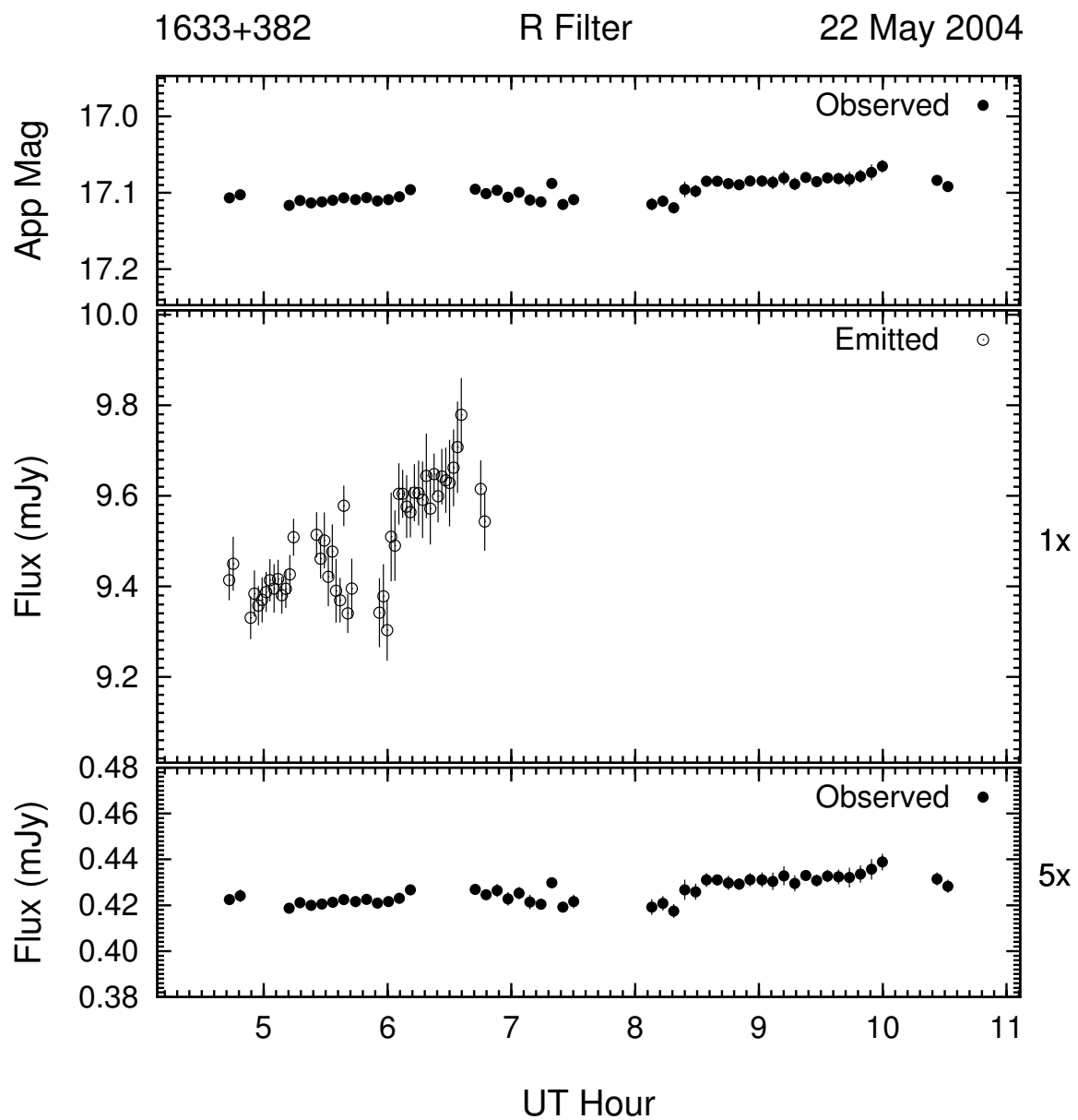


Figure 3.64: Example of the optical microvariability (R band) of 1633 + 382 on the night of 22 May 2004.

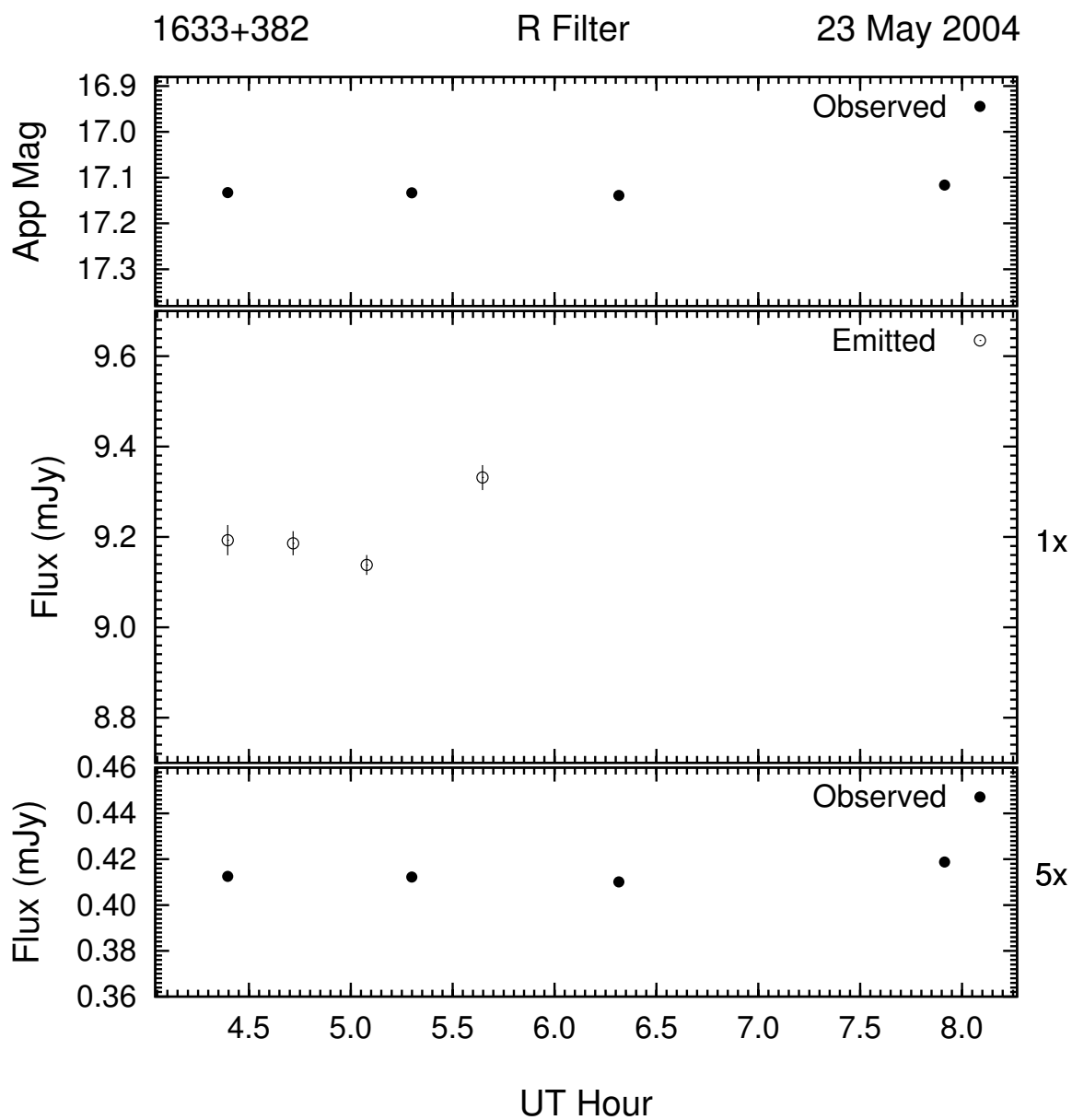


Figure 3.65: Example of the optical microvariability (R band) of 1633 + 382 on the night of 23 May 2004. This night's data was 2-point averaged to improve S/N .

3.2.5 1641 + 399

The OVV Quasar 3C 345 (also known as PKS 1641+399 or simply 1641+399) has a redshift of 0.593 and has exhibited a variability amplitude range of almost 2.5 mag over the time that it has been monitored for this investigation (see Figure 3.66). The data used for 3C 345 is in the R band only, is taken from the PEGA archives, and covers a time period of approximately 12 years. No SMARTS data exists for this object.

The long term light curve of 1641 + 399 shows it in a high state three times: in early 1992, early 1998, and early 2001. It was in an extreme low state between 1994 and 1998.

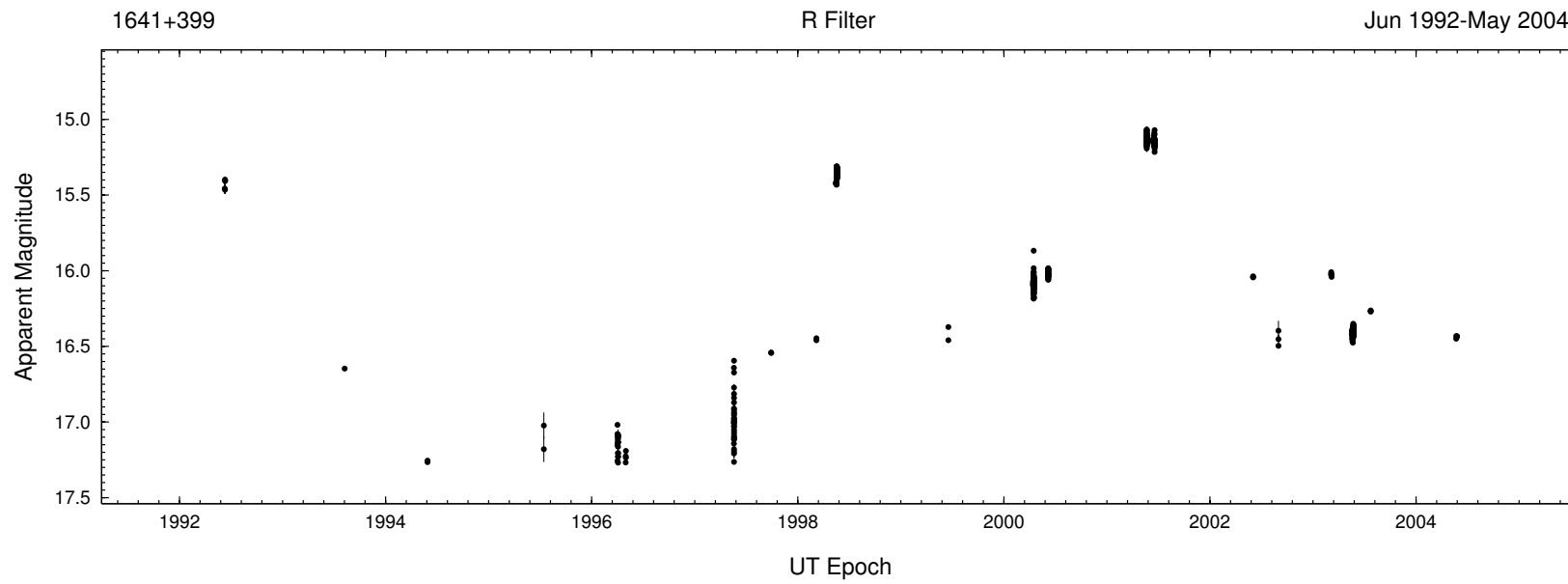


Figure 3.66: Complete R band light curve of 1641 + 399 from 1991 to 2004. The amplitude of variability is ~ 2.5 mag.

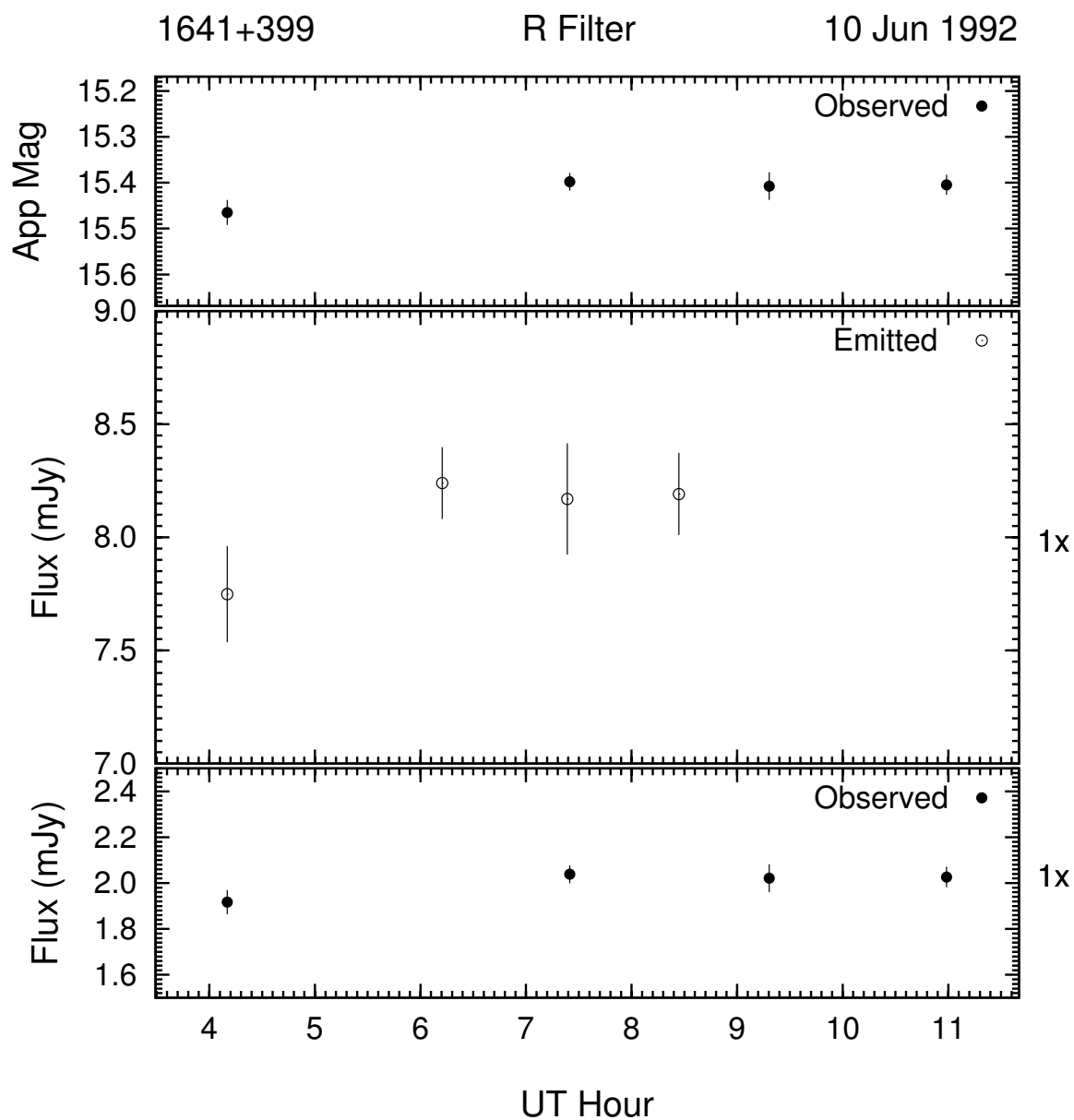


Figure 3.67: Example of the optical microvariability (R band) of 1641 + 399 on the night of 10 Jun 1992.

The first microvariability light curve of 1641 + 399 for the night of 10 Jun 1992 is shown in Figure 3.67. The object was monitored sparsely for 7 hours and the light curve shows no statistically significant variations in amplitude.

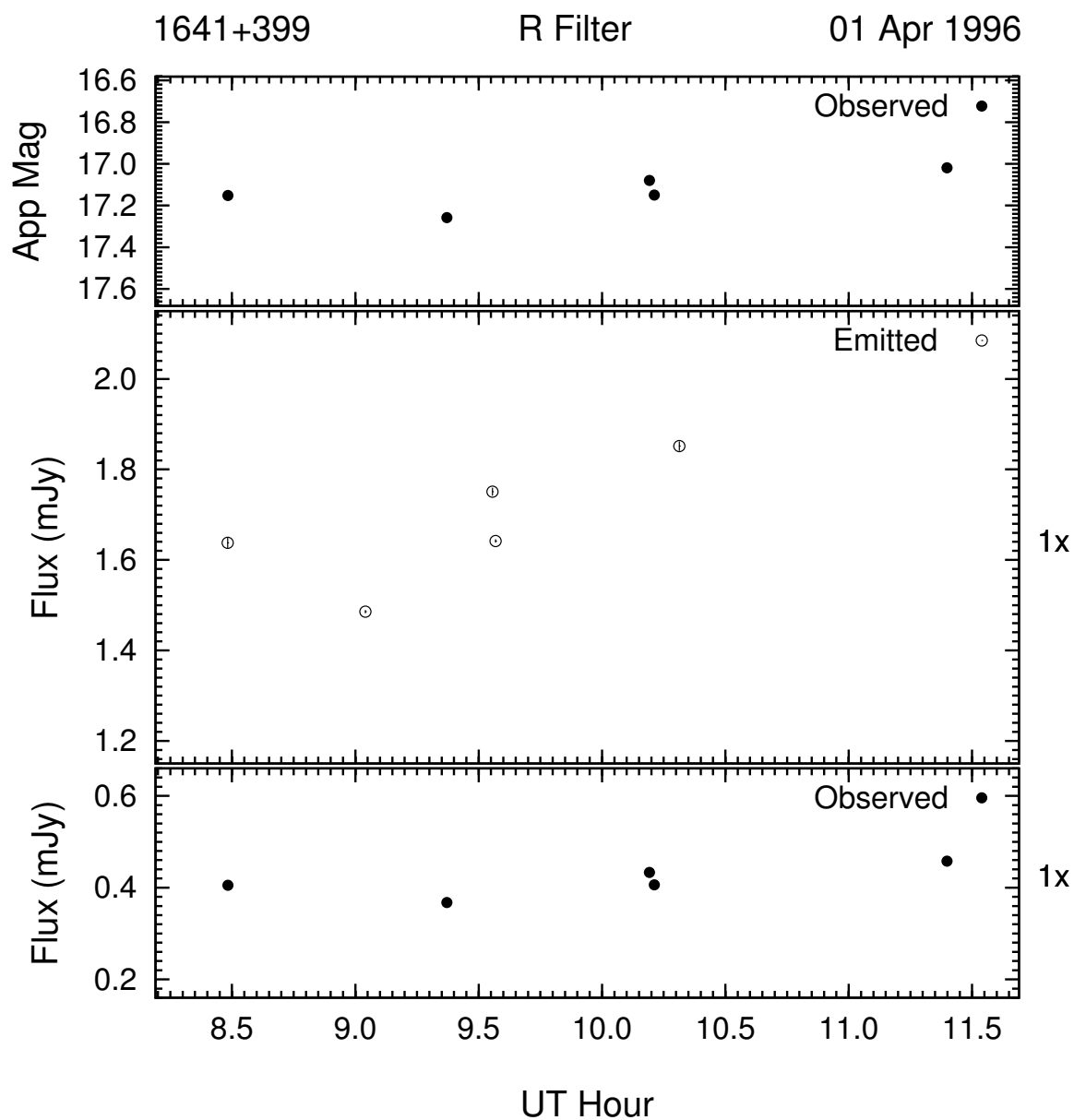


Figure 3.68: Example of the optical microvariability (R band) of 1641 + 399 on the night of 01 Apr 1996.

1641 + 399 was then monitored for 2 nights in April of 1996. On the night of 01 April (Figure 3.68), the object exhibited its largest variation in amplitude in terms of significance level of 46.4σ (0.25 mag) over 3 hours. The peak brightness for this night occurred at the

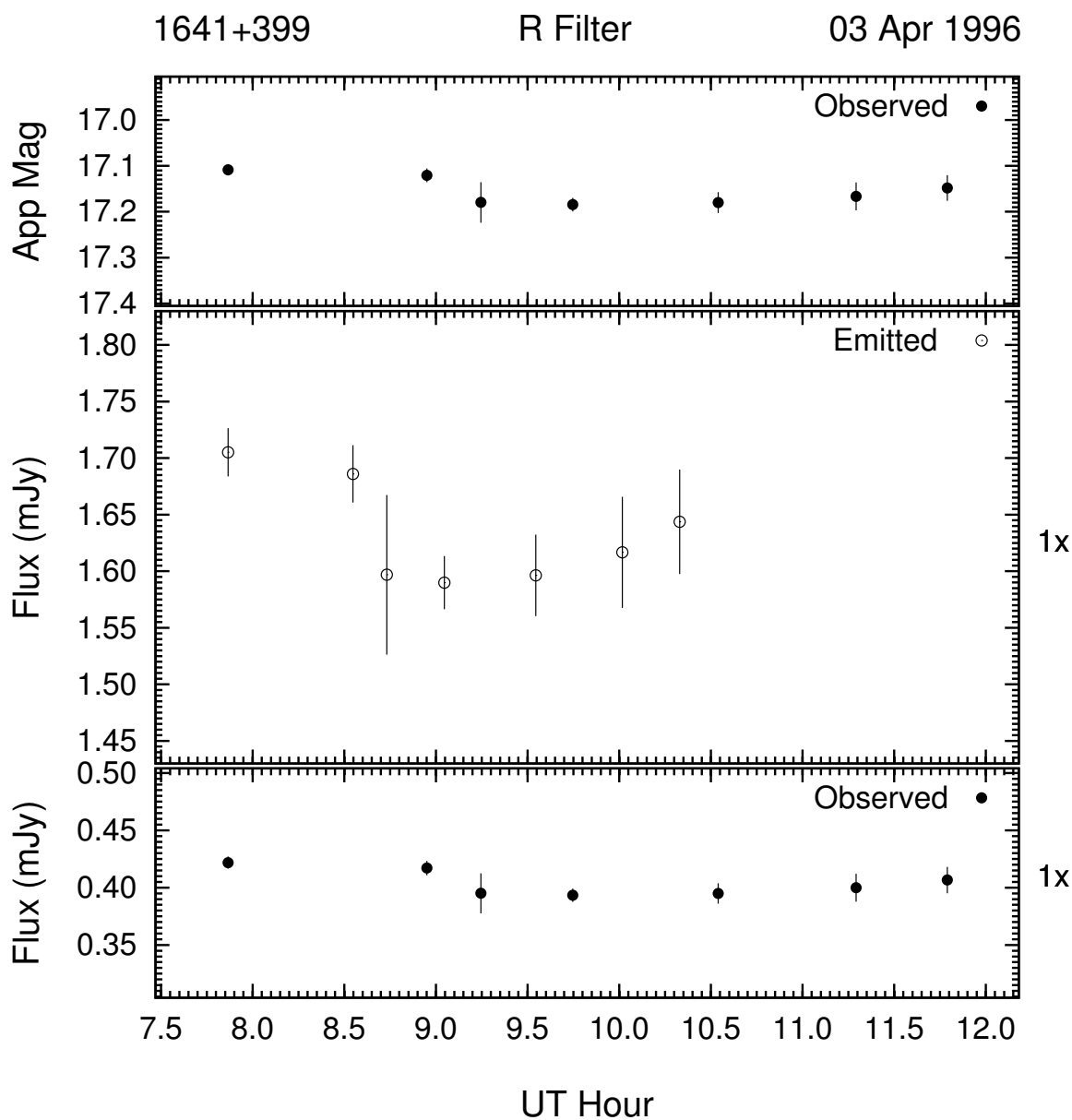


Figure 3.69: Example of the optical microvariability (R band) of 1641 + 399 on the night of 03 Apr 1996. This night's data was 2-point averaged to improve S/N .

end at a level of $R = 17.0$. Two nights later, 1641 + 399 was 0.1 mag dimmer and showed a variation of < 0.1 mag which is not significant given the error of the observations on this night.

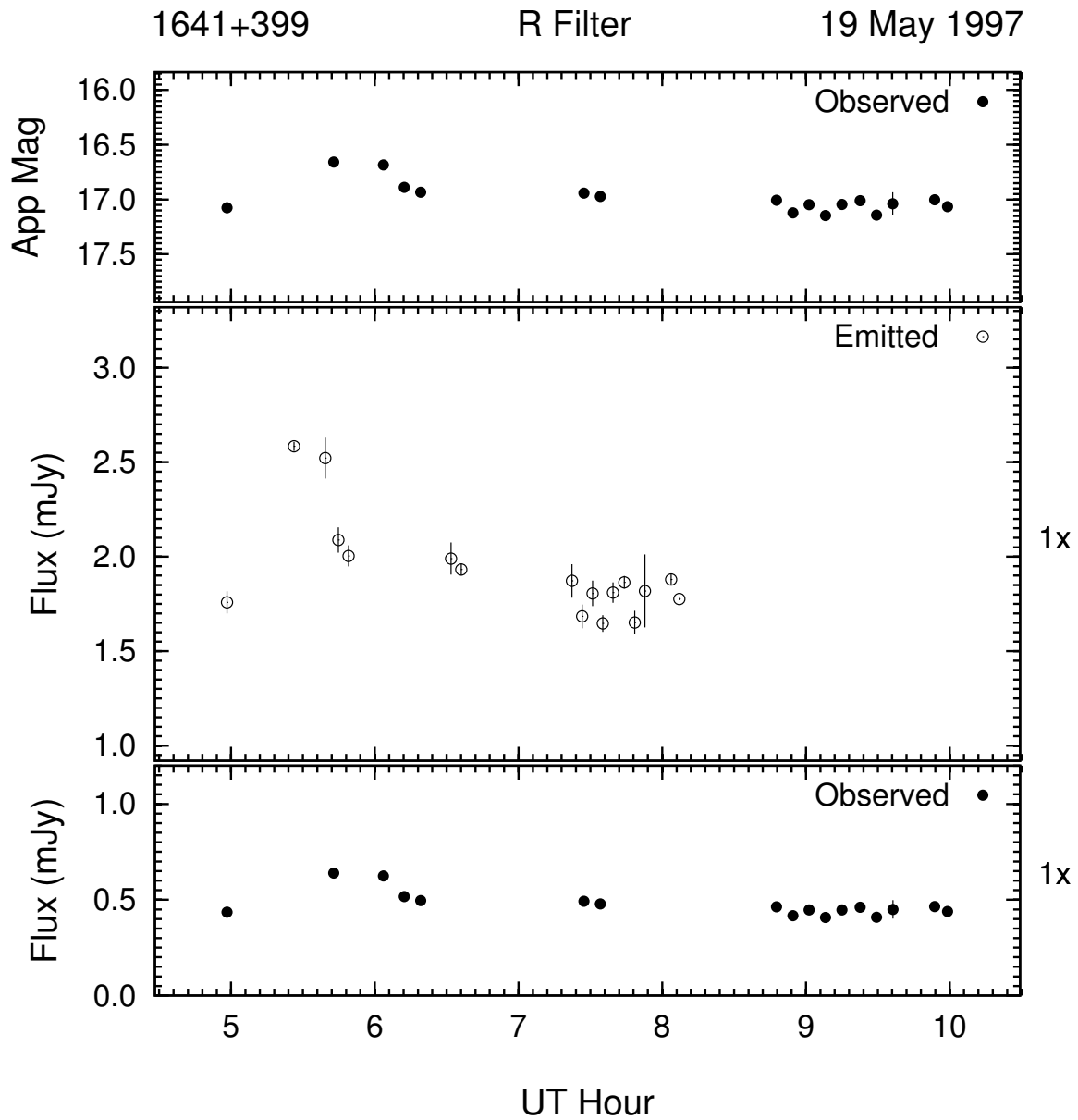


Figure 3.70: Example of the optical microvariability (R band) of 1641 + 399 on the night of 19 May 1997. This night's data was 2-point averaged to improve S/N .

On the night of 19 May 1997, 1641 + 399 showed the largest change in brightness of any night it was observed (0.5 mag), albeit with a significance of only 12.9σ . The light curve shown in Figure 3.70 illustrates this microvariability. Starting at a brightness of $R \simeq 17.1$,

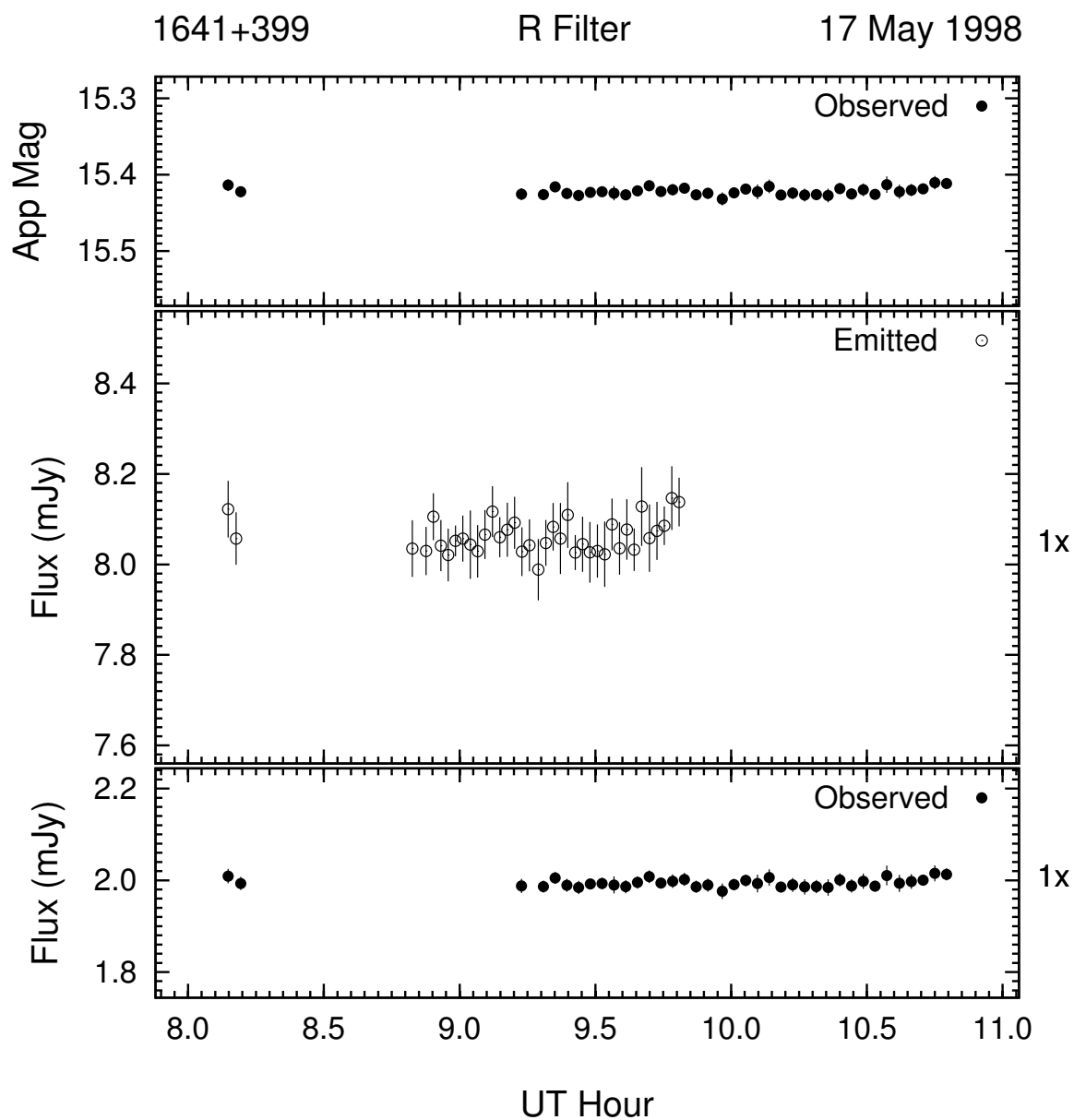


Figure 3.71: Example of the optical microvariability (R band) of 1641 + 399 on the night of 17 May 1998.

1641 + 399 increased in brightness by 0.5 mag in less than an hour. It then dimmed ~ 0.35 mag in less than one half hour, and then the remaining 0.15 mag over the next 3 hours, ending the night at roughly the same brightness level as it began.

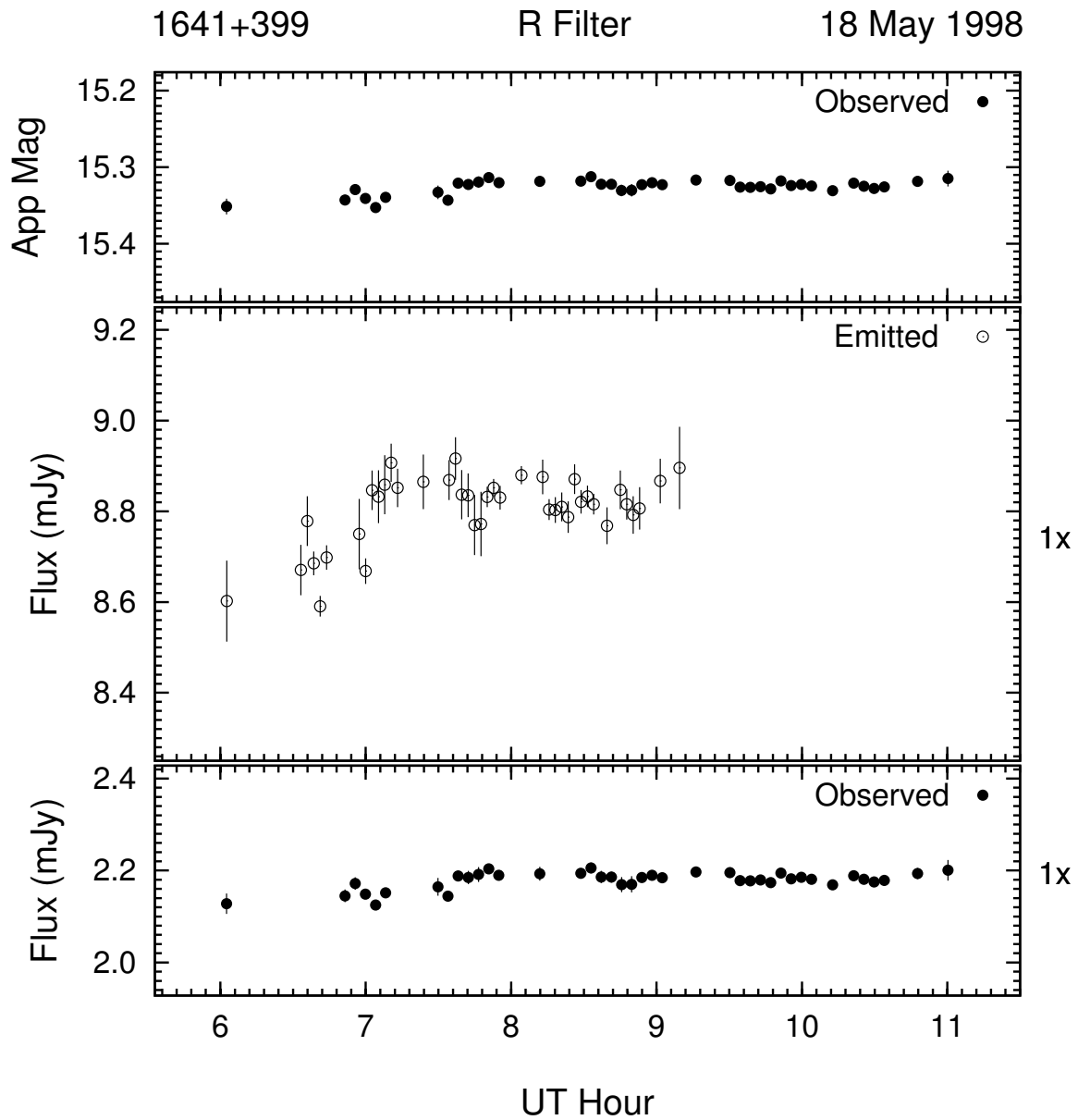


Figure 3.72: Example of the optical microvariability (R band) of 1641 + 399 on the night of 18 May 1998. This night's data was 2-point averaged to improve S/N .

In May of 1998, 1641 + 399 was observed for the 3 consecutive nights at a brightness level ~ 2.5 mag higher than in mid-1997. These observations are shown in the light curves in Figures 3.71 through 3.73. The first night, 17 May, the observations showed no significant

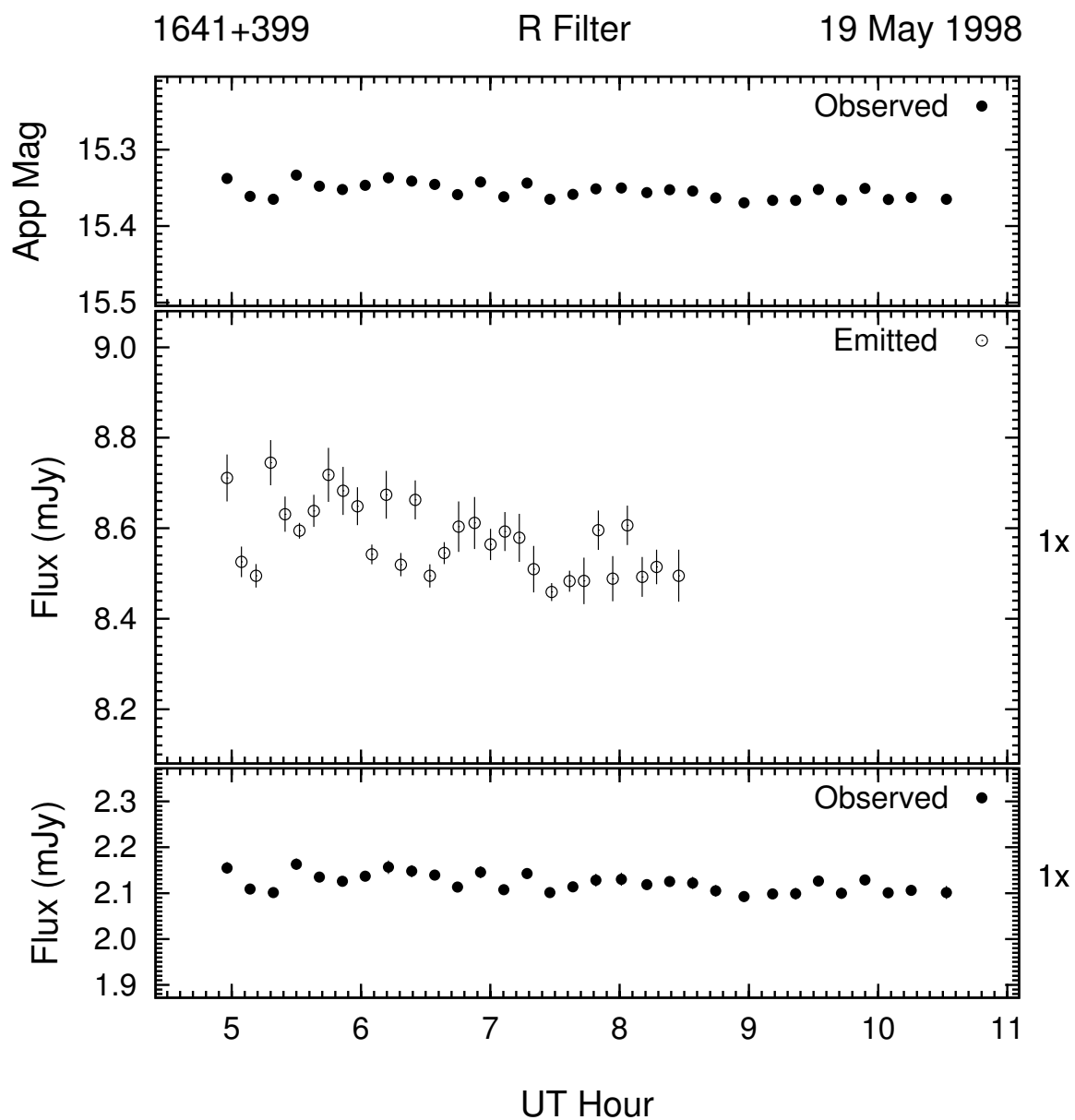


Figure 3.73: Example of the optical microvariability (R band) of 1641 + 399 on the night of 19 May 1998. This night's data was 4-point averaged to improve S/N .

variations, but the remaining 2 nights exhibited variations at $> 5\sigma$ confidence level. On the night of 18 May (Figure 3.72), 1641 + 399 showed a gentle rise in brightness of ~ 0.05 mag over the first half of the night (~ 2.5 hours) and a plateau during the latter half. The next

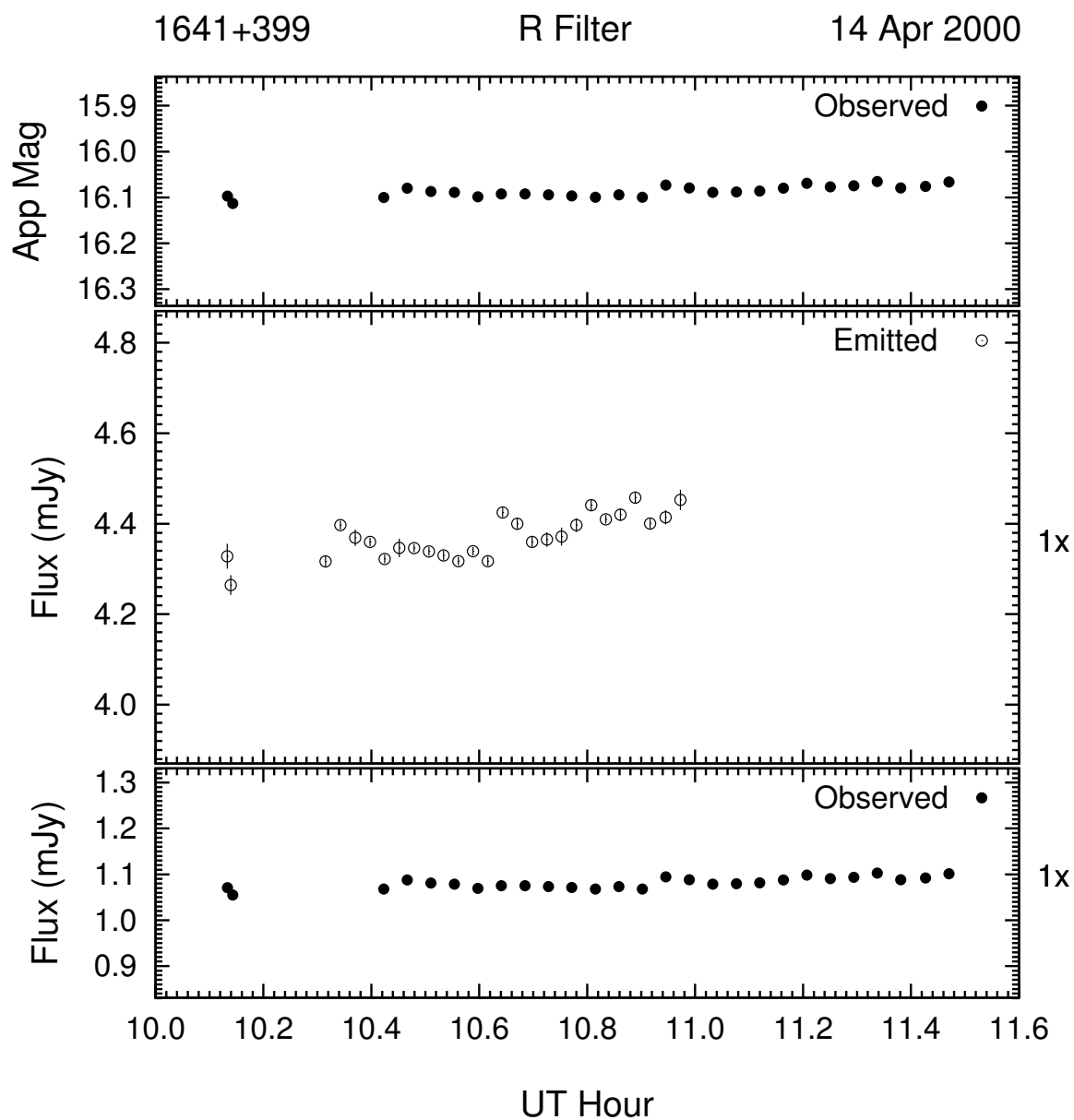


Figure 3.74: Example of the optical microvariability (R band) of 1641 + 399 on the night of 14 Apr 2000.

night (Figure 3.73), 1641 + 399's light curve showed a similar character, but started the night with the plateau and dimmed ~ 0.05 mag. All 3 nights were between the brightness levels of $R = 15.3$ and $R = 15.4$.

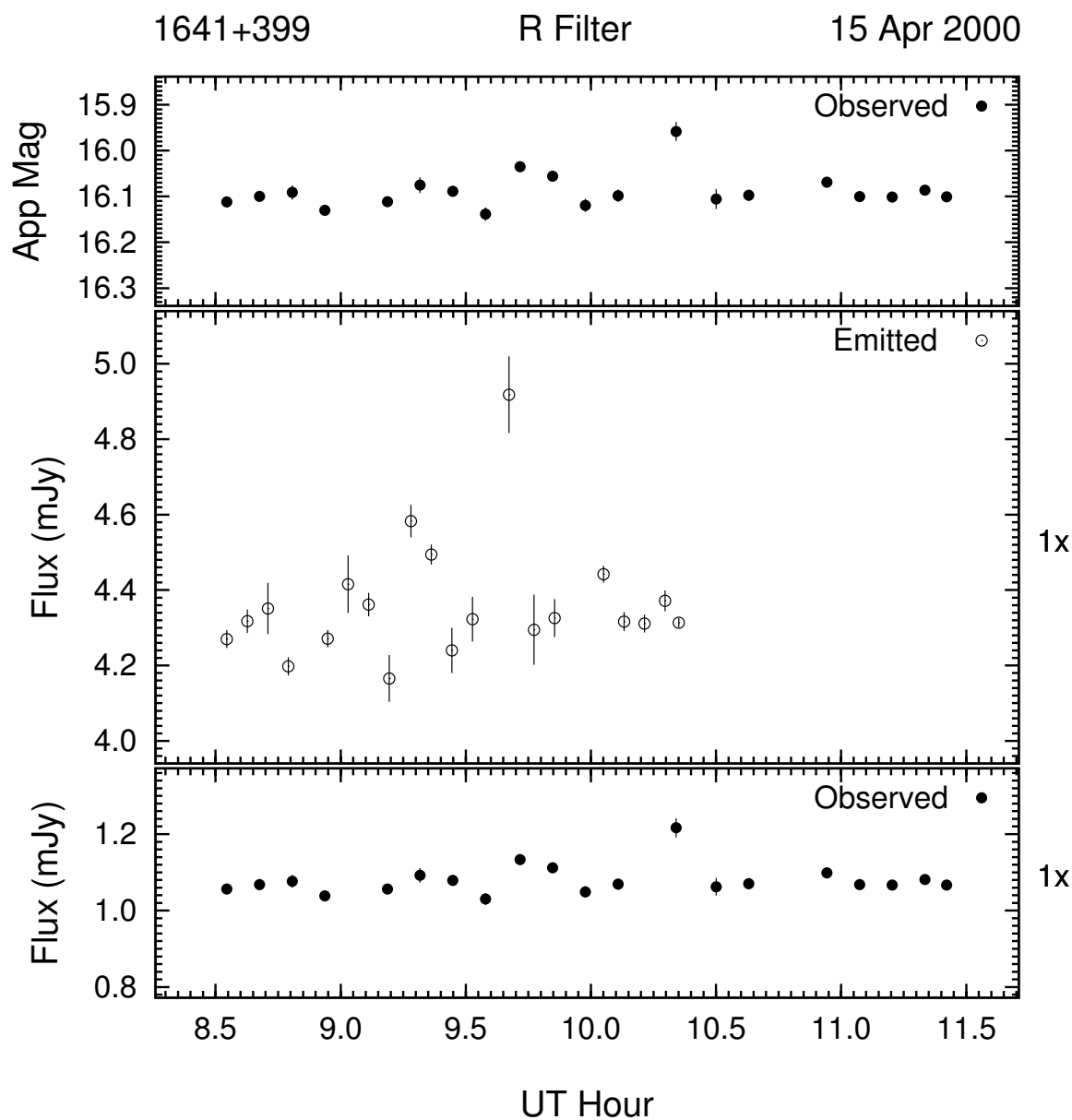


Figure 3.75: Example of the optical microvariability (R band) of 1641 + 399 on the night of 15 Apr 2000. This night's data was 3-point averaged to improve S/N .

The next time 1641 + 399 was monitored for microvariability was in mid-April of 2000. It was 0.7 mag dimmer than in May of 1998 and was observed for 4 consecutive nights from 14 to 17 April, with the corresponding light curves shown in Figures 3.74 through 3.77.

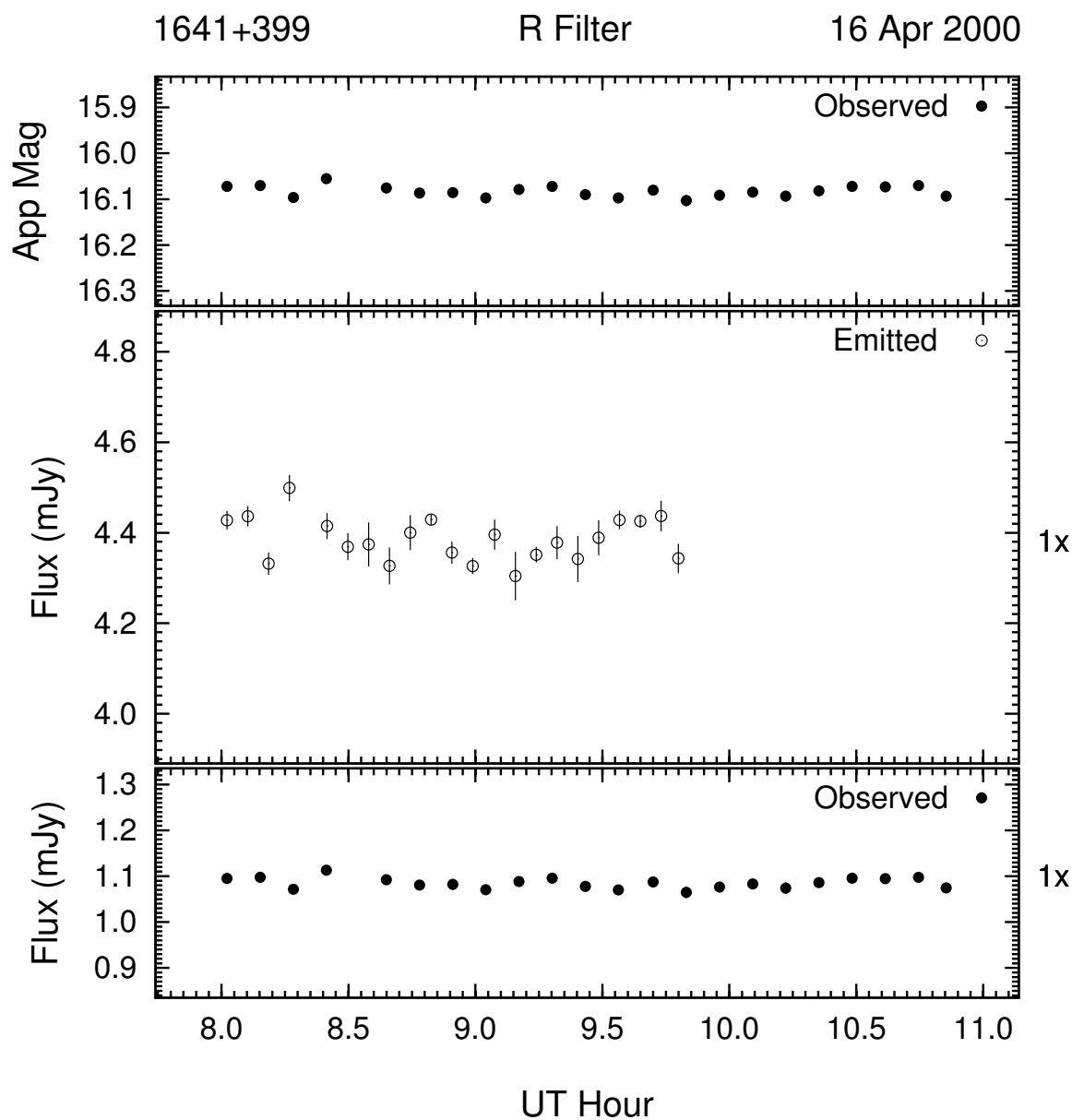


Figure 3.76: Example of the optical microvariability (R band) of 1641 + 399 on the night of 16 Apr 2000. This night's data was 3-point averaged to improve S/N .

On the night of 14 Apr, 1641 + 399 brightened only slightly (0.05 mag) with no significant brightness variations on the trend. The following night (Figure 3.75), the overall variability amplitude was significantly higher (0.2 mag) with $> 2.6\sigma$ brightness variations for durations

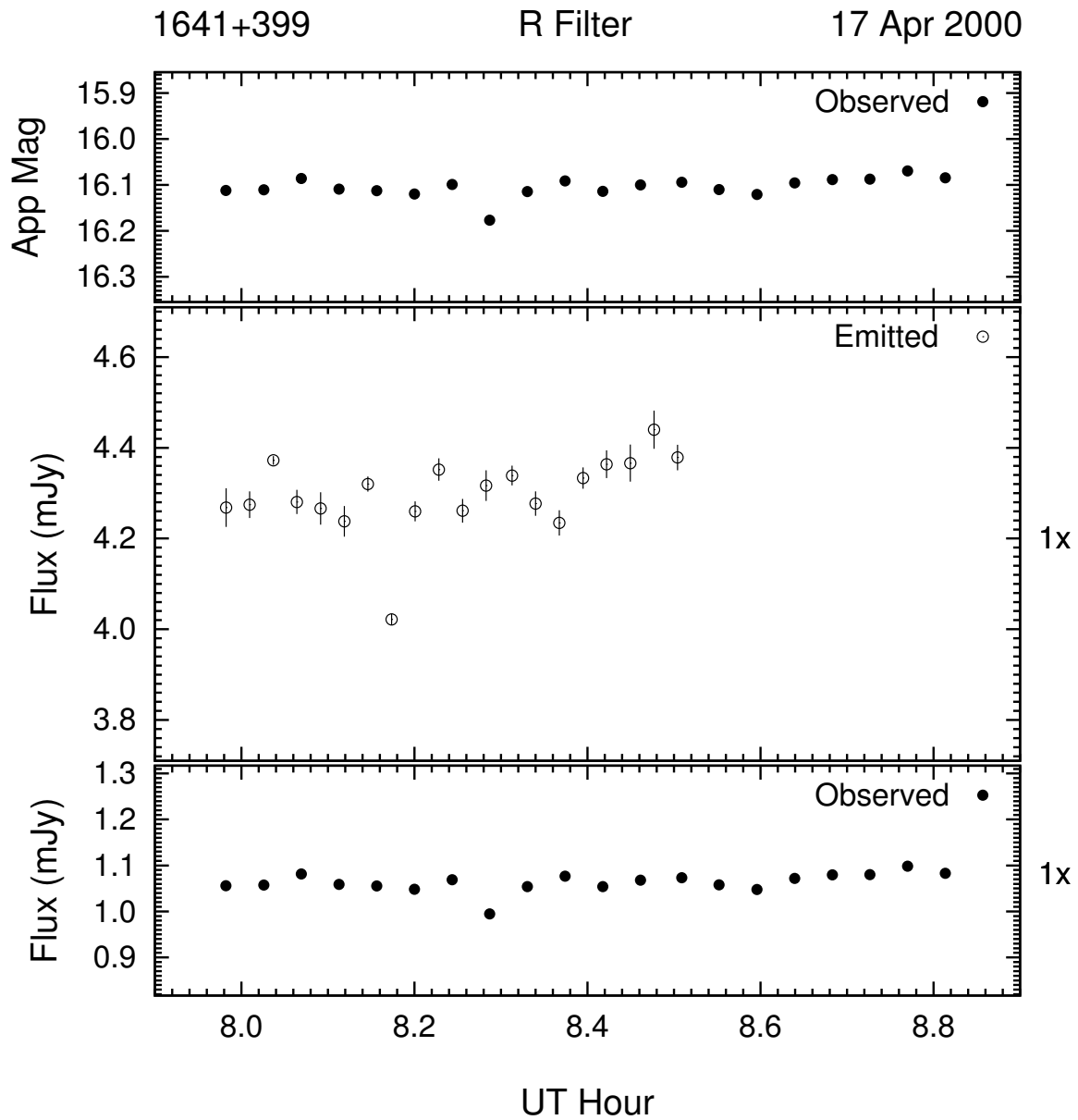


Figure 3.77: Example of the optical microvariability (R band) of 1641 + 399 on the night of 17 Apr 2000.

of ~ 0.5 hour. There was no net brightness change for this night. The variability character of 1641 + 399's light curve on the night of 16 Apr (Figure 3.76) is similar to the previous night. The last night (17 Apr, Figure 3.77), 1641 + 399 exhibited a general increase in brightness

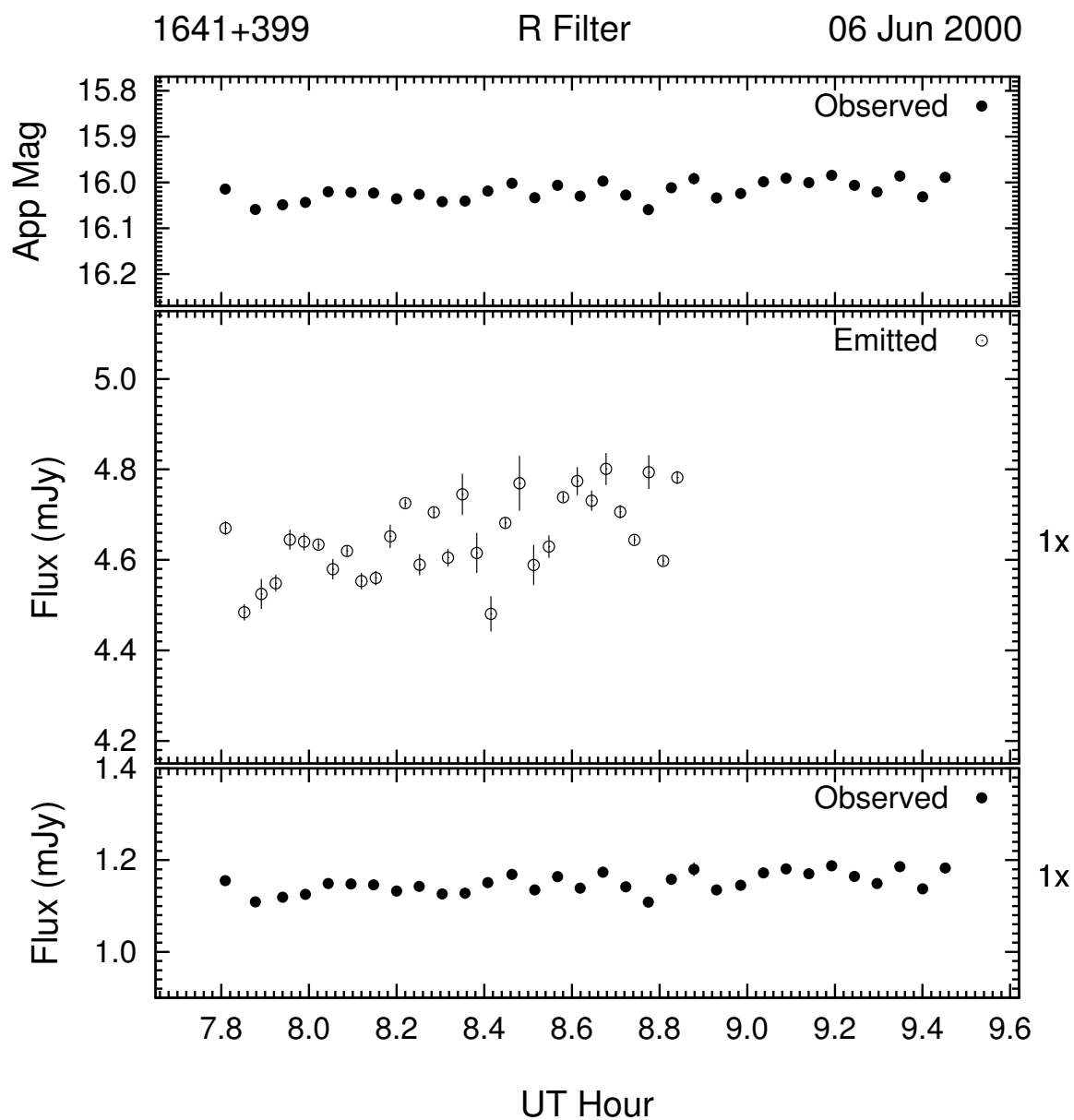


Figure 3.78: Example of the optical microvariability (R band) of 1641 + 399 on the night of 06 Jun 2000.

with a variability character similar to the previous 2 nights. All 4 nights were at a relatively constant brightness level of $R \simeq 16.1$ and the total duration of the observations for all 4 nights was only ~ 8 hours.

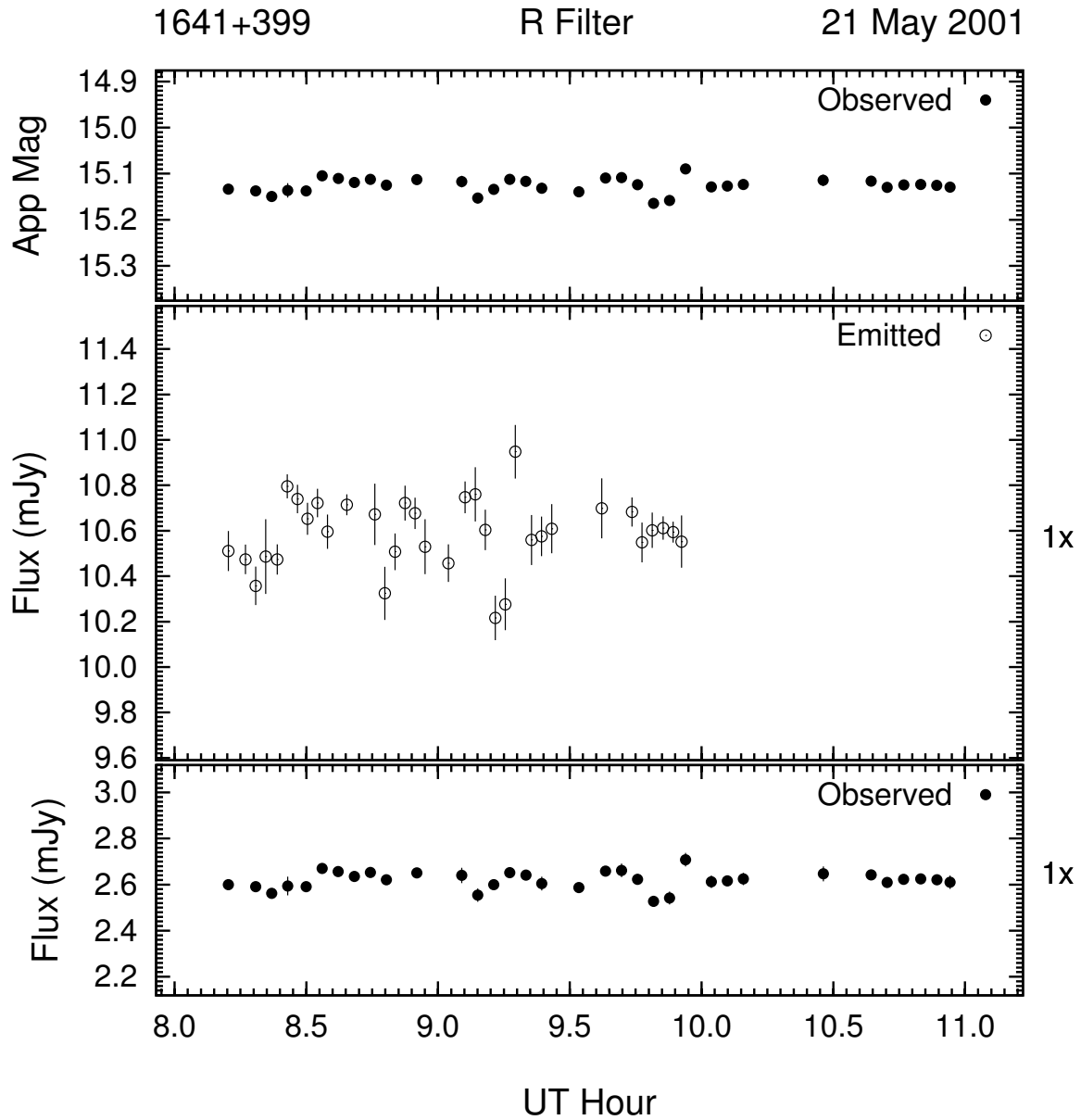


Figure 3.79: Example of the optical microvariability (R band) of 1641 + 399 on the night of 21 May 2001. This night's data was 3-point averaged to improve S/N .

1641 + 399 was monitored for ~ 1.5 hours on the night of 06 Jun 2000 (Figure 3.78). The only statistically significant variation seen was the 0.07 mag rise in brightness from the beginning of the observation to the end. Over the course of almost 3 hours on the night

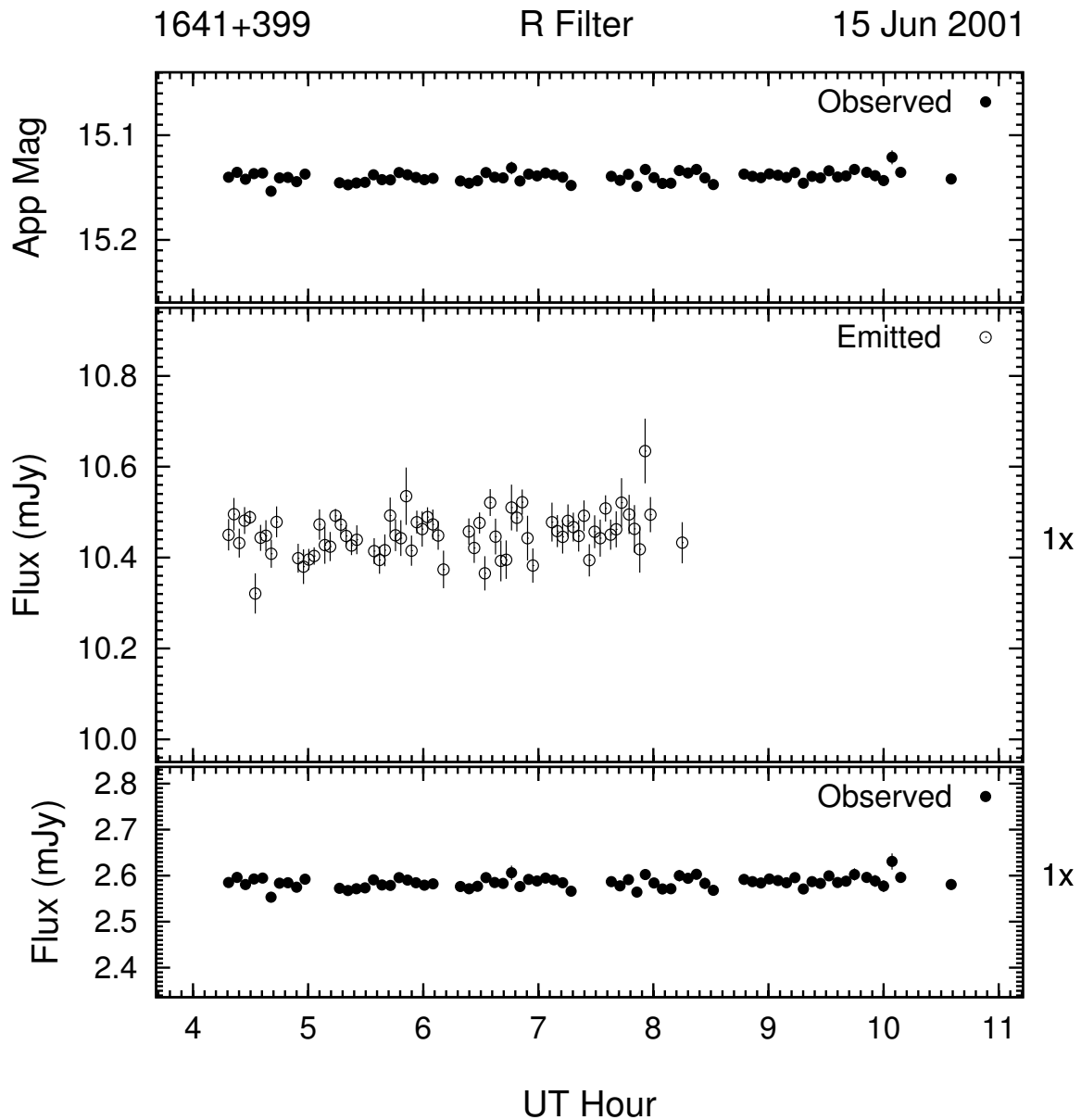


Figure 3.80: Example of the optical microvariability (R band) of 1641 + 399 on the night of 15 Jun 2001. This night's data was 2-point averaged to improve S/N .

of 21 May 2001 (Figure 3.79), 1641 + 399 varied in brightness at approximately the same amplitude, but without the trend in brightness. The brightness level of 1641 + 399 increased by more than 1 mag between these 2 observations.

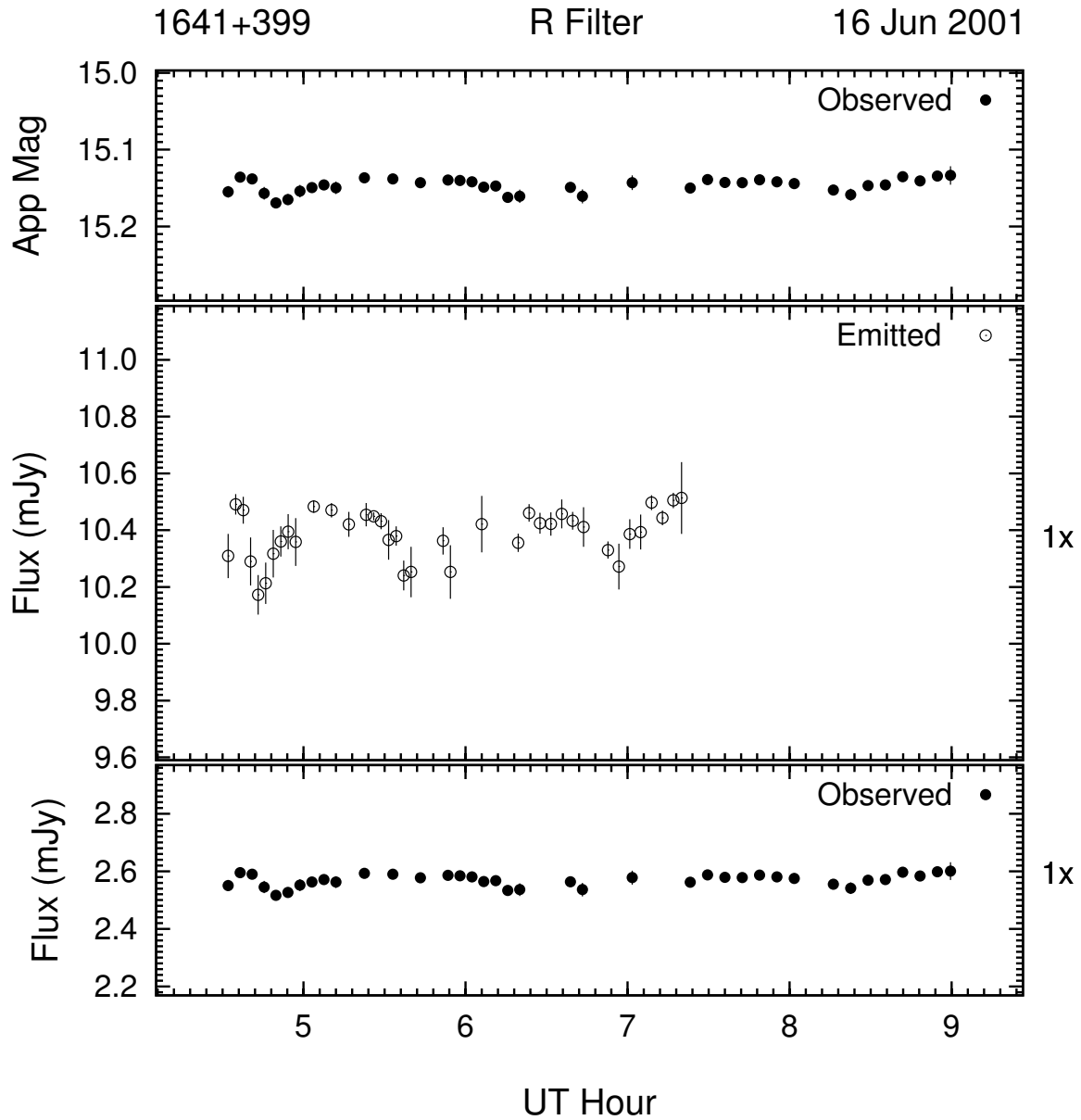


Figure 3.81: Example of the optical microvariability (R band) of 1641 + 399 on the night of 16 Jun 2001. This night's data was 2-point averaged to improve S/N .

In June of 2001, 641 + 399 was observed for 4 consecutive nights between 15 and 18 June (Figures 3.80 through 3.83). It was at about the same brightness level as it was the previous month, $R \simeq 15.15$. It stayed at this level all 4 nights and showed < 0.1 mag

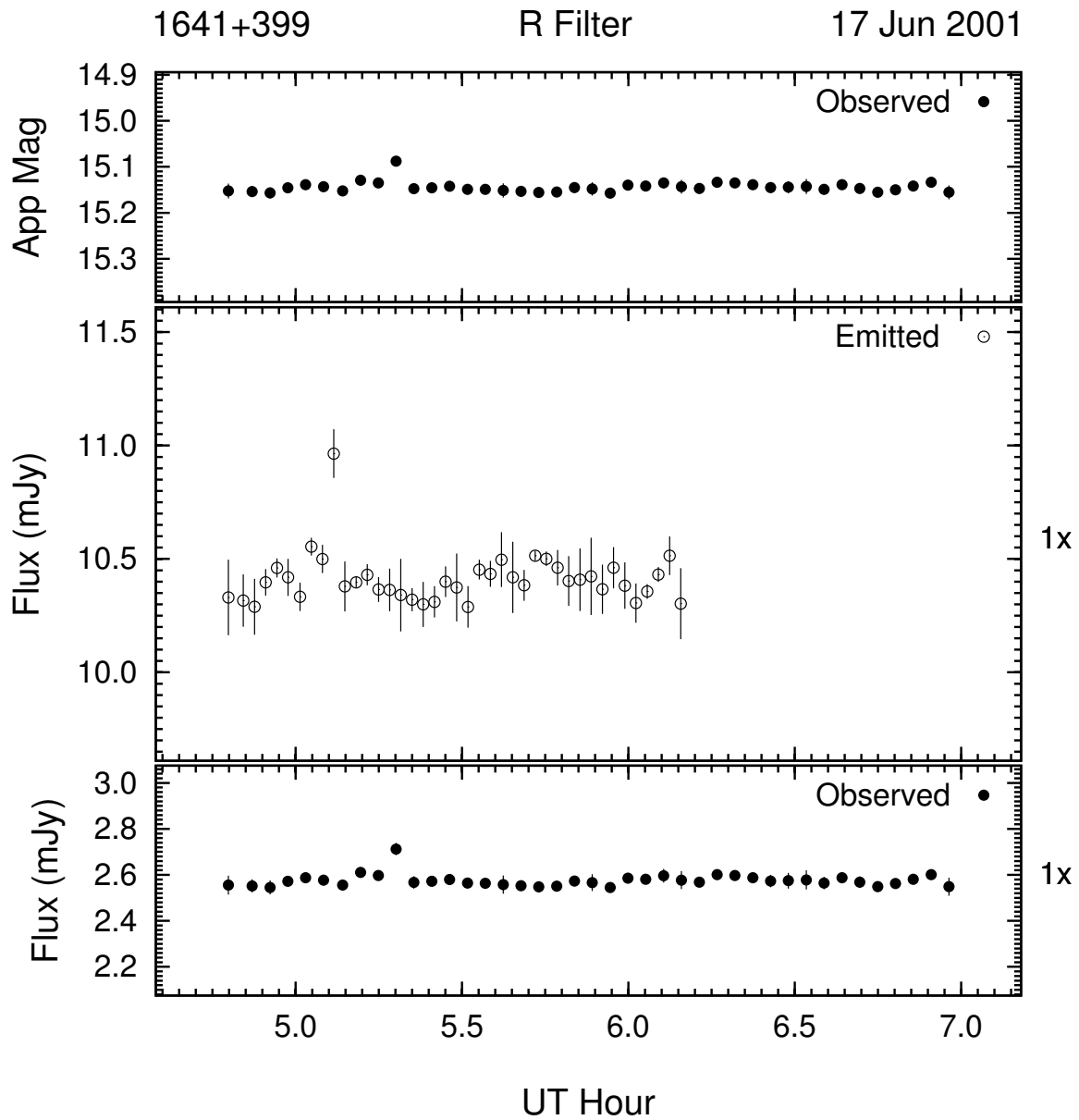


Figure 3.82: Example of the optical microvariability (R band) of 1641 + 399 on the night of 17 Jun 2001.

($< 10\sigma$) changes throughout each night. The only night that stands out is 16 Jun (Figure 3.81) where 1641 + 399's light curve exhibits some discrete brightening followed immediately by a dimming trend, twice over the course of about 3 hours, with a third brightening before

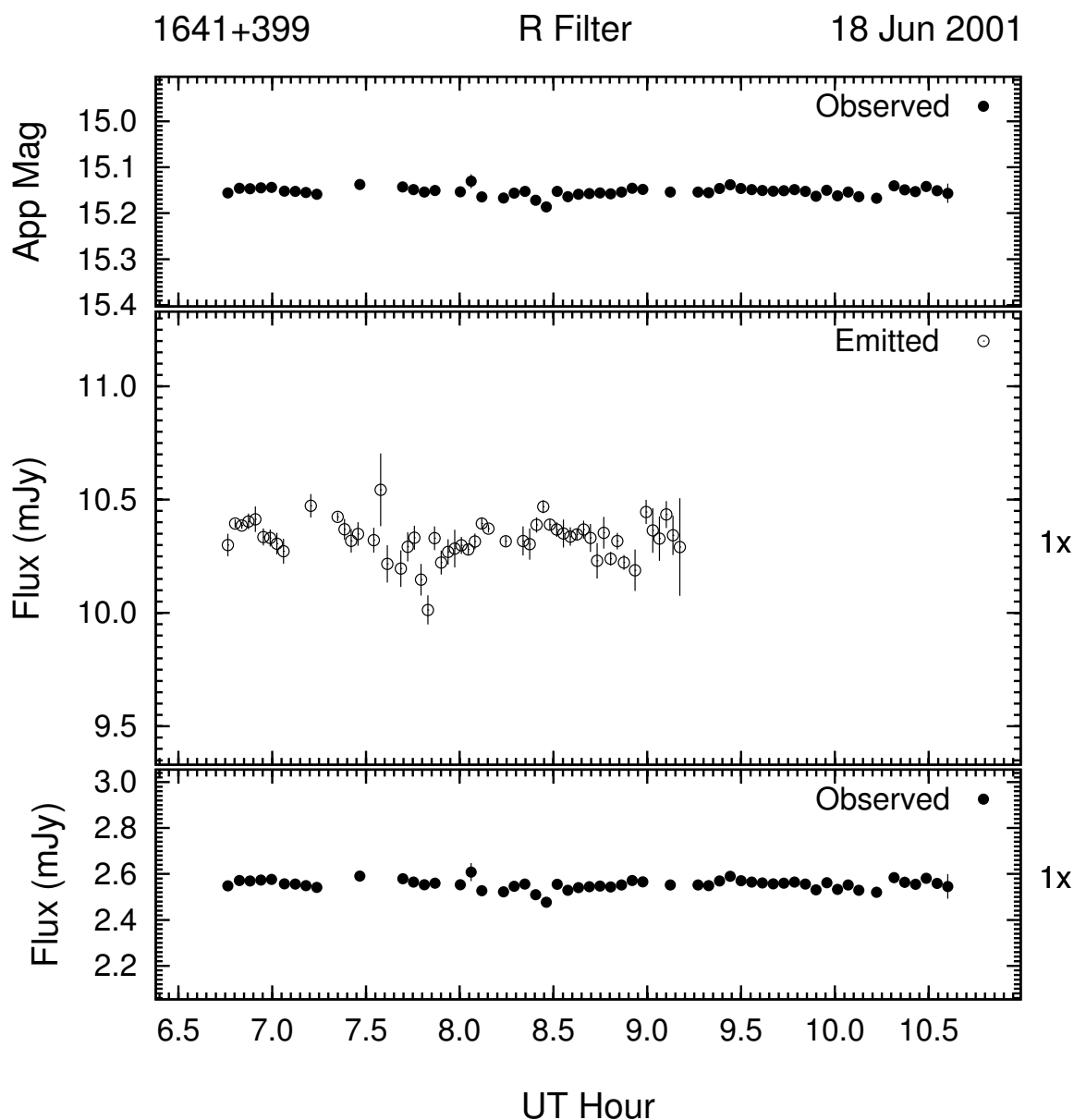


Figure 3.83: Example of the optical microvariability (R band) of 1641 + 399 on the night of 18 Jun 2001. This night's data was 2-point averaged to improve S/N .

the observation's end. The level of these variations is $\sim 5\sigma$.

The final run of microvariability observations for 1641 + 399 occurs in late May of 2004 for the 5 consecutive nights shown in Figures 3.84 through 3.88. The microvariability character

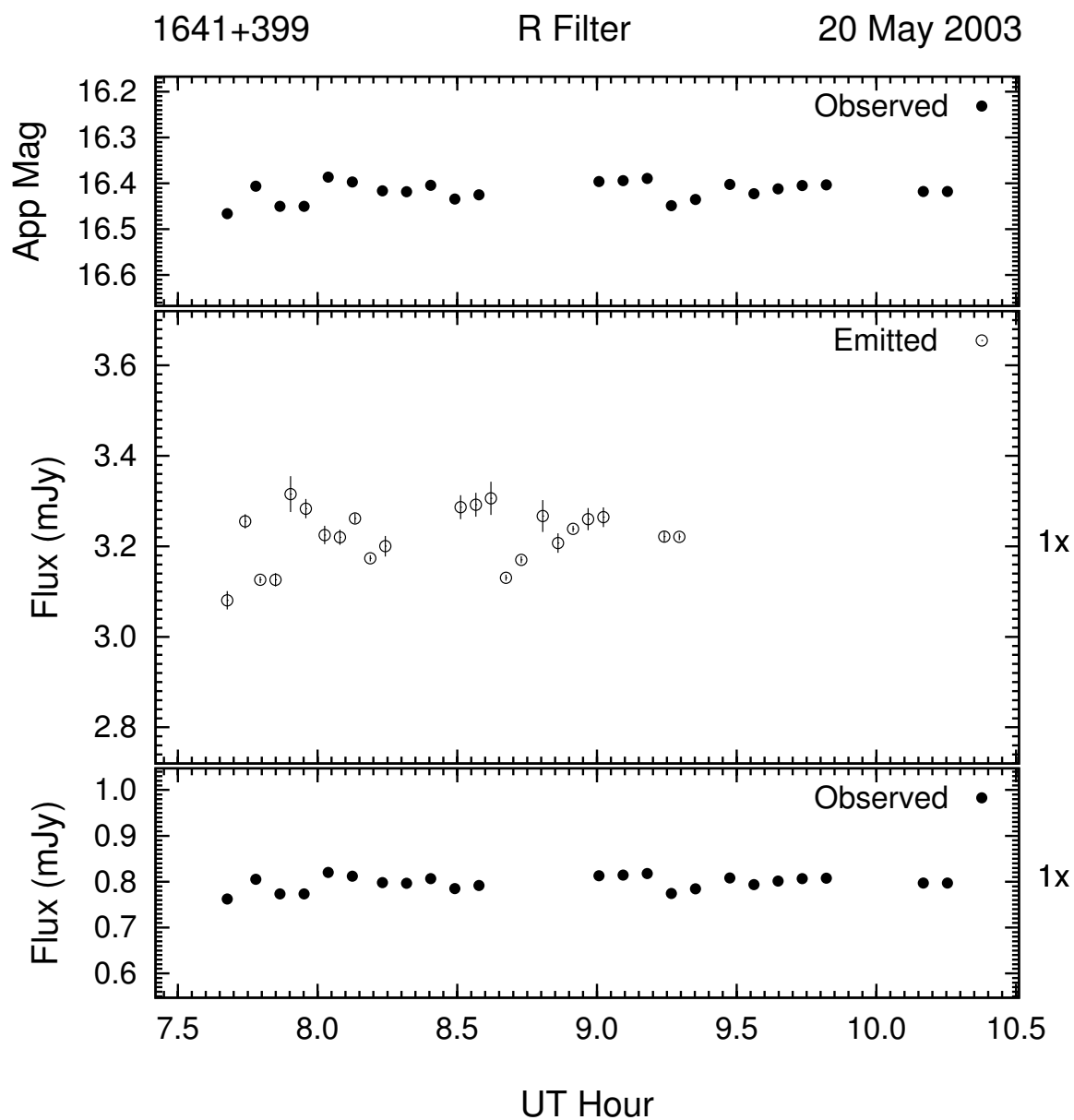


Figure 3.84: Example of the optical microvariability (R band) of 1641 + 399 on the night of 20 May 2003.

is very similar to that in the previous run during June of 2001, but is ~ 1.25 mag dimmer.

On all nights, 1641 + 399 stayed within approximately 0.05 mag of $R = 16.4$.

When shifted into its rest frame, 1641 + 399's redshift of 0.593 causes its variability

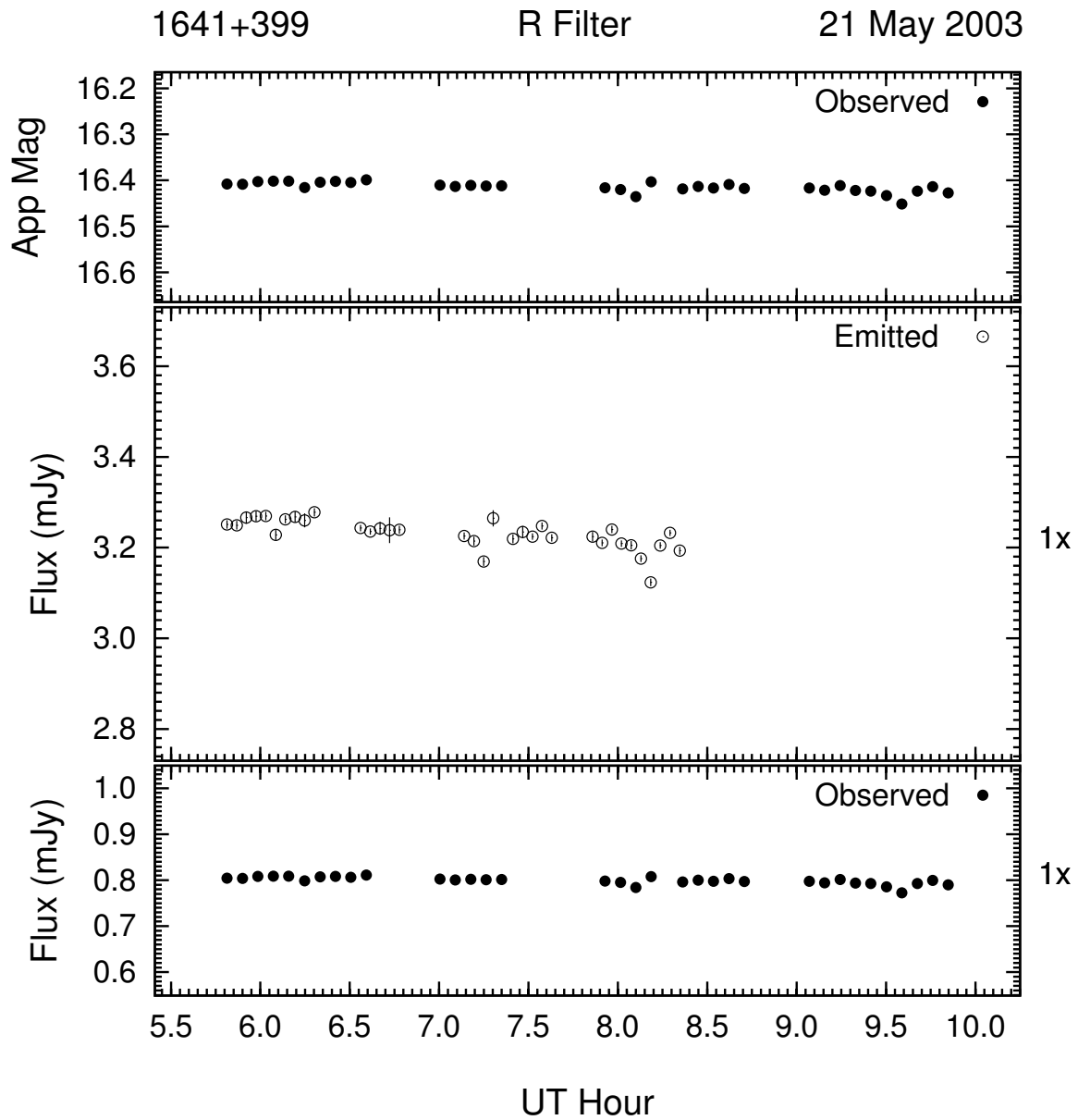


Figure 3.85: Example of the optical microvariability (R band) of 1641 + 399 on the night of 21 May 2003.

amplitudes to be enhanced by a factor of just over 4 and its time-scale is *undilated* by 37%.

The only object for which microvariability is being studied that has a lower enhancement is

BL Lac, the object which is the subject of the next section.

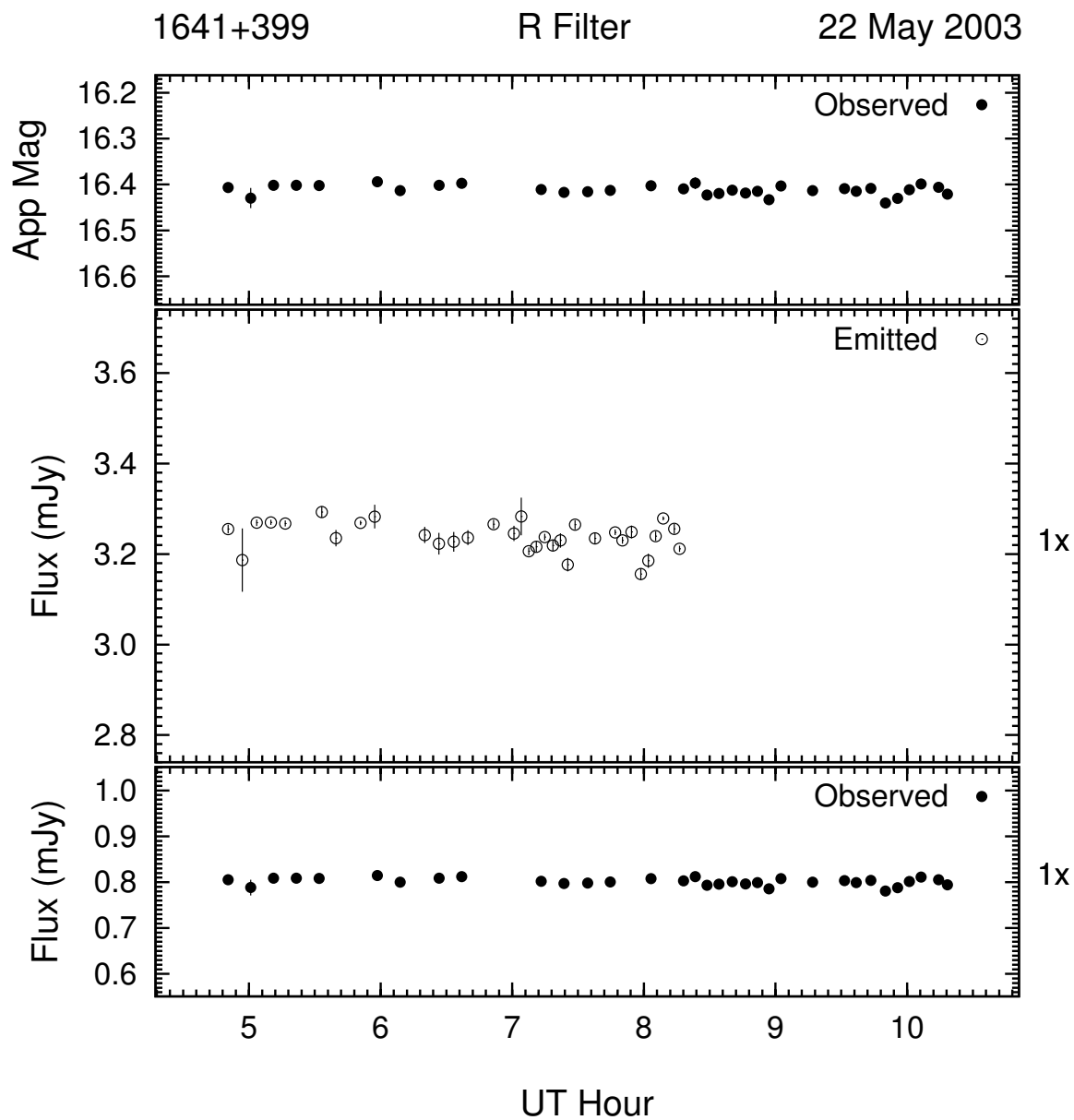


Figure 3.86: Example of the optical microvariability (R band) of 1641 + 399 on the night of 22 May 2003. This night's data was 2-point averaged to improve S/N .

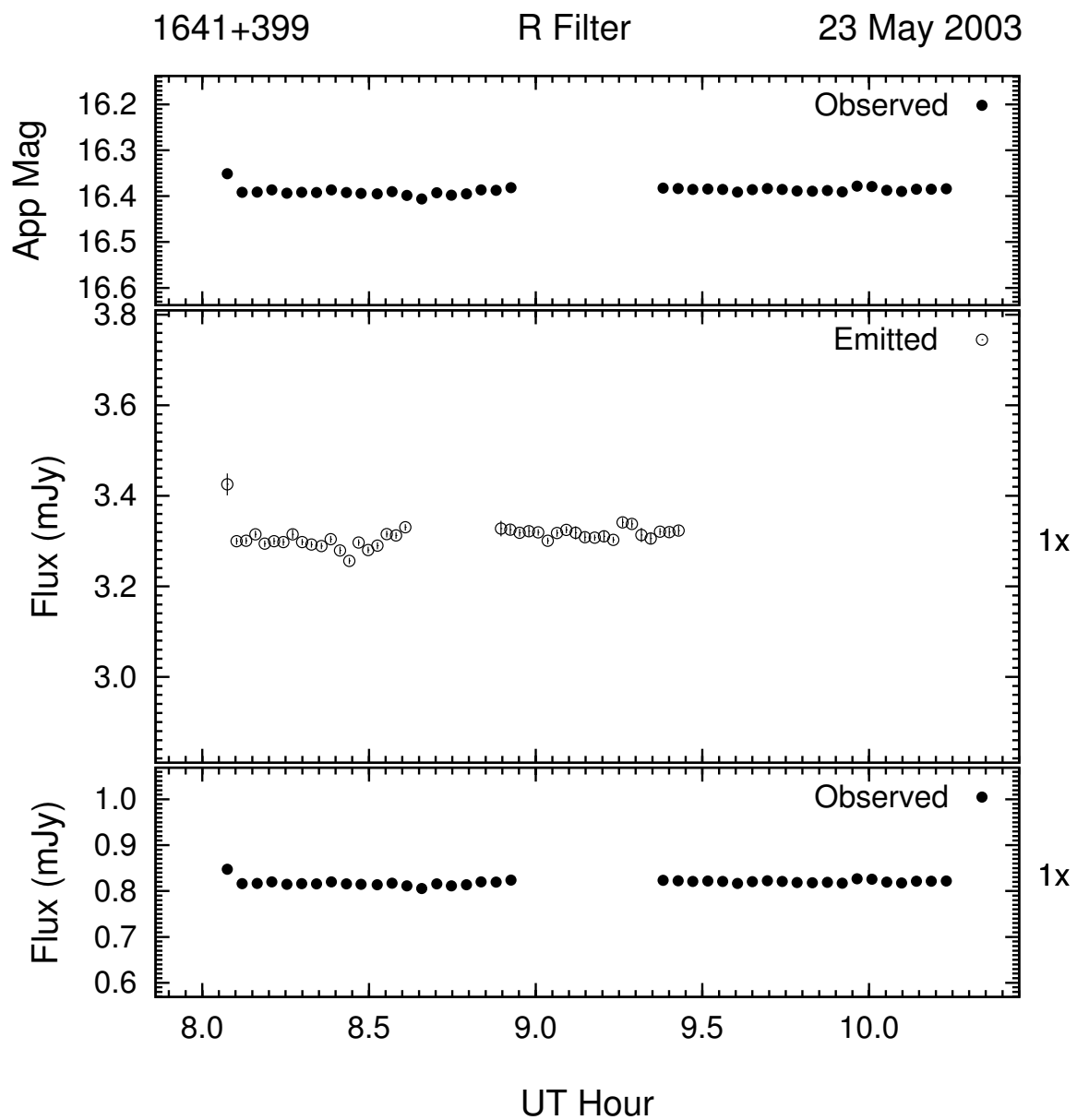


Figure 3.87: Example of the optical microvariability (R band) of 1641 + 399 on the night of 23 May 2003.

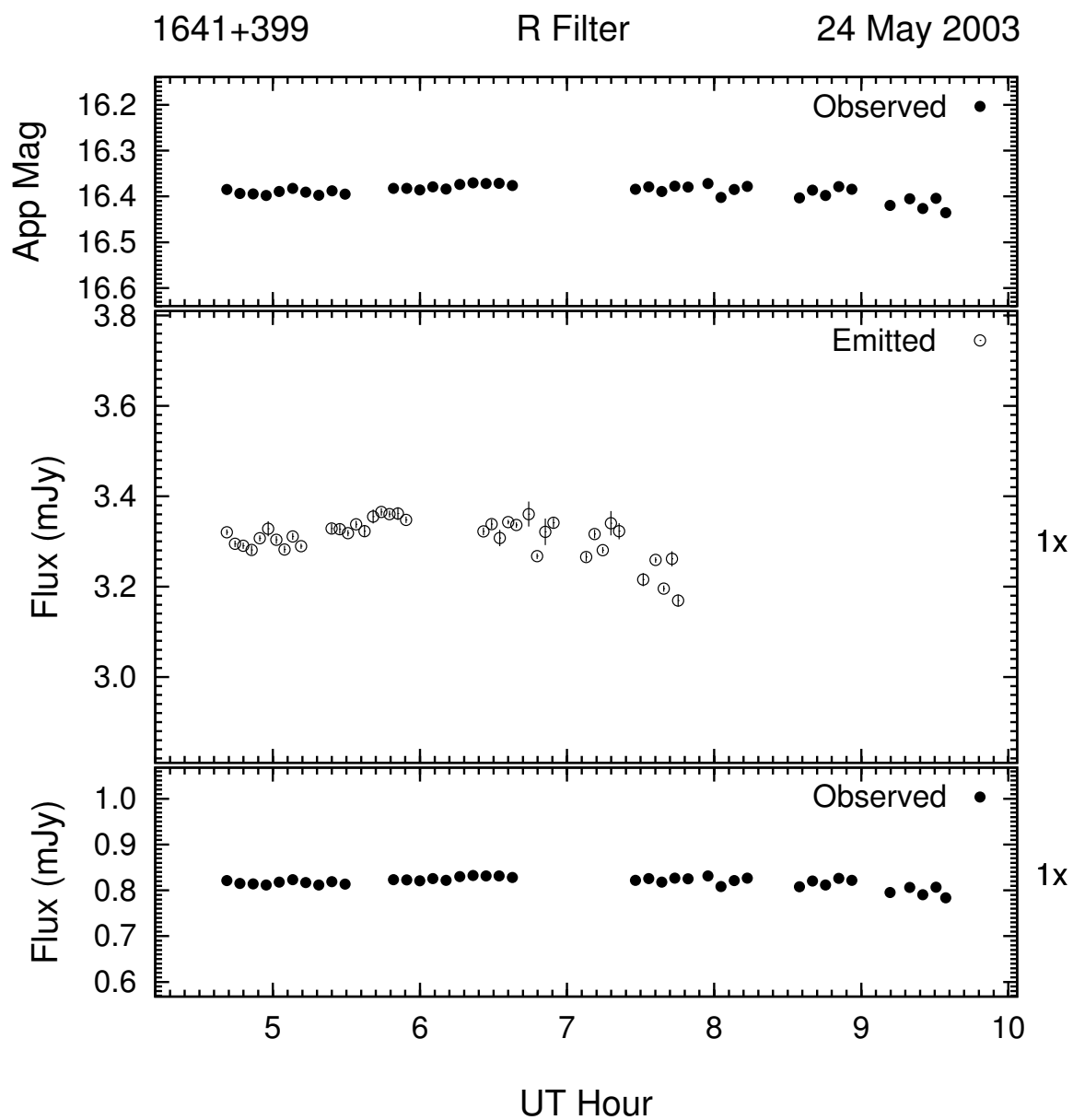


Figure 3.88: Example of the optical microvariability (R band) of 1641 + 399 on the night of 24 May 2003. This night's data was 2-point averaged to improve S/N .

3.2.6 2200 + 420

The BL Lac object BL Lacertae (also known as PKS 2200 + 420 or simply 2200 + 420) has a redshift of 0.069 and has exhibited a variability amplitude range of more than 3 mag over the time that it has been monitored for this investigation (see Figure 3.89). The data used for BL Lac is in the V and R bands only, is taken from the PEGA archives, and covers a time period of approximately 13 years. No SMARTS data exists for this object.

In Figure 3.89 the complete V and R band light curves of BL Lac from 1991 to 2004 are shown. The average color index $V - R = 0.66$ was adopted from near simultaneous observations throughout overlap region to combine the V and R band data. A detailed view showing only the overlap region is seen in Figure 3.90. The following Figures 3.91 through 3.146 show the individual nightly light curves with time periods long enough to detect microvariability.

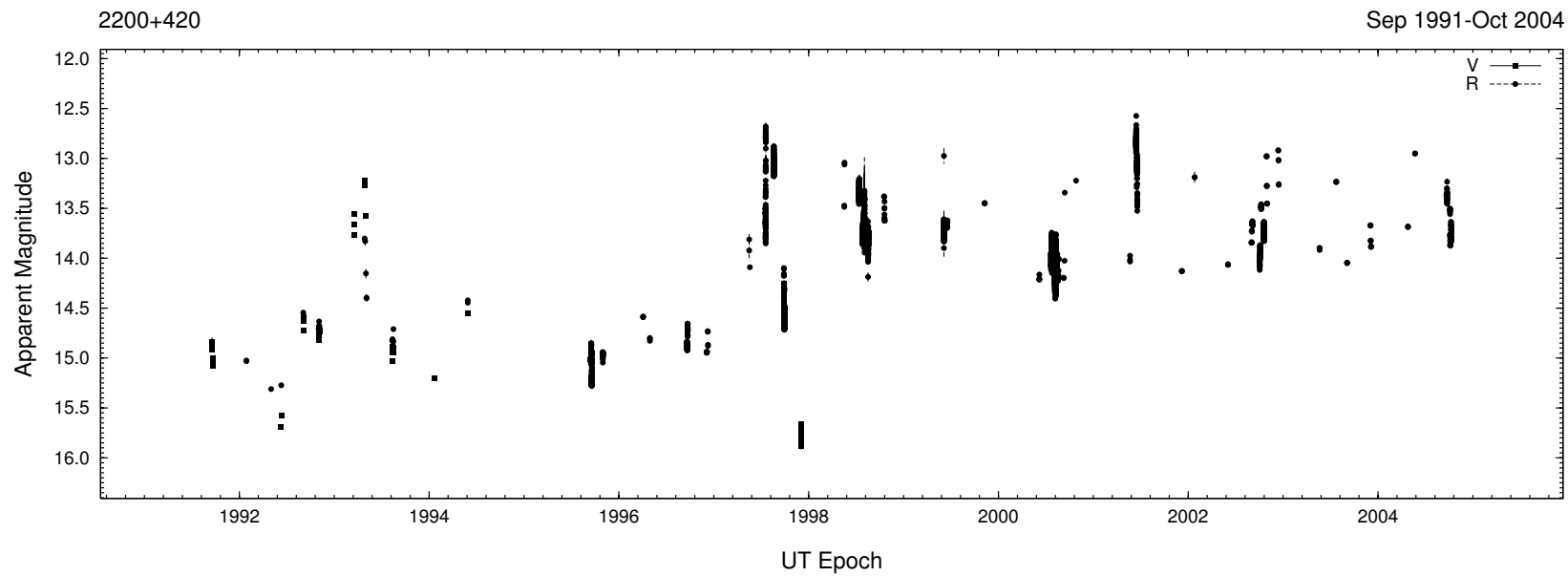


Figure 3.89: Complete V and R band light curve of BL Lac from 1991 to 2004. The amplitude of variability is ~ 3.5 mag.

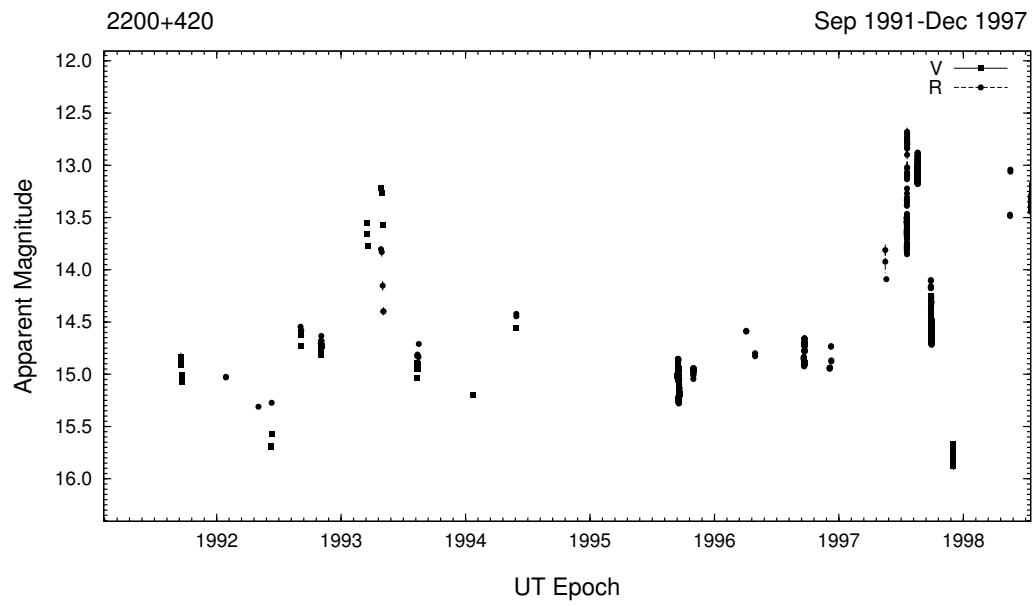


Figure 3.90: Detailed intersection of V and R band light curve of BL Lac from 1991 to 1997. The amplitude of variability is ~ 3.5 mag.

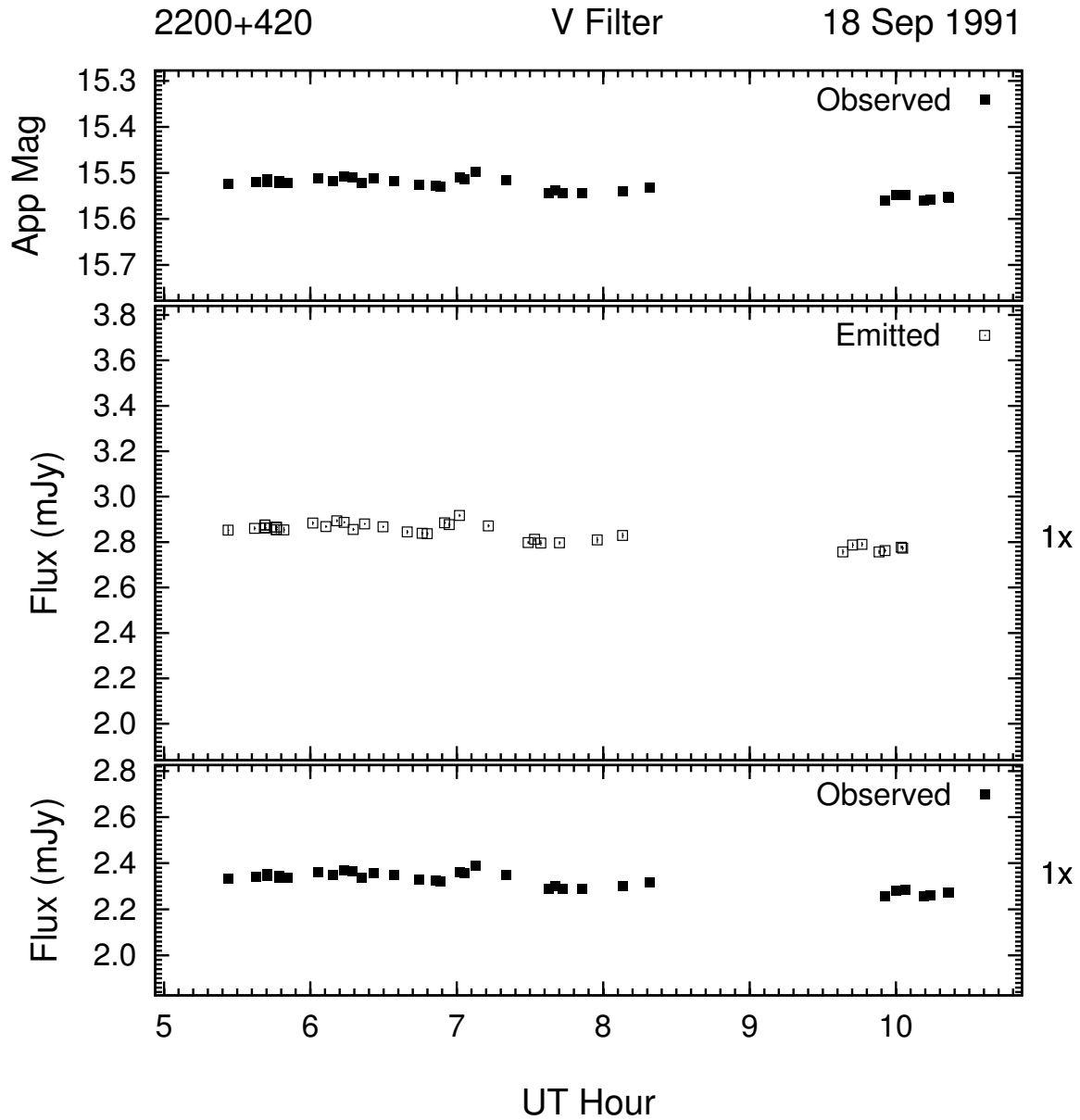


Figure 3.91: Example of the optical microvariability (V band) of 2200 + 420 on the night of 18 Sep 1991. This night's data was 3-point averaged to improve S/N .

The first microvariability light curve for BL Lac is from the night of 18 Sep 1991 and is shown in Figure 3.91. BL Lac started at a brightness level of $V \simeq 15.5$ and dimmed ~ 0.05 mag over 5 hours. There were 2 slight brightenings from this trend at 7.2^h and 8.3^h .

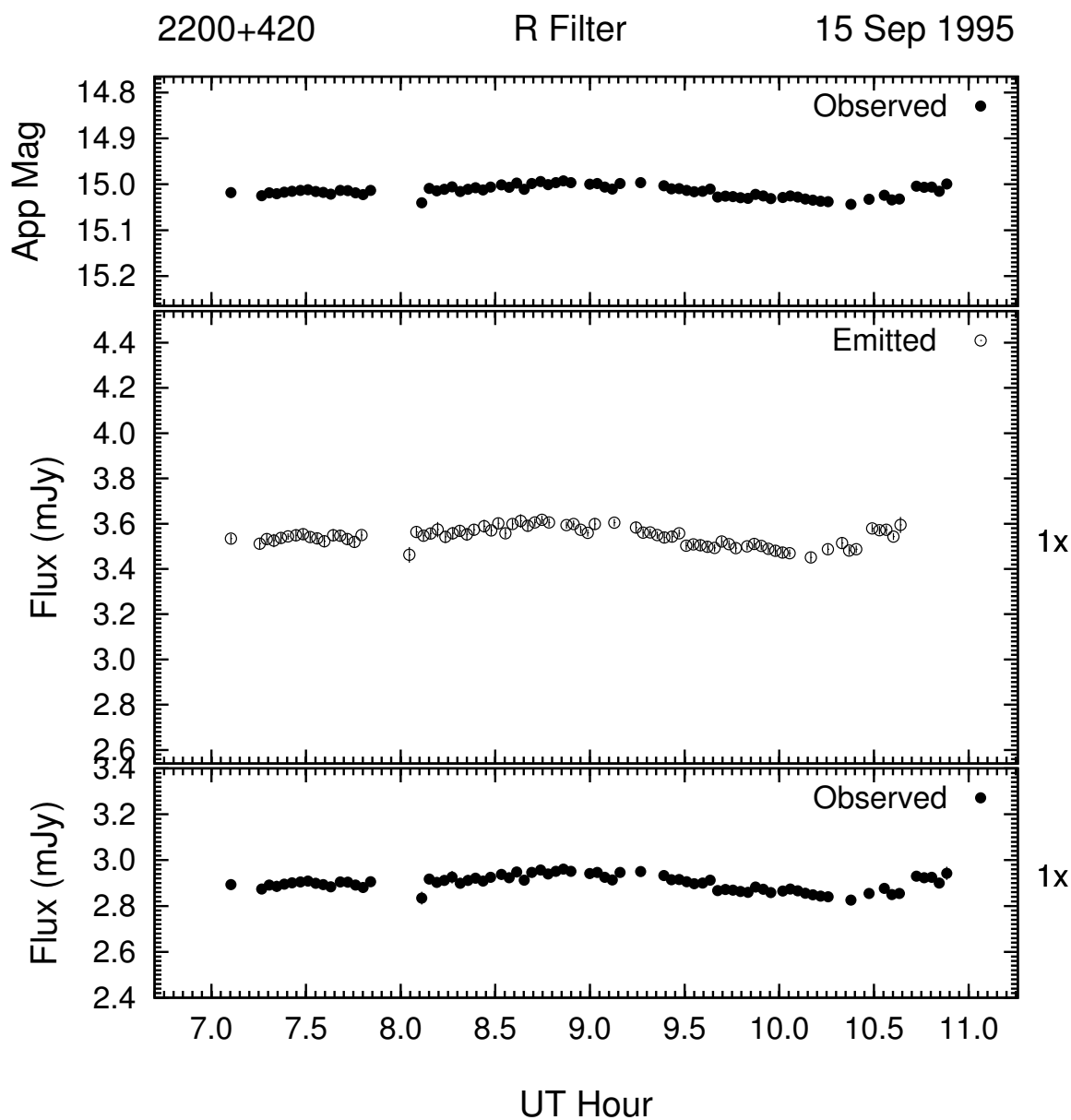


Figure 3.92: Example of the optical microvariability (R band) of 2200 + 420 on the night of 15 Sep 1995.

The next run of observations for BL Lac took place in mid-September of 1995 over 5 consecutive nights and is displayed in Figures 3.92 through 3.96. On the night of 15 Sep (Figure 3.92), BL Lac varied in brightness only 0.05 mag over 4 hours. The variations

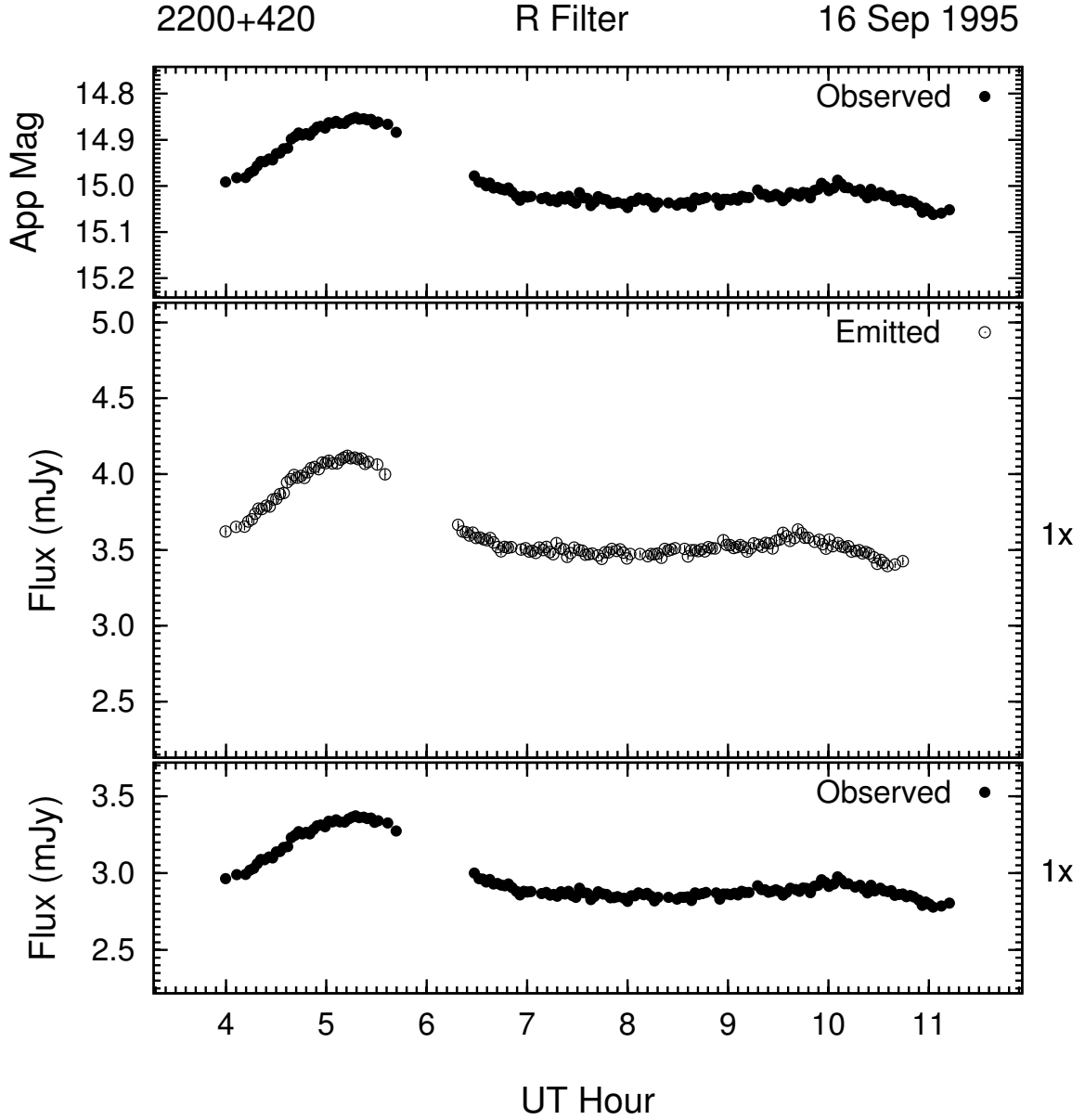


Figure 3.93: Example of the optical microvariability (R band) of 2200 + 420 on the night of 16 Sep 1995.

show a quasi-oscillatory appearance that is rather typical for BL Lac. The following night's observations exemplify this behavior. On 16 Sep (Figure 3.93), BL Lac exhibited a large 0.2 mag flare centered at 5.3^h UT, followed by a smaller flare of $\lesssim 0.1$ mag centered at

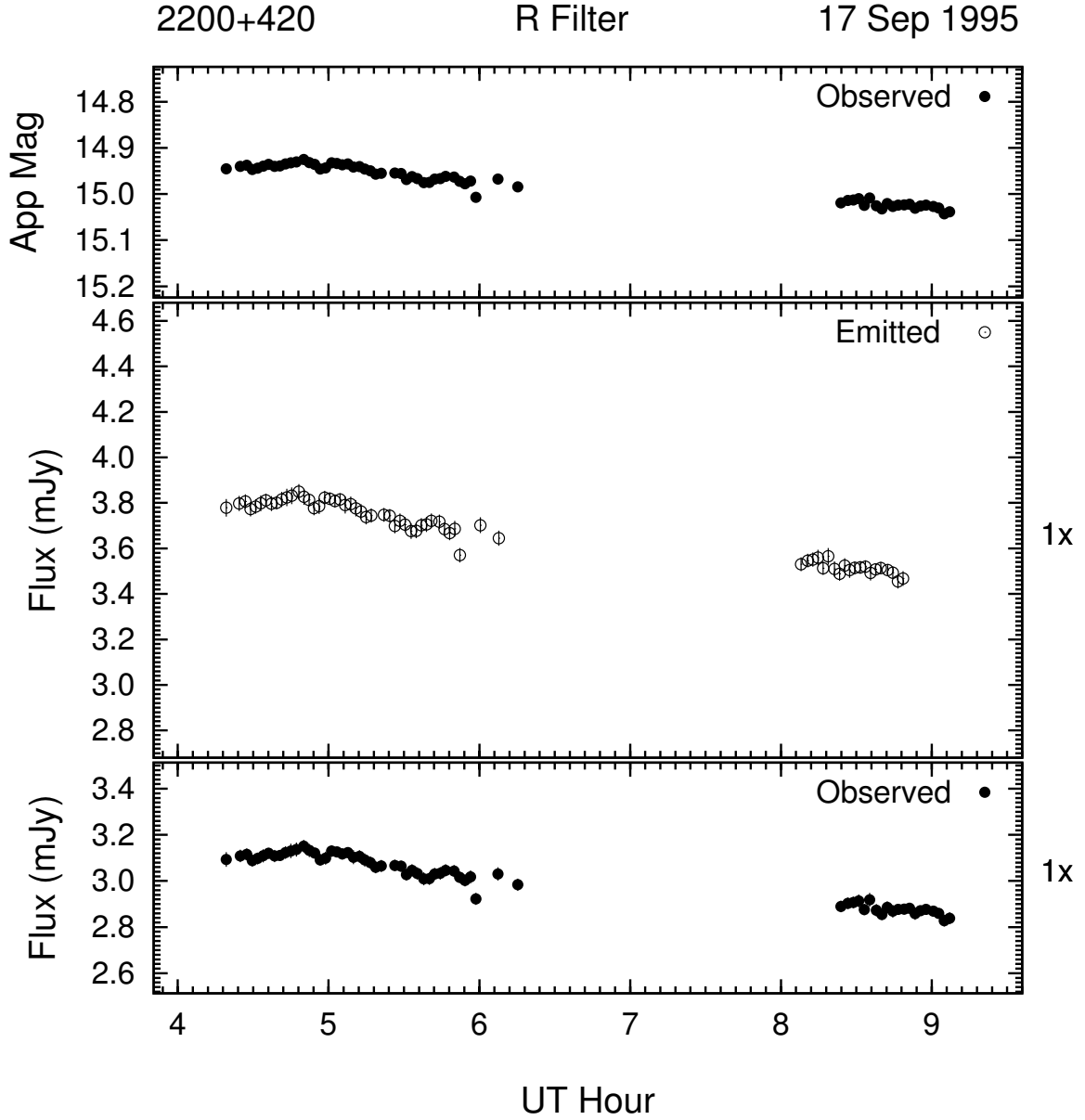


Figure 3.94: Example of the optical microvariability (R band) of 2200 + 420 on the night of 17 Sep 1995.

about 10.2^h UT. The base brightness level for BL Lac over the first two nights was about $R \simeq 15.0$. On the third night, 17 Sep (Figure 3.94), BL Lac decreased in brightness ~ 0.1 mag from $R \simeq 14.95$. There exist some statistically significant low level brightness variations

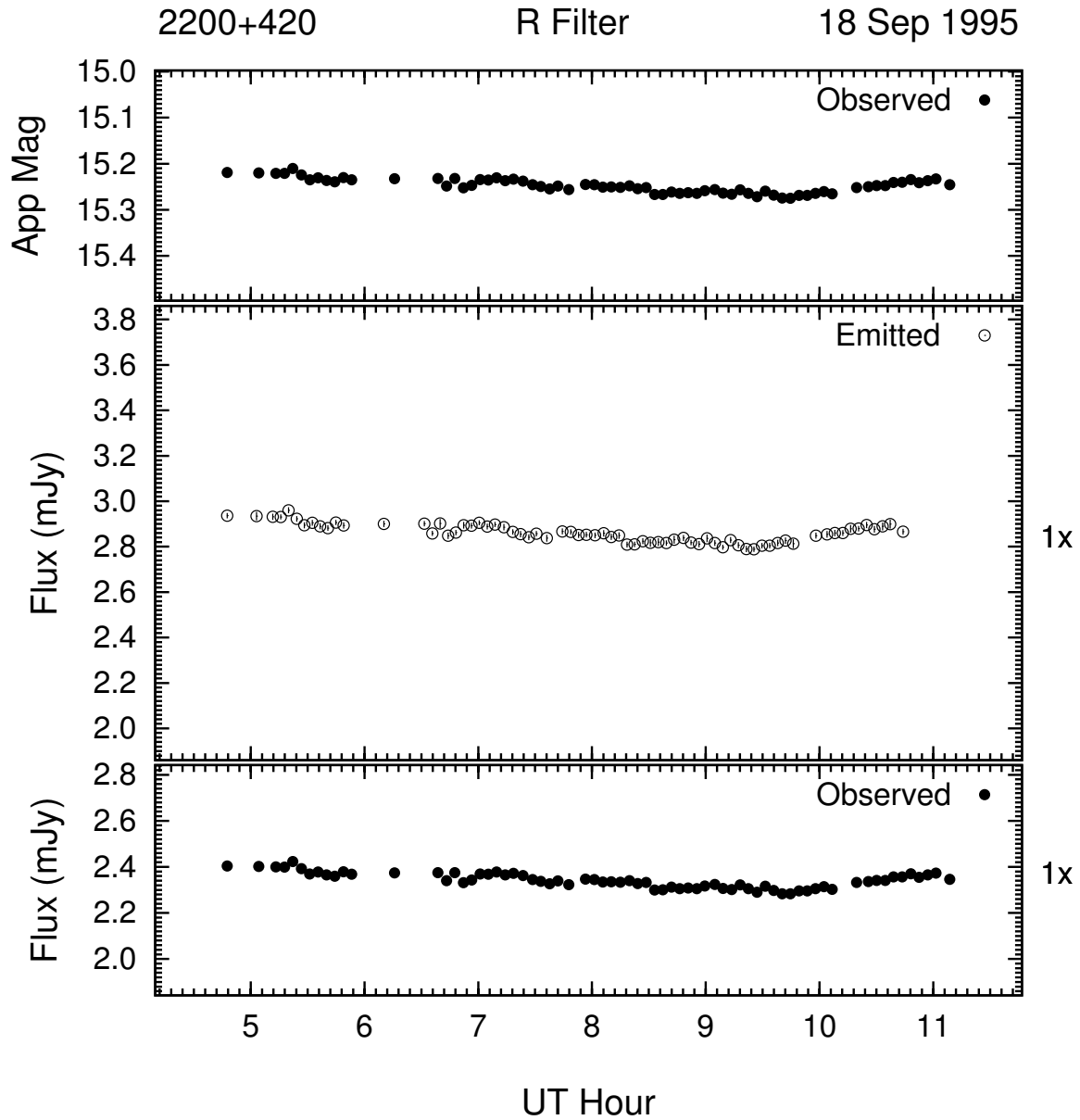


Figure 3.95: Example of the optical microvariability (R band) of 2200 + 420 on the night of 18 Sep 1995. This night's data was 2-point averaged to improve S/N .

superimposed the trend. After a drop in brightness of about 0.15 mag, BL Lac continued the dimming trend on the next night (18 Sep, Figure 3.95). At about 9.7^h UT, the dimming trend reversed and BL Lac returned to roughly the same brightness level of $R \simeq 15.22$ after

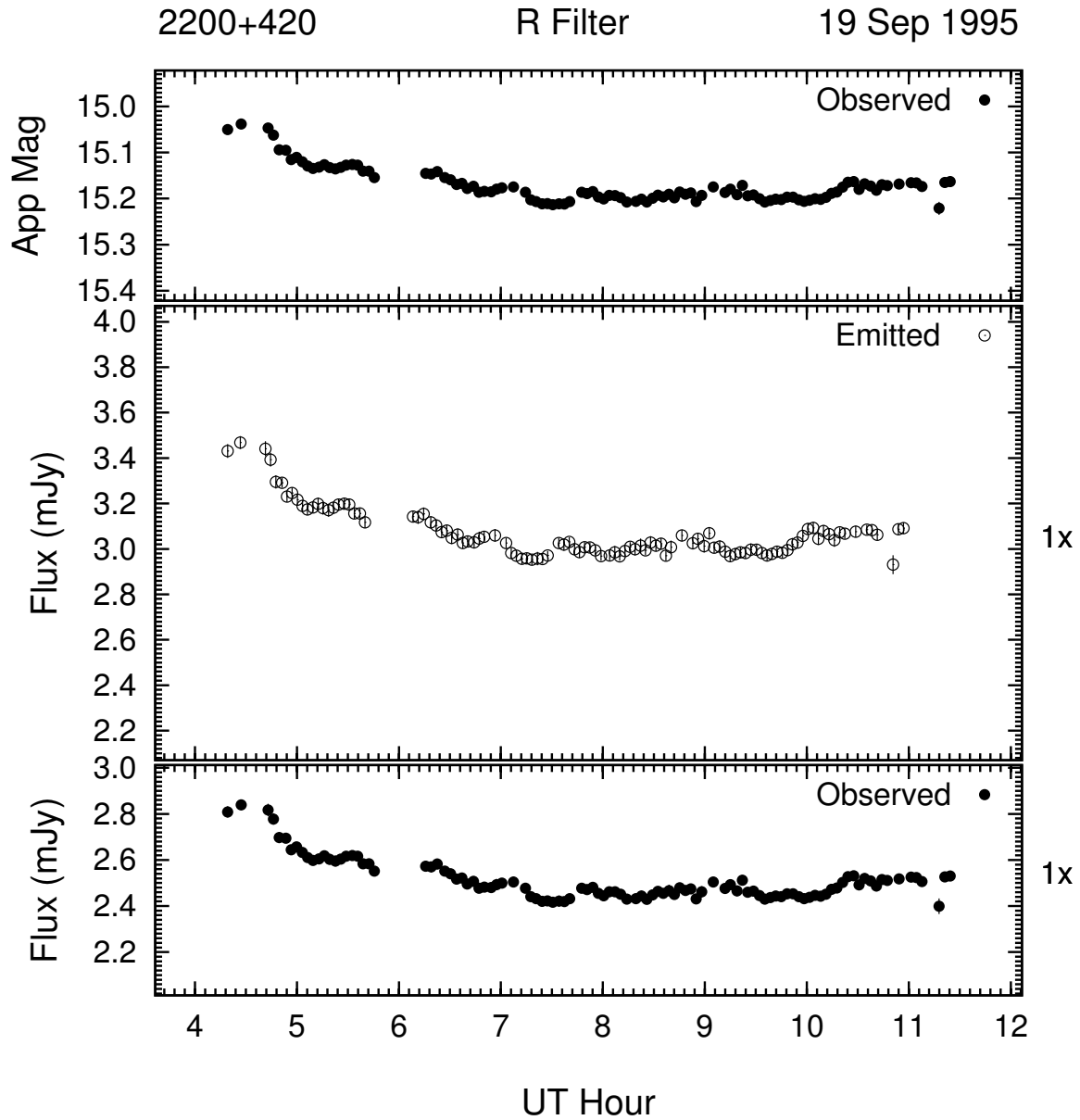


Figure 3.96: Example of the optical microvariability (R band) of 2200 + 420 on the night of 19 Sep 1995.

dimming ~ 0.5 mag. The final night of 19 Sep (Figure 3.96) showed brightness variations for BL Lac almost as large as on the night of 16 Sep. BL Lac dimmed almost 0.2 mag over about 4 hours, only to brighten ~ 0.05 mag over the next 3 hours. Statistically significant

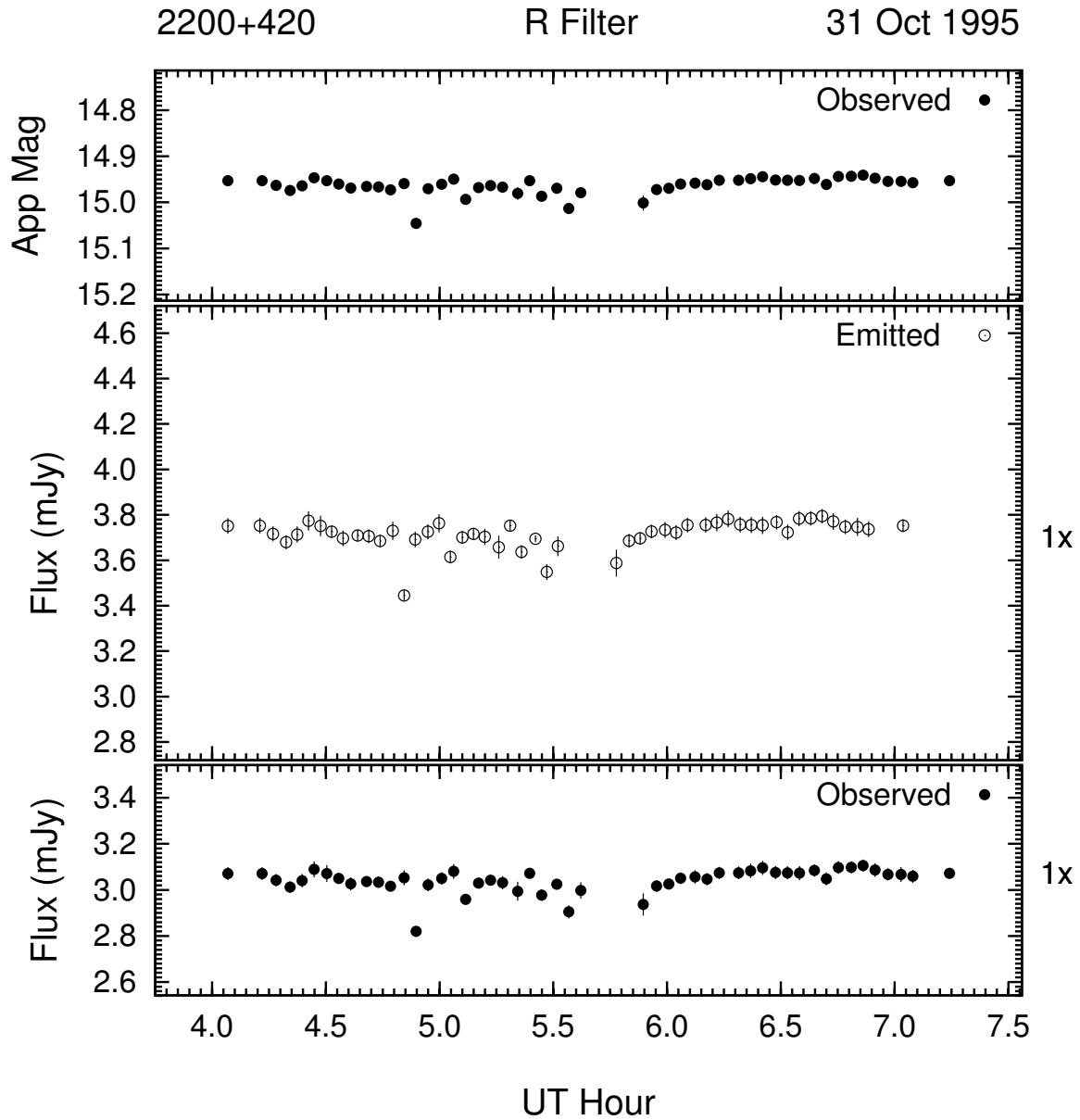


Figure 3.97: Example of the optical microvariability (R band) of 2200 + 420 on the night of 31 Oct 1995.

brightness variations of ~ 1 hour duration are clearly superimposed on this light curve.

The brightness variations of BL Lac on the night of 31 Oct 1995 (Figure 3.97) ranged only 0.1 mag over roughly 3 hours. There appears to be a drop in brightness centered at

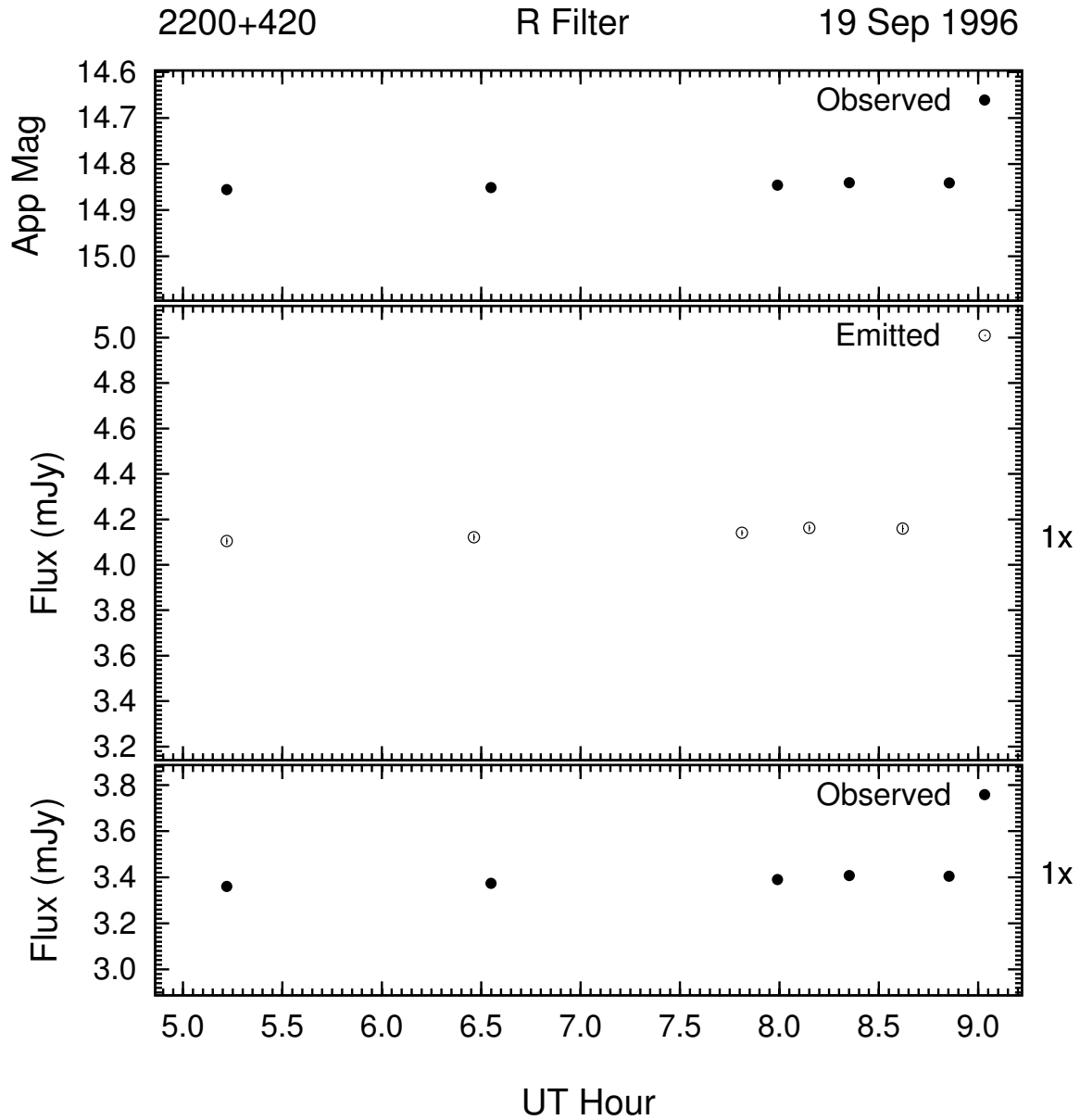


Figure 3.98: Example of the optical microvariability (R band) of 2200 + 420 on the night of 19 Sep 1996. This night's data was 2-point averaged to improve S/N .

about 5.7^h UT. BL Lac's brightness level was near that of the previous run at $R \simeq 15.0$.

The next three figures show the monitoring of BL Lac for three consecutive nights between 19 and 21 Sep 1996. On the first night, seen in Figure 3.98, BL Lac showed no variations

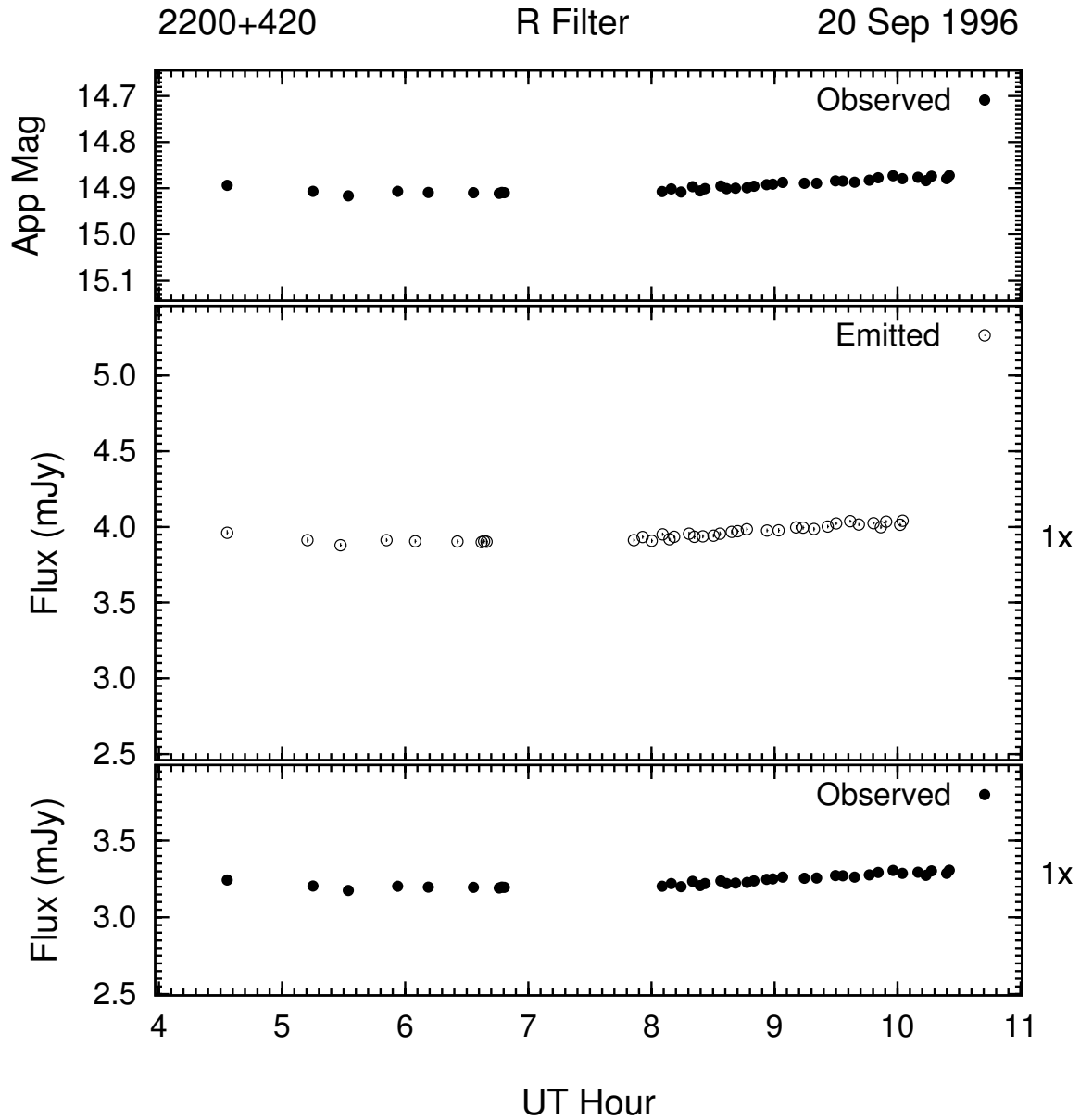


Figure 3.99: Example of the optical microvariability (R band) of 2200 + 420 on the night of 20 Sep 1996. This night's data was 3-point averaged to improve S/N .

in brightness over the course of almost 4 hours. On the following night (Figure 3.99), it exhibited a 0.04 mag rise in brightness in the latter half of the night. BL Lac continued to increase in brightness another 0.12 mag in about 3 hours on the night of 21 Sep (Figure

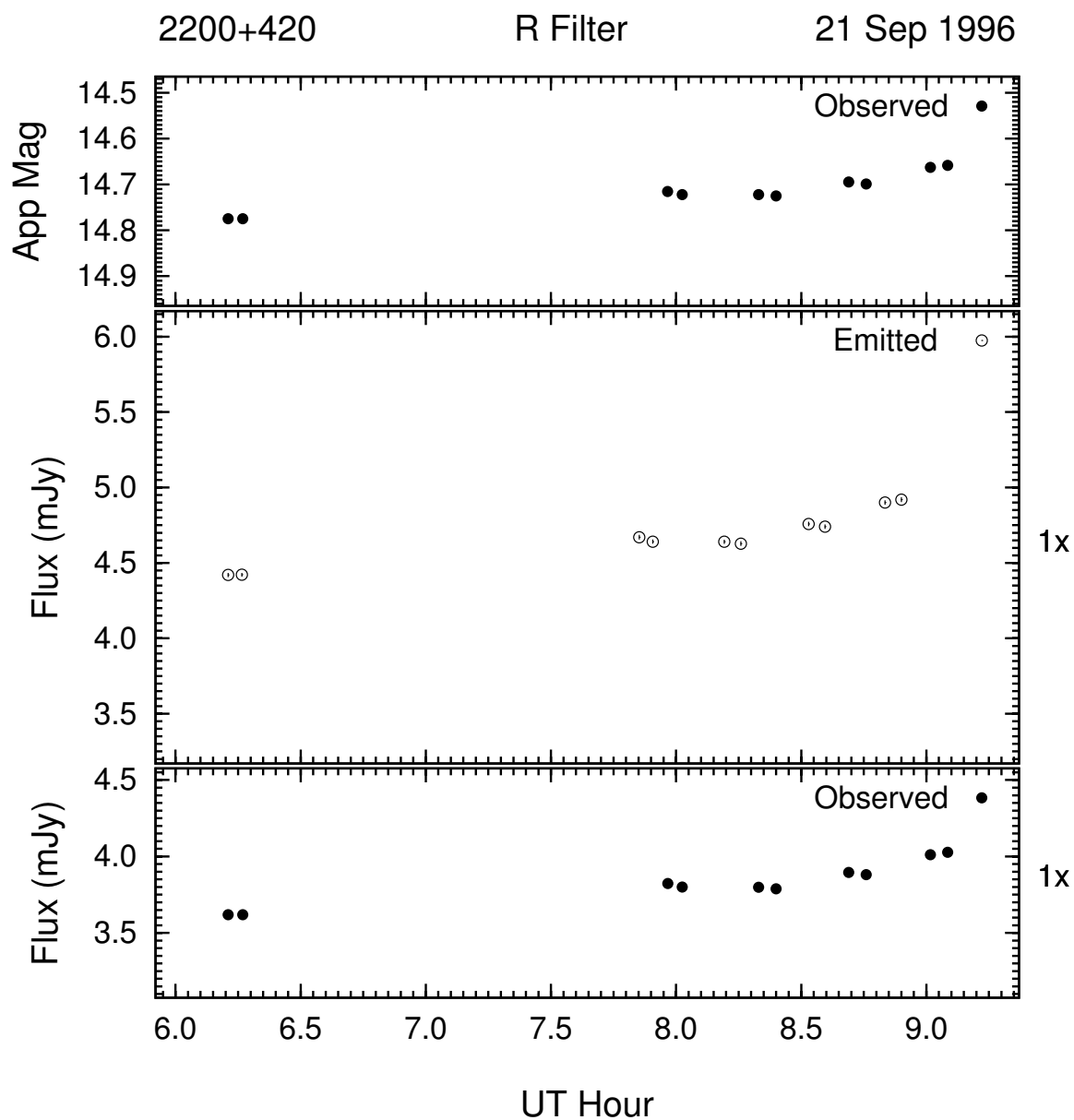


Figure 3.100: Example of the optical microvariability (R band) of 2200 + 420 on the night of 21 Sep 1996. This night's data was 5-point averaged to improve S/N .

3.100). BL Lac's total range of brightness for this run was 0.25 mag, peaking at $R = 14.65$ at the end of the last night.

On the nights of 18 and 19 Jul 1997 (Figures 3.101 and 3.102), BL Lac started out ~ 1

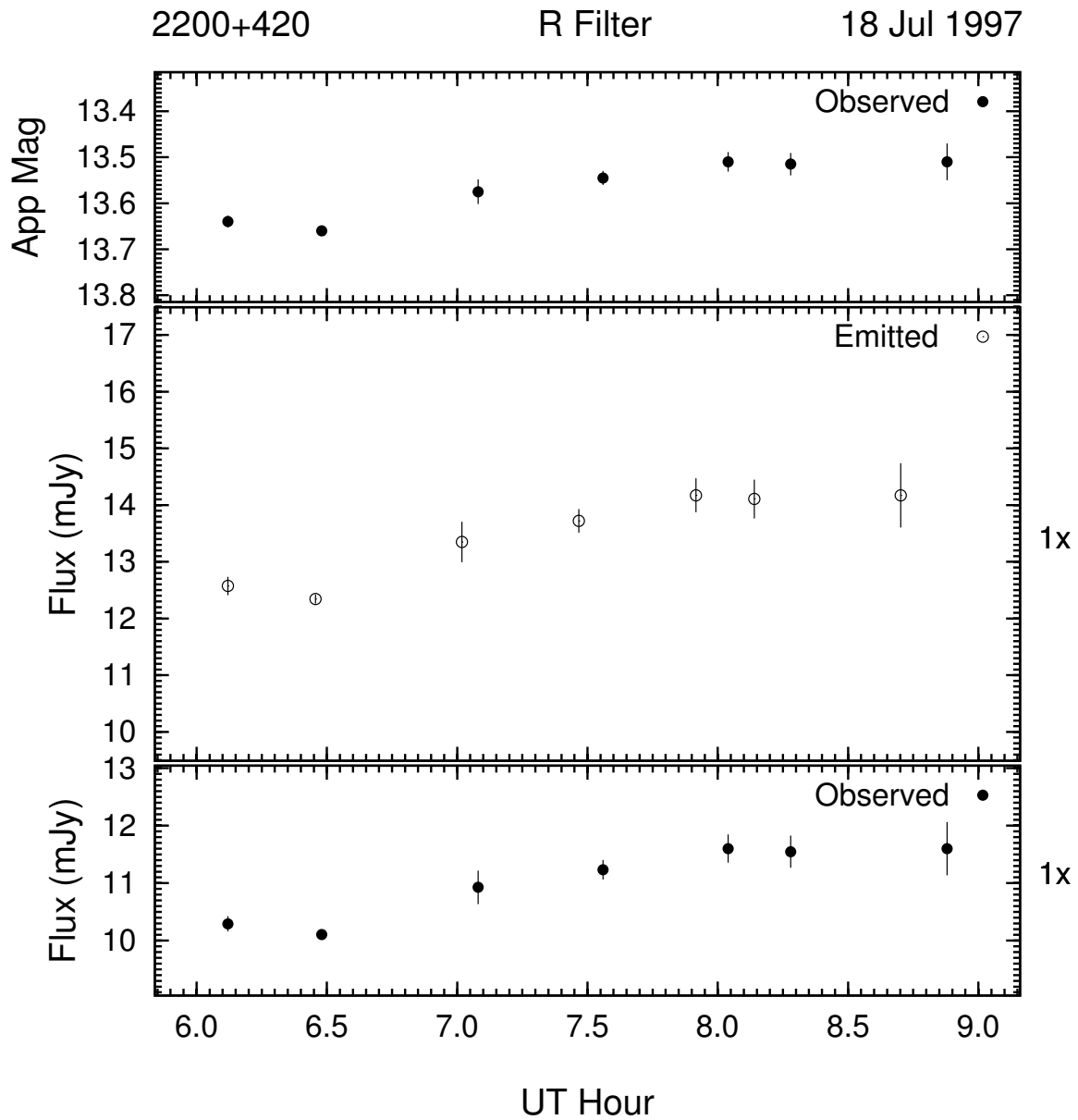


Figure 3.101: Example of the optical microvariability (R band) of 2200 + 420 on the night of 18 Jul 1997. This night's data was 3-point averaged to improve S/N .

mag brighter than September of 1996, increased in brightness 0.15 mag over the 3 hours of the observation on 18 Sep, brightened another 0.8 mag between the 2 nights, and then dropped 0.4 mag over the 4 hours of observations on 19 Sep. The variations on the two

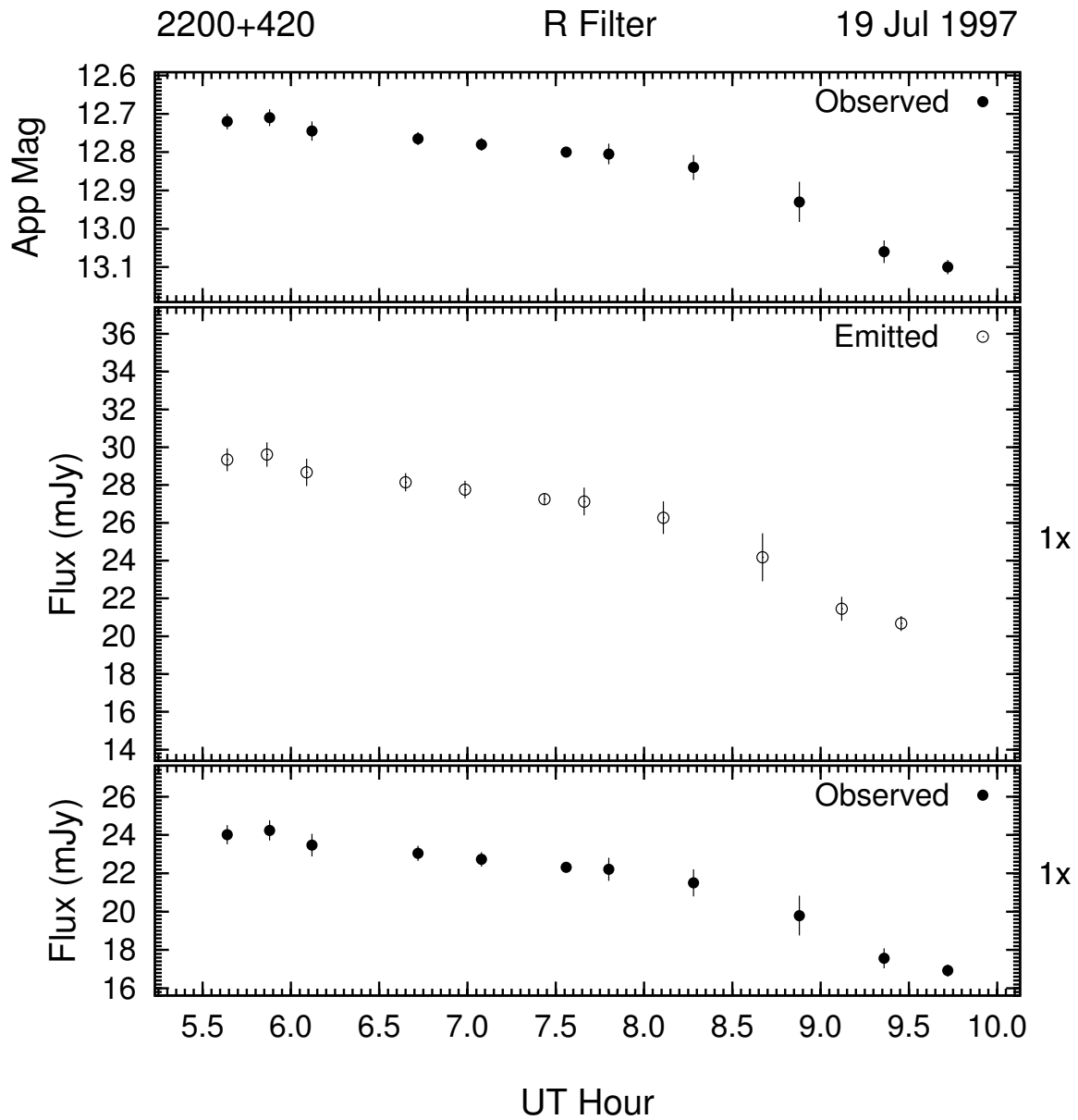


Figure 3.102: Example of the optical microvariability (R band) of 2200 + 420 on the night of 19 Jul 1997. This night's data was 2-point averaged to improve S/N .

nights are at a confidence level of 4.3σ and 11.8σ , respectively. There is little evidence of brightness variations on the trends observed.

On the night of 19 Aug 1997, BL Lac was observed for just over 4 hours (see Figure

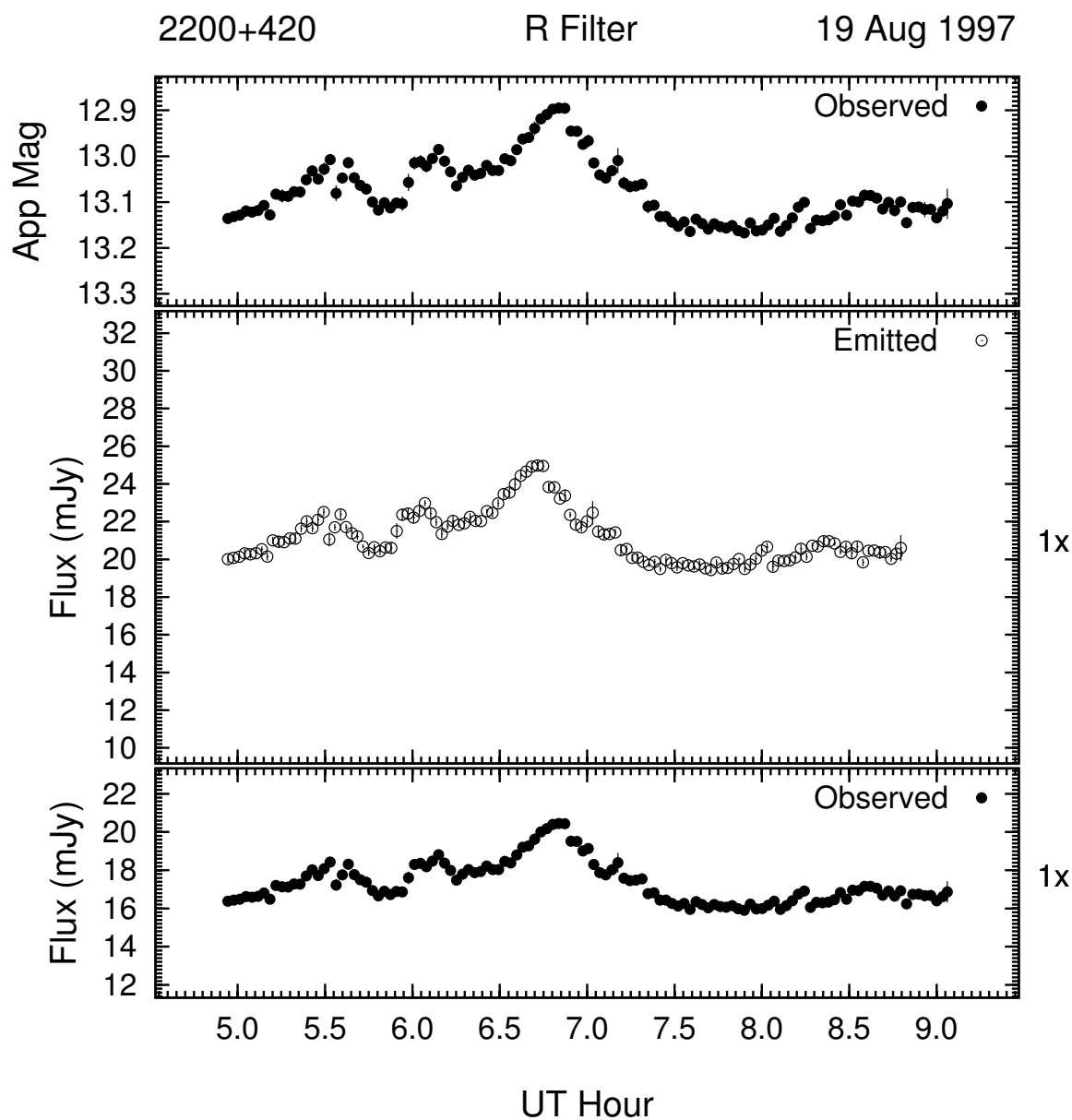


Figure 3.103: Example of the optical microvariability (R band) of 2200 + 420 on the night of 19 Aug 1997. This night's data was 2-point averaged to improve S/N .

3.103). It exhibited an increasing trend in brightness over the first half of the night and a decreasing trend over the last half. Superimposed on the brightening trend were three flares > 0.1 mag at 5.6^h , 6.2^h , and 6.7^h UT. On the dimming trend, the microvariations are at

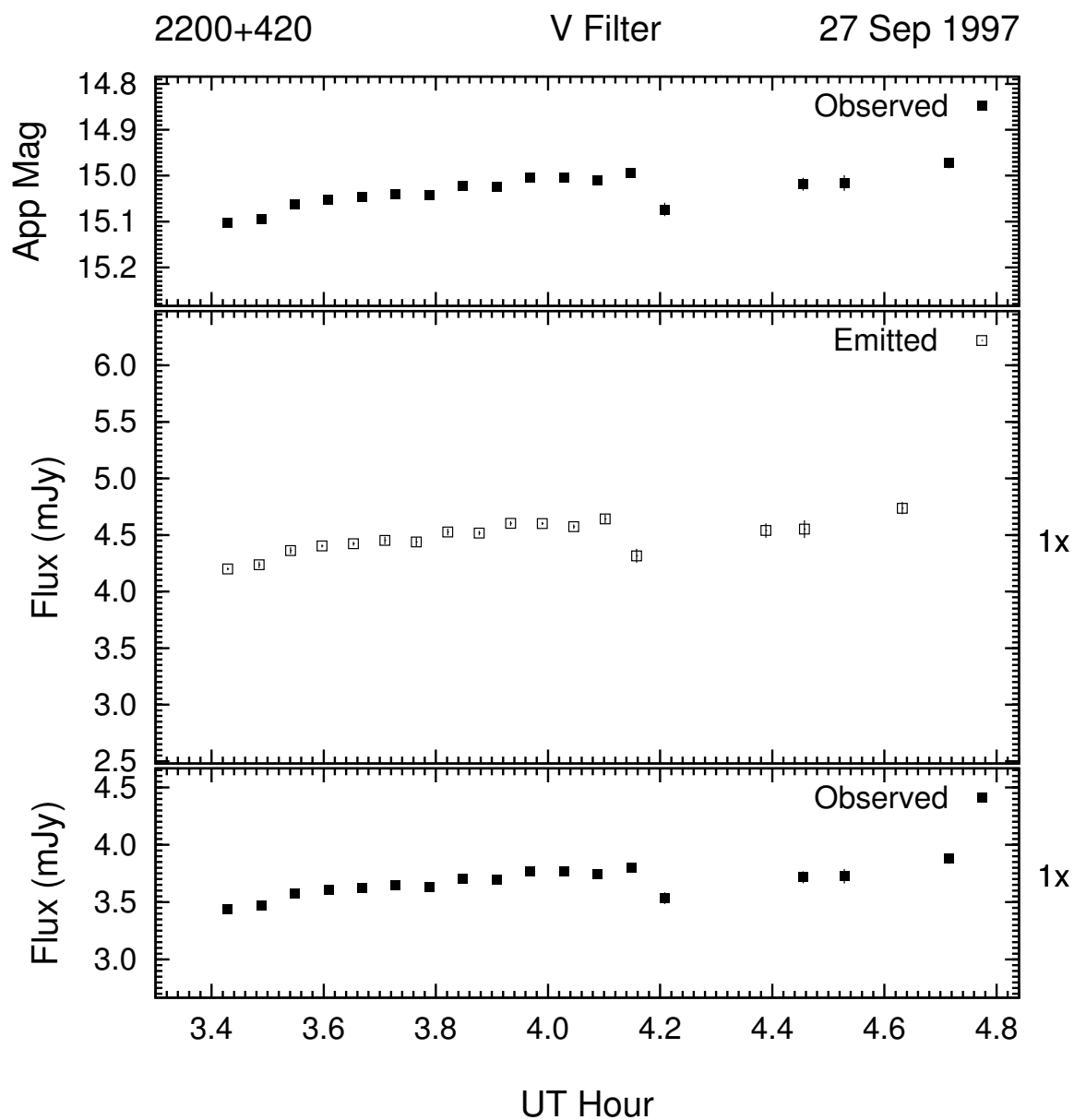


Figure 3.104: Example of the optical microvariability (V band) of 2200 + 420 on the night of 27 Sep 1997. This night's data was 3-point averaged to improve S/N .

a much lower level and are not statistically significant. BL Lac was at roughly the same brightness level as the previous month, $R \simeq 13.1$.

BL Lac was monitored for three consecutive nights in late September of 1997 in both the

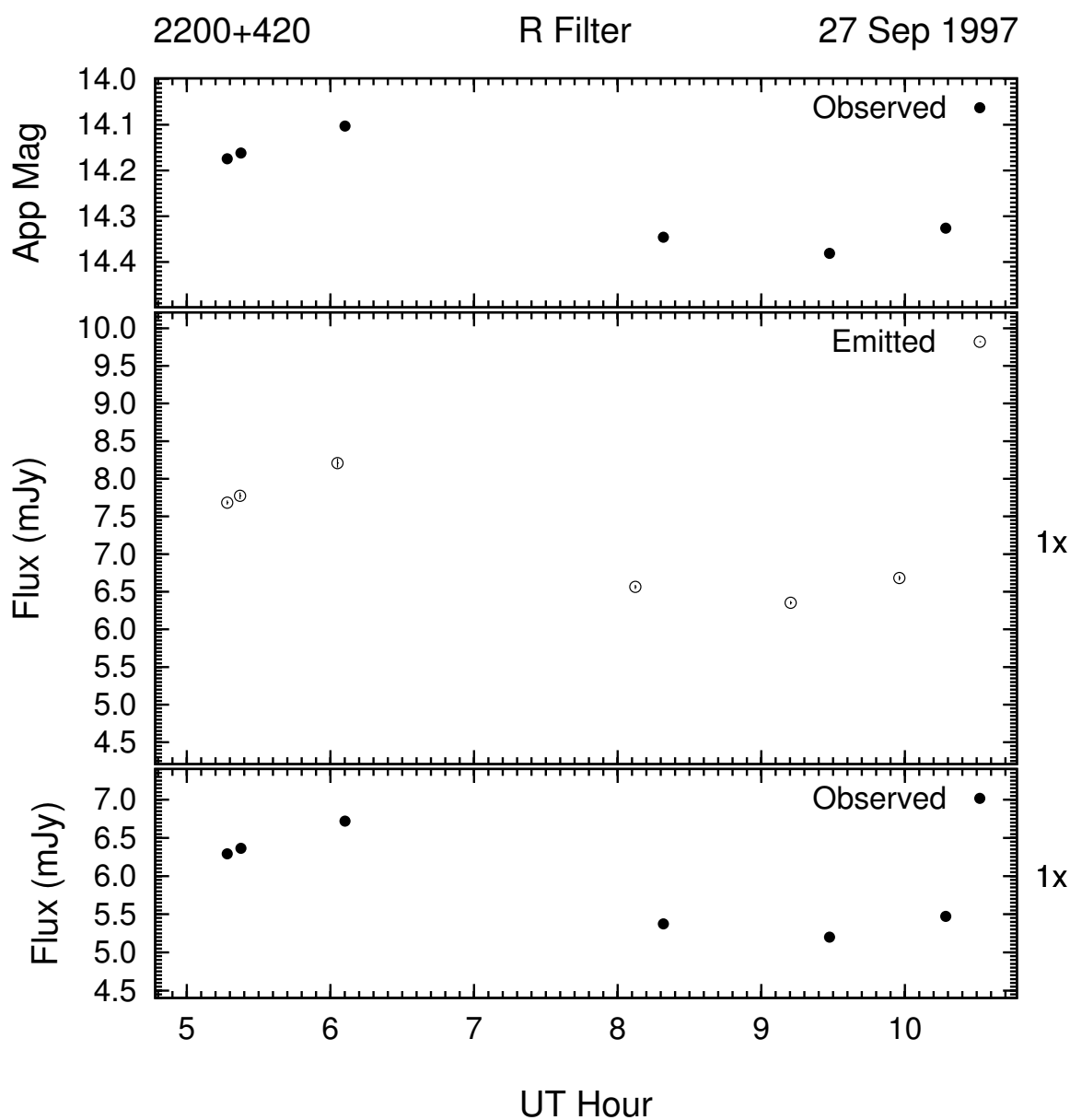


Figure 3.105: Example of the optical microvariability (R band) of 2200 + 420 on the night of 27 Sep 1997. This night's data was 2-point averaged to improve S/N .

R and the V band. These are the only microvariations observed in this way. The observations began on 27 Sep (Figure 3.104) in the V band where BL Lac showed a modest increase of 0.1 mag over less than an hour, a quick drop of < 0.1 mag in just a few minutes, then a

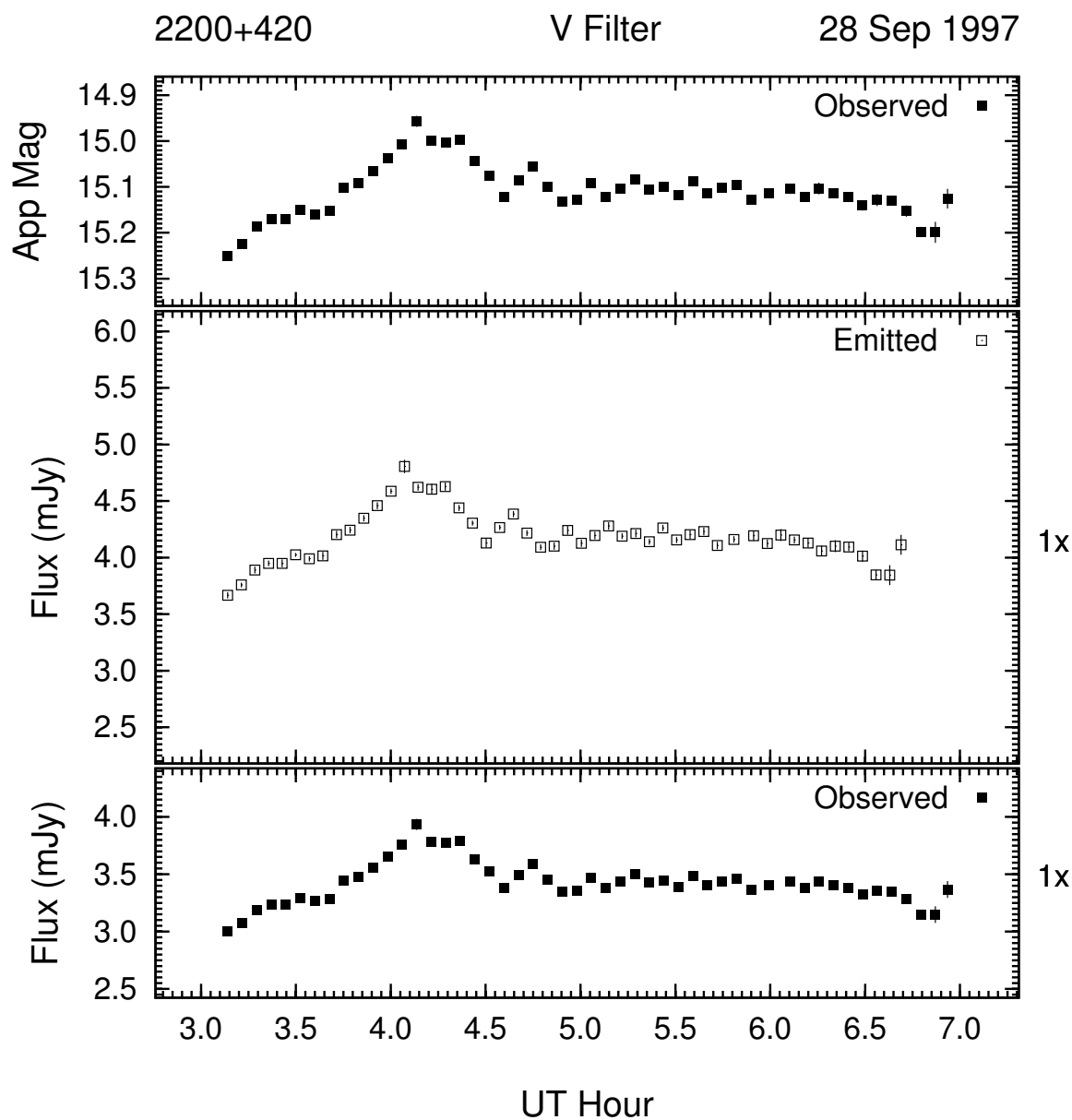


Figure 3.106: Example of the optical microvariability (V band) of 2200 + 420 on the night of 28 Sep 1997. This night's data was 3-point averaged to improve S/N .

resumption of the original trend over the next half hour. The total brightness change was 0.13 mag. This increasing trend was picked up at $R = 14.2$, ~ 0.8 mag brighter in R band (see Figure 3.105), and showed an increase of ~ 0.1 mag for the next hour. At this point,

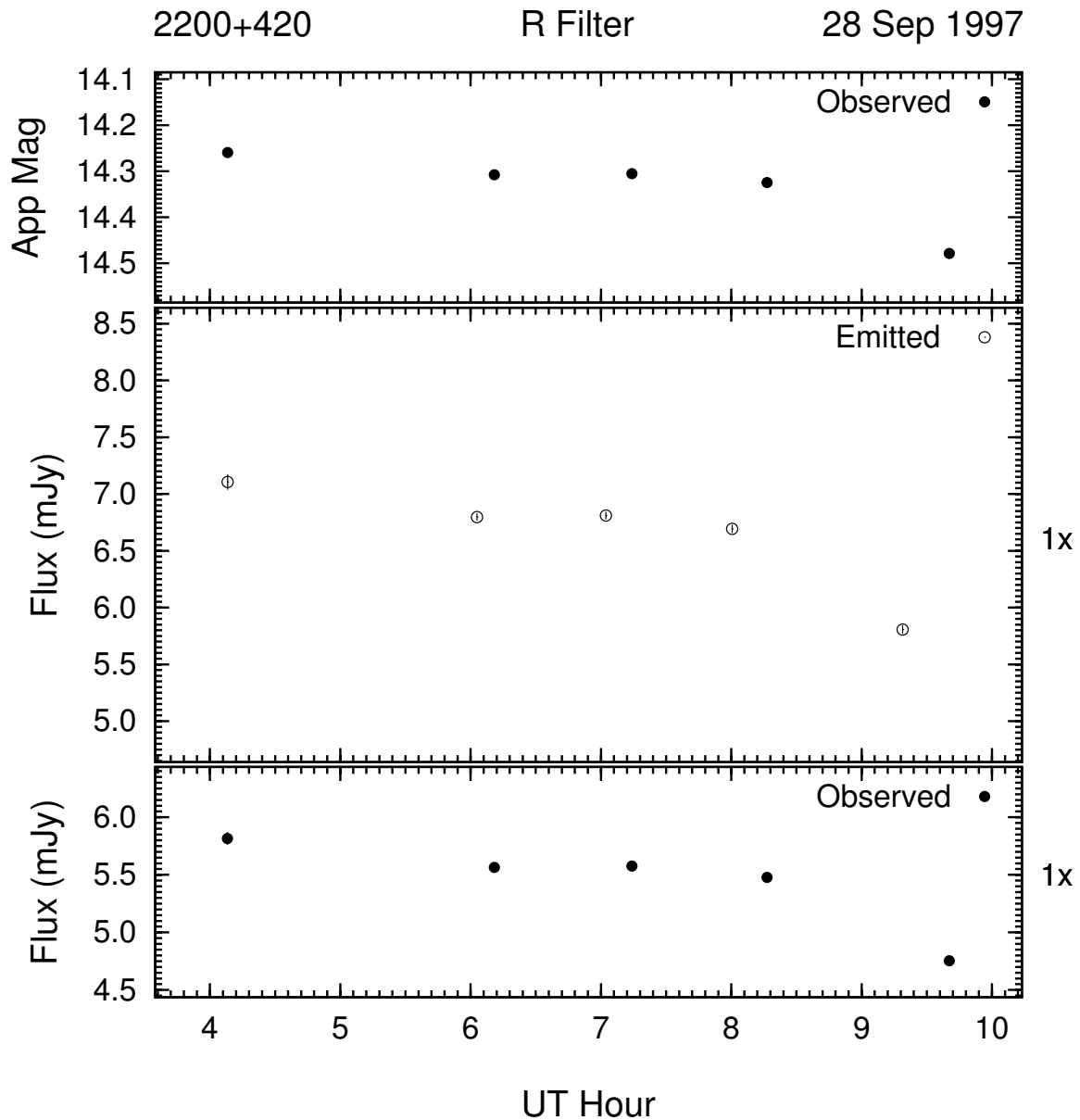


Figure 3.107: Example of the optical microvariability (R band) of 2200 + 420 on the night of 28 Sep 1997. This night's data was 2-point averaged to improve S/N .

BL Lac dimmed ~ 0.25 mag in 2 hours to end the night at roughly the same brightness it began. On the following night, 28 Sep (Figure 3.106), BL Lac exhibited a flare of 0.3 mag in only 1 hour centered at $\sim 4.2^h$ UT, followed by a more modest decrease over the remainder

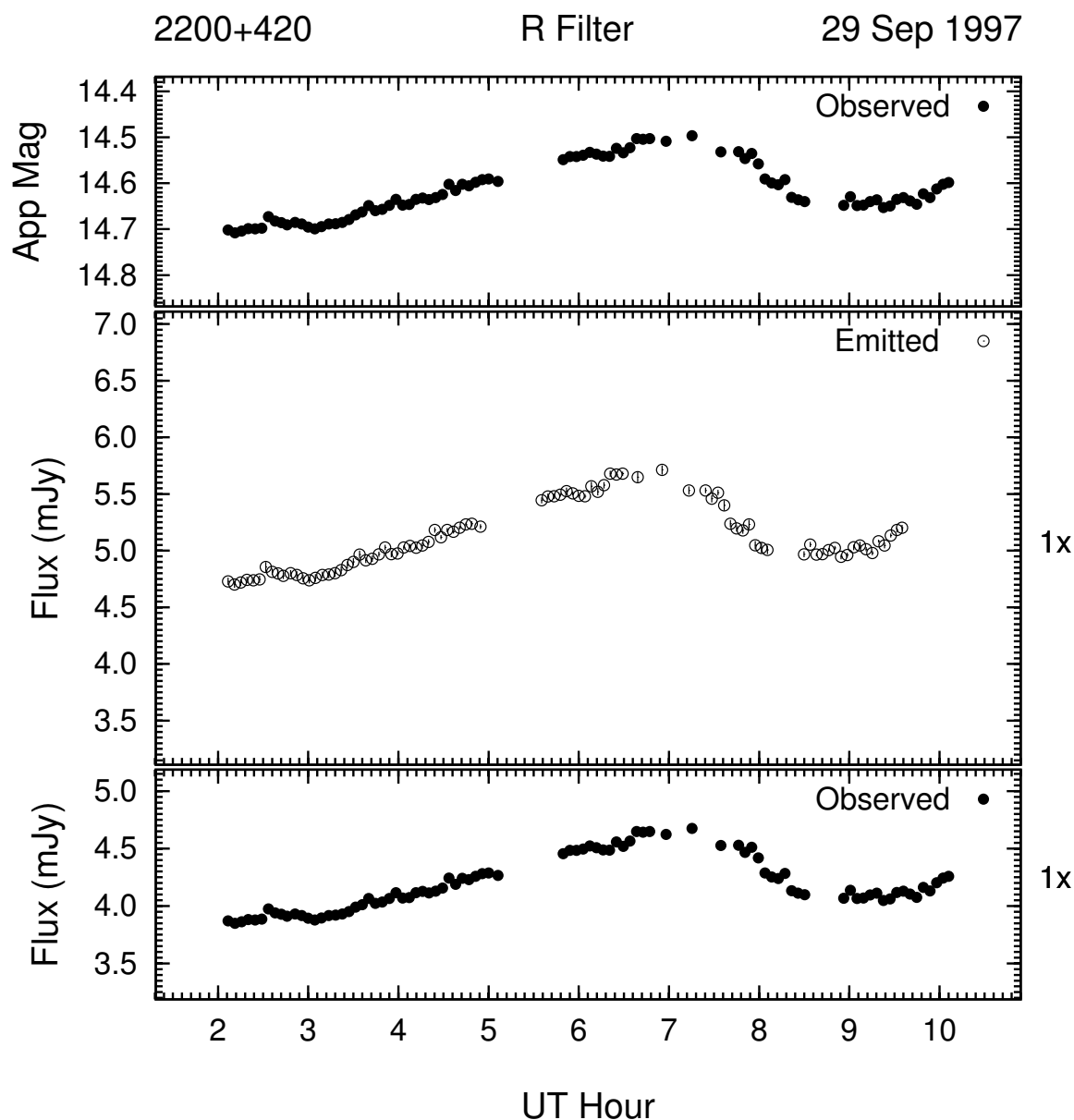


Figure 3.108: Example of the optical microvariability (R band) of 2200 + 420 on the night of 29 Sep 1997. This night's data was 3-point averaged to improve S/N .

of the night. The R band observations (Figure 3.107) overlap the V band observations and parallel them at a $V - R$ of ~ 0.8 as they continue to decrease in brightness back down to the brightness level at the beginning of the night. This $V - R$ is comparable to the average

$V - R$ used to combine the long term V and R band light curves of BL Lac. The last night of this run is on 29 Sep (Figure 3.108) and is in the R band only. On this night BL Lac showed a brightening of 0.2 mag over 5 hours, followed by a dimming of ~ 0.15 in less than 2 hours. BL Lac then continued to brighten until the observations end. This light curve is another example of BL Lac's undulating oscillatory behavior.

The V band light curve of BL Lac on the night of 02 Dec 1997 is shown in Figure 3.109. BL Lac is more than 1.5 mag dimmer than at the end of September, and showed a decrease in brightness of 0.15 mag over 1.5 hours followed by a “flat” trend in which no statistically significant brightness variations were seen for the remaining 2 hours of the observations.

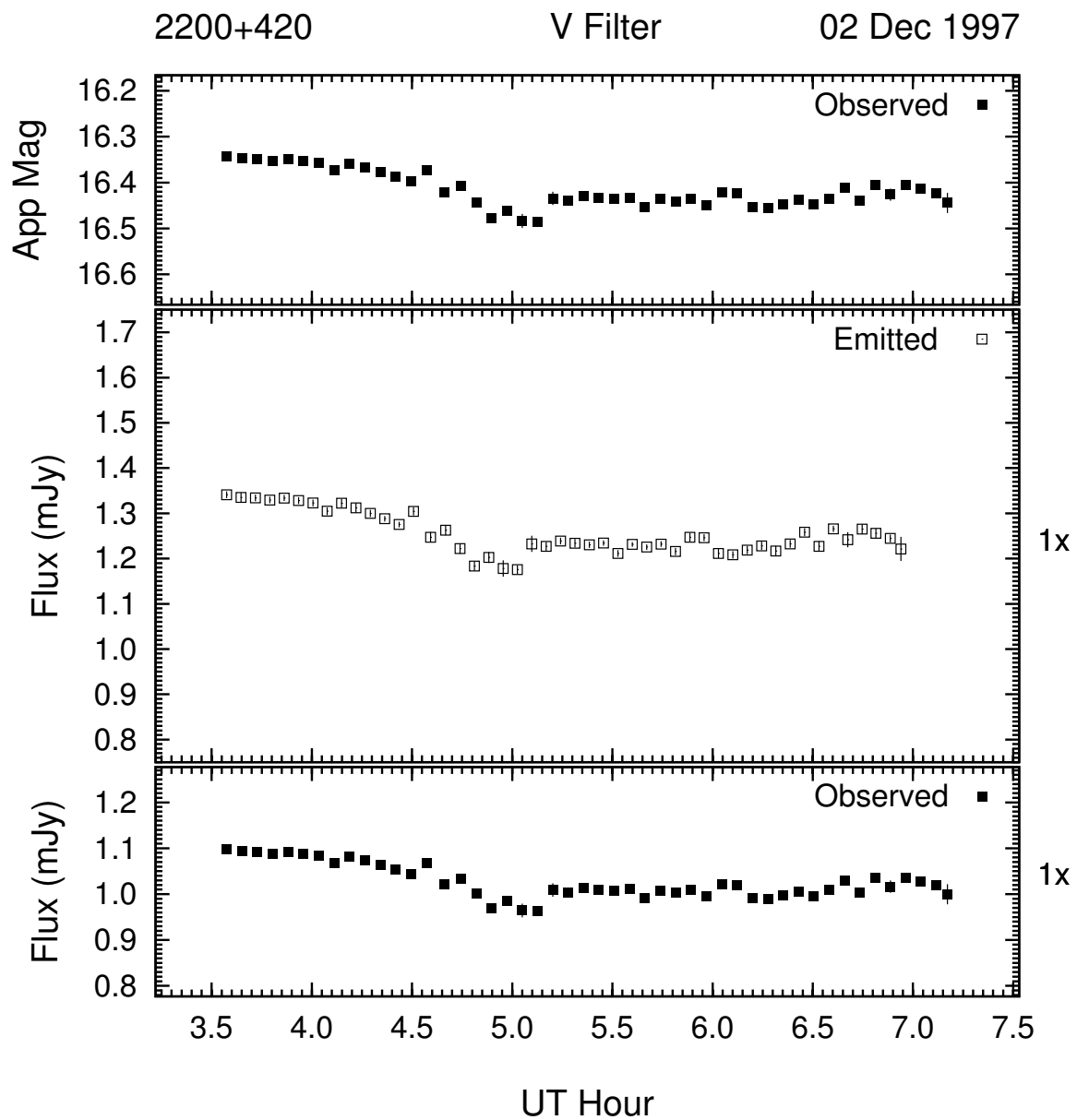


Figure 3.109: Example of the optical microvariability (V band) of 2200 + 420 on the night of 12 Dec 1997. This night's data was 4-point averaged to improve S/N .

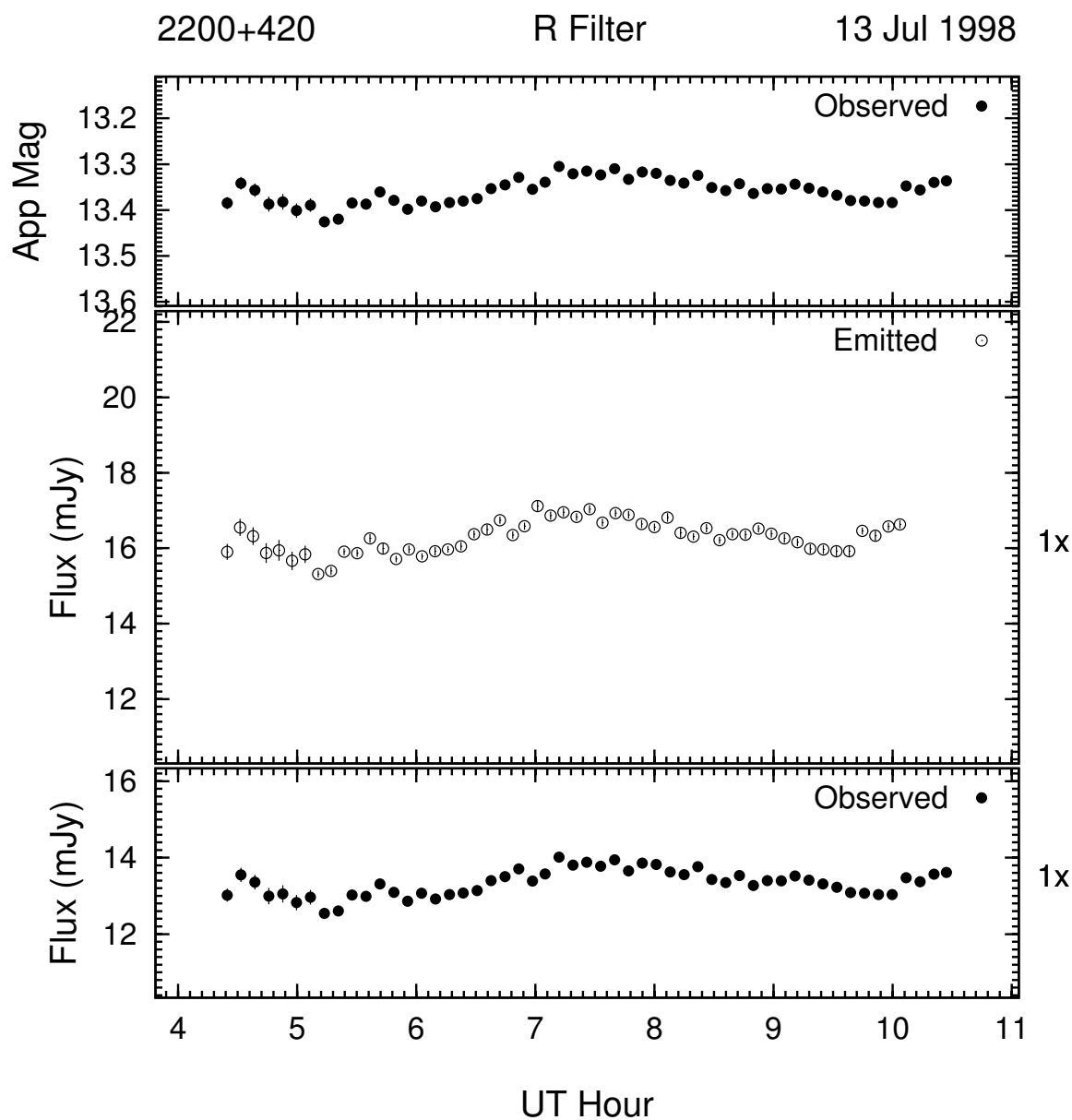


Figure 3.110: Example of the optical microvariability (R band) of 2200 + 420 on the night of 13 Jul 1998. This night's data was 5-point averaged to improve S/N .

Light curves from the observations of BL Lac on the nights of 13 and 14 July of 1998 are shown in Figures 3.110 and 3.111 respectively. BL Lac is roughly 3 mag brighter than in December of 1997. On the first night, BL Lac showed > 0.1 mag oscillations over 6 hours

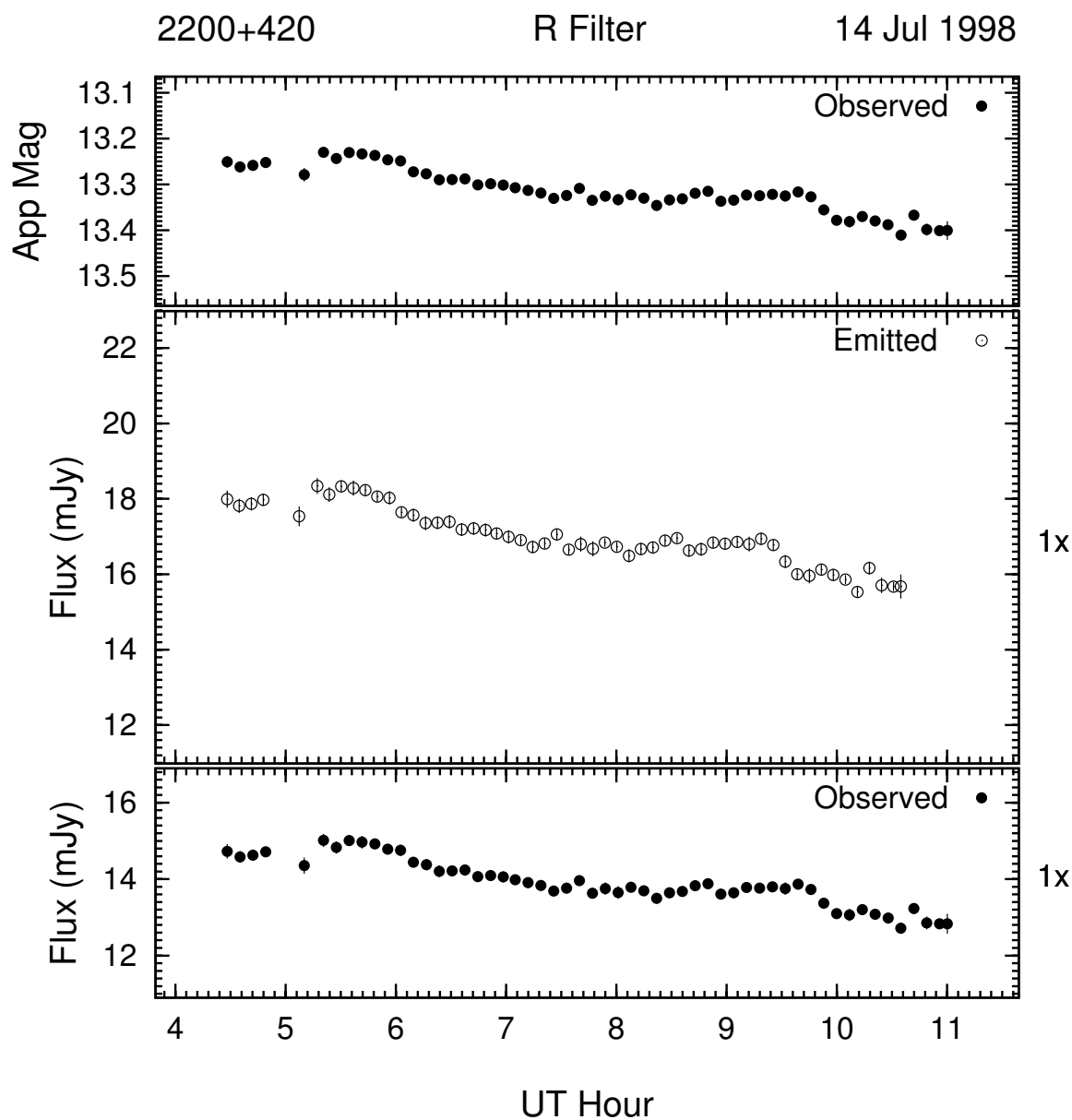


Figure 3.111: Example of the optical microvariability (R band) of 2200 + 420 on the night of 14 Jul 1998. This night's data was 5-point averaged to improve S/N .

with no net change in brightness, while on the second, it showed a dimming trend of almost 0.2 mag over 7 hours with statistically significant brightness variations superimposed.

In late July and early August of 1998, BL Lac was observed again for three non-

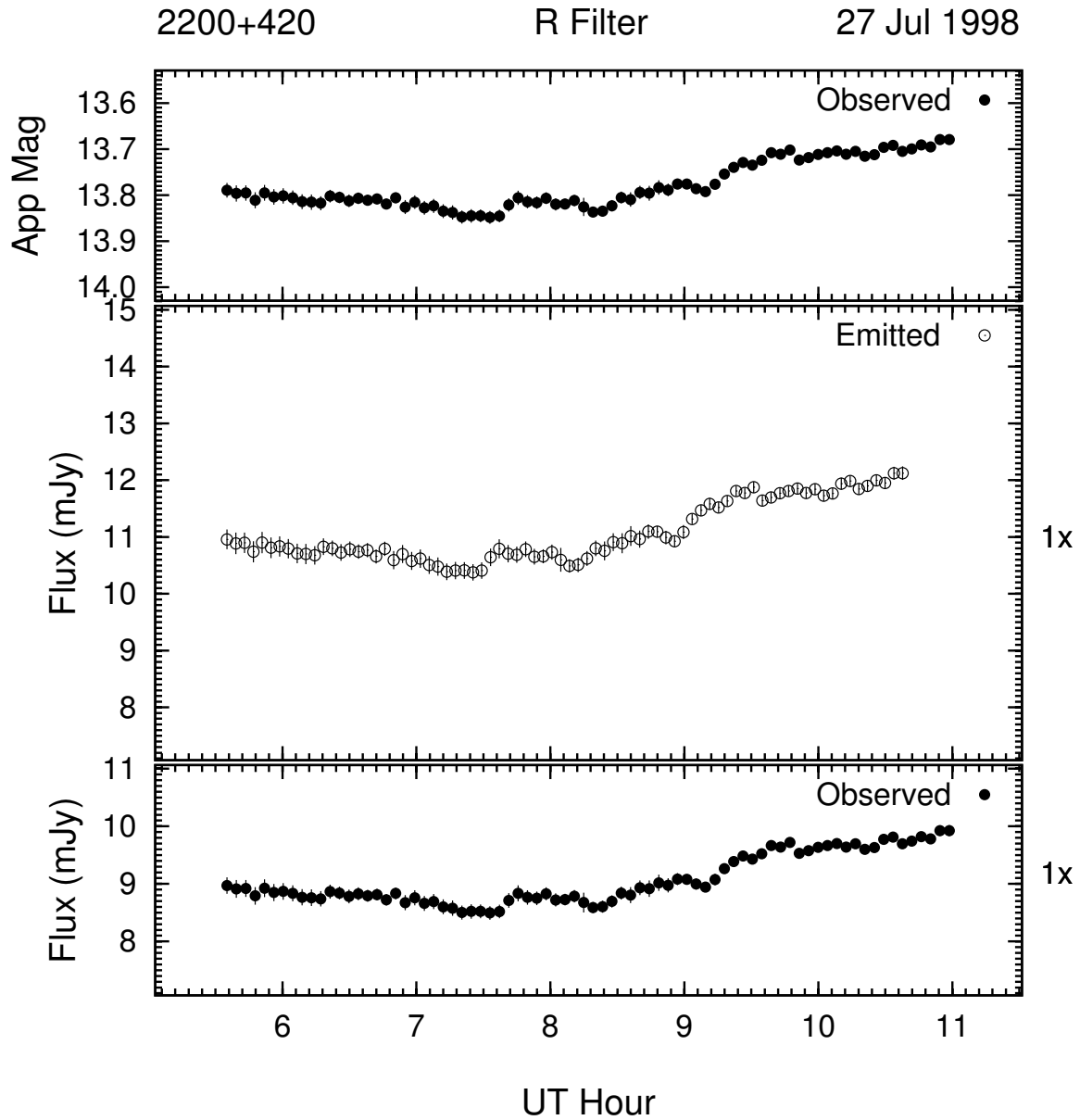


Figure 3.112: Example of the optical microvariability (R band) of 2200 + 420 on the night of 27 Jul 1998. This night's data was 3-point averaged to improve S/N .

consecutive days. On 27 Jul (Figure 3.112), BL Lac was about 0.5 mag dimmer than in July and dimmed slightly before brightening 0.17 mag to $R = 13.7$. The superimposed variability is statistically significant. On 01 Aug (Figure 3.113), BL Lac exhibited small scale

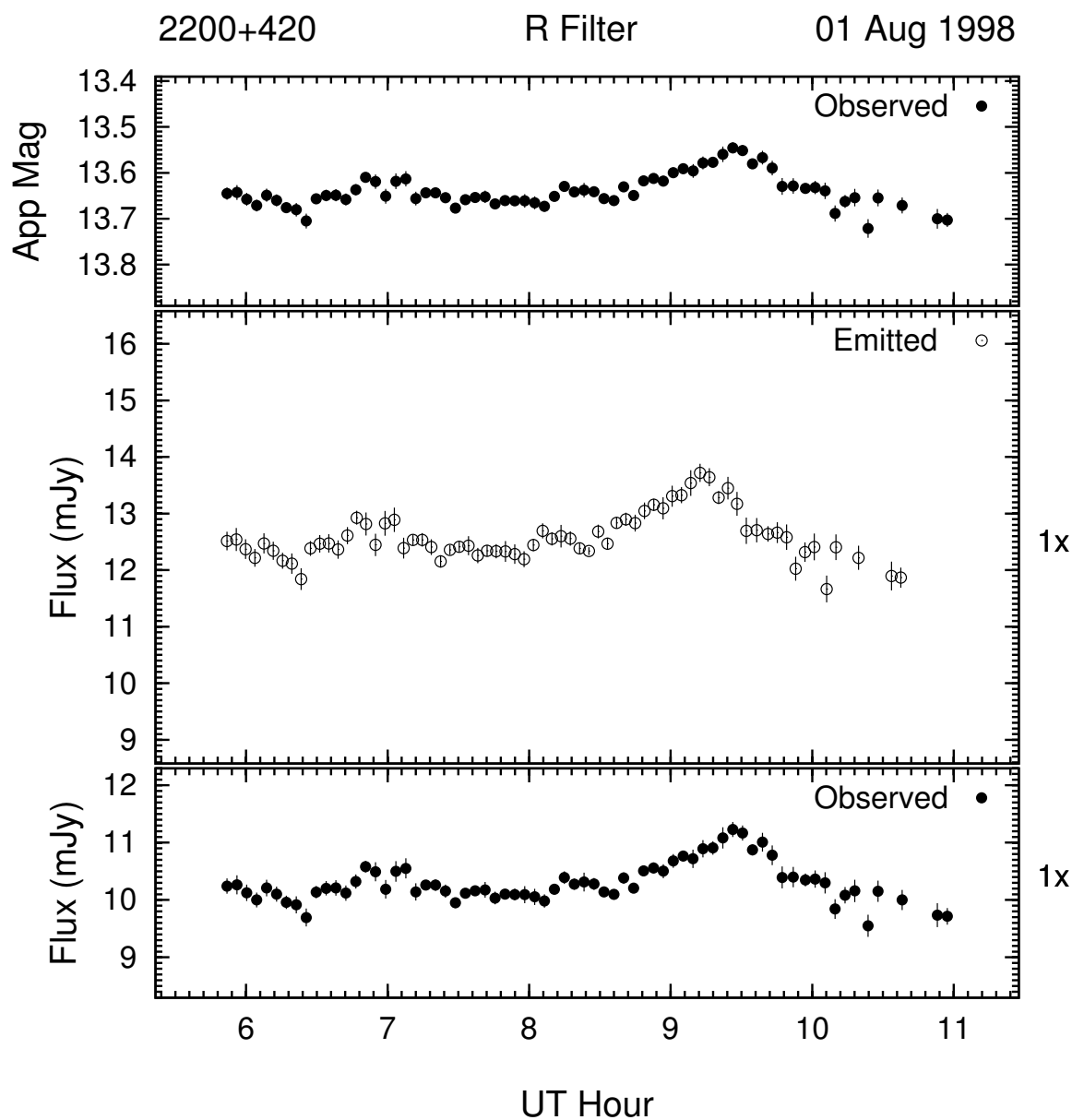


Figure 3.113: Example of the optical microvariability (R band) of 2200 + 420 on the night of 01 Aug 1998. This night's data was 3-point averaged to improve S/N .

(~ 0.1 mag) variations with the duration of approximately 0.5 hour. At 8^h UT, BL Lac started an increase in brightness of almost 0.2 mag over 1.5 hours. This flare can be seen centered at 9.5^h UT. BL lac subsequently dimmed at roughly the same rate. The brightness

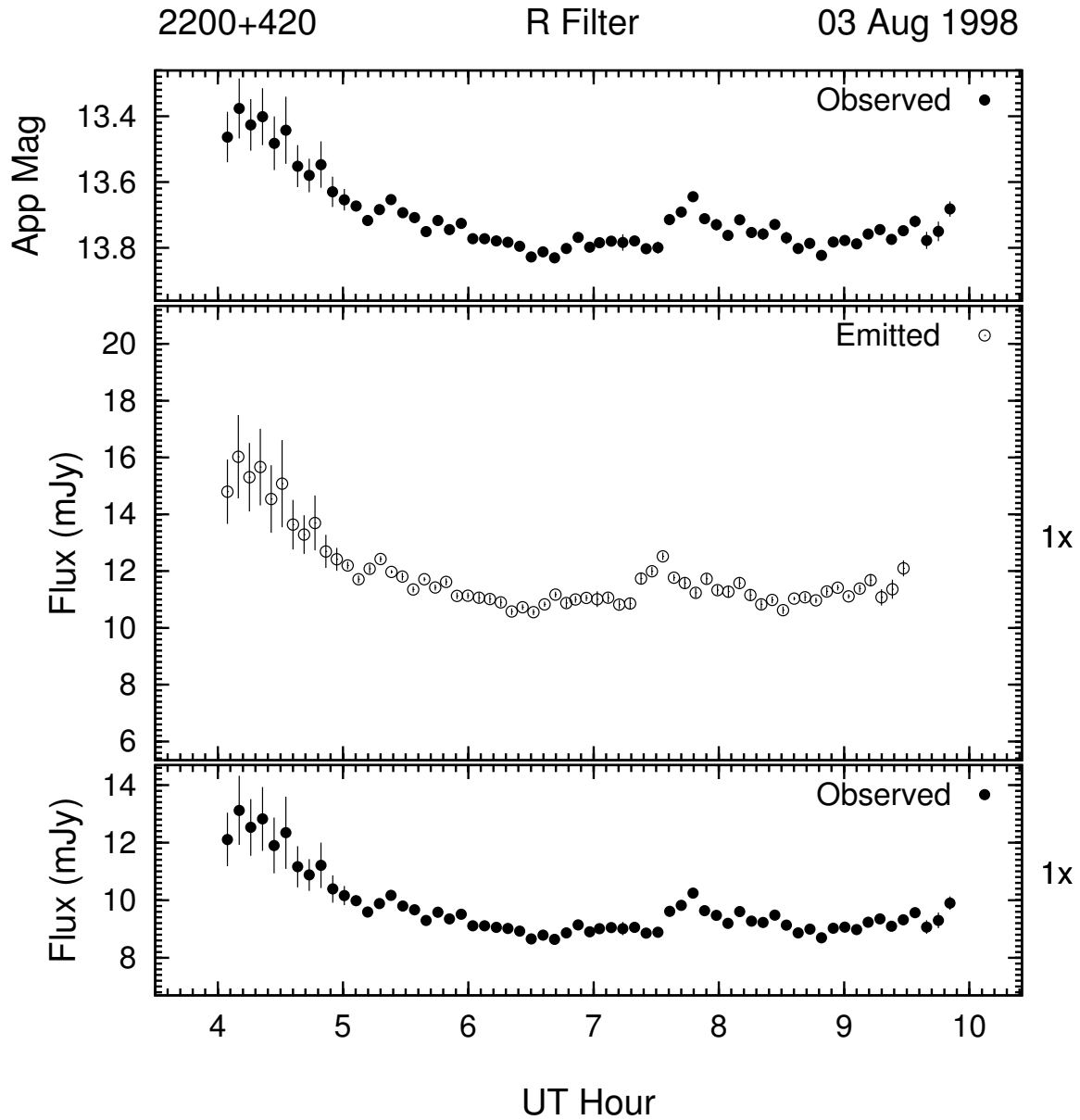


Figure 3.114: Example of the optical microvariability (R band) of 2200 + 420 on the night of 03 Aug 1998. This night's data was 4-point averaged to improve S/N .

variations on the night of 03 Aug (Figure 3.114) are similar to the previous nights, but with a dimming trend of 0.45 mag over 2.5 hours, followed by one small flare at 7.8^h UT.

Later the same month, BL Lac was observed to be exhibiting similar behavior to the

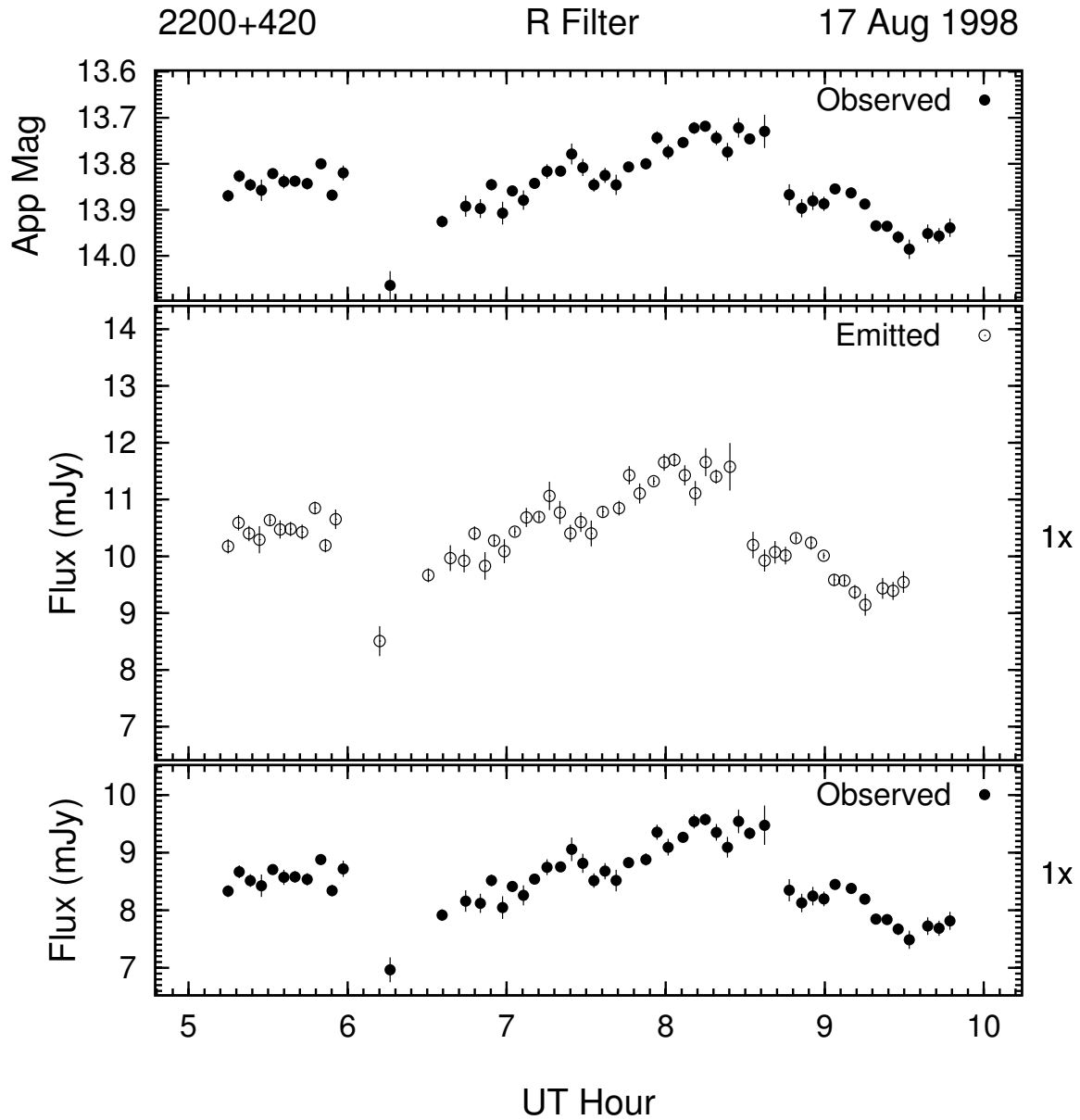


Figure 3.115: Example of the optical microvariability (R band) of 2200 + 420 on the night of 17 Aug 1998. This night's data was 3-point averaged to improve S/N .

previous 3 nights. On the night of 17 Aug 1998 (Figure 3.115), the total variations in brightness were ~ 0.35 mag, most of which occurred in a loosely defined flare centered at $\sim 8.2^h$ UT. The brightness levels and variability character were similar over the next two

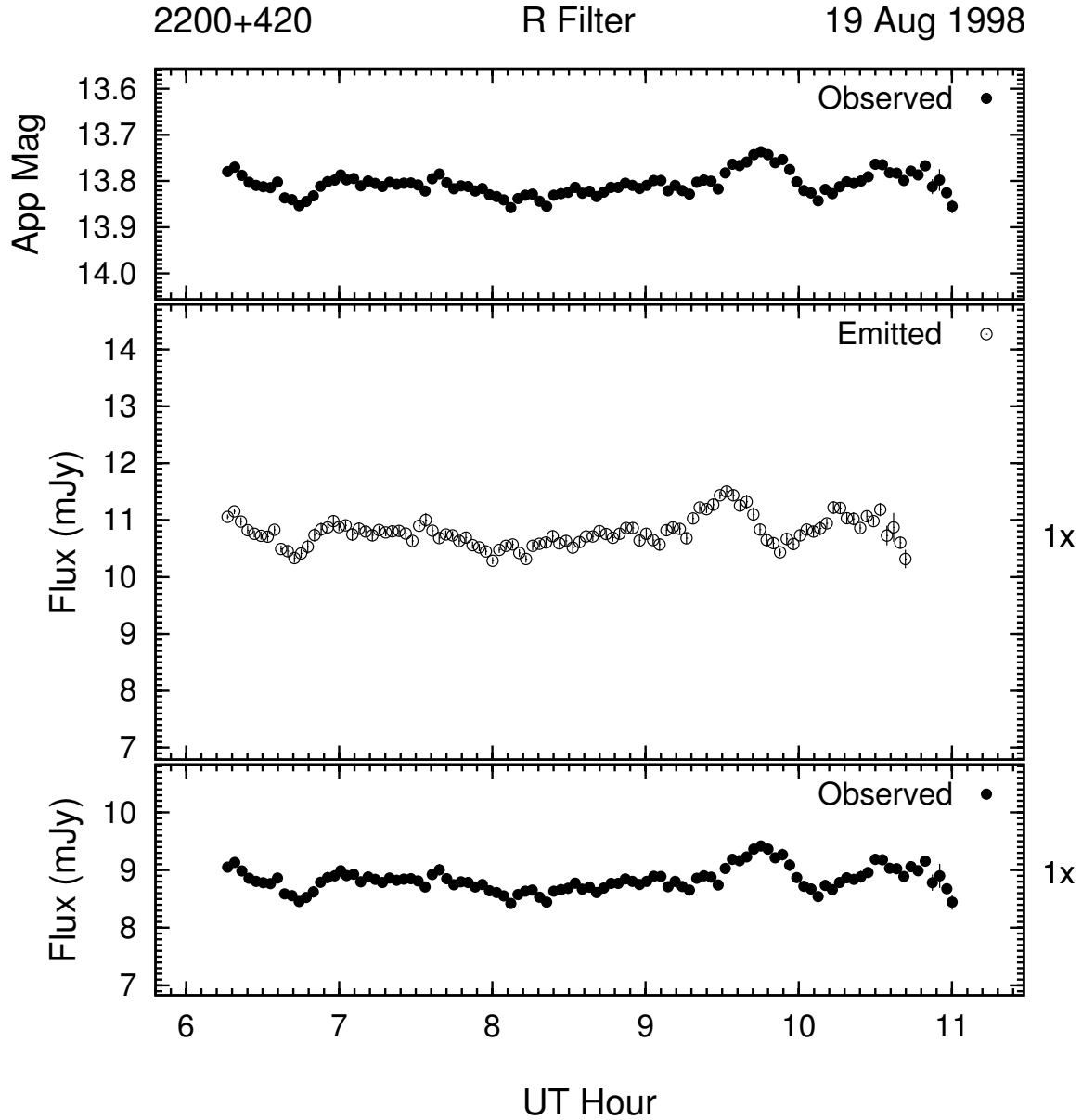


Figure 3.116: Example of the optical microvariability (R band) of 2200 + 420 on the night of 19 Aug 1998. This night's data was 2-point averaged to improve S/N .

nights (19 and 20 August) as seen in Figures 3.116 and 3.117. The variations for both nights were 0.12 and 0.15 mag respectively. On the night of 19 Aug, BL Lac exhibited two well defined flares (9.8^h & 10.6^h UT) but no net change in brightness, and on 20 Aug, it showed

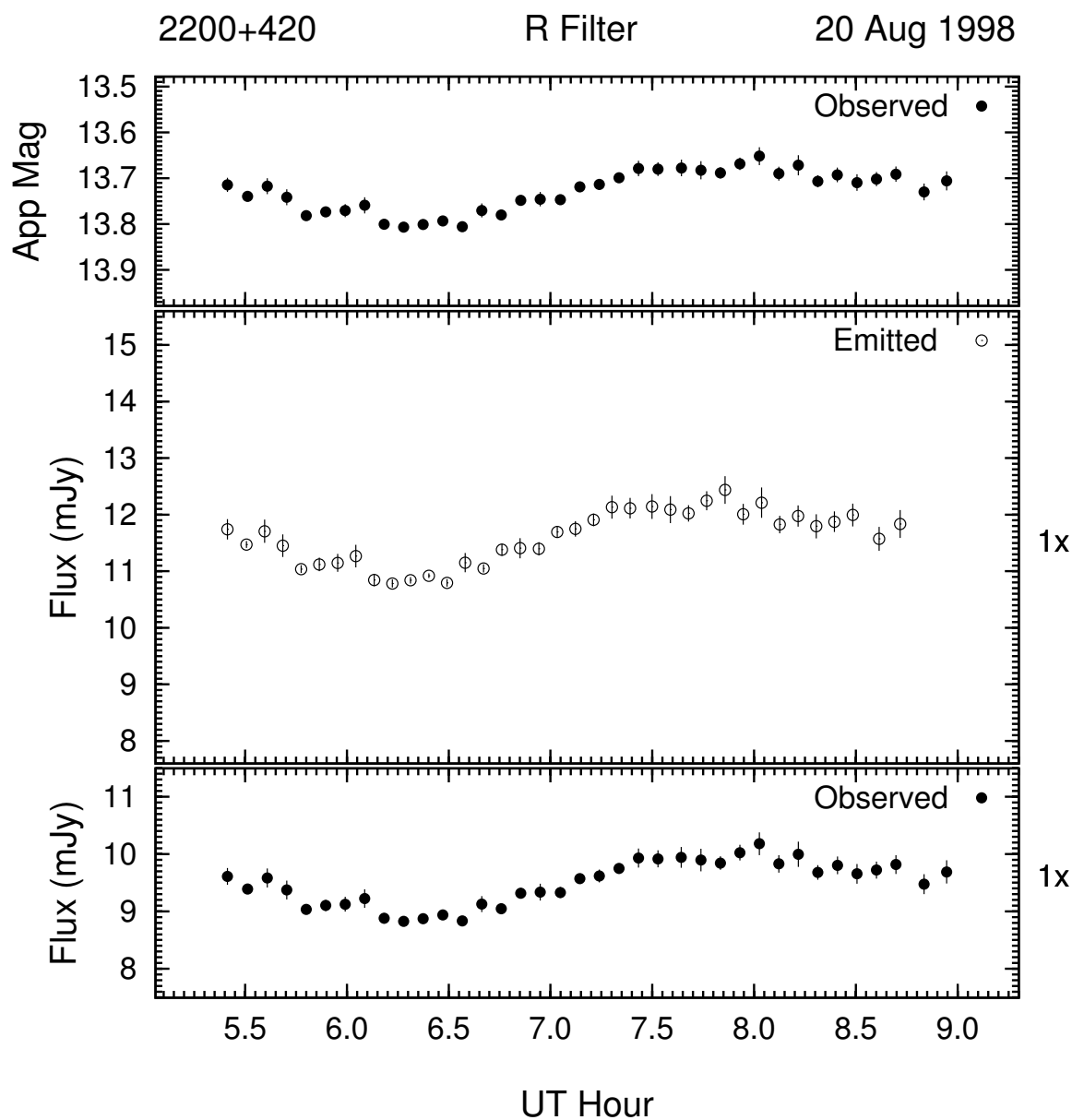


Figure 3.117: Example of the optical microvariability (R band) of 2200 + 420 on the night of 20 Aug 1998. This night's data was 5-point averaged to improve S/N .

more oscillatory behavior at $\gtrsim 0.1$ mag level without any statistically significant brightness variations superimposed upon it.

On the night of 19 Oct 1998, BL Lac again displayed its quasi-oscillatory behavior as

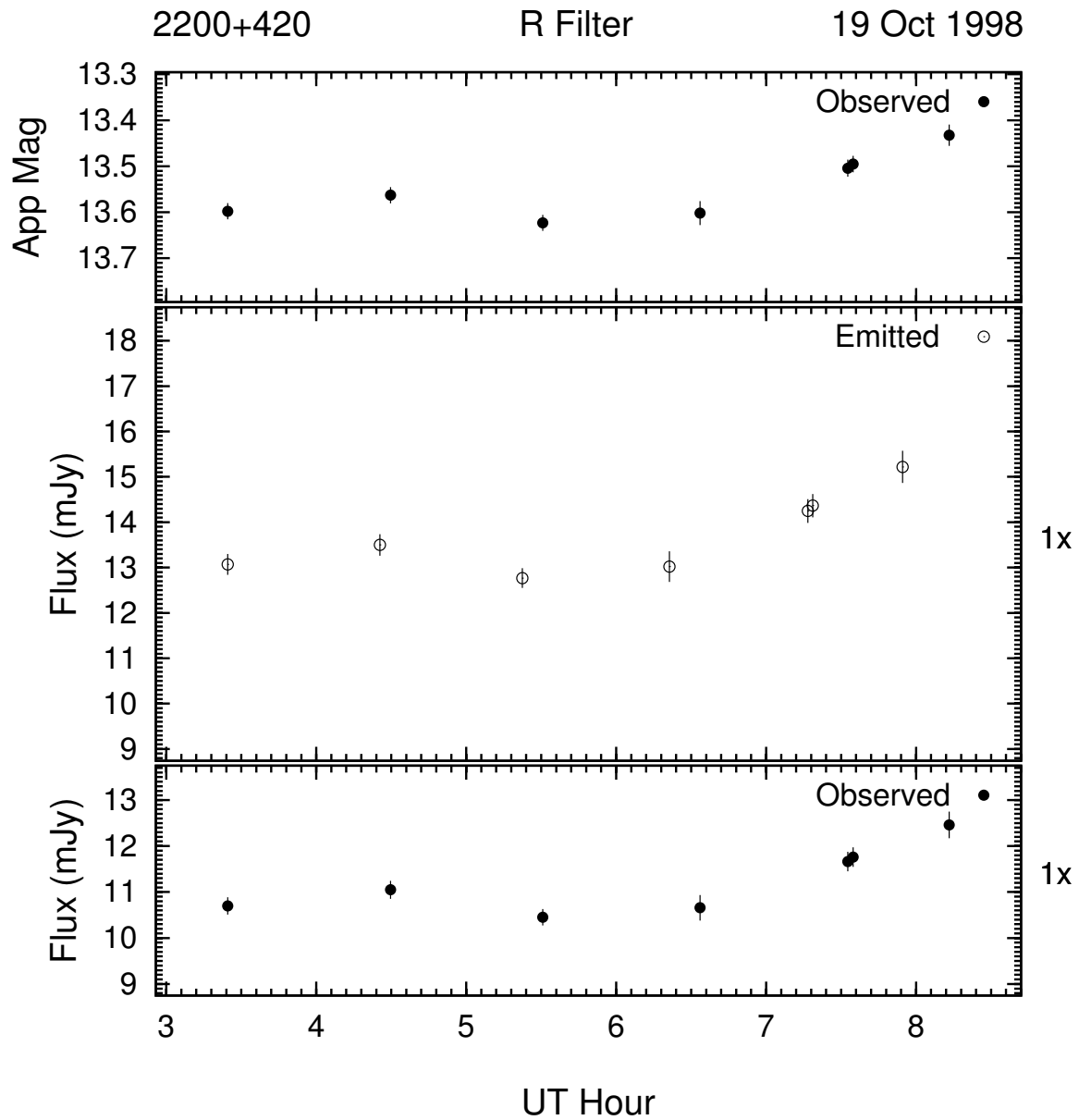


Figure 3.118: Example of the optical microvariability (R band) of 2200 + 420 on the night of 19 Oct 1998.

shown in Figure 3.118. These brightness variations are at a level of 0.2 mag and a significance level of 7.0σ .

A run of 8 nights of microvariability observations begins on 21 Jul 2000 (Figure 3.119). BL

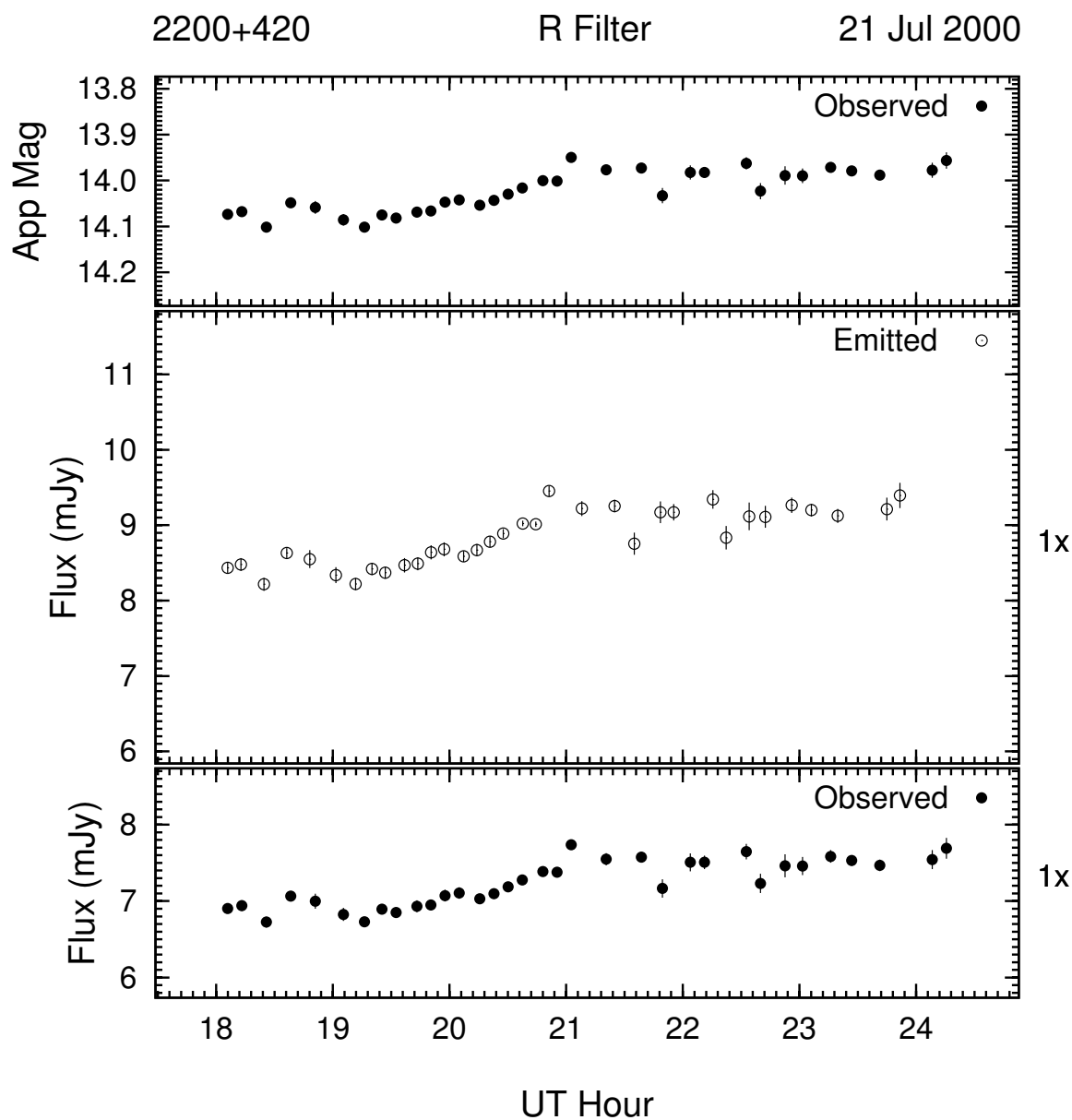


Figure 3.119: Example of the optical microvariability (R band) of 2200 + 420 on the night of 21 Jul 2000. This night's data was 2-point averaged to improve S/N .

Lac is ~ 0.5 mag dimmer than it was in 1998, and showed an increasing trend in brightness of 0.2 mag over the course of 6 hours. On 23 Jul (Figure 3.120), BL Lac exhibited a flare of 0.15 mag (10.5σ) over only 2 hours. It showed yet another, lower level flare about 3 hours

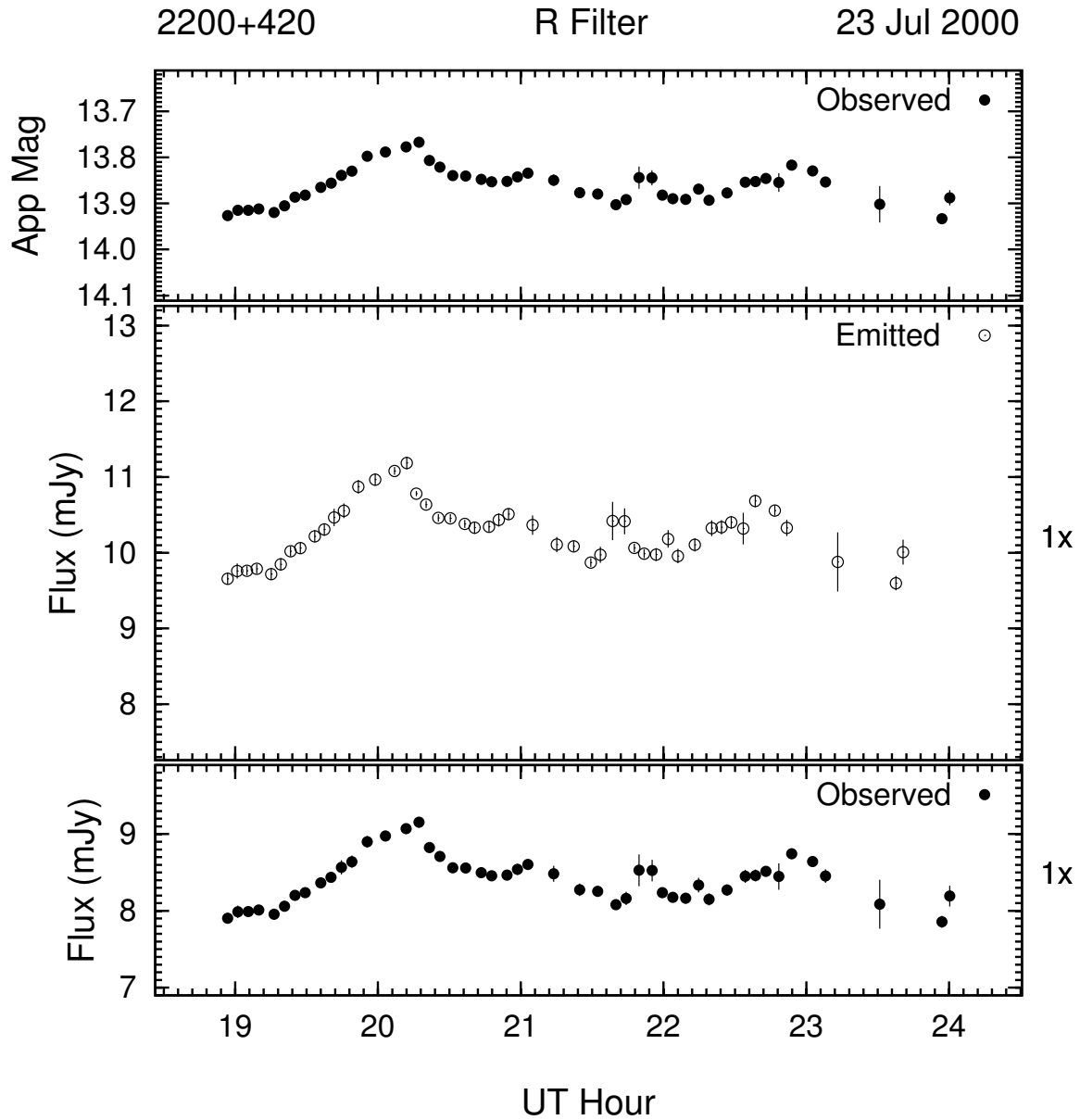


Figure 3.120: Example of the optical microvariability (R band) of 2200 + 420 on the night of 23 Jul 2000. This night's data was 2-point averaged to improve S/N .

later. No net change in brightness was observed for this night. BL Lac dimmed 0.1 mag between 2 plateaus on the night of 25 Jul as seen in Figure 3.121. Figure 3.122 shows BL Lac undergoing 2 discrete flares at -4.0^h and -2.3^h . Both occurred in ~ 1 hour with a

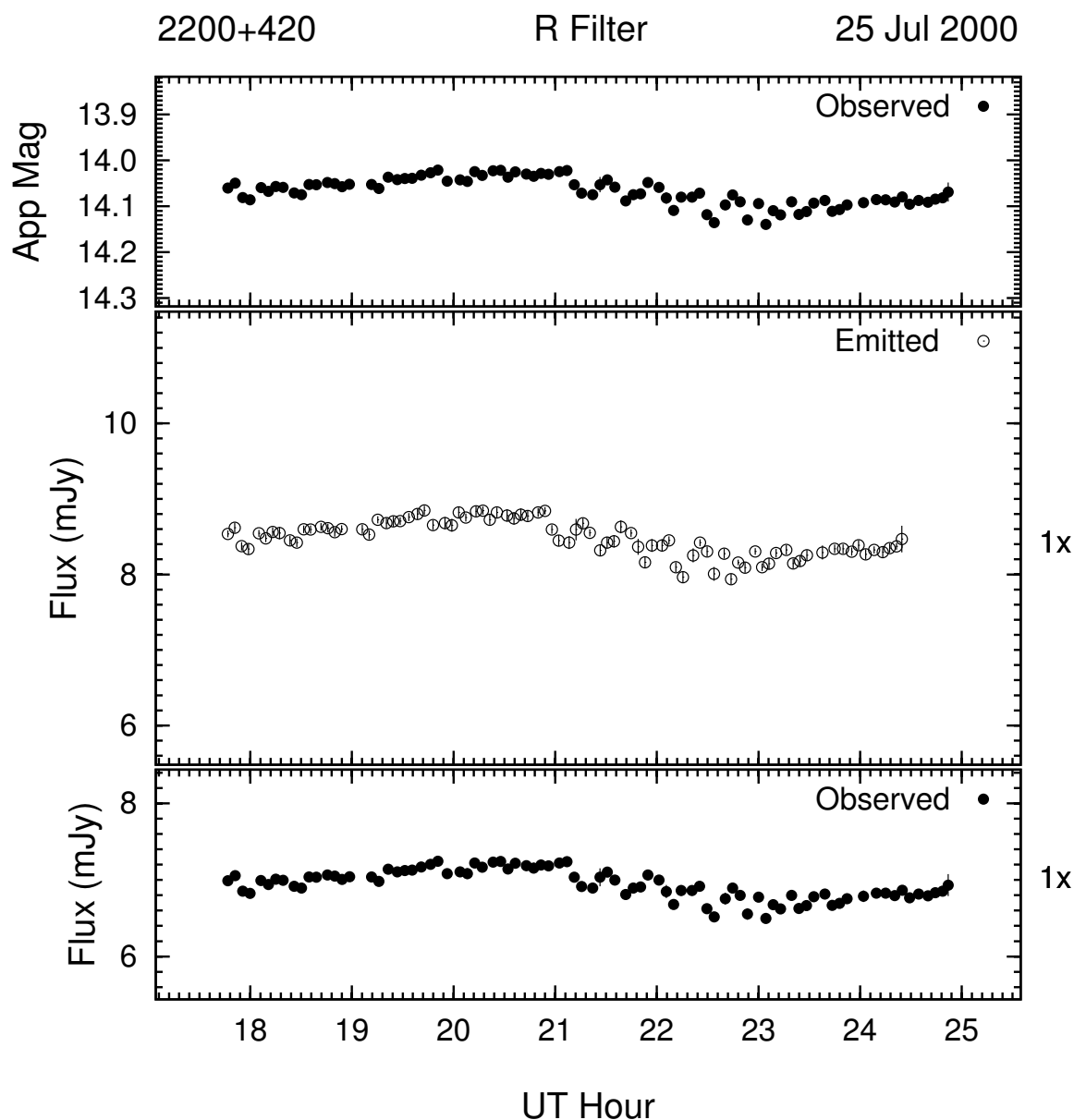


Figure 3.121: Example of the optical microvariability (R band) of 2200 + 420 on the night of 25 Jul 2000. This night's data was 2-point averaged to improve S/N .

change in brightness of 0.3 mag above the lowest level for the night. On the night of 05 Aug (3.123), BL Lac showed one definite flare centered at -5^h UT which lasted ~ 2 hours and another less well defined flare centered at approximately -1^h UT with duration of 4 hours.

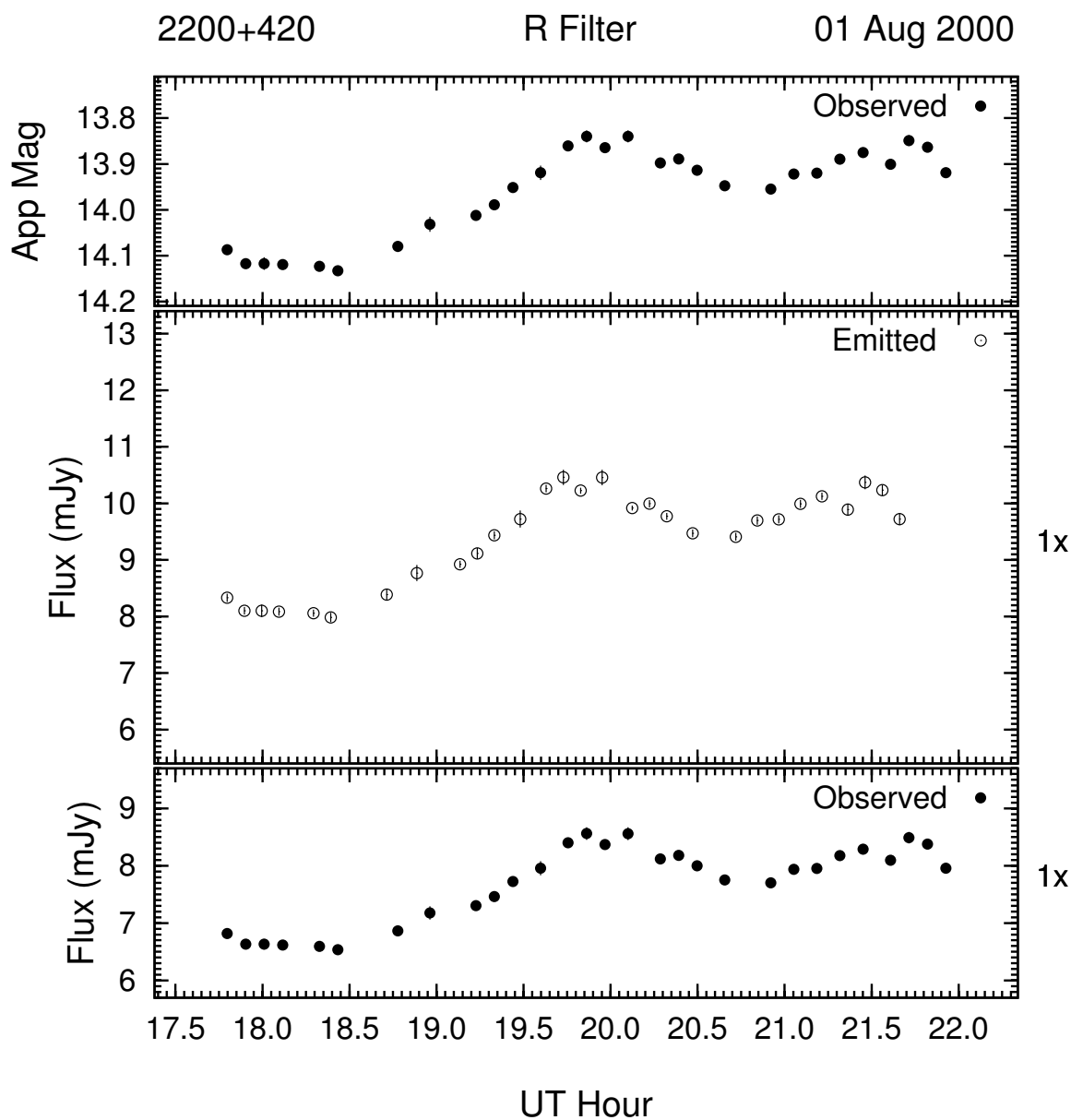


Figure 3.122: Example of the optical microvariability (R band) of 2200 + 420 on the night of 01 Aug 2000. This night's data was 2-point averaged to improve S/N .

BL Lac showed even more oscillatory behavior on the night of 06 Aug (Figure 3.124) with an amplitude of 0.2 mag over 6 hours. This behavior is repeated 2 nights later (08 Aug, Figure 3.125) with an amplitude roughly 2 times greater (0.43 mag) over a longer period.

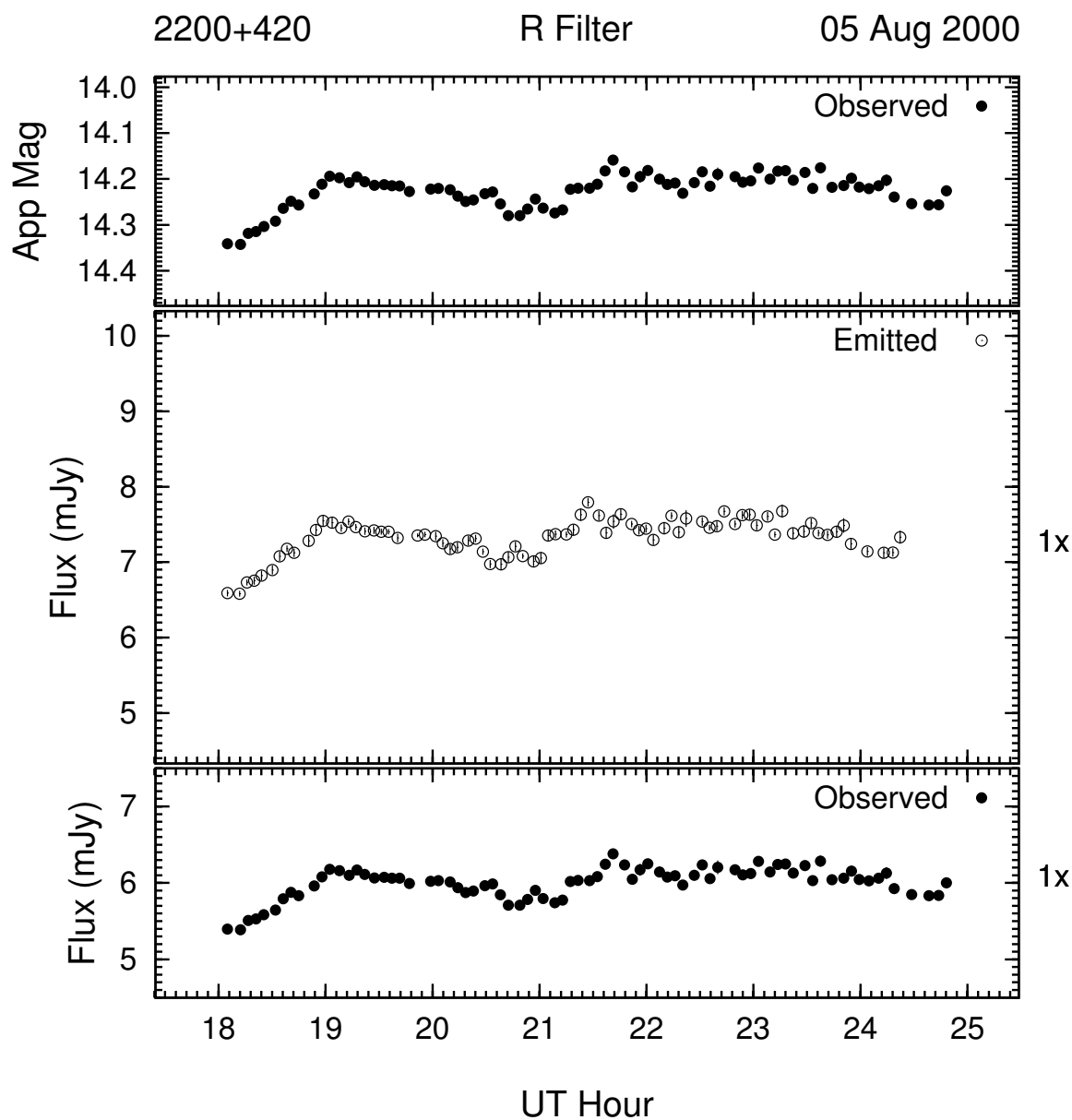


Figure 3.123: Example of the optical microvariability (R band) of 2200 + 420 on the night of 05 Aug 2000. This night's data was 2-point averaged to improve S/N .

This run concludes on 11 Aug (3.126) with BL Lac exhibiting yet more oscillatory brightness variations (0.2 mag), but with some small (~ 0.05 mag) variations superimposed. During this entire run, BL Lac's brightness ranged between $R = 13.8$ and $R = 14.4$.

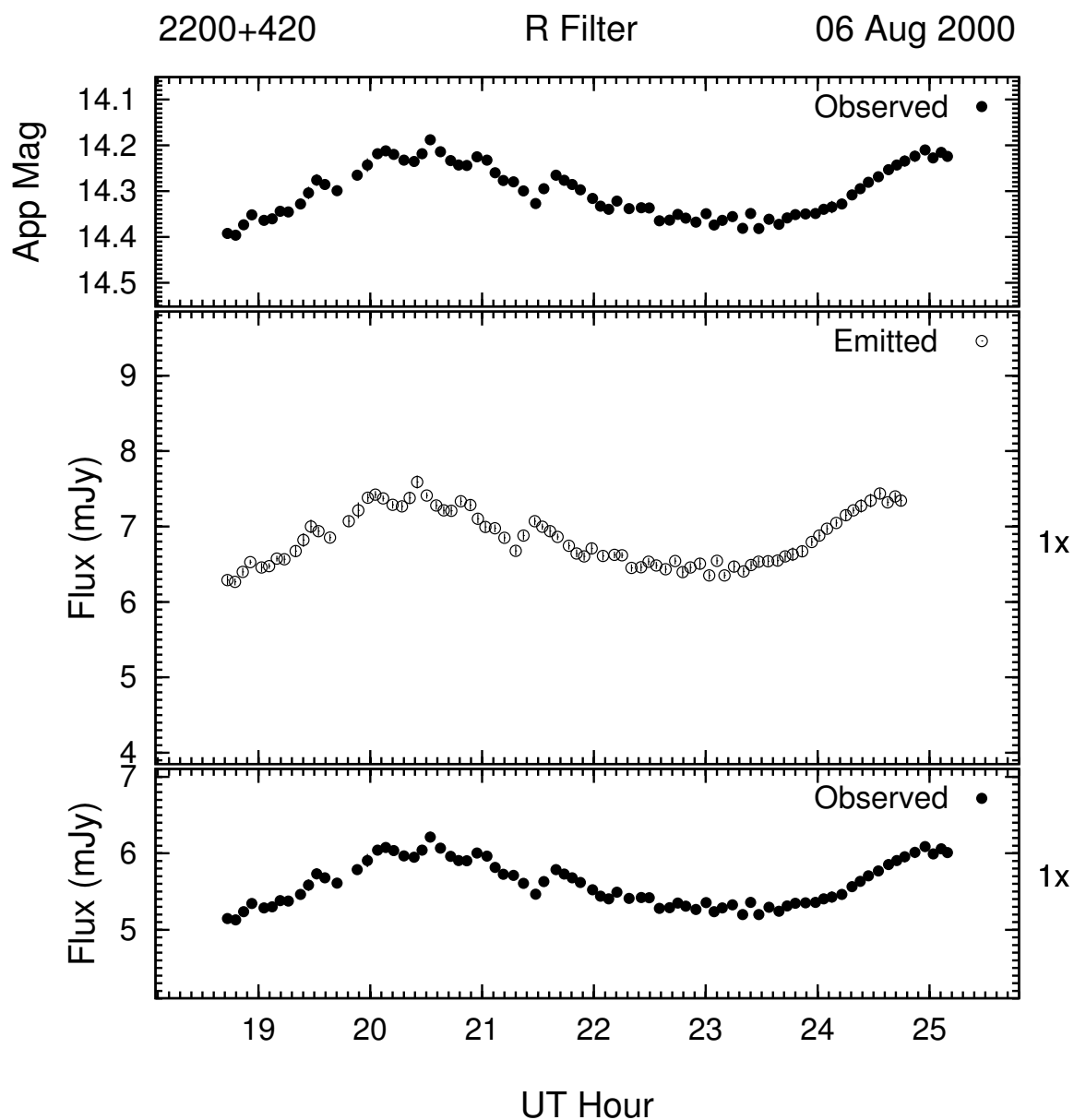


Figure 3.124: Example of the optical microvariability (R band) of 2200 + 420 on the night of 06 Aug 2000. This night's data was 2-point averaged to improve S/N .

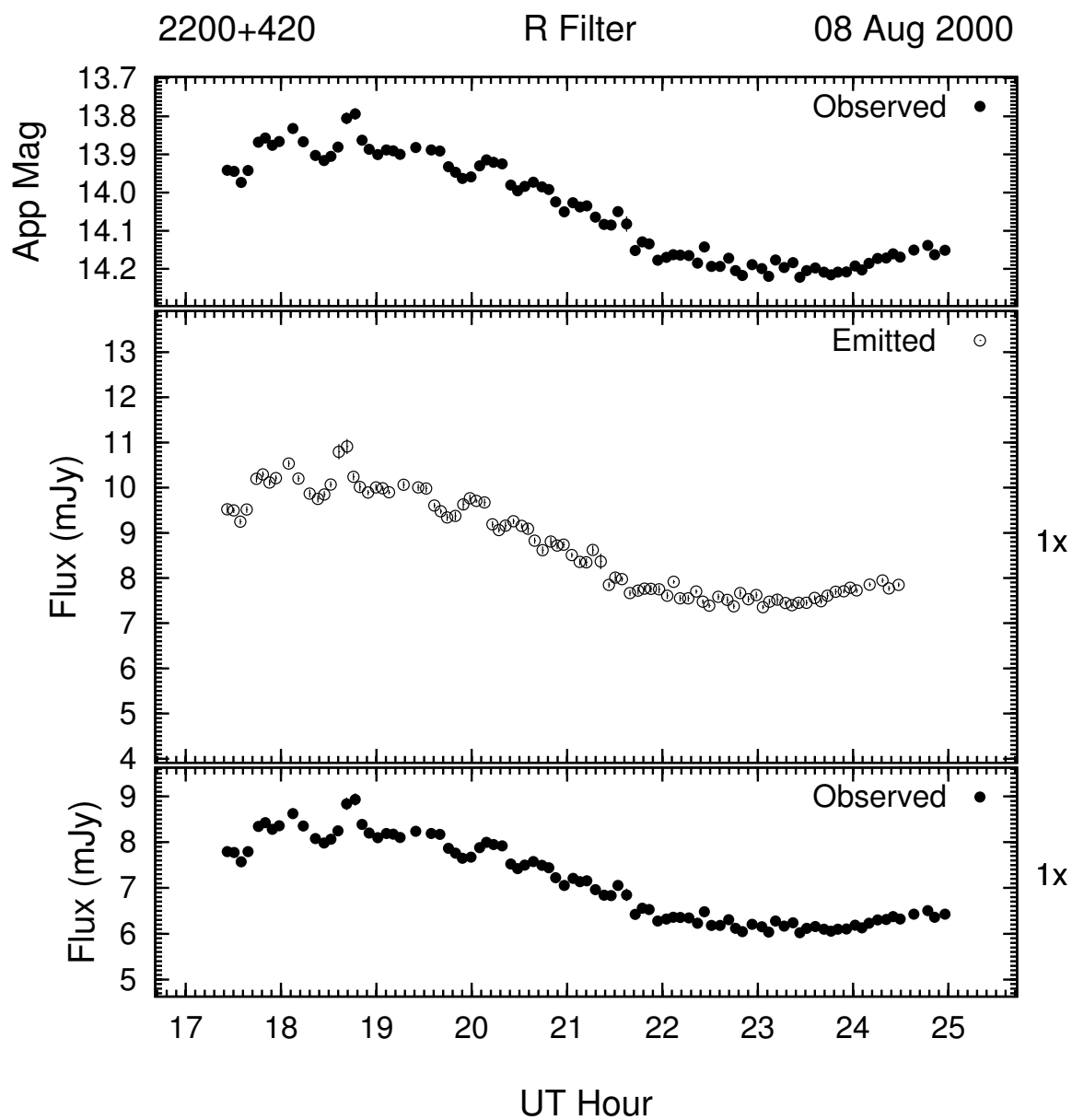


Figure 3.125: Example of the optical microvariability (R band) of 2200 + 420 on the night of 08 Aug 2000. This night's data was 2-point averaged to improve S/N .

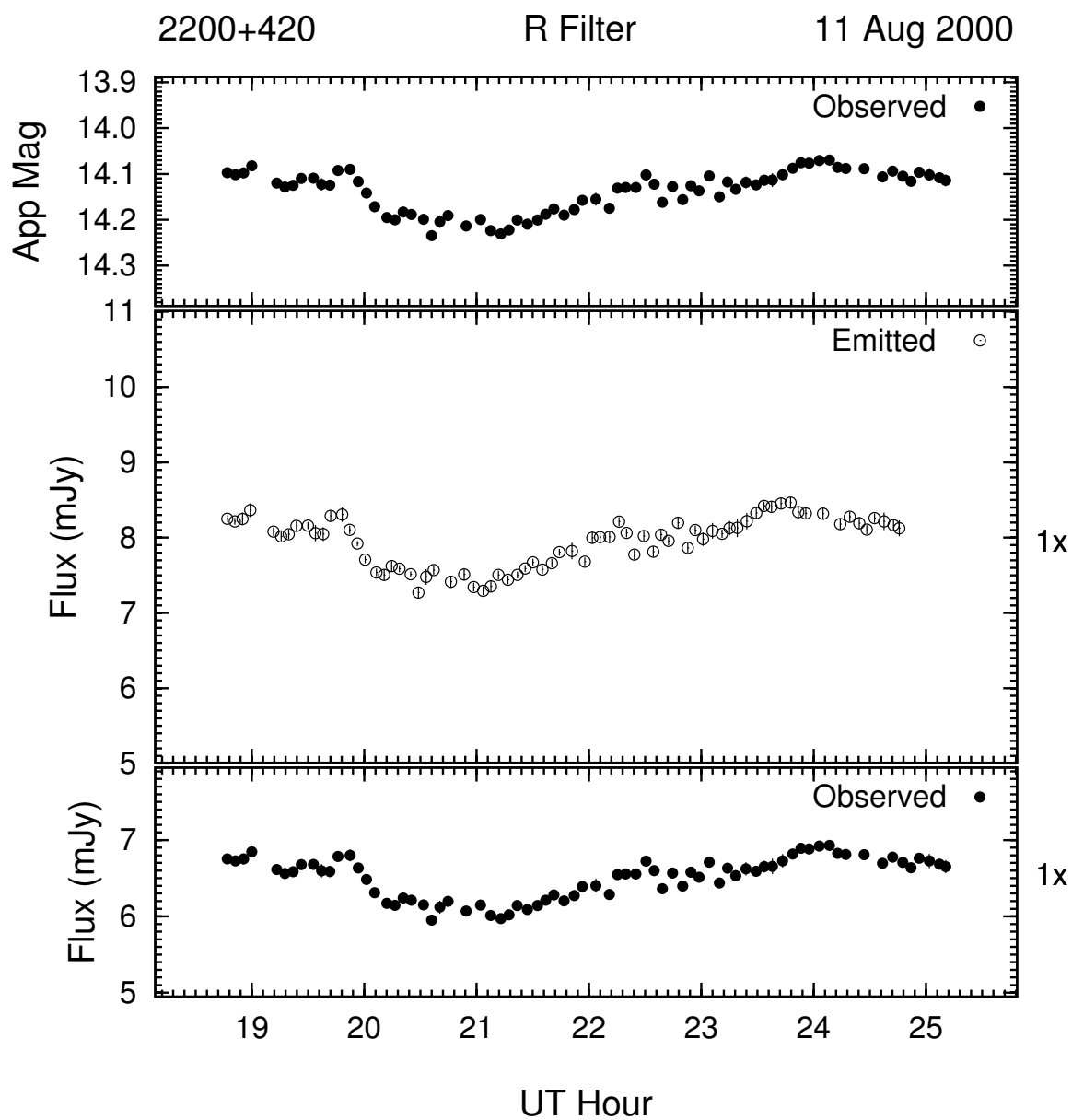


Figure 3.126: Example of the optical microvariability (R band) of 2200 + 420 on the night of 11 Aug 2000. This night's data was 2-point averaged to improve S/N .

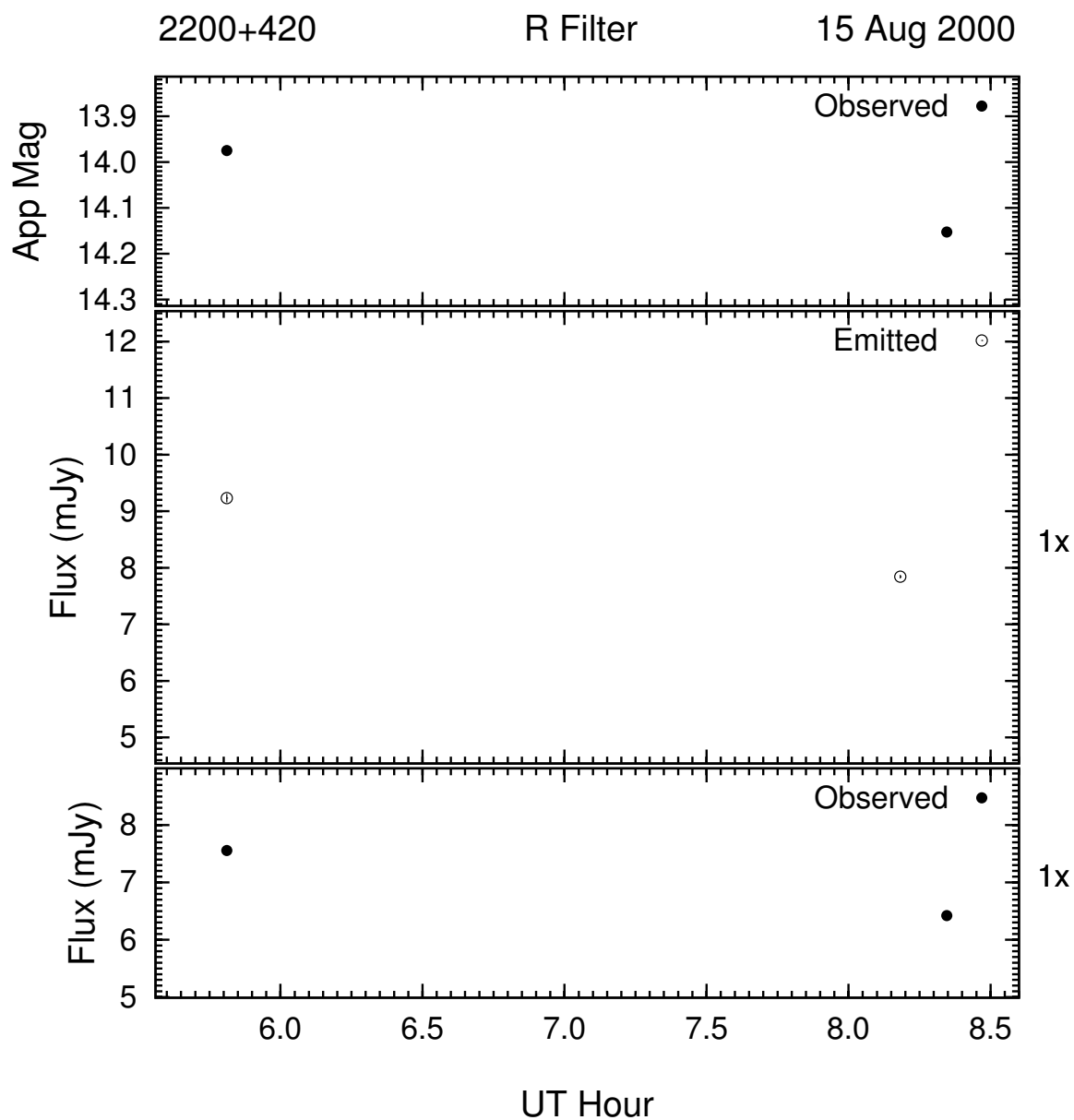


Figure 3.127: Example of the optical microvariability (R band) of 2200 + 420 on the night of 15 Aug 2000. This night's data was 2-point averaged to improve S/N .

The next attempt to find microvariability in BL Lac was in late August of 2000. The light curves for 15, 17, and 19 Aug are in Figures 3.127, 3.128, and 3.129, respectively. The first night it started at a level of $R \simeq 14.0$ and ended 2.5 hours later 0.18 mag dimmer. On

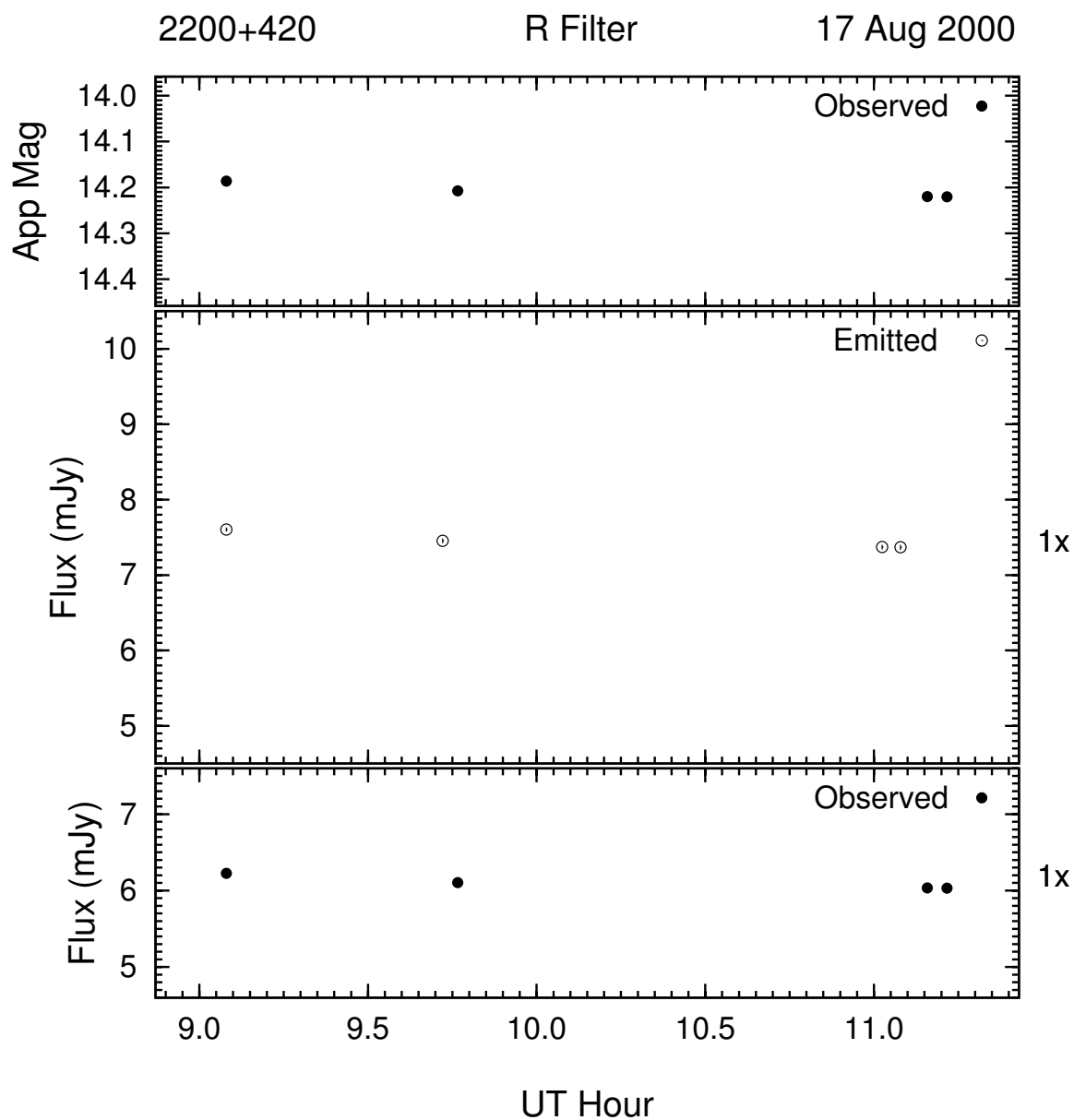


Figure 3.128: Example of the optical microvariability (R band) of 2200 + 420 on the night of 17 Aug 2000. This night's data was 2-point averaged to improve S/N .

the following two nights, BL Lac stayed at approximately that same level ($R = 14.2$) with small amplitude changes in brightness (a slight dimming and brightening respectively).

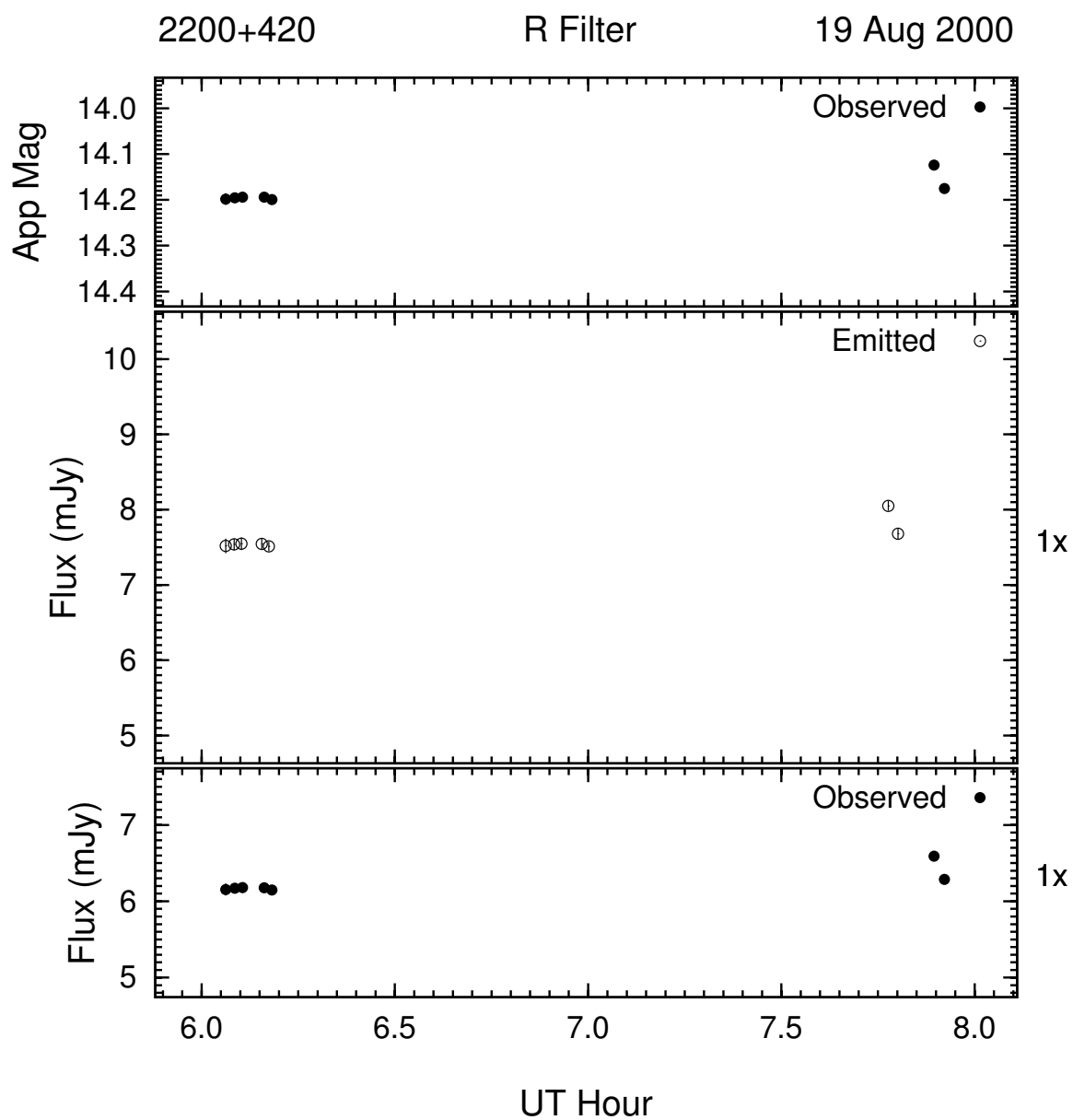


Figure 3.129: Example of the optical microvariability (R band) of 2200 + 420 on the night of 19 Aug 2000.

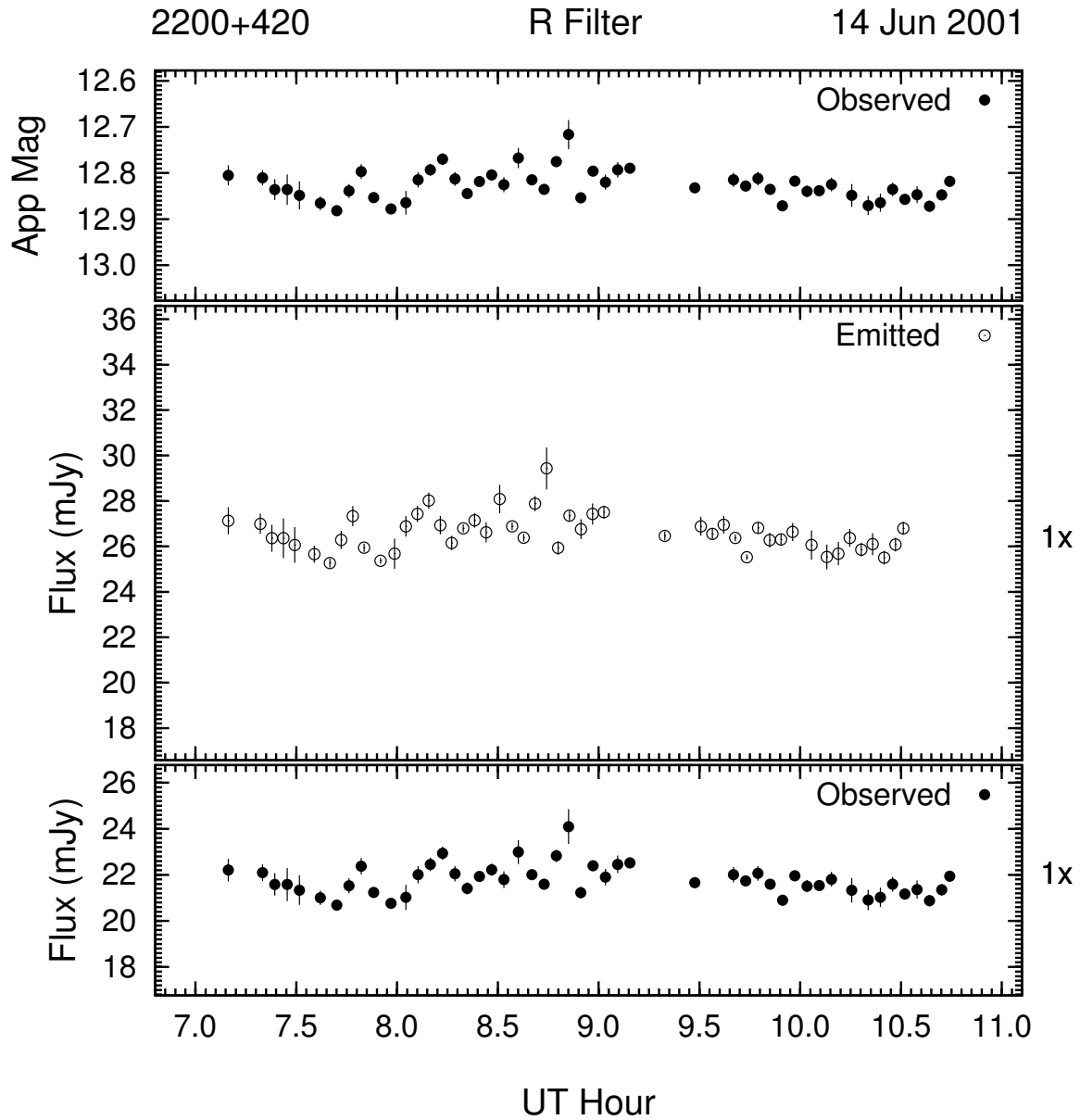


Figure 3.130: Example of the optical microvariability (R band) of 2200 + 420 on the night of 14 Jun 2001. This night's data was 3-point averaged to improve S/N .

Four nights of BL Lac observations between 14 and 18 Jun 2001 are displayed in figures 3.130 through 3.133. On the first night, BL Lac was 1.4 mag brighter than in August of 2000 and exhibited brightness variations of $\lesssim 0.2$ mag over almost 4 hours with no net change in

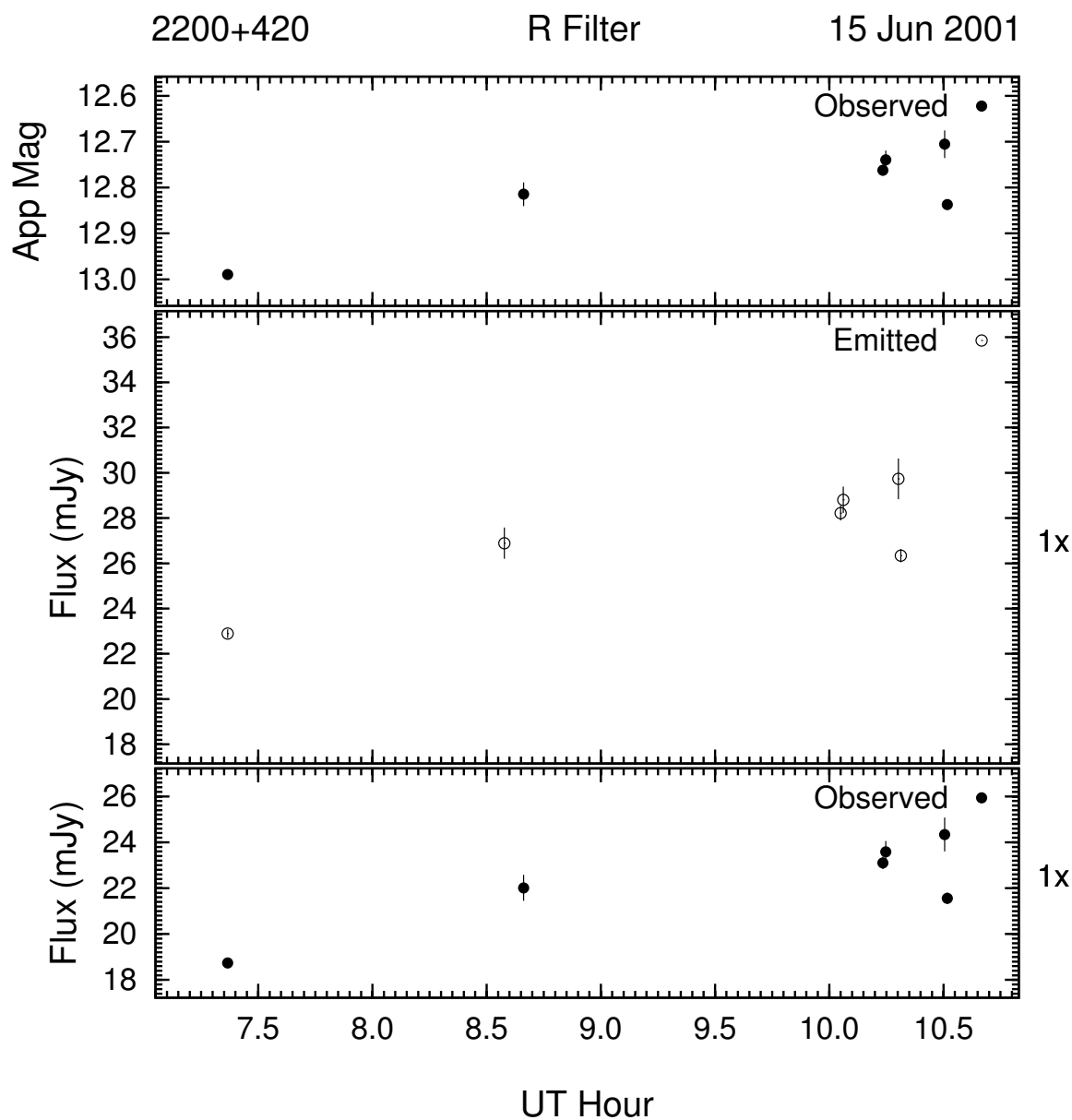


Figure 3.131: Example of the optical microvariability (R band) of 2200 + 420 on the night of 15 Jun 2001.

brightness. On the next night, 15 June (Figure 3.131), BL Lac was in a brightening trend of 0.28 mag over 3 hours, starting at a brightness level of $R = 13.0$. On the night of 17 Jun, BL Lac was again in an increasing trend that started another 0.15 mag dimmer, rising only

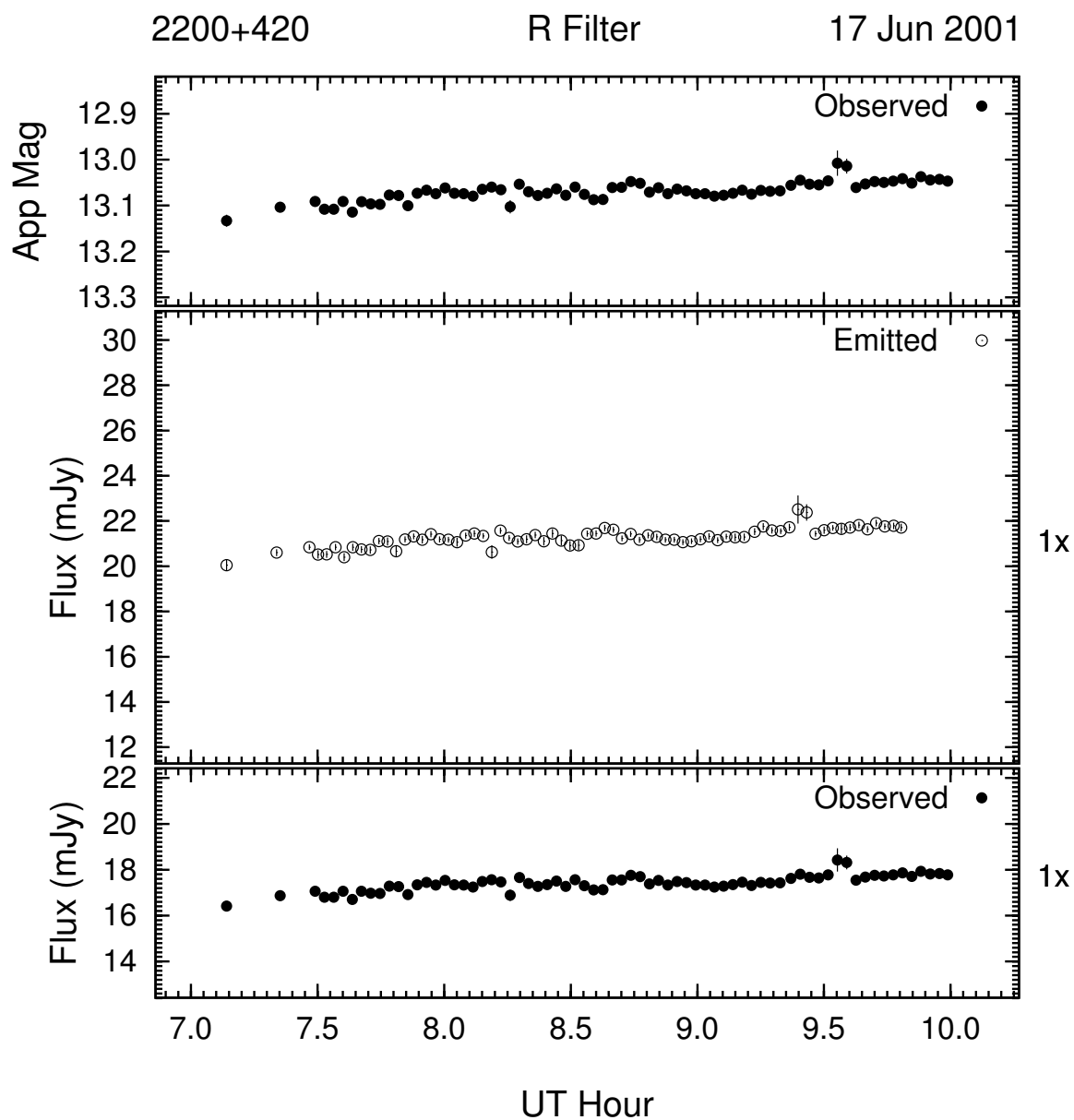


Figure 3.132: Example of the optical microvariability (R band) of 2200 + 420 on the night of 17 Jun 2001. This night's data was 4-point averaged to improve S/N .

0.13 mag (13.2σ). The last night of this run shows that BL Lac increased, then decreased in brightness 0.13 mag over 2 hours.

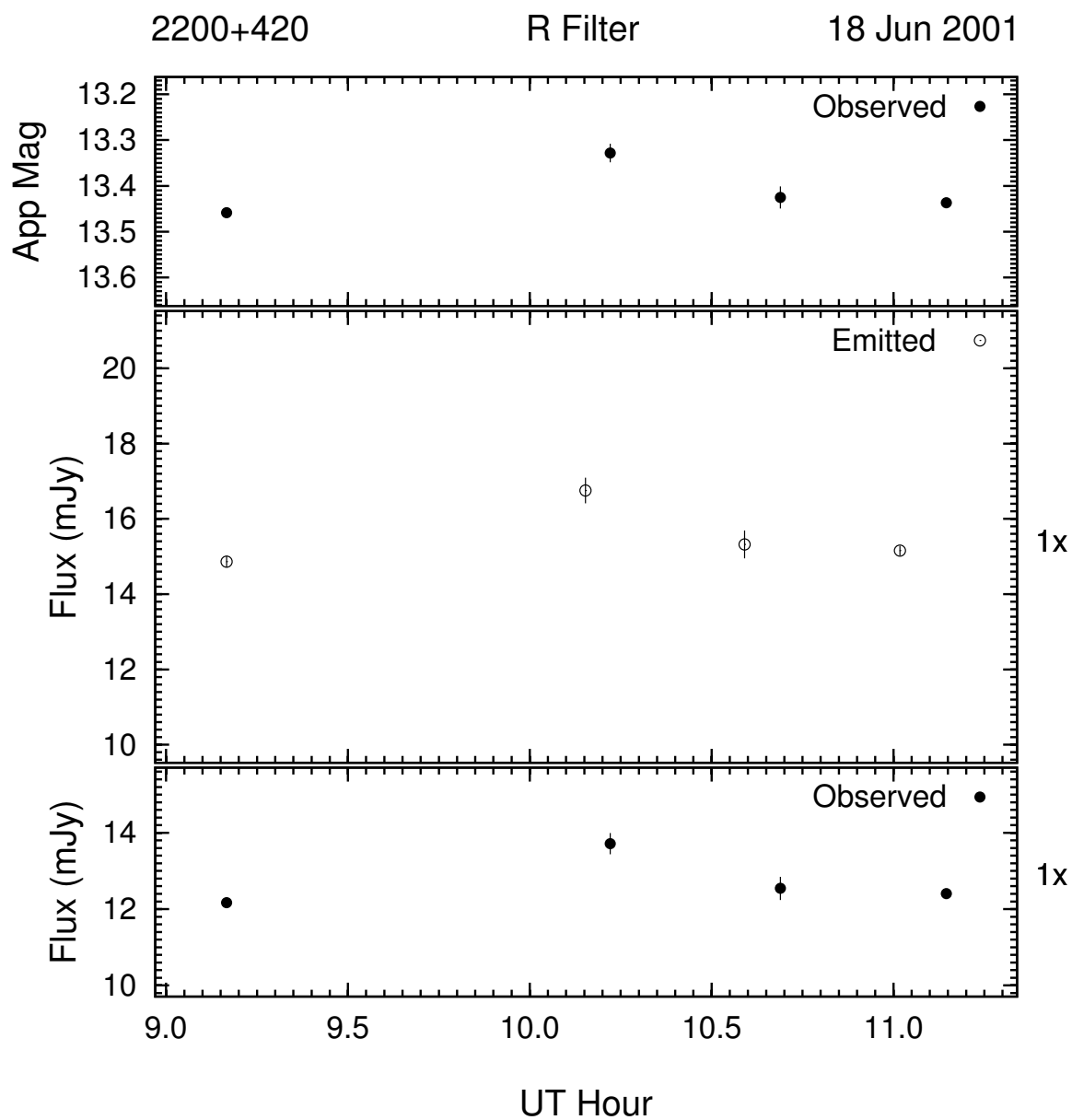


Figure 3.133: Example of the optical microvariability (R band) of 2200 + 420 on the night of 18 Jun 2001. This night's data was 3-point averaged to improve S/N .

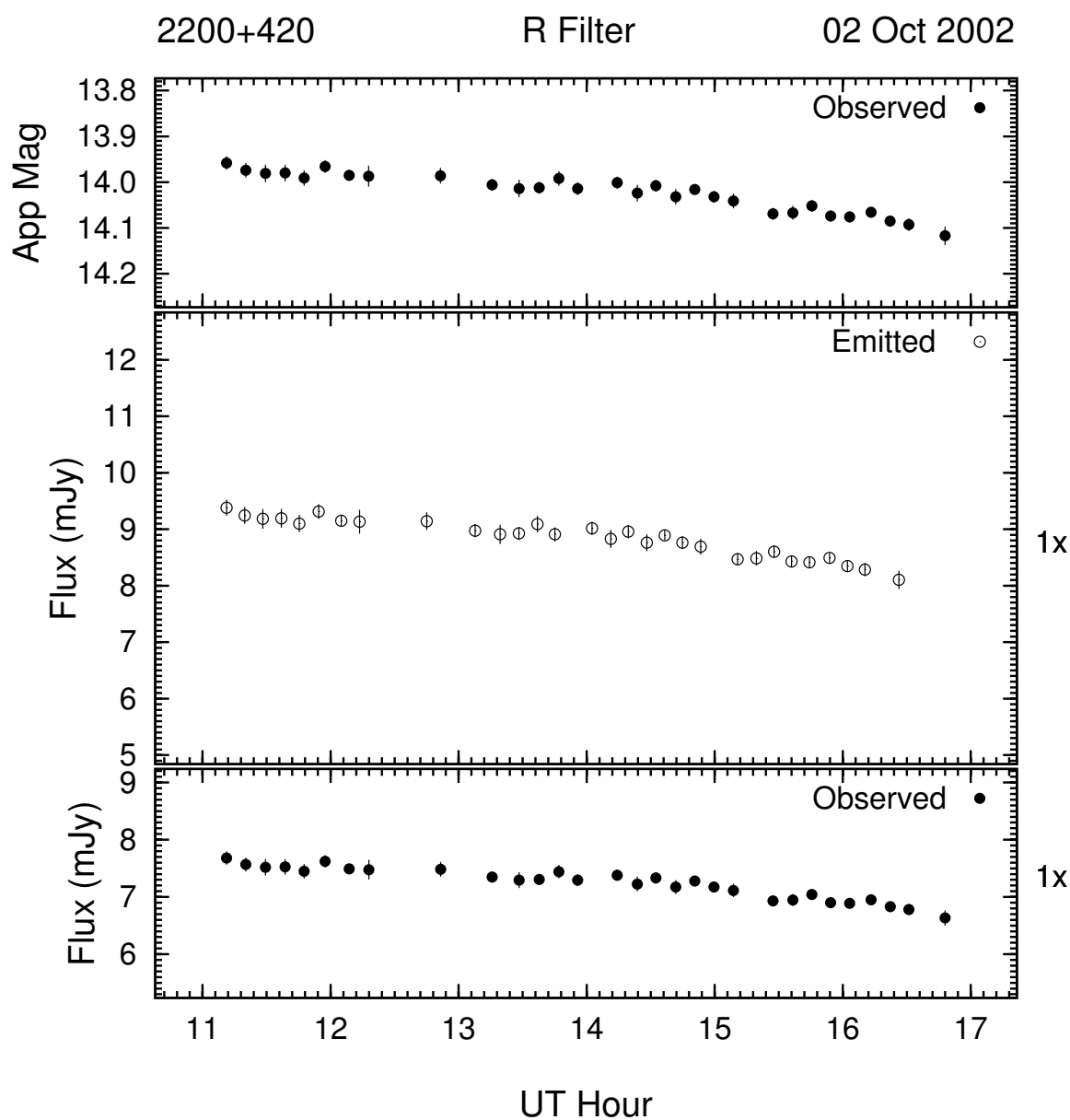


Figure 3.134: Example of the optical microvariability (R band) of 2200 + 420 on the night of 02 Oct 2002.

The nightly brightness variations of BL Lac on 02, 04, and 08 Oct 2002 are shown in Figures 3.134 through 3.136. BL Lac was about 0.5 mag dimmer than in June of 2001 and shows three trends over the 3 nights: a dimming trend of 0.16 mag, a brightening trend of

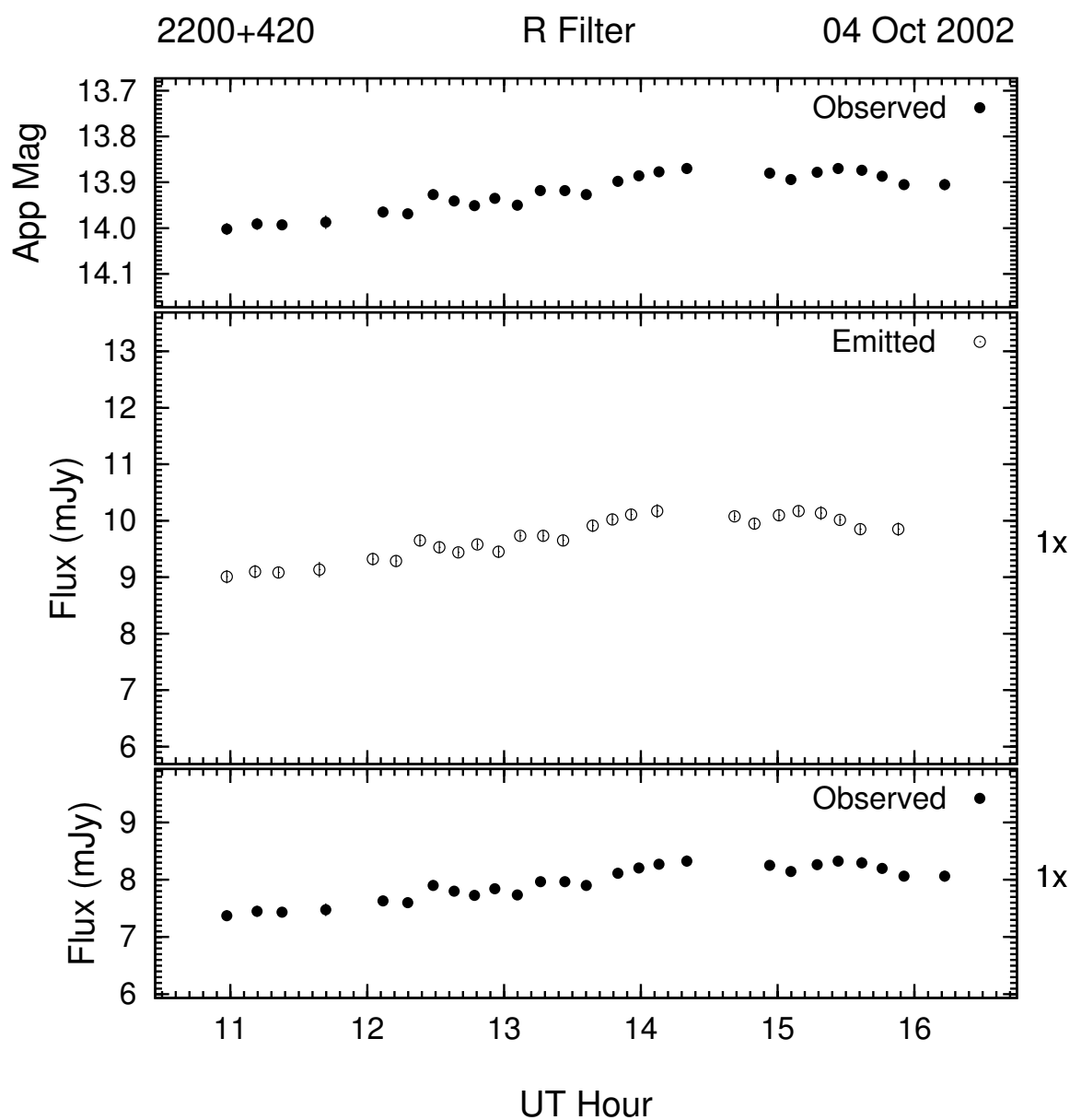


Figure 3.135: Example of the optical microvariability (R band) of 2200 + 420 on the night of 04 Oct 2002.

0.13 mag, and a “flat” trend with small, but significant microvariations in brightness. The object’s brightness increased 0.4 mag between the last 2 nights (Figures 3.135 and 3.136).

On the night of 19 Oct 2002 (Figure 3.137), BL Lac started the night out 0.1 mag dimmer

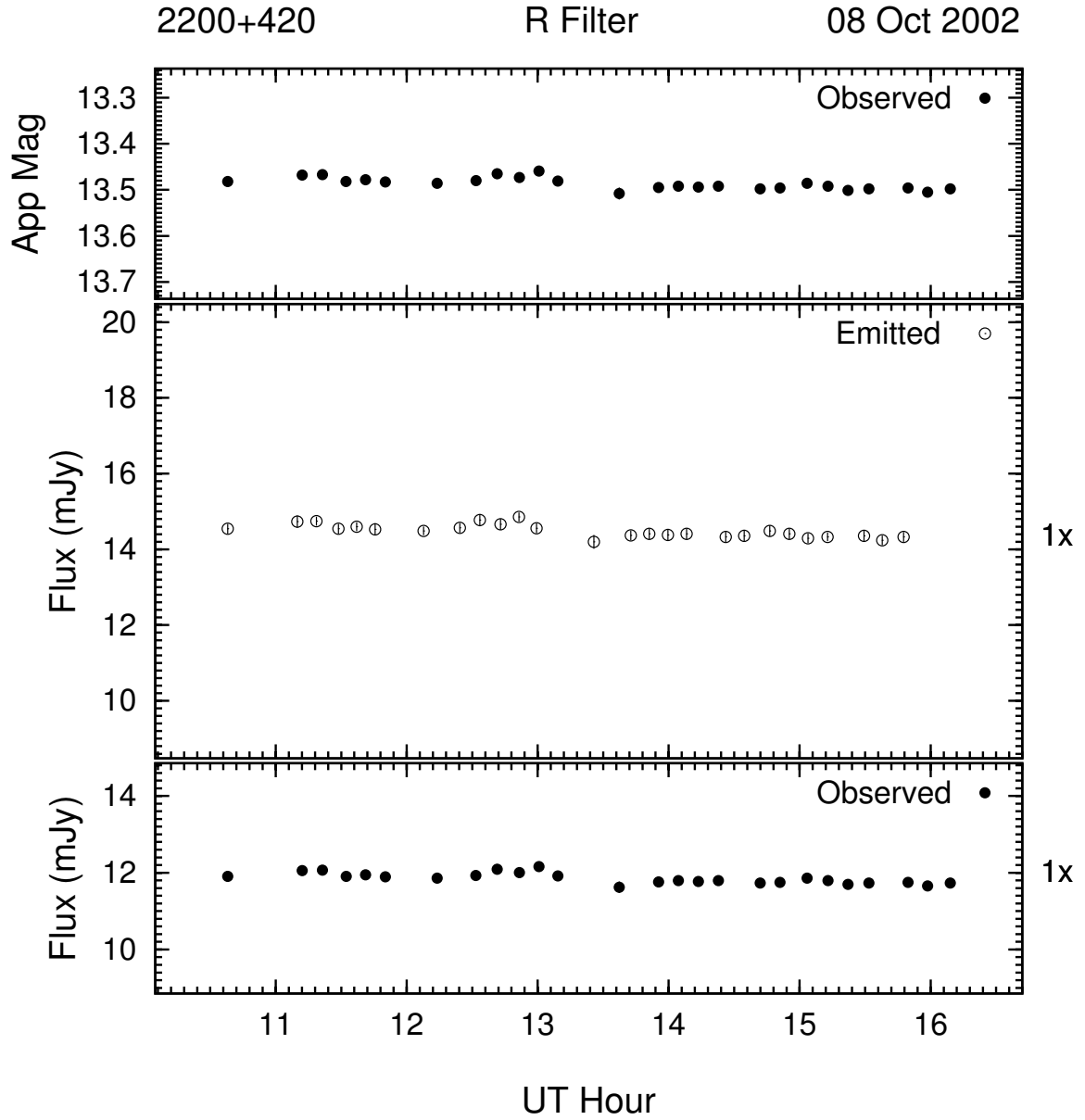


Figure 3.136: Example of the optical microvariability (R band) of 2200 + 420 on the night of 08 Oct 2002.

than the levels earlier in the month. It exhibited a well defined dimming trend over 2.5 hours, followed by two small flares in brightness centered at approximately 5.8^h and 7.5^h UT. The overall change in brightness was 0.18 mag at a significance level of 25.9σ .

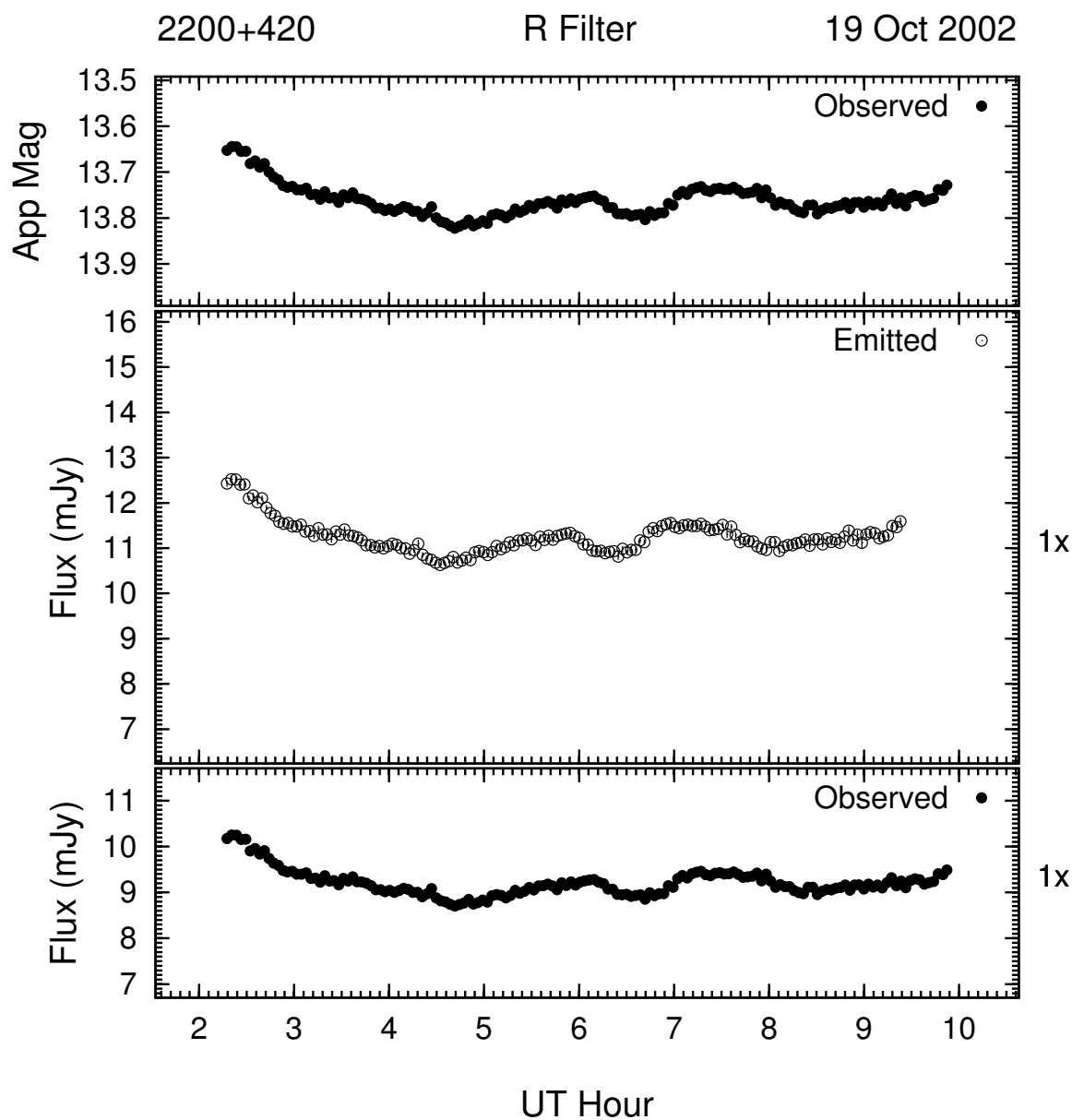


Figure 3.137: Example of the optical microvariability (R band) of 2200 + 420 on the night of 19 Oct 2002. This night's data was 3-point averaged to improve S/N .

BL Lac was observed for microvariability for three consecutive days in late September of 2004. The light curves for these observations are shown in Figures 3.138 through 3.140. The night of 21 Sep is one of only 4 times that BL Lac failed to show any microvariability, and can

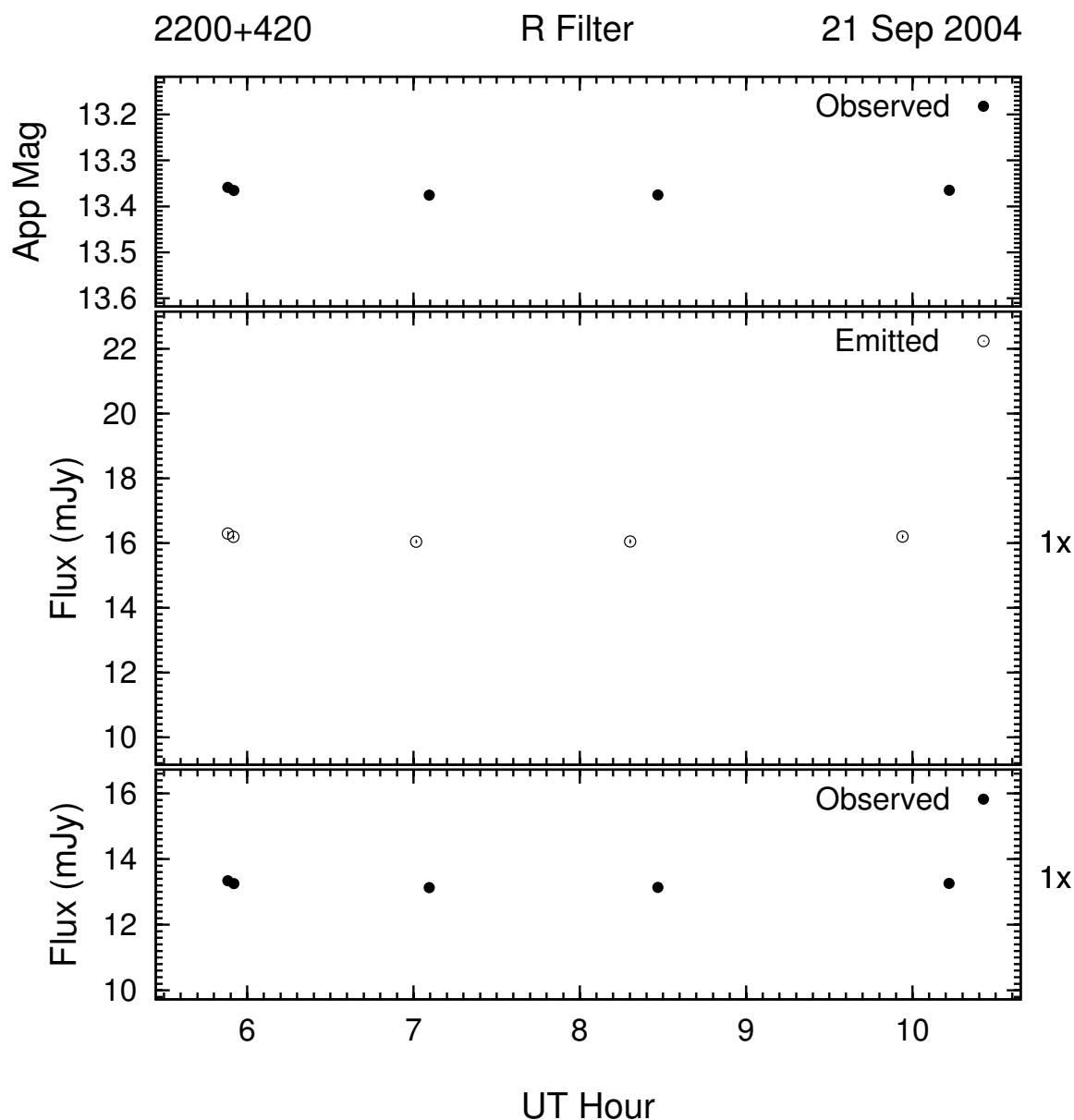


Figure 3.138: Example of the optical microvariability (R band) of $2200 + 420$ on the night of 21 Sep 2004. This night's data was 2-point averaged to improve S/N .

be seen in Figure 3.138. It is ~ 0.3 mag brighter than in October of 2002. The following 2 nights, 22 Sep and 23 Sep (Figure 3.139 and Figure 3.140), show similar oscillatory behavior of 0.09 and 0.17 mag, respectively, over ~ 7 hours each. The brightness level of all three

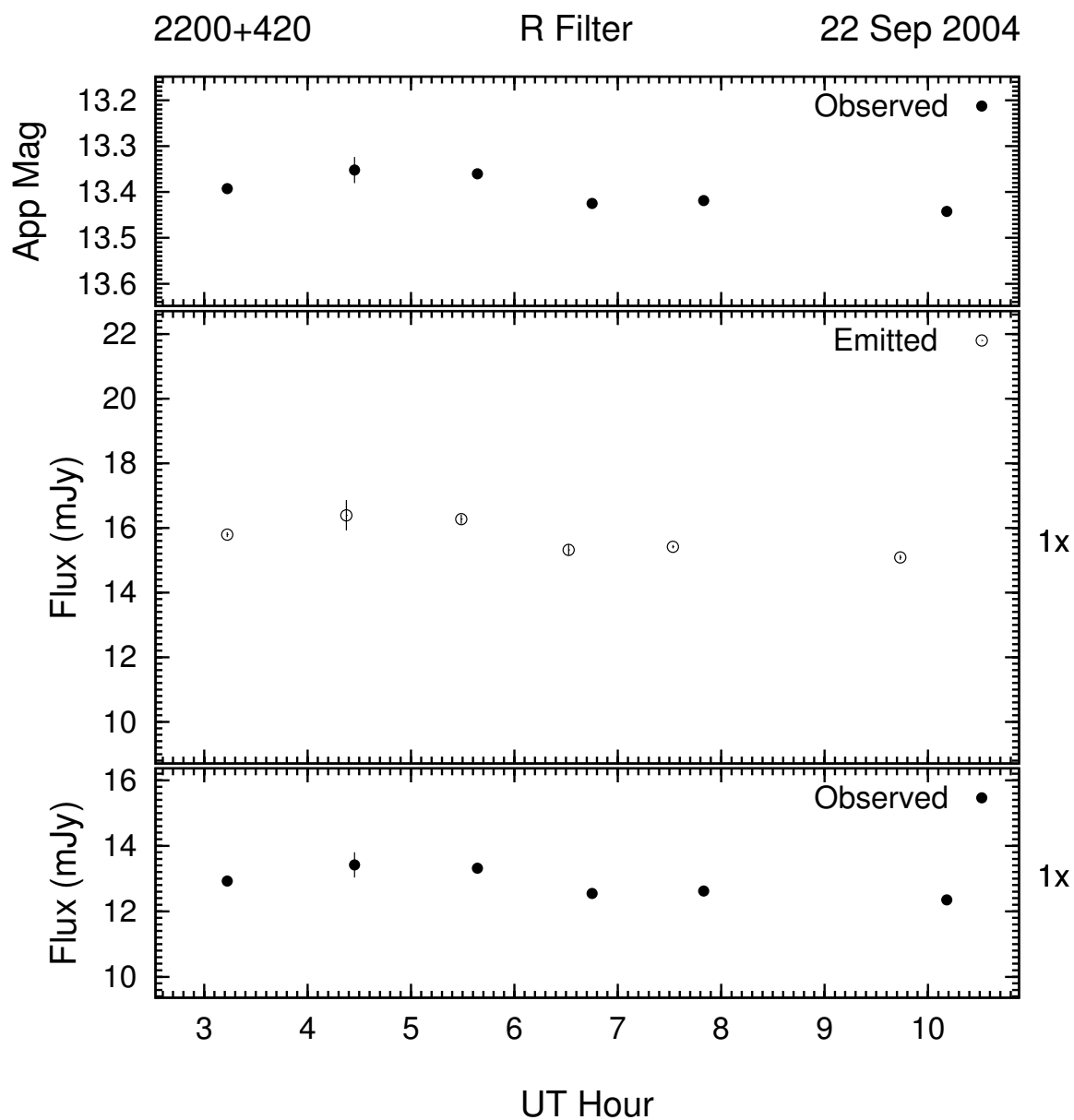


Figure 3.139: Example of the optical microvariability (R band) of $2200 + 420$ on the night of 22 Sep 2004. This night's data was 2-point averaged to improve S/N .

nights was relatively constant at $R \simeq 13.4$.

In the last observations for BL Lac examined, it failed to exhibit statistically significant microvariability on two out of six nights. Light curves for all 6 nights are shown in Figures

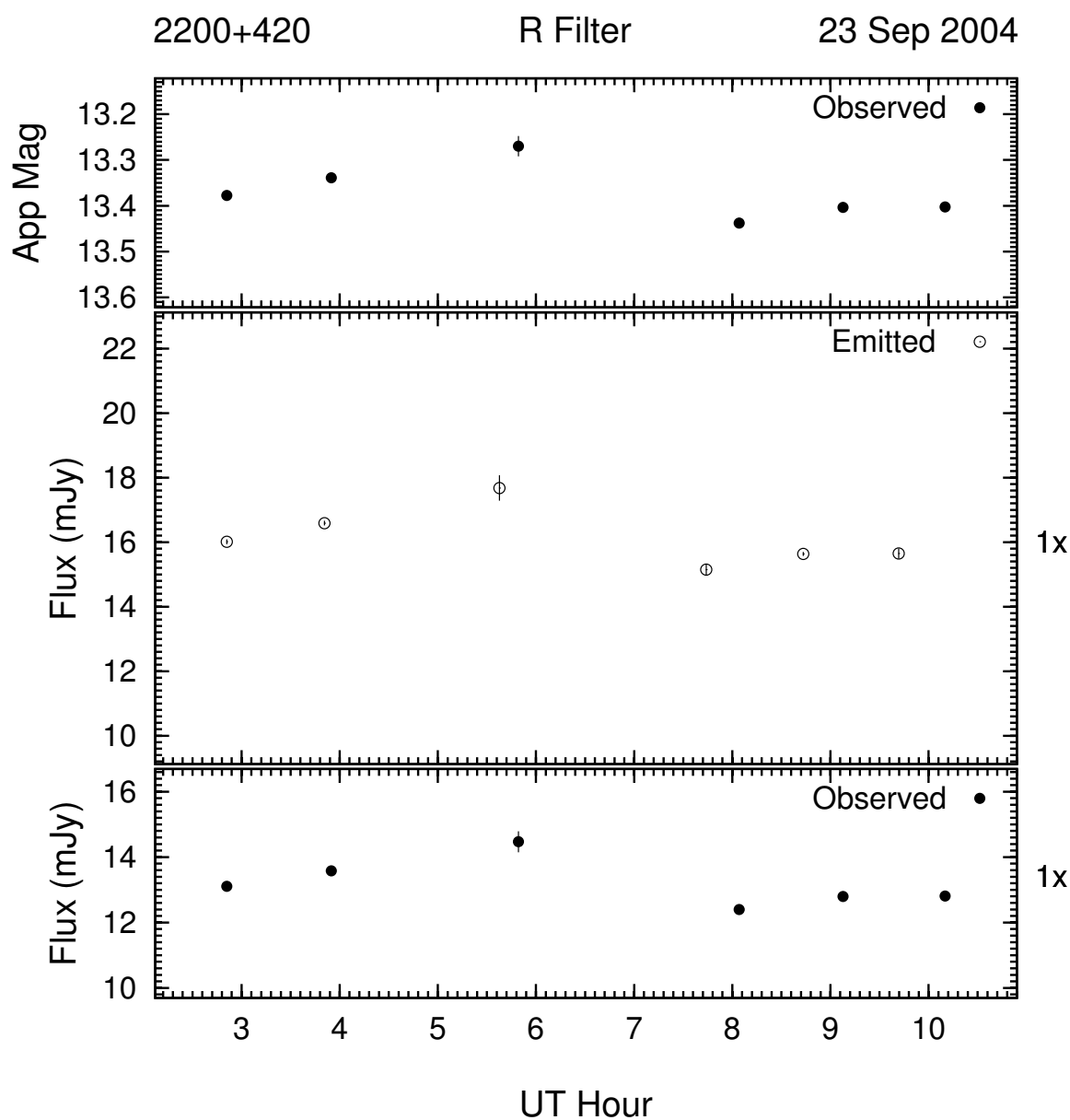


Figure 3.140: Example of the optical microvariability (R band) of 2200 + 420 on the night of 23 Sep 2004. This night's data was 2-point averaged to improve S/N .

3.141 through 3.146. The two nights without microvariability are 04 Oct (Figure 3.141) and 07 Oct (Figure 3.144). The remaining four nights showed brightness variations which mainly took the form of oscillations with durations from several hours to the entire night.

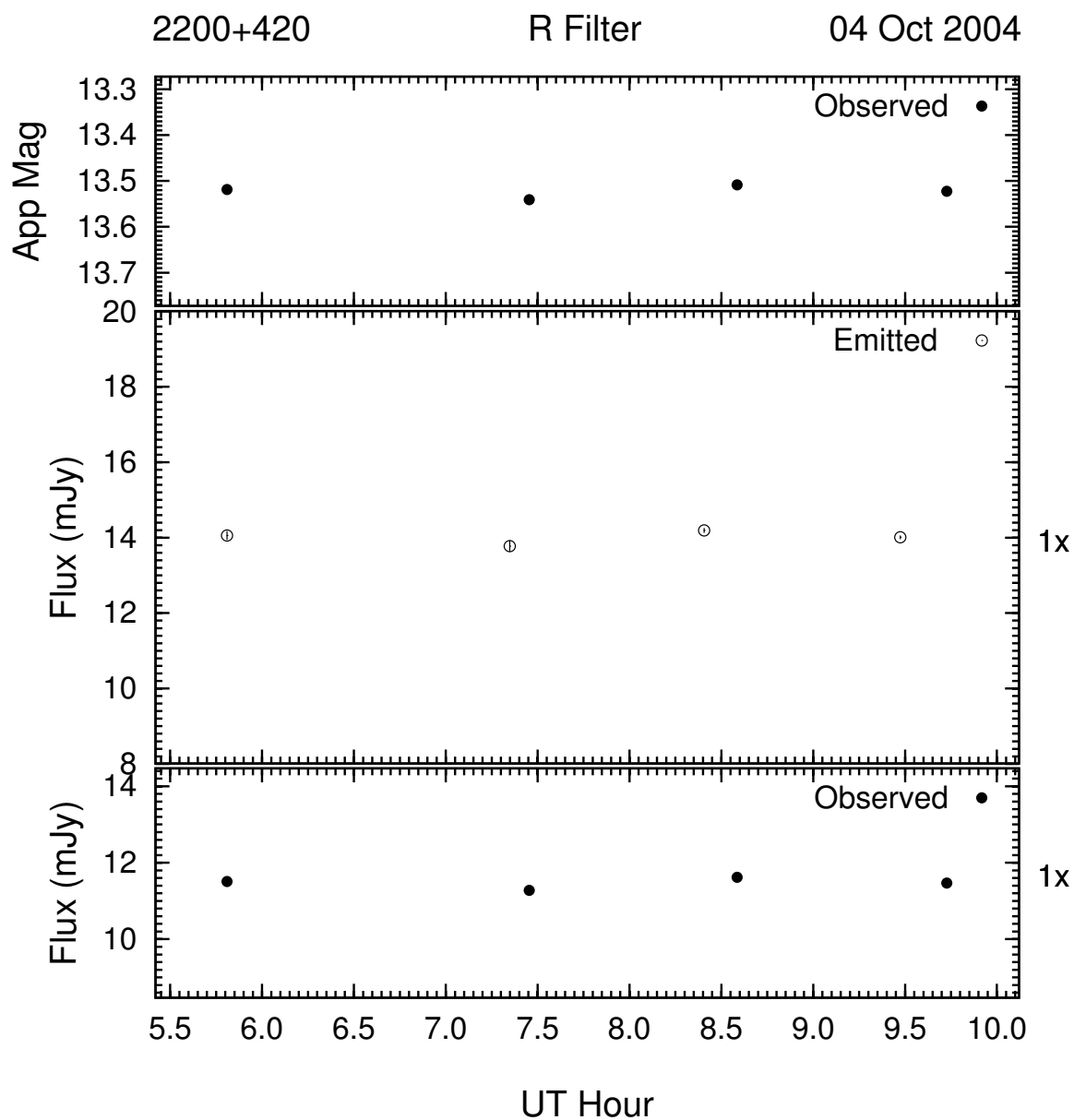


Figure 3.141: Example of the optical microvariability (R band) of $2200 + 420$ on the night of 04 Oct 2004. This night's data was 2-point averaged to improve S/N .

The largest variations took place on the nights of 05 Oct (Figure 3.142) and 09 Oct (Figure 3.146), where BL Lac exhibited dimming of 0.11 and 0.13 mag respectively. The observations of BL Lac for this run started at a brightness level of $R \simeq 13.5$ and took place in a window

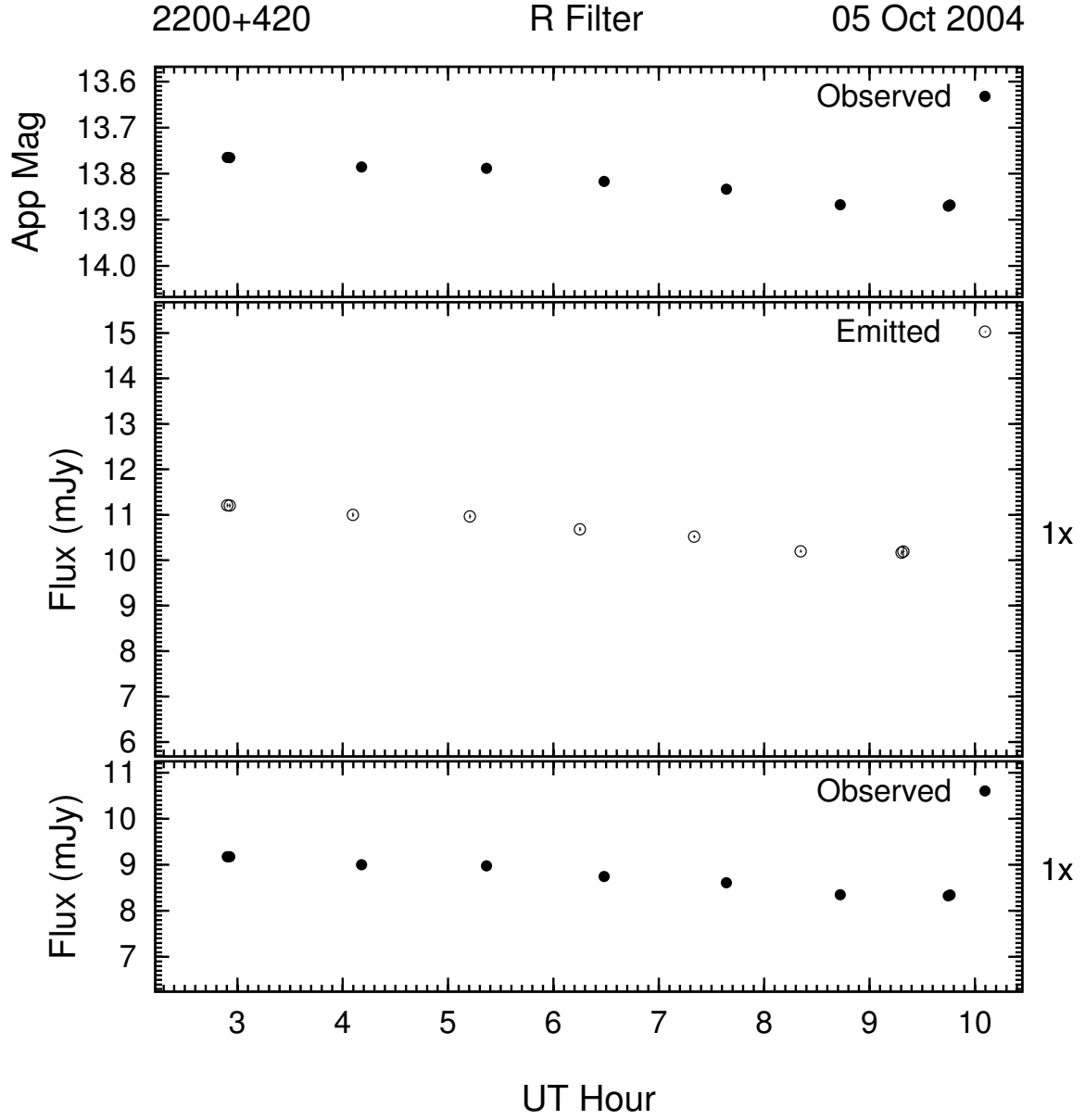


Figure 3.142: Example of the optical microvariability (R band) of $2200 + 420$ on the night of 05 Oct 2004. This night's data was 2-point averaged to improve S/N .

between that level and $R \simeq 13.9$.

BL Lac has the lowest redshift of the sample, 0.069, and therefore shows the least enhancement of the variability amplitude and the smallest change in time-scale: 1.22 and 6.5%

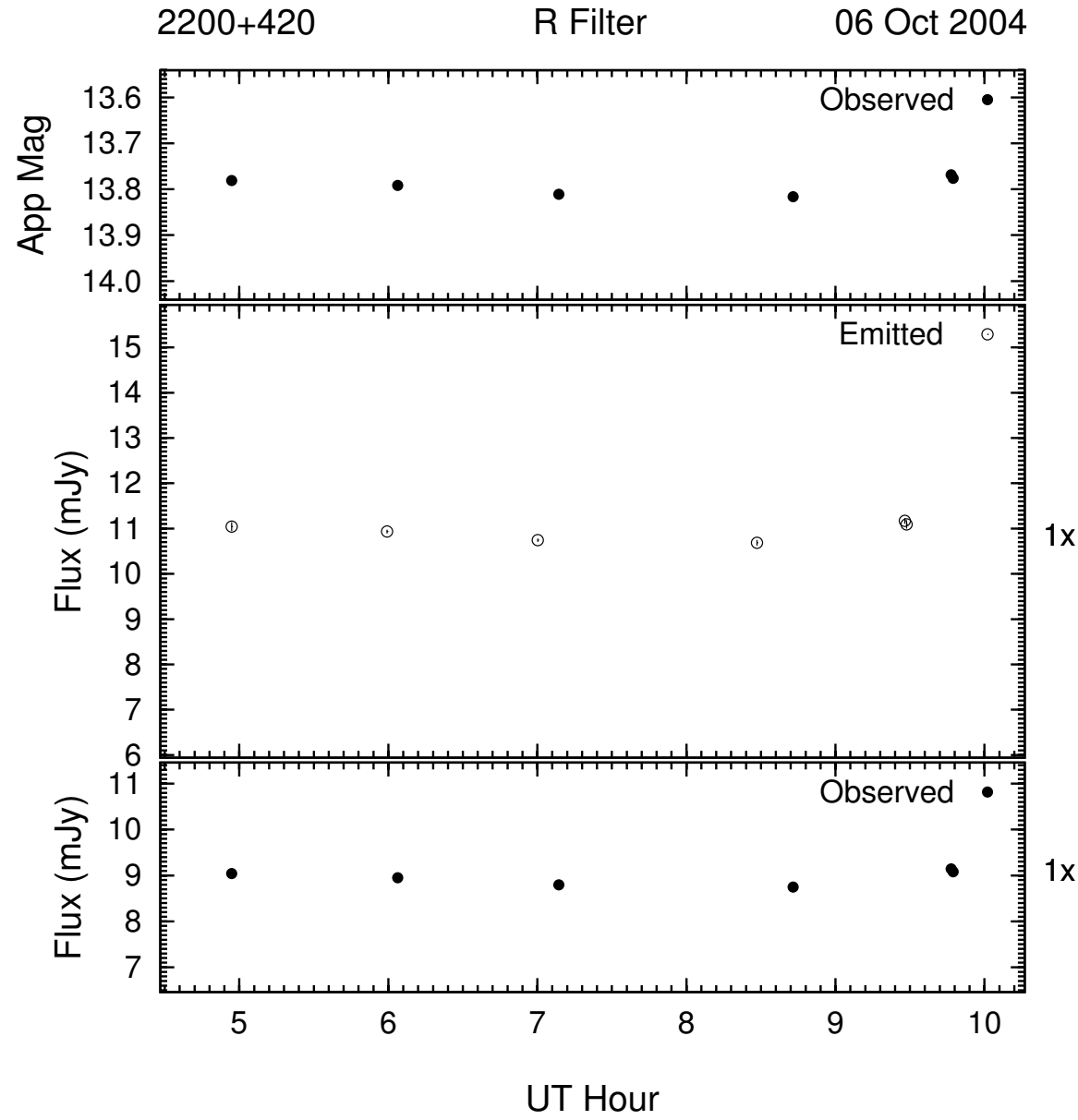


Figure 3.143: Example of the optical microvariability (R band) of 2200 + 420 on the night of 06 Oct 2004. This night's data was 2-point averaged to improve S/N .

respectively.

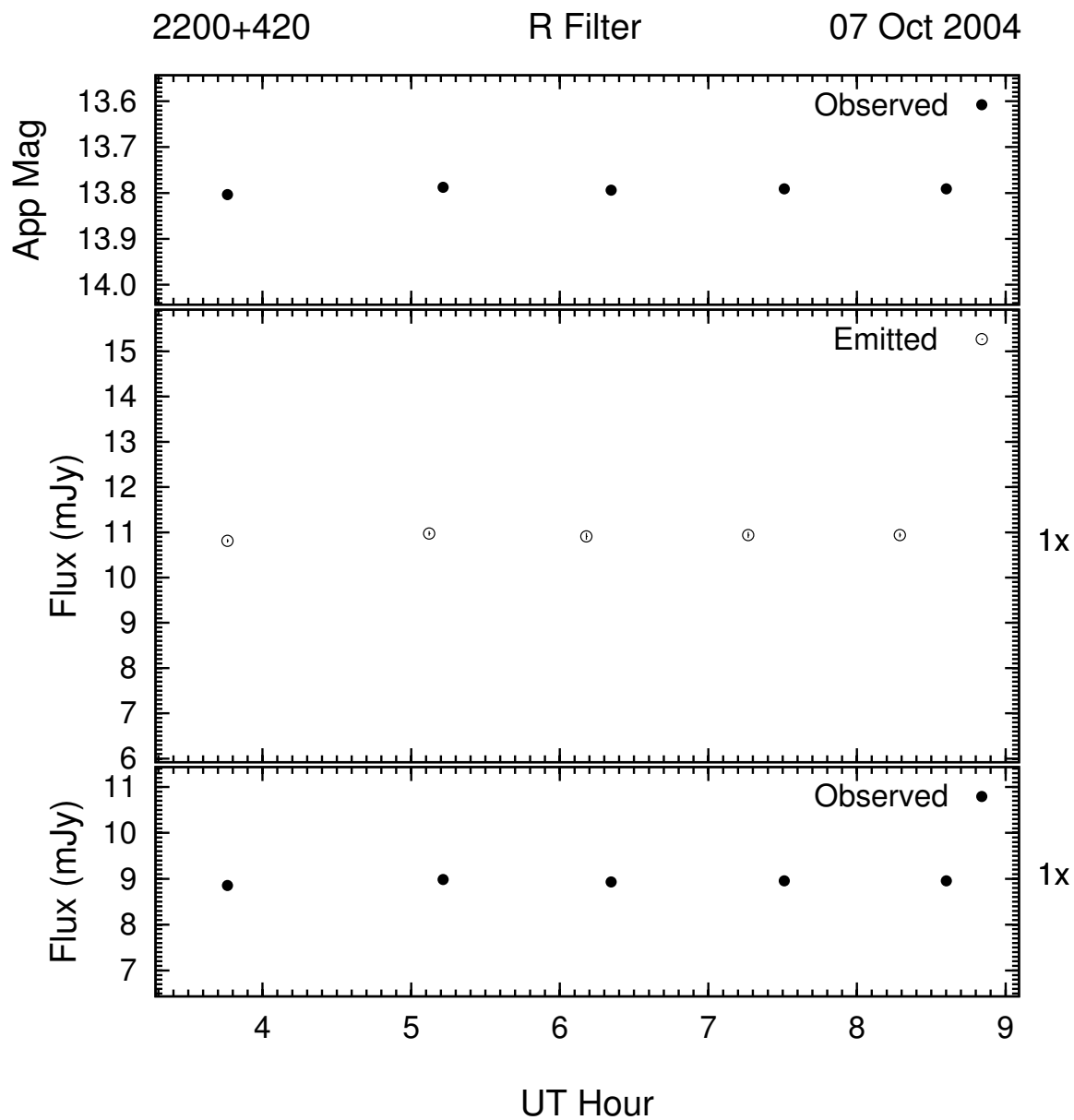


Figure 3.144: Example of the optical microvariability (R band) of 2200 + 420 on the night of 07 Oct 2004. This night's data was 2-point averaged to improve S/N .

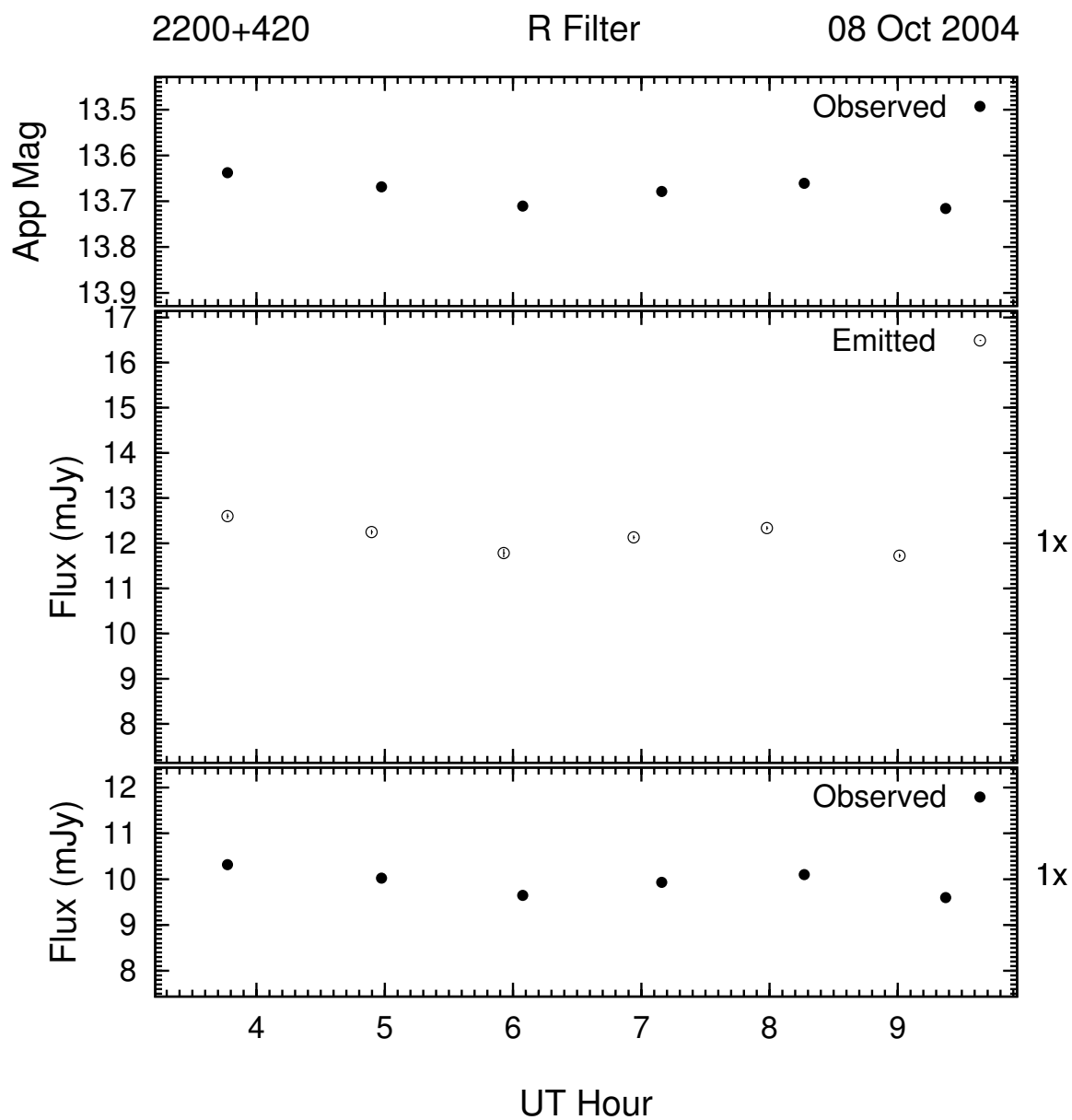


Figure 3.145: Example of the optical microvariability (R band) of 2200 + 420 on the night of 08 Oct 2004. This night's data was 2-point averaged to improve S/N .

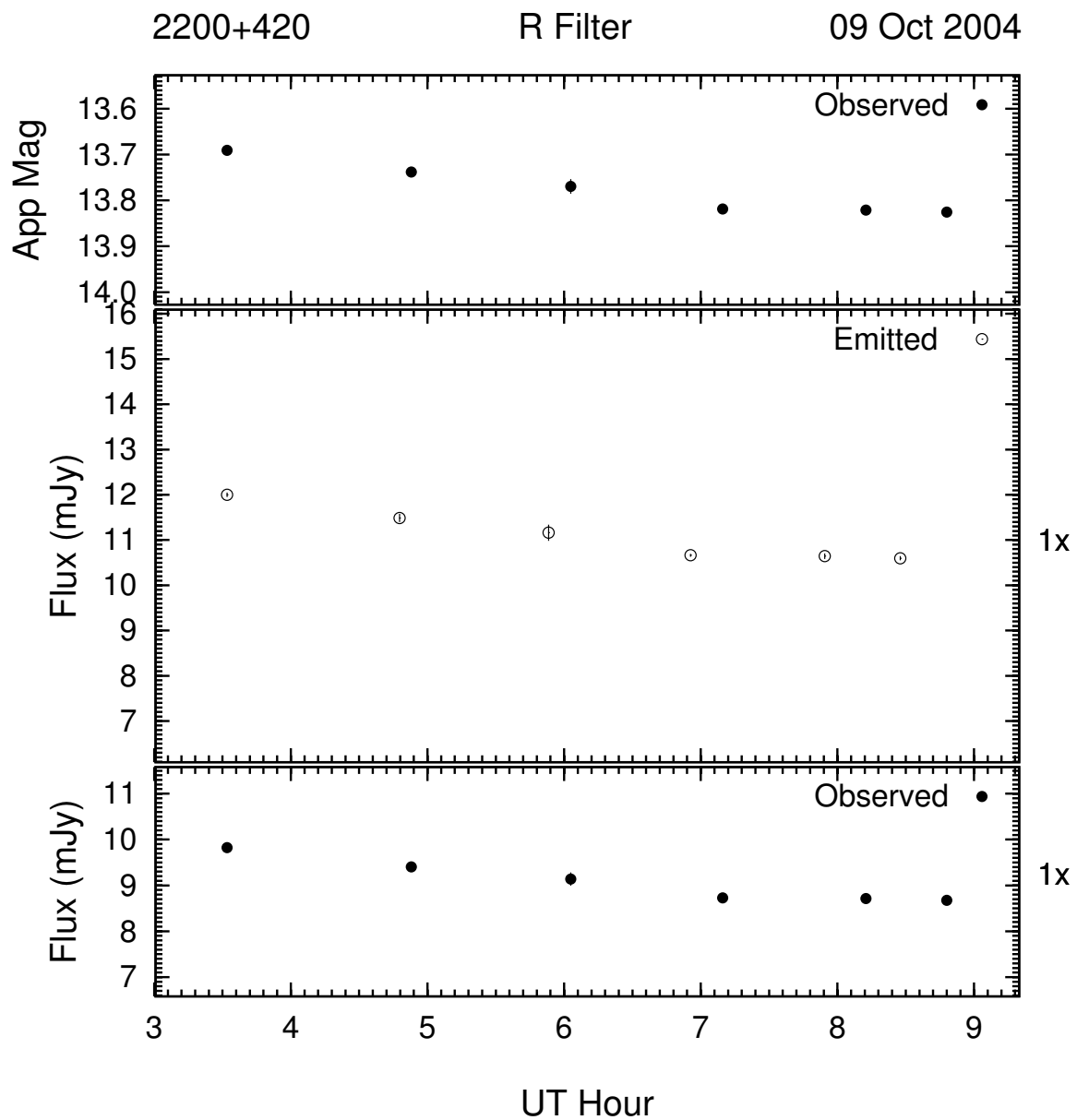


Figure 3.146: Example of the optical microvariability (R band) of 2200 + 420 on the night of 09 Oct 2004. This night's data was 2-point averaged to improve S/N .

3.2.7 2223 – 052

The OVV quasar 3C 446 (also known as PKS 2223 – 052 or simply 2223 – 052) has a redshift of 1.404 and has exhibited a variability amplitude range of approximately 3 mag over the time that it has been monitored for this investigation (see Figure 3.147). The archival data used for 3C 446 was taken from the PEGA archives and is in the R band only. The observations cover a time period of just over 16 years. SMARTS observations exist for this object and are exhibited in §4.1.10. The long term light curve of 3C 446 shows a quasi-periodic character with peaks in 1988, 1995 and 2000.

The short term microvariability observations of 3C 446 shows very large errors of $\gtrsim 0.04$ mag. It is felt that this error is an overestimate of the true error that resulted from the high error of the calibrated comparison stars (average of 0.11 mag) used in the conversion of instrumental magnitudes into real magnitudes.

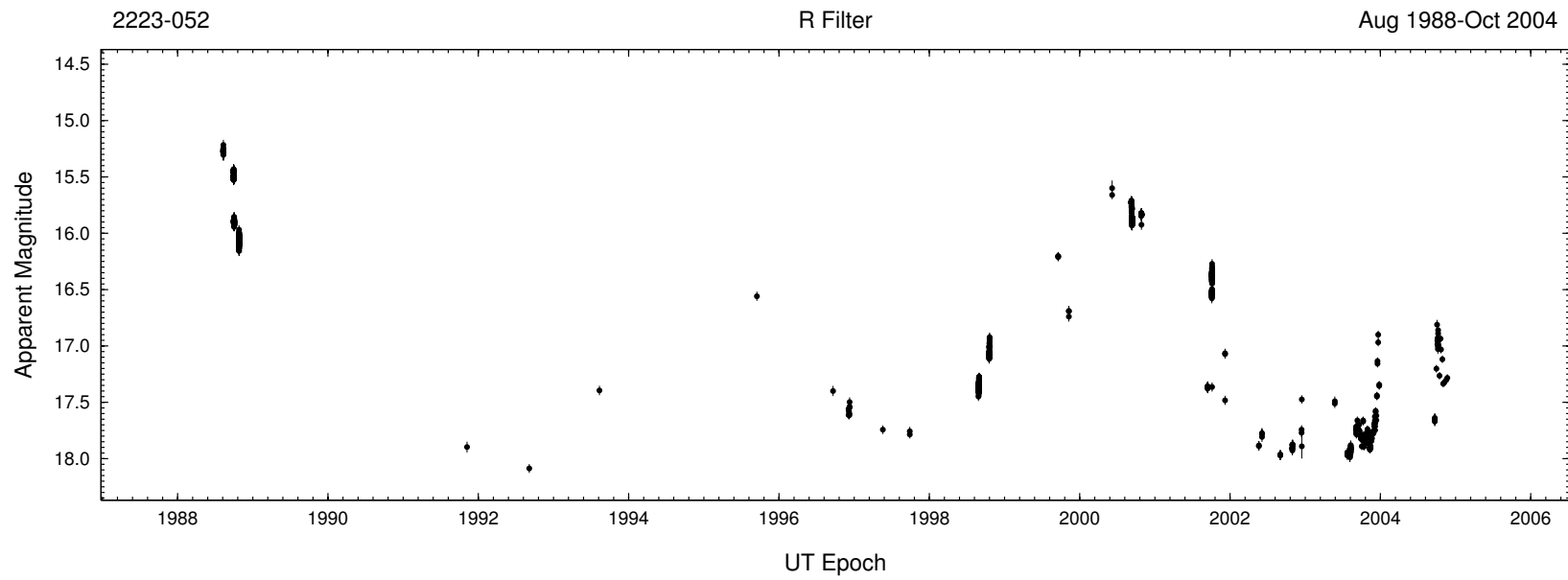


Figure 3.147: Complete R band light curve of 2223 – 052 from 1988 to 2004. The amplitude of variability is ~ 3 mag.

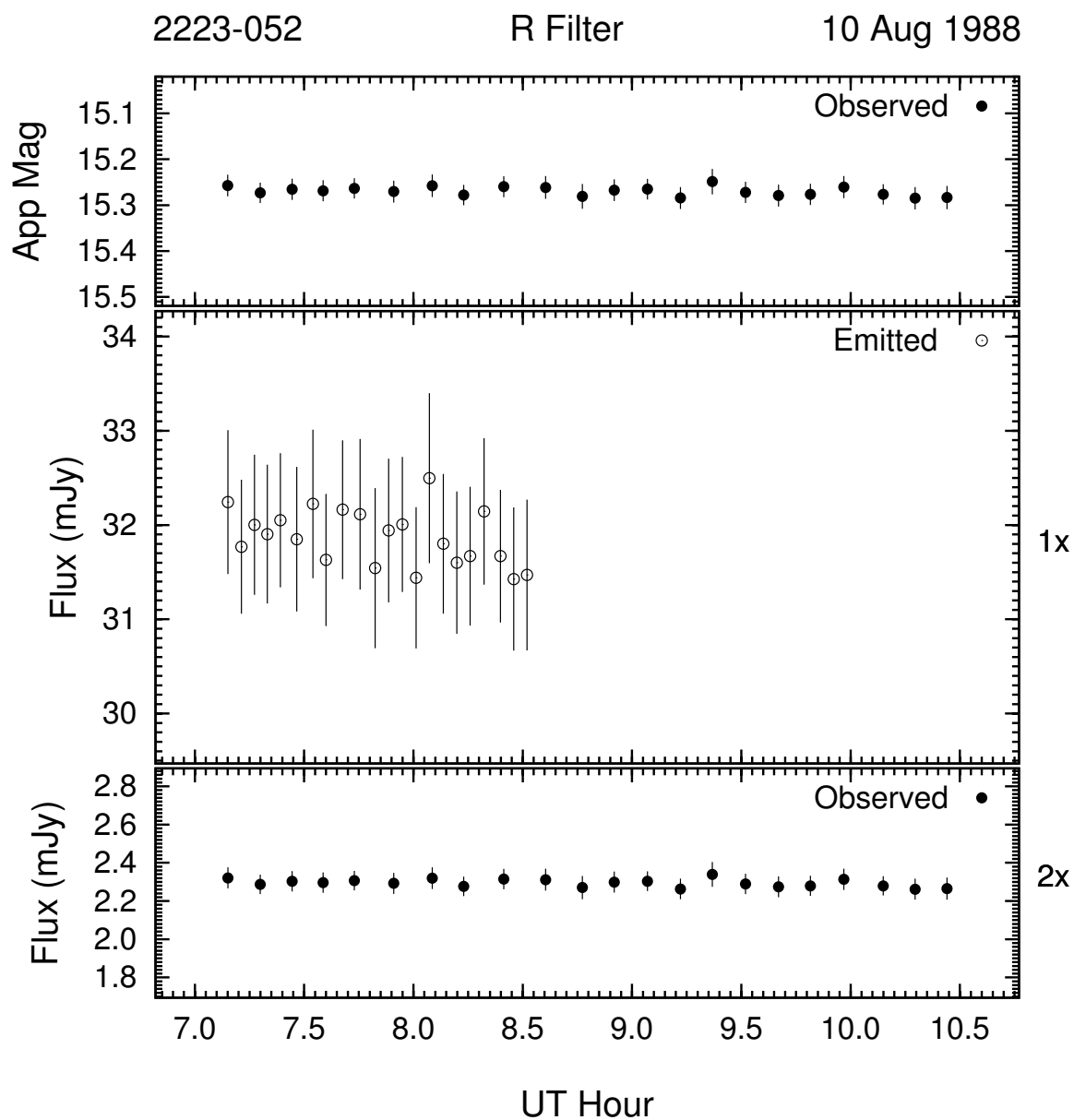


Figure 3.148: Example of the optical microvariability (R band) of 2223 – 052 on the night of 10 Aug 1988. This night's data was 2-point averaged to improve S/N .

The microvariability observations for 3C 446 are shown in Figures 3.148 through 3.173. Statistically significant microvariability for 3C 446 exists for only one night (05 Oct 2001, Figure 3.167) due to the minimum significance level of 2.6σ . This does not mean that the

object shows no other brightness variations, but that it does not exhibit microvariability as defined here. The process of n -point averaging has been employed to attempt to reduce the errors, but only to a level that does not dilute the character of the original observations. It is possible to use this method to reduce the errors to a level where microvariability would be detected, but at a cost of sacrificing the usability (e.g., in structure function analysis) and original character of the observations. One must wonder if it is truly microvariability under these circumstances.

The first attempt at detecting microvariability for 3C 446 was the night of 10 Aug 1988 shown in Figure 3.148. No significant variability was detected in this night, but the object does show a slight dimming trend. The brightness level for this night is $R \simeq 15.3$

The next run of microvariability observations for 3C 446 takes place on 3 consecutive nights from 29 Sep to 01 Oct 1988 (Figures 3.149 through 3.151). No significant microvariability is detected, but there exists a definite downward trend in brightness. The brightness level for this night is $R \sim 15.5$. The levels for the next 2 nights (30 Sep and 01 Oct, Figures 3.150 and 3.151) are at $R \simeq 15.9$, 0.4 mag dimmer. There are no significant brightness variations over the course of either night, but the night of 01 Oct shows a slight decrease, then increase in brightness.

The observations of 3C 446 on the night of 25 Oct 1988 are shown in Figure 3.152. Although there is no significant brightness variations, there appears to be a possible dimming trend. 3C 446 is ~ 0.2 mag dimmer than the previous run.

The next run of microvariability observation are on the four consecutive nights of 27 to 30 Aug 1998 (Figures 3.153 through 3.156). These observations start at a brightness level

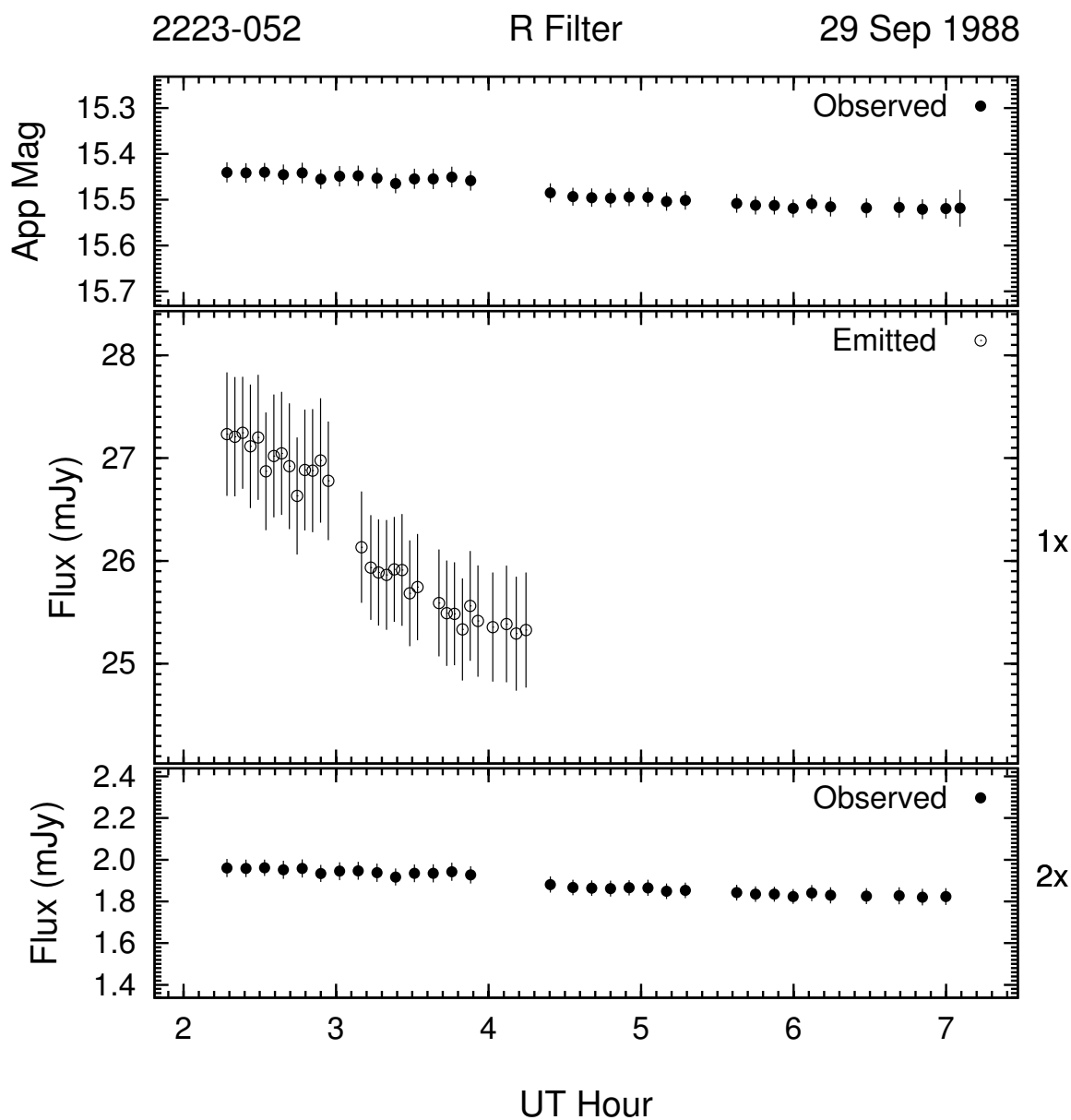


Figure 3.149: Example of the optical microvariability (R band) of 2223 – 052 on the night of 29 Sep 1988. This night's data was 2-point averaged to improve S/N .

of $R \simeq 17.35$, ~ 1.3 mag dimmer than 10 years ago. The brightness level of 3C 446 varied only ± 0.1 mag from this point, with no statistically significant microvariations in any of the nights. There is a hint of positive and negative trends in brightness, but they are not

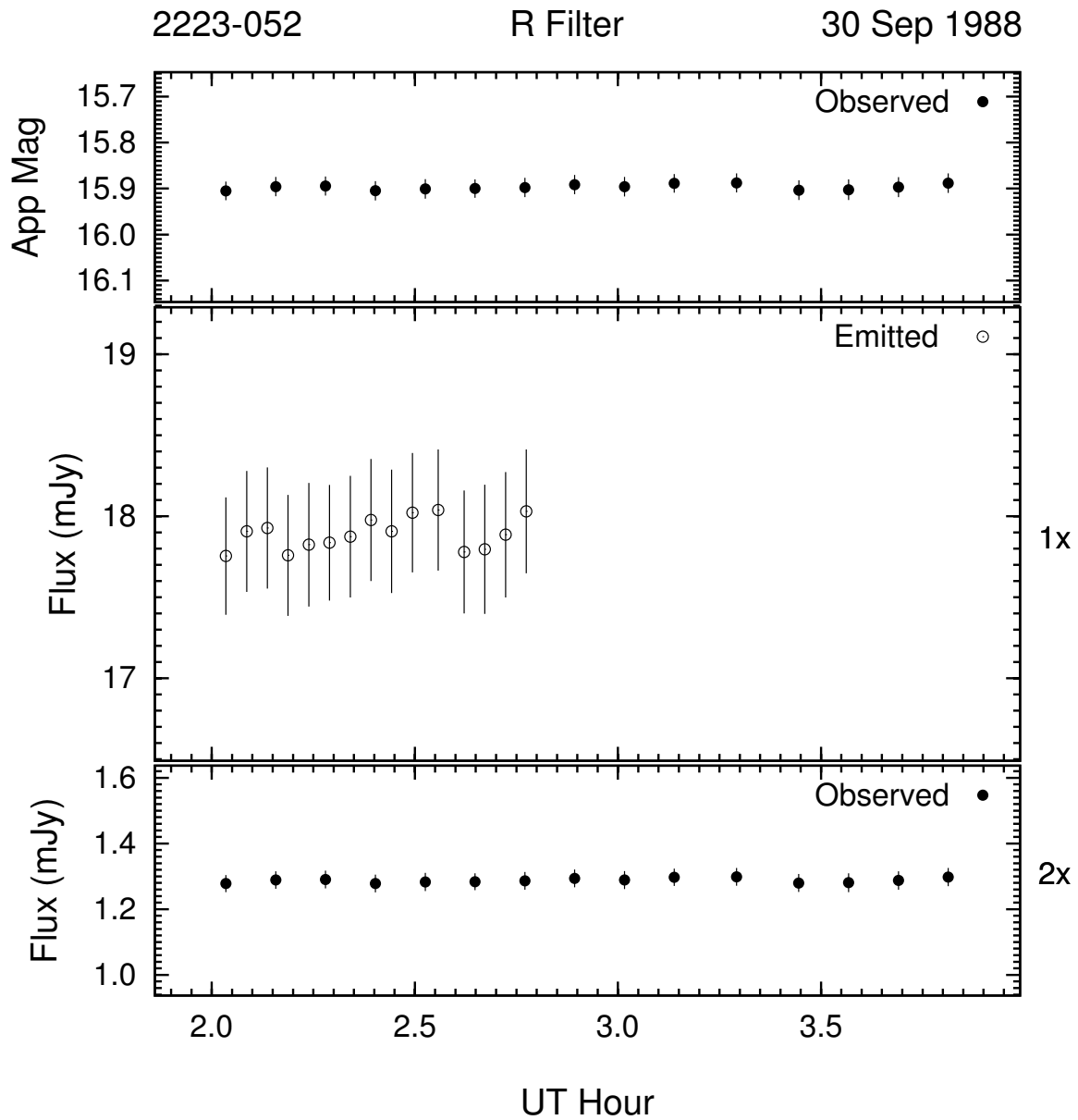


Figure 3.150: Example of the optical microvariability (R band) of 2223 – 052 on the night of 30 Sep 1988. This night's data was 2-point averaged to improve S/N .

conclusive.

Microvariability for 3C 446 was again searched for in 1998 on three consecutive nights (18-20) in October, and is displayed in the Figures 3.157 through 3.159. There are hints

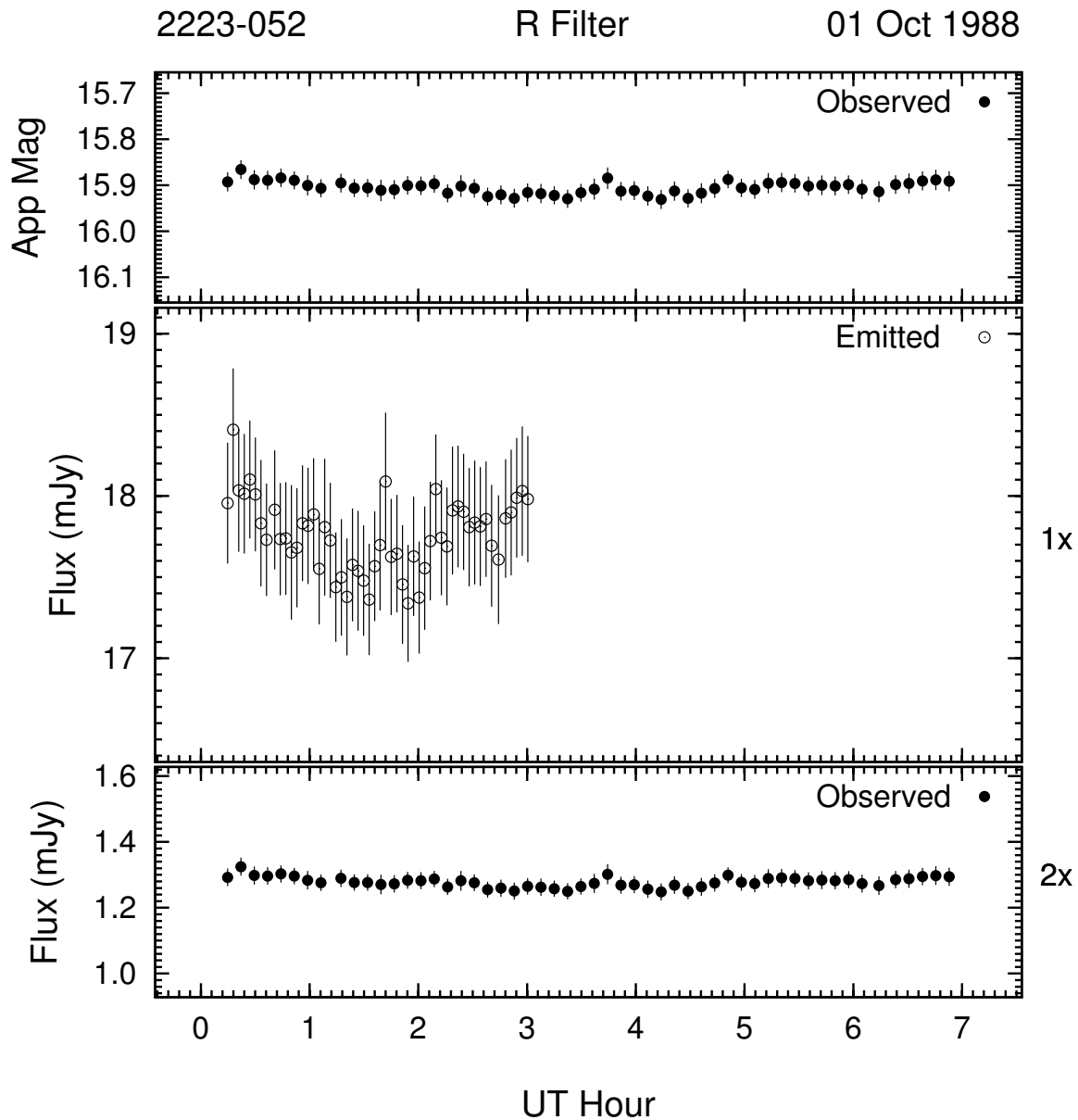


Figure 3.151: Example of the optical microvariability (R band) of 2223 – 052 on the night of 01 Oct 1988. This night's data was 2-point averaged to improve S/N .

of brightening trends in all three nights, but no significant variability is detected. The brightness level is $R \simeq 17.0$, ~ 0.35 mag brighter than in August of this year. 3C 446 is within 0.1 mag of the base level for this run over all 3 nights.

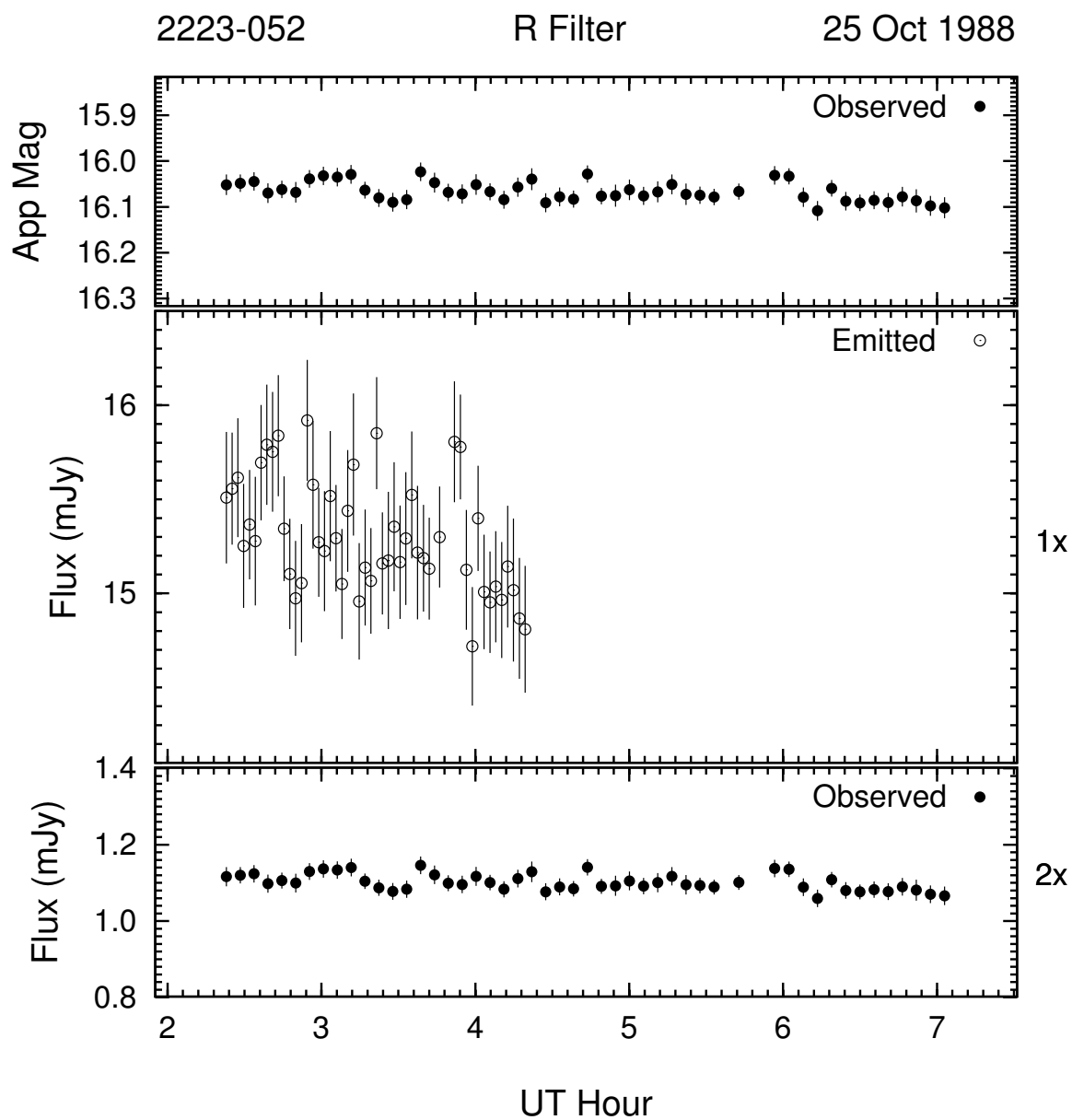


Figure 3.152: Example of the optical microvariability (R band) of 2223 – 052 on the night of 25 Oct 1988. This night's data was 3-point averaged to improve S/N .

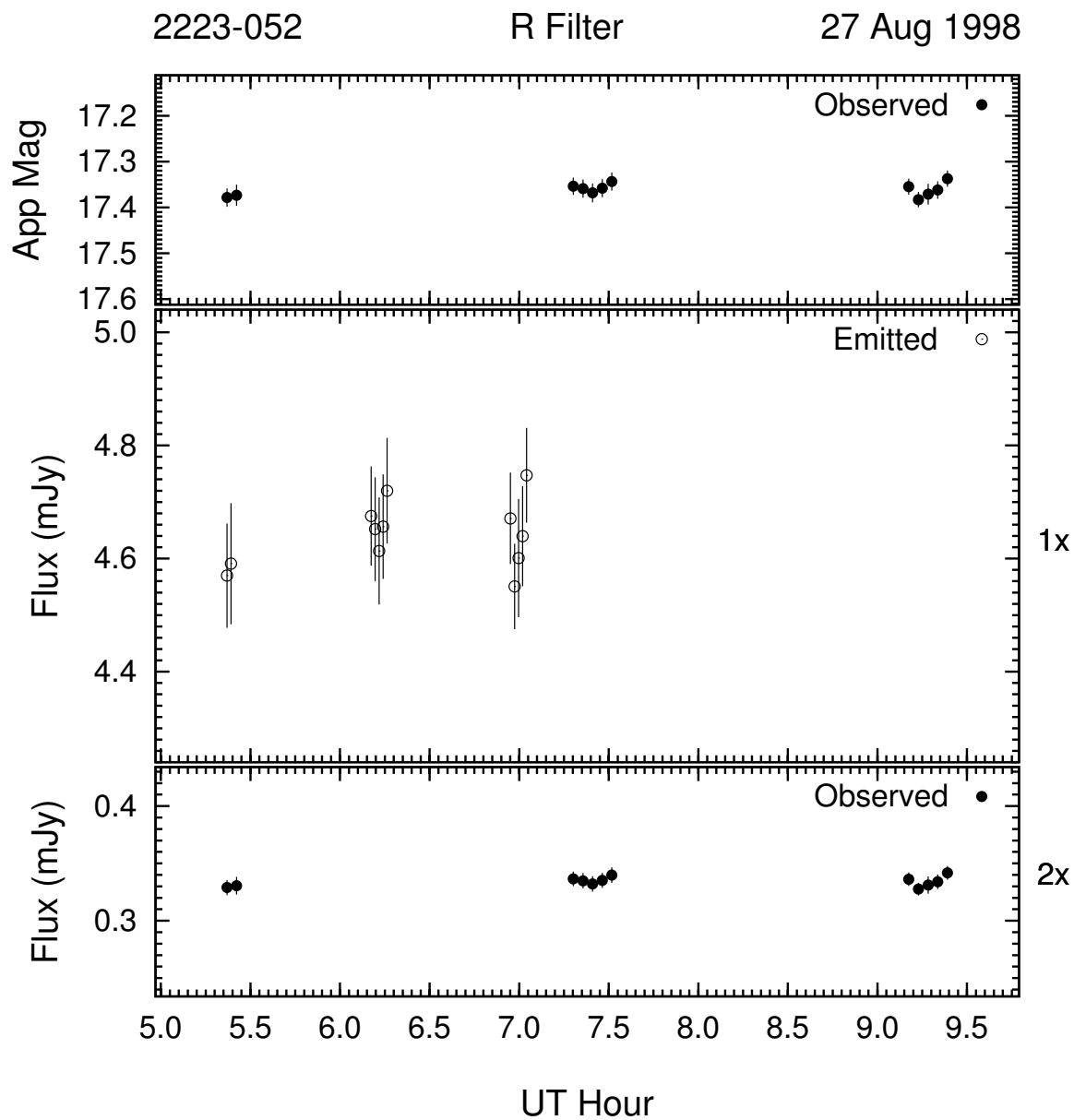


Figure 3.153: Example of the optical microvariability (R band) of 2223 – 052 on the night of 27 Aug 1998. This night's data was 2-point averaged to improve S/N .

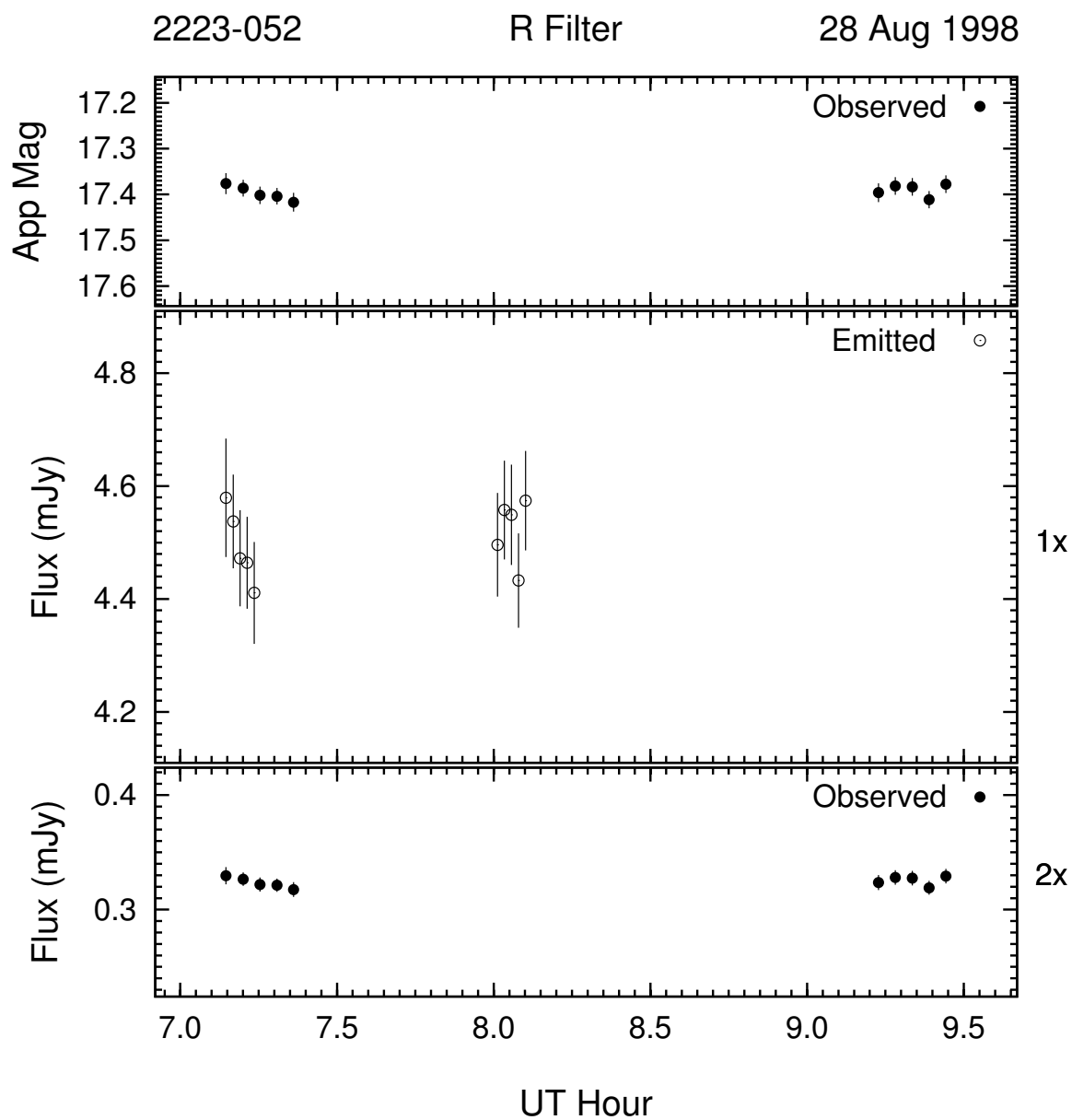


Figure 3.154: Example of the optical microvariability (R band) of 2223 – 052 on the night of 28 Aug 1998. This night's data was 2-point averaged to improve S/N .

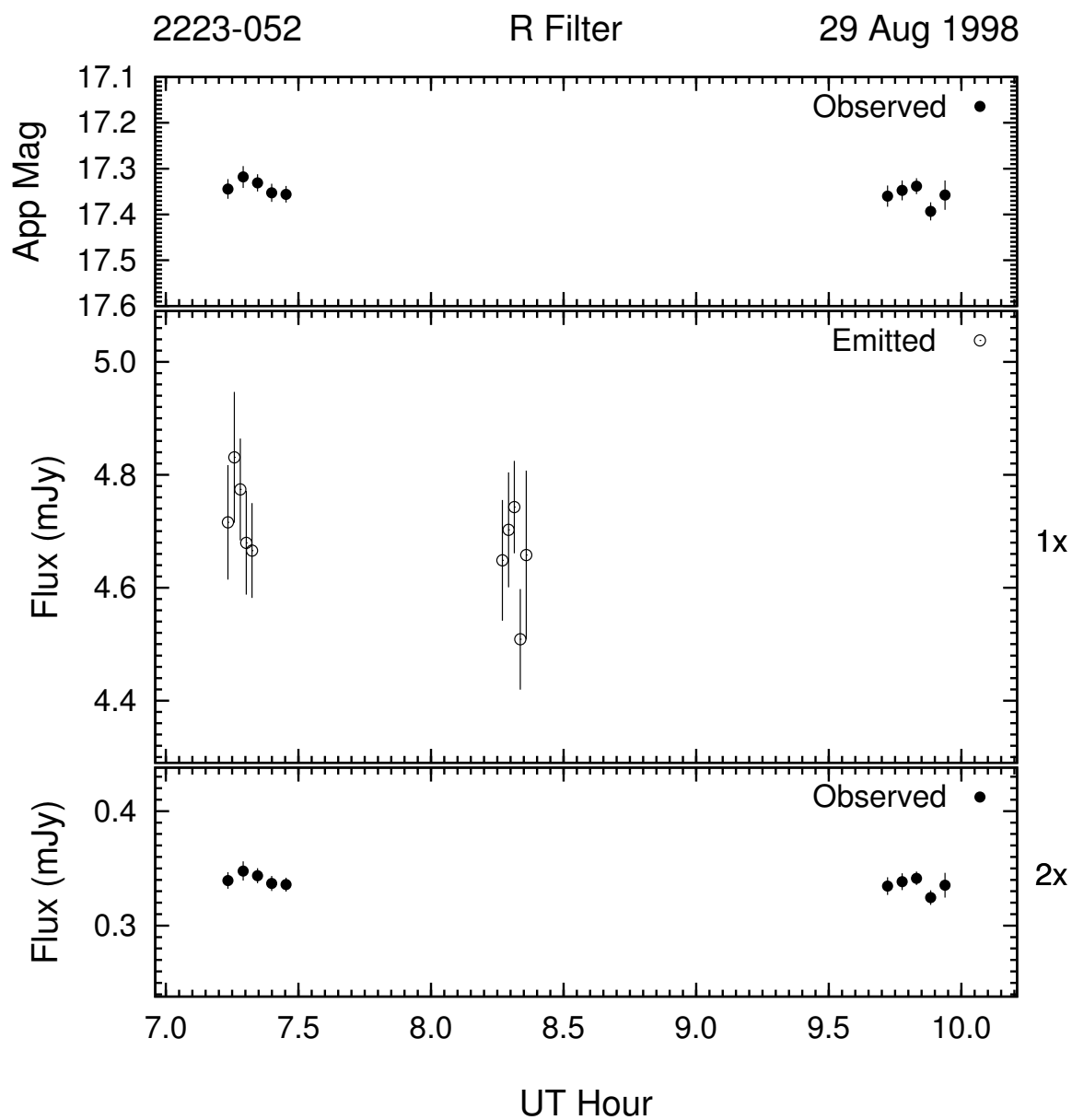


Figure 3.155: Example of the optical microvariability (R band) of 2223 – 052 on the night of 29 Aug 1998. This night's data was 2-point averaged to improve S/N .

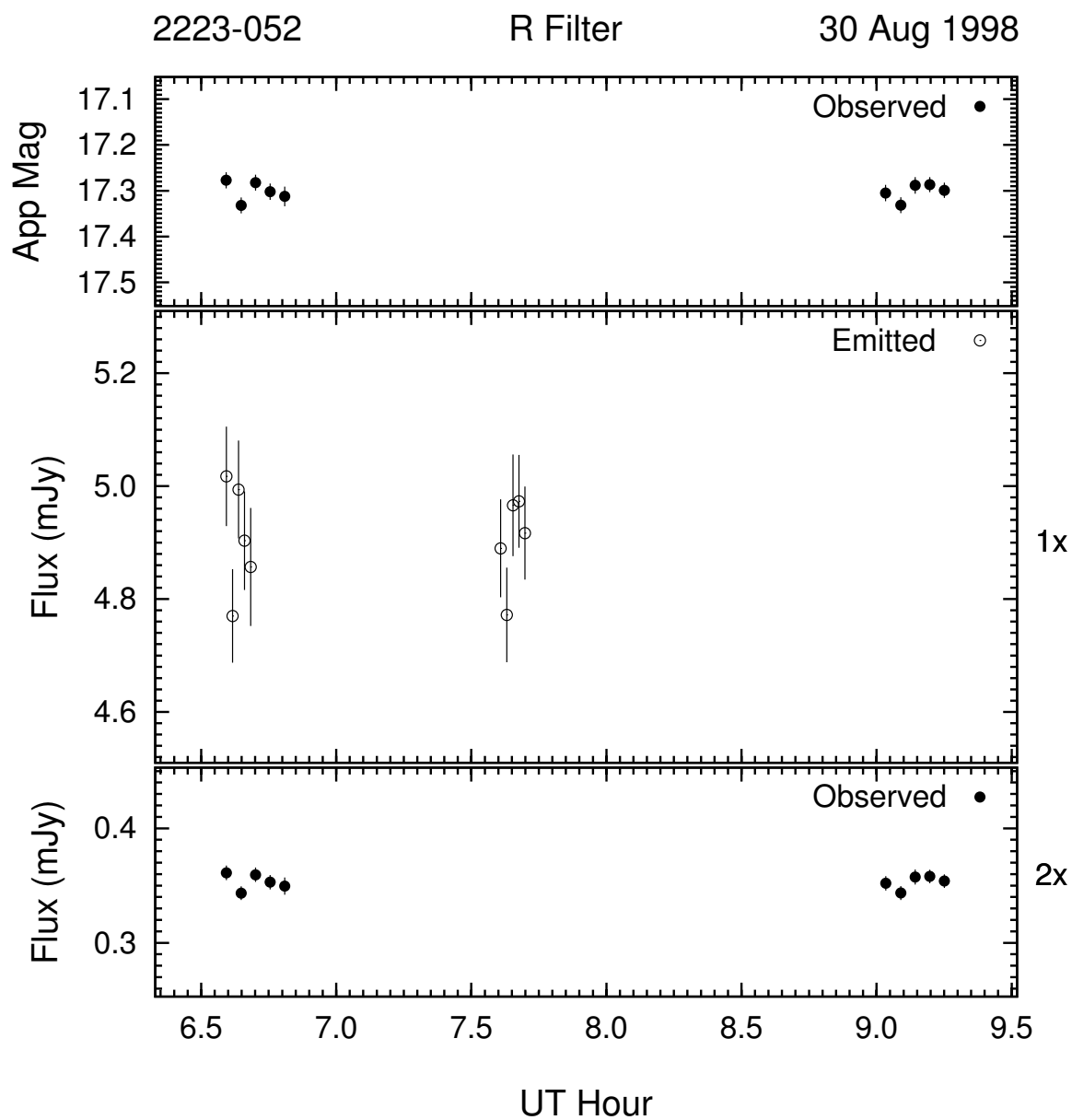


Figure 3.156: Example of the optical microvariability (R band) of 2223 – 052 on the night of 30 Aug 1998. This night's data was 2-point averaged to improve S/N .

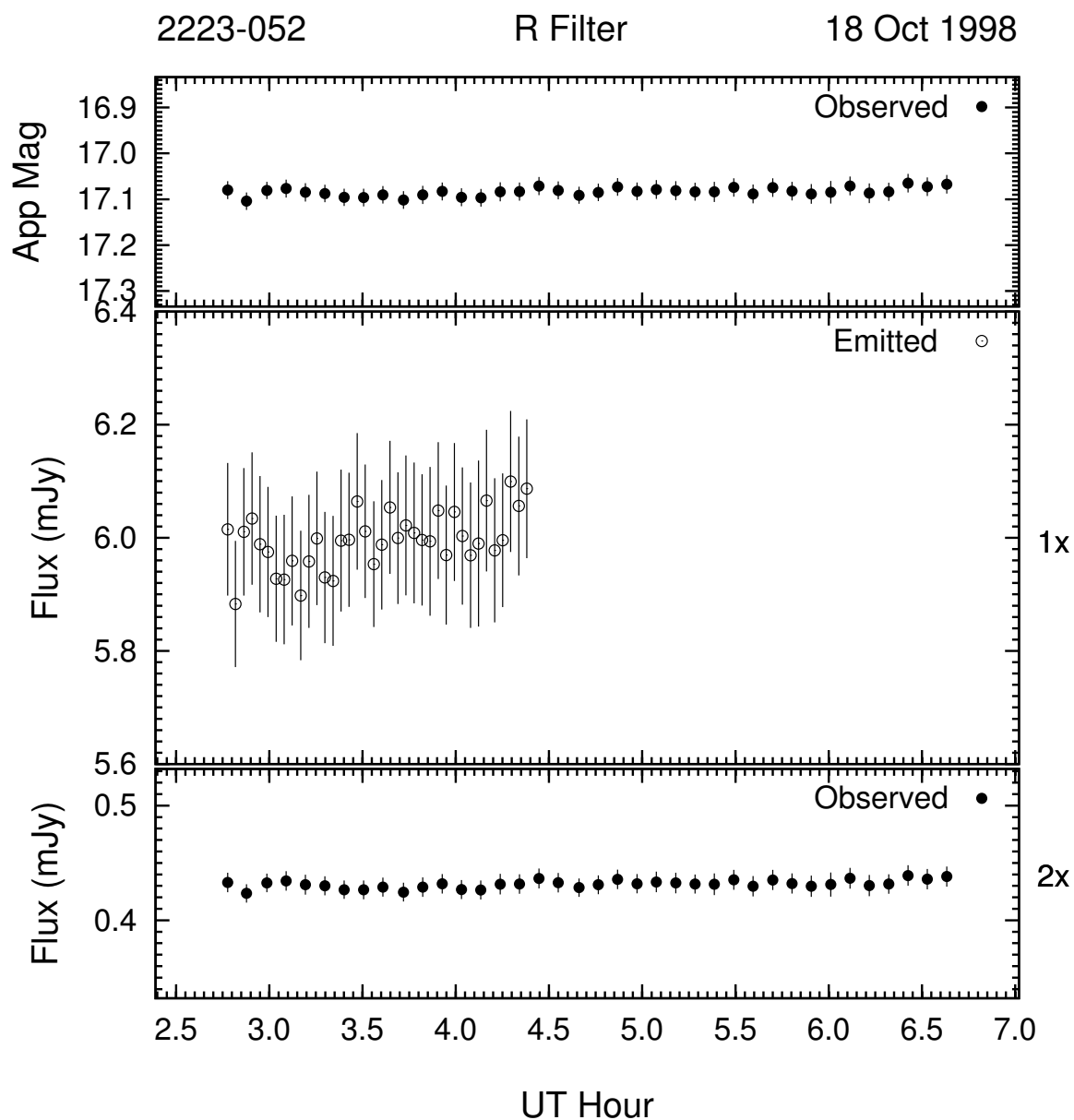


Figure 3.157: Example of the optical microvariability (R band) of 2223 – 052 on the night of 18 Oct 1998. This night's data was 2-point averaged to improve S/N .

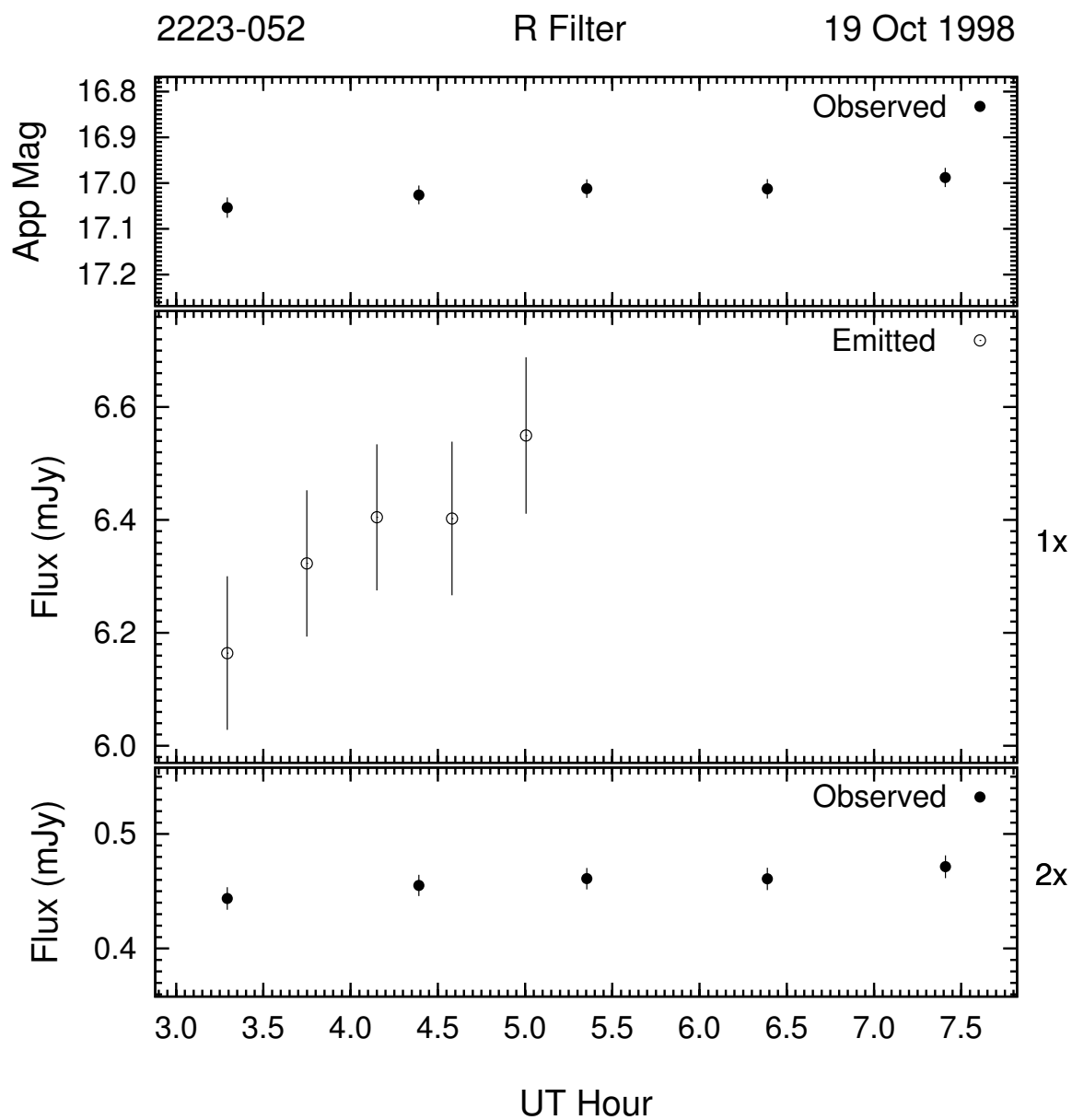


Figure 3.158: Example of the optical microvariability (R band) of 2223 – 052 on the night of 19 Oct 1998. This night's data was 2-point averaged to improve S/N .

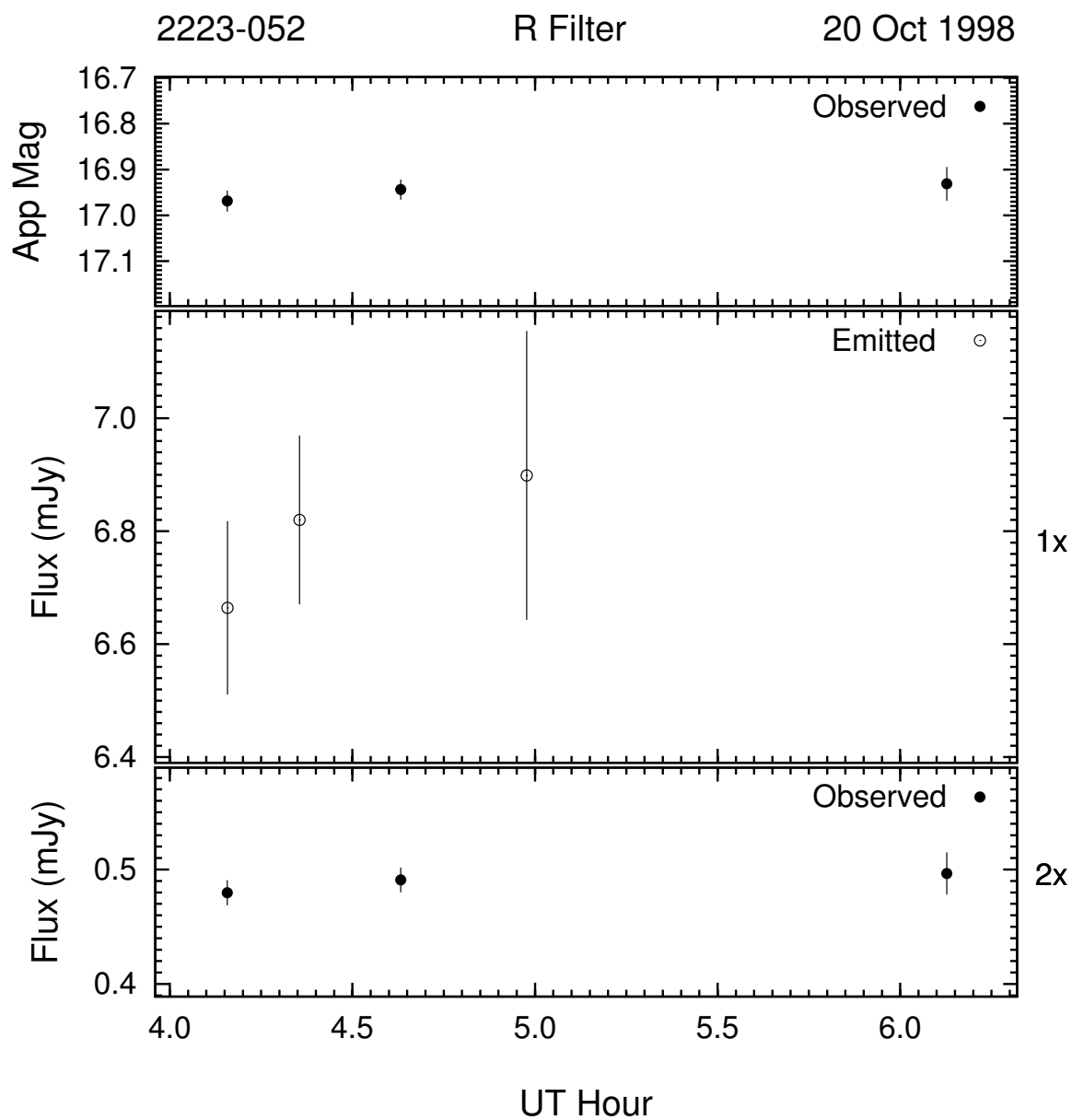


Figure 3.159: Example of the optical microvariability (R band) of 2223 – 052 on the night of 20 Oct 1998. This night's data was 2-point averaged to improve S/N .

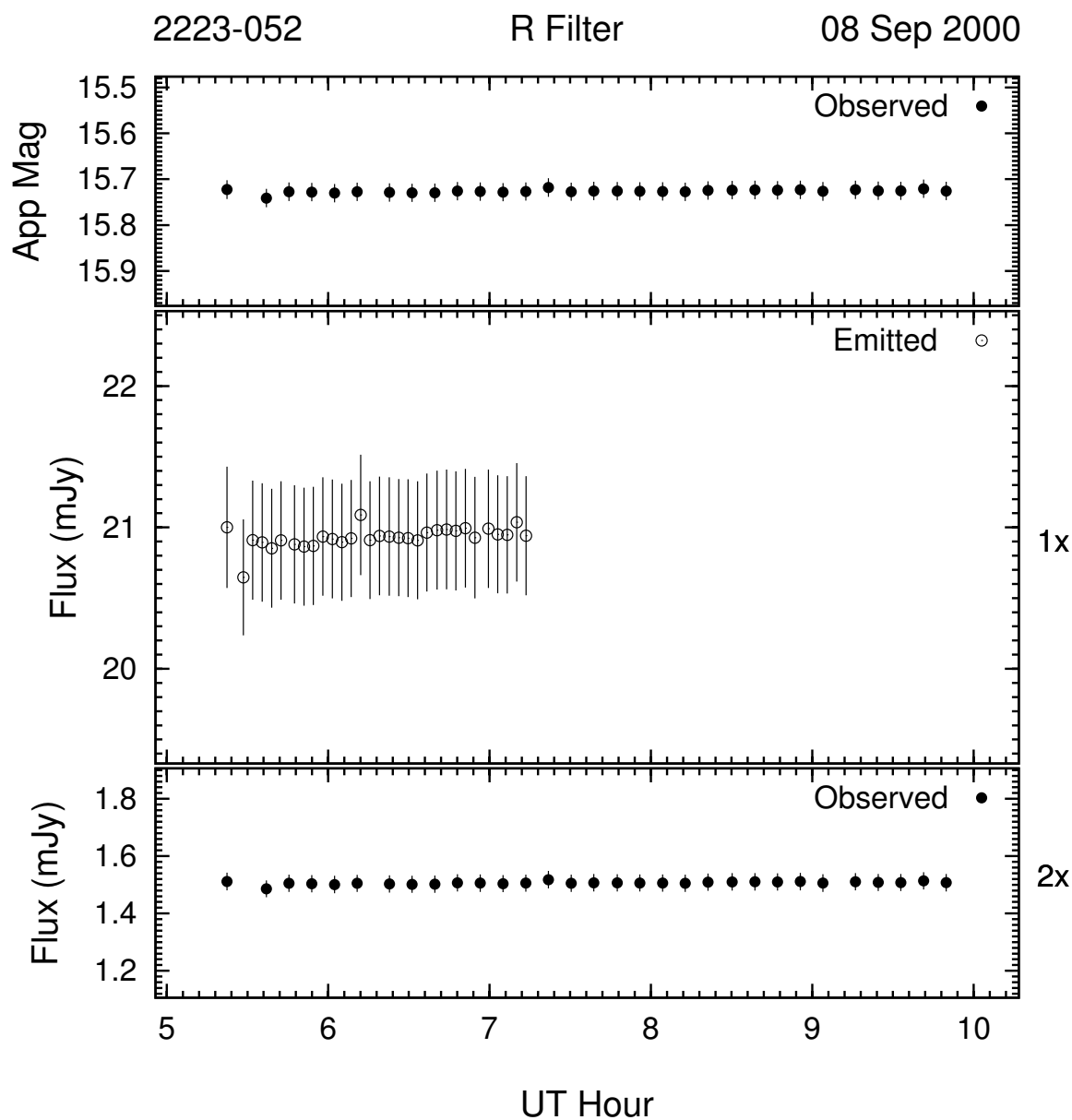


Figure 3.160: Example of the optical microvariability (R band) of 2223 – 052 on the night of 08 Sep 2000. This night's data was 2-point averaged to improve S/N .

The four consecutive nights of observations for 3C 446 on 08 through 11 Sep 2000 are displayed in Figures 3.160 through 3.163. Although there is no detected variability on any night, there are hints of dimming trends in the latter three nights. Indeed, 3C 446 dimmed

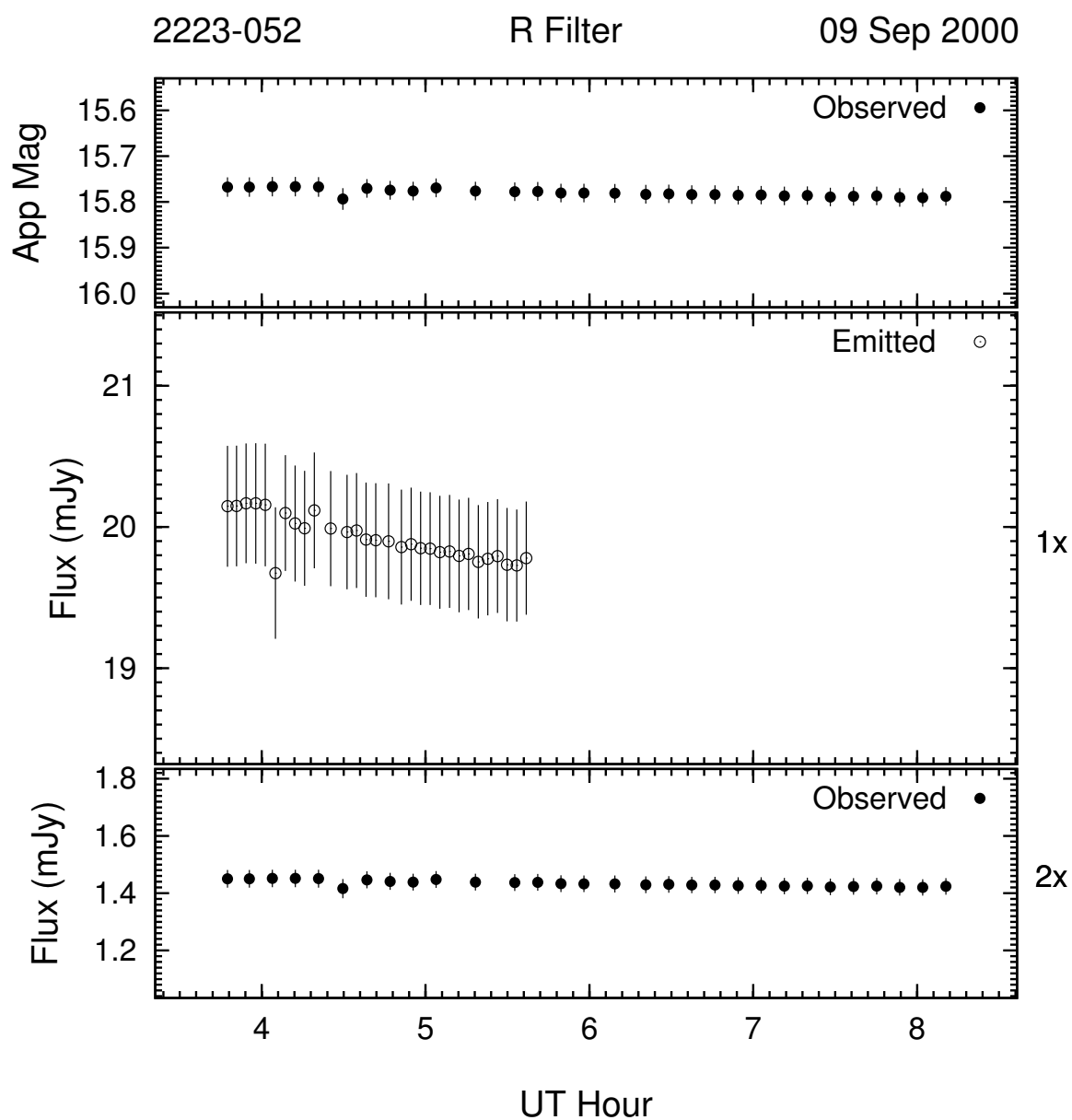


Figure 3.161: Example of the optical microvariability (R band) of 2223 – 052 on the night of 09 Sep 2000. This night's data was 2-point averaged to improve S/N .

from $R \simeq 15.7$ to $R \simeq 15.9$ over these four nights.

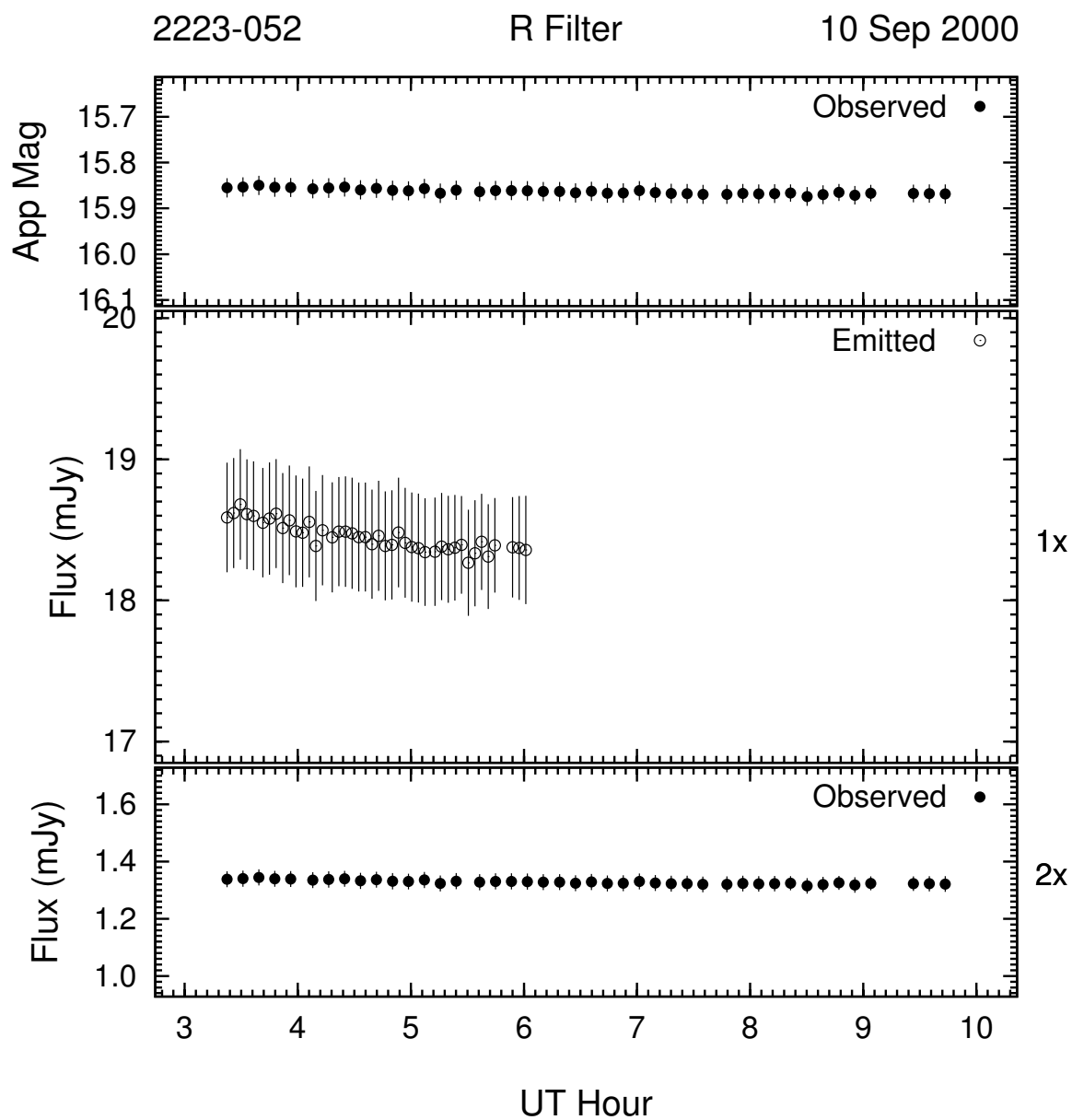


Figure 3.162: Example of the optical microvariability (R band) of 2223 – 052 on the night of 10 Sep 2000. This night's data was 2-point averaged to improve S/N .

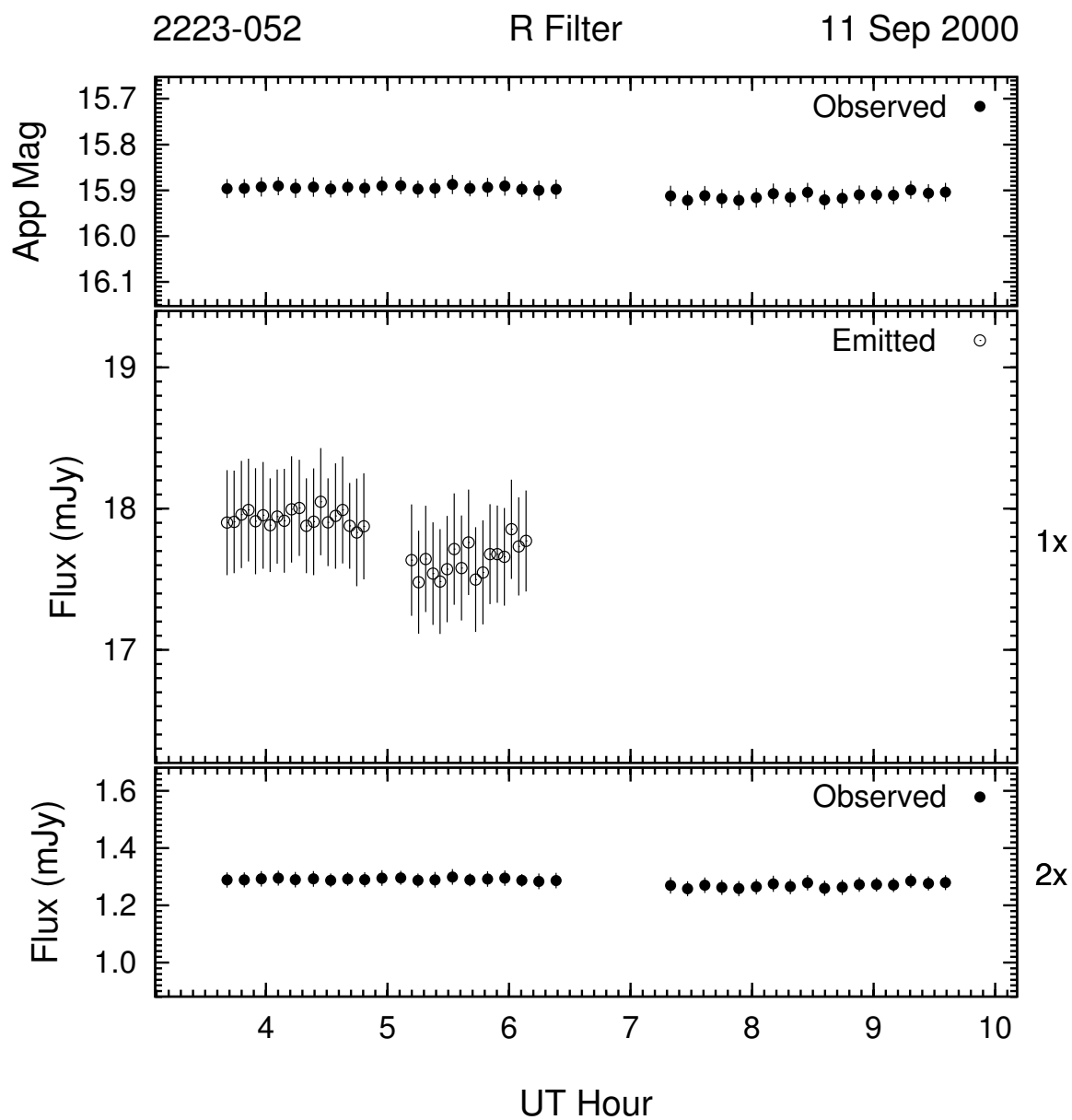


Figure 3.163: Example of the optical microvariability (R band) of 2223 – 052 on the night of 11 Sep 2000. This night's data was 2-point averaged to improve S/N .

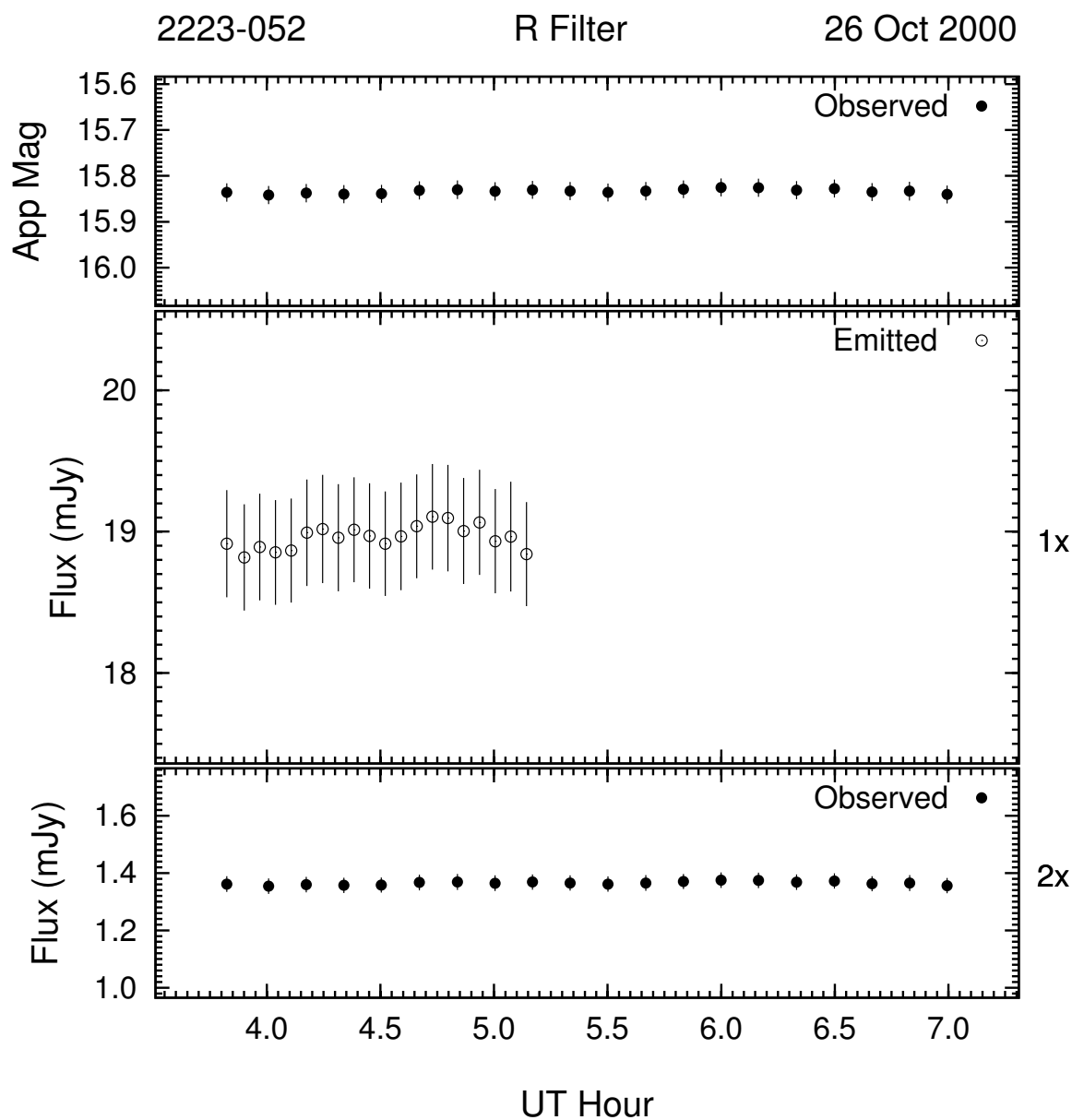


Figure 3.164: Example of the optical microvariability (R band) of 2223 – 052 on the night of 26 Oct 2000. This night's data was 2-point averaged to improve S/N .

The next 3C 446 microvariability observations took place on the nights of 26 and 27 Oct 2000 (Figures 3.164 and 3.165). No significant microvariability was detected. The brightness level was at roughly the same level as the previous run in September.

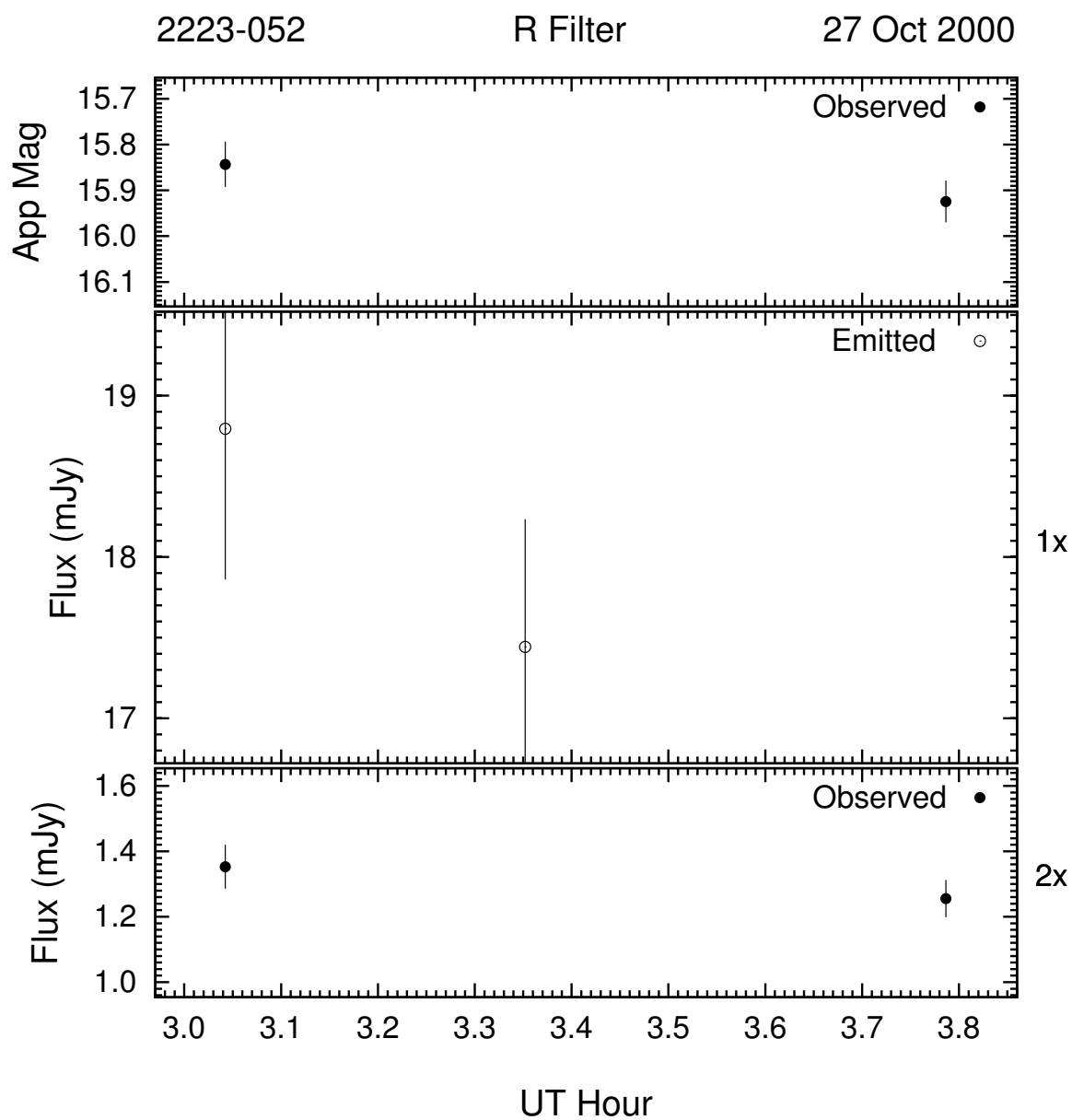


Figure 3.165: Example of the optical microvariability (R band) of 2223 – 052 on the night of 27 Oct 2000.

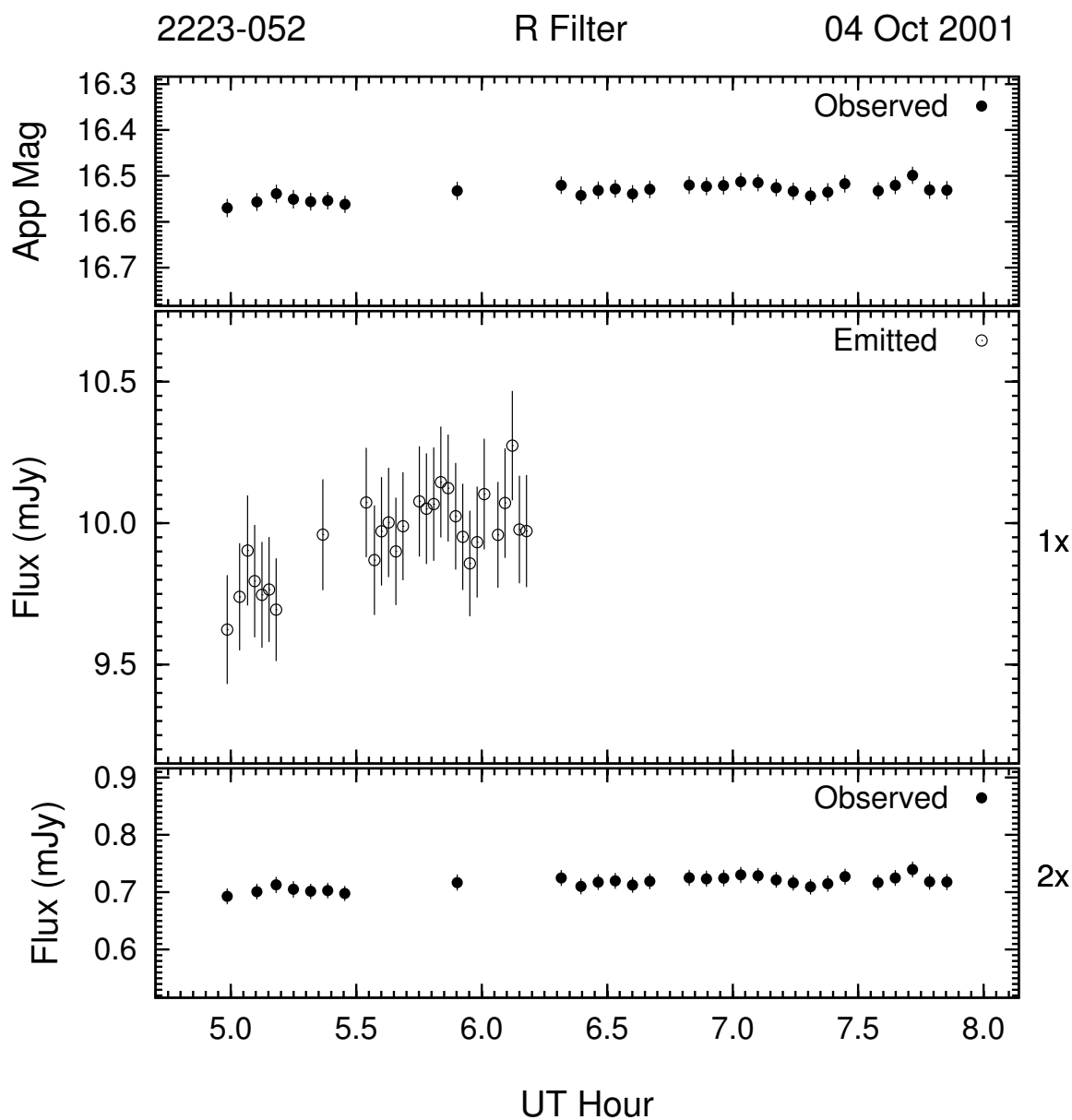


Figure 3.166: Example of the optical microvariability (R band) of 2223 – 052 on the night of 04 Oct 2001. This night's data was 2-point averaged to improve S/N .

The only successful detection of statistically significant microvariability for 3C 446 was during the run in October of 2001. Figures Figure 3.166 and Figure 3.167 show light curves for 4C 446 on 04 and 05 Oct respectively. On the first night, 3C 446 appears to brighten

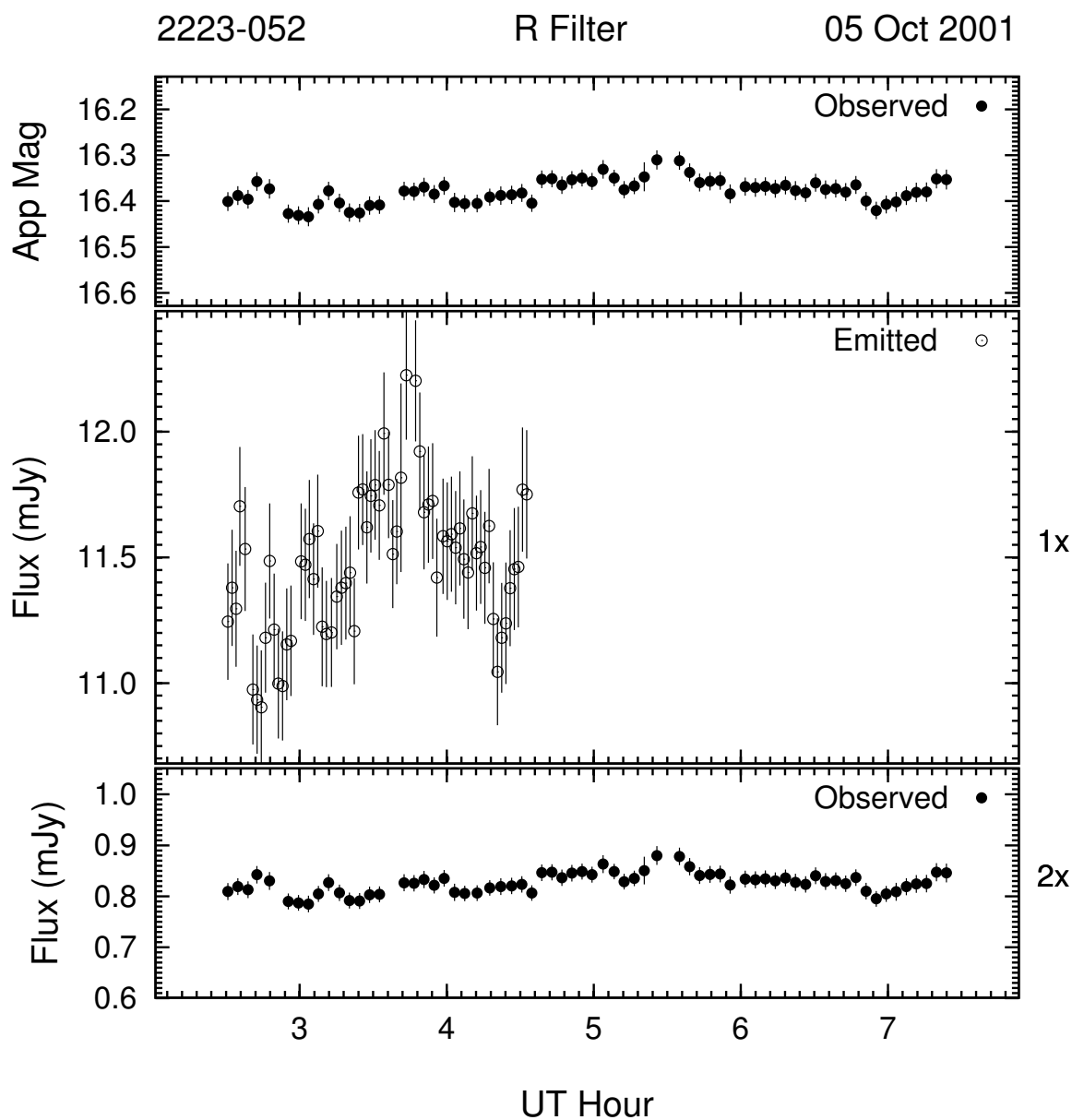


Figure 3.167: Example of the optical microvariability (R band) of 2223 – 052 on the night of 05 Oct 2005. This night's data was 2-point averaged to improve S/N .

~ 0.05 mag, but this variation is not above the 2.6σ confidence level. However, the brightness variations of 3C 446 on the night of 05 Oct (Figure 3.167) *are* statistically significant, and are complex in character superimposed on a rising trend. There exists one peak in the variations

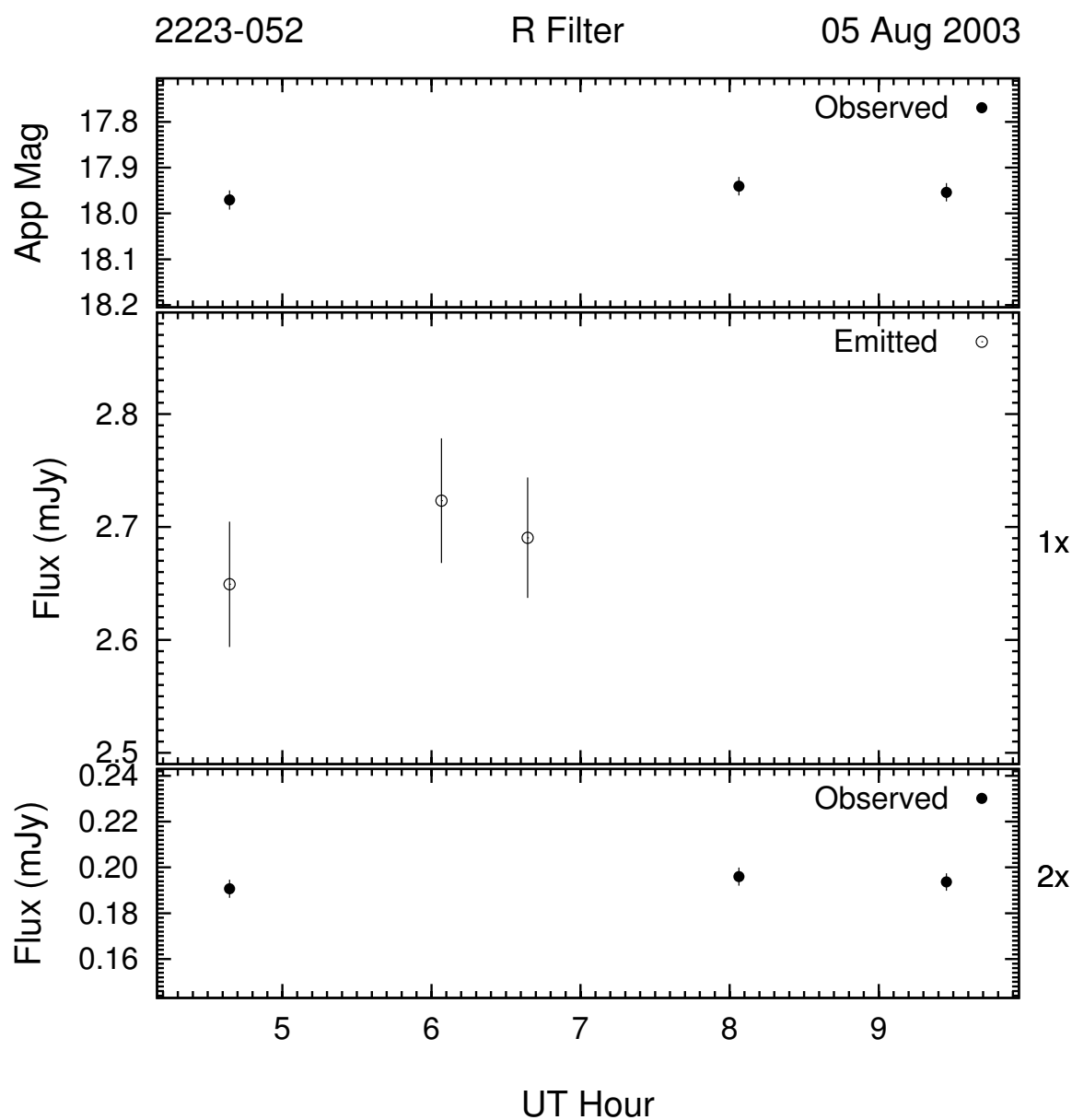


Figure 3.168: Example of the optical microvariability (R band) of 2223 – 052 on the night of 05 Aug 2003. This night's data was 2-point averaged to improve S/N .

at 8^h UT. During this run, 3C 446 is ~ 0.6 mag dimmer than the year before when it was observed at a brightness level of $R \simeq 16.5$.

The observations in early Aug of 2003 show 3C 446 at the lowest brightness level seen in

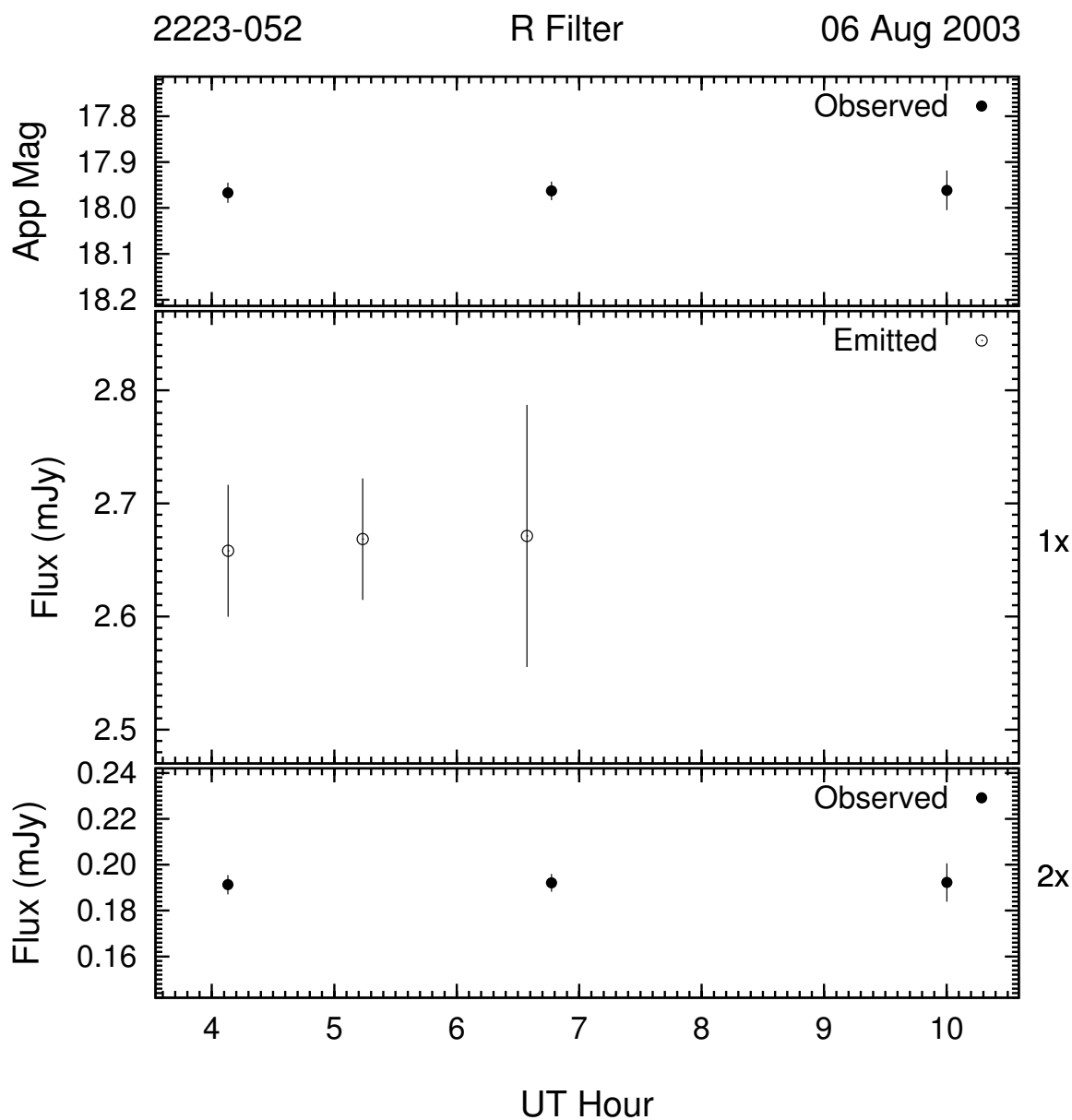


Figure 3.169: Example of the optical microvariability (R band) of 2223 – 052 on the night of 06 Aug 2003. This night's data was 2-point averaged to improve S/N .

the microvariability observations at an average of $R = 17.95$. The light curves for these nights are in Figures 3.168 through 3.172. 3C 446 showed no statistically significant brightness variations in any of the 5 nights.

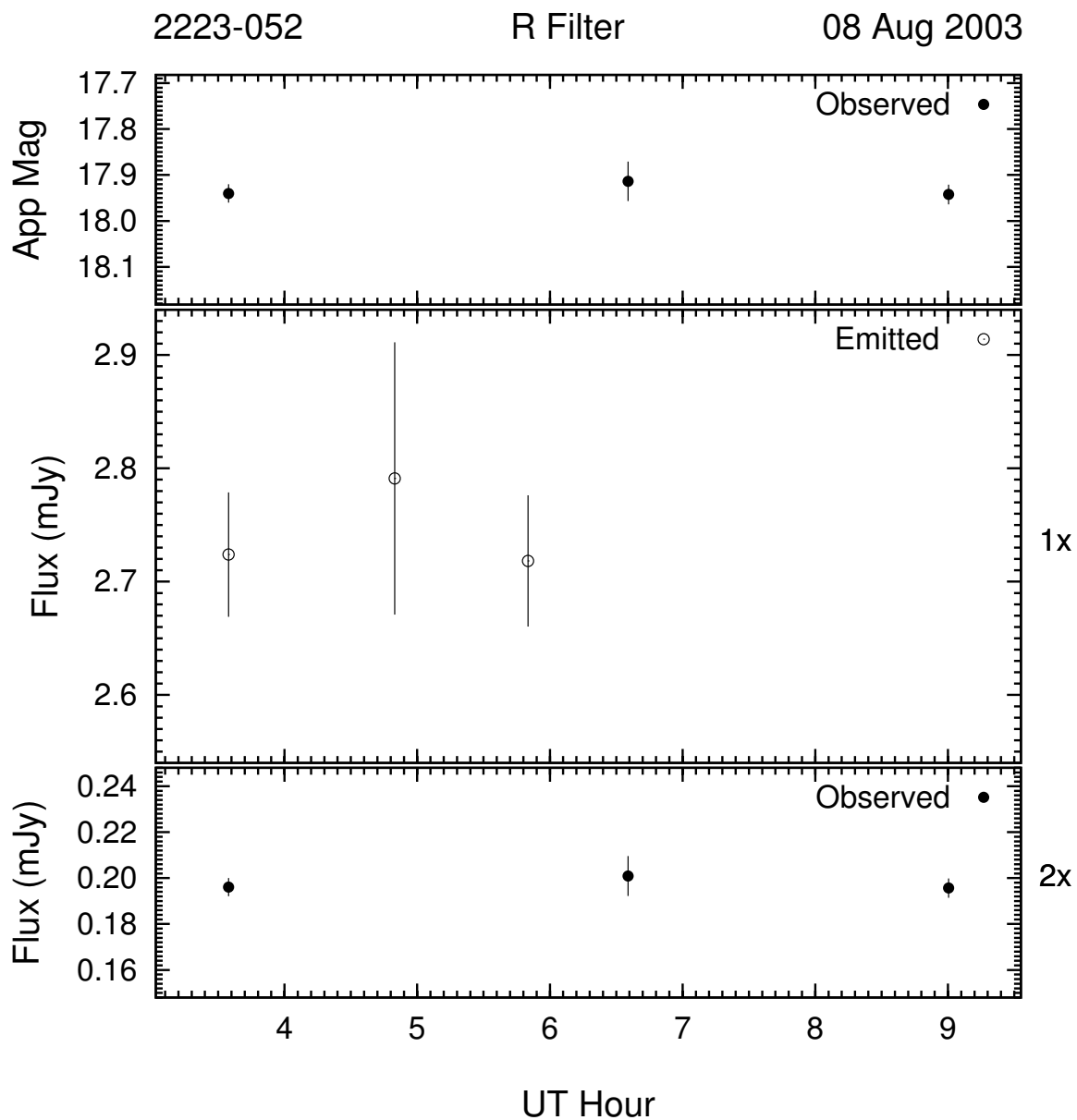


Figure 3.170: Example of the optical microvariability (R band) of 2223 – 052 on the night of 08 Aug 2003. This night's data was 2-point averaged to improve S/N .

The final observations of microvariability for 3C 446 are on the night of 06 Oct 2004 and can be seen in Figure 3.173. There is a hint of a decreasing trend in brightness, but no significant brightness variations. At the time of these observations, 3C 446 was 0.9 mag

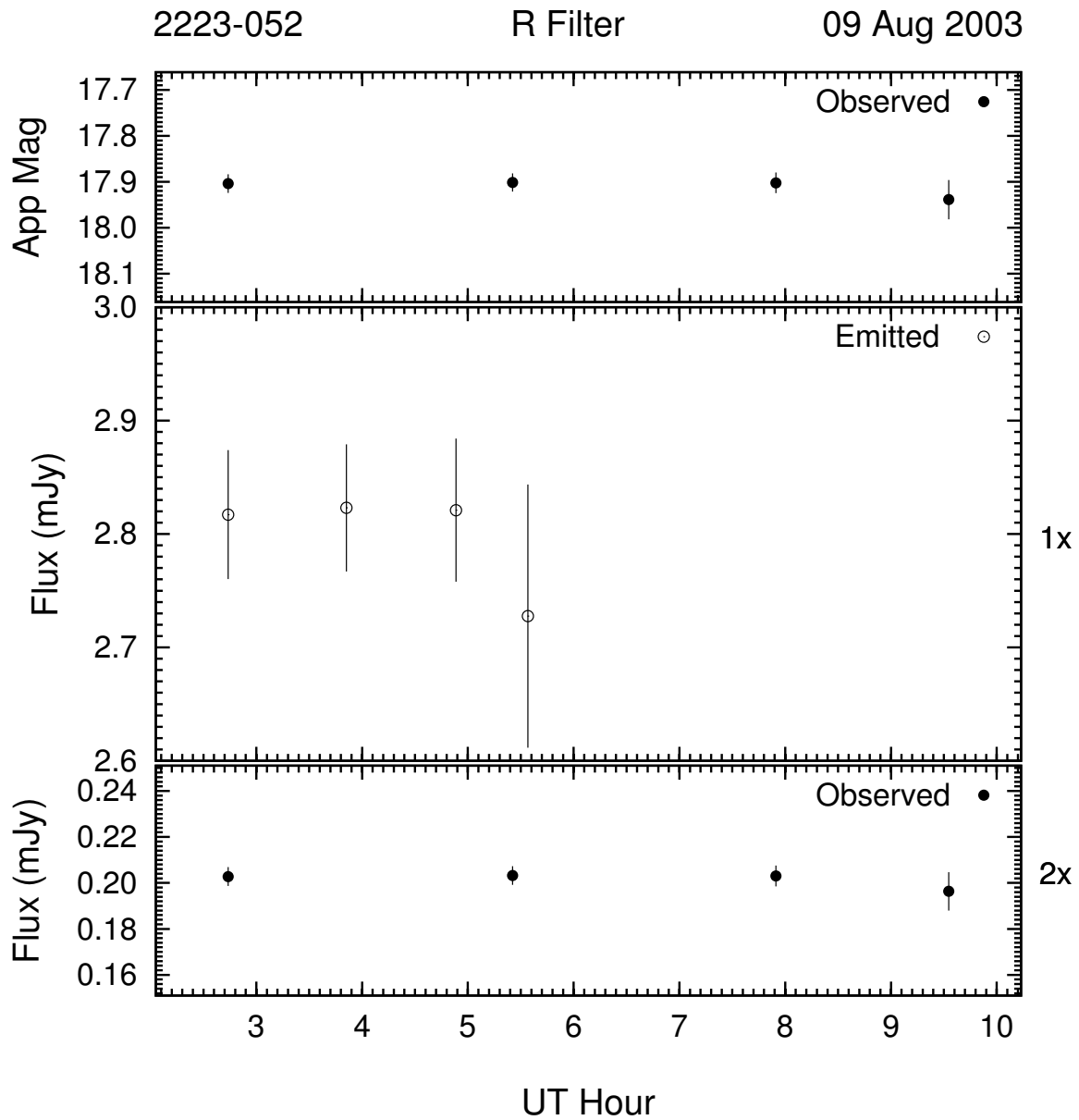


Figure 3.171: Example of the optical microvariability (R band) of 2223 – 052 on the night of 09 Aug 2003. This night's data was 2-point averaged to improve S/N .

brighter than in August of 2003.

At a redshift of 1.404, 3C 446 has the second largest enhancement in variability amplitude at a factor of almost 14, and a time *undilation* factor of almost 60%.

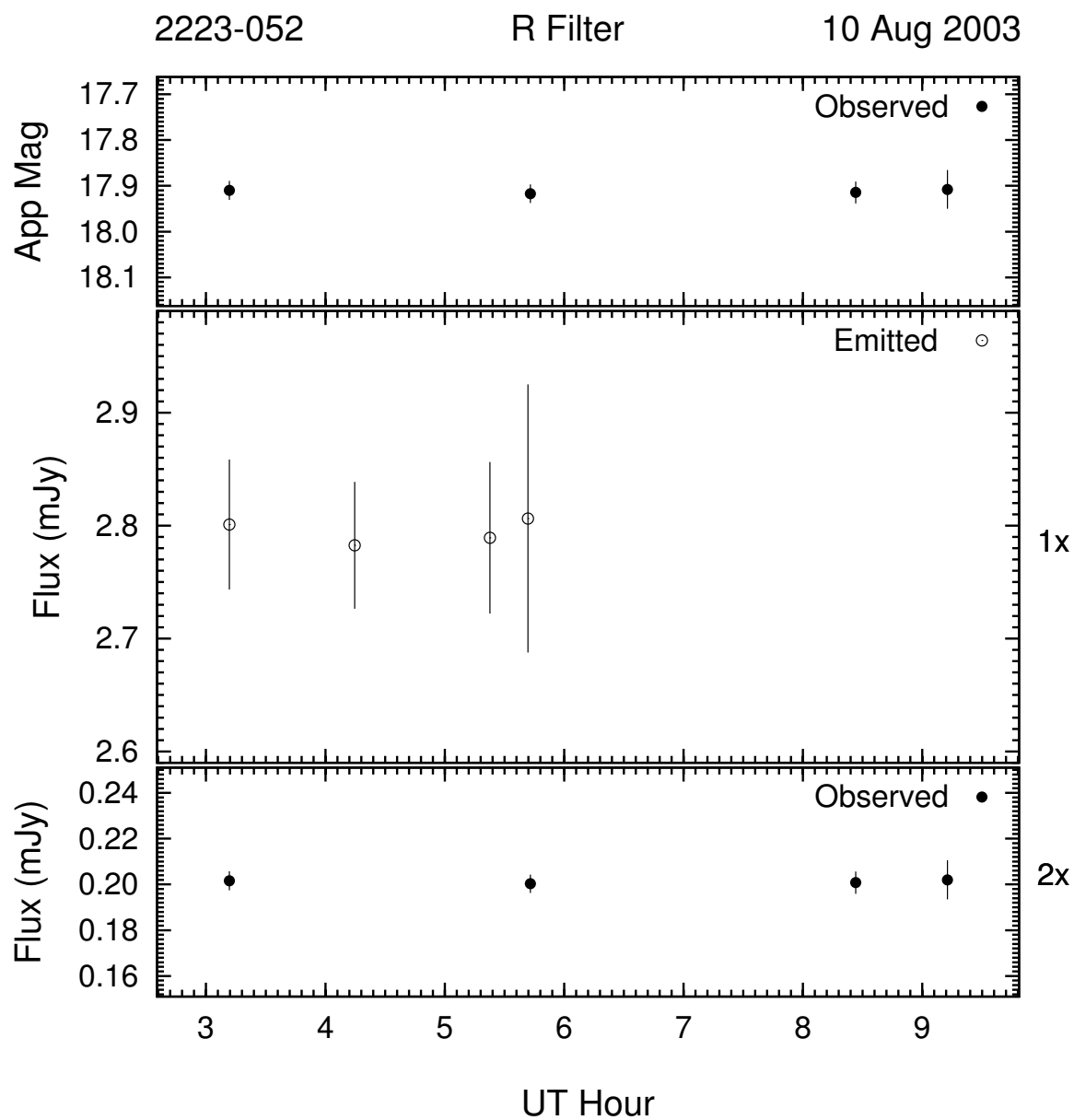


Figure 3.172: Example of the optical microvariability (R band) of 2223 – 052 on the night of 10 Aug 2003. This night's data was 2-point averaged to improve S/N .

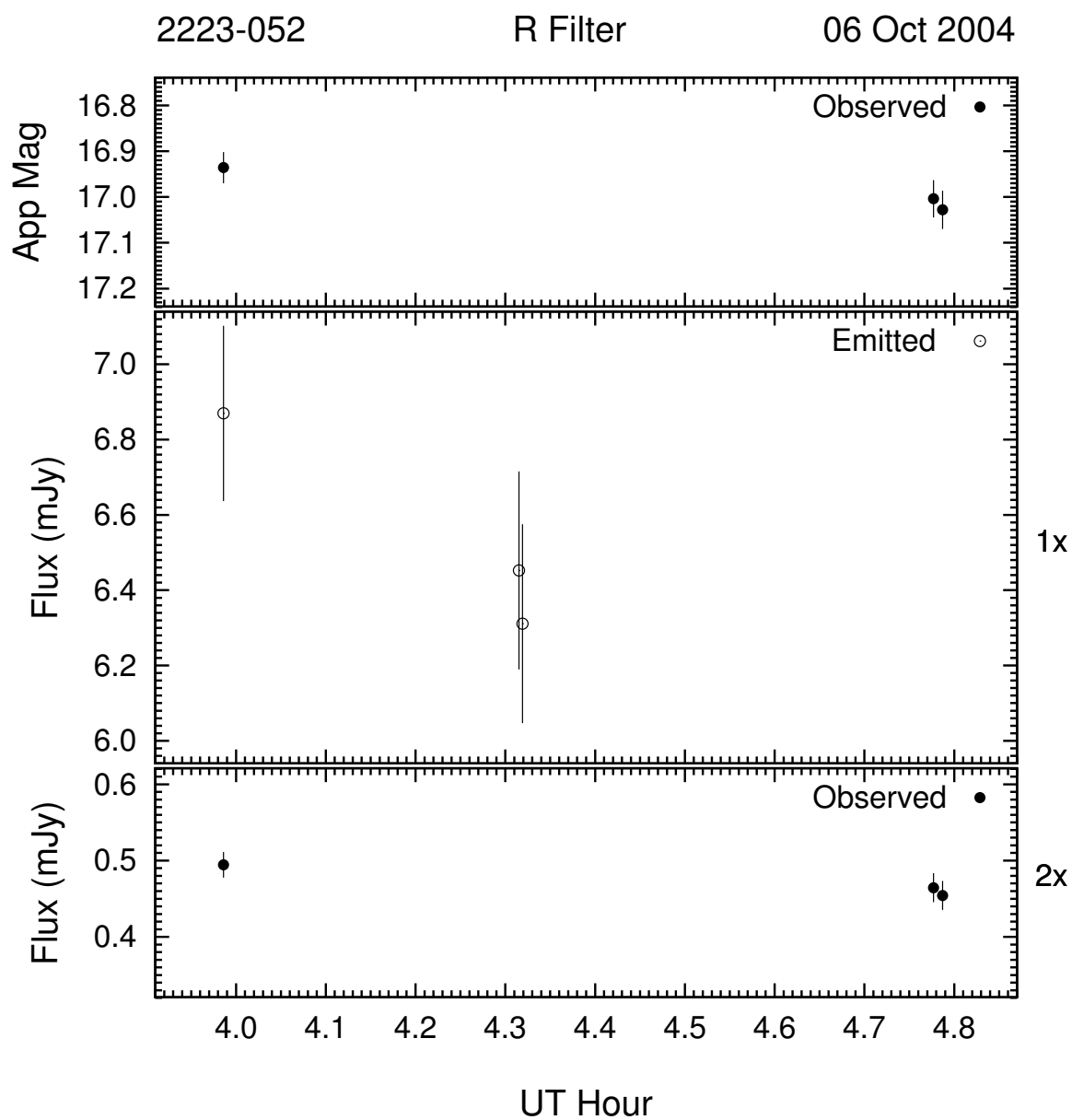


Figure 3.173: Example of the optical microvariability (R band) of 2223 – 052 on the night of 06 Oct 2004.

3.2.8 Comparison in the Rest Frame

The enhancement of the microvariability of any object’s emissions when shifted back into its rest frame (i.e., “corrected” for cosmological effects) is obvious given the arguments in §3.1.1. Not only are the amplitudes enhanced by the factor of $(1+z)^3$, but the time-scale is “undilated” and therefore compressed by a factor of $(1+z)$. By correcting the time-scale to the rest frame, an advantageous side effect is realized: an enhancement of temporal resolution is achieved in the rest frame. By looking at the objects in their rest frame, lower amplitude variations are more pronounced and shorter time-scale events may be detected. This allows more stringent constraints to be placed on the structure of the emitting region. It should be noted that the associated errors are enhanced along side of the variability amplitudes. The implication here is that no new statistically significant variability is detected. This enhancement only allows comparison of objects with different redshifts to each other on similar footing.

In order to compare the microvariability of the corrected, rest frame light curves to each other, it is helpful to have an object with a large base of microvariability observations that is relatively nearby. This allows direct comparison of many variability morphologies, time-scales, and amplitudes of variation. BL Lac is just such an object. Its microvariability light curves (described in §3.2.6) number more than 50, and show variations on time-scales of minutes to hours, and amplitudes ranging from about 0.08 to 8.0 mJy. Its microvariability morphologies range from simple trends (e.g., increasing, decreasing, or “flat”) to complex variations with multiple flares at many different rates of change (e.g., mJy / hour).

Many of the objects in this sample show only modest variability time-scales and am-

plitudes until they are shifted back into their rest frame (c.f. middle panel of light curves in §§3.2.1 through 3.2.7). Table 3.3 lists their variability amplitudes in both observed and emitted (rest) frames as well as their brightness levels. In this section, the rest frame light curves for all objects in this sample will be compared with those of BL Lac. This will not be an exhaustive comparison. One or more light curves from each object will be compared to an analogous one of BL Lac.

BL Lac is a very intriguing object. When shifted back into its rest frame, its variability is characterized by outbursts of 0.5 to 3 hours duration at the 10-20% level (e.g., Figures 3.103, 3.106, and 3.113) and larger, oscillatory variations lasting 4 to 8 hours at levels up to $\sim 30\%$ (e.g., Figures 3.93, 3.118, and 3.125). The character of the variability is similar to that found for other objects in the sample. One can usually find examples of similar time scale and amplitude of variability, but many objects exhibit variations shorter in duration and greater in intensity by up to a factor of two.

One such example is AO 0235 + 16 as seen on the night of 09 Nov 1997 (Figure 3.15). It shows a $\gtrsim 40\%$ change in brightness (as seen in its rest frame) over roughly 2 hours. The comparable BL Lac event is on the night of 17 Aug 1998 (Figure 3.115) where it shows a change in brightness of $\sim 20\%$ over the same time-scale. Another example is 1622 – 297 on the night of 16 May 1997 (Figure 3.35). This object exhibited a $> 40\%$ change in brightness in much less than an hour. The closest BL Lac comes to this is a change of $\sim 30\%$ over a little more than an hour on the beginning of the night of 03 Aug 1998 (Figure 3.114). A similar event is observed for 1633 + 382 where a variation of 30% in 2 hours can be seen in the light curve of 01 Apr 1996 (Figure 3.45).

Some objects show variations very similar to the oscillatory behavior of BL Lac such as 1156 + 295 on the night of 19 Jan 1994 (Figure 3.28). In this light curve, 1156 + 295 rises $\sim 8\%$ over about 2 hours in a quasi-sinusoidal fashion. BL Lac exhibits virtually identical behavior at roughly twice this amplitude on the night of 16 Sep 1995 (Figure 3.93).

Another example of similarity to BL Lac's variability time-scales and amplitudes is 3C 345 on the night of 19 May 1997. In the beginning of this night, displayed in Figure 3.70, 3C 345 exhibited a 40% change in one hour. BL Lac showed comparable variations in the middle of the night of 19 Aug 1997 with a 30% change over the same amount of time. This night's light curve can be seen in Figure 3.103. The last example of variability similarity is seen in the object 3C 446 on the night of 05 Oct 2001 (Figure 3.167). This $\lesssim 15\%$ change over 1 hour is comparable to that seen for BL Lac on the night of 01 Aug 1998 (see Figure 3.113). BL Lac exhibited a change of $\sim 18\%$ on this night over a duration of just one hour.

It is clear when looking at the light curves of all the objects in this sample in their rest frame that the variability is quite similar.

3.3 Analysis Methods

The variability observed for a number of blazars will be analyzed in multiple ways. The rest frame investigation will compare simple light curves for high z blazars with the light curves of 2200 + 420, and a structure function analysis of the light curves and a variability index will be used to characterize the variability. The following sections will describe these methods in detail.

3.3.1 Light Curves

Light curves are a simple, yet powerful tool astronomers use to display and analyze the temporal flux variability detected from astronomical objects. They are extremely useful tools for studying AGN variability. In the case of AGN, light curves can provide limits on the size of emitting region and the estimates of characteristic time scales.

The emission region size estimate is based on light time travel arguments. The basic argument is that the shortest time scale seen (Δt) is directly related to the size of the emission region, R by Equation (3.6) where c is the velocity of light.

$$R \leq c\Delta t \quad (3.6)$$

This equation assumes no relativistic beaming or cosmological effects. When dealing with blazars, whose dominant emission mechanism is believed to be related to a relativistic jet, and whose distances are generally $z \gtrsim 0.1$, these effects are important. Equation (3.7) includes these factors through δ , the Doppler factor (described immediately below) of the relativistic jet, and, z , the redshift of the source. It should be noted the Doppler factor is based on radio measurements of individual or multiple bright spots propagating down a jet, and can therefore be highly variable.

$$R' \leq \frac{\delta c \Delta t}{1 + z} \quad (3.7)$$

Light Curve Analysis

In this investigation, the light curves will be analyzed to determine if there is any variability and, if present, its nature. Visual inspection of the light curve morphology is the first and most basic method to do this. To describe the character of the variability based on this method, a reduced version of the classification scheme of Noble (1995) is used. It is summarized in Table 3.2. It was determined that the 8 bins used in the previous study oversampled the characteristics to an undesirable degree. Therefore the 2+/- designations (a single increase/decrease followed immediately by a decrease/increase) were integrated into C+/-, as both designations indicate variations that exhibit a complex character with the only difference being in degree (i.e., multiple events versus just one). For example, if one were to subsample a “C” light curve (some complex set of increases and decreases) such that only one increase followed by a decrease were seen, the reduced light curve could easily be classified as a 2+ light curve. Examples of the characteristics are illustrated in Figure 3.174.

Table 3.2: Variability Characteristic Classification Scheme (Noble, 1995)

| Class | Description |
|-------|----------------------------------------------------|
| 0 | no change in brightness |
| 1+/1- | trend (increase/decrease) in brightness |
| C | complex structure with no net change in brightness |
| C+/C- | complex structure with a trend (increase/decrease) |

Microvariability is detected when the excursion from the mean or from the trend exceeds a certain value of σ , the average measurement error, over the duration of the light curve in question (30 minute minimum). A $\sigma \geq 2.6$ ensures a 99% confidence level that the measured excursion is statistically significant and can be considered microvariability. It is to

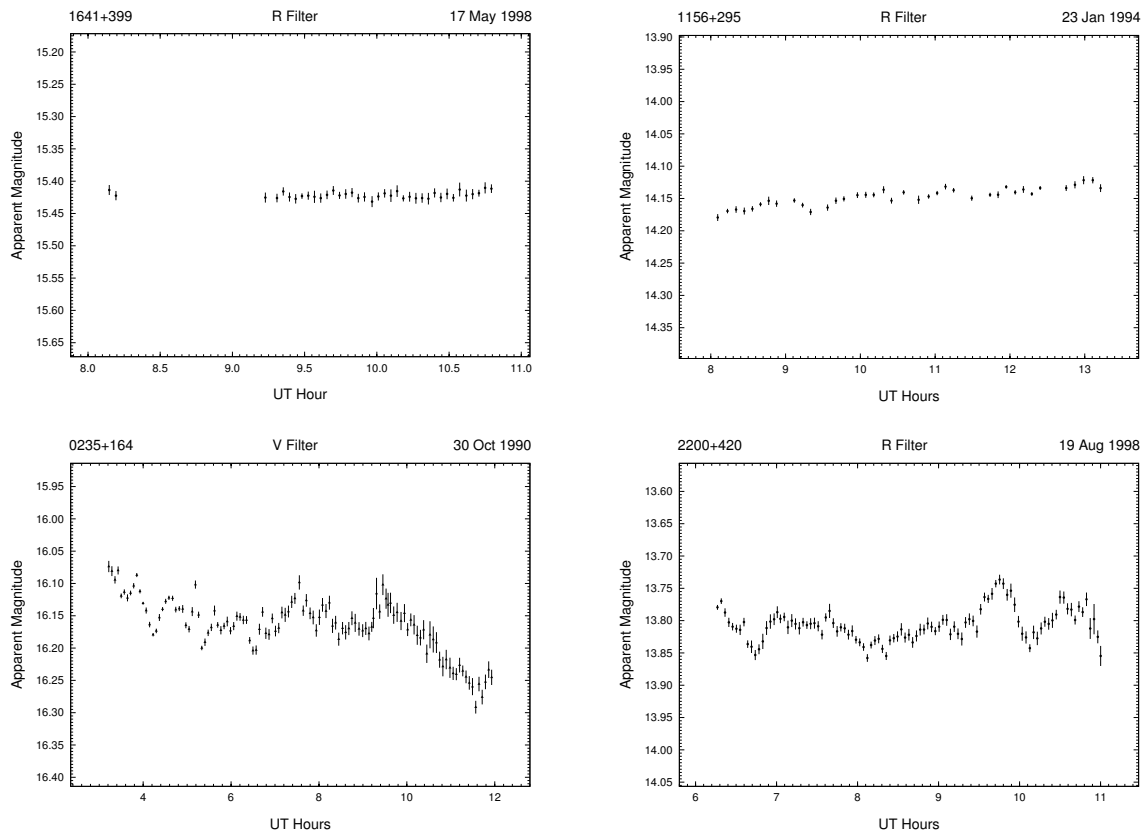


Figure 3.174: Examples of characteristics of microvariability. The upper left panel shows an example of “0”, no microvariability, while the upper right panel shows an increasing trend that would be designated “1+”. The two lower panels show examples of complex variability, with the left exhibiting a decreasing trend (“C–”) and the right exhibiting no trend (“C”).

be noted, however, due to the uncertain nature of any single photometric measurement, so called “single point excursions” can possibly lead to spurious detections of microvariability.

Single point excursions are the phenomenon whereby the point in question is not statistically supported. If only one point is sampled, it is difficult to determine the reliability of a single point conclusively. For this reason, one “observation” is typically composed of two or more closely associated measurements (i.e., closely associated in time for the current context). If two neighboring points show an unreasonable difference (e.g., significantly beyond

3σ), it is difficult to know either point to better than their difference. In this case, the points can either be used with the greater error (e.g., via binning), or can be excluded as spurious data. It is usually in the context of the overall data set that this choice is made.

3.3.2 Structure Function

Analysis of time series data to determine characteristic time-scales and duty cycles is best done with a power density spectrum (PDS). Unfortunately, this method of determining the time scales at which the largest power concentrations occur (i.e., the most common time scales in the series) requires evenly sampled data. Binning of the data in the time dimension can be done with reasonable results; however, the results can be highly dependent on the choice of window function. For this reason, the structure function (SF) has been chosen as a more useful tool rather than the PDS in determining characteristic time scales:

$$D(k) = \frac{1}{N(k)} \sum_{i=1}^N w(i)w(i+k)[f(i+k) - f(i)]^2; \quad (3.8)$$

$$N(k) = \sum_{i=1}^N w(i)w(i+k) . \quad (3.9)$$

The form of the SF used here, from Simonetti et al. (1985), is seen in Equation (3.8) and is the SF of the first order; N is the number of data points, f is the observable (e.g., flux or magnitude), i represents the i th time window, t_i , and k is associated with the size of the time window, $\Delta t = t_k - t_i$. The weighting factor, $w(i)$, has the value 1 when there is a measurement for i , 0 if not. The SF is in the same family of equations as is the cross correlation function (CCF) which will be used in the second main part of the data analysis

included in this dissertation.

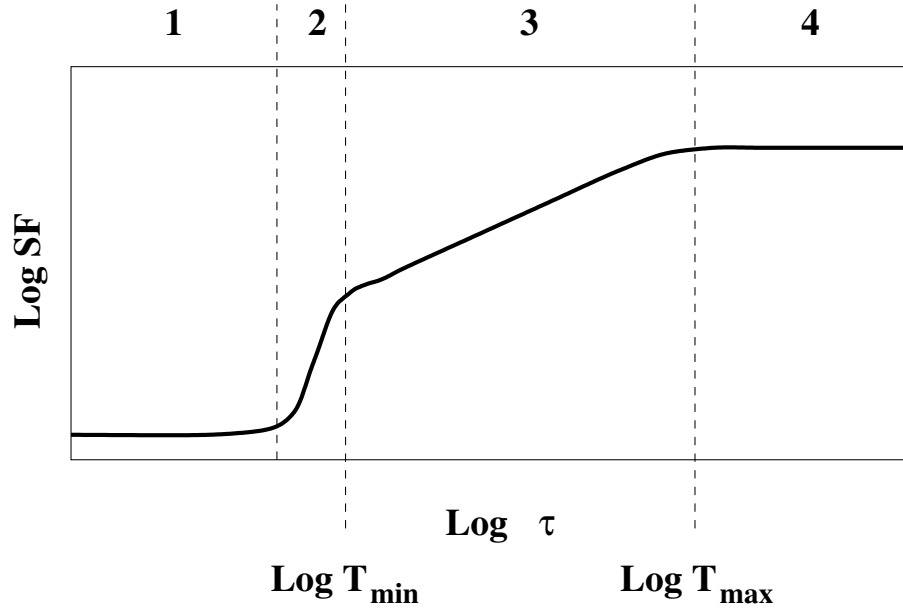


Figure 3.175: Schematic of “ideal” structure function from Paltani (1999).

The SF can be used to determine various characteristics of a light curve. Figure 3.183 illustrates the “ideal” form of the SF. Seldom are the data complete enough in time resolution to fill this “ideal” curve out, but it will be shown that it is not generally necessary in order to obtain useful information. Paltani (1999) gives a good description of the different parts of the SF, but some of the main points of interest for the current study are T_{\min} , the minimum variability time-scale and T_{\max} , the maximum variability time-scale. Together, these can constrain the size of the emitting region (see argument in §3.3.1 and Equations 3.6 & 3.7). One thing to note about the SF is that it is only useful for resolved variability. Therefore any linear trends need to be removed and only light curves where there is resolved variability (i.e., the trend is not the sole source of the variability) will be used.

3.3.3 Variability Index

One method used to quantify the character of the variability is assigning designations to flux changes greater than 2.6σ as in §3.3.1. This nicely quantifies the *character* of the variability, but does little to take into account the *amplitude* or *time scales* of the variability. In order to better quantify these values, a variability index (VI), defined in Equation (3.10), see e.g., Aller (1999), will be used to study its relationships to other properties (e.g., state, object type, reference frame). The VI is the fractional variability whose value is obtained using the maximum and minimum flux level (F_{max} and F_{min} respectively) within a given time window defined by $\Delta t = t_k - t_i$. Multiple time windows are chosen (as suggested by the data) and scanned across the data to obtain an average VI for each time window. This is done to maximize the accuracy of the VI because any individual measurement is highly dependent on both the location and size of the time window. Note the weighting factors (Equation (3.9)) with the same definitions as in §3.3.2

$$VI(k) = \frac{1}{N(k)} \sum_{i=1}^N w(i)w(i+k) \frac{F_{max} - F_{min}}{F_{max} + F_{min}} . \quad (3.10)$$

Similar to the structure function, the VI is properly defined for resolved variability only. The light curves that the VI will be calculated from will also have any linear trends removed. Also note, that the VI and SF are both functions of time, whereas a PDS is a function of frequency.

3.4 Rest Frame Analysis Results

In the following section, the dependence of the variability on luminosity state and redshift will be investigated and discussed. This includes variability characteristics, structure function analysis, and variability index analysis in both the observed and rest frame and as a function of luminosity state.

The results for the microvariability characteristic analysis are summarized in Table 3.3. Columns 1, 2, 3 are the object name, UT date in “CCYYMMDD” format, and filter; columns 4 and 5 are $F_{\nu,o}$, the mean flux for the night in mJy and $\Delta F_{\nu,o}$, the max–min differential flux (i.e., total change in flux), both as measured in the observed frame; column 6 is the confidence level, the largest change of flux in units of σ ; columns 7 and 8 are $F_{\nu,e}$, the mean flux and $\Delta F_{\nu,e}$, the differential flux, both after conversion into the rest frame of the source as described in §3.1.1; and the last 2 columns are C, the character of the variability as described in §3.3.1, and S, the state of the object at the time of observation (H=high, L=low, see §3.4.1).

The superscripts on the dates indicate the degree of n –point averaging of the data points in a given night’s light curve (e.g., ³ implies 3-point averaging) to improve the signal-to-noise ratio (S/N) of the observations. This is done subjectively with the degree chosen to match as close as possible the character of original data while maximizing S/N . See §2.3 for a complete discussion of data binning.

Table 3.3: Microvariability Characteristics of Archival Sample

| Object | UT Date | Filter | $F_{\nu,o}$ | $\Delta F_{\nu,o}$ | Conf | $F_{\nu,e}$ | $\Delta F_{\nu,e}$ | C | S |
|------------|-----------------------|--------|-------------|--------------------|------|-------------|--------------------|----|---|
| 0235 + 164 | 19861013 ⁴ | V | 0.42 | 0.03 | 2.7 | 3.08 | 0.21 | C– | L |

Table 3.3: continued...

| Object | UT Date | Filter | F_{ν_o} | ΔF_{ν_o} | Conf | F_{ν_e} | ΔF_{ν_e} | C | S |
|------------|-----------------------|--------|-------------|--------------------|------|-------------|--------------------|----|---|
| | 19871111 ⁴ | V | 0.26 | 0.05 | 5.6 | 1.89 | 0.34 | C | L |
| | 19901027 ³ | V | 0.90 | 0.06 | 14.3 | 6.57 | 0.42 | 1+ | L |
| | 19901028 ⁵ | V | 0.95 | 0.14 | 17.6 | 6.97 | 1.02 | 1+ | L |
| | 19901029 ⁵ | V | 1.02 | 0.21 | 28.3 | 7.46 | 1.54 | C+ | L |
| | 19901030 ⁵ | V | 1.30 | 0.26 | 19.5 | 9.46 | 1.87 | C− | H |
| | 19901031 ³ | V | 1.00 | 0.06 | 10.4 | 7.30 | 0.45 | C | L |
| | 19911105 ² | V | 6.13 | 1.13 | 15.9 | 44.75 | 8.23 | 1+ | H |
| | 19911106 ² | V | 6.11 | 0.53 | 6.8 | 44.59 | 3.90 | C | H |
| | 19911107 ² | V | 5.73 | 0.38 | 5.0 | 41.81 | 2.76 | C | H |
| | 19911108 ² | V | 7.99 | 1.35 | 15.7 | 58.30 | 9.82 | C− | H |
| | 19961203 | R | 0.07 | 0.08 | 33.0 | 0.53 | 0.57 | C | L |
| | 19971109 ² | V | 0.79 | 0.70 | 57.8 | 5.84 | 3.23 | C+ | L |
| | 19971125 ⁴ | V | 0.35 | 0.34 | 49.0 | 2.53 | 2.51 | C− | L |
| | 19980309 | R | 1.92 | 0.13 | 1.0 | 14.03 | 0.97 | 0 | H |
| | 19981018 ⁴ | R | 1.04 | 0.15 | 4.6 | 7.57 | 1.08 | C+ | H |
| | 19981019 ³ | R | 0.65 | 0.11 | 8.9 | 4.72 | 0.78 | C− | H |
| | 20040113 | R | 0.15 | 0.02 | 6.5 | 1.07 | 0.14 | C− | L |
| | 20040127 | R | 0.16 | 0.02 | 2.9 | 1.16 | 0.17 | C+ | L |
| | 20040209 | R | 0.22 | 0.02 | 1.0 | 1.62 | 0.14 | 0 | L |
| | 20040211 | R | 0.27 | 0.03 | 1.6 | 1.97 | 0.20 | 0 | L |
| | 20040212 | R | 0.23 | 0.03 | 3.0 | 1.69 | 0.23 | C+ | L |
| | 20040214 | R | 0.20 | 0.06 | 6.5 | 1.49 | 0.44 | C− | L |
| | 20040216 | R | 0.19 | 0.06 | 9.0 | 1.35 | 0.44 | C | L |
| 1156 + 295 | 19940119 ² | R | 8.70 | 1.16 | 28.0 | 44.97 | 5.98 | C+ | H |
| | 19940120 ² | R | 8.80 | 0.30 | 5.0 | 45.51 | 1.57 | C | H |
| | 19940121 ² | R | 9.26 | 0.77 | 14.5 | 47.84 | 3.96 | C+ | H |
| | 19940122 ² | R | 6.12 | 0.74 | 23.3 | 31.63 | 3.85 | C+ | H |
| | 19940123 ² | R | 6.45 | 0.34 | 10.0 | 33.33 | 1.77 | 1+ | H |
| | 19940124 ² | R | 5.09 | 0.35 | 7.6 | 26.29 | 1.83 | 1− | H |
| 1622 − 297 | 19970516 ² | R | 0.61 | 0.82 | 16.6 | 3.67 | 4.93 | C | H |
| | 19970823 | R | 0.41 | 0.09 | 20.2 | 2.47 | 0.51 | C+ | H |
| | 19970824 | R | 0.39 | 0.01 | 0.1 | 2.35 | 0.06 | 0 | H |
| | 19970825 | R | 0.47 | 0.07 | 11.3 | 2.83 | 0.42 | C+ | H |
| | 19970826 ² | R | 0.47 | 0.02 | 2.2 | 2.84 | 0.12 | 0 | H |
| | 19970827 ² | R | 0.41 | 0.03 | 2.8 | 2.43 | 0.16 | 1− | H |
| | 20000608 ² | R | 0.37 | 0.11 | 2.0 | 2.20 | 0.68 | 0 | H |
| | 20000609 ² | R | 0.26 | 0.03 | 2.8 | 1.53 | 0.15 | C− | L |
| | 20020520 ³ | R | 0.21 | 0.00 | 1.2 | 1.27 | 0.03 | 0 | L |
| 1633 + 382 | 19960401 ⁴ | R | 0.72 | 0.25 | 29.4 | 16.13 | 5.47 | 1− | H |
| | 19960402 ² | R | 0.60 | 0.05 | 3.9 | 13.43 | 1.04 | C | H |
| | 19960403 ⁴ | R | 0.55 | 0.08 | 9.9 | 12.33 | 1.85 | C | H |

Table 3.3: continued...

| Object | UT Date | Filter | F_{ν_o} | ΔF_{ν_o} | Conf | F_{ν_e} | ΔF_{ν_e} | C | S |
|------------|-----------------------|--------|-------------|--------------------|------|-------------|--------------------|----|---|
| 1641 + 399 | 19960426 ³ | R | 0.34 | 0.00 | 0.2 | 7.55 | 0.11 | 0 | L |
| | 19960427 ² | R | 0.33 | 0.01 | 2.7 | 7.44 | 0.30 | C | L |
| | 19960428 ² | R | 0.34 | 0.00 | 0.3 | 7.65 | 0.08 | 0 | L |
| | 19960429 ² | R | 0.35 | 0.01 | 1.6 | 7.71 | 0.18 | 0 | L |
| | 19960430 ² | R | 0.35 | 0.01 | 4.7 | 7.87 | 0.29 | C+ | L |
| | 19960501 ² | R | 0.37 | 0.01 | 3.1 | 8.18 | 0.26 | C | L |
| | 19980517 | R | 0.35 | 0.01 | 0.2 | 7.71 | 0.12 | 0 | L |
| | 19980518 ² | R | 0.37 | 0.01 | 2.1 | 8.33 | 0.26 | 0 | L |
| | 20000608 ² | R | 0.35 | 0.04 | 7.6 | 7.85 | 0.92 | C | L |
| | 20000609 ² | R | 0.36 | 0.01 | 2.7 | 8.12 | 0.30 | C | L |
| | 20030520 ² | R | 0.34 | 0.01 | 2.9 | 7.59 | 0.27 | C | L |
| | 20030521 ² | R | 0.34 | 0.01 | 1.6 | 7.57 | 0.12 | 0 | L |
| | 20030522 ² | R | 0.34 | 0.02 | 9.3 | 7.60 | 0.48 | C | L |
| | 20030523 ² | R | 0.34 | 0.03 | 6.7 | 7.49 | 0.69 | 1+ | L |
| | 20030524 ² | R | 0.36 | 0.01 | 2.9 | 7.93 | 0.16 | C | L |
| | 20040521 ² | R | 0.43 | 0.01 | 2.6 | 9.63 | 0.21 | C− | L |
| | 20040522 | R | 0.43 | 0.02 | 5.7 | 9.50 | 0.48 | C+ | L |
| | 20040523 ² | R | 0.41 | 0.01 | 5.1 | 9.21 | 0.19 | 1+ | L |
| | 19920610 | R | 2.00 | 0.12 | 0.9 | 8.09 | 0.49 | 0 | H |
| | 19960401 | R | 0.41 | 0.09 | 46.4 | 1.67 | 0.37 | C+ | L |
| | 19960403 ² | R | 0.40 | 0.03 | 1.0 | 1.63 | 0.12 | 0 | L |
| | 19970519 ² | R | 0.48 | 0.23 | 12.9 | 1.92 | 0.94 | C− | L |
| | 19980517 | R | 1.99 | 0.04 | 0.7 | 8.06 | 0.16 | 0 | H |
| | 19980518 ² | R | 2.18 | 0.08 | 5.6 | 8.81 | 0.33 | C+ | H |
| | 19980519 ⁴ | R | 2.12 | 0.07 | 5.0 | 8.58 | 0.29 | C− | H |
| | 20000414 | R | 1.08 | 0.05 | 12.1 | 4.37 | 0.19 | C+ | H |
| | 20000415 ³ | R | 1.08 | 0.19 | 15.0 | 4.36 | 0.75 | C | H |
| | 20000416 ³ | R | 1.08 | 0.05 | 4.4 | 4.39 | 0.19 | C | H |
| | 20000417 | R | 1.06 | 0.10 | 13.1 | 4.30 | 0.42 | C+ | H |
| | 20000606 | R | 1.15 | 0.08 | 11.7 | 4.65 | 0.32 | C+ | H |
| | 20010521 ³ | R | 2.62 | 0.18 | 6.3 | 10.59 | 0.73 | C | H |
| | 20010615 ² | R | 2.59 | 0.08 | 6.9 | 10.45 | 0.31 | C | H |
| | 20010616 ² | R | 2.57 | 0.08 | 4.3 | 10.39 | 0.34 | C | H |
| | 20010617 | R | 2.58 | 0.17 | 5.8 | 10.41 | 0.68 | C | H |
| | 20010618 ² | R | 2.55 | 0.13 | 7.6 | 10.33 | 0.53 | C | H |
| | 20030520 | R | 0.80 | 0.06 | 10.6 | 3.22 | 0.23 | C | L |
| | 20030521 | R | 0.80 | 0.04 | 13.1 | 3.23 | 0.15 | C | L |
| | 20030522 ² | R | 0.80 | 0.03 | 7.2 | 3.24 | 0.14 | C | L |
| | 20030523 | R | 0.82 | 0.04 | 16.3 | 3.31 | 0.17 | C | L |
| | 20030524 ² | R | 0.82 | 0.05 | 15.6 | 3.31 | 0.20 | C+ | L |
| 2200 + 420 | 19910918 ³ | V | 2.33 | 0.13 | 14.4 | 2.84 | 0.16 | 1− | L |

Table 3.3: continued...

| Object | UT Date | Filter | F_{ν_o} | ΔF_{ν_o} | Conf | F_{ν_e} | ΔF_{ν_e} | C | S |
|--------|-----------------------|--------|-------------|--------------------|------|-------------|--------------------|----|---|
| | 19950915 | R | 2.90 | 0.14 | 5.5 | 3.54 | 0.17 | C+ | L |
| | 19950916 | R | 2.97 | 0.59 | 24.5 | 3.63 | 0.73 | C+ | L |
| | 19950917 | R | 3.01 | 0.32 | 10.4 | 3.68 | 0.39 | C+ | L |
| | 19950918 ² | R | 2.34 | 0.14 | 10.6 | 2.86 | 0.17 | C− | L |
| | 19950919 | R | 2.51 | 0.44 | 19.2 | 3.07 | 0.54 | C− | L |
| | 19951031 | R | 3.04 | 0.29 | 8.4 | 3.72 | 0.35 | C− | L |
| | 19960919 ² | R | 3.39 | 0.05 | 1.9 | 4.14 | 0.06 | 0 | L |
| | 19960920 ³ | R | 3.24 | 0.13 | 10.5 | 3.96 | 0.16 | C− | L |
| | 19960921 ⁵ | R | 3.83 | 0.41 | 32.2 | 4.67 | 0.50 | C+ | L |
| | 19970718 ³ | R | 11.04 | 1.50 | 4.3 | 13.49 | 1.83 | C+ | H |
| | 19970719 ² | R | 21.62 | 7.31 | 11.8 | 26.41 | 8.94 | 1− | H |
| | 19970819 ² | R | 17.33 | 4.53 | 23.5 | 21.17 | 5.54 | C+ | H |
| | 19970927 ³ | V | 3.67 | 0.44 | 13.9 | 4.48 | 0.54 | C+ | L |
| | 19970927 ² | R | 5.90 | 1.52 | 49.7 | 7.21 | 1.86 | C− | L |
| | 19970928 ³ | V | 3.42 | 0.93 | 30.2 | 4.18 | 1.14 | C | L |
| | 19970928 ² | R | 5.44 | 1.06 | 29.4 | 6.64 | 1.30 | C− | L |
| | 19970929 ³ | R | 4.19 | 0.83 | 35.7 | 5.11 | 1.01 | C+ | L |
| | 19971202 ⁴ | V | 1.03 | 0.14 | 15.2 | 1.25 | 0.17 | C− | L |
| | 19980713 ⁵ | R | 13.33 | 1.47 | 12.5 | 16.29 | 1.80 | C+ | H |
| | 19980714 ⁵ | R | 13.90 | 2.30 | 14.8 | 16.98 | 2.81 | C− | H |
| | 19980727 ³ | R | 9.06 | 1.43 | 11.0 | 11.07 | 1.75 | C− | H |
| | 19980801 ³ | R | 10.30 | 1.68 | 10.7 | 12.58 | 2.05 | C | H |
| | 19980803 ⁴ | R | 9.69 | 4.48 | 16.1 | 11.84 | 5.48 | C | H |
| | 19980817 ³ | R | 8.52 | 2.61 | 17.8 | 10.41 | 3.19 | C | H |
| | 19980819 ² | R | 8.83 | 1.00 | 11.4 | 10.79 | 1.22 | C | H |
| | 19980820 ⁵ | R | 9.49 | 1.35 | 8.6 | 11.60 | 1.65 | C− | H |
| | 19981019 | R | 11.25 | 2.01 | 7.0 | 13.74 | 2.45 | C+ | H |
| | 20000721 ² | R | 7.24 | 1.01 | 10.5 | 8.84 | 1.24 | C+ | L |
| | 20000723 ² | R | 8.40 | 1.30 | 14.4 | 10.26 | 1.59 | C+ | H |
| | 20000725 ² | R | 6.94 | 0.75 | 11.7 | 8.48 | 0.91 | C+ | L |
| | 20000801 ² | R | 7.70 | 2.03 | 26.8 | 9.40 | 2.47 | C− | L |
| | 20000805 ² | R | 6.00 | 0.99 | 18.3 | 7.33 | 1.21 | C+ | L |
| | 20000806 ² | R | 5.60 | 1.08 | 20.5 | 6.85 | 1.32 | C+ | L |
| | 20000808 ² | R | 7.13 | 2.91 | 46.5 | 8.71 | 3.56 | C+ | L |
| | 20000811 ² | R | 6.51 | 0.98 | 14.9 | 7.95 | 1.19 | C− | L |
| | 20000815 ² | R | 6.99 | 1.14 | 23.8 | 8.54 | 1.39 | 1− | L |
| | 20000817 ² | R | 6.10 | 0.19 | 5.7 | 7.45 | 0.24 | 1− | L |
| | 20000819 | R | 6.24 | 0.44 | 5.1 | 7.63 | 0.54 | 1+ | L |
| | 20010614 ³ | R | 21.77 | 3.41 | 8.7 | 26.59 | 4.16 | C+ | H |
| | 20010615 | R | 22.22 | 5.60 | 11.8 | 27.15 | 6.84 | 1+ | H |
| | 20010617 ⁴ | R | 17.42 | 2.01 | 13.2 | 21.28 | 2.46 | C+ | H |

Table 3.3: continued...

| Object | UT Date | Filter | F_{ν_o} | ΔF_{ν_o} | Conf | F_{ν_e} | ΔF_{ν_e} | C | S |
|------------|-----------------------|--------|-------------|--------------------|------|-------------|--------------------|----|---|
| 2223 – 052 | 20010618 ³ | R | 12.71 | 1.55 | 5.6 | 15.52 | 1.89 | C | H |
| | 20021002 | R | 7.24 | 1.05 | 7.7 | 8.84 | 1.28 | 1– | L |
| | 20021004 | R | 7.94 | 0.95 | 9.4 | 9.69 | 1.16 | C+ | H |
| | 20021008 | R | 11.85 | 0.54 | 2.7 | 14.48 | 0.66 | 1– | H |
| | 20021019 ³ | R | 9.20 | 1.55 | 25.9 | 11.24 | 1.89 | C– | H |
| | 20040921 ² | R | 13.22 | 0.21 | 1.7 | 16.15 | 0.25 | 0 | H |
| | 20040922 ² | R | 12.86 | 1.07 | 6.1 | 15.71 | 1.31 | C– | H |
| | 20040923 ² | R | 13.19 | 2.07 | 14.4 | 16.12 | 2.53 | C+ | H |
| | 20041004 ² | R | 11.47 | 0.34 | 2.3 | 14.01 | 0.42 | 0 | H |
| | 20041005 ² | R | 8.74 | 0.85 | 17.9 | 10.68 | 1.04 | 1– | H |
| | 20041006 ² | R | 8.96 | 0.40 | 5.3 | 10.94 | 0.49 | C– | H |
| | 20041007 ² | R | 8.94 | 0.13 | 0.9 | 10.92 | 0.16 | 0 | H |
| | 20041008 ² | R | 9.93 | 0.72 | 13.6 | 12.14 | 0.88 | C– | H |
| | 20041009 ² | R | 9.08 | 1.15 | 16.2 | 11.09 | 1.40 | 1– | H |
| | 19880810 ² | R | 2.29 | 0.08 | 0.6 | 31.87 | 1.07 | 0 | H |
| | 19880929 ² | R | 1.89 | 0.14 | 1.5 | 26.23 | 1.95 | 0 | H |
| | 19880930 ² | R | 1.29 | 0.02 | 1.2 | 17.89 | 0.28 | 0 | H |
| | 19881001 ² | R | 1.28 | 0.08 | 0.9 | 17.76 | 1.07 | 0 | H |
| | 19881025 ³ | R | 1.10 | 0.09 | 1.8 | 15.30 | 1.20 | 0 | H |
| | 19980827 ² | R | 0.33 | 0.01 | 0.2 | 4.64 | 0.20 | 0 | L |
| | 19980828 ² | R | 0.32 | 0.01 | 0.3 | 4.51 | 0.17 | 0 | L |
| | 19980829 ² | R | 0.34 | 0.02 | 1.2 | 4.69 | 0.32 | 0 | L |
| | 19980830 ² | R | 0.35 | 0.02 | 0.8 | 4.91 | 0.25 | 0 | L |
| | 19981018 ² | R | 0.43 | 0.02 | 0.2 | 6.00 | 0.22 | 0 | L |
| | 19981019 ² | R | 0.46 | 0.03 | 0.9 | 6.37 | 0.39 | 0 | L |
| | 19981020 ² | R | 0.49 | 0.02 | 0.7 | 6.79 | 0.23 | 0 | L |
| | 20000908 ² | R | 1.51 | 0.03 | 0.9 | 20.93 | 0.44 | 0 | H |
| | 20000909 ² | R | 1.43 | 0.04 | 0.8 | 19.92 | 0.49 | 0 | H |
| | 20000910 ² | R | 1.33 | 0.03 | 0.9 | 18.45 | 0.41 | 0 | H |
| | 20000911 ² | R | 1.28 | 0.04 | 0.4 | 17.80 | 0.57 | 0 | H |
| | 20001026 ² | R | 1.36 | 0.02 | 1.2 | 18.96 | 0.29 | 0 | H |
| | 20001027 | R | 1.30 | 0.10 | 0.4 | 18.12 | 1.35 | 0 | H |
| | 20011004 ² | R | 0.72 | 0.05 | 1.4 | 9.95 | 0.65 | 0 | H |
| | 20011005 ² | R | 0.83 | 0.10 | 3.8 | 11.48 | 1.32 | C | H |
| | 20030805 ² | R | 0.19 | 0.01 | 0.6 | 2.69 | 0.07 | 0 | L |
| | 20030806 ² | R | 0.19 | 0.00 | 1.8 | 2.67 | 0.01 | 0 | L |
| | 20030808 ² | R | 0.20 | 0.01 | 1.1 | 2.74 | 0.07 | 0 | L |
| | 20030809 ² | R | 0.20 | 0.01 | 0.7 | 2.80 | 0.10 | 0 | L |
| | 20030810 ² | R | 0.20 | 0.00 | 1.7 | 2.79 | 0.02 | 0 | L |
| | 20041006 | R | 0.47 | 0.04 | 0.4 | 6.54 | 0.56 | 0 | L |

3.4.1 Variability and State

Because all objects in the sample were monitored for a minimum of 6 years, it is likely that a large fraction of the brightness range of each object is adequately sampled. This allows one to determine how the occurrence of microvariability changes as a function of luminosity state (or more succinctly, state). The state of the object is said to be “high” when the average magnitude of the data in question is in the upper half of its range, and “low” when in the lower half. It should be noted that the state referred to here is not an absolute state, rather a relative state based on the observations used. The states are chosen in this way to avoid selection effects whereby only a small, unrepresentative number of observations would be included in the sample if the states were defined with respect to all known observations.

An important result of this study is that for this sample of Blazars, the probability of detecting microvariability is independent of the state of the object (Figure 3.176). The probabilities are 0.74 (59 out of 80) for the high state and 0.71 (59 out of 83) for the low state.

The sample of objects investigated here is comprised of only LBLs (low-energy-cutoff BL Lacs). This allows the opportunity to compare the characteristics of this sample of LBLs with a like sample of HBLs (high-energy-cutoff BL Lacs). Campbell (2004) investigated 7 HBLs in a similar way, and found the probability of microvariability as a function of state for HBLs was 0.31 for the high state and 0.30 for the low state. This compares well with the assertion that the microvariability occurrence is independent of state for blazars as a class. This result also shows that HBLs do indeed exhibit optical microvariability less often than do LBLs, suggesting that the duty cycle is very different for the two classes of objects.

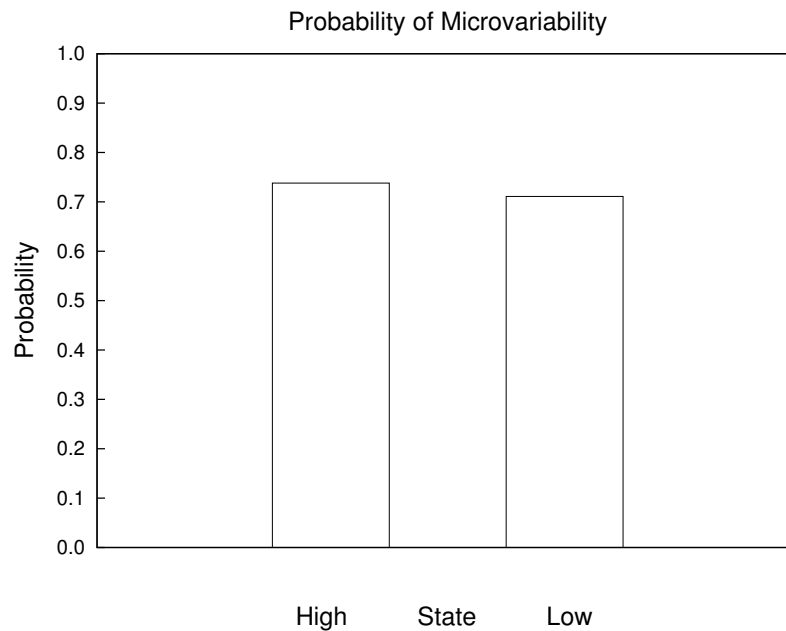


Figure 3.176: The percentage of microvariability as a function of state.

The microvariability characteristics as a function of state are shown in Figure 3.177. Notice the symmetry around the 0,C center, and how characteristics are independent of state. This suggests that variability character is predominantly composed of erratic variations (e.g., flares, drops, etc.) superimposed on the overall intensity level (whether it be rising, falling, or steady) and that this character is constant. This result allows one to confront two possible models for the origin of the microvariability. Blazar microvariability is believed to originate in one of two places: disturbances in relativistic shocks propagating down the jet or discrete events (e.g., flares or hot spots) in the accretion disk. The fact that the state plays no role in the character of the microvariability bolsters the jet model, because the accretion disk variability would be most conspicuous in the low state and nearly absent in the high state (Miller, private communication). This is clearly not the case. This result for LBLs is similar for the case of HBLs as seen in Campbell (2004). The HBLs in that sample also showed

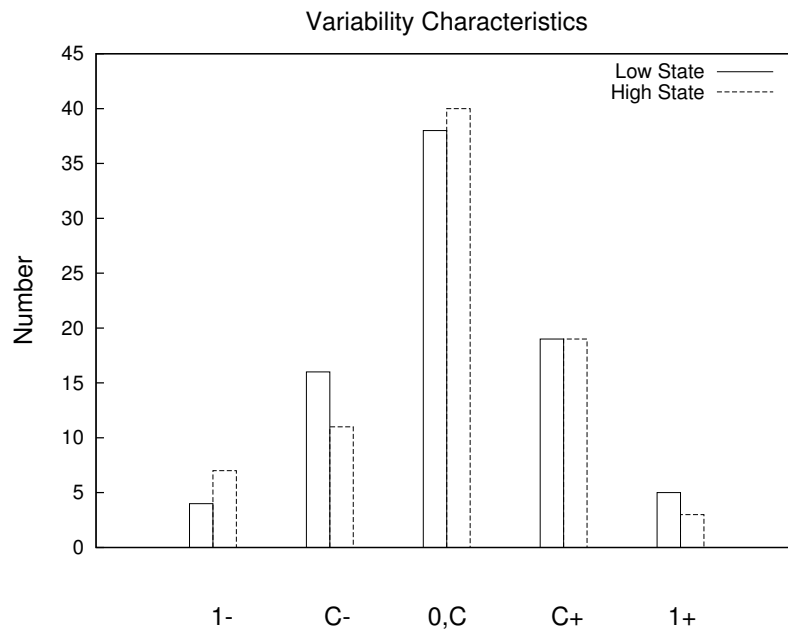


Figure 3.177: The characteristics of microvariability as a function of state.

microvariability that was predominantly complex, or exhibited no variations (C or 0) with very few “clean” positive or negative linear trends.

If the number of occurrences of microvariability is plotted against the total magnitude change as a function of state, it is seen that the amplitude of variability does not change with state (see Figure 3.178). This is the expected result if the energy of a given microvariability event scales with the luminosity state of the object (i.e., $\Delta L \propto L$) and is further evidence for the origin of the emissions responsible for these variations to be in the jet. This was the same conclusion found by Campbell (2004) for the sample of HBLs.

If the number of occurrences of microvariability is plotted against the total flux change as a function of state, the distribution is expected to shift to higher flux levels in the high luminosity state. The amplitude of variability (in flux space) does indeed change with state as seen in both the observed frame and the rest frame (see Figure 3.179) in the direction of

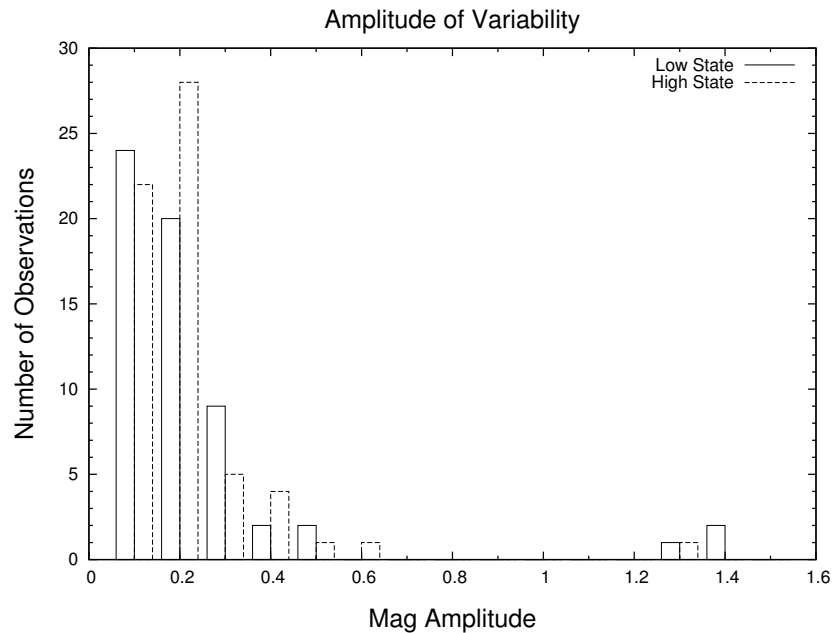


Figure 3.178: The occurrences of microvariability in the observed frame as a function of change in magnitude for all objects.

higher amplitudes in higher states as expected. Significantly more events are concentrated in lower energy flux bins in the low state versus the high state. This is more evident when looking at the observations shifted back into the rest frame. This trend is seen more clearly when the energetics of microvariability is investigated by plotting the average flux change per event as a function of state. Figure 3.180 clearly shows that the average flux change of each event increases by a factor of 3 in the high state (0.13 to 0.39 mJy in the observed frame). When the same observations are shifted into the rest frame of each object, the result is virtually the same: a shift from 0.27 to 0.87 mJy.

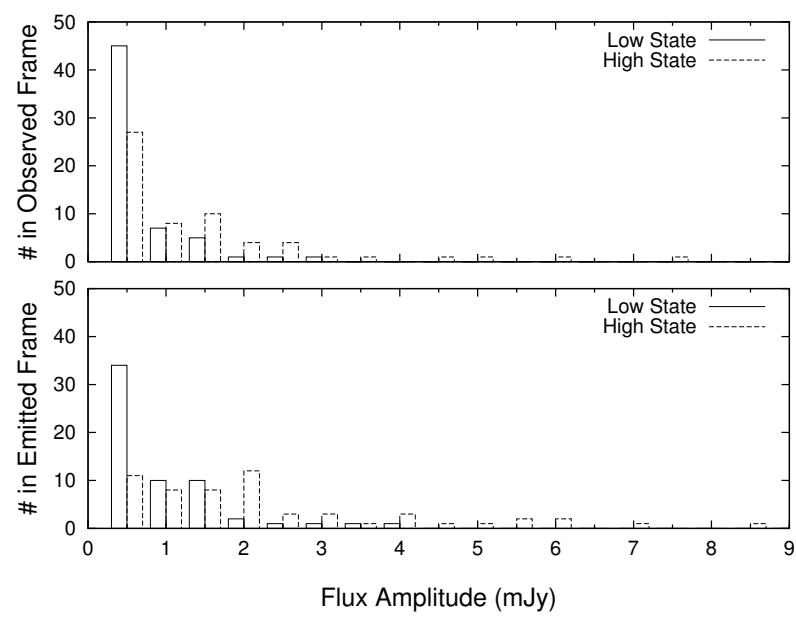


Figure 3.179: The occurrences of microvariability in the observed frame (top panel) and the rest frame (bottom panel) as a function of flux amplitude for all objects.

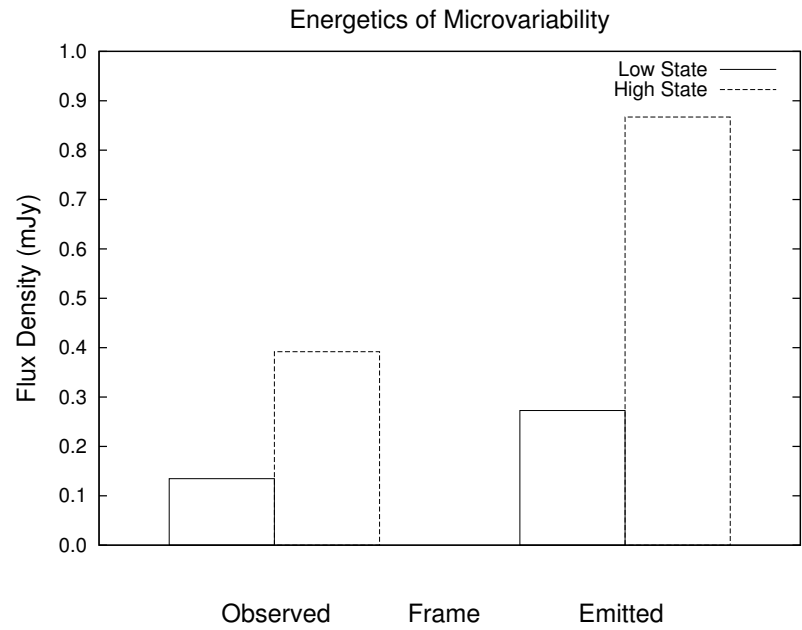


Figure 3.180: The average flux per microvariability event as a function of state and frame of reference.

An investigation of the relationship of the duty cycle³ versus two jet parameters (5 GHz radio flux and apparent transverse speed, $\beta = v/c$, of material in the jet) was undertaken for this sample of LBLs. The values of the 5 GHz radio flux were taken from various sources as compiled by NED⁴, and the β values were an average from Jorstad et al. (2001), Piner and Edwards (2004), and Vermeulen and Cohen (1994). The 5 GHz flux was converted into the rest frame in the same manner as the optical flux (see §3.1). The plots of duty cycle versus 5GHz radio flux and apparent speeds are displayed in Figures 3.181 and 3.182 respectively.

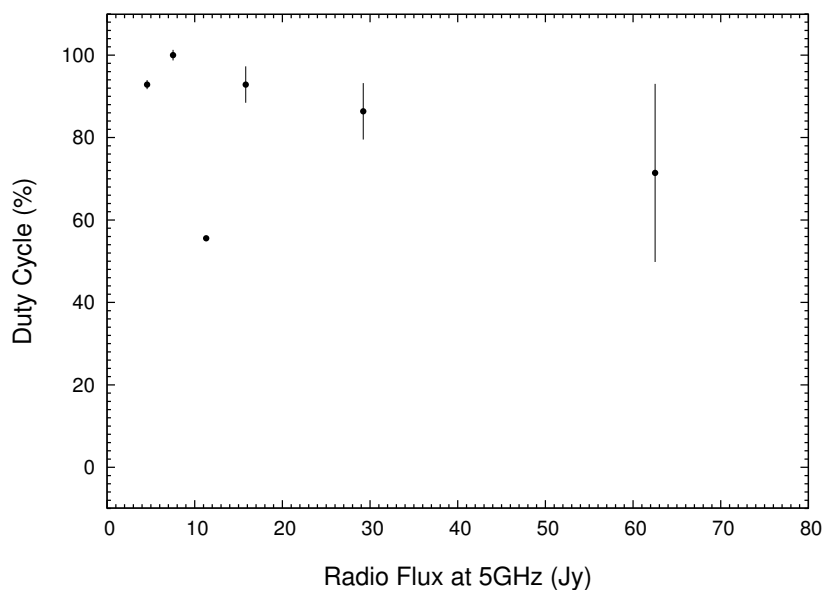


Figure 3.181: Duty cycle of LBLs versus 5 GHz radio flux as converted to the rest frame.

There appears to be no relationship between the duty cycle and either the 5GHz flux or the apparent speed of the jet in this sample of LBLs. This is a very different result from that

³The ratio of the number of nights with detected variability versus the total number of nights with microvariability observations, expressed as a percentage.

⁴NASA/IPAC Extragalactic Database, <http://nedwww.ipac.caltech.edu/>

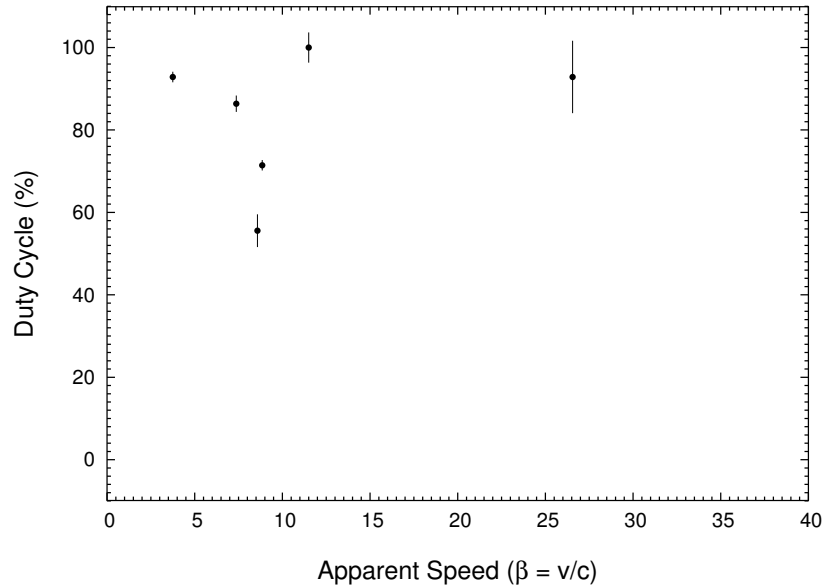


Figure 3.182: Duty cycle of LBLs versus apparent speed $\beta = v/c$.

reached by Campbell (2004), whose sample of HBLs showed a positive linear relationship with both the 5 GHz radio flux and the apparent speed.

3.4.2 Structure Function in the Rest Frame

The interpretation of the various parts of a structure function (SF) for the ideal case was introduced in §3.3.2. The interpretation of actual SFs requires small modifications of these original definitions, see e.g., Sagar et al. (2004). The minimum and maximum time-scales are best determined with an adequately sampled light curve containing temporal sampling in both of those time-scales. Because this is not likely to be achieved in nightly light curves, the time-scale(s) found will indicate *typical* time-scales for the light curve indicated by a local maximum (peaks or plateaus in an increasing part of the SF). If, however, no statistically significant (i.e., $\geq 2.6\sigma$) maxima is seen, only the lower limit of a characteristic time-scale

can be determined from the longest time lag seen.

It should be noted that the time-scales determined from the SF in the observed frame are directly related to those in the rest frame and vice versa. The conversion factor is the same used to shift the observations back into the rest frame. This is illustrated in Equation (3.11), where t_e is the time-scale in the emitted (rest) frame, t_o is the time-scale in the observed frame, and z is the redshift,

$$t_e = t_o(1 + z)^{-1} . \quad (3.11)$$

The SFs for the rest frame light curves⁵ are shown in Figure 3.183 and the values for any time-scales are summarized in Table 3.4 (shown after the figure), where columns 1, 2, and 3 are the object, UT date of the observation, and the filter in which it was observed, respectively. The values of any characteristic timescales are listed in column 4. The values of the time-scales and percent amplitudes of the variability index are listed in columns 5 and 6 respectively (see §3.4.3). All time-scales quoted are rest frame values.

Figure 3.183 displays the first order SFs of all light curves with resolved variability and large enough temporal sampling (i.e., enough observations) to adequately define the SF. For AO 0235 + 16 on the night of 13 Oct 1986, there is a clear indication of a time-scale at ~ 0.3 hours, but no similar indication on the night of 11 Nov 1987. The character of AO 0235 + 16's SF in October of 1990 shows multiple time-scales that are clearly seen in all but the first night at shorter lags as indicated by the various peaks (e.g., ~ 0.3 to 0.4 hour and $\gtrsim 1$ hour). The character of the SF of the light curves November of 1991 is different yet

⁵To remind the reader, the rest frame light curves are flux density versus time in hours.

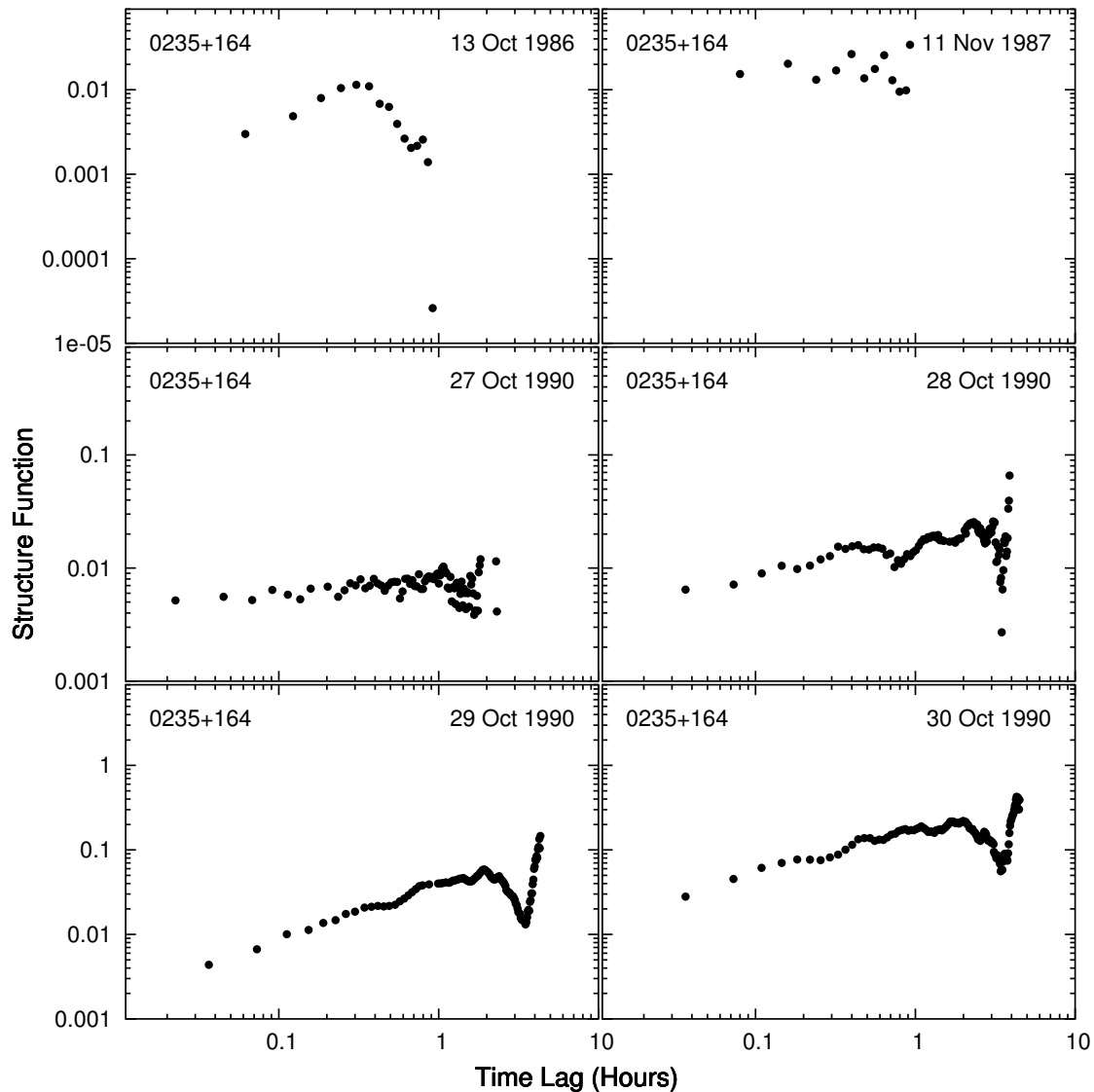


Figure 3.183: Structure functions for the light curves of all objects that showed variability and have a great enough sampling to determine time scales.

again. Most show time-scales of between ~ 0.5 and ~ 2 hours, with two time-scales on the night of 08 Nov. The SF on 25 Nov 1997 shows one time-scale at ~ 1.8 hours. The SFs on the night of 18 Oct 1998 shows a time-scale of about 0.5 hours, while the data on 19 Oct 1998 shows a hint of a similar time-scale. The SF for 13 Jan 2004 shows no time-scale.

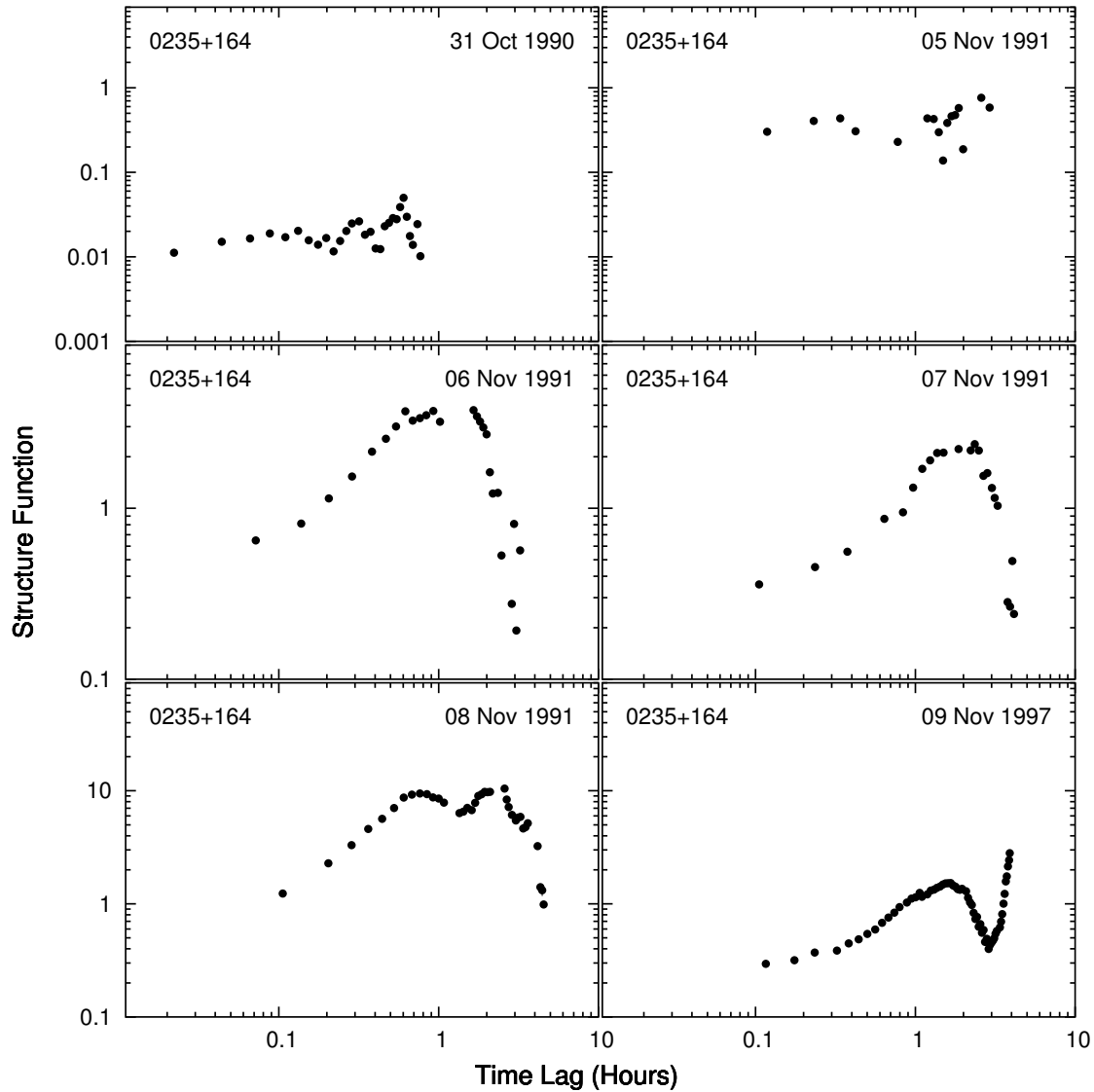


Figure 3.183 (continued)

The SFs for 1156+295 are all very similar. The nights for which they were calculated are 19 through 24 January of 1994. They all show one variability timescale. The last 2 nights are less well sampled and this is seen in the quality of the SF. The typical time-scales are on the order of 1 hour.

The SF for the night of 16 May 1997 for the object 1622 – 297 shows a time-scale around

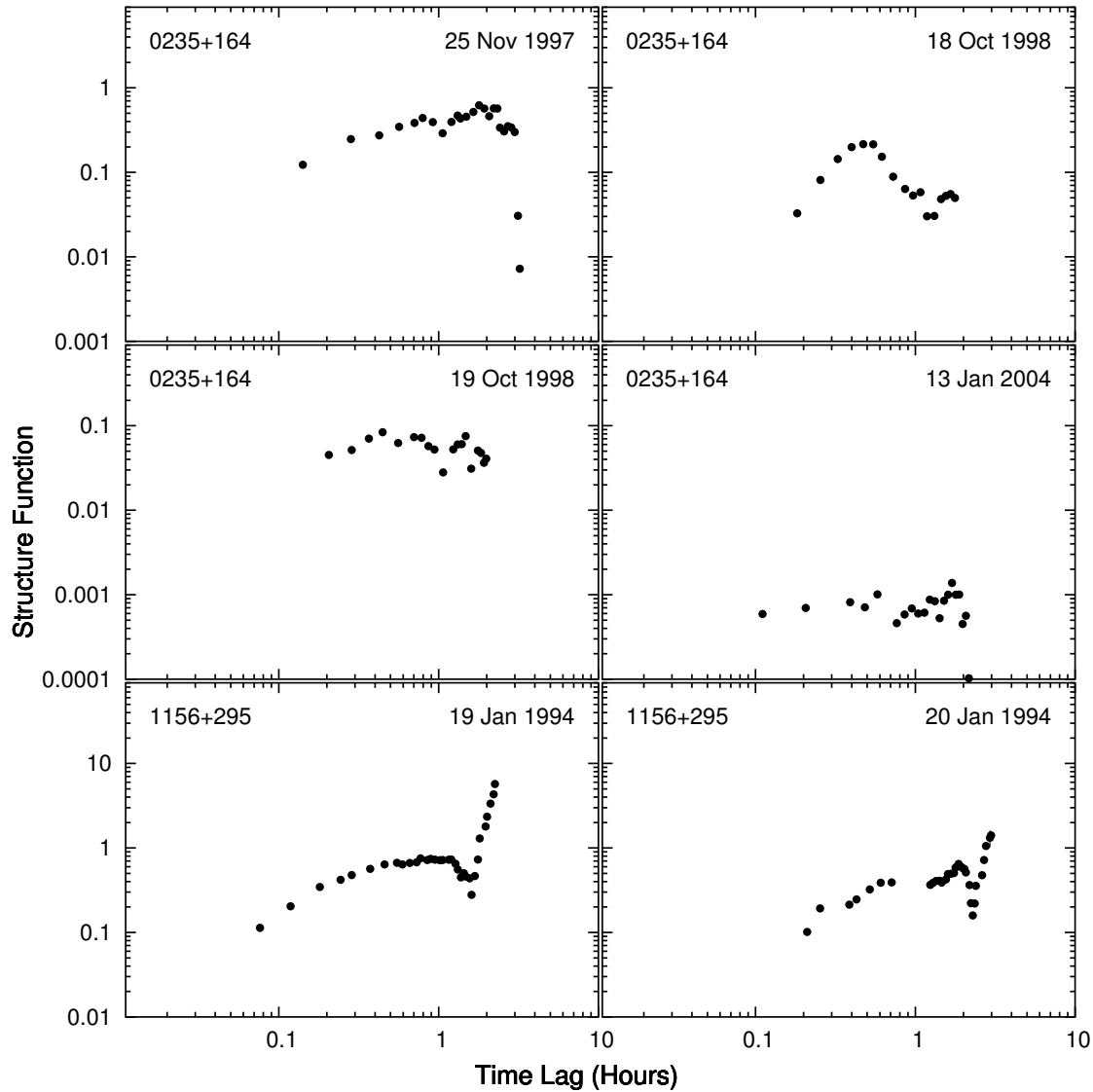


Figure 3.183 (continued)

0.5 hour. On the nights of 23, 25, and 27 Aug 1997, there are time-scales indicated for the first 2 nights of less than one hour, with no time-scale indicated for the last night.

The SF on the night of 01 Apr 1996 shows that 1633+382 has a time-scale of ~ 0.5 hour. On the night of 27 Apr 1996, the character is virtually identical, but with poorer resolution. The nights of 03 Apr 1996 and 08 Jun 2000 both show very similar character in their SF

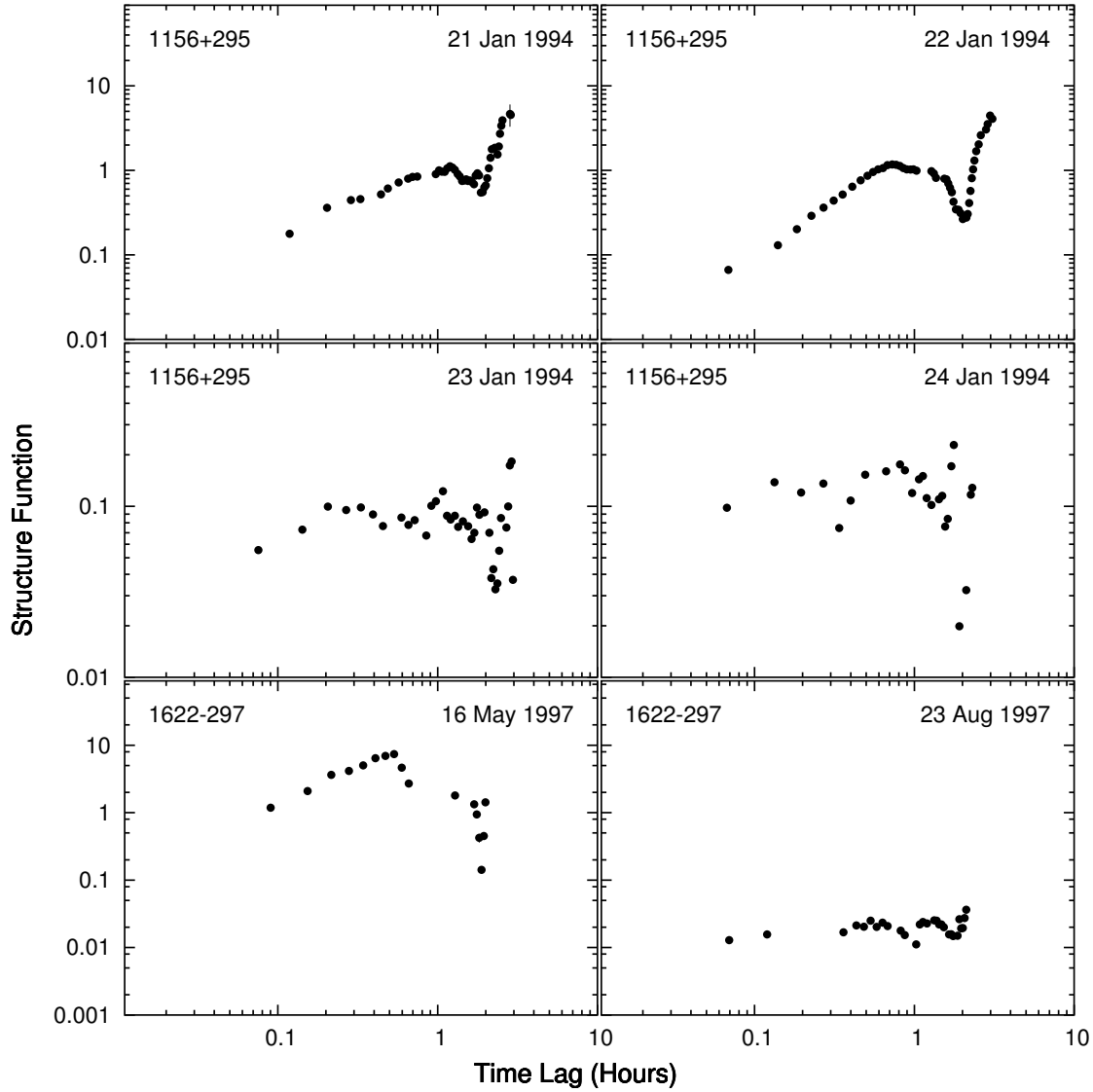


Figure 3.183 (continued)

with time-scales of $\lesssim 2$ hours. The last 2 SFs for 1633 + 382 are from the nights of 21 and 22 May 2004. They each indicate a timescale of about 0.6 and 0.9 hour, respectively.

The object 3C 345 (1641 + 399) has a generally noisier quality to its SFs which start on the night of 19 May 1997 with an indeterminate time-scale. A similar result is seen for 19 May 1998. The nights of 18 May 1998 and 14 Apr 2000 show single timescales of ~ 2 and

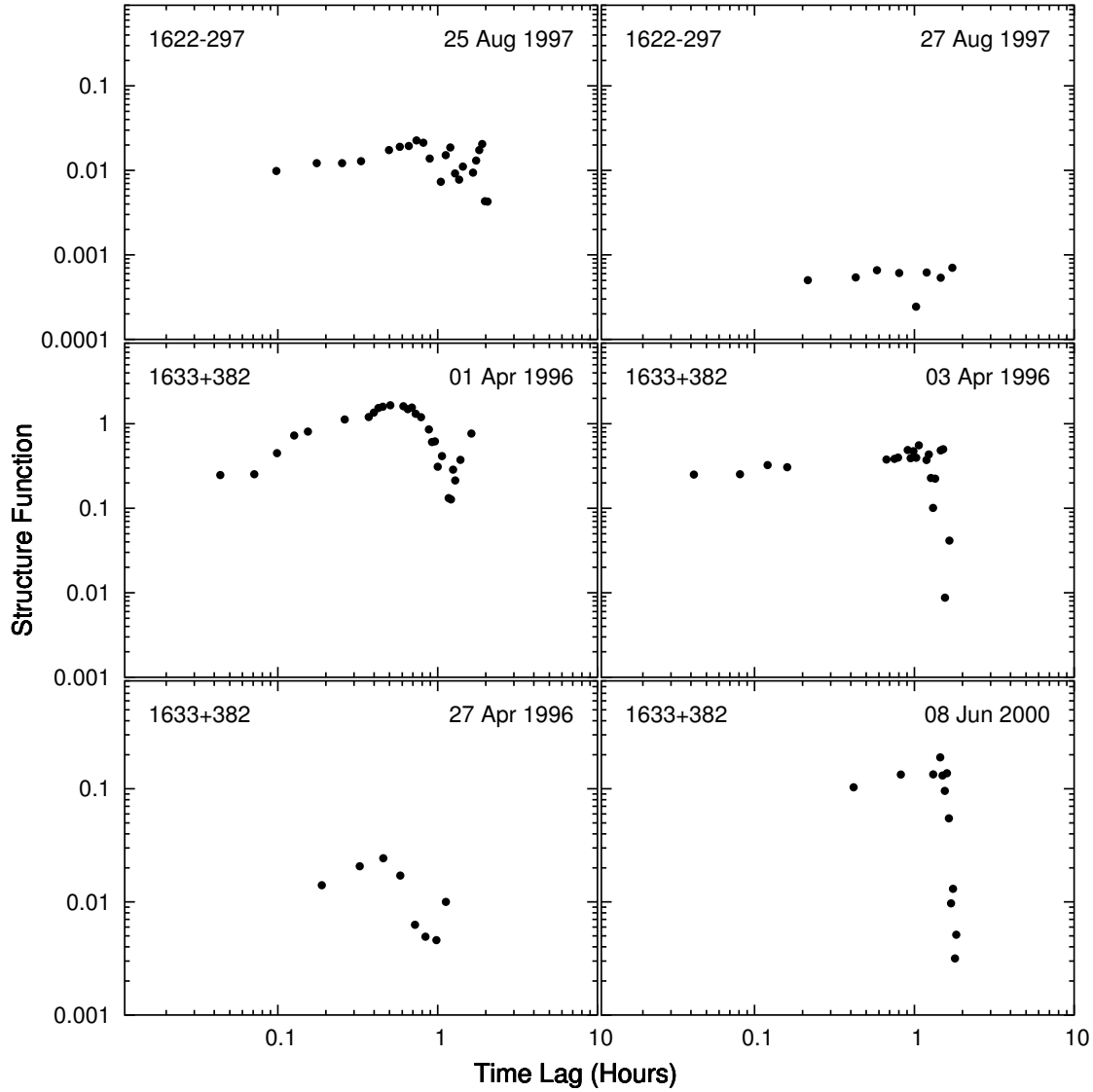


Figure 3.183 (continued)

~ 0.5 hours respectively. The SFs for the nights of 15 and 16 Apr 2000, and 21 May 2001 show time-scales $\gtrsim 1$ hour, and 17 Apr 2000 indicates no time-scale. The nights of 06 Jun 2000 and 15 Jun 2001 show time-scales of about 1.0 and 3.4 hours respectively. 3C 345 on the nights of 16, 17, and 18 Jun 2001 exhibit multiple time-scales between 0.3 and 2.5 hours. The time-scales on the nights of 20 and 21 May 2003 are indeterminate. The last SFs for 3C

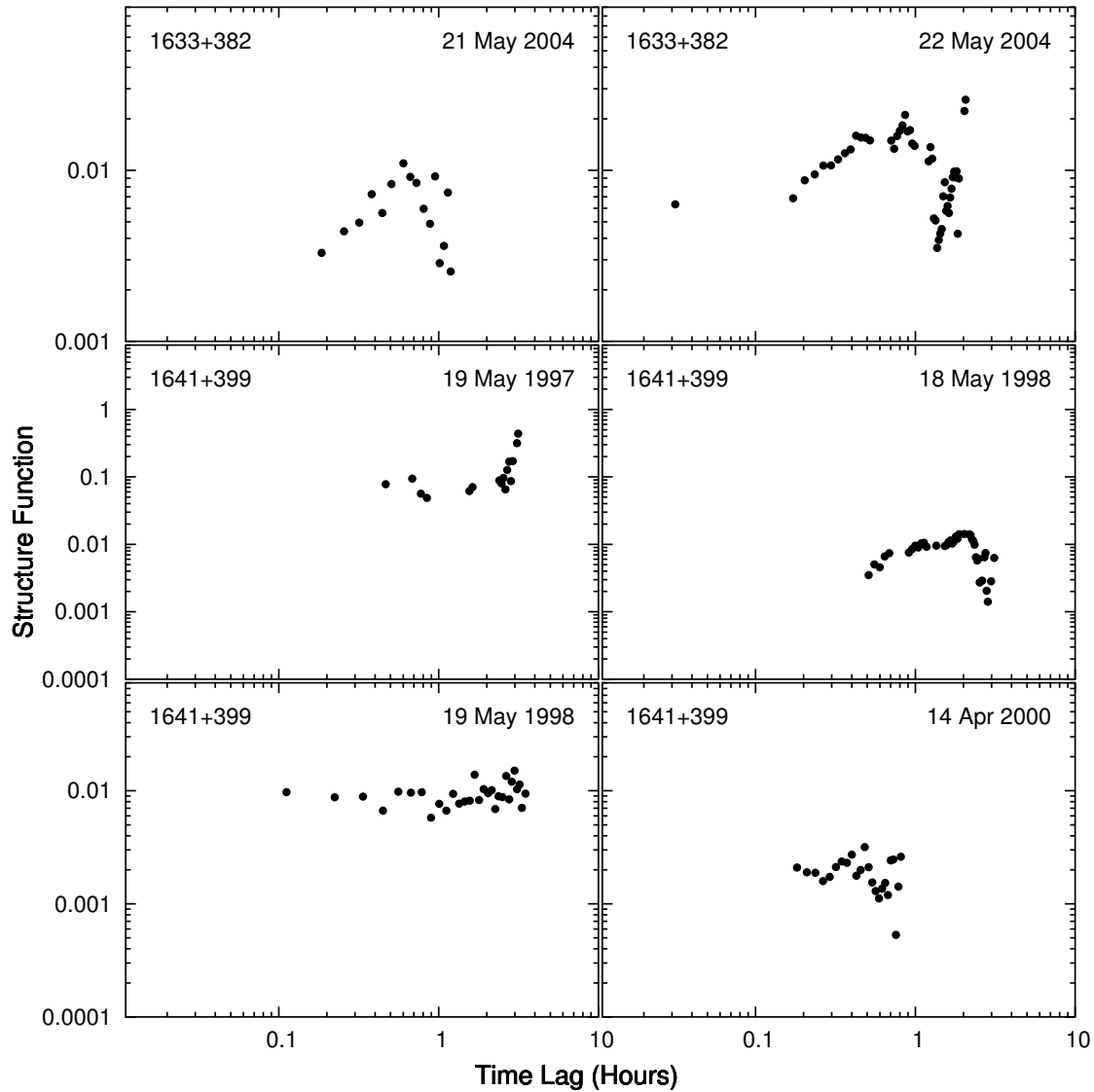


Figure 3.183 (continued)

345 are from the nights of 22, 23, and 24 May and all show different character: a possible time-scale at ~ 0.3 hours and definite one at 1.4 hours for 22 May; a timescale of 0.4 hours for 23 May; and a time-scale of 1.5 hours for 24 May.

The SFs for BL Lac (2200 + 420) are generally very well defined. Most show a definite time-scale which likely arises from BL Lac's oscillatory brightness variations. Due to the

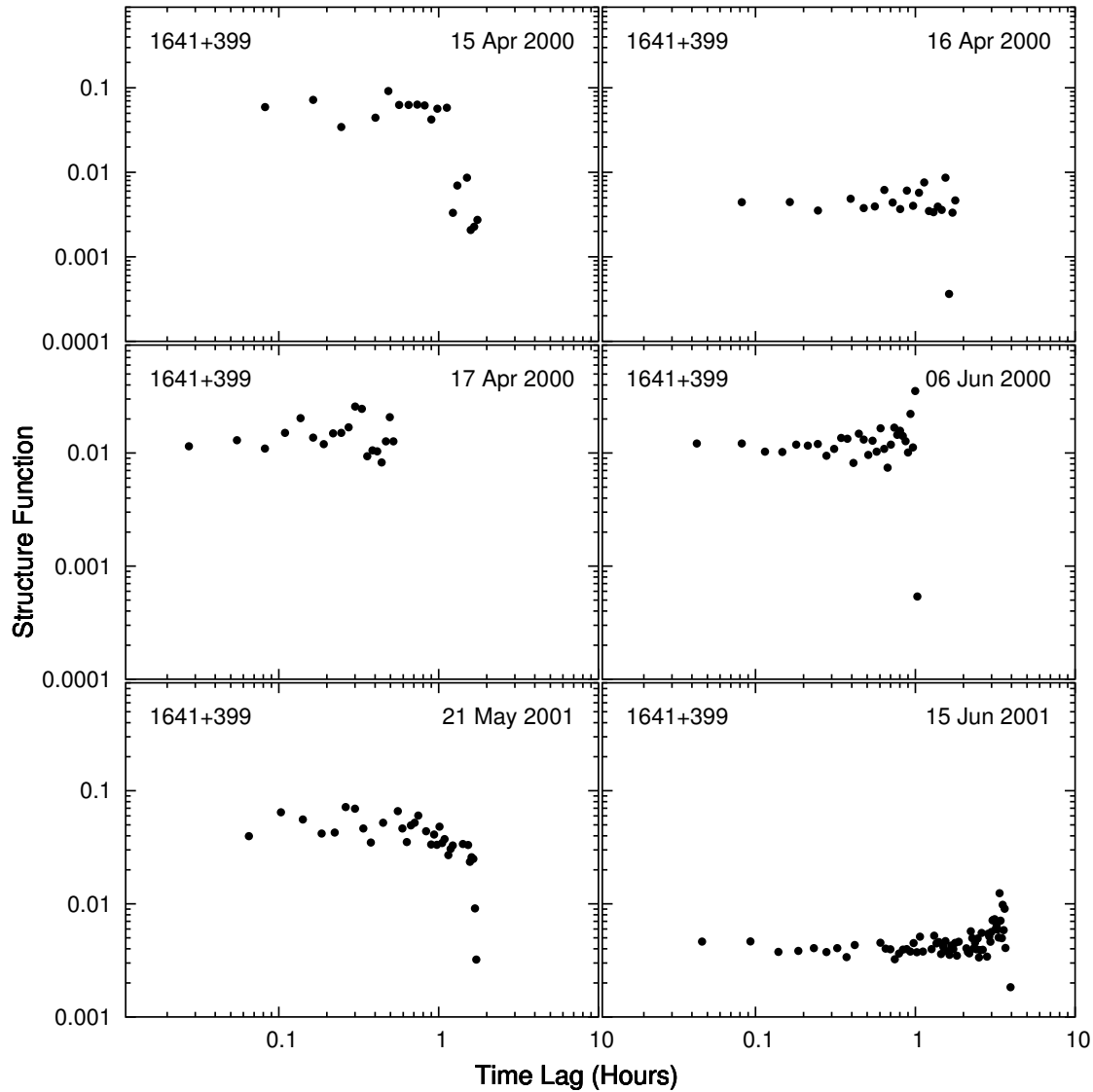


Figure 3.183 (continued)

number of SFs for this object, only a representative sample will be described in detail. The SFs for 15 Sep 1995; 29 Sep 1997; 27 Jul 1998; 20 Aug 1998; 25 Jul 2000; and 06, 08, and 11 Aug 2000 are all excellent examples of a single characteristic time-scale, typically 1-3 hours. The SF from the nights of 16 Sep 1995 and 19 Aug 1997 both show a “double” peak for the typical time-scale. This is due to the multiple events exhibited by BL Lac in those

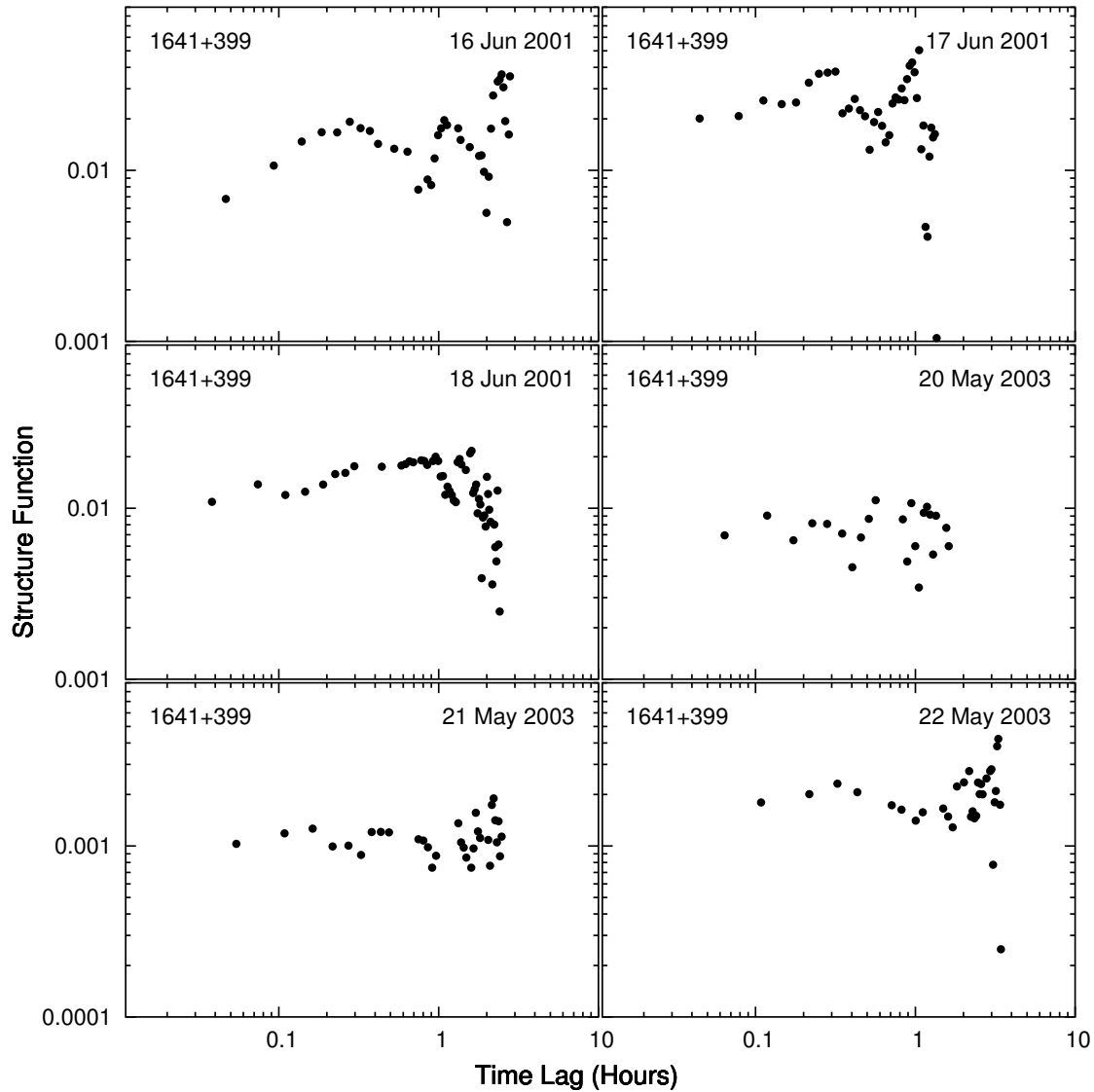


Figure 3.183 (continued)

nights. Many others show a complex character of multiple characteristic time-scales (> 2): 19 Sep 1995, 19 Aug 1998, 23 Jul 2000, and 19 Oct 2002 are all good examples of this class. The remainder of the SFs show similar character or simply indeterminate time-scales due to sparser temporal sampling or noisier data (see e.g., 18 Sep 1991 and 21 Sep 1996). Overall, BL Lac's time-scales are between 0.7 to 5.1 hours inclusively.

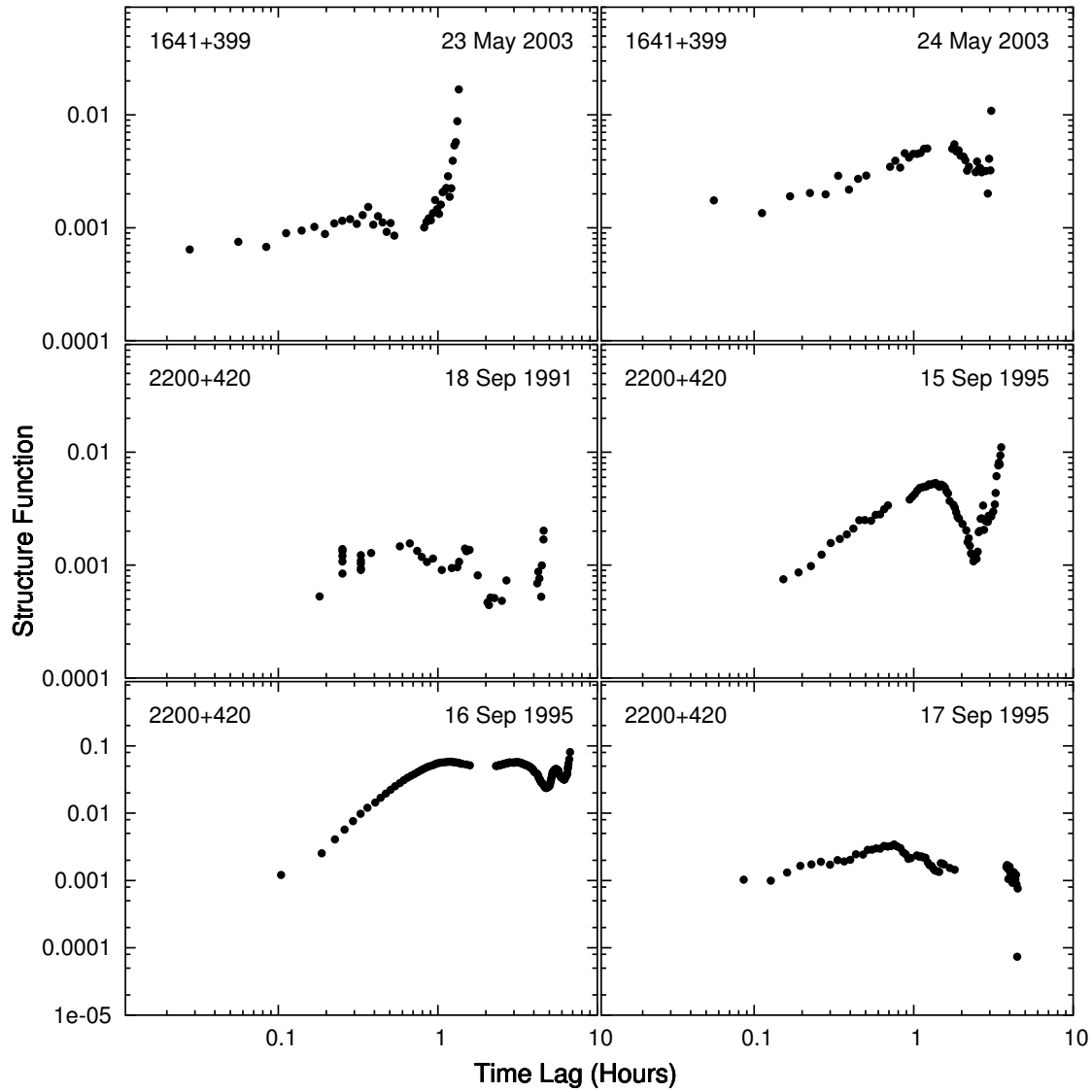


Figure 3.183 (continued)

The SF was calculated for the observations of 3C 446 (2223-052) on only the night of 05 Oct 2001, the only observations with statistically significant microvariability. The SF for this night indicates two time-scales of 0.8 and 1.8 hours.

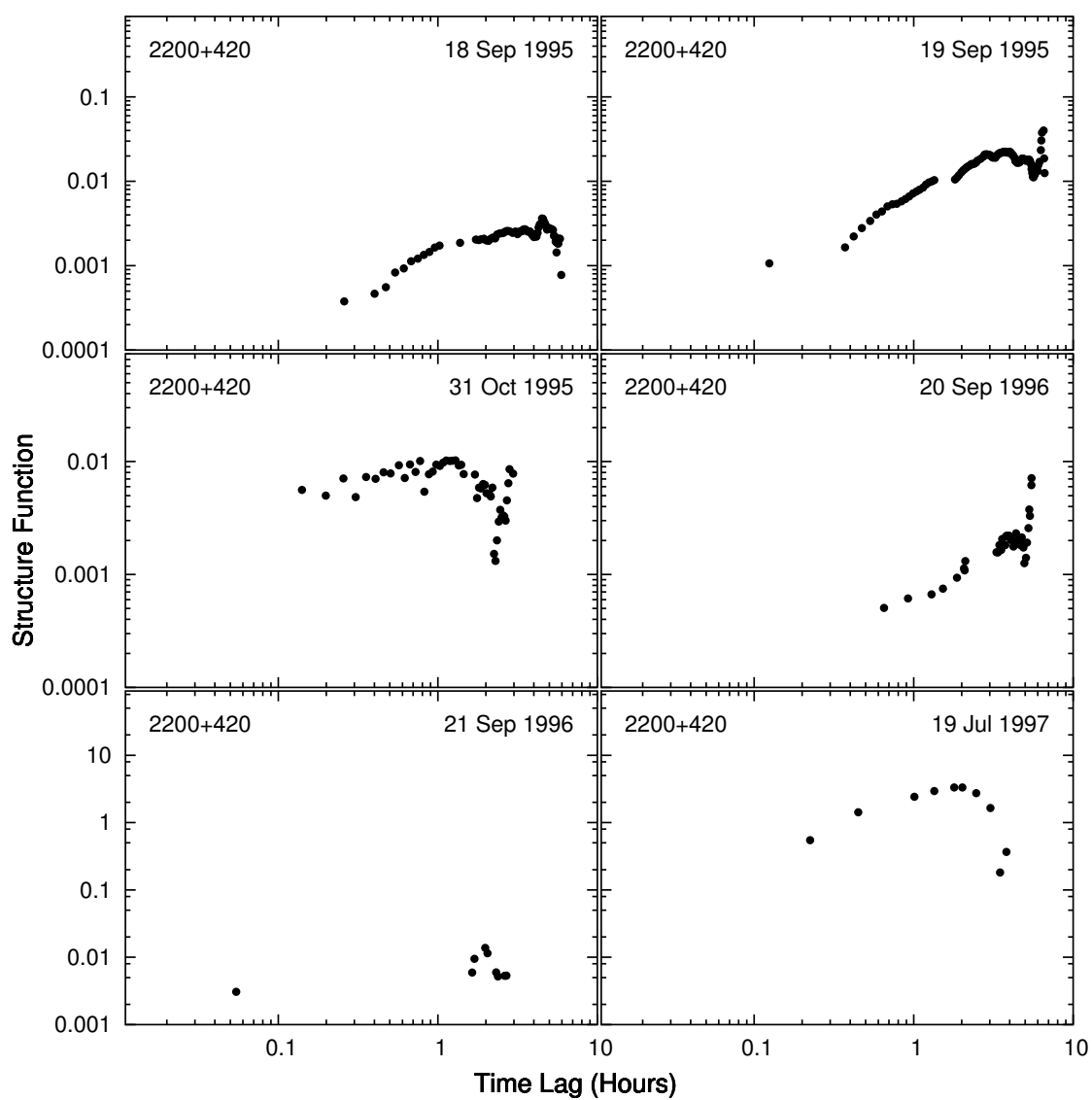


Figure 3.183 (continued)

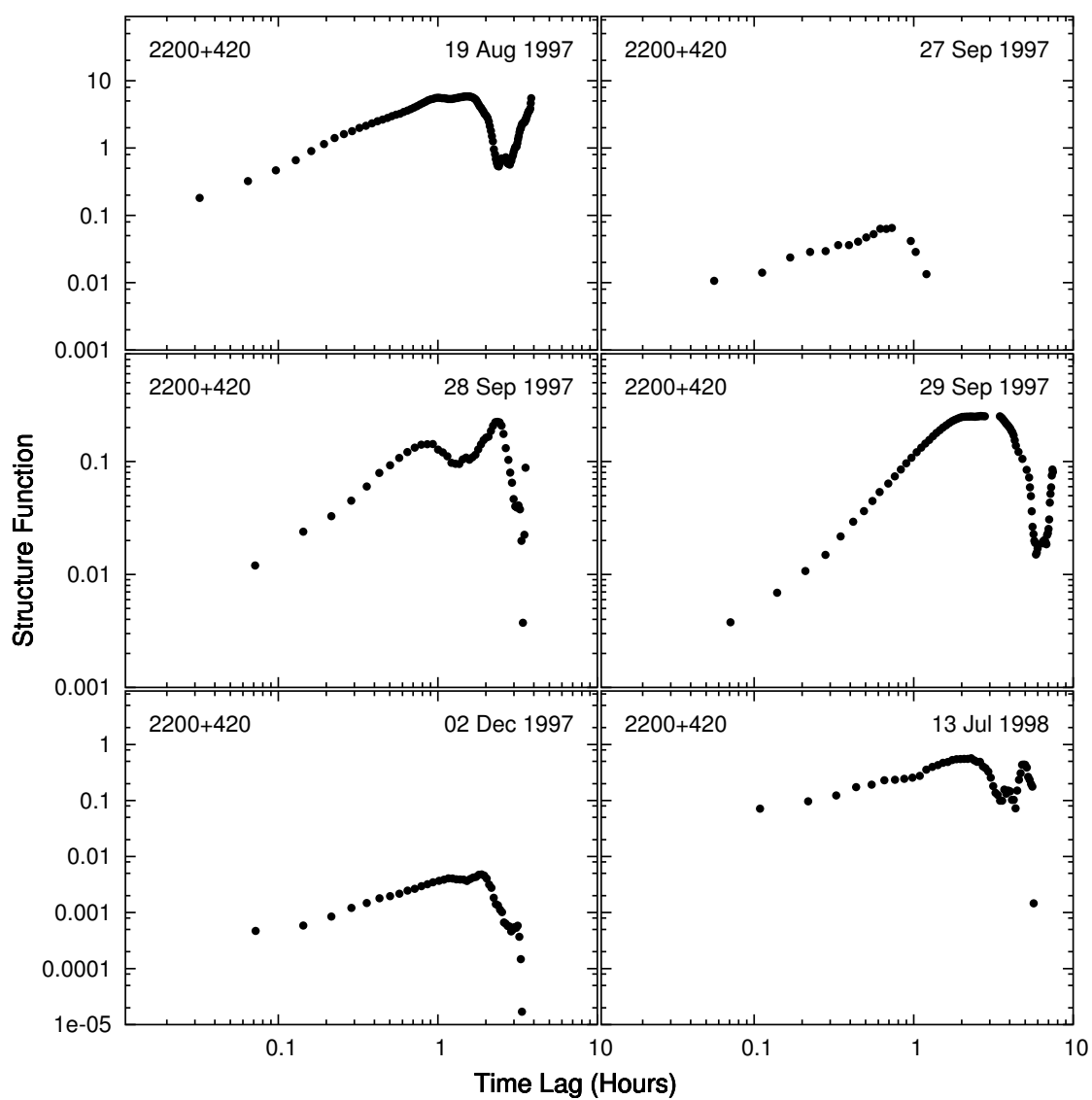


Figure 3.183 (continued)

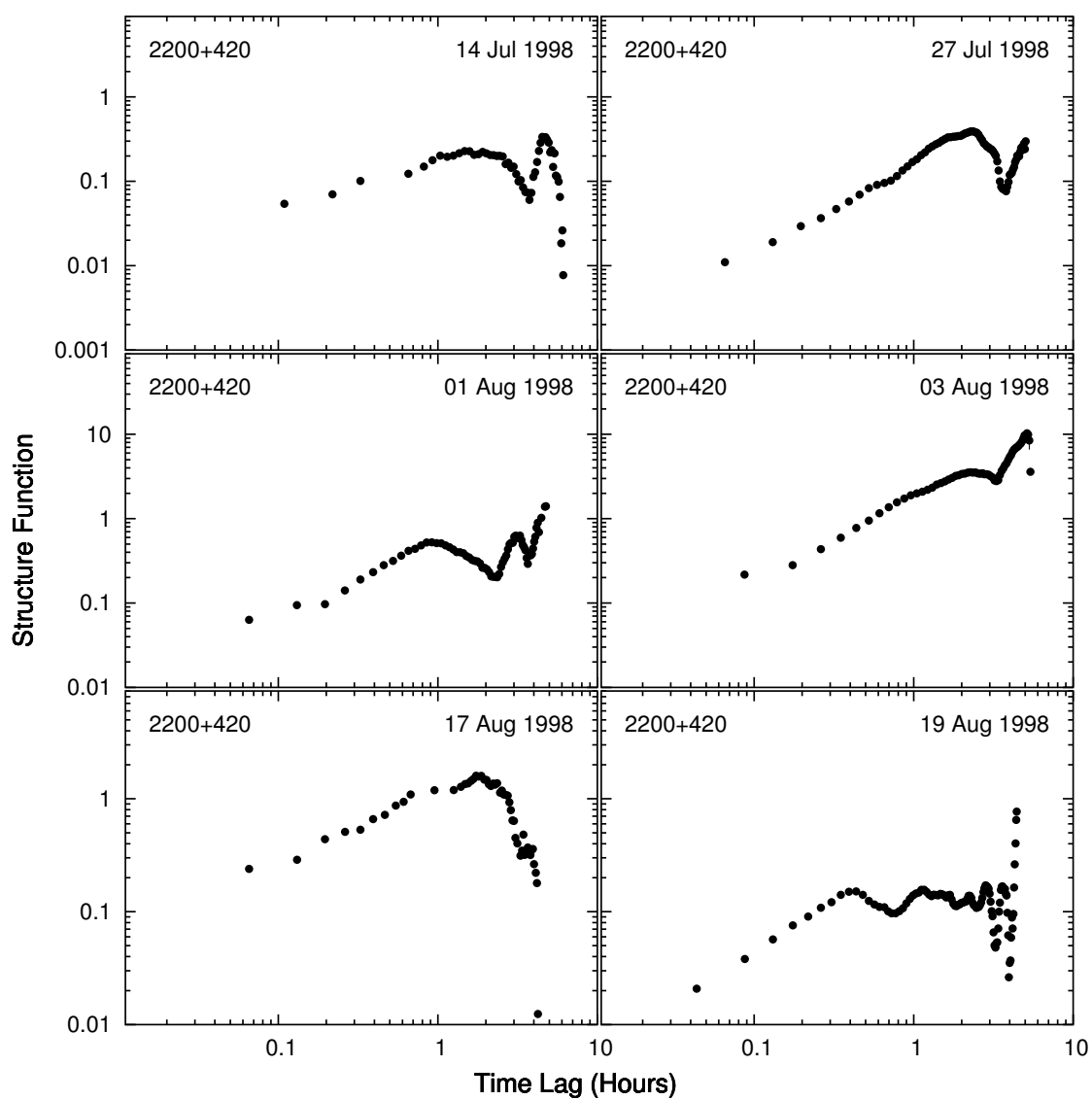


Figure 3.183 (continued)

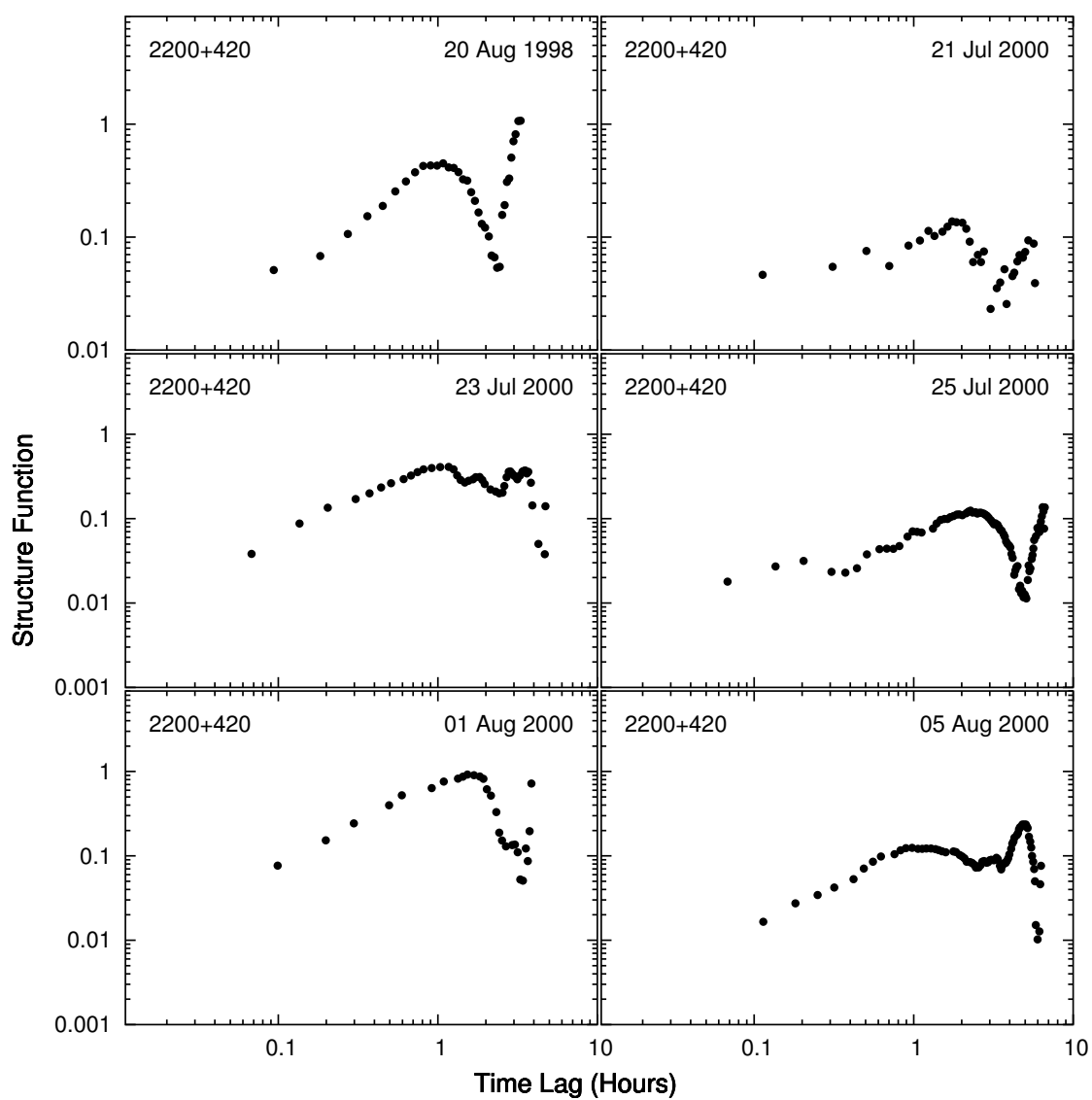


Figure 3.183 (continued)

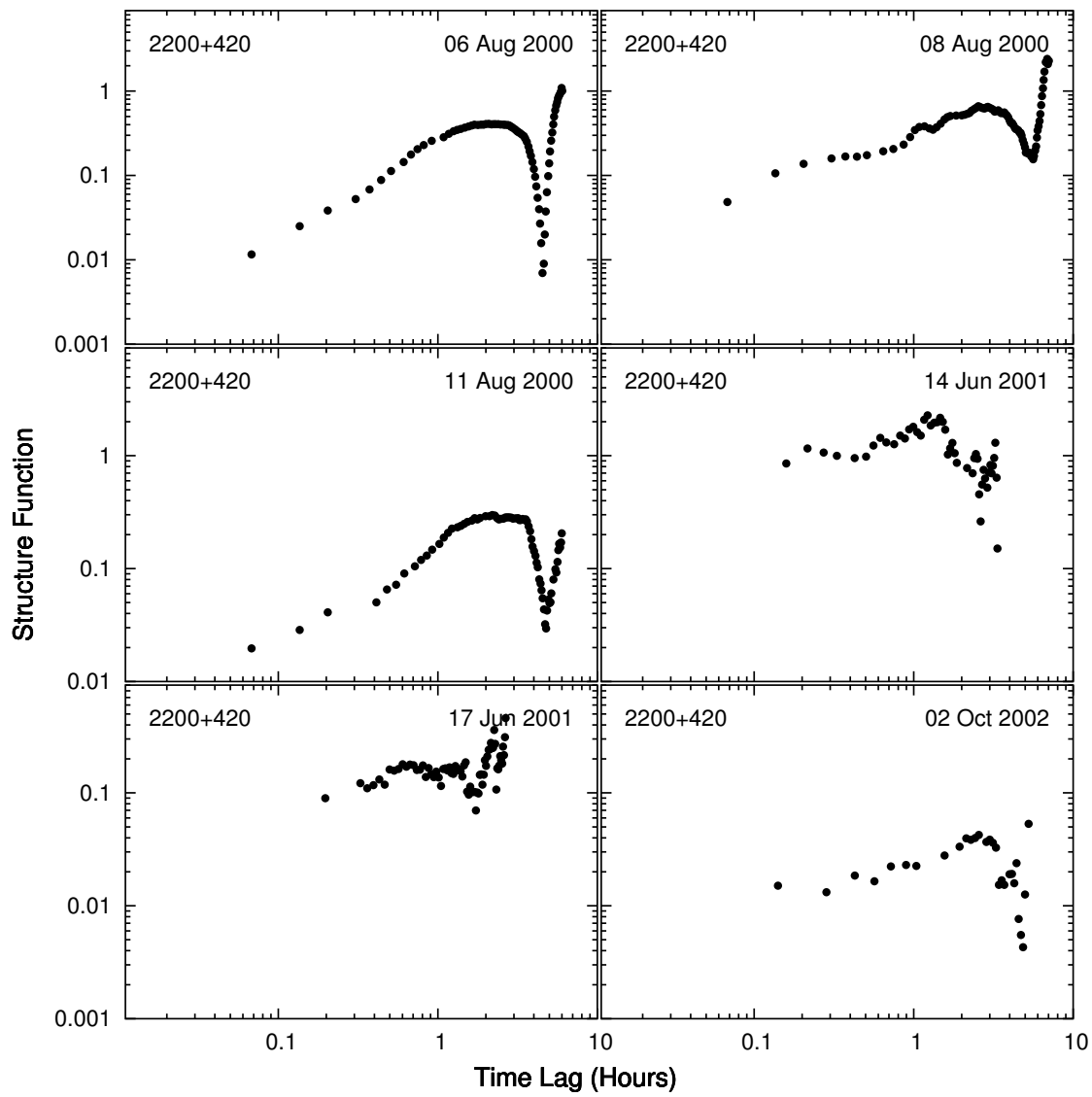


Figure 3.183 (continued)

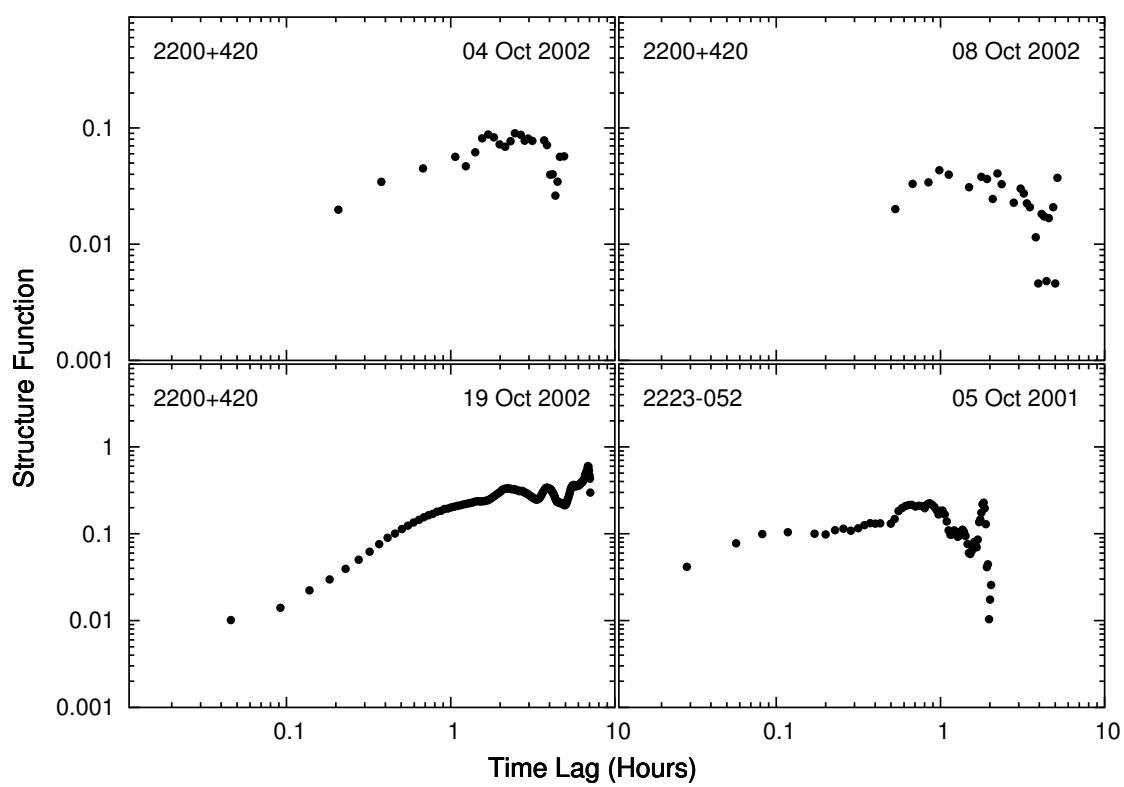


Figure 3.183 (continued)

Table 3.4: SF time-scales, VI time-scales, and VI amplitudes of variability.

| Object | UT Date | Filter | $T_{SF}(\text{hr})$ | $T_{VI}(\text{hr})$ | Amp(%) |
|------------|------------|--------|---------------------|---------------------|--------|
| 0235 + 164 | 1986 10 13 | V | 0.3 | > 0.7 | 3.0 |
| 0235 + 164 | 1987 11 11 | V | ... | > 0.9 | 9.1 |
| 0235 + 164 | 1990 10 27 | V | 1.1 | 1.6 | 2.5 |
| 0235 + 164 | 1990 10 28 | V | 0.4,1.4,2.3,3.1 | > 3.1 | 3.3 |
| 0235 + 164 | 1990 10 29 | V | 1.9 | 2.4 | 4.1 |
| 0235 + 164 | 1990 10 30 | V | 2.0 | 3.3 | 7.2 |
| 0235 + 164 | 1990 10 31 | V | 0.3,0.6 | > 0.8 | 3.0 |
| 0235 + 164 | 1991 11 05 | V | ... | > 2.9 | 1.8 |
| 0235 + 164 | 1991 11 06 | V | 1.3 | > 3.2 | 4.5 |
| 0235 + 164 | 1991 11 07 | V | 1.9 | > 4.1 | 3.5 |
| 0235 + 164 | 1991 11 08 | V | 0.8,1.9 | > 3.9 | 6.7 |
| 0235 + 164 | 1997 11 09 | V | 1.7 | > 2.9 | 41.3 |
| 0235 + 164 | 1997 11 25 | V | 1.8 | > 2.4 | 25.4 |
| 0235 + 164 | 1998 10 18 | R | 0.5 | > 1.3 | 5.6 |
| 0235 + 164 | 1998 10 19 | R | 0.5 | > 1.4 | 8.6 |
| 0235 + 164 | 2004 01 13 | R | ... | 1.8 | 3.4 |
| | | | | | |
| 1156 + 295 | 1994 01 19 | R | 0.9 | > 2.3 | 2.6 |
| 1156 + 295 | 1994 01 20 | R | 1.9 | 1.6 | 1.9 |
| 1156 + 295 | 1994 01 21 | R | 1.2 | > 2.9 | 3.1 |
| 1156 + 295 | 1994 01 22 | R | 0.7 | 3.1 | 4.1 |
| 1156 + 295 | 1994 01 23 | R | 1.1 | > 2.4 | 1.2 |
| 1156 + 295 | 1994 01 24 | R | 0.8 | 1.1 | 2.3 |
| | | | | | |
| 1622 - 297 | 1997 05 16 | R | 0.5 | > 1.5 | 45.7 |
| 1622 - 297 | 1997 08 23 | R | 0.5 | > 1.4 | 7.8 |
| 1622 - 297 | 1997 08 25 | R | 0.7 | 1.2 | 6.8 |
| 1622 - 297 | 1997 08 27 | R | ... | > 1.9 | 1.1 |
| | | | | | |
| 1633 + 382 | 1996 04 01 | R | 0.5 | > 1.1 | 8.0 |
| 1633 + 382 | 1996 04 03 | R | 1.1 | 1.2 | 8.0 |
| 1633 + 382 | 1996 04 27 | R | 0.5 | > 0.8 | 1.7 |
| 1633 + 382 | 2000 06 08 | R | 1.5 | ... | 5.7 |
| 1633 + 382 | 2004 05 21 | R | 0.6 | 1.0 | 0.9 |
| 1633 + 382 | 2004 05 22 | R | 0.9 | 1.2 | 2.1 |
| | | | | | |
| 1641 + 399 | 1997 05 19 | R | ... | 1.0 | 26.7 |
| 1641 + 399 | 1998 05 18 | R | 2.0 | > 2.5 | 1.6 |
| 1641 + 399 | 1998 05 19 | R | ... | > 3.2 | 1.5 |

Table 3.4: continued...

| Object | UT Date | Filter | $T_{SF}(\text{hr})$ | $T_{VI}(\text{hr})$ | Amp(%) |
|------------|------------|--------|---------------------|---------------------|--------|
| 1641 + 399 | 2000 04 14 | R | 0.5 | > 0.8 | 1.4 |
| 1641 + 399 | 2000 04 15 | R | 1.1 | > 1.3 | 8.1 |
| 1641 + 399 | 2000 04 16 | R | 1.6 | > 1.6 | 2.1 |
| 1641 + 399 | 2000 04 17 | R | ... | 0.4 | 4.9 |
| 1641 + 399 | 2000 06 06 | R | 1.0 | 0.7 | 3.2 |
| 1641 + 399 | 2001 05 21 | R | 1.5 | > 1.2 | 3.5 |
| 1641 + 399 | 2001 06 15 | R | 3.4 | > 3.9 | 1.4 |
| 1641 + 399 | 2001 06 16 | R | 0.3,1.1,2.5 | 0.9 | 1.5 |
| 1641 + 399 | 2001 06 17 | R | 0.3,1.1 | > 1.0 | 3.2 |
| 1641 + 399 | 2001 06 18 | R | 1.6 | 1.3 | 2.6 |
| 1641 + 399 | 2003 05 20 | R | ... | 0.8 | 3.5 |
| 1641 + 399 | 2003 05 21 | R | ... | 1.7 | 1.8 |
| 1641 + 399 | 2003 05 22 | R | 1.4 | 1.0 | 1.9 |
| 1641 + 399 | 2003 05 23 | R | 0.4 | 0.5 | 2.6 |
| 1641 + 399 | 2003 05 24 | R | 1.5 | 1.2 | 2.3 |
| | | | | | |
| 2200 + 420 | 1991 09 18 | V | 0.7 | 3.9 | 1.9 |
| 2200 + 420 | 1995 09 15 | R | 1.4 | 2.3 | 2.3 |
| 2200 + 420 | 1995 09 16 | R | 1.2,3.1 | 4.4 | 8.0 |
| 2200 + 420 | 1995 09 17 | R | 0.8 | > 4.0 | 2.7 |
| 2200 + 420 | 1995 09 18 | R | 4.5 | 4.0 | 2.3 |
| 2200 + 420 | 1995 09 19 | R | 3.8 | > 6.6 | 6.6 |
| 2200 + 420 | 1995 10 31 | R | 1.3 | 1.2 | 4.7 |
| 2200 + 420 | 1996 09 20 | R | 4.4 | > 5.5 | 1.9 |
| 2200 + 420 | 1996 09 21 | R | ... | > 2.7 | 1.9 |
| 2200 + 420 | 1997 07 19 | R | 1.8 | 2.6 | 5.5 |
| 2200 + 420 | 1997 08 19 | R | 1.6 | 2.1 | 13.0 |
| 2200 + 420 | 1997 09 27 | V | 0.7 | 0.8 | 4.7 |
| 2200 + 420 | 1997 09 28 | V | 0.9,2.4 | 2.7 | 12.8 |
| 2200 + 420 | 1997 09 29 | R | 2.6 | > 7.5 | 8.5 |
| 2200 + 420 | 1997 12 02 | V | 1.9 | 1.8 | 6.0 |
| 2200 + 420 | 1998 07 13 | R | 2.3 | > 4.8 | 4.8 |
| 2200 + 420 | 1998 07 14 | R | 1.5,4.5 | > 5.9 | 3.1 |
| 2200 + 420 | 1998 07 27 | R | 2.3 | 2.4 | 6.0 |
| 2200 + 420 | 1998 08 01 | R | 0.9,3.3 | > 4.3 | 8.6 |
| 2200 + 420 | 1998 08 03 | R | 2.3,5.1 | > 5.4 | 18.9 |
| 2200 + 420 | 1998 08 17 | R | 1.7 | 1.1 | 17.0 |
| 2200 + 420 | 1998 08 19 | R | 0.4,1.2,2.8,3.6 | > 3.3 | 5.5 |
| 2200 + 420 | 1998 08 20 | R | 1.1 | 2.2 | 5.6 |
| 2200 + 420 | 2000 07 21 | R | 1.8 | 3.0 | 5.2 |
| 2200 + 420 | 2000 07 23 | R | 1.2,1.8,2.9 | 2.2 | 7.6 |

Table 3.4: continued...

| Object | UT Date | Filter | $T_{SF}(\text{hr})$ | $T_{VI}(\text{hr})$ | Amp(%) |
|------------|------------|--------|---------------------|---------------------|--------|
| 2200 + 420 | 2000 07 25 | R | 2.3 | > 4.6 | 4.7 |
| 2200 + 420 | 2000 08 01 | R | 1.5 | 2.0 | 9.0 |
| 2200 + 420 | 2000 08 05 | R | 1.0,5.1 | 3.1 | 6.7 |
| 2200 + 420 | 2000 08 06 | R | 2.1 | 4.4 | 9.4 |
| 2200 + 420 | 2000 08 08 | R | 2.5 | > 6.9 | 12.3 |
| 2200 + 420 | 2000 08 11 | R | 2.2 | 4.2 | 7.4 |
| 2200 + 420 | 2001 06 14 | R | 1.3 | 1.7 | 7.5 |
| 2200 + 420 | 2001 06 17 | R | 0.6,1.5,2.7 | > 2.7 | 3.8 |
| 2200 + 420 | 2002 10 02 | R | 2.6 | 3.7 | 2.1 |
| 2200 + 420 | 2002 10 04 | R | 1.7,2.5 | > 4.9 | 3.3 |
| 2200 + 420 | 2002 10 08 | R | 1.0 | > 3.2 | 2.1 |
| 2200 + 420 | 2002 10 19 | R | 2.2,3.8 | > 7.1 | 7.8 |
| 2223 - 052 | 2001 10 05 | R | 0.8,1.8 | > 2.0 | 5.6 |

3.4.3 Variability Index in the Rest Frame

The results of the variability index (VI) tests indicate overwhelmingly that both the frequency and amplitude of variability increase with observing interval (time window). This is indicated by the fact that *all* plots of VI versus time window show a positive slope. This result is sound regardless of the reference frame and state.

The VI changes little in character when observations are transformed into the rest frame. This is expected because the character of the observations do not change, only the amplitudes and time scales. The only change seen is the difference in variability time-scale as transformed by Equation (3.11), the same factor by which the observations were transformed. The amplitude of the VI does not change simply because it measures fractional changes which are constant under the transform of the observations into the rest frame.

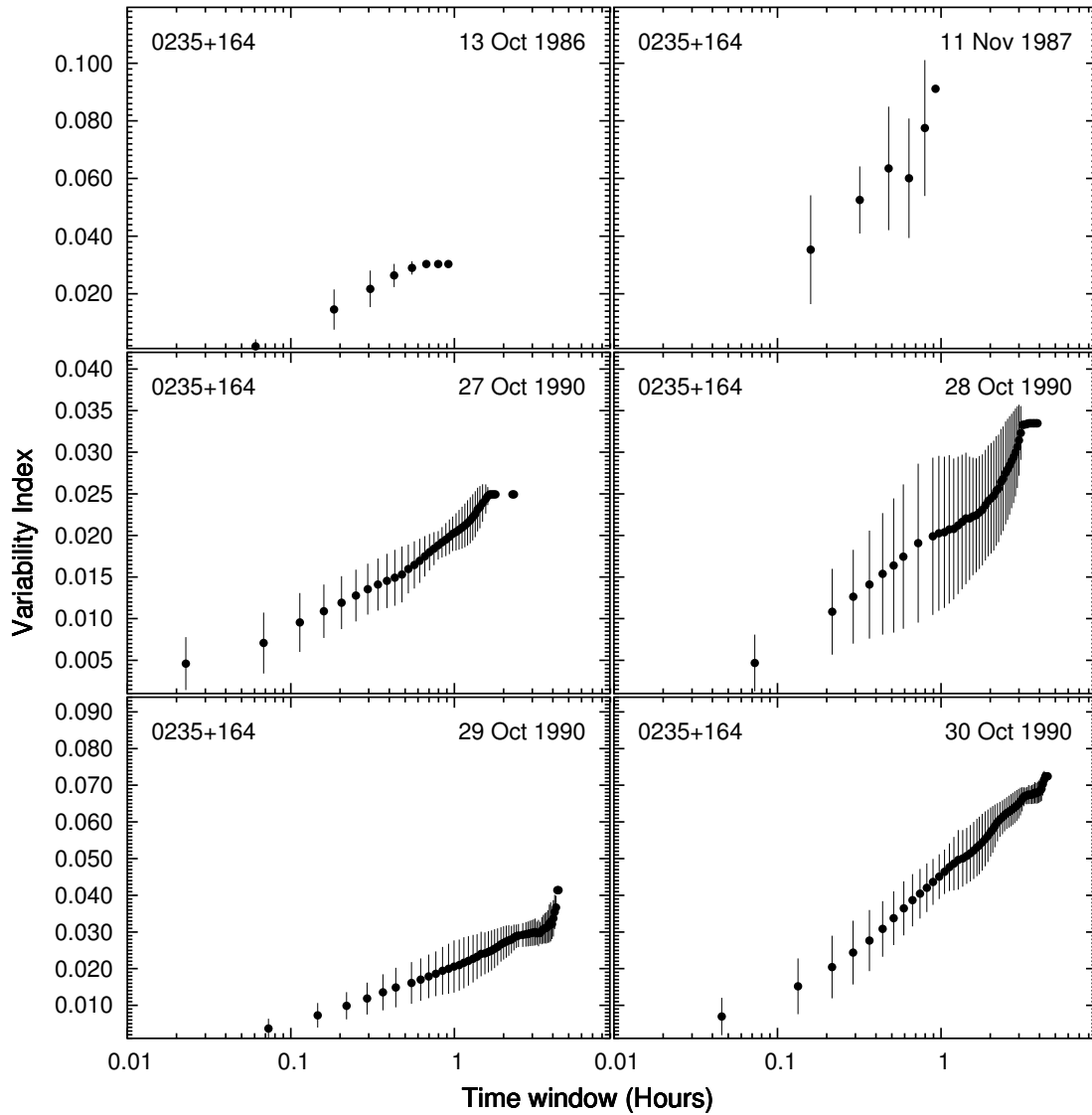


Figure 3.184: Variability indexes for the light curves of all objects for which structure functions were calculated.

Figure 3.184 displays the VIs of all light curves with resolved variability and large enough temporal sampling (i.e., enough observations) to adequately define the VI. This is the same subset used for the SF plots. It should be noted that the error bars simply give an indication of the scatter of the VI values within a particular time window. Large “scatter” bars at small

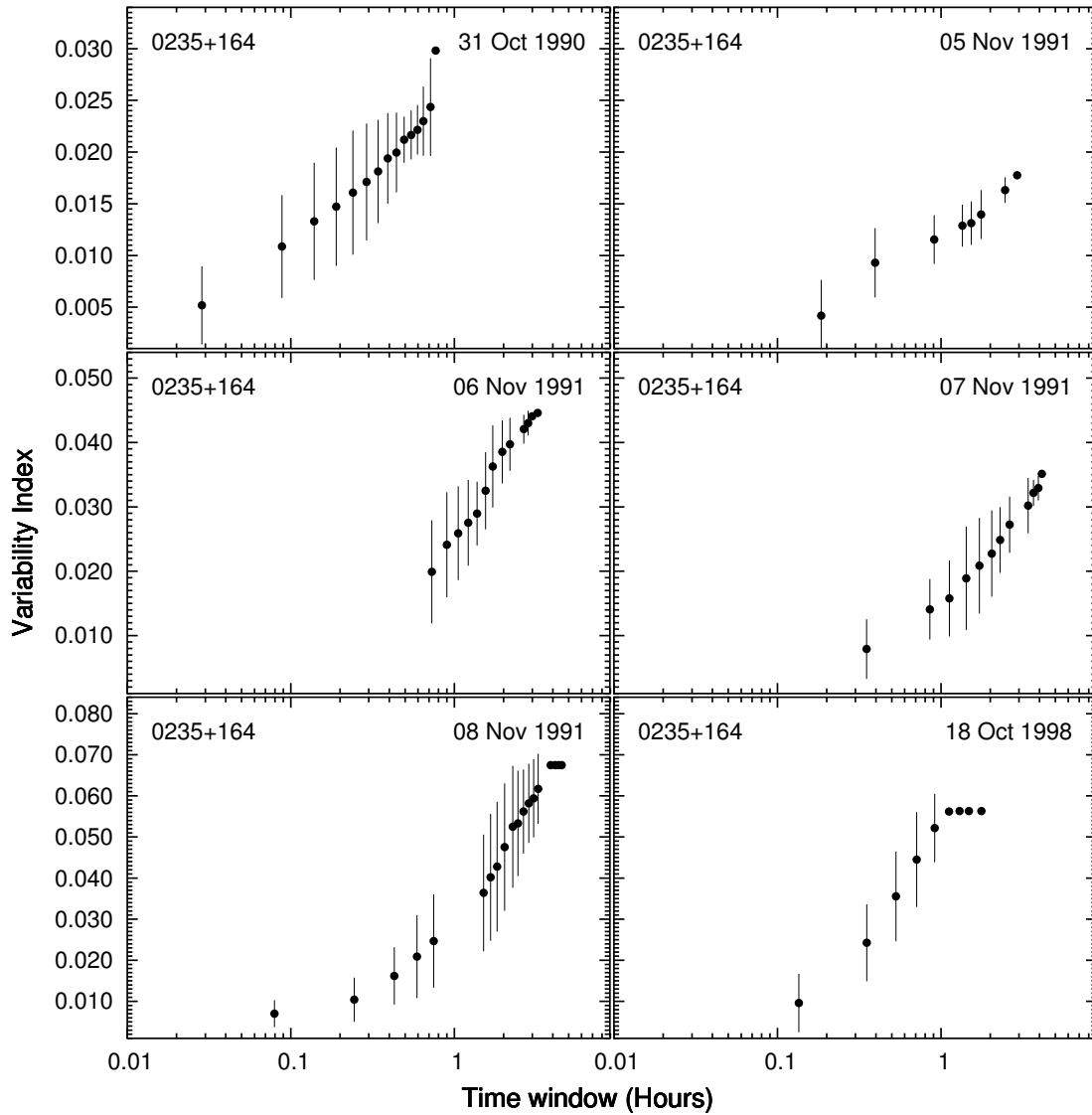


Figure 3.184 (continued)

time windows indicate low S/N (noisy) observations and may provide an indication of the true error of the dataset. At larger time windows, they are more indicative of the amount of variability in the light curve. In many cases, the VI curve ends in a plateau without variation or scatter. This is due to the time window exceeding the temporal difference between the maximum and minimum flux in the dataset, and should not be considered significant.

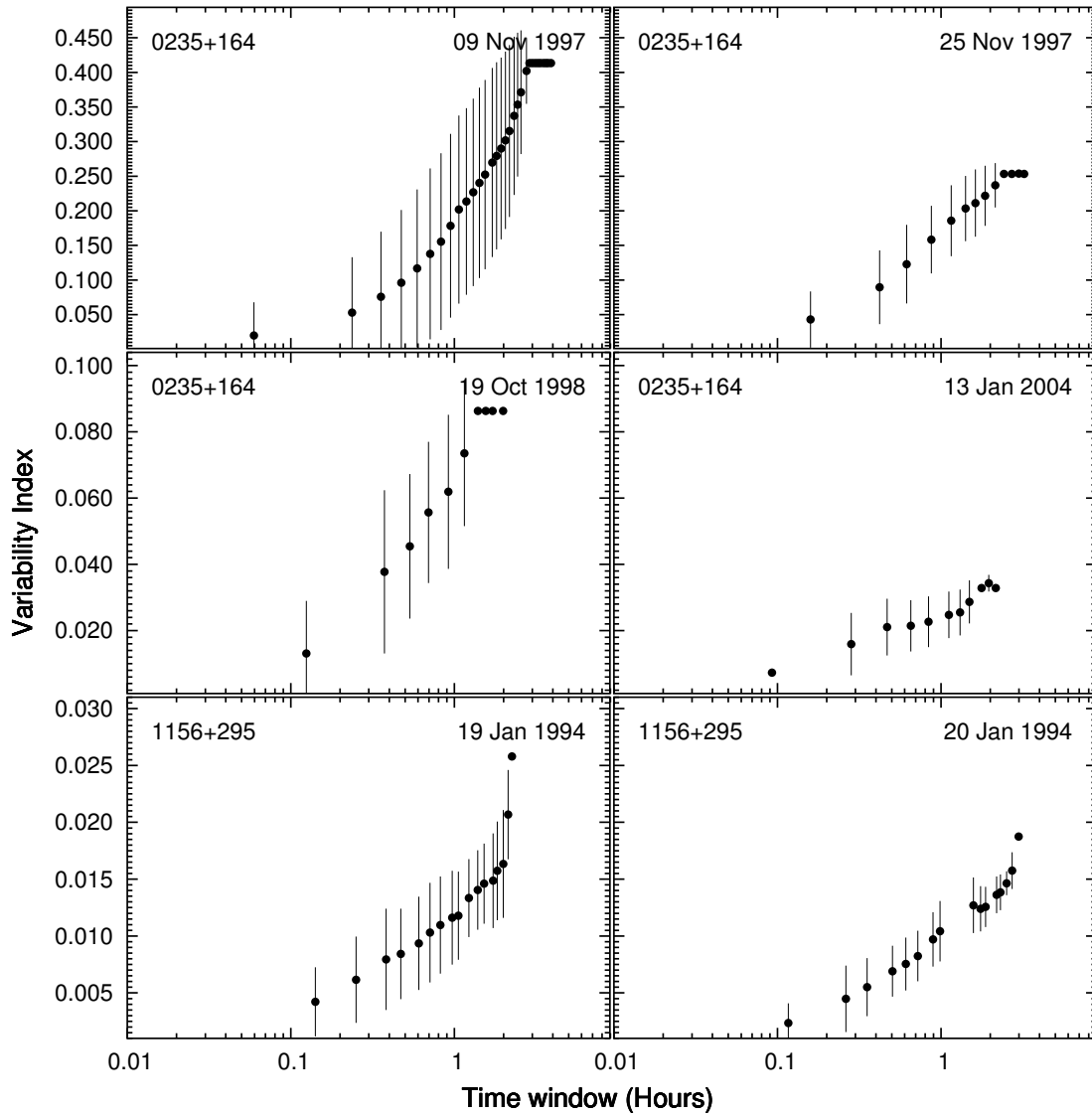


Figure 3.184 (continued)

The interpretation of the VI is similar to the structure function (SF) in that any turnover of a monotonically increasing function can be interpreted as a variability time-scale (e.g., the turnover at 1.5 hours for the night of 27 Oct 1990 for AO 0235 + 16) and a lack of one indicates either unresolved variability within the duration of the observations, or a time-scale that exceeds the duration of the observations (e.g., the night of 07 Nov 1991 for AO

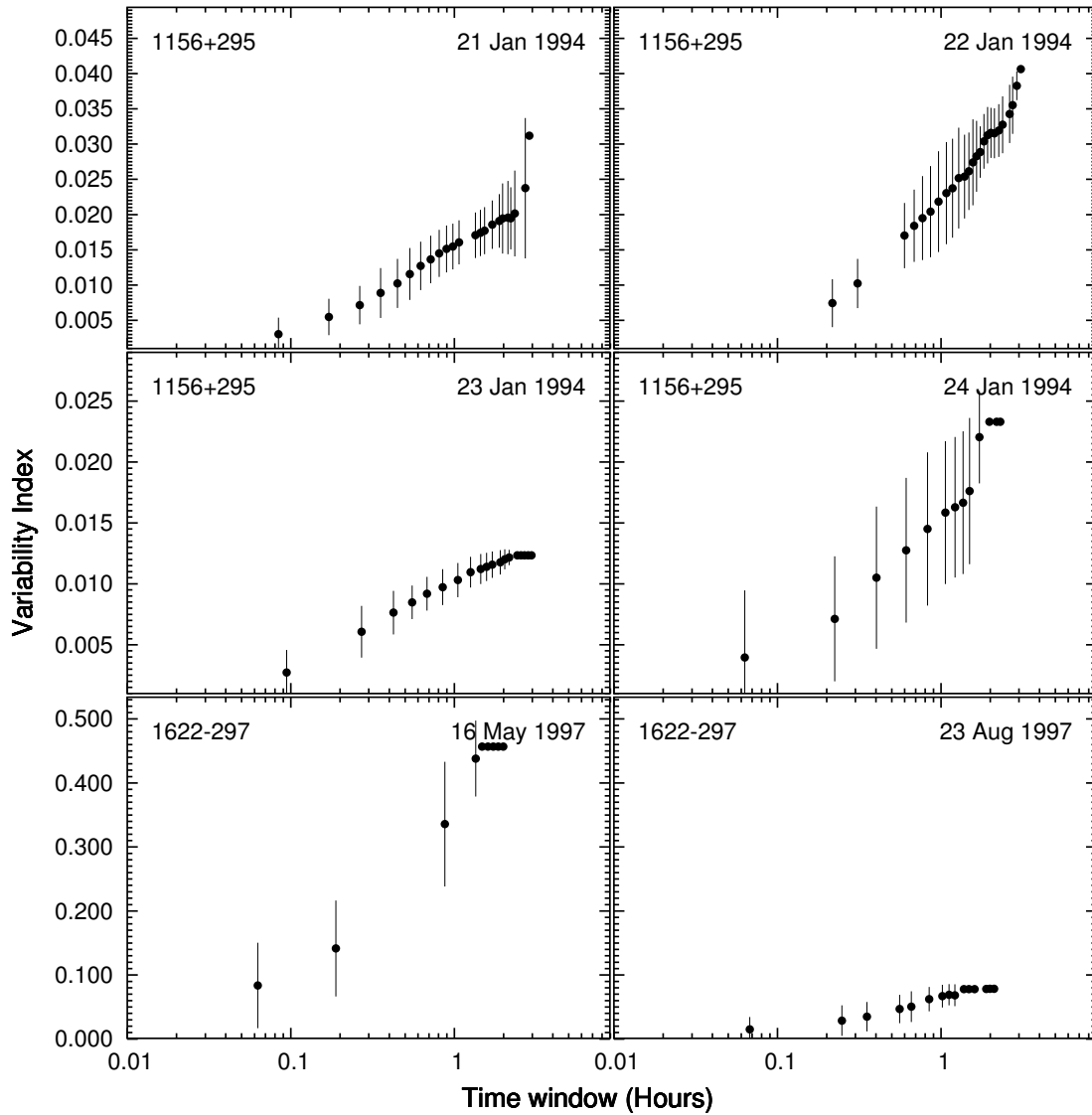


Figure 3.184 (continued)

0235 + 16). There is an exception to this rule in that multiple, well defined time-scales may not always be resolved with the VI. The primary example for this is on the night of 19 Aug 1998 for the object BL Lac (2200 + 420). The SF clearly shows many time-scales of variability, but the VI does not. In this case, the turnover at large time window would indicate only one of the time-scales.

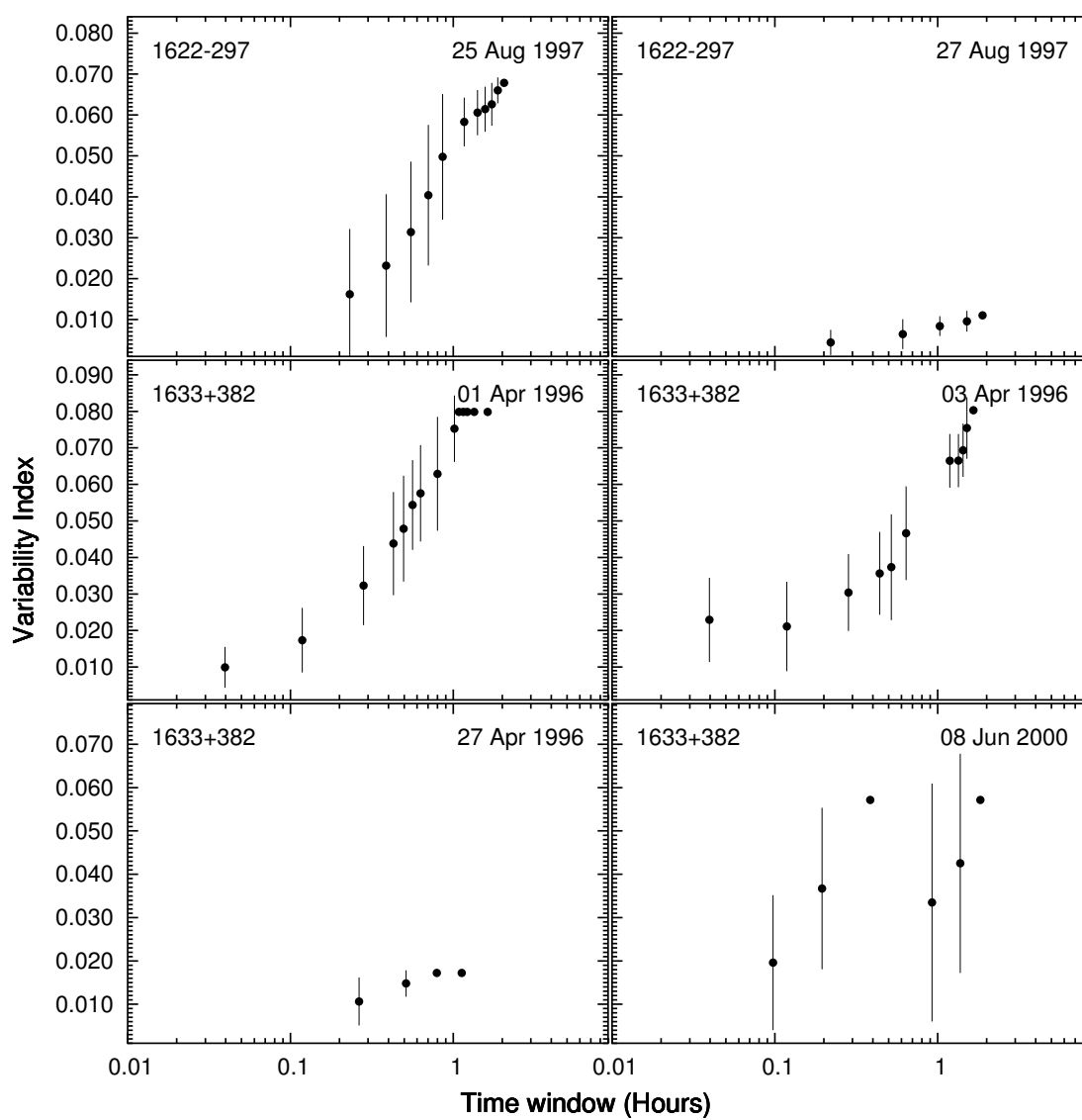


Figure 3.184 (continued)

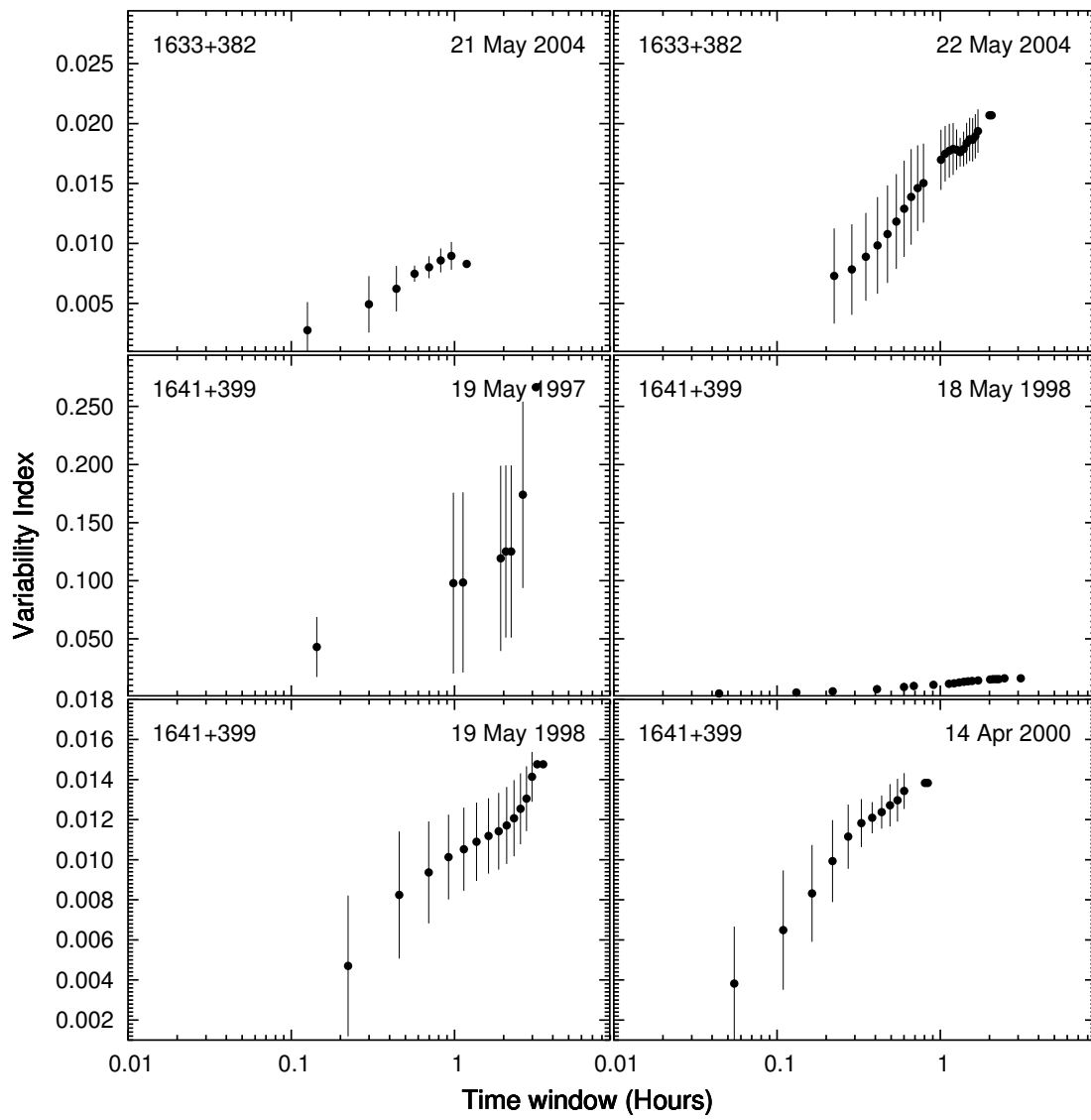


Figure 3.184 (continued)

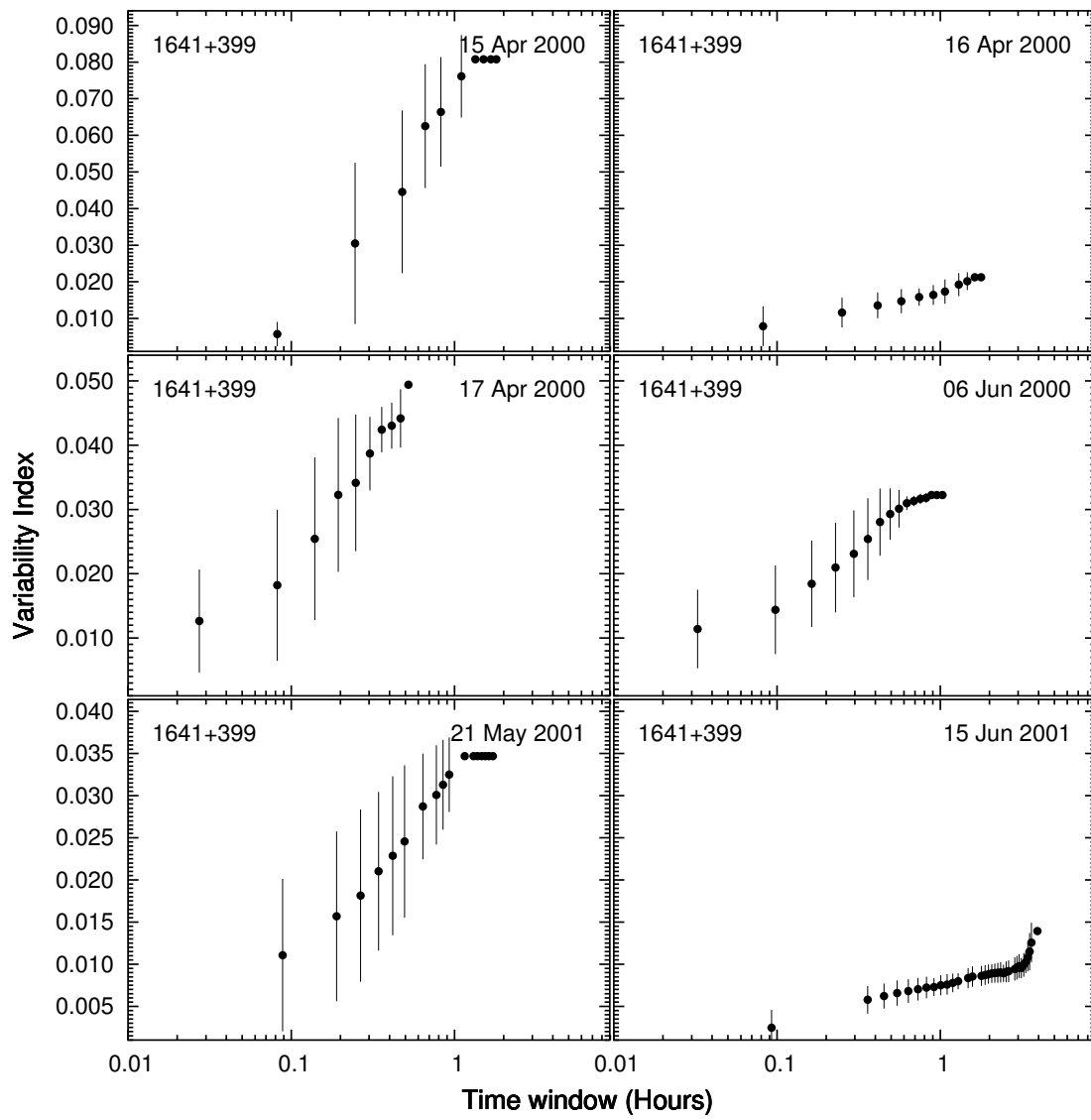


Figure 3.184 (continued)

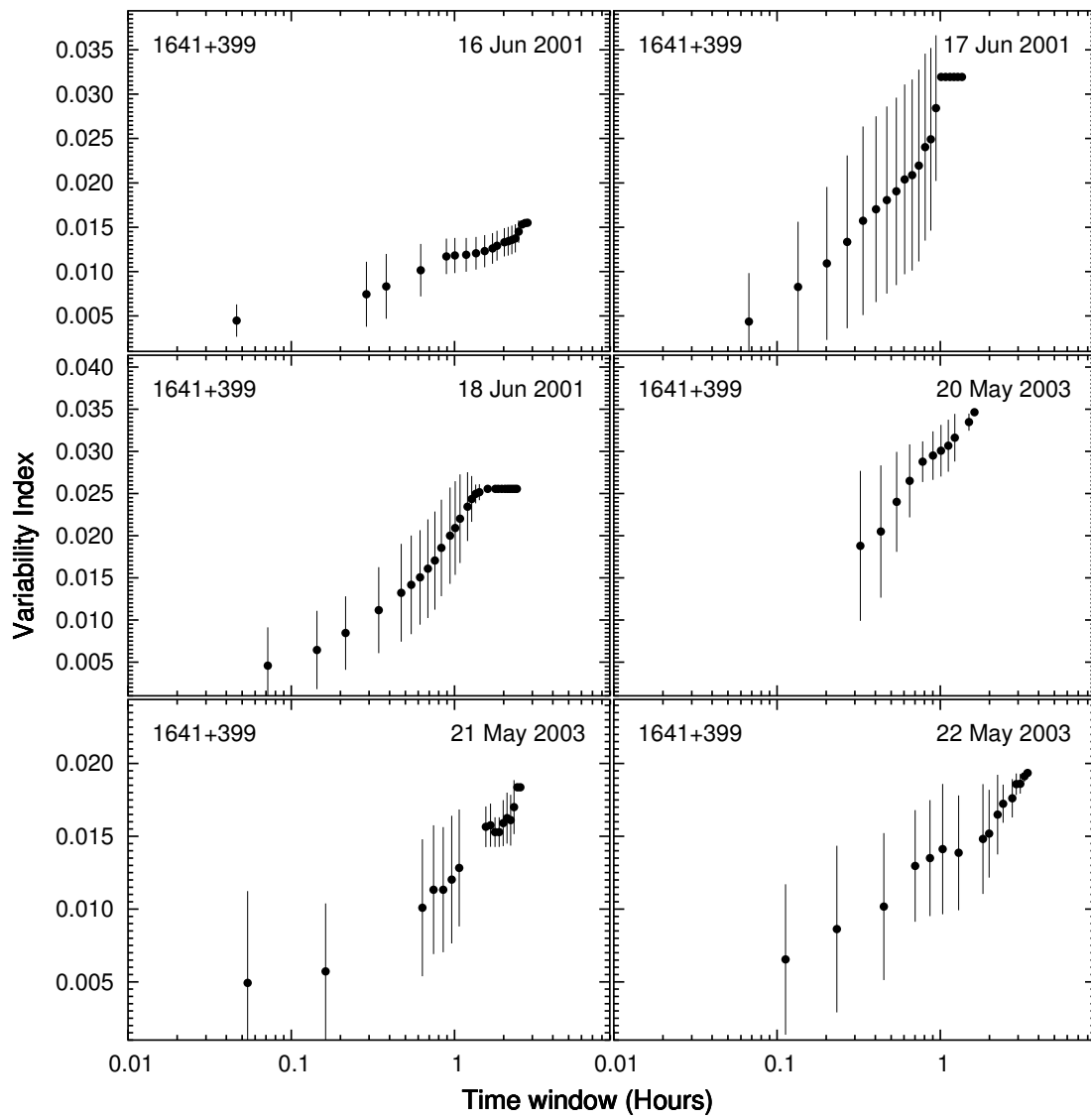


Figure 3.184 (continued)

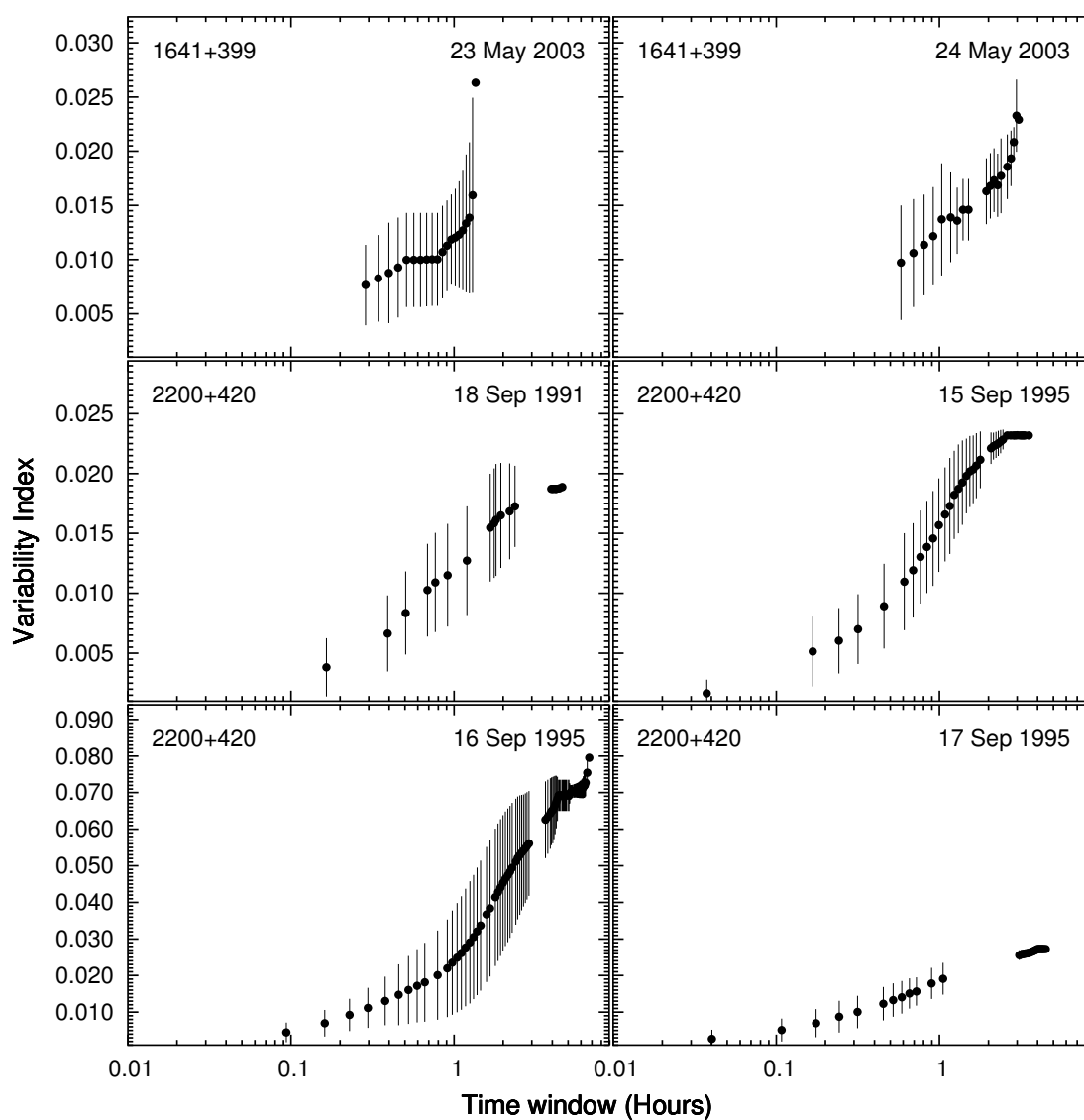


Figure 3.184 (continued)

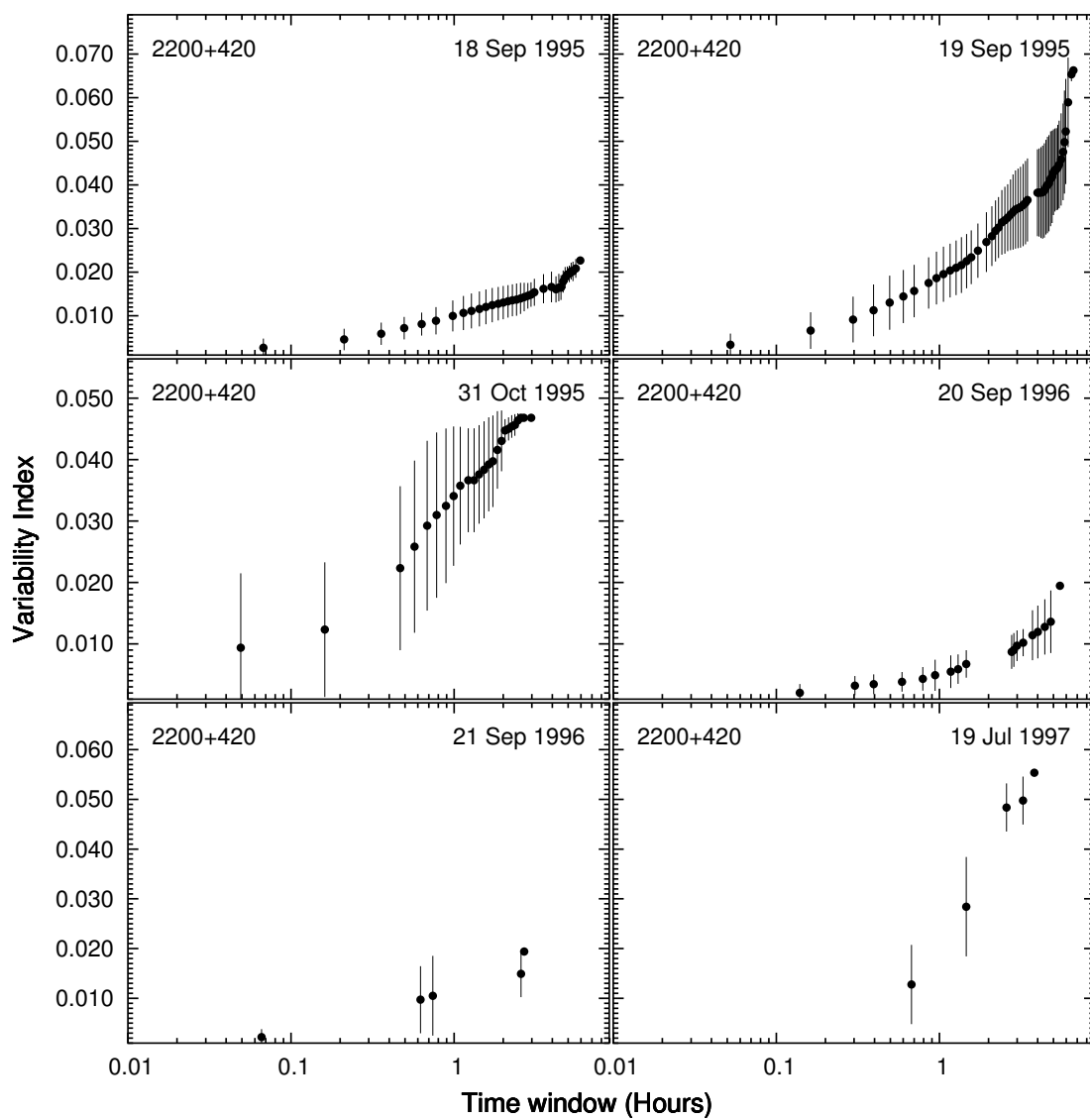


Figure 3.184 (continued)

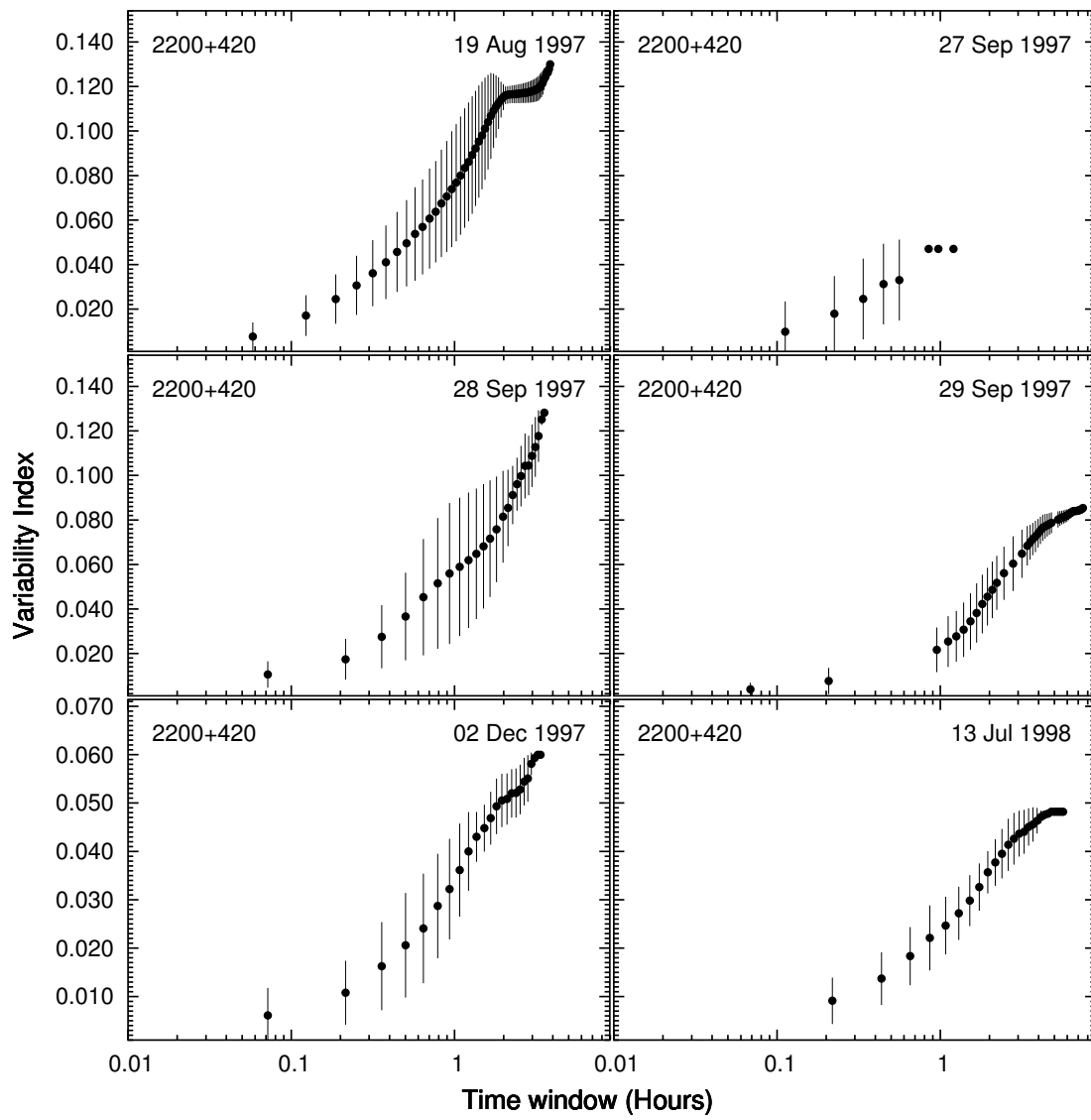


Figure 3.184 (continued)

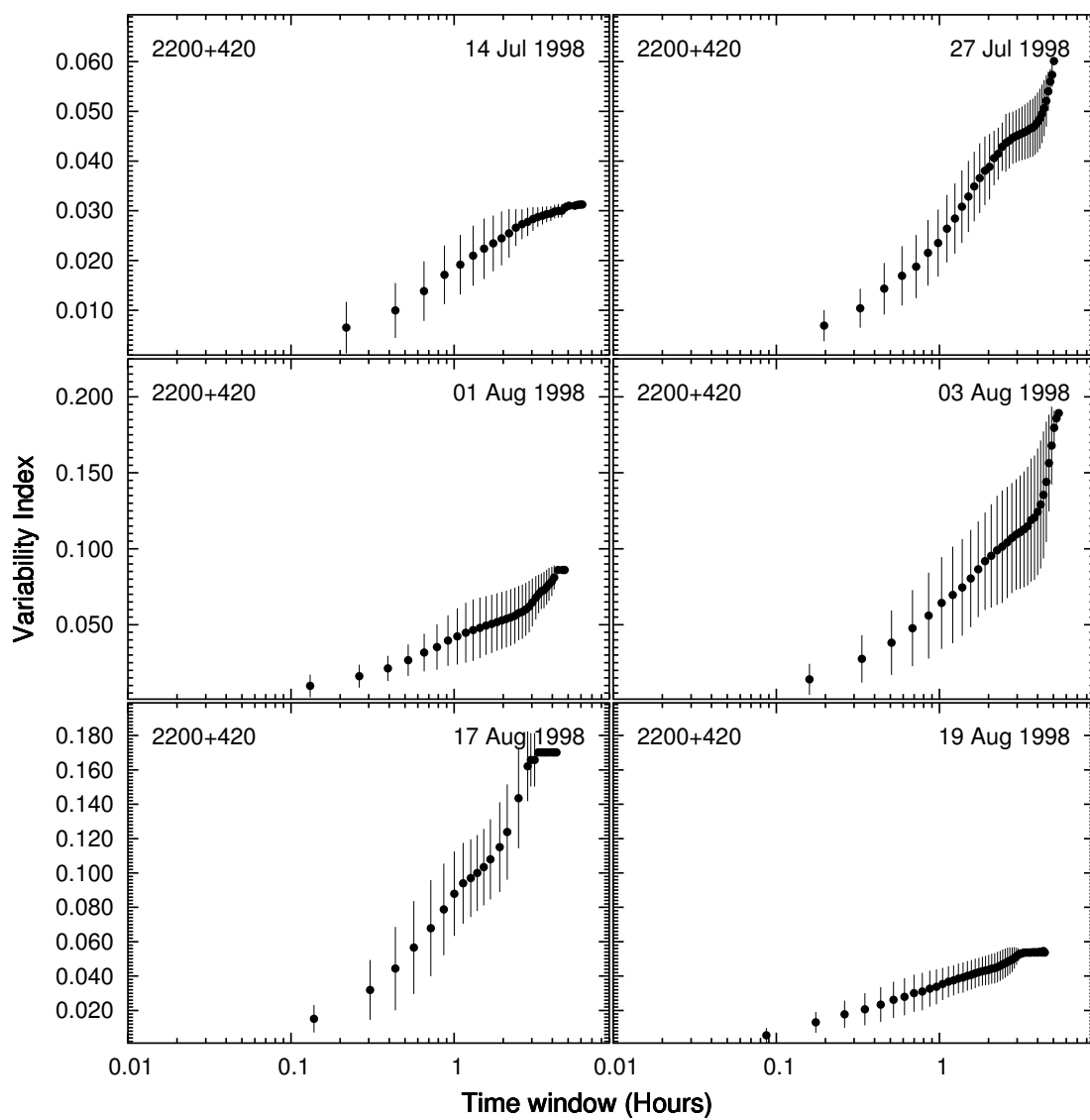


Figure 3.184 (continued)

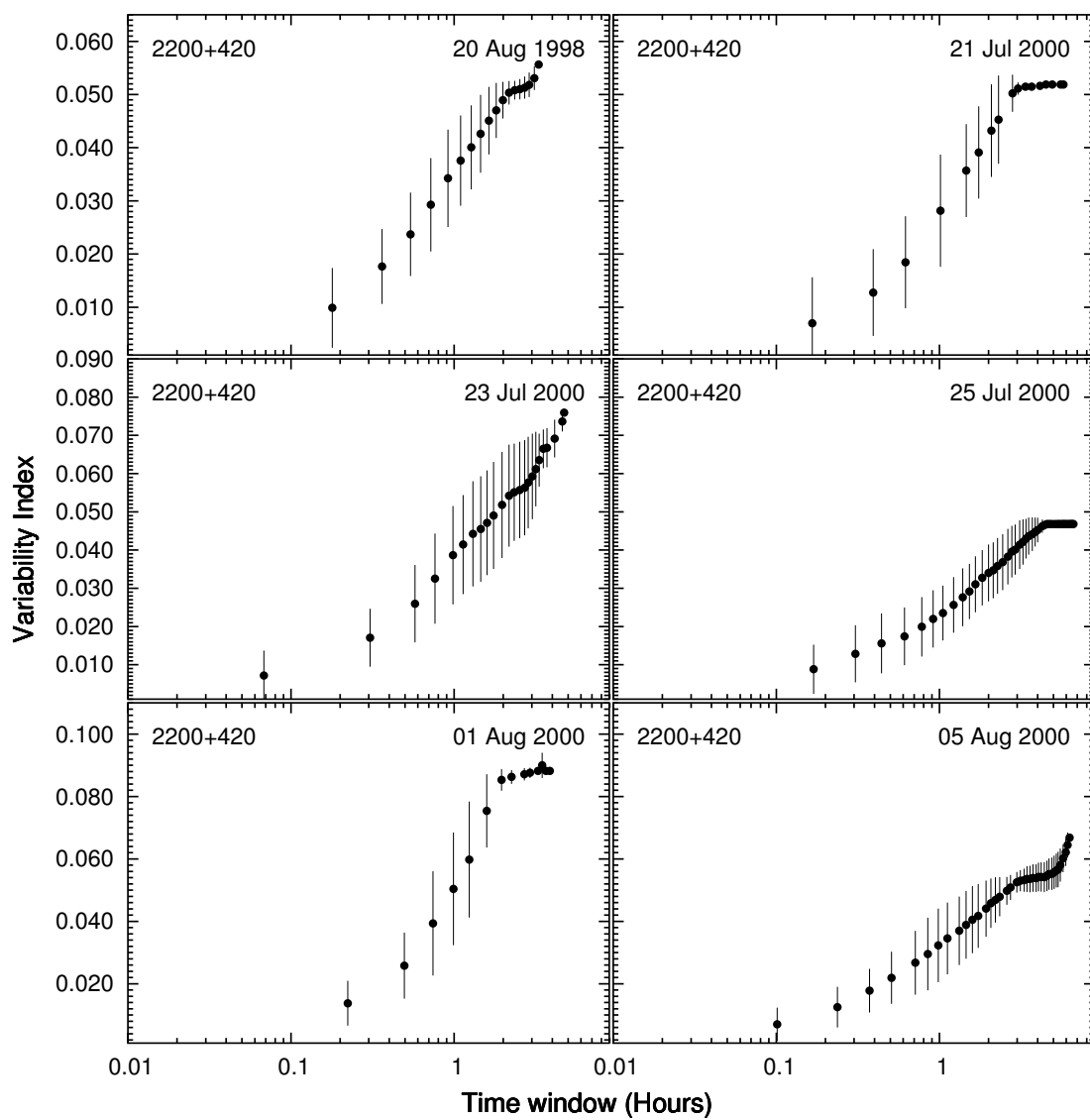


Figure 3.184 (continued)

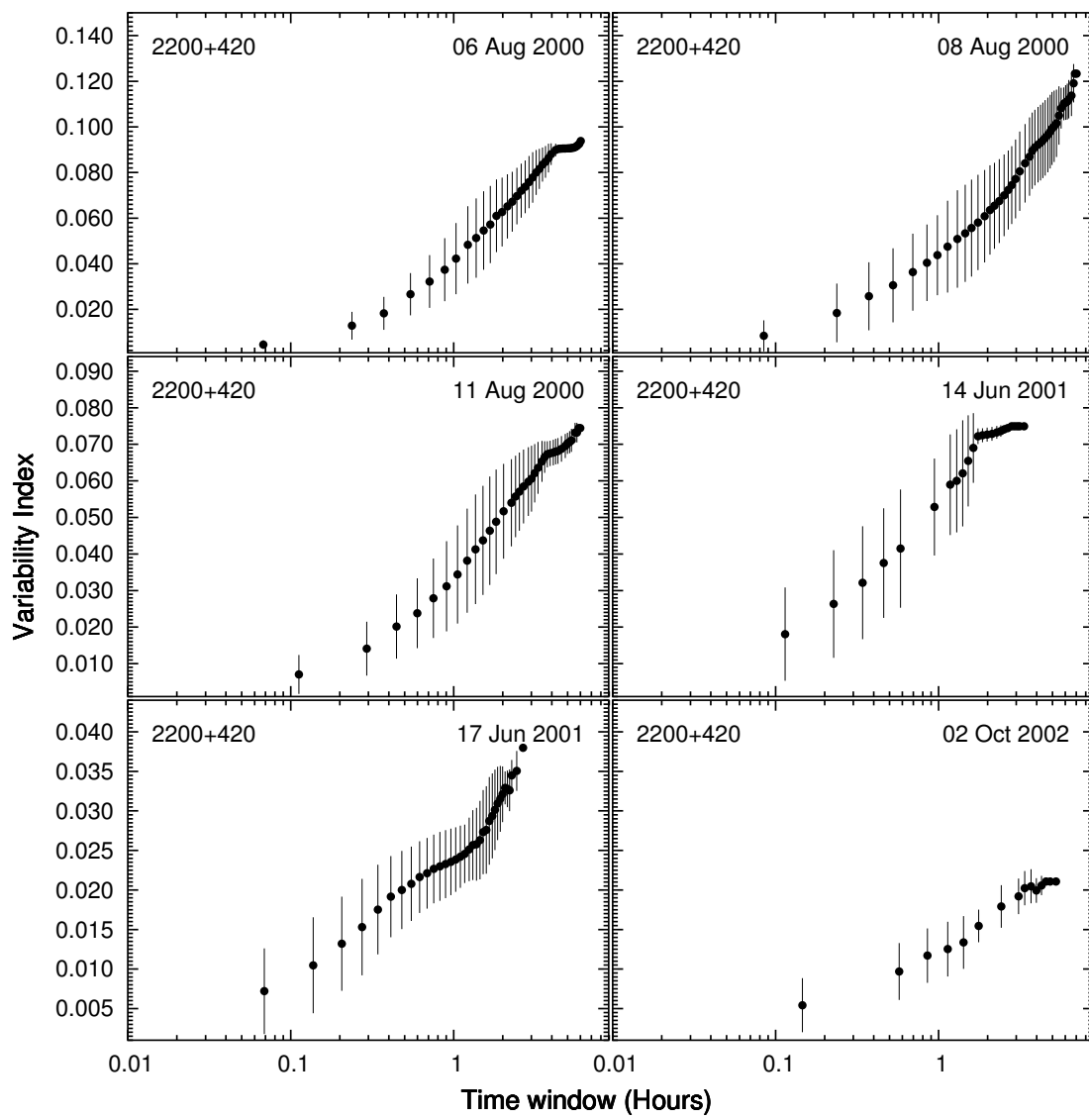


Figure 3.184 (continued)

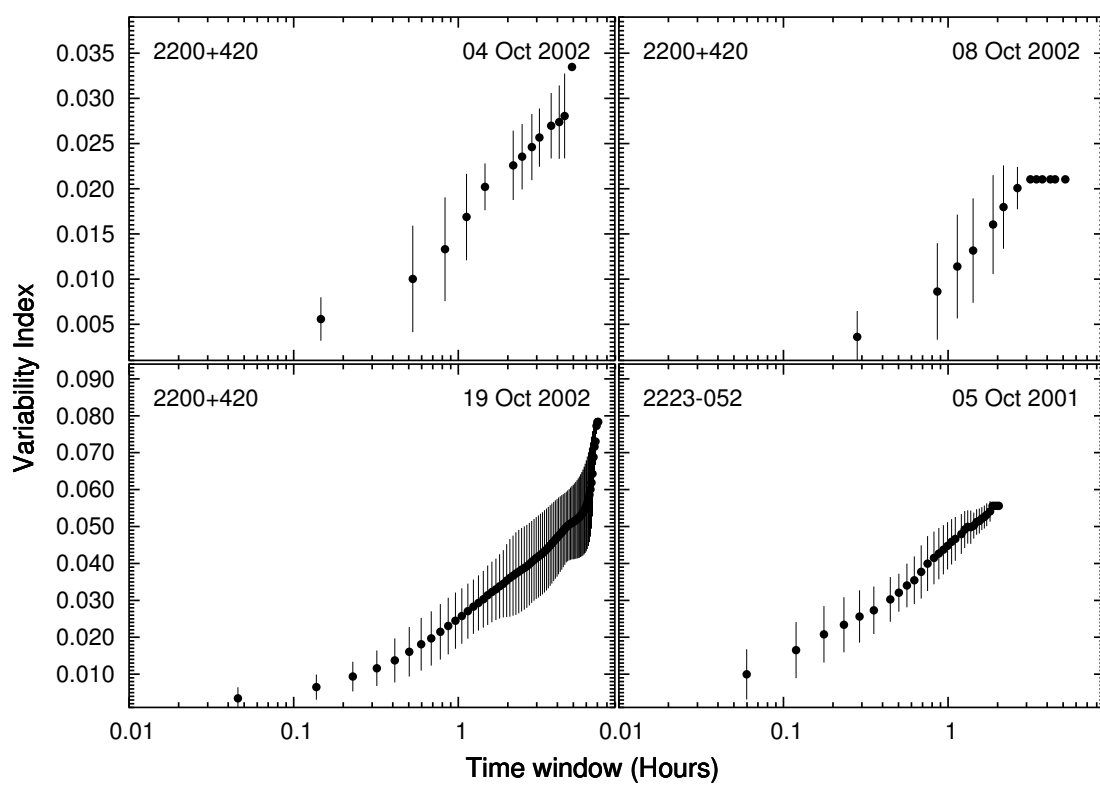


Figure 3.184 (continued)

Chapter 4

Multi-color Analysis

Photometric analysis of astronomical objects has historically used one of two types of data: (1) light curves which represent the brightness of an object at a particular waveband as a function of time and (2) color (e.g., $B - V$) as a function of time. The first set of analyses will use photometric light curves exclusively, while this second set will make use of the light curves and colors simultaneously.

These light curves were sampled uniformly with a sampling frequency of one observation every three days. Each object was observed simultaneously through 4 to 6 different filters ($BVRJHK$). The observations are not strictly simultaneous, but were performed in a 10 minute window due to mechanical restrictions. Because this window is only 0.23% of the sample interval, the claim of “simultaneous” is reasonable.

As mentioned earlier, the data to be used for this investigation was obtained via the SMARTS consortium’s 1.3m telescope equipped with ANDICAM. There were a total of 11 blazars observed over intervals ranging between 7 and 21 months and with variability amplitudes ranging from 0.2 to 3.0 mag. This allows one to investigate possible time lags and variability amplitude differences between the different wavebands.

Investigating how the variability varies versus color has important implications for the

processes involved in the emissions. For example, lags between variations observed at one waveband with respect to that observed at another waveband can test jet models. These models predict that different frequency emissions originate from different locations in the jet.

4.1 SMARTS Data

The SMARTS¹ Consortium telescopes are located at Cerro Tololo Interamerican Observatory (CTIO). A substantial portion of the data used in this dissertation was obtained through observations provided by this consortium. PEGA Team members have acquired spectroscopic data from the 1.5m telescope, optical photometric data from the 0.9m telescope, and optical and near-IR photometric data from the 1.3m telescope.

All the archival data were collected by observers in the PEGA group using a variety of telescopes. The SMARTS AGN data, however, were collected for two years on a continuous basis using the 1.3m telescope and will be discussed in the following sections. The 1.3m SMARTS telescope is equipped with A Novel Double-Imaging CAMera (ANDICAM) which can simultaneously obtain observations in the optical ($UBVRI$) and near-IR ($YJHK$). Data was gathered at the rate of one set of observations per object every 3 days, with the baseline for coverage extending up to 2 years. The filters used in this program were B , V , R , J , H , and K . Due to time constraints, fainter objects were sometimes restricted to only one near-IR filter, namely H , and brighter objects to only two bands, J and K . This filter combination allows one to extend the spectral coverage adequately.

¹Small and Moderate Aperture Research Telescope System

The SMARTS light curves are presented in terms of magnitude versus time (Epoch) and are displayed in 4 panels. The B band (V band in the case of one object) light curve will be shown and described in the upper panel, while the lower three panels will display color indices. The second panel will show $B - V$, the third $V - R$, and the lower panel will show B minus one of the near-IR wavebands. The apparent magnitudes and associated errors for all observations were obtained using the methods described in §2.3 and the errors for the color indices were combined by adding them in quadrature (i.e., $(x_1^2 + x_2^2 + \dots + x_n^2)^{1/2}$).

4.1.1 0420 – 014

The OVV quasar 0420 – 014 (also known as PKS 0420 – 014) has a redshift of 0.915 and has exhibited a variability amplitude range of just under 2 mag over the time that it has been monitored for this investigation (see Figure 4.1). The data used for 0420 – 014 was obtained with the SMARTS 1.3m telescope, is in the B, V, R, H, and K bands, and covers a time period of approximately 14 months.

The character of 0420 – 014’s B band light curve is one of a general decreasing brightness with many small events not quite resolved due to the minimum sample window of 3 days. There are some obvious smaller trends superimposed on the main decline. At the end of 2003, 0420 – 014 was near its brightest state observed, with $B \simeq 16.7$. It exhibited two ~ 0.5 mag flares in the first several months of observing before dimming significantly. In Mar 2004, a shoulder on the decline was observed before it was lost for the season near $B \simeq 18.3$. When the observations were picked up again in September of the same year, 0420 – 014 had brightened a few tenths of a magnitude, peaked several tenths brighter, then

continued a well defined decline. Despite some slight variation near the beginning of 2005, 0420–014 fell to its faintest level at $B \simeq 18.7$, nearly 2 mag below its brightest level observed in late 2003.

The multi-color character of 0420–014 in both $B - V$ and $V - R$ are relatively constant with averages of 0.61 and 0.48 respectively. The character of $B - H$ is much noisier around its average value of 3.25. There is an indication that 0420–014 gets slightly bluer when it is dimmer (see Epochs ~ 2004.25 and ~ 2005.0) that is present in all 3 color indices. The error and scatter in the measurements, especially in $B - H$, do not allow one to claim that this trend is statistically significant.

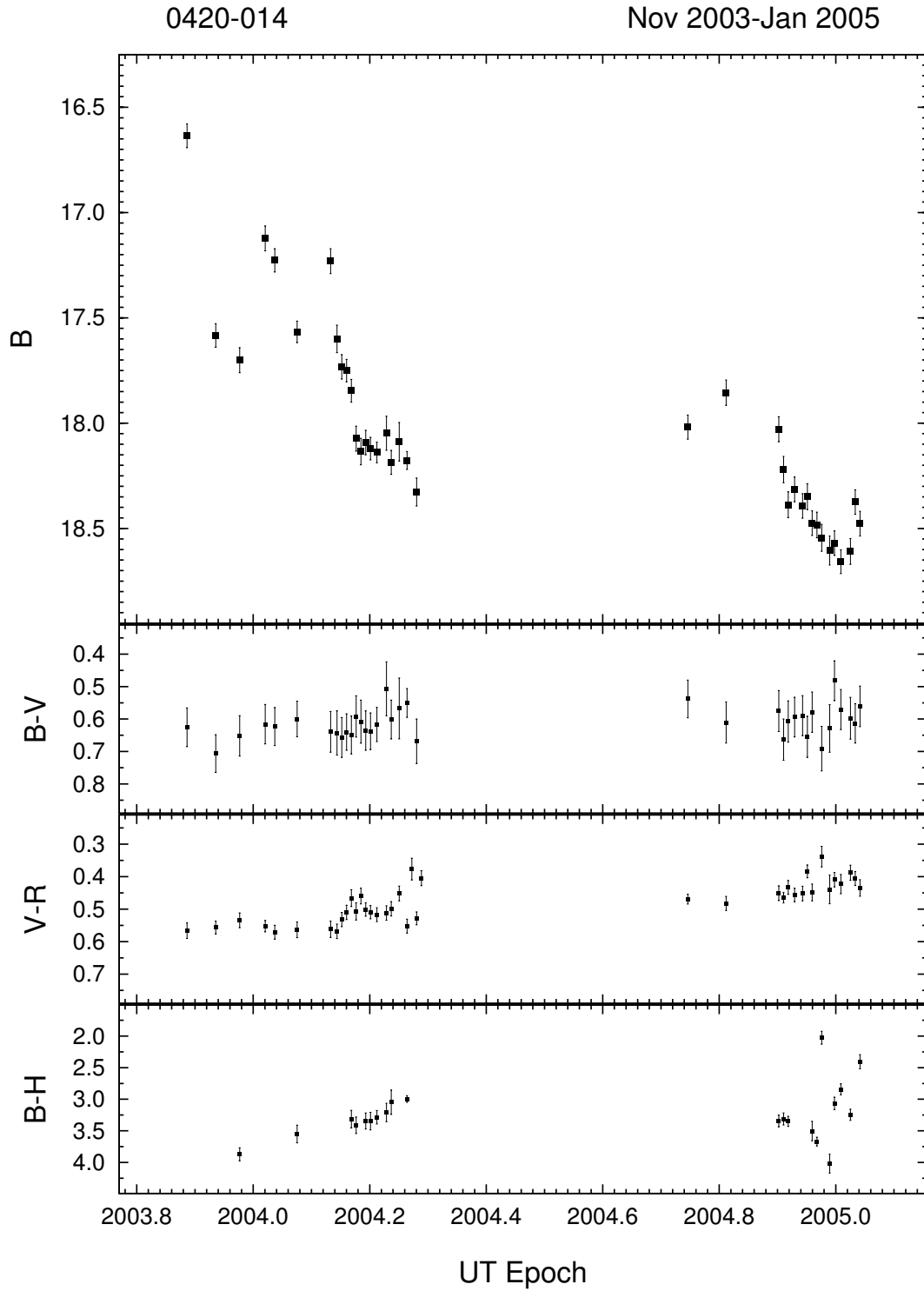


Figure 4.1: SMARTS light curve of 0420 – 014 from Nov 2003 to Jan 2005. The amplitude of variability is ~ 2 mag.

4.1.2 0818 – 128

The BL Lac object OJ –131 (also known as PKS 0818 – 128 or simply 0818 – 128) has no known redshift and has exhibited a variability amplitude range of just under 0.8 mag over the time that it was monitored for this investigation (see Figure 4.2). The data used for OJ –131 was obtained with the SMARTS 1.3m telescope, and is in the B, V, R, H, and K bands, and covers a time period of approximately 14 months.

The B band SMARTS observations of OJ –131 commenced on Nov 2003 where it started at a brightness level of $B \simeq 18.4$ and showed several peaks and dips in brightness before beginning a dimming trend of 0.5 mag which reached a minimum in Mar 2004 at a brightness of $B \sim 18.7$. Following this minimum, OJ –131 steadily increased in brightness until it was no longer observable for the season. It was next observed in September of 2004 near the same level, $B \simeq 18.3$, observed in the Spring. The object steadily declined from September of 2004 to January of 2005. The final observations of OJ –131 show a rapid dimming of 0.4 mag over only 2 months from Dec 2004 to Jan 2005, where it reached its dimmest level of $B = 18.8$.

The colors of OJ –131 are constant within their scatter and have values of $B - V = 0.49$, $\Delta(V - R) = 0.13^2$, and $B - H = 3.14$. No changes in color are indicated by these observations.

²No R band comparison sequence exists for OJ –131, so the color index is a *differential* color index: $(v - c) - (r - c)$

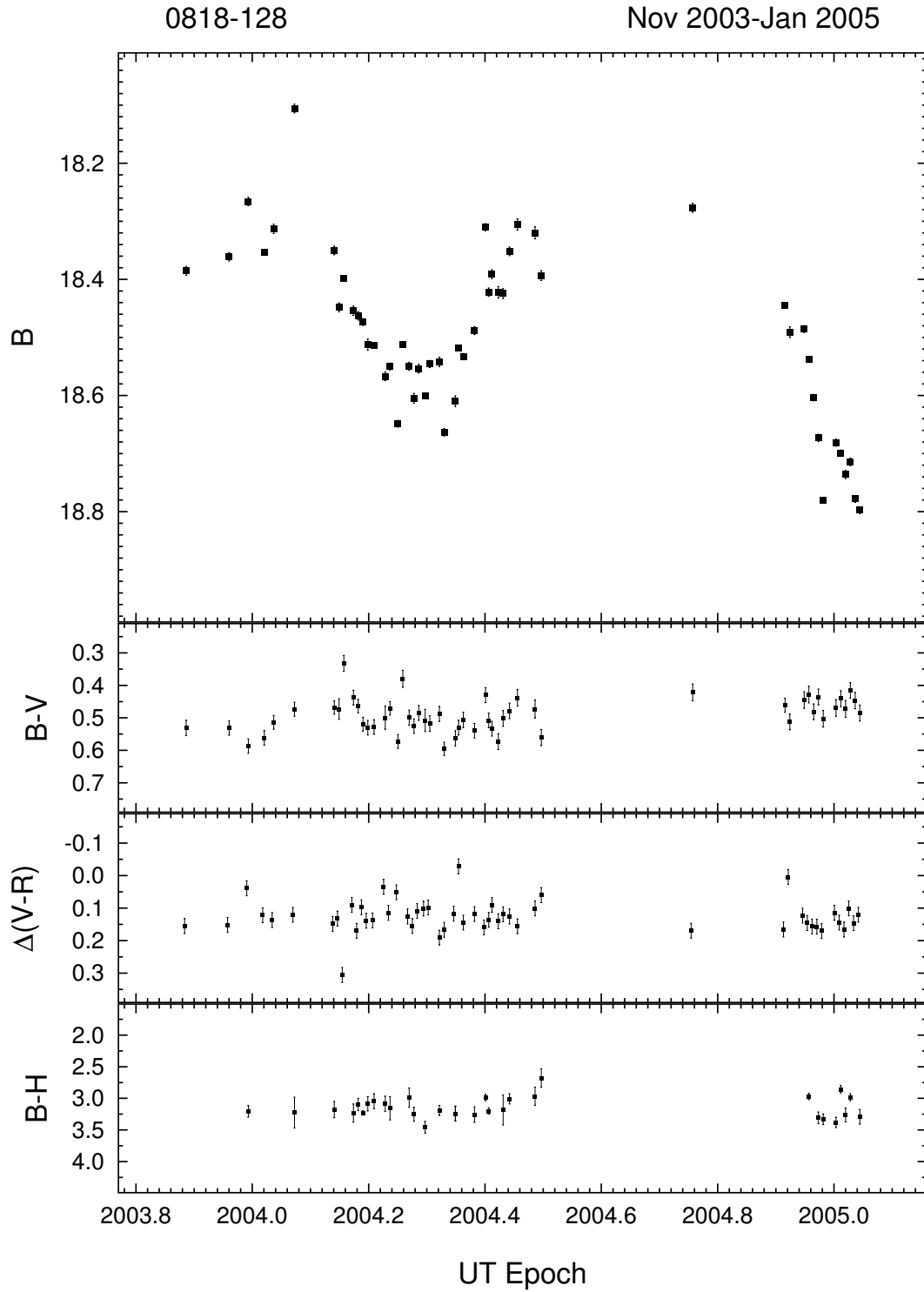


Figure 4.2: SMARTS light curve of 0818 – 128 from Nov 2003 to Jan 2005. The amplitude of variability is ~ 0.8 mag.

4.1.3 1226 + 023

The OVV Quasar 3C 273 (also known as PKS 1226+023 or simply 1226+023) has a redshift of 0.158 and has exhibited a variability amplitude range of less than 0.2 mag over the time that it has been monitored for this investigation (see Figure 4.3). The data used for 3C 273 was obtained with the SMARTS 1.3m telescope, is in the B, V, R, J, and K bands, and covers a time period of approximately 7 months.

Unlike all the other objects in the sample, 3C 273 showed little variability. As seen in Figure 4.3, the amplitude of variability barely exceeded 0.1 mag over the 7 months it was observed (see e.g., Romero et al. (2002) for other instances of low or no variability in this object). 3C 273 maintained a brightness level of $B \simeq 12.9$

The colors of 3C 273 showed the same low variability, remaining roughly constant at levels of $B - V = 0.25$, $V - R = 0.14$, and $B - J = 1.36$.

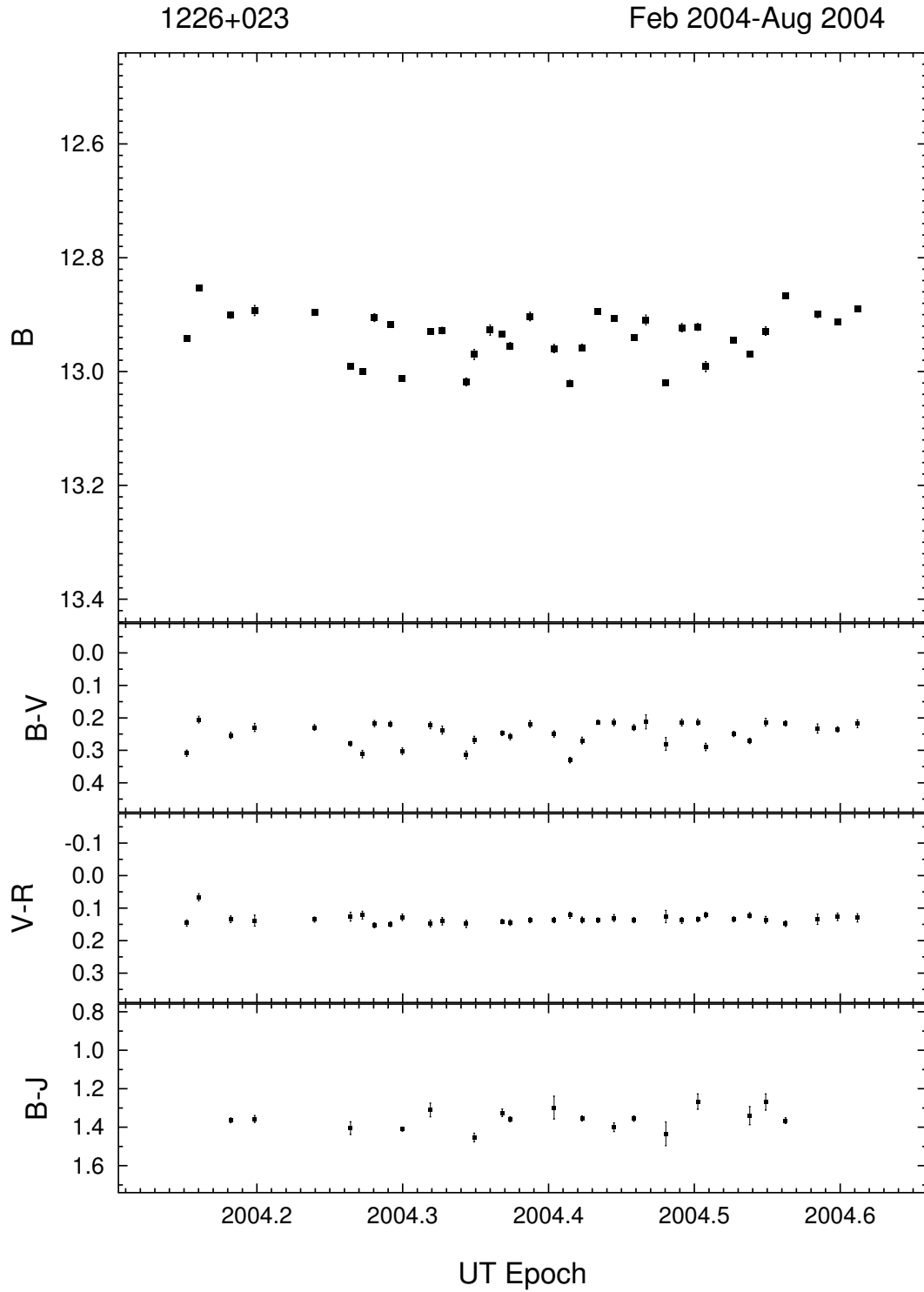


Figure 4.3: SMARTS light curve of 1226 + 023 from Feb 2004 to Aug 2004. The amplitude of variability is ~ 0.1 mag.

4.1.4 1253 – 055

The OVV Quasar 3C 279 (also known as PKS 1253 – 055 or simply 1253 – 055) has a redshift of 0.538 and has exhibited a variability amplitude approaching 2 mag over the time that it has been monitored for this investigation (see Figure 4.4). The data used for 3C 279 was obtained with the SMARTS 1.3m telescope, is in the B, V, R, and H bands, and covers a time period of approximately 12 months.

During the time 3C 279 was observed, it showed substantial variability that can be seen in Figure 4.4. The brightness level of 3C 279 began at $B \simeq 16.1$ in February of 2004 and quickly dimmed 0.8 mag in less than 3 months. It then brightened over the next 3 months in a well-defined flare. The amplitude of this flare is 1.9 mag, peaking in brightness at a level of $B \simeq 15.1$. Following this peak in brightness, 3C 279 dimmed rapidly to approximately the same level it was at the start of the flare. When it was observed again in Jan 2005, 3C 279 had brightened 0.7 mag only to drop rapidly to a brightness level of $B \simeq 16.6$.

The colors of 3C 279 were variable (0.3 mag in both $B - V$ and $V - R$, and 0.8 mag in $B - H$), but showed no correlation with brightness. Their average levels were $B - V = 0.47$, $V - R = 0.56$, $B - H = 3.21$.

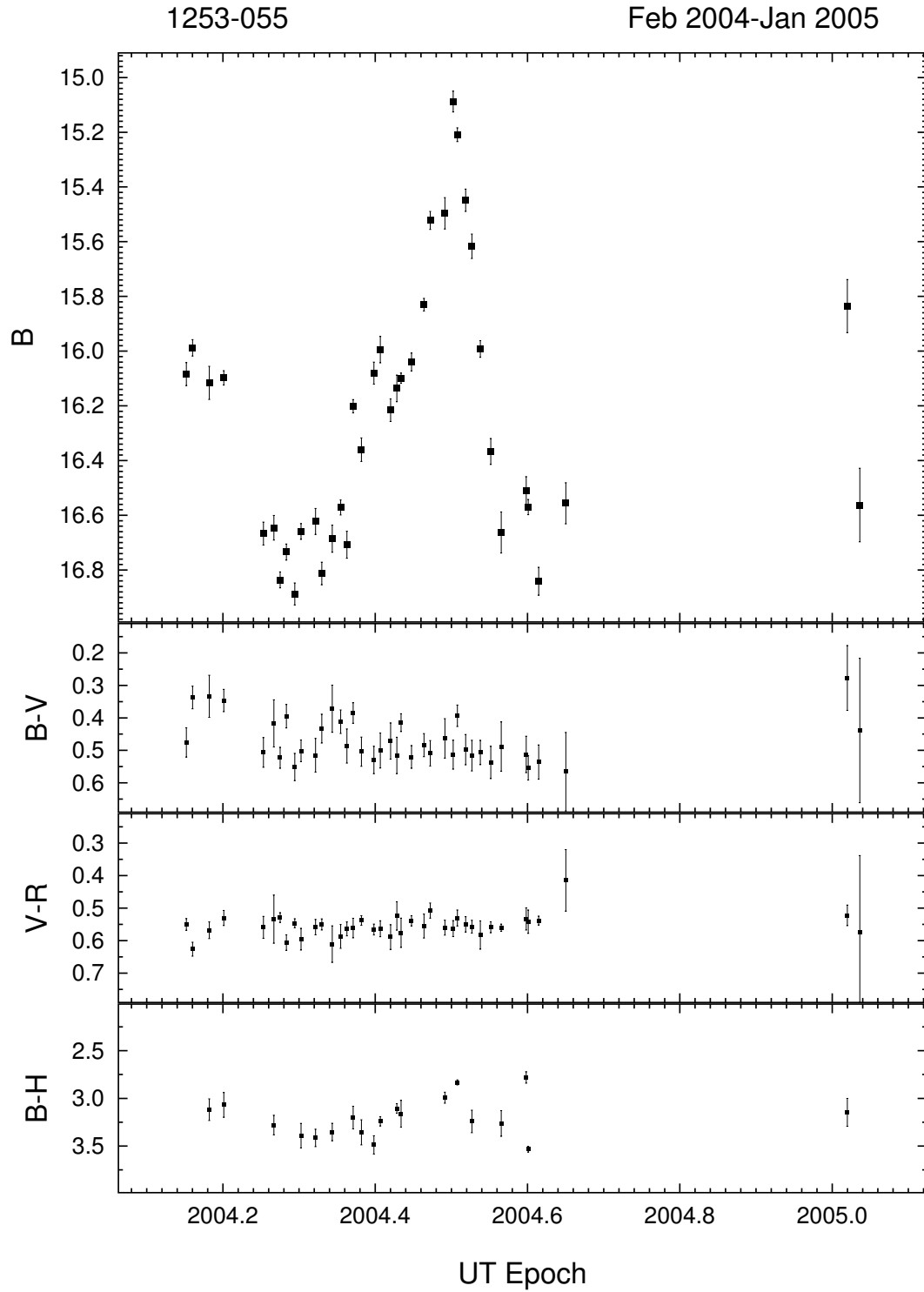


Figure 4.4: SMARTS light curve of 1253 – 055 from Feb 2004 to Jan 2005. The amplitude of variability is ~ 2 mag.

4.1.5 1510 – 089

The OVV Quasar 1510 – 089 (also known as PKS 1510 – 089) has a redshift of 0.360 and has exhibited a variability amplitude range of approximately 1 mag over the time that it has been monitored for this investigation (see Figure 4.5). The data used for 1510 – 089 was obtained with the SMARTS 1.3m telescope, is in the B, V, R, J, H, and K bands, and covers a time period of approximately 20 months.

1510 – 089 is first observed at a brightness level of $B \simeq 17.4$ in February of 2003. It then exhibits a well-defined decline of 0.2 mag followed by a brightening trend of 0.3 mag over the span of 5 months, reaching $B \simeq 17.3$ in Aug 2003. When observations of 1510 – 089 were resumed in April of 2004, it was at nearly the same level of brightness. It immediately showed a dramatic flare over only 3 months, peaking at $B \simeq 16.9$ in July of 2004.

Although modest color variations were present for 1510 – 089 with average values of $B - V = 0.21$, $V - R = 0.44$, $B - H = 2.49$, the color changes were uncorrelated with the brightness of the object.

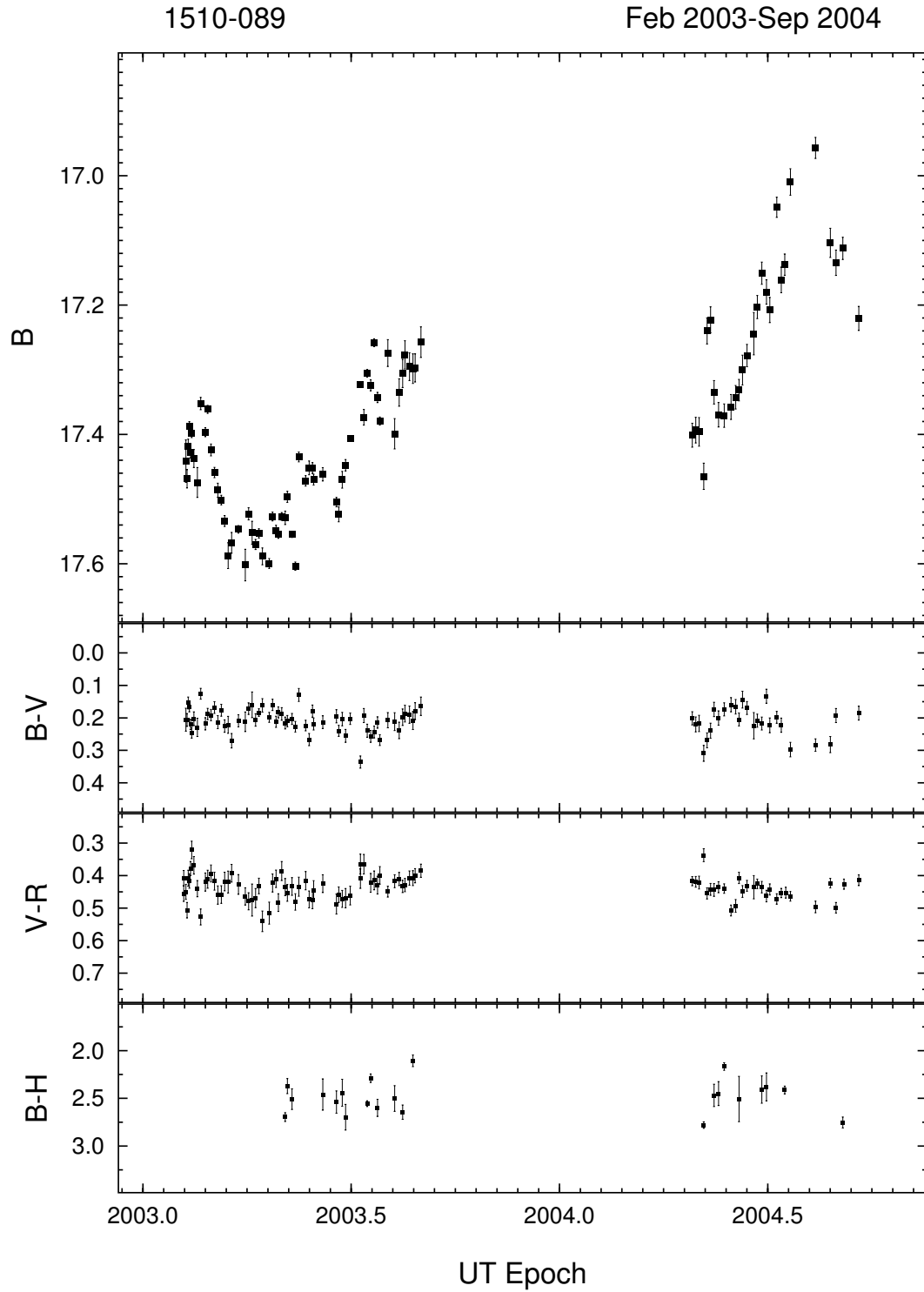


Figure 4.5: SMARTS light curve of 1510 – 089 from Feb 2003 to Sep 2004. The amplitude of variability is ~ 1.2 mag.

4.1.6 1514 – 241

The BL Lac object AP Librae (also known as PKS 1514 – 241 or simply 1514 – 241) has a redshift of 0.049 and has exhibited a variability amplitude range of just above 0.5 mag over the time that it has been monitored for this investigation (see Figure 4.6). The data used for AP Librae was obtained with the SMARTS 1.3m telescope, is in the B, V, R, J, H, and K bands, and covers a time period of approximately 20 months.

The amplitude of variability of AP Lib is near the lowest of all the objects, yet it has shown very complex character. Figure 4.6 shows AP Lib at a brightness level of $B \simeq 16.3$ in February of 2003. It immediately began to brighten 0.3 mag in less than 3 months followed by an even more dramatic dimming of 0.4 mag over only 1 month. From this point (Apr 2003), AP Lib began a somewhat slower decline superimposed with several small flares of ~ 0.2 mag in amplitude. The next observing season commenced with AP Lib near the same level followed by a slight dimming trend superimposed with several ~ 0.2 mag events observed from April to August of 2004.

The color variations for AP Lib were similar to those observed for both 3C 279 and 1510 – 089 (see §§4.1.4 & 4.1.5) showing no correlation with the brightness of the object. The average values were $B - V = 0.95$, $V - R = 0.66$, $B - H = 3.39$.

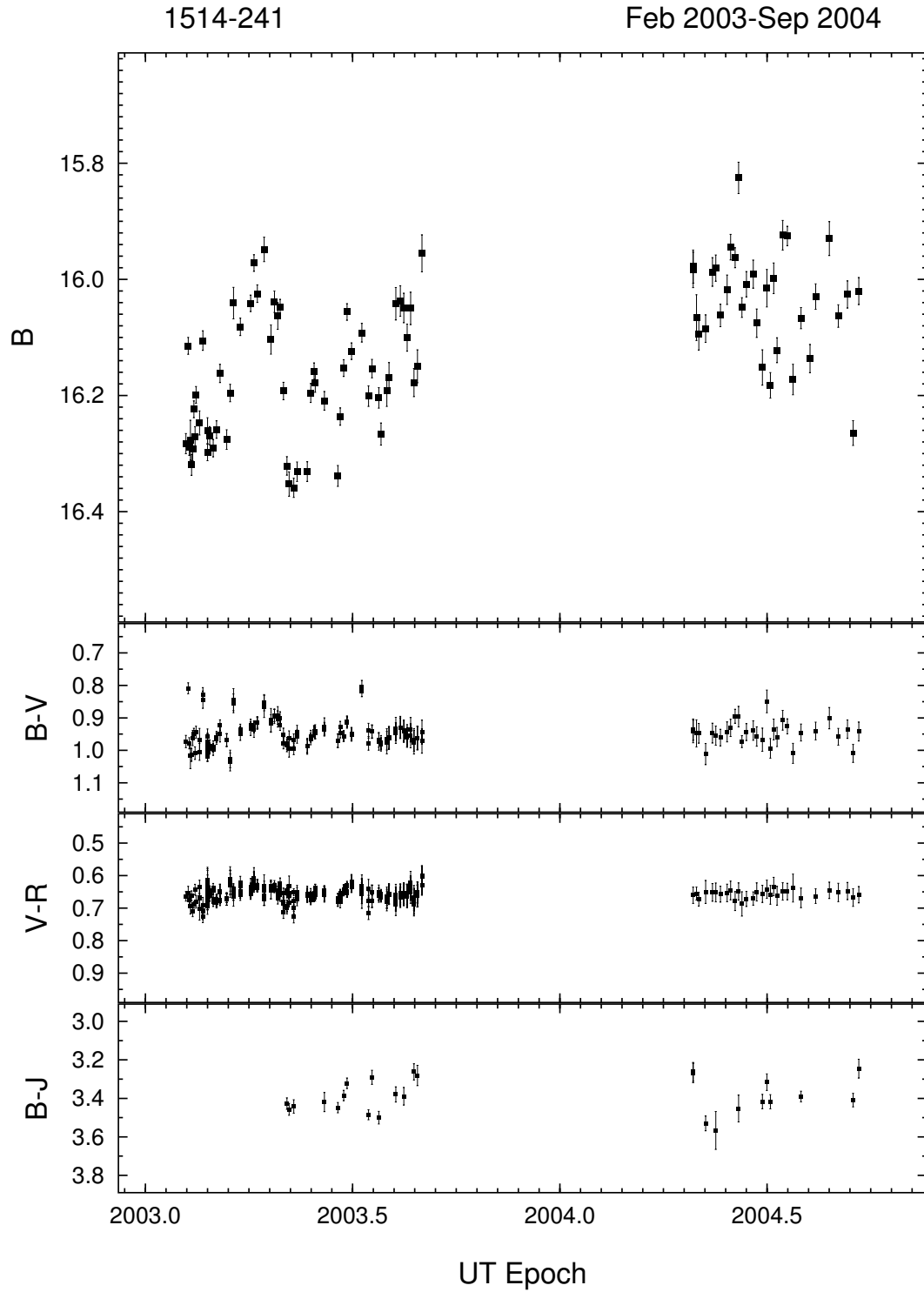


Figure 4.6: SMARTS light curve of 1514 – 241 from Feb 2003 to Sep 2004. The amplitude of variability is ~ 0.6 mag.

4.1.7 1622 – 297

The OVV quasar 1622 – 297 (also known as PKS 1622 – 297) has a redshift of 0.815 and has exhibited a variability amplitude range of approximately 1.3 mag over the time that it has been monitored (see Figure 4.7). The data used for 1622 – 297 was obtained with the SMARTS 1.3m telescope and is in the B, V, R, J, H, and K bands. The observations cover a period of approximately 21 months. See §3.2.3 for the full R band light curve which includes these observations.

In February of 2003, 1622 – 297 was near its faintest observed level of $V \simeq 19.8$. It increased only slightly over the next 4 months until in Jun 2003 a flare of more than 1.2 mag was observed in less than a month! During the decline following this outburst, 1622 – 297 exhibited erratic variations of ~ 0.3 mag. In Apr 2004, 1622 – 297 was observed near a brightness level similar to that observed at the beginning of the previous season, $V \simeq 19.6$. It brightened only slightly over the next several months until in Sep 2004, it flared > 1 mag in less than 2 months! This seasons observations also showed low amplitude (~ 0.2 mag) variations superimposed on the main trends.

The colors of 1622 – 297 changed considerably (~ 0.5 mag in both $\Delta(B - V)^3$ and $V - R$, and $\gtrsim 1.5$ mag in $V - H$) over its observations. There appears to be a trend toward the $V - H$ colors appearing redder during the flare observed in 2003 in all three color indices. However, there appears to be no significant color variations observed during the flare in 2004. The average color indices for 1622 – 297 were $B - V = -0.72$, $V - R = 0.44$, $V - H = 3.72$.

³No B band comparison sequence exists for 1622 – 297, so the color index is a *differential* color index: $(b - c) - (v - c)$

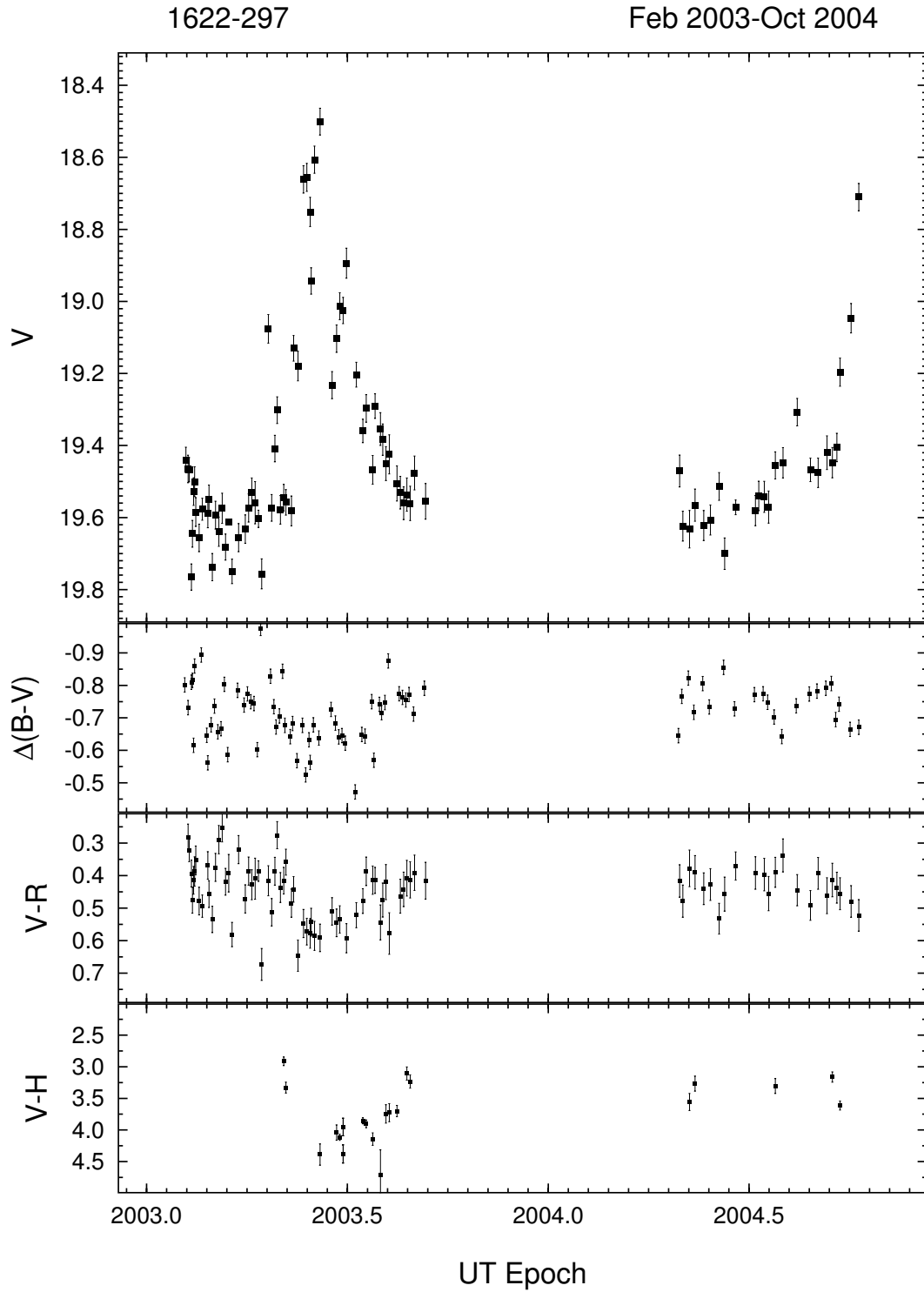


Figure 4.7: SMARTS light curve of 1622 – 297 from Feb 2003 to Oct 2004. The amplitude of variability is ~ 2 mag.

4.1.8 2005 – 489

The BL Lac object 2005 – 489 (also known as PKS 2005 – 489) has a redshift of 0.071 and has exhibited a variability amplitude range of approximately 0.6 mag over the time that it has been monitored for this investigation (see Figure 4.8). The data used for 2005 – 489 was obtained with the SMARTS 1.3m telescope, is in the B, V, R, J, H, and K bands, and covers a time period of approximately 16 months.

Over the course of the observations of 2005 – 489, it exhibited a steep decline in brightness followed by a slower increase in brightness that is punctuated by rapid variations of 0.2 to 0.4 mag. The monitoring of 2005 – 489 began in late October of 2003 with the source at a brightness level of $B \simeq 14.2$. It decreased monotonically by more than 0.2 mag in early December. In late April of 2004, 2005 – 489 was observed at a brightness level of $B \sim 14.6$ and steadily increased ~ 0.4 mag over the next five months with ~ 0.2 mag excursions superimposed on this trend. In October, the brightness of 2005 – 489 leveled out near $B \sim 14.3$.

The colors indices show little variations with all three indicating a slight trend that suggests 2005 – 489 gets bluer as it brightens. The average values for all the indices were $B - V = 0.46$, $B - R^4 = 0.83$, $B - J = 2.19$.

⁴Normally, the $V - R$ color index is used because of its wide familiarity, but due to the limited V band coverage for 2004 – 489, it is replaced by the B band for this color index.

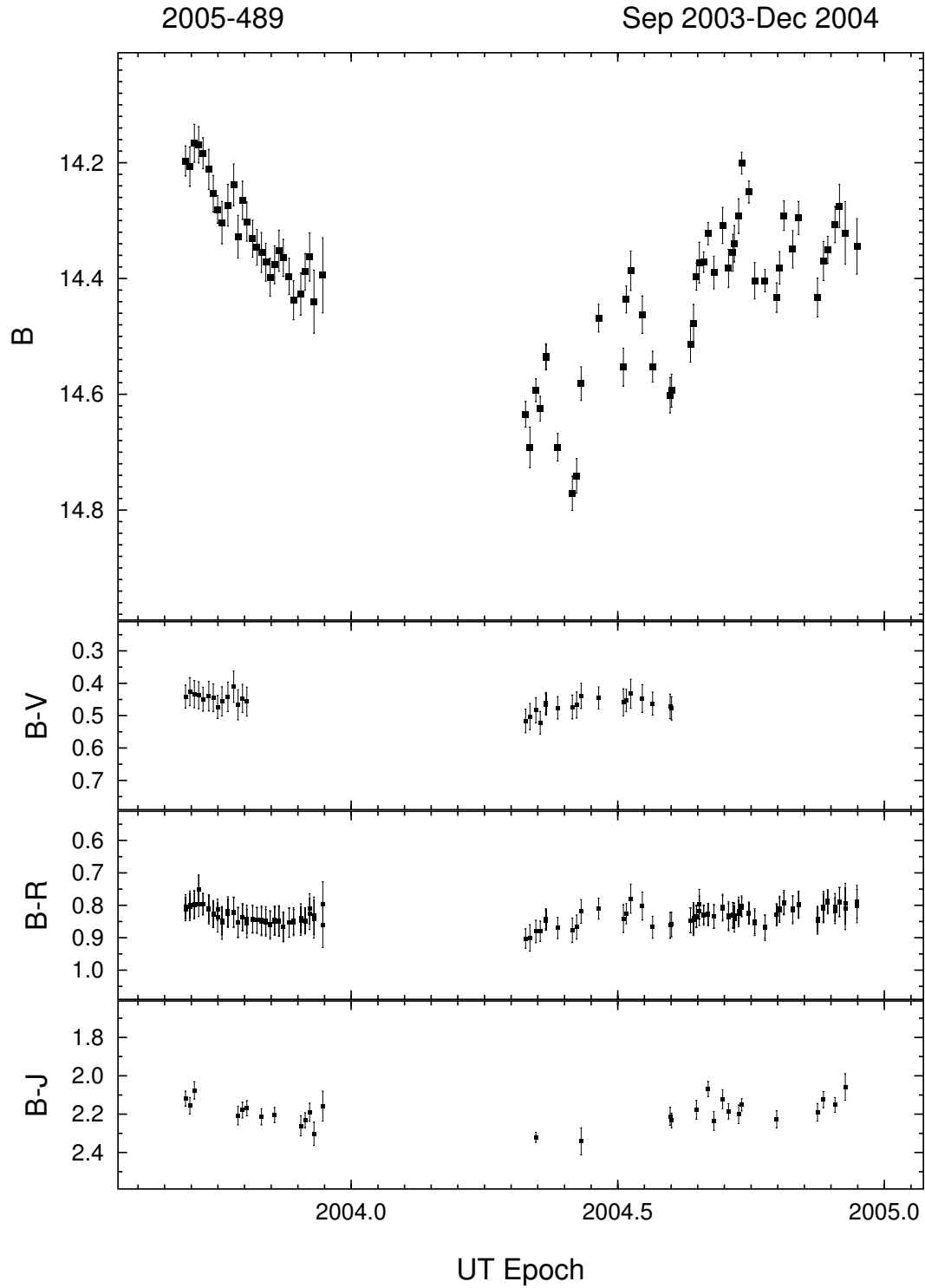


Figure 4.8: SMARTS light curve of 2005 – 489 from Sep 2003 to Dec 2004. The amplitude of variability is ~ 0.5 mag.

4.1.9 2155 – 304

The BL Lac object 2155 – 304 (also known as PKS 2155 – 304) has a redshift of 0.117 and has exhibited a variability amplitude range of nearly 1.5 mag over the time that it has been monitored for this investigation (see Figure 4.9). The data used for 2155 – 304 was obtained with the SMARTS 1.3m telescope, is in the B, V, R, J, H, and K bands, and covers a time period of approximately 21 months.

2155 – 304 exhibits a very interesting character in its variability. In March of 2003, observations of 2155 – 304 found the source near a brightness level of $B \simeq 13.9$. The object then dimmed significantly over the next 5 months to a level of $B \simeq 14.5$. It then increased in brightness at a similar rate until it reached a brightness level near $B \simeq 13.6$ in Dec 2003. There was some low level ($\lesssim 0.2$ mag) variability superimposed on these trends. 2155 – 304 was next observed in late Apr 2004 near this same level. The object exhibits 2 small flares over the next 3 months, only to flare to its maximum brightness level of $B \simeq 13.2$ in late August. It then decreased rapidly at a rate of ~ 0.25 mag per month to a plateau brightness level near $B \sim 13.7$ in October of 2004.

2155 – 304's colors appear very well behaved, deviating $\lesssim 0.1$ mag in $B - V$ and $V - R$, and ~ 0.5 mag in $B - H$. None of the colors show any correlation with the object's brightness and were at average levels of $B - V = 0.35$, $V - R = 0.29$, $B - H = 1.88$.

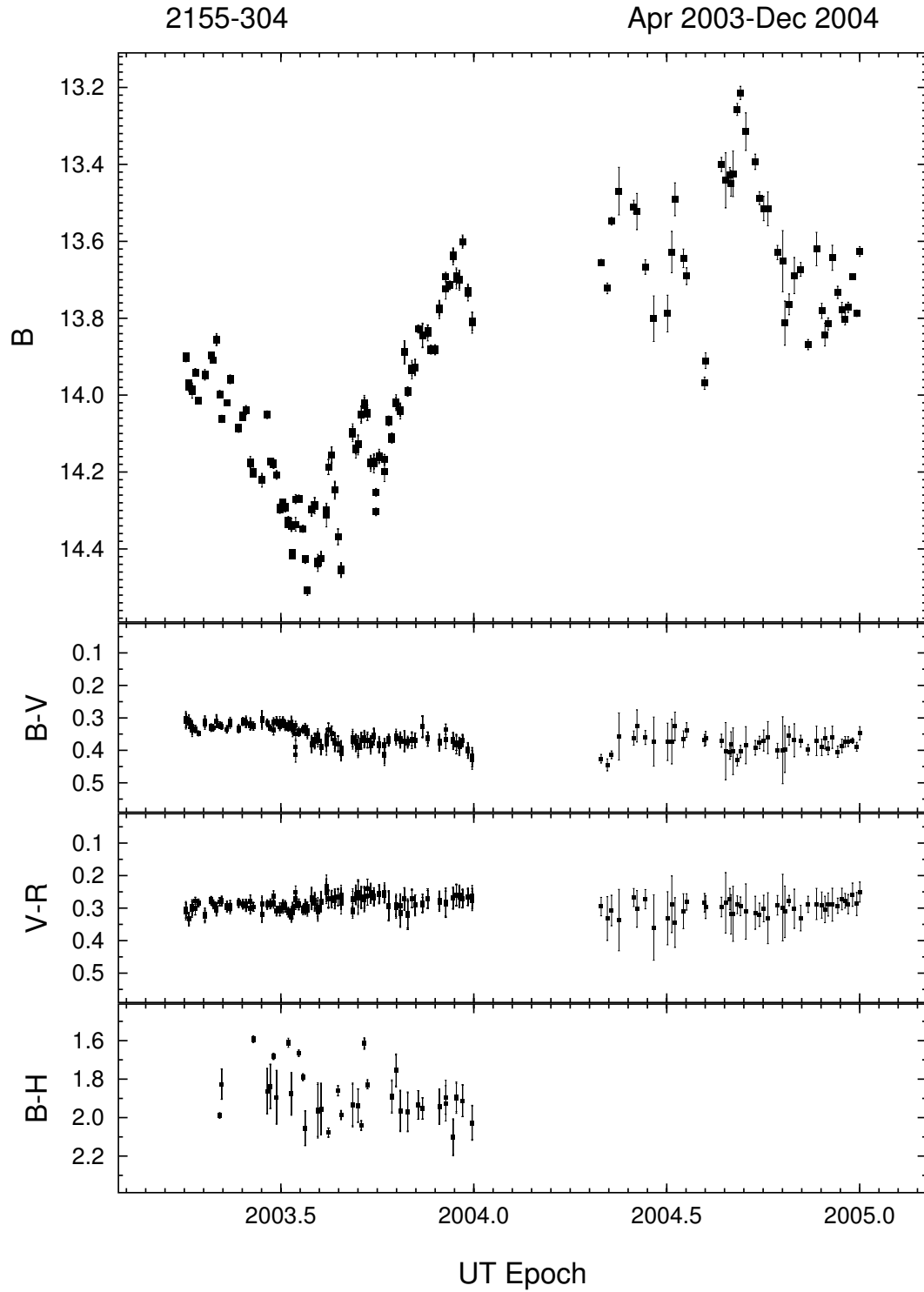


Figure 4.9: SMARTS light curve of 2155 – 304 from Apr 2003 to Dec 2004. The amplitude of variability is ~ 1.5 mag.

4.1.10 2223 – 052

The OVV quasar 3C 446 (also known as PKS 2223 – 052 or simply 2223 – 052) has a redshift of 1.404 (the second largest in the sample) and has exhibited a variability amplitude range of approximately 1.2 mag (see Figure 4.10) during approximately 15 months of monitoring.

The SMARTS observations begin in September of 2003 with some low level variations of $\lesssim 0.2$ mag for several months at an average brightness of $B \sim 18.7$. It then flares dramatically by 0.8 mag over 1 month at the end of the observing season, reaching a brightness level of $B \simeq 17.9$. When it was next observed in August of 2004, it showed erratic variations over 2 months of ~ 0.3 mag with a decline to $B \sim 18.4$ in December 2004.

The colors of 3C 446 showed variations that are not correlated with the brightness of the object in any consistent fashion. Both $B - V$ and $V - R$ exhibit variations of ~ 0.2 mag, while $B - H$ varies ~ 0.5 mag. The average levels of the color indices are $B - V = 0.43$, $V - R = 0.48$, $B - H = 2.89$.

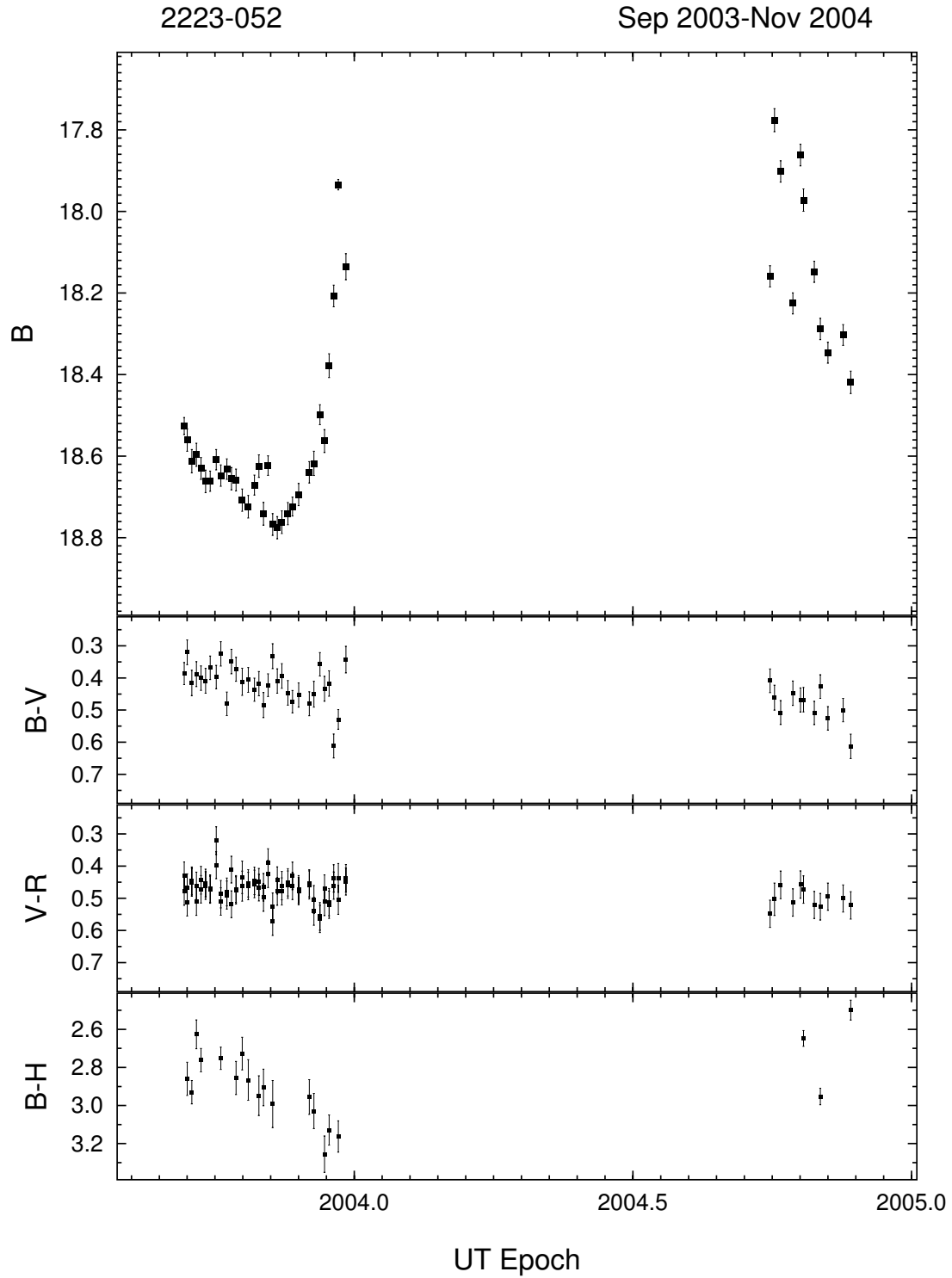


Figure 4.10: SMARTS light curve of 2223 – 052 from Sep 2003 to Nov 2004. The amplitude of variability is ~ 1.2 mag.

4.1.11 2345 – 167

The OVV Quasar 2345 – 167 (also known as PKS 2345 – 167) has a redshift of 0.576 and has exhibited a variability amplitude range of near 3 mag over the time that it was monitored for this investigation (see Figure 4.11). The data used for 2345 – 167 was obtained with the SMARTS 1.3m telescope, is in the B, V, R, J, H, and K bands, and covers a time period of approximately 14 months.

The observations for 2345 – 167 appear somewhat noisier overall than many of the SMARTS objects. The observations for this object begin in September of 2003 when the object was rising rapidly in brightness by ~ 2.5 mag starting at a brightness level of $V \simeq 18.3$. It then decreased in brightness more slowly over the next several months to a brightness level $V \sim 17.8$. A second rapid flare of ~ 1 mag was observed in late January of 2004. When it was next observed in September, it was decreasing in brightness ~ 1 mag with two $\gtrsim 0.5$ flares superimposed, reaching a minimum brightness level of $V \sim 18.6$ in Jan 2005.

The optical color indices showed a correlation with the brightness of 2345 – 167 such that it gets bluer when it dims. This can be seen at Epochs 2004.0 and 2004.9. The optical/near-IR color index is uncorrelated due to its large scatter and limited coverage. The mean levels of all 3 color indices are: $B - V = 0.58$, $V - R = 0.31$, $B - H = 2.81$.

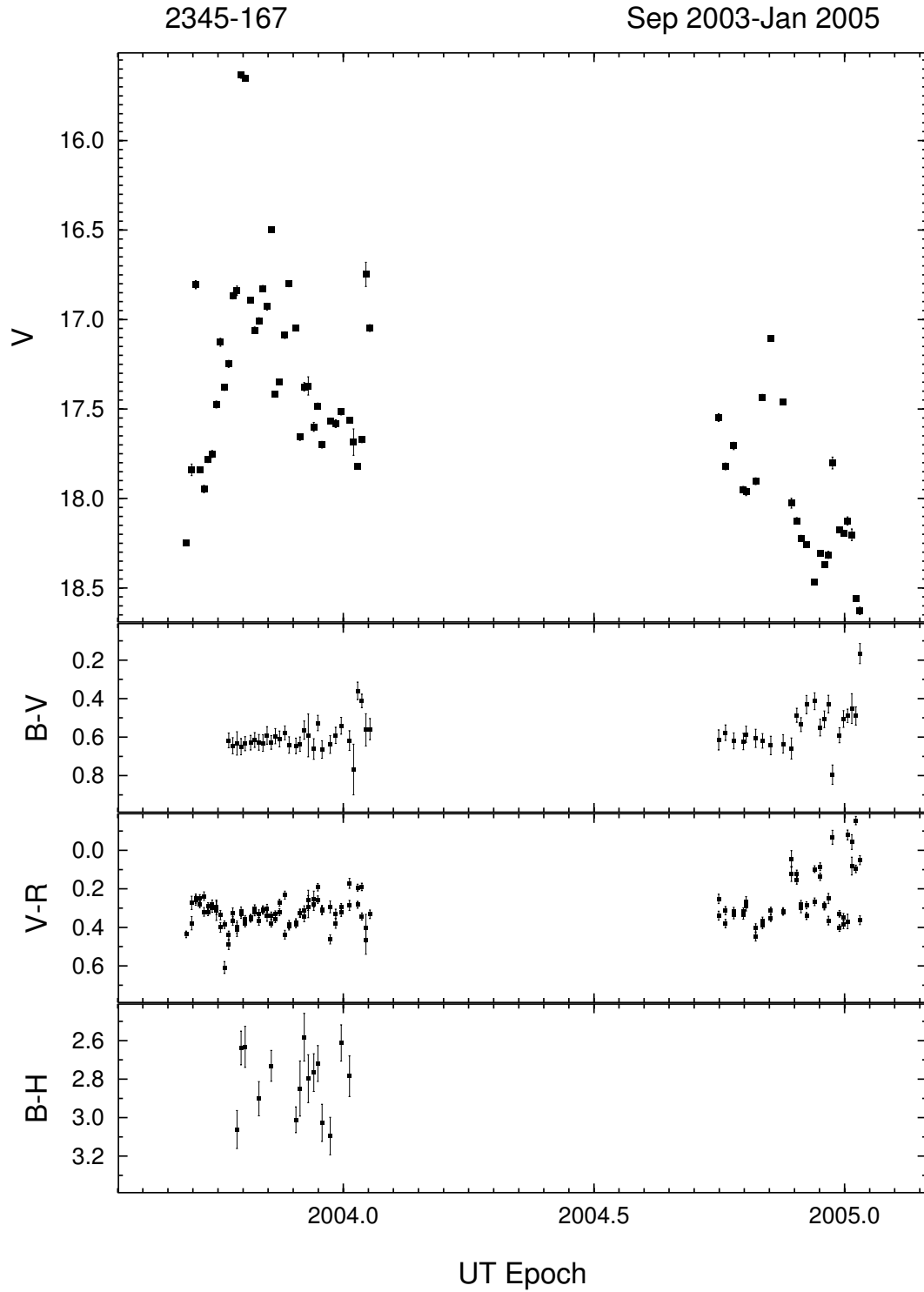


Figure 4.11: SMARTS light curve of 2345 – 167 from Oct 2003 to Jan 2005. The amplitude of variability is ~ 3.5 mag.

4.2 Analysis Methods

The first analysis method involves comparing discrete events in different wavebands to investigate if there is a wavelength-dependence associated with the amplitude of the variability. This is done using the color indices described in the previous sections. If an appreciable change in a color index is associated with a change in brightness, a second analysis method will be employed to investigate if there are any variability shifts with color (i.e., time lags or leads). This method utilizes a cross correlation function (CCF). This compares any two time series (e.g., B band light curve and H band light curve), that are matched in time against each other, such that any similarities show up as a peak at a time difference correlated with the similarities. For instance, an auto correlation function (the CCF of a time series with itself) will show a peak at 0 time difference, or lag.

4.2.1 Cross Correlation Function

The cross correlation function (CCF) used for this investigation is the standard CCF defined in Equation (4.1), where L is the time lag; x , y , \bar{x} , and \bar{y} are the observables to be correlated and their averages respectively; and N is the number of observations. This simple version is chosen because the data has been sampled in such a way (one observation in each filter virtually simultaneously) that data binning is unnecessary except to improve data quality.

$$CCF(L)_{xy} = \frac{\sum_{k=0}^{N-L} (x_{k+L} - \bar{x})(y_k - \bar{y})}{(\sum_{k=0}^{N-1} (x_k - \bar{x})^2)(\sum_{k=0}^{N-1} (y_k - \bar{y})^2)} \quad (4.1)$$

4.3 Multi-color Analysis Results

Several objects exhibited color variations with respect to their brightness. These variations of the objects will be summarized here with respect to the variability amplitudes of their colors and investigated for any possible time leads or lags in the following subsections.

4.3.1 Amplitudes of Colors

The first object to show a possible correlation between color and variability amplitude was 0420 – 014. There were two points at which a correlation appeared to exist and both were at a minimum in brightness. The first event was at an Epoch of ~ 2004.25 (see Figure 4.1). $B - V$ appeared to get bluer (decrease in value of the color index), but the error is too high to be statistically significant. The color index $V - R$ shows a very similar picture. The $B - H$ color index shows a definite increase in value (redder color), but this may not be real given the large scatter in the observations around Epoch 2005.0. The second event is much more weakly correlated in all color indices. If real, the magnitude of the change of amplitude with brightness is in the direction of a greater increase in blueness in the redder wavebands. In effect, the amplitudes of variation decrease in the longer wavelengths.

1622 – 297 is the second object to show a possible correlation of color with brightness. The main event showing this is located at Epoch 2003.4 in Figure 4.7. There exists a reddening (an increase in value of the color index) as the object increases in in brightness in both the $V - R$ and $V - H$ color indices. The $\Delta(B - V)$ differential color index shows a similar indication, but the correlation is weaker. The amplitudes of variation are smaller at longer wavelengths.

The object 2005 – 489 shows correlations that are different from that seen for other objects exhibiting color variations (see Figure 4.8). There are no statistically significant correlations with either $B - V$ or $B - R$ color indices, but the $B - J$ color index shows a possible change in color such that the object gets *bluer* (i.e., smaller color index values) as it increases in brightness. This indicates that the shorter wavelengths show a greater amplitude of variability.

The final object showing a possible correlation of color with variability amplitude is 2345 – 167 (Figure 4.11). The situation here is virtually identical to that for 0420 – 014. The $B - V$ and $V - R$ color indices show a correlation such that the object gets bluer when it is dimmer. The points of interest are at Epochs 2004.0 and 2004.9.

4.3.2 Leads and Lags

If the four objects that showed (possible) color variations are examined qualitatively, no clear evidence for leads or lags are seen between the different wavebands. Below is a description of the quantitative comparison (i.e., CCFs) of these variations.

Figure 4.12 shows the results of the correlative analysis for 0420 – 014. The dotted line is the auto correlation function (ACF) of the B band light curve (ACF_B), the short dashed line is the CCF of the B band light curve with respect to the V band light curve (CCF_{BV}), the long dashed line is the CCF of the V band light curve with respect to the R band light curve (CCF_{VR}), and the solid line is the CCF of the B band light curve with respect to the H band light curve (CCF_{BH}). There are obviously no definite lags in any of the 4 correlation functions because they all peak strongly at 0 lag, but there is an indication of a positive lag

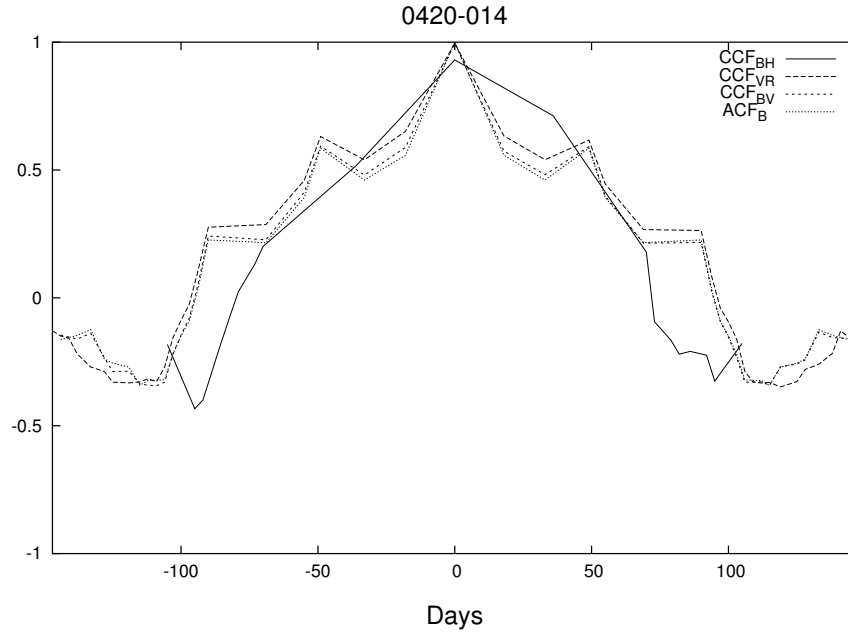


Figure 4.12: Cross Correlation Function of 0420 – 014.

in CCF_{BH} . There is, however, no way to determine a reliable value for this lag. It should be noted that for this correlation curve and those that follow, only the ACF peaks identically at a coefficient of unity. All the CCFs peak at a value slightly lower than this value.

Figure 4.13 shows the correlation functions for 1622 – 297. They are ACF_V , CCF_{BV} , CCF_{VR} as indicated by the short dashed, long dashed, and solid lines respectively. Here again, all functions are strongly peaked at 0 lag. The light curve of the V band data was cross correlated with that of the H band and unrealistic results were obtained (i.e., a broad asymmetry of more than 100 days on one side, and an incomplete correlation curve on the other) and is not being displayed to avoid confusion with the other curves.

Figure 4.14 shows the correlation functions for 2005 – 489. They are ACF_B , CCF_{BV} , CCF_{BR} as indicated by the short dashed, long dashed, and solid lines respectively. Again, all functions are strongly peaked at 0 lag. The light curve of the b band data was cross correlated

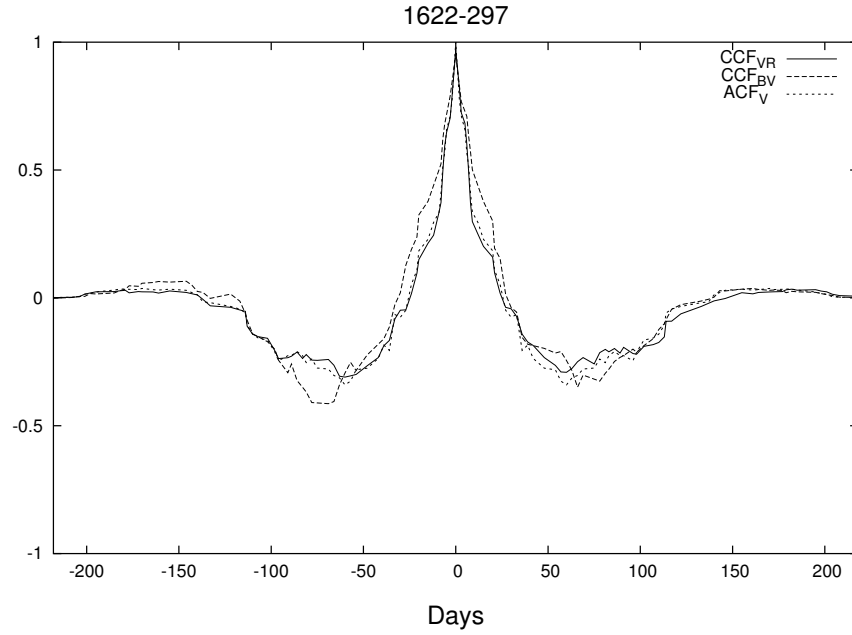


Figure 4.13: Cross Correlation Function of 1622 – 297.

with that of the H band and unrealistic results were obtained (i.e., a -30 day positive peak and a +30 negative peak with incomplete endpoints) and is not being displayed to avoid confusion with the other curves.

Lastly, Figure 4.15 shows the correlation functions for 2345 – 167. They are ACF_B , CCF_{BV} , CCF_{VR} , as indicated by the short dashed, long dashed, and solid lines respectively. Yet again, all functions are strongly peaked at 0 lag. There might exist slight asymmetries indicating lags in both CCF_{BV} and CCF_{VR} , but they are at such low levels that no reliable lags could be found.

None of the CCFs run on the data showed any clear evidence of leads or lags. This is likely due to the coarseness of the sampling (3 days) and the magnitude of the expected lags or leads ($\lesssim 1$ day), or it may be due to a lack of a lag altogether. They all do, however, show a high degree of symmetry, which is expected of such closely matched observations.

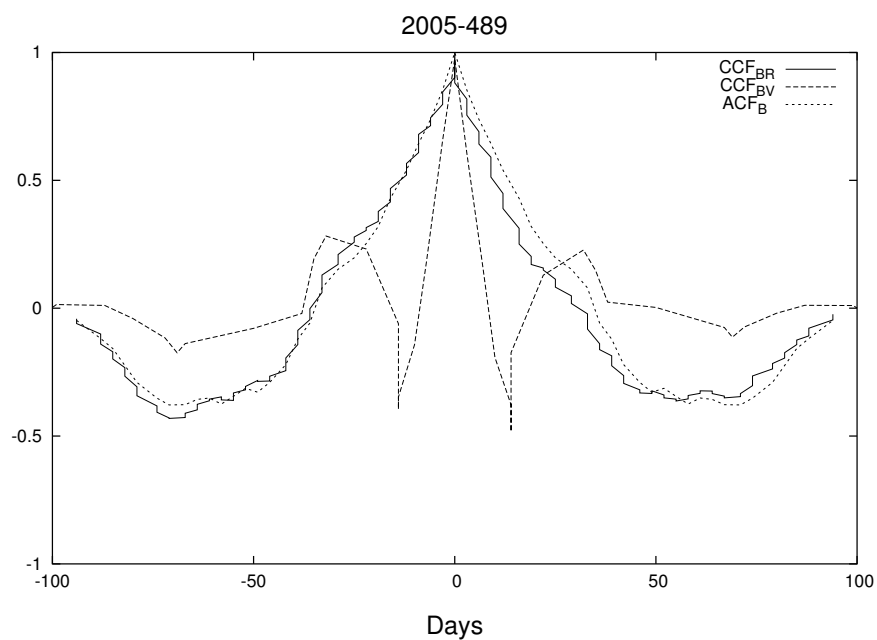


Figure 4.14: Cross Correlation Function of 2005 – 489.

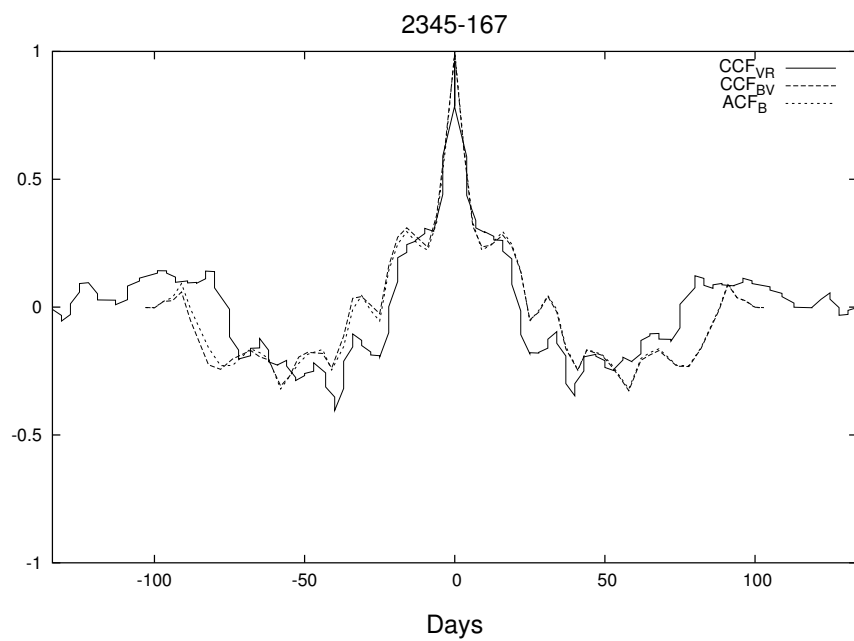


Figure 4.15: Cross Correlation Function of 2345 – 167.

4.3.3 Rest Frame Correlations

The set of SMARTS observations is sampled uniformly in time (every 3 days) for a minimum of 7 to 21 months with definite large scale brightness variations easily resolved. This allows an investigation of the sizes of emitting regions on scales larger than light days through the use of an auto-correlation function (ACF). The observations were shifted into the rest frame of the source using the methods described in §3.1. This shift into the rest frame only takes into consideration cosmological effects. The Doppler boosting factor δ , which contains information about bulk relativistic motions within the jet (Γ) and opening angles (θ), is not accounted for because (1) the emissions in the rest frame are being investigated, not the inner workings of the jets, and (2) conversions based on these factors are inherently inaccurate due to the lack of accurate values of the factors.

Table 4.1: The source region size estimates from the auto-correlation functions of the SMARTS light curves in the rest frame.

| OBJECT | FWHM |
|------------|-----------|
| 0420 – 014 | ... |
| 1226 + 023 | 2.6 days |
| 1253 – 055 | 11.7 days |
| 1510 – 089 | 6.6 days |
| 1514 – 241 | 4.8 days |
| 1622 – 297 | 3.3 days |
| 2005 – 489 | 11.2 days |
| 2155 – 304 | 21.5 days |
| 2223 – 052 | 1.6 days |
| 2345 – 167 | 2.5 days |

Table 4.1 and Figure 4.16 displays the results of the ACF for the ten objects in the SMARTS sample with redshifts. The ACFs for the various objects are far from uniform in

width. This indicates that the sizes of the source regions for the different objects over the sample interval are different. The full width at half maximum (FWHM) shown in column 2 can be compared to the time it takes information to cross the emitting region, and may act as an upper limit to the size of the source region (c.f., Equation (3.6)).

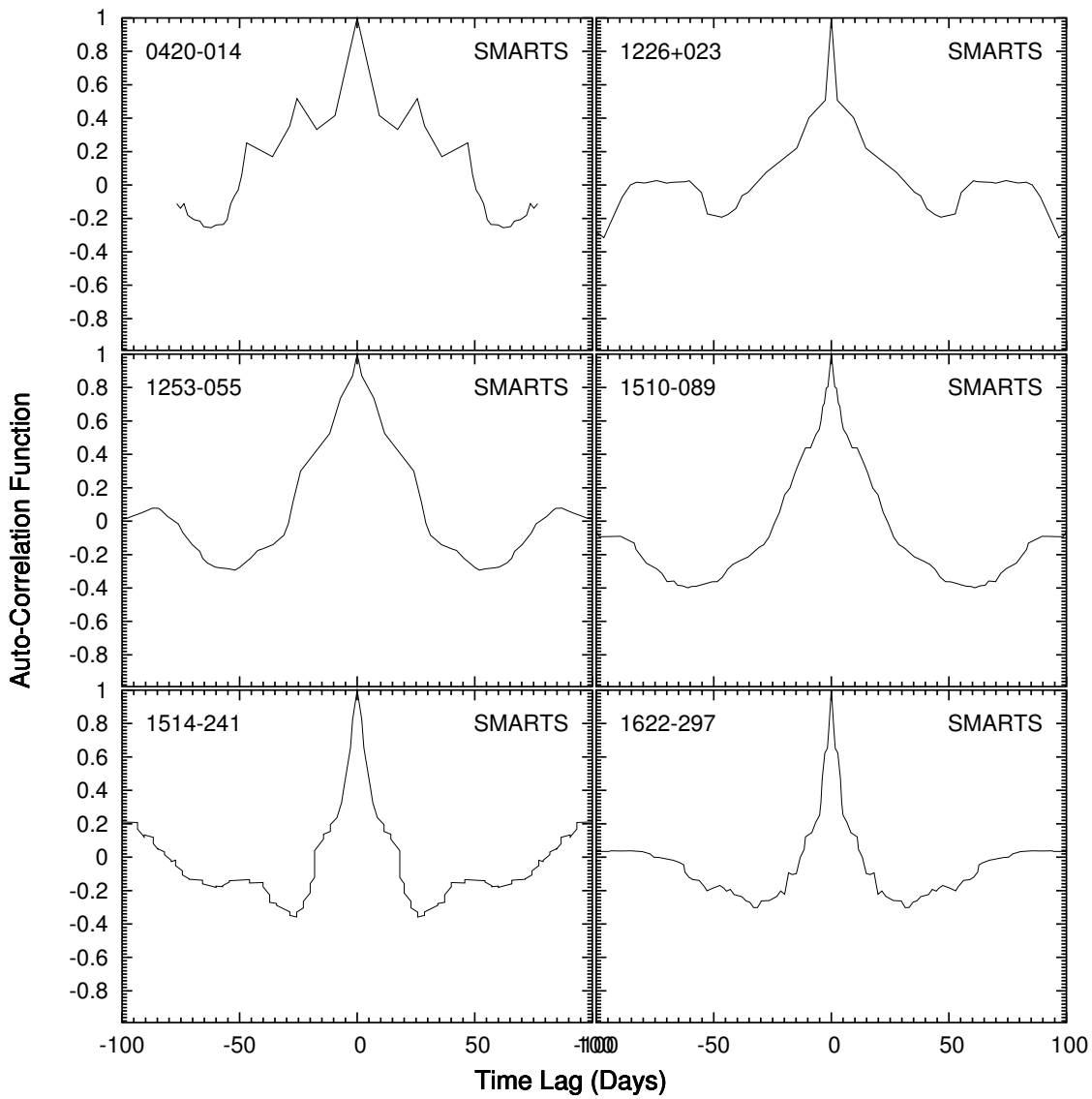


Figure 4.16: SMARTS Auto-Correlation Functions

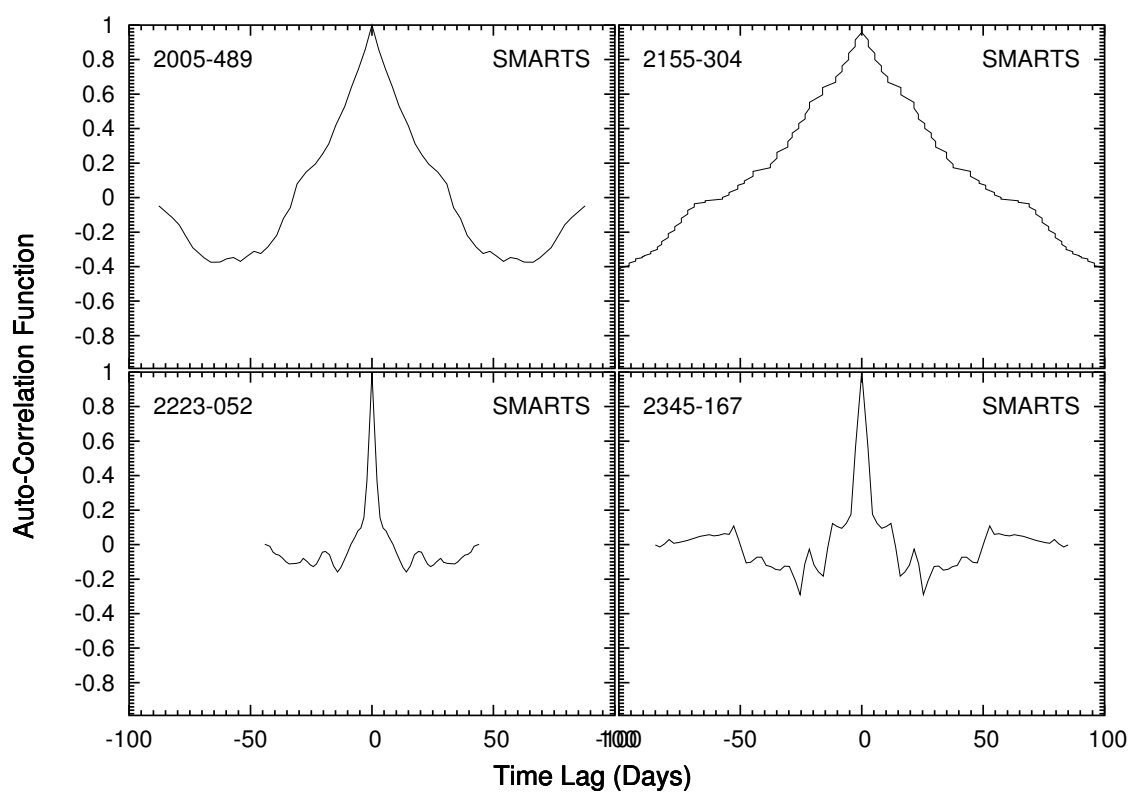


Figure 4.16 (continued)

Chapter 5

Discussion and Future Work

5.1 Discussion

The model of blazars is that they are the type of radio loud AGN that have their jets oriented nearly in line with the observer. This has strong consequences for how their emissions are modified before they are intercepted by the observer. Doppler boosting (or beaming) by the relativistic jet ensures that the approaching jet is seen to far greater distances than the receding jet. This can lead to a selection effect in which blazars at very large distances may be seen preferentially over other AGN in general, and there may be boosting induced distinctions even among different subclasses of blazars. The general picture now has BL Lac objects as the boosted versions of FR I radio galaxies, while OVV's are the boosted version of FR II radio loud quasars. (Urry and Padovani, 1995)

It is believed that shocks propagating down the jet give rise to variations both in brightness and in color. By analyzing short term (< 1 day) variations in flux and longer term (months to years) variations in flux through multiple wavebands, clues to the location and structure of the processes creating the variations can be obtained. To this end, sixteen blazars of widely different redshifts have been investigated for intrinsic variability character-

istics at multiple time-scales. This was done by looking at the flux variations as they would appear in the rest frame of the source and by looking at color variations as a function of brightness.

5.1.1 Variability in the Rest Frame

The intrinsic flux variability investigation utilized existing data in the PEGA archives of 11 blazars observed for total durations of between 8 and 18 years. The typical sampling frequency in the observed frame was $\lesssim 10$ minutes for a minimum of one hour up to a full night of observations. The observations were primarily done in the R band, but older observations in the V band were included to supplement the dataset. The observations were shifted into the emitted, or rest frame, of the source using the accepted emission-line redshift for each source.

By shifting observations into the rest frame, they are changed in two significant ways: (1) the amplitude of the variability is enhanced by 3 factors of $(1 + z)$, demonstrating that the intensity of the measured variability has been deamplified by cosmological effects; and (2) the duration of any events detected are less by one factor of $(1 + z)$ due to cosmological time dilation. The enhancement effect reveals as yet unseen variability and often strengthens the seen variability to levels far greater than were immediately noticed. There error of the observations are also enhanced, so no new statistically significant variability is seen. The time *undilation* effect has the tremendous advantage of allowing smaller time-scales of variability to be investigated, time-scales that were not earlier accessible. This augmentation of temporal resolution reduces the lower detection limit of the size of source regions.

The methods of analysis began with the simple determination of the duty cycles of each blazar by calculating which nights showed statistically significant ($\gtrsim 2.6\sigma$) variations in brightness. These duty cycles were used in many different lines of investigation.

The first line of investigation was how the duty cycles of the blazars in the sample were affected by the state of the object. It was found that the duty cycles of the sample as a whole, and for select blazars with large numbers of light curves (i.e., AO 0235+16 and BL Lac), were independent of state. One implication of this is the location of the source of the variability. If the primary source of variability was flares in a thermal accretion disk for instance, one would expect that the contrast between these variations and the non-thermal jet emissions would be greatest in the lowest luminosity state and least in the highest luminosity state. This is clearly not what is seen. This does not exclude thermal emissions from an accretion disk as a source of variability, but lessens the role it plays, bolstering the model of the jet as the dominant source of variability.

When the duty cycles of the blazars in this sample (all low-energy-cutoff BL Lac objects or LBLs) were compared to the duty cycles of HBLs (high-energy-cutoff BL Lac objects), the long standing assertion that HBLs are less variable as a class than LBLs was confirmed. The result from the duty cycle versus state investigation showed that HBLs do indeed exhibit optical microvariability less often than do LBLs (by a factor of more than 2), suggesting that the duty cycle is very different for the two classes of objects. This may possibly be a selection effect due to an intrinsic difference between the two classes. There exists evidence that HBLs have jets with wider opening angles leading to a marked decrease in amplification from relativistic beaming (e.g., Gopal-Krishna et al. (2004)). This is seen in lower measured

Lorentz factors and lower $\beta = v/c$ (see e.g., Vermeulen and Cohen (1994), Jorstad et al. (2001), and Piner and Edwards (2004)). Lower amplification of the variable emissions in HBLs means that it is much more difficult to detect the resulting brightness variations.

The next line of investigation using the duty cycles was to search for a correlation between the duty cycle of the LBLs in this sample and their 5 GHz radio flux. Previous studies (Campbell, 2004) have found that the duty cycles of HBLs are correlated with the 5 GHz radio flux. No such correlation is found for the LBLs in this sample. Furthermore, upon investigation of the possible relationship between duty cycle and apparent speed $\beta = v/c$ of material in the jet, no correlation was found. This too was in disagreement with the results of Campbell (2004) for HBLs. This supports the findings of Sagar et al. (2004) and Stalin et al. (2004) that report that high optical polarization is a stronger indicator of high duty cycles of optical microvariability for LBLs than the radio jet properties.

The analysis methods continued with determination of microvariability morphology of the nightly light curves. The morphology of the light curves was split into 6 bins of 3 types of morphologies: -1, -C, C, 0, C+, 1+ indicating a light curve with a negative slope, one with a negative slope and superimposed variations, variations without a trend, no detectable variations whatsoever, a variable light curve with a positive slope, and one with only a positive slope, respectively. Each light curve was examined and assigned to one of these classes. The initial result of this line of investigation is that the variability morphology of the LBLs in this sample is primarily complex in nature, which agrees with the results of Campbell (2004). The vast majority of variations seen are complex and very few “clean” trends are seen.

The morphology of LBLs was also investigated as a function of luminosity state. The result of this investigation was that luminosity state played virtually no role in the morphology of the light curves. This result, like the result of duty cycle being independent of luminosity state, argues the dominant source of variations is from a region whose variations are equally visible regardless of luminosity state (i.e., turbulence behind shocks in a jet, as suggested by e.g., Marscher and Travis (1996)).

Another line of investigation used the amplitude of variability, in both the observed and rest frame, to see if there was any dependence on state. The standard model of blazars is that a relativistic jet provides the vast majority of the luminosity. If the dominant source of variability were not in the jet, but in the accretion disk for example, the luminosity of the jet would play no role in the amplitude of variability and, in flux space, the amplitude of variation would remain constant (it would decrease in magnitude space). If, however, the dominant source of variability resided in the jet, one would expect the flux variability amplitude to scale with state (i.e., remain constant in Δ mag). This suggests that a change in variability amplitude scales with luminosity state $\Delta L \propto L$. This is exactly what is seen. Whether these values are investigated in the observed or rest frame of the source, the picture remains the same. If the average flux amplitude of variability per event is compared in both the high and low luminosity state, the difference is a factor of three in both the observed and rest frame. The rest frame variations exhibit roughly twice the average variability amplitude of the observed frame for both luminosity states.

Two more analysis methods were used to analyze the microvariability data: the structure function and the variability index. They both have the characteristic that the time-scales

indicated in the observed frame can be directly scaled into the rest frame by dividing by the factor $(1 + z)$. This allows simple and direct comparison of sources at different distances.

The structure function (SF) analysis is a powerful method, related mathematically to the cross correlation function, to determine time-scales in unevenly sampled light curves. Any turnover from a monotonically increasing function gives a characteristic time-scale. All of the microvariability data with detected microvariability and enough observations to adequately describe that variability were analyzed in this fashion. The results show that the typical time-scales ranged from 0.3 hours up to 5.1 hours, with BL Lac showing the largest time-scales (which makes sense because it is the least time *undilated*). Of course, any longer time-scales could not be seen in the data which rarely covered more than 7 hours. It is important to note that the SFs of these light curves generally show different character from night to night and different time-scales from night to night. There are exceptions to this SF variability, but they show that, in general, the source regions responsible for the emission are in a constant state of change on time-scales of a day or less.

The variability index (VI) analysis is somewhat similar to the SF analysis in that it can detect characteristic time-scales, but can also determine fractional variability which is independent of reference frame. The interpretations of the VI plots are similar to those of the SFs in that turnovers in monotonically increasing slopes indicate characteristic time-scales. The VI appears less sensitive to certain types of variability (e.g., noisy data or multiple, discrete variability time-scales within one light curve), and may not be a reliable method to detect variability time-scales. That said, the time-scales determined for the microvariability data analyzed here (the same as analyzed with the SF) range from 0.7 to 8.5 hours, roughly

double the time-scale indicated by the SF analysis, and fractional variability amplitudes from 0.01 to 0.45 are seen. The most important result from the VI analysis is not the time-scales or the fractional variability amplitudes, but the predominant shape of the VI for all data analyzed here. For *all* light curves analyzed, the VI has always increased with the time window. This indicates that the amplitude of variability scales with the observation interval and that larger intervals will increase the chances of detecting variability. Another result, similar to that revealed by the SF, is that the slope and shape of the VI changes from night to night, indicating a very dynamic source region.

5.1.2 Color variability

The color variability investigation utilized newly acquired data from the SMARTS consortium that was virtually simultaneous in up to 6 filters (3 optical and 3 near-IR: *BVRJHK*). The data were gathered for 11 objects for periods ranging from 7 to 21 months. This allowed the color properties of the blazars in this sample (mostly LBLs) to be investigated.

The objects studied showed very large scale variations from ~ 0.1 mag up to ~ 5 mag on time-scales ranging from as short as a week up to several months or more. Many of the objects (3C 279, 1510 – 089, 1622 – 297, 2155 – 304, 3C 446, and 2345 – 167) showed very dramatic flares, ranging in amplitude from 0.5 up to more than 2 mag, and but one (3C 273) has shown virtually no variability at all, varying less than 0.2 mag over the 7 months it was observed.

The overall morphology of the variations seen in these long-term light curves mirrors those of the microvariability light curves. In both cases, trends, with and without superimposed

variations are seen; flares of different magnitude (0.2 to 2 mag) show very similar structure; and the overall complex structure is seen on both time-scales. This argues for similar physics in the emitting regions but at far different sizes and time-scales.

The primary method of analysis for multi-color observations was plotting both light curves and color indices versus time. This allowed the direct comparison of the amplitude of variability with any color changes in the sources. All sources showed color variation with time in all color indices, but few gave a hint of correlation with the amplitudes of variability of the source. The optical data were of high S/N with a mean error of $\lesssim 0.05$ mag, so it is not likely that poor data prevented the discovery of correlation within the optical regime. It is more likely that the spectral width traversed gave too little leverage to find the differences. It was for this reason, in part, that near-IR data were obtained as well. Unfortunately, due to severe time constraints (only 0.5 hour to observe 6 objects in 6 filters in each observing block), the quality of the near-IR data (error of $\lesssim 0.2$ mag) was insufficient to properly characterize the color variability, but some positive indications were derived despite this. With three objects (0420 – 014, 1622 – 297, and 2345 – 167), all LBLs, there *appears* to be a trend toward the objects getting redder as they brighten. This is consistent with the increase of the synchrotron peak red-ward of the optical/near-IR window with increasing luminosity (i.e., a change in spectral slope). One of the 2 HBLs, 2005 – 489, showed a possible trend of getting bluer with increasing brightness. This is consistent with its synchrotron peak being blue-ward of the optical/near-IR window.

To determine if there were any measurable time lags associated with the the color changes, a cross correlation function (CCF) was run on the 4 objects that showed the possible color

variations with amplitude. All the optical CCFs were very similar to the ACF of the B band light curve, but only one IR band light curve (H band for 0420 – 014) was well behaved enough to show a realistic result. None of the CCFs showed a measurable lead or lag. There were some slight indications, but no definite positive result. This is likely due to combination of 2 factors: (1) too narrow spectral width, and (2) too coarse temporal sampling, or it may be that any lags simply do not exist.

Another method of analysis afforded by the well sampled data was rest frame auto correlation functions (ACFs). The idea is that for long-term light curves, the full width at half maximum of the ACF may be related to a characteristic time-scale, perhaps an upper limit to the larger scale source regions. The best sampled optical band light curve of each object with a known redshift was shifted back into the rest frame of the source to allow a more intrinsic comparison. Only cosmological effects were taken into account with this conversion, and no corrections were made for the beaming of the emissions because the desire was to investigate rest frame variations, not jet physics, and because of substantial inherent inaccuracies in the determination of the jet parameters used in such a conversion. The result of this investigation was that the source region sizes, as indicated by the FWHM of the ACFs, varied quite a bit from source to source. In comparing these values with those derived from the structure function and variability index analyses, it is seen that the time-scales from the FWHM are orders of magnitude larger than the SF/VI sizes, which is consistent if they are to be considered upper limits. If the FWHM value derived for each object is compared to the light curve of the object, the indicated time-scale is typically the shortest resolved time-scale for some and an intermediate time-scale for others. There appears to be no other

correlation of these derived sizes.

5.2 Future Work

Investigations like the ones just summarized are not just done for one purpose. They are an ongoing discovery of the nature of the objects investigated. The most obvious continuation of these investigations is to include more objects into the sample to give a more accurate picture of the processes defining blazars as a class, and to fill in any gaps in redshift. Also, adding a greater number of nights of microvariability observations per object helps improve the statistics for all the rest frame investigations.

The second most obvious continuation is to improve the quality of the multi-color data, particularly the near-IR observations. It is very important in determining reliable color differences and time lags to have improved temporal resolution (i.e., $\lesssim 1\text{day}$) as well as much higher S/N observations in this regime.

Another logical offshoot of the present investigations is to integrate more HBLs into the sample to directly investigate the differences of the two classes. This can only lead to greater understanding of the the processes that make these two classes different and the ones which give them similar characteristics (e.g., Doppler boosting.)

The null results of the duty cycle versus the radio jet properties is an important investigation to pursue. It will allow investigations into jet properties that were inadequately covered in this dissertation.

The overall future goal is to develop better ways to organize and handle the data that is used in these investigations. More than 50,000 raw frames (both calibration and science)

were used to yield the final results of this dissertation. Reducing data is one of the most time consuming and tedious aspects of astronomical studies and no other aspect has as far reaching implications. The final results can be no better than the quality of the data that went into it.

Appendix A

Scripts

A.1 pegasort

The `pegasort` script sorts the output (.log format) of the CCDPHOT multi-aperture photometry program. It is used to pre-process data for use with the `pegaplot` script. It transposes multiple lines per frame into one line that contains time information for the frame, FWHM, peak counts (in ADU), and instrumental magnitudes for the object and all comparison stars. The object name must not have any spaces and the comparison stars must be named “checkX”, where X is a numeric or alphabetic designation. The comparison stars must be listed in increasing order with numeric preceding alphabetic designations.

```
#!/bin/bash

# pegasort by J.P.M. 2000-07-15
#
# usage: pegasort ccdphot_logfile_without_extension [no_header]
#
# This script takes Marc Buie's CCDPhot output file and converts it to
# something more usable for the PEGA team
#
# The logfile name (without .log extension) is required, but the
# no_header argument is optional.
#
# At this time, there is a limitation to this script. If the CCDPhot
# .log file has multiple entries for the same frame, the sorting is
# imperfect. To avoid redundancy, simply remove the unwanted extra
# entries and re-sort.
#
# Also, if the check stars are out of order (the proper order is numeric
# before alphabetic), it is problematic for pegaplot.
#

LOGFILE=$1
```



```

# see how we were called
if [ "$LOGFILE" = "" ] || [ ! -f $LOGFILE.log ] ; then
    echo
    echo "usage: pegasort ccdphot_log_file_without_extension [no_header]"
    echo "logfile name required (sans the .log extension)"
    echo "the header is prepended if no second argument included"
    echo
    exit 1
fi

# no need to append to the dat file
if [ -f "$LOGFILE.txt" ] ; then
    echo ".txt file exists. Moving to backup file . . . "
    mv -fv $LOGFILE.txt $LOGFILE.txt.bak
fi

# check the version of the .log file
#
# older versions
# filename object filter JD exptime gain rad sky1 sky2 serial xpos ypos
#   fwhm maxcnt mag err bad
#
# newer version (has "PHOTFILE v1.0" as the first line)
# filename object filter JD exptime gain rad sky1 sky2 serial xpos ypos
#   fwhm maxcnt sky skyerr mag err bad
#
PHOTFILE=$(grep PHOTFILE $LOGFILE.log)
COLUMNS=$(awk '{print NF}' $LOGFILE.log | sort | uniq)
if [ "$PHOTFILE" == "PHOTFILE v1.0" ] ; then
    OV=2
    grep -v PHOTFILE $LOGFILE.log > $LOGFILE.new
    mv -f $LOGFILE.new $LOGFILE.log
elif [ $COLUMNS -eq 19 ] ; then
    OV=2
elif [ $COLUMNS -eq 17 ] ; then
    OV=0
else
    echo -e "\n.log file in unknown format!"
    echo -e "Please check and try again.\n"
    exit 2
fi

```

```

# get a list of the objects plus checks in the .log file
OBJ_LIST=$(gawk -F "' " '{gsub(/ /,".", $2) ; print $2}' $LOGFILE.log |
            sort | uniq)

# initialize the number of checks counter
n=0;k=0

# separate the object from the checks and assign the checks a number
for j in $(echo $OBJ_LIST)
do
    if [ "$(echo $j | grep check)" != "" ] ; then
        CHK_LIST="$CHK_LIST\n$j"
        CHK_LIST=$(echo -e $CHK_LIST)
        n=$((n+1))
    else
        OBJECT=$j
        OBJ=$(echo $j | gawk '{gsub(/\./,"", $0) ; print $0}')
    fi
done

# print out the object and check stars
echo ""
echo "The object in this log file is $(echo $OBJECT |
                                     gawk '{gsub(/\./,"", $0) ;
                                     print $0}')"

echo ""
echo "The list of check stars is as follows:"
echo "$CHK_LIST"
echo ""

# write the header to the output file
if [ "$2" = "" ] ; then
    HEADER="image filter JD exptime RJD PixAp ArcAp '${OBJ}'FWHM
            '${OBJ}'cts '${OBJ}'mag"
    for b in $(echo $CHK_LIST) ; do
        HEADER="$HEADER '${b}'FWHM '${b}'cts '${b}'mag"
    done
    echo $HEADER > $LOGFILE.txt
fi

# start the sorting
# pull out all the dates and get the object info for each date
LIST=$(gawk -v OV=$OV '{print $(NF-13-OV)}' $LOGFILE.log | uniq)
for i in $LIST ; do

```

```

echo -ne "Now sorting Julian Date $i\r"
CURRENT_JD=$(grep $i $LOGFILE.log |
              gawk '{gsub(/\./,"",$2) ; print $0}')
m=0

until [ ! "$CURRENT_JD" ] ; do
    CURRENT_OBJ=$(echo "$CURRENT_JD" | head -n1)
    if [ "$(echo $CURRENT_OBJ | grep $OBJECT)" ] ; then
        FRAME=$(echo $CURRENT_OBJ |
                gawk -v OV=$OV '{print $1,$(NF-14-OV),$(NF-13-OV),
                $(NF-12-OV),"--",$(NF-10-OV),"--",$(NF-4-OV),$(NF-3-OV),
                $(NF-2)}')
        CURRENT_JD=$(echo "$CURRENT_JD" | grep -v "$CURRENT_OBJ")
    fi

    for a in $(echo $CHK_LIST) ; do
        CURRENT_OBJ=$(echo "$CURRENT_JD" | head -n1)
        if [ "$(echo $CURRENT_OBJ | grep $a)" ] ; then
            FRAME="$FRAME $(echo $CURRENT_OBJ |
                            gawk -v OV=$OV '{print $(NF-4-OV),$(NF-3-OV),
                            $(NF-2)}') "
            CURRENT_JD=$(echo "$CURRENT_JD" | grep -v "$CURRENT_OBJ")
        else
            FRAME="$FRAME -- -- --"
        fi
    done
    # write each date to the output file
    echo $FRAME >> $LOGFILE.txt
    FRAME='echo $FRAME | cut -d ' ' -f 1-10'
    m=$((m+1))
    if [ $k -lt $m ] ; then k=$m ; fi
done
done

if [ $k -gt 2 ] ; then
    echo ""
    echo ""
    echo " * * * * * "
    echo " *                               WARNING                               * "
    echo " * * * * * "
    echo " * "
    echo " *      Duplicate entries MAY exist in OUTPUT file!      * "
    echo " * "
    echo " *      Check the INPUT file for duplicate entries.      * "

```


A.2 pegaplot

The `pegaplot` script is capable of creating publication quality plots by acting as a front-end to the `gnuplot` program (www.gnuplot.info). It is a very extensive script with full usage instructions built in. It will plot the output files of `pegasort` (.txt format), and will automatically handle 2 column (time, observable) or 3 column (time, observable, error) data files with a .dat extension, and can handle arbitrary columns using `gnuplot`'s syntax (e.g., 1:2:3 for the first three columns as time, observable, error, respectively).

```
#!/bin/bash

#
# pegaplot by J.P.M. 2001-06-19, 2001-06-25
#
# usage: pegaplot pegasort_txtfile
#         pegaplot -h (for additional options)
#
# This script is for generating data graphs via GnuPlot.
#
# The data to be plotted MUST be the output of the pegasort script.
# Any other input files will only yield unpredictable results.
#
# The default output of the script is in GNUPlot X format, but can
# easily be publication quality postscript files.
#
# For more information, type "pegaplot -h" or contact the author at
# <jpm@chara.gsu.edu>
#

if [ $# -lt 1 ] ; then
    echo ""
    echo "usage: pegaplot data_file.txt"
    echo ""
    echo "Try \"pegaplot -h\" for detailed usage."
    echo ""
    exit 1
fi

GAWK="gawk -v OFMT=%.6f"
SORT="sort -g"

# r=range, h=help, O=object, f=filter, d=date, j=JD_format
```

```

# e=no_error_bars, c=bar_cross_size, T=tic_inc, N=num_tic
# t=terminal, o=output_gnuplot, a=aspect, b=base_output_filename
# p=portrait, l=landscape, s=symbol_index, J=JD_padding

while getopts :r:O:f:d:j:e:c:T:X:Y:N:x:y:t:oa:hpls:S:qkJmDE:b:B: NAME
do
  case $NAME in
    r) DELTA_MAG=$OPTARG
      ;;

    O) OBJECT=$OPTARG
      ;;

    f) FILTER=$OPTARG
      ;;

    d) CCYYMMDD=$OPTARG
      ;;

    j) BAS_JD=$OPTARG
      ;;

    e) STYLE="errorbars"
      if [ $OPTARG = 0 ] ; then
        POINT_SIZE=1
        ERR_INDEX=0
        ERROR=0
      else
        POINT_SIZE=0
        ERR_INDEX=0
        ERROR=$OPTARG
      fi
      ;;

    c) BAR_SIZE=$OPTARG
      ;;

    T) XTIC_INC=$OPTARG
      YTIC_INC=$OPTARG
      ;;

    X) XTIC_INC=$OPTARG
      ;;
  esac
done

```

[illegible]


```

p) TERMINAL="postscript portrait"
   SIZE="1.0, 0.6"
   POSTSCRIPT=1
;;

l) TERMINAL="postscript landscape"
   SIZE="1.0, 1.0"
   POSTSCRIPT=1
;;

a) SIZE="ratio $OPTARG"
;;

q) QUIET=1
;;

k) KEEP=1
;;

m) MAX=1
;;

D) DAT=1
;;

E) NUM_ENTRY=$(echo $OPTARG | $GAWK -F ":" '{print NF}')
```

```

    if [ $NUM_ENTRY -eq 2 ] ; then
        X=$(echo $OPTARG | $GAWK -F ":" '{print $1}')
```

```

        Y=$(echo $OPTARG | $GAWK -F ":" '{print $2}')
```

```

        COLUMNS=2
```

```

    elif [ $NUM_ENTRY -eq 3 ] ; then
        X=$(echo $OPTARG | $GAWK -F ":" '{print $1}')
```

```

        Y=$(echo $OPTARG | $GAWK -F ":" '{print $2}')
```

```

        Z=$(echo $OPTARG | $GAWK -F ":" '{print $3}')
```

```

        COLUMNS=3
```

```

    fi
;;

b) XLABEL=$OPTARG
;;

B) YLABEL=$OPTARG
;;

```

```

*) echo ""
   echo "usage: pegaplot data_file.txt"
   echo ""
   echo "Try \"pegaplot -h\" for detailed usage."
   echo ""
   exit 1
;;
esac
done
shift $((OPTIND - 1))

DATA_FILE=$1

if [ ! "$ERR_INDEX" ] ; then
    ERR_INDEX=1
fi
if [ ! "$DELTA_JD" ] ; then
    DELTA_JD=10
fi
if [ ! "$DELTA_MAG" ] ; then
    DELTA_MAG=0.5
fi
if [ ! "$CCYYMMDD" ] ; then
    CCYYMMDD=$(echo $DATA_FILE | $GAWK -F. '{print $1}')
fi

DATE=$(date -d $CCYYMMDD +%d %b %Y)
LINES=$(wc -l $DATA_FILE | $GAWK '{print $1}')
if [ ! $COLUMNS ] ; then
    COLUMNS=$(($GAWK '{print NF}' $DATA_FILE | $SORT | uniq)
fi

if [ "$(echo $DATA_FILE | grep dat)" ] || [ $DAT ] ; then
#
# Free format .dat file
#
#
# set default columns
#
if [ $COLUMNS -eq 2 ] ; then
    if [ ! $X ] ; then
        X=1
    fi
    if [ ! $Y ] ; then

```

```

        Y=2
    fi
    if [ $ERROR ] ; then
        Z="($ERROR)"
        ENTRY="$X:$Y:$Z"
        if [ ! $STYLE ] ; then
            STYLE="errorbars"
        fi
    else
        ENTRY="$X:$Y"
        if [ ! $STYLE ] ; then
            STYLE="points"
        fi
    fi
elif [ $COLUMNS -ge 3 ] ; then
    if [ ! $X ] ; then
        X=1
    fi
    if [ ! $Y ] ; then
        Y=2
    fi
    if [ ! $Z ] ; then
        Z=3
    fi
    ENTRY="$X:$Y:$Z"
    if [ ! $STYLE ] ; then
        STYLE="errorbars"
    fi
fi
#
# get the time range
#
DELTA_TIME=$DELTA_JD
TOT_TIME=$(($GAWK -v TIME=$X '{print $TIME}' $DATA_FILE)
MIN_TIME=$(echo "$TOT_TIME" | $SORT | head -n1 | $GAWK '{print $1}')
MAX_TIME=$(echo "$TOT_TIME" | $SORT | tail -n1 | $GAWK '{print $1}')
DEL_TIME=$(($GAWK -v max=$MAX_TIME -v min=$MIN_TIME -v d=$DELTA_TIME
            'BEGIN {print (min==max) ? d/100 : (max-min)*d/100}'))
MIN_TIME=$(($GAWK -v min=$MIN_TIME -v del=$DEL_TIME
            'BEGIN {print min-del}'))
MAX_TIME=$(($GAWK -v max=$MAX_TIME -v del=$DEL_TIME
            'BEGIN {print max+del}'))
#
# set some fundamental plot parameters

```

```

#
if [ ! "$ERROR" ] ; then
    ERROR=0
fi
if [ ! "$POINT_SIZE" ] ; then
    POINT_SIZE=1
fi
if [ ! "$POINT_TYPE" ] ; then
    POINT_TYPE=3
fi
if [ ! "$BAR_SIZE" ] ; then
    BAR_SIZE=0.0
fi
if [ ! "$TERMINAL" ] ; then
    TERMINAL="X"
fi
if [ ! "$OBJECT" ] ; then
    OBJECT="Unknown Object"
fi
if [ "$TERMINAL" = "postscript eps" ] ||
    [ "$TERMINAL" = "postscript portrait" ] ; then
    TITLE="'$OBJECT          $FILTER Filter          $DATE'
          0.0,0.0 \"Helvetica, 18\""
else
    TITLE="'$OBJECT
          $FILTER Filter
          $DATE' 0.0,0.0 \"Helvetica, 18\""
fi
if [ ! "$XLABEL" ] ; then
    XLABEL="Time (unknown base)"
fi
if [ ! "$YLABEL" ] ; then
    YLABEL="Magnitude or Flux"
fi
#
# get the mag range
#
if [ ! "$(echo $Y | egrep [[:punct:]])" ] ; then
    TOT_MAG=$(($GAWK -v MAG=$Y '!/JD/ && !/99.9990/ && !/--/ {print $MAG}'
               $DATA_FILE)
else
    #
    # in case the y value is complex (e.g. 2-3)
    #

```

```

Y1=$(echo $Y | sed 's/[[:punct:]]/ /g' | awk '{print $1}')
Y2=$(echo $Y | sed 's/[[:punct:]]/ /g' | awk '{print $2}')
SIGN=$(echo $Y | sed 's/[[:digit:]]//g')
TOT_MAG=$(($GAWK -v MAG1=$Y1 -v MAG2=$Y2 -v SIGN=$SIGN
            '!/JD/ && !/99.9990/ && !/--/ {print $MAG1-$MAG2}'
            $DATA_FILE)
Y=$(echo $Y | sed 's/[[:digit:]]/$&/g')
if [ $COLUMNS -eq 2 ] ; then
    if [ $ERROR ] ; then
        Z="($ERROR)"
        ENTRY="$X:($Y):$Z"
        if [ ! $STYLE ] ; then
            STYLE="errorbars"
        fi
    else
        ENTRY="$X:($Y)"
        if [ ! $STYLE ] ; then
            STYLE="points"
        fi
    fi
elif [ $COLUMNS -ge 3 ] ; then
    ENTRY="$X:($Y):$Z"
fi
fi
AVG_MAG=$(echo "$TOT_MAG" | $GAWK -v x=0 '{x+=$1} END
            {print x/NR}')
MIN_MAG=$(($GAWK -v avg=$AVG_MAG -v del=$DELTA_MAG 'BEGIN
            {print avg-(del/2)}')
MAX_MAG=$(($GAWK -v avg=$AVG_MAG -v del=$DELTA_MAG 'BEGIN
            {print avg+(del/2)}')
#
# now plot it
#
echo -e "
    set nokey
    set title $TITLE
    set xlabel '$XLABEL' 0.0,-1.0 \"Helvetica, 18\"
    set ylabel '$YLABEL' 0.0,0.0 \"Helvetica, 18\"
    set xrange [$MIN_TIME:$MAX_TIME]
    set yrange [$MAX_MAG:$MIN_MAG]
    set format y \"%.2f\"
    set format x \"%.2f\"
    set data style $STYLE
    set bar $BAR_SIZE

```

```

set clip points
set clip one
set tics in
set xtics $XTIC_INC
set mxtics $XTIC_NUM
set ytics $YTIC_INC
set mytics $YTIC_NUM
set bmargin 4
set lmargin 10
set rmargin 7
set tmargin 3
set terminal $TERMINAL
set size $SIZE
set output '$CCYMMDD.ps'
plot \"$DATA_FILE\" using $ENTRY pt $POINT_TYPE ps
    $POINT_SIZE" > . $CCYMMDD.gp

gnuplot -persist . $CCYMMDD.gp

if [ "$POSTSCRIPT" ] && [ ! "$QUIET" ] ; then
    gv . $CCYMMDD.ps
fi

if [ ! "$KEEP" ] ; then
    rm . $CCYMMDD.ps
else
    mv -i . $CCYMMDD.ps $CCYMMDD.ps
fi

if [ ! "$GNUPLOT" ] ; then
    rm . $CCYMMDD.gp
else
    mv -i . $CCYMMDD.gp $CCYMMDD.gp
fi
else
#
# Standard format .txt file
#
if [ ! $(($GAWK '/JD/ {print $1}' $DATA_FILE) ) ] ; then
    echo ""
    echo "The data file needs to have the header information."
    echo "Rerun \"pegasort\" on the .log file and try again."
    echo ""
    exit 2

```

```

fi

#
# For the above, use "gawk -F. '{print $NF}' $DATA_FILE" to get the
# extension. If it is .log or the above is true, offer to run pegasort
# on the file. Else proceed with the rest of the script.
#
# Also, put in a switch to allow preprocessing through pegasort by
# default.
#

# there should be a better way to do this . . .
if [ ! "$BAS_JD" ] ; then
    BAS_JD="$($GAWK 'FNR==2 {print $3}' $DATA_FILE | cut -b 1-3)0000"
fi
TOT_JD=$($GAWK '/JD/ {print $3}' $DATA_FILE)
MIN_JD=$(echo "$TOT_JD" | $SORT | head -n1 | $GAWK -v BAS=$BAS_JD
    '{print $1-BAS}')
MAX_JD=$(echo "$TOT_JD" | $SORT | tail -n1 | $GAWK -v BAS=$BAS_JD
    '{print $1-BAS}')
DEL_JD=$($GAWK -v max=$MAX_JD -v min=$MIN_JD -v d=$DELTA_JD
    'BEGIN {print (min==max) ? d/100 : (max-min)*d/100}')
MIN_JD=$($GAWK -v min=$MIN_JD -v del=$DEL_JD 'BEGIN {print min-del}')
MAX_JD=$($GAWK -v max=$MAX_JD -v del=$DEL_JD 'BEGIN {print max+del}')

#
# Need mechanism to determine number of check stars.
#

if [ ! "$OBJECT" ] ; then
    OBJECT=$($GAWK '/JD/ {print $10}' $DATA_FILE | cut -d '"' -f2)
fi
if [ ! "$FILTER" ] ; then
    FILTER=$($GAWK '/JD/ {print $2}' $DATA_FILE | uniq | tail -n1)
fi

CHK_NUM=$($GAWK '/JD/ {for (i=0;i<((NF-10)/3);i++) print (3*i+13)}'
    $DATA_FILE)
CHK_NAM=$($GAWK '/JD/ {for (i=0;i<((NF-10)/3);i++) print $(3*i+13)}'
    $DATA_FILE)
OBJ_LIST=$($GAWK '/JD/ {for (i=0;i<((NF-10)/3);i++)
    print (3*i+13)$(3*i+13)}' $DATA_FILE)
OBJ_LIST="10'$(echo "$OBJECT" | sed -e 's/ //g')'mag $OBJ_LIST"

```

```

# echo $OBJ_LIST -> 10'object'mag 13'check1'mag 16'check2'mag . . .
#
# do OBJECT wrt CHKn and then CHKn wrt CHKm . . .

# $10 below should be variable and that entire statement
# should be in a for loop.
#

#
# initialize the best std dev and other variable
#
BEST_SD=unknown

if [ ! "$ERROR" ] ; then
    ERROR=0
fi

if [ ! "$POINT_SIZE" ] ; then
    POINT_SIZE=1
fi

if [ ! "$POINT_TYPE" ] ; then
    POINT_TYPE=3
fi

if [ ! "$BAR_SIZE" ] ; then
    BAR_SIZE=0.0
fi

if [ ! "$TERMINAL" ] ; then
    TERMINAL="X"
fi

if [ "$TERMINAL" = "postscript eps" ] ||
    [ "$TERMINAL" = "postscript portrait" ] ; then
    TITLE="'$OBJECT          $FILTER Filter
          $DATE' 0.0,0.0 \"Helvetica, 18\""
else
    TITLE="'$OBJECT
          $FILTER Filter
          $DATE' 0.0,0.0 \"Helvetica, 18\""
fi

```



```

for i in $(echo $OBJ_LIST) ; do
for j in $(echo $OBJ_LIST) ; do

    INDEX_1=$(echo $i | cut -d '"' -f1)
    INDEX_2=$(echo $j | cut -d '"' -f1)

    if [ $INDEX_1 -ge $INDEX_2 ] ; then
        continue
    fi

    OBJ=$(echo $i | cut -d '"' -f2)
    CHK_STAR=$(echo $j | cut -d '"' -f2)
    TOT_MAG=$(($GAWK -v CHK1=$INDEX_1 -v CHK2=$INDEX_2 '!/JD/ && !/99.9990/
        {if (($CHK1 != "--") && ($CHK2 != "--")) print $CHK1-$CHK2}'
        $DATA_FILE)
    AVG_MAG=$(echo "$TOT_MAG" | $GAWK -v x=0 '{x+=$1} END
        {print x/NR}')
    MIN_MAG=$(($GAWK -v avg=$AVG_MAG -v del=$DELTA_MAG 'BEGIN
        {print avg-del/2}')
    MAX_MAG=$(($GAWK -v avg=$AVG_MAG -v del=$DELTA_MAG 'BEGIN
        {print avg+del/2}')

    #
    # variance = (1/n)*sum((x_i-avg(x))**2)
    # std_dev = sqrt(variance) <---- best describes the error
    # std_err = std_dev/sqrt(n)
    # pnt_var = sqrt((x_i-avg(x))**2)
    #

    # This doesn't make sense if it's obj-chk . . .
    if [ $INDEX_1 -ne 10 ] ; then
        STD_DEV=$(echo "$TOT_MAG" | $GAWK -v AVG=$AVG_MAG -v x=0
            '{x+=$(1-AVG)**2} END {print (NR>1) ? sqrt(x/(NR-1)) :
            sqrt(x/NR)}')
        if [ $MAX ] ; then
            echo "Standard Deviation for $OBJ-$CHK_STAR is $STD_DEV"
        fi
        CHANGED=$(echo $STD_DEV $BEST_SD |
            $GAWK '{print ($1<$2 ? 1 : 0)}')
        if [ $CHANGED -eq 1 ] ; then
            BEST_SD=$STD_DEV
            BEST_COMP1="$OBJ"
            BEST_COMP2="$CHK_STAR"

```

```

        BEST_IDX1="$INDEX_1"
        BEST_IDX2="$INDEX_2"
    fi
    if [ $ERR_INDEX -ne 0 ] ; then
        ERROR=$STD_DEV
        POINT_SIZE=0
    fi
fi

#
# Start the actual plot
#

#
# Only plot everything if asked for it
#
if [ $MAX ] ; then

    echo -e "
        set nokey
        set title $TITLE
        set xlabel 'Julian Date (+$BAS_JD)' 0.0,-1.0 \"Helvetica, 18\"
        set ylabel 'Diff Mag ($OBJ - $CHK_STAR)' 0.0,0.0 \"Helvetica, 18\"
        set xrange [$MIN_JD:$MAX_JD]
        set yrange [$MAX_MAG:$MIN_MAG]
        set format y \"%.2f\"
        set format x \"%.2f\"
        set data style errorbars
        set bar $BAR_SIZE
        set clip points
        set clip one
        set tics in
        set xtics $XTIC_INC
        set mxtics $XTIC_NUM
        set ytics $YTIC_INC
        set mytics $YTIC_NUM
        set bmargin 4
        set lmargin 10
        set rmargin 7
        set tmargin 3
        set terminal $TERMINAL
        set size $SIZE
        set output '.$CCYYMMDD.$OBJ-$CHK_STAR.ps'
        plot \"$DATA_FILE\" using

```

```

        (\$3-$BAS_JD):(\$$INDEX_1-\$$INDEX_2):("$ERROR") pt $POINT_TYPE
        ps $POINT_SIZE" > .\$CCYYMMDD.$OBJ-$CHK_STAR.gp

gnuplot -persist .\$CCYYMMDD.$OBJ-$CHK_STAR.gp

if [ "$POSTSCRIPT" ] && [ ! "$QUIET" ] ; then
    gv .\$CCYYMMDD.$OBJ-$CHK_STAR.ps
fi

if [ ! "$KEEP" ] ; then
    rm .\$CCYYMMDD.$OBJ-$CHK_STAR.ps
else
    mv -i .\$CCYYMMDD.$OBJ-$CHK_STAR.ps \$CCYYMMDD.$OBJ-$CHK_STAR.ps
fi

if [ ! "$GNU PLOT" ] ; then
    rm .\$CCYYMMDD.$OBJ-$CHK_STAR.gp
else
    mv -i .\$CCYYMMDD.$OBJ-$CHK_STAR.gp \$CCYYMMDD.$OBJ-$CHK_STAR.gp
fi
fi
done
done

#
# Now plot the minimum if the maximum wasn't asked for
#

if [ ! $MAX ] ; then

    if [ $ERR_INDEX -ne 0 ] ; then
        ERROR=$BEST_SD
        POINT_SIZE=0
    fi

    OBJ_LIST="10'$OBJECT $BEST_IDX1'$BEST_COMP1 $BEST_IDX2'$BEST_COMP2"

    for i in $(echo $OBJ_LIST) ; do
        for j in $(echo $OBJ_LIST) ; do

            INDEX_1=$(echo $i | cut -d '"' -f1)
            INDEX_2=$(echo $j | cut -d '"' -f1)

            if [ $INDEX_1 -ge $INDEX_2 ] ; then

```

```

    continue
fi

OBJ=$(echo $i | cut -d " " -f2)
CHK_STAR=$(echo $j | cut -d " " -f2)
TOT_MAG=$(($GAWK -v CHK1=$INDEX_1 -v CHK2=$INDEX_2 '!/JD/ &&
    !/99.9990/ {if (($CHK1 != "--") && ($CHK2 != "--"))
        print $CHK1-$CHK2}' $DATA_FILE)
AVG_MAG=$(echo "$TOT_MAG" | $GAWK -v x=0 '{x+=$1} END
    {print x/NR}')
MIN_MAG=$(($GAWK -v avg=$AVG_MAG -v del=$DELTA_MAG 'BEGIN
    {print avg-del/2}')
MAX_MAG=$(($GAWK -v avg=$AVG_MAG -v del=$DELTA_MAG 'BEGIN
    {print avg+del/2}')

echo -e "
    set nokey
    set title $TITLE
    set xlabel 'Julian Date (+$BAS_JD)' 0.0,-1.0 \"Helvetica, 18\"
    set ylabel 'Diff Mag ($OBJ - $CHK_STAR)' 0.0,0.0 \"Helvetica, 18\"
    set xrange [$MIN_JD:$MAX_JD]
    set yrange [$MAX_MAG:$MIN_MAG]
    set format y \"%.2f\"
    set format x \"%.2f\"
    set data style errorbars
    set bar $BAR_SIZE
    set clip points
    set clip one
    set tics in
    set xtics $XTIC_INC
    set mxtics $XTIC_NUM
    set ytics $YTIC_INC
    set mytics $YTIC_NUM
    set bmargin 4
    set lmargin 10
    set rmargin 7
    set tmargin 3
    set terminal $TERMINAL
    set size $SIZE
    set output '.$CCYYMMDD.$OBJ-$CHK_STAR.ps'
    plot \"$DATA_FILE\" using
        (\$3-$BAS_JD):(\$$$INDEX_1-\$$$INDEX_2):("$ERROR") pt $POINT_TYPE
        ps $POINT_SIZE" > .\$CCYYMMDD.$OBJ-$CHK_STAR.gp

```

```

gnuplot -persist .$CCYMMDD.$OBJ-$CHK_STAR.gp

if [ "$POSTSCRIPT" ] && [ ! "$QUIET" ] ; then
    gv .$CCYMMDD.$OBJ-$CHK_STAR.ps
fi

if [ ! "$KEEP" ] ; then
    rm .$CCYMMDD.$OBJ-$CHK_STAR.ps
else
    mv -i .$CCYMMDD.$OBJ-$CHK_STAR.ps $CCYMMDD.$OBJ-$CHK_STAR.ps
fi

if [ ! "$GNUPLLOT" ] ; then
    rm .$CCYMMDD.$OBJ-$CHK_STAR.gp
else
    mv -i .$CCYMMDD.$OBJ-$CHK_STAR.gp $CCYMMDD.$OBJ-$CHK_STAR.gp
fi
done
done
fi

echo -e "\nThe best error value is $BEST_SD obtained from
        $BEST_COMP1-$BEST_COMP2.\n"
fi

```

A.3 pegacalib

The `pegacalib` script takes the output of `pegasort` and calbrates the instrumental magnitudes into real apparent magnitudes using an appropriately formatted calibration file containing the comaprison star magnitudes and errors in the filtger of interest. See the script for the format of the comparison file and usage syntax.

```
#!/bin/bash

# pegacalib: convert relative magnitudes to apparent magnitudes

# example .comp file:
# B u=16.27(0.09) b=14.52(0.04) v=12.78(0.04) r=11.93(0.05) i=11.09(0.06)
# C u=15.53(0.06) b=15.09(0.03) v=14.19(0.03) r=13.69(0.03) i=13.23(0.04)
# H u=16.64(0.08) b=15.68(0.03) v=14.31(0.05) r=13.60(0.03) i=12.93(0.04)
# K u=16.48(0.08) b=16.26(0.05) v=15.44(0.03) r=14.88(0.05) i=14.34(0.10)
#
# Column 1 is the comparison star designation, and the remaining columns
# are the the magnitude and error for each filter: filter=mag(err). The
# filter letter MUST be lower case, and the comparison star designation
# should be upper case or a number.
#

while getopts d:i: NAME ; do
    case $NAME in
        d) DELETE=$(echo $OPTARG | sed 's/ /|/g')
            ;;
        i) INCLUDE=$(echo $OPTARG | sed 's/ /|/g')
            ;;
        esac
done
shift $((OPTIND - 1))

if [ $# -lt 3 ] ; then
    echo -e "\nUsage:\t tpega-calib data_file.txt comp_file.comp filter\n"
    exit 1
fi

GAWK="gawk -v OFMT=%.6f"

DATA_FILE=$1
COMP_FILE=$2
FILT_NAME=$(echo $3 | tr [:upper:] [:lower:])
```

```

if [ ! -f $COMP_FILE ] ; then
    echo "${COMP_FILE}_missing"
    exit 2
fi

OBJECTS=$(($GAWK '/image.filter/ {for (a=1;a<=NF;a++)
    if ($a ~ /mag/) print a$a}' $DATA_FILE |
    $GAWK -F '"' '{print $1"."$2}' | grep -v image.filter)
OBJECT=$(echo "$OBJECTS" | grep -v check)
CHECKS=$(echo "$OBJECTS" | grep check)

if [ "$INCLUDE" != "" ] ; then
    COMP_CHKS=$(awk '{print $1}' $COMP_FILE | egrep $INCLUDE)
elif [ "$DELETE" != "" ] ; then
    COMP_CHKS=$(awk '{print $1}' $COMP_FILE | egrep -v $DELETE)
else
    COMP_CHKS=$(awk '{print $1}' $COMP_FILE)
fi
COMP_DATA=$(for i in $COMP_CHKS ; do egrep ^${i} $COMP_FILE |
    sed -e 's/ /|/g' ; done)
FILE_DATA=$(sed -e 's/ /|/g' $DATA_FILE | grep -v image.filter)
HEADER=$(grep image.filter $DATA_FILE)
echo $HEADER

for i in $(echo $FILE_DATA) ; do
    for j in $(echo $CHECKS) ; do
        CHECK=$(echo "$j" | $GAWK -F "check" '{print $2}')
        CHK_IND=$(echo "$j" | $GAWK -F "." '{print $1}')
        MAG=$(echo "$COMP_DATA" | $GAWK -F "|" -v CHECK=$CHECK
            '{if($1 == CHECK) print $0}' | $GAWK -F "|" -v FILT=$FILT_NAME
            '{for (a=1;a<=NF;a++) if ($a ~ FILT) print $a}' |
            $GAWK -F= '{print $2}')
        if [ $MAG ] ; then
            MAG_VAL=$(echo $MAG | $GAWK -F "(" '{print $1}')
            MAG_ERR=$(echo $MAG | $GAWK -F "(" '{print $2}' |
                $GAWK -F ")" '{print $1}')
            OFFSET=$(echo $i | $GAWK -F "|" -v VAL=$MAG_VAL -v IND=$CHK_IND
                '{if ($IND !~ /--/ && $IND !~ 99.9990) print VAL-$IND}')
            if [ $OFFSET ] ; then
                MAG_DIFF="$MAG_DIFF\n$OFFSET"
                CAL_ERR="$CAL_ERR\n$MAG_ERR"
            fi
        fi
    fi
fi

```

```

done
MAG_OFF=$(echo -e "$MAG_DIFF" | $GAWK '{if ($1) print $1}' |
    $GAWK -v x=0 '{x+=$1} END {print x/NR}')
CAL_ERR=$(echo -e "$CAL_ERR" | $GAWK '{if ($1) print $1}' |
    $GAWK -v x=0 '{x+=$1**2} END {print sqrt(x)/NR}')
VAL_ERR=$(echo -e "$MAG_DIFF" | $GAWK '{if ($1) print $1}' |
    $GAWK -v x=0 -v AVG=$MAG_OFF '{x+=(AVG-$1)**2} END
    {if (x!=0) print (NR>1) ? sqrt(x/(NR-1)) : sqrt(x/NR)}')
ERROR=$(echo "$CAL_ERR $VAL_ERR" | $GAWK -v x=0 '{for (a=1;a<=NF;a++)
    x+=$a**2} END {print sqrt(x)/NF}')
unset MAG_DIFF CAL_ERR
OUTPUT=$(echo $i | $GAWK -F "|" -v OFF=$MAG_OFF -v ERR=$ERROR '{for
    (i=10;i<=NF;i+=3) $i=($i!="--" ? $i+OFF : "--") ; $(NF+1)=ERR ;
    $(NF+2)=OFF} {gsub(/\|/, " ", $0) ; print $0}')
echo $OUTPUT
done

```


Appendix B

Analysis Code

B.1 pegabin

The `pegabin` C program bins data into bins containing N points. See §2.3 for more information on the algorithms used.

```

/*****
 * pegabin.c
 *
 * Read in a 3 column file and bin the time, mag/flux, and error.
 *
 *****/

#include <stdio.h>
#include <stddef.h>
#include <stdlib.h>
#include <string.h>
#include <math.h>
#include "functions.h"

#define NRANSI
#include "nrutil.h"

#define LINE_LEN 255 /* standard array size for strings */

int main(int argc, char *argv[])
{
/* Declarations * * * * *
int n = 0, i, j, k, kk, factor, num, length, index = 0;
char line[LINE_LEN] = "", dummy[LINE_LEN] = "";
char file[LINE_LEN] = "", *ext, *filename, sfactor[LINE_LEN] = "";
double **data, **bin, var;
FILE *datafile, *binfile;

/* check the arguments * * * * *

```

```

if(argc<2) {
    fprintf(stderr, "\nusage: %s datafile [binning_factor]\n\n",
        argv[0]);
    exit(1);
}
if (argv[2]) {
    factor = atoi(argv[2]);
} else {
    factor = 3;
}

/* Check the data file * * * * *
if ((datafile = fopen(argv[1], "r")) == NULL) {
    fprintf(stderr, "\ncannot open file: %s\n\n", argv[1]);
    exit(1);
}

for(;;) {
    fgets(line, LINE_LEN, datafile);
    if(feof(datafile)) {
        break;
    }
    n++;
}
rewind(datafile);

/* Create the appropriate arrays * * * * *
if (n%factor == 0) {
    num = n/factor;
} else {
    num = n/factor + 1;
}
data = dmatrix(0, 2, 0, n );
bin  = dmatrix(0, 2, 0, num);

/* Read in the data file * * * * *
//printf("Reading in data file . . .\n");
for(i = 0; i < n; i++) {
    fscanf(datafile, "%lf %lf %lf", &data[0][i], &data[1][i],
        &data[2][i]);
}
fclose(datafile);

/* bin the data from data[] [] to bin[] [] * * * * *

```

```

//printf("Binning datafile by a factor of %d . . .\n", factor);
/* create new name: file+"b"+factor+ext */
strcpy(dummy, argv[1]);
length = strlen(dummy);
for(i = length-1; i >= 0 ; i--) {
    if (dummy[i] == '.') {
        index = i;
        break;
    }
}
strncpy(file, dummy, index+1); /* base filename */
ext = strrchr(dummy, '.'); /* extension */
/* convert (int) factor into (string) sfactor */
itoa(factor, sfactor);
filename = strcat(strcat(strcat(file, "b"), sfactor), ext);
if ((binfile = fopen(filename, "w")) == NULL) {
    fprintf(stderr, "\ncannot open file: %s\n\n", dummy);
    exit(1);
}

j = 0;
for(i = 0; i < num; i++) {
    bin[0][i] = bin[1][i] = bin[2][i] = 0; /* initialize arrays */
    for(k = 0; k < factor ; k++) {
        bin[0][i] += data[0][j]; /* linear sum for time */
        bin[1][i] += data[1][j]; /* linear sum for data */
        bin[2][i] += data[2][j]*data[2][j]; /* quadratic sum for error */
        j++; /* running increment */
        if (j == n) {
            k++; /* k is number of points actually binned */
            break;
        }
    }
}
/* average the time and data, the error must wait */
bin[0][i] /= k;
bin[1][i] /= k;
/* average the SD of the dispersion of the data with the averaged
 * error */
if (k > 1) {
    j -= k; /* rewind j */
    var = 0;
    for(kk = 0; kk < k; kk++) {
        var += (data[1][j]-bin[1][i])*(data[1][j]-bin[1][i]);
        j++;
    }
}

```

```

    }
    var /= (k-1); /* var = variance = sd^2 */
    bin[2][i] = sqrt(var + bin[2][i]) / (k+1);
} else {
    bin[2][i] = sqrt(bin[2][i]) / k;
}
}

for(i = 0; i < num; i++) {
    fprintf(binfile, "%f %f %f\n", bin[0][i], bin[1][i], bin[2][i]);
}
fclose(binfile);

fprintf(stderr,
    "data binned by %d and output to file %s . . . \n", factor,
    filename);

/* Free the matrices * * * * * */
free_dmatrix(data, 0, 2, 0, n );
free_dmatrix(bin, 0, 2, 0, num);

return 0;
}

```

B.2 mag2flux

The `mag2flux` C program converts apparent magnitudes into the equivalent flux density in units of Janskys (Jy). See the code for details.

```

/*****
 * mag2flux.c
 *
 * Read in a 3 column file and convert the data and error from real
 * magnitudes to flux densities.
 *
 *****/

#include <stdio.h>
#include <stddef.h>
#include <stdlib.h>
#include <string.h>
#include <math.h>
#include <getopt.h>

#define NRANSI
#include "nrutil.h"

#define LINE_LEN 255 /* standard array size for strings */

int main(int argc, char *argv[])
{
/* Declarations * * * * *
long n = 0, i, x, reverse = 0;
char line[LINE_LEN] = "", dummy[LINE_LEN] = "", filter[LINE_LEN];
double **data, fnu0;
FILE *datafile, *fluxfile;

/* check the arguments * * * * *
while ((x = getopt(argc, argv, "r")) != -1) {
    switch (x) {
        case 'r':
            reverse = 1;
            break;
    }
}
argc -= optind-1;
argv += optind-1;

```

```

if(argc<3) {
    fprintf(stderr,
        "\nusage: %s [-r] datafile (filter_letter|zero-point_flux)\n",
        argv[0]);
    fprintf(stderr,
        "The option -r reverses the sense of conversion\n\n");
    exit(1);
}

/* check the data file * * * * * */
if((datafile = fopen(argv[1], "r")) == NULL) {
    fprintf(stderr, "\ncannot open file: %s\n\n", argv[1]);
    exit(1);
}

/* find the proper filter * * * * * */
strcpy(filter, argv[2]);
switch (filter[0]) {
    case 'u':
    case 'U': fnu0 = 1823 * 1000;
               break;
    case 'b':
    case 'B': fnu0 = 4130 * 1000;
               break;
    case 'v':
    case 'V': fnu0 = 3781 * 1000;
               break;
    case 'r':
    case 'R': fnu0 = 2941 * 1000;
               break;
    case 'i':
    case 'I': fnu0 = 2635 * 1000;
               break;
    case 'j':
    case 'J': fnu0 = 1603 * 1000;
               break;
    case 'h':
    case 'H': fnu0 = 1075 * 1000;
               break;
    case 'k':
    case 'K': fnu0 = 667 * 1000;
               break;
    default:  fnu0 = strtod(filter, NULL);
}

```

```

/* count the number of records * * * * * */
for(;;) {
    fgets(line, LINE_LEN, datafile);
    if(feof(datafile)) {
        break;
    }
    n++;
}
rewind(datafile);

/* Create the appropriate arrays * * * * * */
data = dmatrix(0, 2, 0, n);

/* Read in the data file * * * * * */
fprintf(stderr, "Reading in data file . . .\n");
for(i = 0; i < n; i++) {
    fscanf(datafile, "%lf %lf %lf", &data[0][i], &data[1][i], &data[2][i]);
}
fclose(datafile);

/* create the output file name * * * * * */
strcpy(dummy, argv[1]);
if (!reverse) {
    if ((fluxfile = fopen(strcat(dummy, ".flux"), "w")) == NULL) {
        fprintf(stderr, "\ncannot open file: %s\n\n", dummy);
        exit(1);
    }
} else {
    if ((fluxfile = fopen(strcat(dummy, ".mag"), "w")) == NULL) {
        fprintf(stderr, "\ncannot open file: %s\n\n", dummy);
        exit(1);
    }
}

/* print out the reference frame file * * * * * */
if (!reverse) {
    for(i = 0; i < n; i++) {
        fprintf(fluxfile, "%.5f %.6f %.6f\n", data[0][i],
            fnu0*pow(10, -0.4*data[1][i]),
            data[2][i]*(fnu0*pow(10, -0.4*data[1][i])));
    }
} else {
    for(i = 0; i < n; i++) {

```

```

        fprintf(fluxfile, "%.5f %.6f %.6f\n", data[0][i],
            -2.5*log10(data[1][i]/fnu0),
            data[2][i]/data[1][i]);
    }
}
fclose(fluxfile);

/* Free the matrices * * * * * */
free_dmatrix(data, 0, 2, 0, n);

return 0;
}

```


B.3 obs2ref

The `obs2ref` C program converts time and flux densities into the rest frame values based on the redshift given. See the code for details.

```

/*****
 * obs2ref.c
 *
 * Read in a 3 column file and convert the time, data and error to the
 * reference frame of the given redshift.
 *
 *****/

#include <stdio.h>
#include <stddef.h>
#include <stdlib.h>
#include <string.h>
#include <math.h>

#define NRANSI
#include "nrutil.h"

#define LINE_LEN 255 /* standard array size for strings */

int main(int argc, char *argv[])
{
/* Declarations * * * * *
long n = 0, i;
char line[LINE_LEN] = "", dummy[LINE_LEN] = "";
double **data, z;
FILE *datafile, *reffile;

/* check the arguments * * * * *
if(argc<3) {
    fprintf(stderr, "\nusage: %s datafile redshift\n\n", argv[0]);
    exit(1);
}

/* check the data file * * * * *
if((datafile = fopen(argv[1], "r")) == NULL) {
    fprintf(stderr, "\ncannot open file: %s\n\n", argv[1]);
    exit(1);
}

```

```

/* convert and assign the redshift * * * * * */
z = strtod(argv[2], NULL);

/* count the number of records * * * * * */
for(;;) {
    fgets(line, LINE_LEN, datafile);
    if(feof(datafile)) {
        break;
    }
    n++;
}
rewind(datafile);

/* Create the appropriate arrays * * * * * */
data = dmatrix(0, 2, 0, n);

/* Read in the data file * * * * * */
fprintf(stderr, "Reading in data file . . .\n");
for(i = 0; i < n; i++) {
    fscanf(datafile, "%lf %lf %lf", &data[0][i], &data[1][i], &data[2][i]);
}
fclose(datafile);

/* create the output file name * * * * * */
strcpy(dummy, argv[1]);
if ((reffile = fopen(strcat(dummy, ".ref"), "w")) == NULL) {
    fprintf(stderr, "\ncannot open file: %s\n\n", dummy);
    exit(1);
}

/* print out the reference frame file * * * * * */
for(i = 0; i < n; i++) {
    fprintf(reffile, "%.5f %.4f %.6f\n", data[0][i]/(1+z),
        data[1][i]*pow((1+z), 3), data[2][i]*pow((1+z), 3));
}
fclose(reffile);

/* Free the matrices * * * * * */
free_dmatrix(data, 0, 2, 0, n);

return 0;
}

```

B.4 strfun

The `strfun` C program is the front end for the `structure` function seen in §B.7 which implements the structure function algorithm described in §3.3.2. It reads in the datafile, runs the function on it, then returns the results into a file with the extension “.sf” added to the original name.

```

/*****
 * strfun.c
 *
 * Read in a 3 column file and calculate the structure function as a
 * function of time step.
 *
 *****/

#include <stdio.h>
#include <stddef.h>
#include <stdlib.h>
#include <string.h>
#include <math.h>
#include "functions.h"

#define NRANSI
#include "nrutil.h"

#define LINE_LEN 255 /* standard array size for strings */

int main(int argc, char *argv[])
{
/* Declarations * * * * *
long n = 0, i;
char line[LINE_LEN] = "", dummy[LINE_LEN] = "";
double **data, **sf, **sfl;
double sum = 0, avg, a, b, siga, sigb, chi2, q;
FILE *datafile, *sffile;

/* Check the data file * * * * *
if ((datafile = fopen(argv[1], "r")) == NULL) {
    fprintf(stderr, "\ncannot open file: %s\n\n", argv[1]);
    exit(1);
}

for(;;) {

```

```

    fgets(line, LINE_LEN, datafile);
    if(feof(datafile)) {
        break;
    }
    n++;
}
rewind(datafile);

/* Create the appropriate arrays * * * * * */
data = dmatrix(0, 2, 0, n );
sf    = dmatrix(0, 4, 0, n-1);
sfl   = dmatrix(0, 4, 0, n-1);

/* Read in the data file * * * * * */
fprintf(stderr, "Reading in data file . . .\n");
for(i = 0; i < n; i++) {
    fscanf(datafile, "%lf %lf %lf", &data[0][i], &data[1][i],
           &data[2][i]);
    sum += data[1][i];
}
avg = sum / n;
fclose(datafile);

/* Fit the data to a line and remove the linear trend * * * * * */
fit(data[0]-1, data[1]-1, n, data[2]-1, 1, &a, &b, &sig_a, &sig_b, &chi2,
    &q);
for(i = 0; i < n; i++) {
    data[1][i] -= (a + b * data[0][i]) - avg;
}

/* Calculate the Structure Function * * * * * */
fprintf(stderr, "Calculating Structure Functions . . .\n");
strcpy(dummy, argv[1]);
if ((sffile = fopen(strcat(dummy, ".sf"), "w")) == NULL) {
    fprintf(stderr, "\ncannot open file: %s\n\n", dummy);
    exit(1);
}
/* sf[0] = time step, sf[1] = 1st order SF, sf[2] = 1st order SF err */
/* sf[3] = 2nd order SF, sf[3] = 2nd order SF err */
structure(data[0], data[1], data[2], n, sf[0], sf[1], sf[2], sf[3],
    sf[4]);
for(i = 0; i < n-1; i++) {
    if(sf[0][i] > 0.0) {
        sfl[0][i] = log10(sf[0][i]);
    }
}

```

```

    } else {
        sfl[0][i] = 0.0;
    }
    if(sf[1][i] > 0.0) {
        sfl[1][i] = log10(sf[1][i]);
    } else {
        sfl[1][i] = 0.0;
    }
    if(sf[2][i] > 0.0) {
        sfl[2][i] = fabs (sf[2][i] * sfl[1][i]);
    } else {
        sfl[2][i] = 0.0;
    }
    if(sf[3][i] > 0.0) {
        sfl[3][i] = log10(sf[3][i]);
    } else {
        sfl[3][i] = 0.0;
    }
    if(sf[4][i] > 0.0) {
        sfl[4][i] = fabs (sf[4][i] * sfl[3][i]);
    } else {
        sfl[4][i] = 0.0;
    }

    fprintf(sffile, "%g %g %g %g %g %g %g %g %g\n", sf[0][i],
        sf[1][i], sf[2][i], sf[3][i], sf[4][i], sfl[0][i], sfl[1][i],
        sfl[2][i], sfl[3][i], sfl[4][i]);
}
fclose(sffile);

/* Free the matrices * * * * *
free_dmatrix(data, 0, 2, 0, n );
free_dmatrix(sf, 0, 4, 0, n-1);
free_dmatrix(sfl, 0, 4, 0, n-1);

return 0;
}

```

B.5 varind

The `varind` C program is the front end for the `vi` function seen in §B.7 which implements the variability index algorithm described in §3.3.3. It reads in the datafile, runs the function on it, then returns the results into a file with the extension “.vi” added to the original name.

```

/*****
 * varind.c
 *
 * Read in a 3 column file and calculate the variability index as a
 * function of time window.
 *
 *****/

#include <stdio.h>
#include <stddef.h>
#include <stdlib.h>
#include <string.h>
#include <math.h>
#include "functions.h"

#define NRANSI
#include "nrutil.h"

#define LINE_LEN 255 /* standard array size for strings */

int main(int argc, char *argv[])
{
/* Declarations * * * * * */
    long n = 0, i;
    char line[LINE_LEN] = "", dummy[LINE_LEN] = "";
    double **data, **vim;
    double sum = 0, avg, a, b, siga, sigb, chi2, q;
    FILE *datafile, *vifile;

/* Check the data file * * * * * */
    if ((datafile = fopen(argv[1], "r")) == NULL) {
        fprintf(stderr, "\ncannot open file: %s\n\n", argv[1]);
        exit(1);
    }

    for(;;) {

```

```

    fgets(line, LINE_LEN, datafile);
    if(feof(datafile)) {
        break;
    }
    n++;
}
rewind(datafile);

/* Create the appropriate arrays * * * * * */
data = dmatrix(0, 2, 0, n );
vim  = dmatrix(0, 2, 0, n/2);

/* Read in the data file * * * * * */
fprintf(stderr, "Reading in data file . . .\n");
for(i = 0; i < n; i++) {
    fscanf(datafile, "%lf %lf %lf", &data[0][i], &data[1][i],
        &data[2][i]);
    sum += data[1][i];
}
avg = sum / n;
fclose(datafile);

/* Fit the data to a line and remove the linear trend * * * * */
fit(data[0]-1, data[1]-1, n, data[2]-1, 1, &a, &b, &sig_a, &sig_b, &chi2,
    &q);
for(i = 0; i < n; i++) {
    data[1][i] -= (a + b * data[0][i]) - avg;
}

/* Calculate the Variability Index * * * * * */
fprintf(stderr, "Calculating the Variability Index . . .\n");
strcpy(dummy, argv[1]);
if ((vifile = fopen(strcat(dummy, ".vi"), "w")) == NULL) {
    fprintf(stderr, "\ncannot open file: %s\n\n", dummy);
    exit(1);
}
vi(data[0], data[1], data[2], n, vim[0], vim[1], vim[2]);
for(i = n/2-1; i >=0; i--) {
    fprintf(vifile, "%f %f %f\n", vim[0][i], vim[1][i], vim[2][i]);
}
fclose(vifile);

/* Free the matrices * * * * * */
free_dmatrix(data, 0, 2, 0, n );

```

```
    free_dmatrix(vim, 0, 2, 0, n/2);  
    return 0;  
}
```


B.6 ccfdcf

The `strfun` C program is the front end for the `structure` function seen in §B.7 which implements the CCF described in §4.2.1. It reads in the datafile, runs the function on it, then returns the results into a file with the extension “.acf” or “ccf” added to the original name, dependent upon whether one or two input files were given.

```

/*****
 * ccfdcf.c
 *
 * Read in 2 2 column files and calculate the cross
 * correlation function and discrete [binned] correlation function.
 *
 *****/

#include <stdio.h>
#include <stddef.h>
#include <stdlib.h>
#include <string.h>
#include <math.h>
#include "functions.h"

#define NRANSI
#include "nrutil.h"

#define LINE_LEN 255 /* standard array size for strings */

int main (int argc, char *argv[])
{
/* Declarations * * * * * */
    long n = 0, i, m=1, mn;
    char line[LINE_LEN] = "", dummy1[LINE_LEN] = "",
          dummy2[LINE_LEN] = "";
    double **data1, **data2, **ccf;
    FILE *datafile1, *datafile2, *ccffile;
    int isccf = 0;

/* Check the arguments * * * * * */
    if (argc < 2) {
        fprintf(stderr, "\nusage: %s datafile1 [datafile2]\n\n", argv[0]);
        exit(1);
    } else if (argc > 2) {
        isccf = 1;

```

```

}

/* Check the data file(s) * * * * * */
if ((datafile1 = fopen(argv[1], "r")) == NULL) {
    fprintf(stderr, "\ncannot open file: %s\n\n", argv[1]);
    exit(1);
}
for(;;) {
    fgets(line, LINE_LEN, datafile1);
    if (feof(datafile1)) {
        break;
    }
    n++;
}
rewind(datafile1);
if (isccf) {
    if ((datafile2 = fopen(argv[2], "r")) == NULL) {
        fprintf(stderr, "\ncannot open file: %s\n\n", argv[1]);
        exit(1);
    }
}
mn = m*n-(m-1);

/* Create the appropriate arrays * * * * * */
data1 = dmatrix(0, 1, 0, n);
data2 = dmatrix(0, 1, 0, n);
ccf = dmatrix(0, 1, 0, 2*mn-1);

/* Read in the data file * * * * * */
for(i = 0; i < n; i++) {
    fscanf(datafile1, "%lf %lf", &data1[0][i], &data1[1][i]);
}
fclose(datafile1);
if (isccf) {
    for(i = 0; i < n; i++) {
        fscanf(datafile2, "%lf %lf", &data2[0][i], &data2[1][i]);
    }
    fclose(datafile2);
}

/* Caclulate the Cross-Correlation Function * * * * * */
if (isccf) {
    strcpy(dummy1, argv[1]);
    strcpy(dummy2, argv[2]);
}

```

```

    if ((ccffile = fopen(strcat(strcat(strcat(dummy1, "-"), dummy2),
        ".ccf"), "w")) == NULL) {
        fprintf(stderr, "\ncannot open file: %s\n\n",
            strcat(strcat(dummy1, dummy2), ".ccf"));
        exit(1);
    }
    iccf(m, data1[0], data1[1], data2[0], data2[1], n, ccf[0],
        ccf[1]);
    for(i = 0; i < 2*mn-1; i++) {
        fprintf(ccffile, "%f %f\n", ccf[0][i], ccf[1][i]);
    }
    fclose(ccffile);
} else {
    strcpy(dummy1, argv[1]);
    if ((ccffile = fopen(strcat(dummy1, ".acf"), "w")) == NULL) {
        fprintf(stderr, "\ncannot open file: %s\n\n", dummy1);
        exit(1);
    }
    iccf(m, data1[0], data1[1], data1[0], data1[1], n, ccf[0],
        ccf[1]);
    for(i = 0; i < 2*mn-1; i++) {
        fprintf(ccffile, "%f %f\n", ccf[0][i], ccf[1][i]);
    }
    fclose(ccffile);
}

/* Free the matrices * * * * *
free_dmatrix(data1, 0, 1, 0,      n);
free_dmatrix(data2, 0, 1, 0,      n);
free_dmatrix(ccf,   0, 1, 0, 2*mn-1);

return 0;
}

```

B.7 functions

The `functions` C source file contains all the functions required to implement the programs described above. It includes source from *Numerical Recipes in C* (Press et al., 2002), that is designated where applicable.

```

/*****
 *
 * functions.c file
 *
 *****/

#include <stdio.h>
#include <stdlib.h>
#include <string.h>
#include <math.h>

#define NRANSI
#include "nrutil.h"

#define TWOPID 6.2831853071795865
#define SWAP(a,b) tempr=(a);(a)=(b);(b)=tempr
#define MOD(a,b) while(a >= b) a -= b;
#define MACC 4

/*
 * itoa, K&R's inverse to 'atoi'
 */
void
itoa (int n, char s[])
{
    int c, i, j, sign;

    if ((sign = n) < 0) {
        n = -n;
    }
    i = 0;
    do {
        s[i++] = n % 10 + '0';
    } while ((n /= 10) > 0);
    if (sign < 0) {
        s[i++] = '-';
    }
}

```

```

    s[i] = '\0';
    for (i = 0, j = strlen(s)-1; i < j; i++, j--) {
        c = s[i], s[i] = s[j], s[j] = c;
    }
}

void
fastsort(double data[], long left, long right, long max)
{
    long l_hold, r_hold, hold;
    double swap, status;

    status=((double)left / (double)max) * 100.;
    fprintf(stderr, "%.4f%% complete\r", status);

    l_hold = left;
    r_hold = right;
    swap = data[left];
    while (left < right)
    {
        while ((data[right] >= swap) && (left < right))
            right--;
        if (left != right)
        {
            data[left] = data[right];
            left++;
        }
        while ((data[left] <= swap) && (left < right))
            left++;
        if (left != right)
        {
            data[right] = data[left];
            right--;
        }
    }
    data[left] = swap;
    hold = left;
    left = l_hold;
    right = r_hold;
    if (left < hold)
        fastsort(data, left, hold-1, max);
    if (right > hold)
        fastsort(data, hold+1, right, max);
}

```

```

/*
 * "structure function" function
 *
 * time    = time array
 * f       = flux or magnitude array
 * err     = error on flux or magnitude
 * n       = total number of points
 * deltata = return array of time steps
 * sf1     = first order structure function return array
 * err1    = first order sf error return array
 * sf2     = second order structure function return array
 * err2    = second order sf error return array
 * i,j     = general purpose counters
 * fnew    = f array holder (don't modify original data)
 * sumf    = summatioin of "f" values
 * avef    = average of "f" values
 * sf_1    = value holder for 1st order SF
 * sf_2    = value holder for 2nd order SF
 *
 */
void
structure(double time[], double f[], double err[], long n,
          double deltata[], double sf1[], double err1[], double sf2[],
          double err2[])
{
    long i, j;
    double fnew[n];
    double sumf = 0.0, sume = 0.0, avef, avee, vare, sf_1, sf_2;

    /* sum f=(flux or diff mag) */
    for(i = 0; i < n; i++) {
        sumf += (double) f[i];
    }

    /* average */
    avef = sumf / (double) n;

    /* subtract off the mean. */
    for(i = 0; i < n; i++) {
        fnew[i] = (double) f[i] - avef;
    }

    /* calculate the 1st and 2nd order structure functions. */

```

```

for(i = 1; i < n; i++){
    /* initialize holders */
    sf_1 = 0.0;
    sf_2 = 0.0;
    sume = 0.0;
    for(j = 0; j < n-i; j++){
        /* first order SF */
        sf_1 += (fnew[j+i] - fnew[j]) *
                (fnew[j+i] - fnew[j]);
        /* second order SF */
        sf_2 += (fnew[j+i] - 2*fnew[j+i/2] + fnew[j]) *
                (fnew[j+i] - 2*fnew[j+i/2] + fnew[j]);
        /* sum of measurement error */
        sume += err[j];
    }
    /* calculate each time step and normalize the SFs */
    deltat[i-1] = (double) time[i] - (double) time[0];
    sf1[i-1] = sf_1 / (double) (n-i);
    sf2[i-1] = sf_2 / (double) (n-i);
    avee = sume / (double) (n-i);
    sume = 0.0;
    for (j = 0; j < n-i; j++){
        sume += (err[j] - avee) * (err[j] - avee);
    }
    if (n-i > 1) {
        vare = sume / (double) (n-i-1);
    } else {
        vare = sume / (double) (n-i); /* will be zero */
    }
    err1[i-1] = 8. * vare * sf1[i-1] / (double) (n-i);
    err2[i-1] = 24. * vare * sf2[i-1] / (double) (n-i);
}
}

/*
* "variability index" function
*
* time      = time array
* data      = flux or magnitude data array
* errin     = error input on flux or magnitude
* n         = total number of points
* deltat    = return array of time steps
* vi        = variability index (VI) return array
* errout    = VI error return array

```

```

* i,j,k,m = general counters
* vi1      = primary calculation array
* vi2      = secondary calculation array
* valhi    = the highest valued point in a given window
* vallo    = the lowest valued point in a given window
*
*/
void
vi(double time[], double data[], double errin[], long n,
   double deltat[], double vi[], double errout[])
{
    long i = 0, j, k;
    unsigned long m;
    double vi1[n], vi2[n], valhi, vallo;

    /* calculate the time windows */
    while(i < n/2) {
        deltat[i] = time[n-1-i] - time[i];
        i++;
    }
    /* "i" array counts the time window */
    for(i = n/2; i >= 0; i--) {
        /* "j" array counts all the points within an individual window */
        for(j = 0; j < n; j++) {
            fprintf(stderr, "computing time window % 7.5f . . .\r",
                deltat[i]);
            /* find the highest and lowest valued points */
            valhi = vallo = data[j];
            k = (j+1);
            while((k < n) && ((time[k] - time[j]) < deltat[i])) {
                valhi=DMAX(valhi, data[k]);
                vallo=DMIN(vallo, data[k]);
                k++;
            }
            /* calculate the variability index for this time step and window */
            vi1[j] = fabs((valhi - vallo) / (valhi + vallo));
            if(k >= (n-1)) {
                break;
            }
        }
    }
    /* transfer the values to the secondary array and zero the primary */
    m=0;
    for(j = 0; j < n; j++) {
        if(vi1[j] != 0.0) {

```



```

        vi2[m++] = vi1[j];
    }
    vi1[j] = 0.0;
}
/* sum, average, and calculate the standard deviation for all
 * values in this time window */
if(m > 1) {
    vi[i] = 0.0;
    for(j = 0; j < m; j++) {
        vi[i] += vi2[j]; /* sum */
    }
    vi[i] /= m; /* average */
    errout[i] = 0.0;
    for(j = 0; j < m; j++) {
        errout[i] += (vi2[j] - vi[i])*(vi2[j] - vi[i]); /* variance sum */
    }
    errout[i] = sqrt(errout[i] / (m-1)); /* std dev = sqrt(variance) */
    //errout[i] /= sqrt(m); /* testing with std error = sd / sqrt(n) */
} else {
    /* If only one measurement, set error to zero */
    vi[i] = vi2[0];
    errout[i] = 0.0;
}
}
printf ("\n");
}

void
bubblesort(double data0[], double data1[], long n)
{
    long i, j;
    double temp[2];

    for(i = n-1; i >= 0; i--)
    {
        for(j = 1; j <= i; j++)
        {
            if(data0[j-1] > data0[j])
            {
                temp[0] = data0[j-1];
                temp[1] = data1[j-1];
                data0[j-1] = data0[j];
                data1[j-1] = data1[j];
                data0[j] = temp[0];
            }
        }
    }
}

```

```

        data1[j] = temp[1];
    }
}
}

void
linearinterp(double data1[], double data2[], long m, long n)
{
    long i, j;
    double dy, dt, slope;

    for(i = 1; i < n ; i++) {
        dy = data2[m*i] - data2[m*i-m];
        dt = data1[m*i] - data1[m*i-m];
        slope = dy / dt;
        for(j = 1; j < m; j++) {
            //      t = t_0          + (m-j) fraction of dt
            data1[m*i-j] = data1[m*i-m] + (dt          * (m-j)/m);
            //      y = y intercept + fraction of dt * slope
            data2[m*i-j] = data2[m*i-m] + (dt*(m-j)/m * slope );
        }
    }
}

/*
 * "'interpolated'" CCF" function
 *
 * m      = number of points to interpolate
 * t1     = time array of first dataset
 * f1     = flux or mag array of first dataset
 * t2     = time array of second dataset
 * f2     = flux or mag array of second dataset
 * n      = number of elements in the arrays
 *         (assumed to be the same for all)
 * deltat = time difference (lag) return array
 * ccf     = CCF return array
 * i,j     = general counters
 * mn      = largest size of arrays
 *
 */
void
iccf(long m, double t1[], double f1[], double t2[], double f2[], long n,
     double deltat[], double ccf[])

```

```

{
    long i, j, mn = m*n-(m-1);
    /* Create the necessary arrays */
    double data1[2][mn], data2[2][mn];
    double sumf1 = 0.0, sumf2 = 0.0, varf1 = 0.0, varf2 = 0.0;
    double avef1, avef2, varf, ccf_1, ccf_2;

    /* Initialize the arrays */
    for(i = 0; i < n; i++) {
        data1[0][i*m] = t1[i];
        data1[1][i*m] = f1[i];
        data2[0][i*m] = t2[i];
        data2[1][i*m] = f2[i];
    }

    /* Interpolate empty data points to increase resolution */
    linearinterp(data1[0], data1[1], m, n);
    linearinterp(data2[0], data2[1], m, n);

    /* Sum the interpolated and real function data over n. */
    for(i = 0; i < mn; i++) {
        sumf1 += data1[1][i];
        sumf2 += data2[1][i];
    }

    /* Average . . . */
    avef1 = sumf1 / (double) mn;
    avef2 = sumf2 / (double) mn;

    /* Subtract off the mean. */
    for(i = 0; i < mn; i++) {
        data1[1][i] -= avef1;
        data2[1][i] -= avef2;
    }
    /* Calculate the variance */
    varf1 += data1[1][i] * data1[1][i];
    varf2 += data2[1][i] * data2[1][i];
    }
    varf = sqrt(varf1) * sqrt(varf2);

    /* Calculate the crosscorrelation function. */
    for(i = 0; i < mn; i++){
        ccf_1 = 0.0;
        ccf_2 = 0.0;
        for(j = 0; j < mn-i; j++){

```

```

        ccf_1 += (data1[1][j] * data2[1][j+i]);
        if(i != 0) {
            ccf_2 += (data2[1][j] * data1[1][j+i]);
        }
    }
    deltat[mn-1+i] = data1[0][i] - data1[0][0];
    ccf[mn-1+i] = ccf_1 / varf;
    if(i != 0) {
        deltat[mn-1-i] = data1[0][0] - data1[0][i];
        ccf[mn-1-i] = ccf_2 / varf;
    }
}
}

void fit(double x[], double y[], int ndata, double sig[], int mwt,
        double *a, double *b, double *siga, double *sigb, double *chi2,
        double *q)
{
    double gammq(double a, double x);
    int i;
    double wt,t,sxoss,sx=0.0,sy=0.0,st2=0.0,ss,sigdat;

    *b=0.0;
    if (mwt) {
        ss=0.0;
        for (i=1;i<=ndata;i++) {
            wt=1.0/SQR(sig[i]);
            ss += wt;
            sx += x[i]*wt;
            sy += y[i]*wt;
        }
    } else {
        for (i=1;i<=ndata;i++) {
            sx += x[i];
            sy += y[i];
        }
        ss=ndata;
    }
    sxoss=sx/ss;
    if (mwt) {
        for (i=1;i<=ndata;i++) {
            t=(x[i]-sxoss)/sig[i];
            st2 += t*t;
            *b += t*y[i]/sig[i];

```

```

    }
} else {
    for (i=1;i<=ndata;i++) {
        t=x[i]-sxoss;
        st2 += t*t;
        *b += t*y[i];
    }
}
*b /= st2;
*a=(sy-sx*(b))/ss;
*sigma=sqrt((1.0+sx*sx/(ss*st2))/ss);
*sigb=sqrt(1.0/st2);
*chi2=0.0;
if (mwt == 0) {
    for (i=1;i<=ndata;i++)
        *chi2 += SQR(y[i]-(*a)-(*b)*x[i]);
    *q=1.0;
    sigdat=sqrt((*chi2)/(ndata-2));
    *sigma *= sigdat;
    *sigb *= sigdat;
} else {
    for (i=1;i<=ndata;i++)
        *chi2 += SQR((y[i]-(*a)-(*b)*x[i])/sig[i]);
    *q=gamma(0.5*(ndata-2),0.5*(chi2));
}
}
}
/* (C) Copr. 1986-92 Numerical Recipes Software 3#(11,1&0(9p#3. */

double gammq(double a, double x)
{
    void gcf(double *gammcf, double a, double x, double *gln);
    void gser(double *gamser, double a, double x, double *gln);
    void nrerror(char error_text[]);
    double gamser,gammcf,gln;

    if (x < 0.0 || a <= 0.0) nrerror("Invalid arguments in routine gammq");
    if (x < (a+1.0)) {
        gser(&gamser,a,x,&gln);
        return 1.0-gamser;
    } else {
        gcf(&gammcf,a,x,&gln);
        return gammcf;
    }
}
}

```

```

/* (C) Copr. 1986-92 Numerical Recipes Software 3#(11,1&0(9p#3. */

#define ITMAX 100
#define EPS 3.0e-7
#define FPMIN 1.0e-30
void gcf(double *gammcf, double a, double x, double *gln)
{
double gammln(double xx);
void nrerror(char error_text[]);
    int i;
    double an,b,c,d,del,h;

    *gln=gammln(a);
    b=x+1.0-a;
    c=1.0/FPMIN;
    d=1.0/b;
    h=d;
    for (i=1;i<=ITMAX;i++) {
        an = -i*(i-a);
        b += 2.0;
        d=an*d+b;
        if (fabs(d) < FPMIN) d=FPMIN;
        c=b+an/c;
        if (fabs(c) < FPMIN) c=FPMIN;
        d=1.0/d;
        del=d*c;
        h *= del;
        if (fabs(del-1.0) < EPS) break;
    }
    if (i > ITMAX) nrerror("a too large, ITMAX too small in gcf");
    *gammcf=exp(-x+a*log(x)-(*gln))*h;
}
#undef ITMAX
#undef EPS
#undef FPMIN
/* (C) Copr. 1986-92 Numerical Recipes Software 3#(11,1&0(9p#3. */

#define ITMAX 100
#define EPS 3.0e-7
void gser(double *gamser, double a, double x, double *gln)
{
double gammln(double xx);
void nrerror(char error_text[]);
    int n;

```

```

double sum,del,ap;

*gln=gammln(a);
if (x <= 0.0) {
    if (x < 0.0) nrerror("x less than 0 in routine gser");
    *gamser=0.0;
    return;
} else {
    ap=a;
    del=sum=1.0/a;
    for (n=1;n<=ITMAX;n++) {
        ++ap;
        del *= x/ap;
        sum += del;
        if (fabs(del) < fabs(sum)*EPS) {
            *gamser=sum*exp(-x+a*log(x)-(*gln));
            return;
        }
    }
    nrerror("a too large, ITMAX too small in routine gser");
    return;
}
}
#undef ITMAX
#undef EPS
/* (C) Copr. 1986-92 Numerical Recipes Software 3#(11,1&0(9p#3. */

double gammln(double xx)
{
    double x,y,tmp,ser;
    static double cof[6]={76.18009172947146,-86.50532032941677,
        24.01409824083091,-1.231739572450155,
        0.1208650973866179e-2,-0.5395239384953e-5};
    int j;

    y=x=xx;
    tmp=x+5.5;
    tmp -= (x+0.5)*log(tmp);
    ser=1.000000000190015;
    for (j=0;j<=5;j++) ser += cof[j]/++y;
    return -tmp*log(2.5066282746310005*ser/x);
}
/* (C) Copr. 1986-92 Numerical Recipes Software 3#(11,1&0(9p#3. */

```

References

- Aller, M. F., (1999) Radioband Variability Properties of BL Lac Objects. *ASP Conf. Ser. 159: BL Lac Phenomenon*, page 31.
- Barbieri, C., Vio, R., Cappellaro, E., and Turatto, M. (1990). The Optical Variability of the Quasar 3C 446. *The Astrophysical Journal*, 359:63–66.
- Blandford, R., McKee, C., and Rees, M. (1977). Super-luminal Expansion in Extragalactic Radio Sources. *Nature*, 267:211–216.
- Campbell, A. (2004). The Character of Optical Variability for X-Ray Selected Blazars. Ph.D., Georgia State Univeristy, Atlanta, Georgia.
- Carini, M., Miller, H., and Goodrich, B. (1990). The Timescales of the Optical Variability of Blazars. I. OQ 530. *The Astronomical Journal*, 100(2):347–355.
- Carini, M., Miller, H., Noble, J., and Goodrich, B. (1992). The Timescales of the Optical Variability of Blazars. III. OJ 287. *The Astronomical Journal*, 104(1):15–27.
- Carini, M., Miller, H., Noble, J., and Sadun, A. (1991). The Timescales of the Optical Variability of Blazars. II. AP Librae. *The Astronomical Journal*, 101(4):1196–1201.
- Carini, M. T. (1990). *The Timescales of the Optical Variability of Blazars*. Ph.D., Georgia State Univeristy, Atlanta, Georgia.
- Carini, M. T., Noble, J. C., and Miller, H. R. (1998). The Timescales of the Optical Variability of Blazars. V. 3C 371. *The Astronomical Journal*, 116:2667–2671.
- Fath, E. A. (1908). *Bulletin Number 149 - The Spectra of Some Spiral Nebulae and Globular Star Clusters*. *Lick Observatory Bulletin*, 5:71–77
- Gopal-Krishna, Dhurde, S., and Wiita, P.J. (2004). Do the Mildly Superluminal VLBI Knots Exclude Ultrarelativistic Blazar Jets? *The Astrophysical Journal Letters*, 615:L81–L84.
- Heidt, J., and Wagner, S. (1996). Statistics of Optical Intraday Variability in a Complete Sample of Radio-Selected BL Lacertae Objects. *Astronomy & Astrophysics*, 305:42–52.
- Jorstad, S., Marscher, A., Mattox, J., Wehrle, A., Bloom, S., and Yurchenko, A. (2001). Multiepoch Very Long Baseline Array Observations of EGRET-Detected Quasars and BL Lacertae Objects: Superluminal Motion of Gamma-Ray Bright Blazars. *The Astrophysical Journal Supplement Series*, 134:181–240.

- Marscher, A.P. and Travis, J.P. (1996). Synchrotron Self-Compton Interpretation of Multi-waveband Observations of Gamma-Ray Bright Blazars. *Astronomy & Astrophysics Supplement Series*, 120:537–540.
- Mattox, J. R. and Wagner, S. J., (1996) An Intense Gamma-ray Flare of PKS 1622-297. *ASP Conf. Ser. 110: Blazar Continuum Variability*, page 352.
- McFarland, J.P., Miller, H.R., Ferrara, E.C., Wilson, J.W., Daya, A.B., Fried, R.E., Noble, J.C. (1999). The Variability of the Blazar, OF 038. *American Astronomical Society, 195th AAS Meeting, #16.05; Bulletin of the American Astronomical Society*, 31:1397.
- Noble, J. C. (1995). *The Nature of Optical Microvariability of Blazars*. Ph.D., Georgia State University, Atlanta, Georgia.
- Padovani, P., and Giommi, P. (1995). The Connection Between X-ray- and Radio-selected BL Lacertae Objects. *The Astrophysical Journal*, 444:567–581
- Paltani, S. (1999). Constraining BL Lac Models Using Structure Function Analysis. In Takalo, L., and Sillanpaa, A., editors, *BL Lac Phenomenon ASP Conference Series*, volume 159, pages 293–296, New York, NY.
- Peterson, B. M. (1997). *An Introduction to Active Galactic Nuclei*. Cambridge University Press, 40 West 20th Street, New York, first edition.
- Piner, B., and Edwards, P. (2004). The Parsec-Scale Structure and Jet Motions of the TeV Blazars 1ES 1959+650, PKS 2155-304 and 1ES 2344+514. *The Astrophysical Journal*, 600:115–126.
- Press, W. H., Teukolsky, S. A., Vetterling, W. T., and Flannery, B. P. *Numerical Recipes in C: The Art of Scientific Computing*. Cambridge University Press, 40 West 20th Street, New York, second edition.
- Sagar, R., Stalin, C., Gopal-Krishna, and Wiita, P. J. (2004). Intranight Optical Variability of Blazars. *Monthly Notices of the Royal Astronomical Society*, 348:176–186.
- Schmidt, M. (1963). 3C 273: A Star-Like Object with Large Red-Shift. *Nature*, 197:1040.
- Schmidt, M. (1968). Quasi-Stellar Sources. *Mitteilungen der Astronomischen Gesellschaft*, 25:13–17
- Simonetti, J., Cordes, J., and Heeschen, D. (1985). Flicker of Extragalactic Radio Sources at Two Frequencies. *The Astrophysical Journal*, 296:46–59.
- Slipher, V. (1917). The Spectrum and Velocity of the Nebula NGC 1068 (M 77). *Lowell Observatory Bulletin*, 3:59–62.
- Spiegel, E. (1978). Invited Talk on BL Lac Objects. Pittsburgh Conference on BL Lac Objects.

- Stalin, C., Gopal-Krishna, Sagar, R., and Wiita, P. J. (2004). Intranight Optical Variability of Radio-Quiet and Radio Lobe-Dominated Quasars. *Monthly Notices of the Royal Astronomical Society*, 350:175–188.
- Urry, C., and Padovani (1995). Unified Schemes for Radio-Loud Active Galactic Nuclei. *Publication of the Astronomical Society of Japan*, 107:803–845.
- Urry, C. (1996). *Continuum Variability of Blazars*. Miller, H.R. Webb, J.R., and Noble. J.C., editors, *Blazar Continuum Variability, ASP Conference Series*, volume 110, pages 391–402, San Francisco, CA.
- Vermeulen, R., and Cohen, M. (1994). Superluminal Motion Statistics and Cosmology. *The Astrophysical Journal*, 430:467–494.
- Wurtz, R., Stocke, J. T., and Yee, H. (1996). The Canada-France-Hawaii Telescope Imaging Survey of BL Lacertae Objects. I. Properties of the Host Galaxies. *The Astrophysical Journal Supplement Series*, 103:109–144.